ISSN 1738-1142

Volume 17(1) **2019**

KOREAN RADIOACTIVE WASTE SOCIETY

2019 춘계학술논문요약집

| 일시 |

2019. 5. 8(수) ~ 5. 10(금)

| 장소 |

부산 해운대그랜드호텔

Abstracts of Proceedings of the
Korean Radioactive Waste Society
SPRING 2019

사단법인 한국방사성폐기물학회
Korean Radioactive Waste Society

2019 춘계학술발표회

이 발표논문집은 2019년도 정부재원(과학기술진흥기금 및 복권기금)으로
한국과학기술단체총연합회의 지원을 받아 발간되었음

ISSN 1738-1142

Volume 17(1) 2019

KOREAN RADIOACTIVE WASTE SOCIETY

2019 춘계학술논문요약집

| 일시 |

2019. 5. 8(수) ~ 5. 10(금)

| 장소 |

부산 해운대그랜드호텔

Abstracts of Proceedings of the
Korean Radioactive Waste Society
SPRING 2019

사단법인 한국방사성폐기물학회
Korean Radioactive Waste Society

Contents

KOREAN
RADIOACTIVE WASTE
SOCIETY

1분과 핵주기정책·규제 및 비확산 (Oral)

09:00~09:20 A Study on Considerations to Apply Technical Security Controls for Nuclear Facilities ····· 19
Chaechang Lee [KINAC]

09:20~09:40 Risk-Informed Based Graded Approach and Consequence Assessment on Cyber Security Measure in Nuclear Facilities ····· 21
Soo Min Lim [KINAC]

09:40~10:00 Two Classification Algorithms for Nuclear Fuel Cycle Related Documents ·· 23
Tongkyu Park, Yunpil Jeong, and Byoungchan Han [FNC], Sang Jun Lee, Chan Seo Lee, and Dong-hoon Shin [KINAC]

10:00~10:20 Legal Policy Study on Revision of Korea Tax Acts About a New Nuclear Fuel Tax ····· 25
Daesung Lee, Sungjin Choi, and Jaeyoung Bang [KAERI]

11:20~11:40 Algorithm Development for Tracking Process Material on Surveillance Camera in Pyroprocessing Based on Deep Learning Techniques ····· 27
Byung Hee Won, Se Hwan Park, Hee-Sung Shin, and Seong-Kyu Ahn [KAERI]

11:40~12:00 Nuclear Material Diversion Detection Using Intelligent Surveillance Based on Deep Learning ····· 29
Se-Hwan Park, Byung-Hee Won, Hee-Sung Shin, and Seong-Kyu Ahn [KAERI], Shin-Dong Kang [IDOSI]

12:00~12:20 Laser-induced Breakdown Spectroscopy Analysis for Addressing Copycat Crime of Alexander Litvinenko (Polonium-laced Tea) ····· 31
Yunu Lee and Sungyeol Choi [KAIST]

12:20~12:40 Measurement of Uranium in LiCl-KCl Salt Using LIBS ····· 33
Seul-Ki Han, Se-Hwan Park, and Seong-Kyu Ahn [KAERI]

1분과 핵주기정책·규제 및 비확산 (Poster)

P0101 Analyzing and Suggesting on the Practical Measures to Prevent Illicit Activities on Nuclear Materials and Radioactive Sources ····· 37
Jae San Kim [KINAC]

P0102 The Current Status and Prospects of INPRO and GIF Proliferation Resistance Evaluation Methodology ····· 39
Ji-song Jeong [UST], Ho-Dong Kim and Seung-kyu Ahn [KAERI]

P0103 IAEA Concept for Exemption and Clearance ····· 41
Jeong-Guk Kim, Won Hyuk Jang, MalGoBalGaeBitNaLa Yoo, Yujeong Choi, Jongjin Kim, Seeun Chang, Hee-Seoung Park, and Dae-Seok Hong [KAERI]

P0104 Identifying Radioactive Materials in Dirty Bomb Terror Scene Using Laser-Induced Breakdown Spectroscopy ····· 43
Hyeongbin Kim, Yunu Lee, and Sungyeol Choi [KAIST]

P0105 An Analysis of the Contributions of KAERI's Operation to the Daejeon Regional Economy ····· 45
Dong Hoon Lee, Jieun Joo, Man-Ki Lee, and Chae Young Lim [KAERI]

P0106 A Study of Training and Qualification of Security Personnel at Nuclear Facilities ····· 47
Hyun-Kyung Lee [KINAC]

P0107 A Literature Study on Simulation Methods With Respect to Denuclearization ··· 49
Jinyoung Lee [KINAC]

2분과 사용후핵연료 처분전관리 (Oral)

09:00~09:20 Calibration of Effective Material Properties of Spent Nuclear Fuel Rod ·· 53
Sanghoon Lee [Keimyung Univ.]

09:20~09:40 Thermal Analysis of HISTORM-100 Dry Storage Cask With Oxidation Considered Heterogeneous WH14X14 Fuel Assembly Using COMSOL MULTIPHYSICS Program ····· 55
SunWoo Park and KwangHeon Park [Kyung Hee Univ.]

09:40~10:00 Cutoff Frequency for Rigid Body Acceleration of KORAD21 Cask in Drop Accidents ····· 57
Sang Soon Cho, Yun Young Yang, Jaehoon Lim, Ki-Seog Seo, and Woo-Seok Choi [KAERI], Sang-Hwan Lee, Chang-Min Shin, and Chang-Yeal Baeg [KORAD]

10:00~10:20 Development of a Reinforcement Device, SAFER, to Ensure the Handling Integrity of PWR Spent Nuclear Fuel for Dry Storage in Korea ····· 59
Hyeong Koo Kim, Jae Jun Lee, Dong Geun Ha, Gyu Cheol Sin, Sung Ki Lee, and Jong Sung Yoo [KEPCO NF]

11:20~11:40 Fatigue Life Characterization of Simulated Fuel Cladding to Hydride Contents for Normal Transportation Integrity ····· 61
Kang-Hee Lee, Heung-Seok Kang, Jae-Yong Kim, Yong-Sik Yang, and Donghak Kook [KAERI]

11:40~12:00 Reduction of Metal Oxides Compounds by Lithium Metal as a Reductant in Molten LiCl Salt ····· 63
Eun-Young Choi, Min Ku Jeon, and Sung-Wook Kim [KAERI]

12:00~12:20 Micro-cantilever Tests on Hydride Blister and Zirconium Matrix of Zircaloy-4 Cladding Tube ····· 65
Ho-a Kim and Yong-soo Kim [Hanyang Univ.], Jae-soo Noh [ACT Co., LTD], Ju-seong Kim [KAERI]

2분과 사용후핵연료 처분전관리 (Poster)

P0201 Effect of the Crucible Cover on the Distillation of Cadmium ····· 69
S.W. Kwon, J.H. Jung, and S.J. Lee [KAERI]

P0202 Review of Design Requirements for SNF Dry Storage System ····· 70
Sunghwan Chung, Taehyeon Kim, and Yunchang Jeong [KHNP-CRI]

P0203 An Applicable Study on the Fast Neutron Detection for Nuclear Material Accountancy ····· 72
Seonkwang Yoon [UST], Chaehun Lee, Byung Hee Won, Seong-Kyu Ahn, and Ho-Dong Kim [KAERI], Hee Seo [Chonbuk Natl. Univ.]

P0204 Measurement of Threshold Stress Intensity Factor of Delayed Hydride Cracking for Unirradiated Zircaloy-4 Cladding ····· 74
Jong-Dae Hong, Euijung Kim, and Donghak Kook [KAERI]

P0205 Characteristics of Vacuum Drying for Canister ····· 76
Seung-hwan Yu, Ju-chan Lee, Kyung-sik Bang, and Woo-seok Choi [KAERI]

P0206 The Direction of Extension of the AMORES Code Capability ····· 78
Daesik Yook, Ara Go, Gyeong-uk Kang, and Haiyong Jung [KINS]

P0207 Review on the Control of the Direction of Hydride in Zirconium Clad Tube in Terms of Manufacturing Process ····· 80
Tae-Sik Jung and Seong-Ki Lee [KEPCO NF]

P0208 Benefits of the ISA Application to Pyroprocessing Facilities ····· 82
Gilsung You, Seokjun Seo, Woojin Jo, Siwan Noh, Hyojik Lee, Hohee Lee, Seungnam Yu, and Jeonghoe Ku [KAERI]

P0209 Effect of Long-term Cooling on the Hydride Reorientation of Non-irradiated Zircaloy-4 Cladding Tube : 1M, 3M & 6M ····· 84
DaeHo Kim, JongDae Hong, Jegeon Bang, IkSung Lim, EuiJung Kim, and Donghak Kook [KAERI]

P0210 Experimental Investigation of Temperature Profiles in Spent Fuel Model 86
Dong-seok Oh, Chang-hwan Shin, and Dong-hak Kook [KAERI]

P0211 Dynamic Buckling Test of Cell Setting Spacer Grid and Normal Spacer Grid ··· 88
Hong-Ryoul Oh, Jae-Yong Kim, Kyung-Ho Yoon, Sung-Uk Lee, and Donghak Kook [KAERI]

P0212 Review of Chloride-Induced Stress Corrosion Cracking Issue and Mitigation Technology of Spent Fuel Dry Storage Canister ····· 90
Donghee Lee and Yongdeog Kim [KHNP-CRI]

P0213 Preliminary Study of Annular Fuel Fabrication Using Hot Extrusion Method ··· 92
Sang-Gyu Park, Kiho Kim, and Jeong-Yong Park [KAERI]

P0214 Speculation on the Boundary Conditions of Spent Fuel Evaluation During Transportation ····· 94
Donghyo Lee, Seongki Lee, and Jongsung Yoo [KEPCO NF]

P0215 Research Status on Long-term Performance of Seals for Spent Fuel Transport and Storage Casks ····· 96
Yun-young Yang, Jongmin Lim, and Woo-seok Choi [KAERI]

P0216 Performance of the Reaction of Rare Earth and UCl_3 in the LiCl-KCl Salt ··· 98
Seungwoo Paek, Dal-Sung Yoon, Gha-Young Kim, Junhyuk Jang, and Sung-Jai Lee [KAERI]

P0217 Concentration Change of Electro-refining Salt With the Conditions of a Reduced Fuel ····· 100
Seungwoo Paek, Chang Hwa Lee, and Sung-Jai Lee [KAERI]

P0218 Mass Transfer Analysis on a Rotating Cylinder Electrode in the Molten-salt Electrolyte ····· 102
Kwang-Rag Kim, Sung-Ki Kim, and Hyo-On Nam [KAERI]

P0219 Determination of Alkali and Alkaline Earth Metal Oxide Solubility in Molten LiCl Salt at 923 K ····· 104
Dokyu Kang, Seokjoo Yoon, and Sungyeol Choi [KAIST],
Byung Heung Park [Korea Natl. Univ. Transportation]

P0220 Characterization of U-10wt.%Zr-5wt.%RE Fuel Remelt Residue for Recycle of Metallic Fuel Scrap ····· 106
Ki-Hwan Kim, Seong-Jun Ha, Seung-Uk Mun, Seok-Jin Oh, Seoung-Woo Kuk, and Jeong-Yong Park [KAERI]

P0221 Purification of LiCl Salt Waste Using Enhanced Melt-crystallization Method ···· 108
Jung-Hoon Choi, Ki-Rak Lee, Seung-Youb Han, Hyun-Woo Kang, and Hwan-Seo Park [KAERI]

P0222 Numerical Method to Estimate Uncertainties Associated With Positioning Error of Stain Measurement in Drop Test of Radioactive Waste Transport Casks ···· 110
Jongmin Lim and Woo-seok Choi [KAERI]

P0223 Development of Si-Al-P Composites for Immobilization of Radioactive Waste Salt ····· 112
Ki Rak Lee, Hwan-Seo Park, Jung-Hoon Choi, Seung Youb Han, Hyun Woo Kang, Daegwon Eun, and Seona Jung [KAERI]

P0224 Development of Spent Fuel Nuclear Characteristic Evaluation System ·· 114
Jae-Han Kim and Hyung-Moon Kwon [KAERI], Young-Suk Jung, Young-Il Oh, and Eun-Kyung Lee [ACT Co., Ltd.]

P0225 Collection of Uranium Metal From the Salt Mixture Using Yttrium Metal ·· 116
Joon-Bo Shim, Dal-Sung Yoon, Si-Hyung Kim, and Sung-Jai Lee [KAERI]

P0226 Preparation of the Pin-loading Tension Test for Evaluation of Fracture Toughness in PWR Cladding Tubes ····· 118
Myungchul Park, Jae-Yong Kim, Dosik Kim, and Sangbok Ahn [KAERI]

P0227 Dry Atmosphere Test of Pyroprocess Automation Mockup Using Dried Air Supply and Drying System Operation ····· 120
Jonghui Han, Byungsuk Park, and Seungnam Yu [KAERI]

P0228 Design of Modular Electrolytic Reduction Equipment ····· 122
Jong Kwang Lee, Sung-Wook Kim, Dong-Seok Ryu, Sun Seok Hong, and Eun-Young Choi [KAERI]

P0229 Evaluation of the Accident Frequency Analysis for the Integrated Safety Analysis in Nuclear Fuel Cycle Facility ····· 124
Woo Jin Jo, Seok-Jun Seo, Siwan Noh, Hyo Jik Lee, and Seung Nam Yu [KAERI]

P0230 Current Status of ACPF Argon Cell System ····· 126
Byungsuk Park, Jongkwang Lee, and Eunyoung Choi [KAERI]

P0231 Studies on the Chlorination Reaction of Uranium Using Zinc Dichloride ··· 128
Chang Hwa Lee, Tack Jin Kim, Dalsung Yoon, and Sungjai Lee [KAERI]

P0232 Demonstration of Basket Transportation Between a Station and Equipment Using Automation System in PAVM ····· 130
Dongseok Ryu, Jongkwang Lee, Jonghui Han, and Seungnam Yu [KAERI]

P0233 Storage and Decommission of Obsolete Cask ····· 132
Woo-Seok Choi, Sang soon Cho, Seung-hwan Yoo, Jongmin Lim, Ju-chan Lee, Ki-seog Seo, Kyong-Sik Bang, Yun-young Yang, Gileon Jung, and Jaehoon Lim [KAERI]

P0234 Investigation of Trapping Characteristics of Iodine From CsI ····· 134
Seok-Min Hong, Do Yeon Lee, Yeoung Soon Lee, and Yung-Zun Cho [KAERI]

P0235 Transportation Analysis of the 14OFA PWR Fuel Assembly ····· 135
Sung-Uk Lee, Jae-Yong Kim, Hong-Ryoul Oh, Kyung-Ho Yoon, Hyo-Chan Kim, and Donghak Kook [KAERI]

P0236 Round Robin Test Result of Pendulum Impact Testers for Low Burn-up Spacer Grids Operated by Three Different Laboratories ····· 137
JaeYong Kim, KyungHo Yoon, HongRyoul Oh, SungGeun Kim, and Donghak Kook [KAERI], Younglk Yoo [KEPCO NF]

P0237 Analysis on Remoteness of Spent Nuclear Fuel Assembly for Disassembling ····· 139
Younghwan Kim, Yungzon Cho, and Youngsoon Lee [KAERI]

3분과 고준위폐기물처분 (Oral)

09:00~09:20 Interpretation of Geological Deformation History by Integrated Analysis of Field and Borehole Survey Around KURT Area ····· 143
Soolim Jung, Kyung-Woo Park, Sung-Hoon Ji, and Kyung-Su Kim [KAERI]

09:20~09:40 Hydrogeochemical Approaches on the Evaluation of Redox Environments in Granitic Bedrock Through New Borehole Drilling in the KURT ····· 145
Jihye Jeong, Jang-Soon Kwon, Yong-Kwon Koh, and Jae-Kwang Lee [KAERI]

09:40~10:00 Buffer Retardation Experiment for Radionuclides Under the Elevated Temperature Conditions: In-situ Synchrotron X-ray Powder Diffraction Study for the Korean Bentonite Under the Dry Conditions ····· 147
Tae-Jin Park, Ji-Hun Ryu, and Jae-Kwang Lee [KAERI], Donghoon Seoung [Chonnam Natl. Univ.]

10:00~10:20 Buffer Retardation Experiment for Radionuclides Under the Elevated Temperature Conditions: In-situ Synchrotron X-ray Powder Diffraction Study for the Korean Bentonite Under the KURT Groundwater Saturated Conditions ····· 149
Donghoon Seoung [Chonnam Natl. Univ.], Tae-Jin Park [KAERI]

11:20~11:40 A Prediction on the Behavior of a Multi-layer Repository Using Thermo-Hydro-Mechanical Damage (THM_D) Model for HLW Disposal ·· 151
Jin-Seop Kim and Geon-Young Kim [KAERI], Jun-Seo Jeon [KAIST]

11:40~12:00 Spherical Gas Migration Modelling Using Mechanical Damage Model ··· 153
Jaewon Lee, Changsoo Lee, and Geon Young Kim [KAERI]

12:00~12:20 Development of a GoldSim Module for Sequential Bayesian Updating for Better Probabilistic Safety Assessment of an HLW Repository ····· 155
Youn-Myoung Lee and Dong-Keun Cho [KAERI]

12:20~12:40 Application of the Adjustment Factor Approach for the Quantification of Model Uncertainty ····· 157
Jongtae Jeong and Dong-Keun Cho [KAERI]

3분과 고준위폐기물처분 (Poster)

P0301 The Methodology for the Decision of Groundwater Monitoring Points Around a Nuclear Facility ····· 161
Kyung-Woo Park, Sung-Hoon Ji, and Jang-Soon Kwon [KAERI]

P0302 Simulations of In-situ Tracer Tests at a Single Borehole With a Wall Having Locally Variable Hydraulic Property ····· 163
Nak-Youl Ko, Kyung-Woo Park, and Sung-Hoon Ji [KAERI]

P0303 Training Course on Geological Disposal of Radioactive Waste at Mizunami URL Part I. Introduction to MIU and Practical Training in MIU ····· 165
Yongheum Jo and Sol-Chan Han [KAIST], Naon Chang [Hanyang Univ.], Sangsu Park [POSTECH], HyungJin Byun [UNIST], JiHwan Boo [Jeju Natl. Univ.], Wonjae Lee [KINGS], Jiwoo Lee [Kyung Hee Univ.], Hyunseok Lee [Seoul Natl. Univ.], Han Young Joo [Dongguk Univ.], Chang-Lak Kim [KINGS]

P0304 Sensitivity Analysis of Thermal Conductivity on Thermal Dimensioning of SNF Direct Disposal System ····· 167
In-Young Kim, Heui-Joo Choi, and Dong-Keun Cho [KAERI]

P0305 Training Course on Geological Disposal of Radioactive Waste at Mizunami URL Part II. Study About the Geological Environment and HLW Disposal in Korea ·· 169
Naon Chang [Hanyang Univ.], Yongheum Jo and Sol-Chan Han [KAIST], Sangsu Park [POSTECH], HyungJin Byun [UNIST], JiHwan Boo [Jeju Natl. Univ.], Wonjae Lee [KINGS], Jiwoo Lee [Kyung Hee Univ.], Hyunseok Lee [Seoul Natl. Univ.], Han Young Joo [Dongguk Univ.], Chang-Lak Kim [KINGS]

P0306 Effect of Temperature on the Interaction of Nuclide With Metal Corrosion Products Under Anaerobic Alkaline Conditions ····· 171
Hyo-Jin Seo, Seung Yeop Lee, and Jae-Kwang Lee [KAERI]

P0307 Review of Finnish Posiva Methodology for the Canister Lifetime Assessment … 173
Heui-Joo Choi, Dong-Keun Cho, and Sung-Hoon Ji [KAERI]

P0308 Corrosion Behavior of SKB Copper in KURT Environment …… 175
Minsoo Lee and Sung-Hoon Ji [KAERI]

P0309 Coupling Multi Scaled Components of Geological Disposal System in APro (Advanced Process-based Total System Performance Assessment Framework for a Geological Disposal System) …… 177
Jung-Woo Kim, Jaewon Lee, Kyung Woo Park, and Dong-Keun Cho [KAERI]

P0310 Preliminary Study on the Development of a Horizontal Disposal Concept for PWR Spent Fuels …… 179
Jong-youl LEE, Heui-joo CHOI, In-young Kim, Hyun-a KIM, and Dong-keun CHO [KAERI]

4분과 중저준위폐기물관리 (Oral)

09:00~09:20 Modification of Granular-Sized Natural Zeolite for Enhancing Practical Use … 183
Seok-ju Hong and Wooyong Um [POSTECH]

09:20~09:40 The Applicability of New Biological and Chemical Decontamination Technology to Nuclear Power Plant and Economic Analysis …… 185
YoungJu Son and Yongbaek Kim [KEPCO E&C], Seung Yeop Lee [KAERI], Junggyu Nam [KEPCO], JaeYeon Jung [KHNP], Chang-Lak Kim [KINGS]

09:40~10:00 Revisit of Recycling of Disposed Radioactive Metal Waste as a Potential Inadvertent Human Intrusion Scenario at a Near-Surface Repository … 187
Wang Hyeon Lee and Jae Hak Cheong [Kyung Hee Univ.]

10:00~10:20 Identification of Redox Reactions of Nb in Molten LiCl-KCl Eutectic for Pyrochemical Decontamination …… 189
Gwan Yoon Jeong, Younghwan Jeon, Jungho Hur, Hyeongjin Byeon, and Jaeyeong Park [UNIST]

11:20~11:40 Studies on ANS 16.1 Leaching Test of Vitrified Forms for the Korean Low-level Radioactive Solid Wastes and Their Leaching Mechanism … 191
Miae Kim, Min-Ji Kang, and Kyong-Soo Hong [KBSI], Mihyun Lee and Cheonwoo Kim [KHNP-CRI]

11:40~12:00 The Activity Calculation Based on Operation History Comparing With Effective Full Power Operation for Decommissioning Plant …… 193
YoungJae Maeng, HyunChul Lee, KyungSik Kim, SungHoon Yoo, and ChoonSung Yoo [KRIST]

12:00~12:20 Revisit of the Feasibility of Controlling the Limit of Gross Alpha Activity and Corresponding Definition of Source Terms in Safety Assessment of Near-Surface LILW Repository in Korea …… 195
Ki Nam Kwon and Jae Hak Cheong [Kyung Hee Univ.]

12:20~12:40 Review on the Possibility of Distinguishing Between "Packaging Container" and "Transport Container" in Domestic Nuclear Regulations …… 197
Moonoh Kim and Nakhoon Sung [KONES Corp.], Jihoon Lee [KHNP-CRI]

4분과 중저준위폐기물관리 (Poster)

P0401 Development of Low-contaminated Sludge Radioactive Nuclides Separation Technology ····· 201
HeeJin Ahn, MiHyun Lee, and KangOk Cho [KHNP-CRI]

P0402 Construction of a Plasma Melting Facility for Developing the Treatment & Disposal Technology of Radioactive Waste ····· 203
Hyun-Je Cho and Mi-Hyun Lee [KHNP-CRI], Jun-Ho Seo [Chonbuk Natl. Univ.]

P0403 Study on Radiological Inventory Assessment of K 1 Reactor Vessel ·· 205
Young Hwan Hwang, Seok-Ju Hwang, and Ju-Young Yoon [KHNP-CRI]

P0404 Development Status of Radioactive Waste Container Package for Decommissioning Nuclear Power Plant ····· 207
Mi-Hyun Lee and Hee-Jin Ahn [KHNP-CRI]

P0405 Manufacture of RWTF Cement Waste Form Including Low-level Liquid Waste for Final Disposal ····· 209
Gi Yong Kim, Junhyuck Im, Jong Sik Shon, and Dae Seok Hong [KAERI]

P0406 Evaluation of Measurement Uncertainty in the Determination of ^{59}Ni in Radioactive Wastes Using Low Energy Photon Spectrometry ····· 211
ChangHeon Lee, SeChul Sohn, KeChun Choi, Preun Kim, and SeungMin You [NDRI]

P0407 Analysis on US NRC Regulatory Position for Blending Radioactive Waste ···· 213
Jungjin Kim, Jeheon Bang, Chan Woo Jeong, and Jinyong Park [KINS]

P0408 A Study on the Comparison of WTS for Establishment of Radioactive Waste Management ····· 215
Ki Tae Yang, Sun Il Kim, and Jong Soon Song [Chosun Univ.]

P0409 Development of Pretreatment Technology of Radioactive HVAC Filter Waste ··· 217
NakJeom Kim, MinHwan Mo, YongHo Cho, and HeeCheol Yoon [KEPCO KPS]

P0410 Review on the Potential Measure for Inadvertent Human Intrusion into LILW Disposal Facility ····· 219
Sangho Lee, Hayan Lim, Yohan Kim, and Jinyong Park [KINS]

P0411 Evaluation of Shielding Performance Effect of Liner Attenuation Coefficient During Radiation Shielding ····· 221
Jin Koh and Eun-duk Han [KORAD]

P0412 Adsorption of Krypton on Porous Carbon at Low Temperature ····· 223
Ju Ho Lee, Seok-Min Hong, Jae-Won Lee, and Yung-Zun Cho [KAERI]

P0413 A Study on the Applicability of Foreign Test Requirements for Type IP-2 Soft Bag Container ····· 225
Hyosub Kim, Moonoh Kim, Jaewoo Park, Dong-gyu Lee, and Nakhoon Sung [KONES Corp.], Jihoon Lee [KHNP-CRI]

P0414 Development of the Practical Technology for Thermal-Chemical Treatment of Low-Level Spent Resin ····· 227
Hyeon-Oh Park, Kyu-Tae Park, and Young-Ku Choi [Sunkwang T&S Co.,Ltd.], Hee-chul Yang [KAERI]

P0415 Fabrication and Characterization of New Glass Wasteforms for Radioactive Iodine Immobilization ····· 229
Min-Ji Kang, Miae Kim, and Kyong-Soo Hong [KBSI]

P0416 Experimental Study of the Analysis Method for Paste Content in the Waste Concrete ····· 231
Donghee An, Hyunkook Choi, and Jaeyoung Kim [SungShin Cement Res. Development]

P0417 Criticality Analysis for Washing of the UF_6 Cylinder and Treatment of the Waste Water Facility ····· 233
Janghwan Lim, Manseok Do, Seongki Lee, and Jongsung Yoo [KEPCO NF]

P0418 A Study on the Clearance Strategy of Surface Contaminated Radioactive Waste Using Mass to Surface Ratio ····· 235
Ji Young Song, Ki Baek Shin, Dong-Ju Lee, and Junhyuck Im [KAERI]

P0419 Structure Stability of Porous Materials to Extract Alkanes From Liquid Radwastes : Preliminary Results ····· 237
Jongjin Kim and Junhyuck Im [KAERI], Hyungwoo Kim and Donghoon Seoung [Chonnam Natl. Univ.]

P0420 Study on the Method to Determine Grouping Analysis Range for KAERI's Radioactive Waste Using Concentration Averaging Method ····· 239
Dong-Ju Lee, Junhyuck Im, and Dae Seok Hong [KAERI]

P0421 Dose Calculation of Landfill Workers Based on the Concrete Landfill Method ·· 241
Byeonglk Park, Hun Kim, and Chang-Lak Kim [KINGS]

P0422 A Convertible Plasma Torch System for Treatment of Low and Intermediate Level Radioactive Waste ····· 243
Jun-Ho Seo, Junseok Nam, In-Mok Yang, Min-Gyu Choi, Mi-Yeon Lee , Hyo-Jeong Kim, Ho-Sang Lee, and Shi-Young Yang [Chonbuk Natl. Univ.]

5분과 제염해체 (Oral)

09:00~09:20 SACER: A Computer Program for Decommissioning Schedule Analysis and Cost Estimate of Nuclear Power Plants ····· 247
Tongkyu Park, Byoungchan Han, and Kibeom Park [FNC]

09:20~09:40 Study on the Functional Group Affinity Toward Aqueous Cesium ····· 249
Il-Kwon Jung and Jong-Il Yun [KAIST], Youngho Sihn [KAERI]

09:40~10:00 Characterization of Ceramicrete Waste Form for Disposal of Concrete Waste of Decommissioned Nuclear Power Plant ····· 251
Jae-Young Pyo and Jong Heo [POSTECH]

10:00~10:20 Optimal Scenario Selection Methodology for Treatment Decontamination of Decommissioning Waste ····· 253
Daehyeon Kim and Jae Hak Cheong [Kyung Hee Univ.], Inhye Hahm, Daeseo Koo, Kwanseong Jeong, Jaehyun Ha, Seungkook Park, Sangbum Hong, and Bum Kyoung Seo [KAERI]

11:20~11:40 An Approach to Reconstruct Digital Mockup Based on Three-dimensional Scan Data for Nuclear Dismantling Process Evaluation System ····· 255
Jonghwan Lee, Ikjune Kim, Sungmoon Joo, and Dongjun Hyun [KAERI]

11:40~12:00 Development of Contaminated Soil Decontamination Technology for NPP's Using Selective Nuclide Adsorption Technique and Micro-bubble Vortex Breakdown Based on High Pressure Cleaning ····· 257
Woohyeon Rhee, Dukwon Kang, Seungil Kim, Pilyong Jeon, and Damhyang Kim [Elim-global Inc.]

12:00~12:20 Study on Activation Evaluation of the Kori Unit 1 Bioshield Concrete ···· 259
Ju-Young Yoon and Young Hwan Hwang [KHNP-CRI]

12:20~12:40 A Study for Dismantling Method of Bio-shield in Kori Unit 1 Nuclear Power Plant ····· 261
Kwang-Soo Park, Han-Sol Im, and Hee-Dong Sohn [Doosan Heavy Industries & Construction], Ju-Young Yoon [KHNP-CRI]

5분과 제염해체 (Poster)

P0501 The Implementation Strategy of Stakeholder Involvement Plan for Decommissioning of Nuclear Facilities ····· 265
KwanSeong Jeong, DaeSeo Koo, InHye Hahm, JaeHyun Ha, SangBum Hong, and BumKyoung Seo [KAERI]

P0502 Underwater Laser Cutting for Dismantling Nuclear Facilities ····· 267
Jae Sung Shin, Seong Yong Oh, Hyunmin Park, Gwon Lim, Taek-Soo Kim, Lim Lee, Chin-Man Chung, and Jonghwan Lee [KAERI]

P0503 Simulation Modeling for Planning a Soil Remediation Process ····· 269
David Kessel, Chang-Lak Kim, Jihan Jeon, and Eui-taek Lee [KINGS]

P0504 Development of Decommissioning Process of the Kori Unit 1 Reactor Vessel Internal Using Full-scale Mockup ····· 271
Sunghoon Hong and Young Hwan Hwang [KHNP-CRI]

P0505 Radiation Shielding Evaluation for Existing Transport Container Containing Decommissioning Waste of KORI Unit 1 ····· 273
Jae-Hun Ko, Dong-Gyu Lee, and Nak-Hoon Sung [KONES Corp.], Ji-Hoon Lee [KHNP-CRI]

P0506 Event/accident Simulation Model of the Reactor Pressure Vessel Internal Segmentation Activity ····· 275
Chang-Su Nam and Byung-Sik Lee [Dankook Univ.]

P0507 Consideration Factors for Public Dose Assessment During Decommissioning of Nuclear Power Plant ····· 277
Kwang-Ho Jo and Su-Hee Lee [KHNP-CRI]

P0508 Analyzes the Status of Patents and Utility Models Related to Domestic Self-Disposal ····· 279
ByeongMok-Park, JeongMi-Lee, AhRan-Cha, CheolWan-Park, Sang Hwan-Jun, DoYeong-Jung, and JaeSeok-Park [SAE-AN Enertech Corp.]

P0509 Preliminary Study on HyBRID Chemical Decontamination Demonstration for the Reactor Coolant Pump Shaft ····· 281
Ki-Chul Kim, Bum-Chul Seo, Sun-sik Yoon, Jung-Yeop Cha, Nam-Kyun Kim, Kwang-Hee Joo, Do-Yong Kwon, Dong-Yeon Kim, Keun-Woo Kim, and Ju-Hyeon Park [KEPCO KPS]

P0510 Effect of Raw Amount of $CuSO_4$ on Precipitation of Cu_2O in the HyBRID Decontamination of Magnetite ····· 283
Byung-Chul Lee [Hannam Univ.], Seon-Byeong Kim and Jei-Kwon Moon [KAERI]

P0511 Underwater Laser Cutting Using High-Pressure Supersonic Nozzle ···· 285
Seong Y. Oh, Jae Sung Shin, Taek Soo Kim, Hyunmin Park, Lim Lee, Chin-Man Chung, and Jonghwan Lee [KAERI]

P0512 Metal Oxide Solubility in Deep Eutectic Solvents – Applications in Decontamination in Decommissioning ····· 287
James T. M. Amphlett and Sungyeol Choi [KAIST]

P0513 Consideration About Assessment of Radiation Source Term When Decommissioning of Nuclear Power Utilization Facilities ····· 289
ByeongMok-Park, JeongMi-Lee, CheolWan-Park, and AhRan-Cha [SAE-AN Enertech Corp.]

P0514 Effect of Alkyl Chain Length of Ionic Liquids on Extraction Efficiency and Phase Separation in the Ionic Liquids Solid-liquid Cs^+ Extraction System ··· 291
Jung-Weon Choi, Hayeon Ryu, Myogwang Kim, Wonzin Oh, and Sang-June Choi [Kyungpook Natl. Univ.]

P0515 Molecular Binding Affinity of Aqueous Uranyl Tricarbonate Towards Basic Surface Functional Groups ····· 293
Youngho Sihn [KAERI], Jong-Il Yun [KAIST]

P0516 Planning for Document Management System Setup of Decommissioned Waste ·· 295
Daeseo Koo, Kook-Nam Park, Sang Bum Hong, In Hye Hahm, and Bum Kyoung Seo [KAERI]

P0517 Separation of Clay Minerals Using Polyethylenimine-coated Magnetic Nanoparticles ····· 297
June-Hyun Kim and Sang-June Choi [Kyungpook Natl. Univ.], Sung-Man Kim, In-Ho Yoon, and Il-Gook Kim [KAERI]

P0518 Removal of Cesium From the Field Soil Using Chemical Extraction ···· 299
Sung Man Kim and So-Jin Park [Chungnam Natl. Univ.], Chan Woo Park, Il-Gook Kim, Jun-Hyun Kim, and In-ho Yoon [KAERI]

P0519 Studies on UVC Photo-Fenton Decomposition of Oxalate Waste Depending on the Reactor Size ····· 301
Yoon-Ji Park, Hyun-Kyu Lee, Sae-Binna Lee, Wonzin Oh, and Sang-June Choi [Kyungpook Natl. Univ.], Hak-Soo Kim and Cho-Rong Kim [KHNP-CRI], Ki-Chul Kim [KEPCO KPS]

P0520 Radioactive Aerosol Modeling in Metal Cutting Process During NPP Decommissioning and Dismantling ····· 303
Hwa Jeong Han, Woong Ryul Choi, Jae Hong Yim, Yeong Sang Jo, and Byung Gi Park [Soonchunhyang Univ.]

P0521 Review and Preliminary Application of SADRWMS Methodology to Decommissioning Waste From NPPs ····· 305
Ji Su Kang, Na Yoon Choi, and Jae Hak Cheong [Kyung Hee Univ.]

P0522 Status of Tritium Permeation Analysis Tool for HCCR TBS ····· 307
Hyung Gon Jin, Dong Won Lee, Jae Sung Yoon, Suk Kwon Kim, Eo Hwak Lee, Seong Dae Park, and Chang Wook Shin [KAERI], Seungyon Cho [NFRI]

P0523 Extraction of Radioactive Ions Using Entrainer and Supercritical Decontamination Technic Equipped With Ultrasonic-horn ····· 309
Jaebin Shin, Kwangheon Park, and Tae hun Kim [Kyung Hee Univ.]

P0524 Status of Development of Final Decommissioning Plan for Kori Unit 1 ···· 311
Suk Bon Yoon, Su Hee Lee, and Jin-Won Son [KHNP-CRI]

P0525 A Review on Generation Characteristics of Sludge Waste During Decommissioning of Nuclear Power Plant ····· 313
Hang-Rae Cho and Ji-Hoon Lee [KHNP-CRI]

P0526 Radiolysis of Hydrazine in a Reductive Decontamination Solution ····· 315
Naon Chang and Yongsoo Kim [Hanyang Univ.], Huijun Won, Sangyoon Park, Heechul Eun, and Seonbyeong Kim [KAERI]

P0527 Studies on Precipitation Characteristics of Mn^{2+} and SO_4^{2-} by $Ba(OH)_2$ ··· 317
Hyun-Kyu Lee, Sae-Binna Lee, Yoon-Ji Park, Myo-Gwang Kim, Wonzin Oh, and Sang-June Choi [Kyungpook Natl. Univ.], Ju-Hyeon Park, Bum-Chul Seo, and Ki-Chul Kim [KEPCO KPS]

P0528 Sampling for Characterizing Radioactive Aerosol From Activated Metal During Cutting With Plasma Arc Torch for Internal Dose Assessment ····· 319
Wonseok Yang, Nakkyu Chae, Minho Lee, and Sungyeol Choi [KAIST]

P0529 3D Underwater Scanning for Nuclear Decommissioning: Laser Beam Distortion ·· 321
Sungmoon Joo, Jonghwan Lee, Ikjune Kim, and Dongjun Hyun [KAERI]

P0530 A Study on the Volume Reduction of Concrete Waste by Sintering Method ····· 323
Dasom Yang [Kyungpook Natl. Univ.], Woojung Shon, Kwangwook Kim, and Keunyoung Lee [KAERI]

P0531 Removal of Cs From Contaminated Aquatic Environments by Water-powered Janus Micromotor Adsorbent ····· 325
Chan Woo Park, Juri Hwang, In-Ho Yoon, and Hee-Man Yang [KAERI], Inae Lee [Sungkyunkwan Univ.]

P0532 Development of Radioactive Waste Tracking System (WATS) for Decommissioning of NPPs ····· 327
Ji-Hoon Lee and Kang-Ok Cho [KHNP-CRI]

6분과 방사선환경 및 안전 (Oral)

초청발표

09:00~09:30 Long Term History of Radiocaesium Activity Concentration in Seawater in the Western North Pacific Ocean and Adjacent Seas Since 1950's Until 2018 ··331
Michio Aoyama [Univ. Tsukuba]

09:30~09:50 In-Situ Gamma-Ray Spectrometry for Radioactivity Analysis Using the Scintillation Detector ·····333
Jun-Ho Lee and Dong Myung Lee [UST], Jong-In Byun [KINS]

09:50~10:10 Verification Method for the in Situ Measurement for Decommissioning Characterization ·····335
Sang Bum Hong, Byung Chae Lee, Jun Ha Kim, Young Yong Ji, In Hye Hahm, and Bum Kyoung Seo [KAERI]

11:20~11:40 Environmental Radiation Analysis of Ulsan Metropolitan City Region Around Kori and Wolseong Nuclear Power Plants ·····337
UkJae Lee, Chanki Lee, and Hee Reyoung Kim [UNIST]

11:40~12:00 Wind Tunnel Performance Test for Shrouded Probes ·····339
Ho Young Kim [LabWoks Inc.],
Maria D. King, John S. Haglund, and Ahmed A. Kalbasi [Texas A&M AgriLife Res.]

12:00~12:20 Development of Leak Position Detection System Using Noise and Reflected Wave Remove Technique ·····341
Minsoo Kim, Yongho Hong, Sooyeun Park, Hyungmin Park, Heekyung Kim, Taegyu Lee, Youngseok Jung, and Eunseok Choi [ACT Co., Ltd.]

12:20~12:40 Review on Revision History of ANSIANS-18.1 and PWR-GALE Along With Its Potential Impact to Anticipated Radioactive Source Terms to Environment From PWRs ·····343
Ji Woo Lee, Ji Su Kang, Sae Gun Lee, and Jae Hak Cheong [Kyung Hee Univ.]

6분과 방사선환경 및 안전 (Poster)

P0601 Environmental Radiation Survey Using Airborne Gamma-Ray Spectrometry Based on Manned and Unmanned Aerial Vehicles ·····347
Young-Yong Ji, Kun Ho Chung, and Mun Ja Kang [KAERI],
Taehyung Lim [SI Detection Co., Ltd.], Jang Hee Lee and Eun Young Song [Busan Metrop. City]

P0602 Calculation of Effective Dose Coefficient to Workers Due to Inhalation of Radon at Groundwater Treatment Facility ·····349
Kwang Pyo Kim, Jung Hwan Jang, Jae Kwon, Se Jong Lee, Seung Woo Ji, and Jae Kook Lee [Kyung Hee Univ.]

P0603 Evaluation of CH_3I Removal Performance and Physical Characteristics for New TEDA Impregnated Activated Carbon Stored in Nuclear Power Plants ·····351
Hak-Soo Kim and Cho-Rong Kim [KHNP-CRI]

P0604 Laboratory Establishment for Measuring Uranium Radioactivity in Urine ··353
Cheol Hyun Kang and Jong Il Lee [KAERI]

P0605 Development of Freshwater Foodchain Model for Calculating Tritium Transfer in Aquatic Organisms in Freshwater Following Nuclear Accident ·····355
Sora Kim, Kyung-suk Suh, Byung-Il Min, Kihyun Park, Byung-Mo Yang, and Jiyoon Kim [KAERI]

P0606 A Method for Improvement of Operation Efficiency of Chemical Cleaning Liquid Waste Equipment ·····357
Kyung-Wook Shin, Jeong-Nam Jeong, Yun-Soon Jeong, Dae-Woo Lee, Gyung-Sun Chae, and Hee-Kon Jang [SAE-AN ENGINEERING CO.]

P0607 Experience in Lancing Process of Steam Generator at PWR Nuclear Power Plants ·····359
Kyung-Wook Shin, Yoon-Ki Min, Young-Suk Choi, Tae-Hwa Kim, Gyung-Sun Chae, and Hee-Kon Jang [SAE-AN ENGINEERING CO.]

P0608 Development of De-burring Machine in Hot Cell ·····361
Y.M. Jung, G. S. Kim, Y.G. Jin, and G. S. Heo [KAERI]

P0609 Comparison of Atmospheric Dispersion Factors Using Different Approaches in Decommission of a Nuclear Power Plant ·····363
Seung-hee Lee and Chang-Lak Kim [KINGS], Won-tae Hwang [KAERI]

P0610 Radioactive Waste Management System of ARTI ·····365
Hyun-Jin Lee, Chong-Yeal Kim, Gyo-Seong Jeong,
and Sang-Bong Lee [Chonbuk Natl. Univ.], Jin-Woo Lee [KAERI]

P0611 Human Exposure to High Natural Background Radiation in Bangladesh ···367
Gazi Muhammad Borhan Uddin and Juyoul Kim [KINGS]

P0612 Assessment of Annual Indoor Effective Dose Around Mrima Area in Kenya ··369
Tarus Kiplabat and Juyoul Kim [KINGS]

P0613 Derivation and Comparison of Preliminary Derivation Concentration Guideline Level (DCGL) According to Scenarios of Kori Unit 1 Using RESRAD-BUILD ···371
SangJune Park, Jihyang Byon, and Seokyoung Ahn [Pusan Natl. Univ.]

P0614 Development of a Numerical Model to Evaluate the Terrestrial Behavior of Radionuclides ·····373
Byung-Il Min, Kihyun Park, Sora Kim, Byung-Mo Yang, Jiyoon Kim, and Kyung-Suk Suh [KAERI]

P0615 Analysis of Area Factor According to Scenario ·····375
Jihyang Byon, Sangjune Park, and Seokyoung Ahn [Pusan Natl. Univ.]

P0616 Measurement of the Radioactivity on the Air Sampling Filter Using the Alpha Spectrometer ·····377
Sung-Kyun Park, Jeong-Min Park, and Yi-Sub Min [KAERI]

P0617 The Annual Environmental Radiation Measurement and Analysis in KOMAC ··379
Jeong-Min Park, Yi-Sub Min, Sung-Kyun Park, and Jin-Nyeong Choi [KAERI]

P0618 Study on the Calculating Method of Atmospheric Diffusion Coefficient Using Turbulence Observation Data on Field Experiments ····· 381
Yoonhee Jung, Jeong-mi Kim, and Hyun-jun Jo [KHNP-CRI]

P0619 Status of Overseas Technical Standards for Exemption Levels of NORM and Disposal Limits of NORM Waste ····· 383
Na Yoon Choi and Jae Hak Cheong [Kyung Hee Univ.]

P0620 Radiation Hazards to Consider During the Decommissioning of NPP for Radiation Protection ····· 385
Gi-Lim Kim and Hyung-Woo Seo [KHNP-CRI]

P0621 A Study on the Radiological Safety Assessment Method Establishment of Recycling Workers of Very Low Level Radiological Metallic Wastes in Decommissioning Nuclear Power Plants ····· 387
Sang Heon Lee and Jong Soon Song [Chosun Univ.], Byung Gi Park and Hwa Jeong Han [Soonchunhyang Univ.]

7분과 방사화학 (Oral)

초청발표

09:10~09:40 DFT Study on the Actinide Complexes in Water ····· 391
Keunhong Jeong [KMA]

09:40~10:00 Chemical Behavior and Solubility of $Ca_2UO_2(CO_3)_3 \cdot 10H_2O(cr)$ at T = 22 and 80℃ in Dilute and Saline NaCl Systems ····· 393
Jun-Yeop Lee, Vanessa Montoya, David Fellhauer, Xavier Gaona, and Marcus Altmaier [KIT, Germany]

10:00~10:20 Luminescence Properties of U(VI) Surface Species on Amorphous Silica ·· 395
Euo Chang Jung, Tae-Hyeong Kim, Hee-Kyung Kim, Hye-Ryun Cho, Wansik Cha, and Min Hoon Baik [KAERI], Yongheum Jo and Jong-Il Yun [KAIST]

11:20~11:40 Spectroscopic and Computational Studies on Am(III)-Dicarboxylate Complexes ··· 397
H.K. Kim, H.R. Cho, E. C. Jung, and W. Cha [KAERI], K. Jeong [KMA], K. Kwak [Korea Univ.]

11:40~12:00 Performance of Mullite as Reference Electrode Membrane During the Electrochemical Reduction and Electrorefining Process ····· 399
Seokjoo Yoon, Dokyu Kang, and Sungyeol Choi [KAIST]

12:00~12:20 Desorption of α , β , and γ Emitting Nuclides in the Mixed Ion-Exchange Resin Using High-Performance Microwave Digestion System ····· 401
Kwang-Soon Choi, Jae-seok Lee, Simon Oh, and Tae-Hong Park [KAERI]

12:20~12:40 Feasibility Study on Hydrogen Isotope Exchange Reaction by Ultraviolet Light ··· 403
JiEun Yang [Chungnam Natl. Univ.], TaeJun Kim and Minsik Kim [UST], Jei-Won Yeon [KAERI]

7분과 방사화학 (Poster)

P0701 Use of Macroporous Resin to Reduce Released Corrosion Products During Shutdown Evolution ····· 407
Jinsoo Choi, Kahee Jeong, and Wook Sohn [KHNP-CRI]

P0702 Study on Cell Design of Electrorefining Process for Decontamination Using Molten Salt ····· 409
Jungho Hur, Gwan Yoon Jeong, Younghwan Jeon, Hyeongjin Byeon, and Jaeyoung Park [UNIST]

P0703 Meso-scale Multi-physics Modeling of CRUD Layer With Water Radiolysis Reactions ····· 411
Seungjin Seo and Sungyeol Choi [KAIST], Byunggi Park [Soonchunhyang Univ.]

P0704 Nonlinear Dynamic Partial Least Squares Modeling for Prediction of Strontium Concentrations in Underground Water (South Korea) ····· 413
Jiseon Jang, Soon Il Ok, and Jae-Yeol Cheong [KORAD], Dae Sung Lee [Kyungpook Natl. Univ.]

P0705 Experimental Study on Mass Transfer of Lanthanide Ions During Reduction by Li Metal in Molten LiCl-KCl/Bi System ····· 414
Jae Hong Yim, Beom Kyu Kim, Hwa Jeong Han, and Byung Gi Park [Soonchunhyang Univ.]

P0706 Effect of Scavengers on Oxalic Acid Degradation Using Ionizing Radiation ···· 416
Kang Lee [Korea Univ.], TaeHun Kim, JaeSon Kim, Seungjoo Lim, Joonpyo Jeun, and Seungho Yu [KAERI]

P0707 A Study on the Pure Separation for Determination of Molybdenum Isotopes in a Simulated Fuel Solution ····· 418
Jung Suk Kim, Kyungwon Suh, Byungman Kang, Yang-Soon Park, and Yeong Keong Ha [KAERI]

P0708 Study on Decomposition Characteristics of Oxalic Acid and Hydrazine by Electron Beam Irradiation ····· 420
DongWoo Kim [Jeonju Univ.], Kang Lee, KiHwan Park, KyungHoon Jung, and Seungjoo Lim [KAERI]

1분과

핵주기정책·규제 및 비확산(Oral)

A Study on Considerations to Apply Technical Security Controls for Nuclear Facilities

Chaechang Lee*
Korea Institute of Nuclear Nonproliferation and Control, 1534, Yuseong-daero, Yuseong-gu, Daejeon, Republic of Korea
*chiching@kinac.re.kr

1. Introduction

Nuclear facilities in South Korea and the United States should implement cyber security programs in accordance with their respective regulatory standards. 'Technical Security Controls', which contains about 70 security requirements, is part of the cyber security programs required by regulatory standards, originated from NIST in the United States [1, 2]. It is difficult to expect these security controls to be implemented properly on the site simply by listing the 70 requirements set forth by regulatory standards and to apply them uniformly at once. Therefore, this paper presents considerations for efficiently applying the requirements of RG 5.71 to nuclear facilities.

2. Considerations to Apply Technical Security Controls

2.1 Cyber Security Control Assessments

The Nuclear Energy Institute (NEI) of the U.S. has established NEI 13-10, Cyber Security Assessments, to streamline requirements for security controls and U.S. nuclear licensees are implementing them with the endorsement of U.S. NRC [3]. The NEI document classifies Critical Digital Assets (CDAs) based on their software and hardware characteristics. It also presents whether or not the attack vectors, corresponding to each security control, exist by the characteristics of the classified types. Based on this, it gives what security controls should be implemented and what security controls are not applicable.

Thus, nuclear licensees could reduce the burden of documenting for the justifications that cannot be applied to technical security controls, once they classify their own CDAs in accordance with the document.

2.2 Alternative Controls

NEI 13-10 referred to other technical security controls in RG 5.71 when presenting alternative security controls for each type of CDAs. That is, one security control can be implemented as an alternative to another. With the analysis of the security controls which refer to alternative security controls, it helps licensees to identify the security controls that they should apply with priority. As a result of the analysis, 'Access Enforcement' and 'Separation of Functions' were cited the most as alternative controls, 10 times.

2.3 Periodic Monitoring and Review

Some technical security controls in RG 5.71 demand periodic monitoring and review. These security requirements should be noticed separately to ensure that the involved employees at the site, such as engineers, do not miss the period they should implement the security activities. The table below outlines the items of technical controls that require periodic review and monitoring.

Table 1. The Technical Security Controls that Should Be Periodically Reviewed and Monitored

Section	Technical Security Controls
Access Control	Account Management
	Information Flow Enforcement
	Wireless Access Restrictions
	Access Control for Portable and Mobile Devices
Audit and Accountability	Response to Audit Processing Failures
Identification and Authentication	Password Requirements
	Non-authenticated Human Machine Interface Security
	Authenticator Management
System Security Hardening	Removal of Unnecessary Services and Programs
	Hardware Configuration

2.4 Role based Access Control

Lots of security controls in RG 5.71 are involved in Role-based Access Control (RBAC). RBAC is a method of access control where access is allocated to roles rather than granting access to individual users. The table below shows an example of implementation of RBAC-applied technical security controls, which can be used to meet the various requirements listed in RG 5.71 at a time.

Table 2. The Example of RBAC Applied by the Security Controls in RG 5.71

Account	Role	Security Function	Non-Security Function
Administrator	Engineers	Scan, Account management	Install and delete, Change set points
	Cyber Security Personnel	Change security configurations	None
User	Operators	Scan	Control, Monitoring
	3rd party personnel	None	Logic management (accompanied by engineers)

3. Conclusions

In this paper, a couple of considerations were presented for applying technical controls in RG 5.71. Cyber security personnel at a nuclear facility should be able to clearly identify what goals of the security controls are intended to achieve. It is up to licensees to find optimal methods to ensure that technical security controls are implemented properly considering the environment of each nuclear facility.

REFERENCES

[1] NIST SP 800-53, Rev. 3, “Recommended Security Controls for Federal Information Systems,” National Institute of Standards and Technology, Gaithersburg, MD, August 2009.

[2] U.S. NRC, Regulatory Guide 5.71, “Cyber Security Programs for Nuclear Facilities”, 2010.

[3] NEI, 13-10, “Cyber Security Controls Assessments”, 2013.

Risk-Informed Based Graded Approach and Consequence Assessment on Cyber Security Measure in Nuclear Facilities

Soo Min Lim*

Korea Institute of Nuclear Nonproliferation and Control, 1534, Yuseong-daero, Yuseong-gu, Daejeon, Republic of Korea

*s2min@kinac.re.kr

1. Introduction

Under the Act on Physical Protection and Radiological Emergency (APPRE)[1], Licensees of ROK are required to establish a Cyber Security Plans and Program that meets cyber security requirements for computer and information system at nuclear facilities security. Regulatory Standards, KINAC/RS-015[2] and KINAC/RS-019[3], are developed to ensure licensee to comply the regulatory requirements for cyber security. Moreover, independent guidelines and procedures for the reviews and inspections are developed to leverage the regulation quality of cyber security. In this paper, a practical methodologies are considered to take into account the effectiveness and efficiency of implementation on security measures with referenced methodologies. Further study for calculate or estimated that regulation of cyber security are effectively implemented, are remained.

2. Research Approach on Security Measures

2.1 Lessons Learned from US and ROK

According to Regulatory Guidance 5.71[4] and 10CFR73.54[5], US licensees are to apply the 150 cyber security measures onto their Critical System and Critical Digital Assets. Depends on the characteristic of the nuclear facility, about hundreds and thousands of CDAs were classified as a result. Excessive efforts for application of a hundred security measures were required to the licensee and much time has to be spent on regulatory inspection and implementation. ROK regulatory situation are similar to US that about 2/3 of all systems are CS with APR1400 based plant and more than 60% of the total critical systems are found out to be a digital system. Table 1 describes the draft result of classification of CDA by each plant type. Those number for CS and CDA are not specified due to the information confidence of licensee.

Table 1. Draft Result of CS and CDA

Plant Type	No. of CS	No. of CDA
WEC	80~100	200~500
CANDU	120~130	100~200
Framatone	100~110	160~170
System80	110~120	490~500
KSNP	100~110	900~1000
OPR1000	100~110	100~1100
APR1400	100~110	1400~1500

Based on the draft result and basic principle, single CDA needs to address 101 security controls and 101,000 security controls are to evaluate the application of the security controls.

2.2 NEI 13-10 [6]

The main concept of the document, NEI 13-10, is to screen low-consequence CDAs and provide criteria to categorize the existing CDAs into four different functions types, such as, Emergency Preparedness (EP), Balance-of-Plant (BOP), Indirect, as Non-Direct (ND), and Direct CDAs. Based on the categorization result, it also provides the minimum security controls for CDAs. Fig. 1 describes the consequence assessment that provides and illustrate the guidance of categorizing low consequence CDAs into Emergency Preparedness, Balance of Plant, and Indirect CDAs.

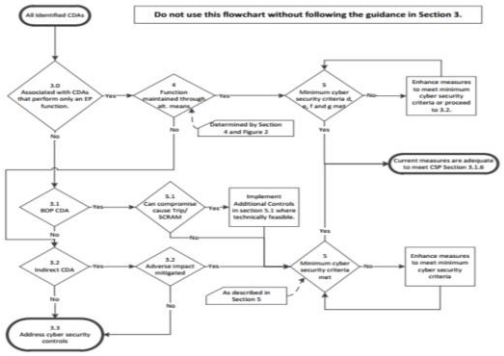

Fig. 1. Consequence Assessment in NEI13-10.

2.3 Consequence-Based Approach on ROK

Initial plan and process for applying NEI 13-10 were reviewed. Security measures and the method for categorizing current CDAs were reviewed as well. Based on the consequence assessment, current CDAs were screening into Direct and ND CDAs.

Direct CDA						Non-Direct CDA		
Safety Related & Security						Indirect	BOP	EP
A1	A2	A3	B1	B2	B3	ITS Q1,2,3,4,6	ITS Q5 only	EP function only
Depends on • Software attributes • Hardware attributes • Location						Baseline Controls a. Physical protection b. No wireless connection c. Air-gapped or isolation device d. PMMD control e. Configuration control f. Periodically check g. Monitoring & assessment		Baseline Controls • d • e • f • g

Fig. 2. Classification Criteria for Direct and ND CDA.

For Direct CDAs, necessary security controls are addressed base on their attributes and for Non-Direct CDAs are streamlined the means into baseline controls.

3. Conclusion and Further Study

As a result, an estimated number of CDA for a single facility was almost 1700. After taking consequence assessment on CDAs, it is categorized into 600 for Direct CDAs, and 1100 for Non Direct CDAs. From this result, the estimated reduction of evaluation process for application of security controls is almost one-third of applying 101 security controls for all CDAs. Further study for finding efficiency and effectiveness of implementation methods, verifying on alternate measures, and detailed verification for implementation method are remained for further study.

REFERENCES

[1] Enforcement of Regulation Act on Physical Protection and Radiological Emergency, Nuclear Laws of ROK, Dec. 2017

[2] Regulatory Standard for Security for Computer and Information System of Nuclear Facility, KINAC/RS-015, Dec. 2015

[3] Regulatory Standard for Classification on Critical Digital System of Nuclear Facility, KINAC/RS-019, Dec. 2015

[4] Cyber Security Program for Nuclear Facilities, RG5.71, Apr. 2015

[5] Protection of Digital Computer and Communication Systems and Networks, 10CFR73.54, Aug. 2017

[6] Cyber Security Control Assessment, NEI 13-10, Aug. 2017

Two Classification Algorithms for Nuclear Fuel Cycle Related Documents

Tongkyu Park[a,*], Yunpil Jeong[a], Byoungchan Han[a], Sang Jun Lee[b], Chan Seo Lee[b], and Dong-hoon Shin[b]

[a] FNC Technology Co., Ltd., 32F, 13 Heungdeok 1-ro, Giheung-gu, Yongin-si, Gyeonggi-do, Republic of Korea

[b] Korea Institute of Nuclear Nonproliferation and Control, 1534, Yuseong-daero, Yuseong-gu, Daejeon, Republic of Korea

[*]tongkyu@fnctech.com

1. Introduction

The Korea Institute of Nuclear Nonproliferation and Control (KINAC) is currently developing a collection and analysis system for nuclear fuel cycle related R&D projects and activities aiming at fulfilling the additional protocol with the IAEA[1] because information of nuclear fuel cycle related products and activities supported by governmental funding needs to be reported to the IAEA according to the additional protocol. This paper presents two algorithms to be implemented into the collection and analysis system for the automatic classification of fuel cycle related documents.

2. Classification Algorithms

The natural language processing (NLP) should be done as a first step for classifying collected documents. To achieve this, a well-known TF-IDF (Term Frequency and Inverse Document Frequency) method was used in this research. Consequently, two classification algorithms, i.e., SVM (Support Vector Machine)[2] and XGBoost (Extreme Gradient Boosting)[3], were coupled with TF-IDF.

2.1 Support Vector Machine

SVMs[2] have been proven as one of the most powerful learning algorithm for text categorization. Let's define *N* is the number of features, and then the goal of this algorithm is to find a hyperplane in an *N*-dimensional space that distinctly classifies the data points. To separate the two classes of data points, there are many possible hyperplanes that could be chosen. In this research the Radial Basis Function (RBF) kernel SVM was selected. In the kernel, two parameters (gamma and *C*) should be predetermined by user. The gamma parameter defines how far the influence of a single training example reaches, with low values meaning far and high values meaning close while the *C* parameter trades off correct classification of training examples against maximization of the decision function's margin.

2.2 Extreme Gradient Boosting

The XGBoost algorithm[3] is an optimized distributed gradient boosting library designed to be highly efficient, flexible and portable. The key concept of this algorithm is so-called decision tree ensembles consisting of a set of classification and regression trees (CART). Several parameters, such as learning_rate, min_child_weight, max_depth, colsample_bytree, and so on, need to be determined by performing sensitivity analyses. The learning_rate is the step size shrinkage used in update to prevent overfitting while the_child_weight is a minimum sum of instance weight needed in a child. The max_depth and colsample_bytree are a maximum depth of a tree and the subsample ratio of columns when constructing each tree, respectively.

3. Numerical Results

To verify the effectiveness and efficiency of the two proposed classification algorithms coupling with TF-IDF as a NLP tool, a series of sensitivity analyses were performed for two test problems listed in Table 1. Among the 900 documents in each group, 80% (720 documents) were used as training data and thus a total of 360 documents including 180 fuel cycle related documents in each problem were automatically classified with the proposed algorithms.

Table 1. Number of training and test documents

Problem Number	Fuel cycle documents	Non-fuel cycle documents[a)]	Non-nuclear documents
1	900	0	900
2	900	900	0

[a)] Documents in nuclear science or engineering

3.1 Support Vector Machine

A total of 48 cases with different values of *C* and gamma each other, was defined for each problem. Table 2 shows that F1 score for the first problem is 0.995 when *C* and gamma were set to 10 and 0.1. It means only 2 or 3 documents among 360 documents were misclassified when the TF-IDF/SVM algorithm was applied. Noted that it is hard to classify the documents in the second problem since all the documents were technical papers in the nuclear science field. It is larger than 0.95 in the aspect of F1 score, and thus it is expected that this algorithm is powerful to classify fuel cycle related documents.

Table 2. Numerical results obtained from SVM

Problem Number	F1 score	Parameters	
		C	gamma
1	0.995	10	0.1
2	0.959	5	1

3.2 Extreme Gradient Boosting

A total of 324 cases with different values for the 4 parameters mentioned above were defined for each problem. F1 scores were 0.998 and 0.956, respectively, for the two problems. It can be carefully concluded that this algorithm is also powerful.

4. Conclusion

In this study, two classification algorithms were proposed and their effectiveness and efficiency were verified by examining two test problems. Numerical results show that the proposed algorithms were powerful to classify the fuel cycle related documents and can be effectively used as main classification algorithms in the collection and analysis system.

ACKNOWLEDGEMENT

This work was supported by the Nuclear Safety Research Program though the Korean Foundation Of Nuclear Safety (koFONS) using the financial resource granted by the Nuclear Safety and Security Commission (NSSC) of Korea. (No. 1803021)

REFERENCES

[1] Sung-ho Yoon and Dong-hoon Shin, “A Conceptual Design of the Information Analysis System for Searching Nuclear Fuel Cycle Related R&D Projects”, Proc. of the KRS 2018 Autumn Conference, 16(2), October 31 – November 2, 2018, Jeju.

[2] C. Cortes and V. Vapnik, “Support Vector Networks”, Machine Learning 20, p.273, 1995.

[3] Tianqi Chen and Carlos Guestrin, “XGBoost: A Scalable Tree Boosting System”, Proc. of the 22nd Conference on Knowledge Discovery and Data Mining, p.785, 2016, San Francisco.

Legal Policy Study on Revision of Korea Tax Acts About A New Nuclear Fuel Tax

Daesung Lee*, Sungjin Choi, and Jaeyoung Bang
Korea Atomic Energy Research Institute, 111, Daedeok-daero 989beon-gil, Yuseong-gu, Daejeon, Republic of Korea
*dslee@kaeri.re.kr

1. Introduction

In January 2019, member of the 20th National Assembly, Jumin Park(Democratic Party) initiated the revision of 'Local Tax Act', 'Framework Act On Local Taxes', and 'Local Finance Act' in relation to nuclear power generation. Since the tax bases for the 'Local Resource And Facility Tax' for the nuclear power generation under the current law is based on the operation of the power plant, if the amount of nuclear power generation is reduced or the nuclear power plant is shut down in accordance with the energy conversion policy of the present government, it leads to a decrease in tax revenue of the region. Therefore, Park proposed to amend the existing taxation system of 'Local Resource And Facility Tax' and to propose a new 'Nuclear Fuel Tax' to secure necessary resources for the maintenance of the living environment and safety measures in the location of the nuclear power plant and its surrounding areas. The purpose of this study is to review the major contents of the amendment of each law related to nuclear power generation and the reason for the legislative process, to examine the effects and prospects of the passage of the bill, and to describe the matters to be considered.

2. Revision of Tax Act Legislation for Nuclear Power Plants

2.1 The Current 'Local Resource and Facility Tax' and 'Nuclear Fuel Tax'

The current 'Local Tax Act' imposes 'Local Resource and Facility Tax' on the amount of electricity generated by nuclear power plants for those who develop using nuclear power to offset the direct and incidental effects of nuclear power directly and indirectly on neighboring areas. The purposes of the 'Local Resource and Facility Tax' is to secure financial resources necessary for protecting and developing local resources, such as underground and marine resources, tourism resources, water resources and special geographical features, for conducting safety management projects, such as fire-fighting activities and prevention of specific disasters in a region, and for performing projects for environment protection and improvement and projects for balanced regional development, or in order to cover the expenses incurred in fire-fighting facilities, waste disposal facilities, irrigation facilities and other public facilities.

In Japan, nuclear fuel tariffs are imposed on nuclear fuel injected into power generating reactors, but Korea is not yet subject to any additional taxation on nuclear fuel.

2.1.1 Amendment of 'Local Resource and Facility Tax' in 'Local Tax Act'. The amendment to the 'Local Tax Act' contains the conversion of the 'Local Resource and Facility Tax' tax bases for nuclear power plants from 'amount of generation'(1 won per kWh) to 'generation capacity'(5,000 won per kW, yearly basis, 2,500 won per kW for permanently suspended power plants). In this case, it is possible to secure tax revenue even if nuclear power generation is reduced or the nuclear power plant is shut down according to the energy conversion policy.

2.1.2 New Plan for 'Nuclear Fuel Tax' under

'Local Tax Act'. Unlike Japan, Korea is not subject to any additional taxation on nuclear fuel that is currently inserted into power generation reactors. The amendment to the 'Local Tax Ac' contains a report on the creation of a 'Nuclear Fuel Tax' that allows nuclear power companies to report and pay 10 percent of the value of nuclear fuel materials to local governments in nuclear power plants by ordinance.

2.2 Amendment to the 'Framework Act on Local Taxes'

The revision bill of the 'Framework Act on Local Taxes' is based on the revision of the 'Local Tax Act', which defines the 'Nuclear Fuel Tax' as target tax, special tax, metropolitan tax, or special autonomy tax. The time of establishing the tax liability for 'Nuclear Fuel Tax' is 'when inserting nuclear fuel material into a nuclear reactor for power generation'. This is to revise the related regulations simultaneously according to the revision of the 'Local Tax Act'.

2.3 Amendment to the 'Local Finance Act'

According to the current law, 65% of the local subsidies levied on thermal power and nuclear power are distributed to the city and county where the power plant is located, and the revised bill is revised according to the revision of the 'Local Tax Act'. The same amount of 65% is allocated to cities and counties where nuclear power plants are located. This is to revise the related regulations simultaneously according to the revision of the 'Local Tax Act'.

3. Impact and Prospects when Passing Legislation

The amendment to the 'Local Tax Act' includes the change of existing 'Local Resource and Facility Tax' levy from 'amount of generation' to 'generation capacity' regardless of the operation rate of the nuclear power plant. And it contains contents that the nuclear fuel tax is newly established and the obligation of the nuclear power plant to obligation to bear the burden of fuel loading. It is expected that when passing the bill, it will be possible to secure additional 55.7 billion won for the 'Local Resource and Facility Tax' of the province and 90 billion won of 'Nuclear Fuel Tax' and it will be possible to secure necessary resources for the maintenance of the living environment of cities and counties around the power plant where the tax amount will be reduced due to the energy conversion policy and for the preparation of safety measures. And it is also expected that it will help to preserve the effects of external uncertainties on the neighboring areas due to nuclear power generation

4. Conclusion

We looked at the Amendment of 'Local Resource and Facility Tax' and new plan for 'Nuclear Fuel Tax'. It is necessary to grasp the legislative intention of the existing 'Local Resource and Facility Tax' for conservation of the external irregularity effect on the neighboring region due to nuclear power, and detailed examining the present energy situation of our country is also needed for the revision. In this process, the new legislation can make a good balance between safe and economic nuclear power generation, which can secure a sustainable nuclear power generation, and protection and development of regional resources near nuclear power plants by listening to the opinions of various stakeholders.

REFERENCES

[1] Chulhoon Ham, "Atomic Energy Law", Bubyoungsa, 2009.

[2] Yunwon Park, Chulhoon Ham, "Nuclear Safety Law", Jinwonsa, 2016.

[3] Korea National Assembly Bill Information http://likms.assembly.go.kr/bill/main.do

Algorithm Development for Tracking Process Material on Surveillance Camera in Pyroprocessing Based on Deep Learning Techniques

Byung Hee Won*, Se Hwan Park, Hee-Sung Shin, and Seong-Kyu Ahn

Korea Atomic Energy Research Institute, 111, Daedeok-daero 989beon-gil, Yuseong-gu, Daejeon, Republic of Korea

*wonbh@kaeri.re.kr

1. Introduction

Surveillance system is considered as one of the important safeguards approaches in a facility handling nuclear material. In particular, optical monitoring device is useful for monitoring movement of process material containing nuclear material. Video images are not only difficult to artificially manipulate, but also is easy to provide clues to abnormal activities. Especially, the role of optical monitoring device is expected to be considerably important in pyroprocessing facility because pyroprocessing processes of are designed to be located in isolated structures such as argon or air cell. However, there is still a limit to simply increase these useful surveillance camera because a lot of human resources may be required to review video image data.

In this study, the algorithm to automatically monitor process material movement in electro-refining cell was developed to minimize human resources based on the hypothetical surveillance camera. The algorithm was designed to track movement of the main crane and identify specific behaviors in order to understand process material movement. It is expected that this method can be utilized in actual facilities and the performance of surveillance system can be greatly improved while minimizing human resources.

2. Method & Results

The hypothetical video images showing electro-refining cell where main pyroprocessing processes are being operated has been utilized in this study. The crane in electro-refining cell remotely transfers process material between process equipment based on prescribed operation scenario. Therefore, it is important to detect and track the crane to identify movement of process material. The cascade classifier, which is a type of conventional machine learning technique, had been applied to detect crane in last study [1]. However this technique showed a limitation of tracking the crane completely because correct detection efficiency was only 65.45%. In this study, faster R-CNN (Region based Convolutional Neural Network) [2], which is a type of deep learning technique and expected to show more improved performance, has been applied. 1,226 images has been utilized to train the faster R-CCN algorithm. These images contain crane and its location information called Region of Interest (ROI). Training time took about 63 hours in a workstation having high performance GPU (NIVIDA GeForce RTX 2080 Ti). Fig. 1 shows the detection result according to various crane positions. As shown in the figure, the trained algorithm is detectable the crane with confidence of 99% or more in most positions, except when the position of the crane is too forward of the camera.

In the next step, another algorithm based on the CNN for classification has been developed to distinguish whether the crane detected by the faster R-CNN has a process material or not. This is an essential requirement for tracking and understanding process material movements.

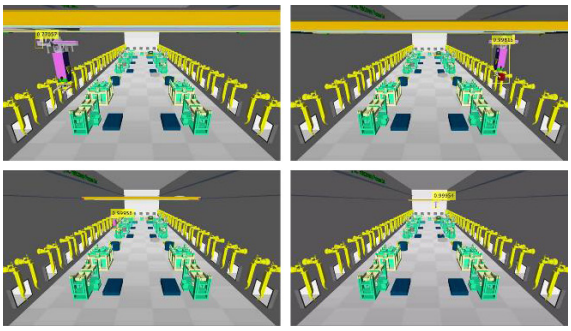

Fig. 1. Results of the Crane Detection using Faster R-CNN.

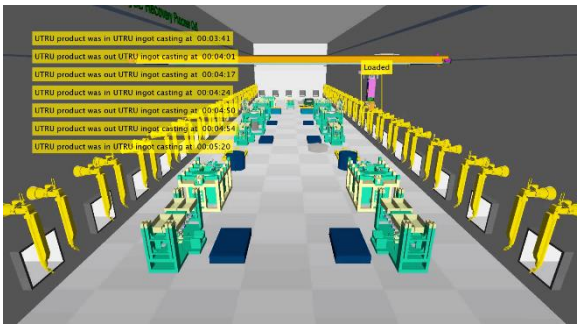

Fig. 2. Result of Tracking Process Material.

A total of 11,105 crane images were automatically detected by the faster R-CNN algorithm and manually classified into 5,065 images having loaded condition and 6,040 images having unloaded condition. 70% of the total data set were used for training and 30% were used for validation. Training time took about less than 2 minutes in the same workstation. The trained algorithm showed the performance with validation accuracy of 97%.

Although the two algorithms used to check condition of the crane show fairly good performance, there is still a difficulty in fully grasping process material movement because they cannot show perfect performance. So a deterministic algorithm has been added to complement this problem. The algorithm examines each frame based on results of back and forth frames and corrects errors in the frame. In the final step, the algorithm records time and name of equipment when the condition of the crane is changed. For example, if condition of the crane is changed from ‘unloaded’ to ‘loaded’, it means that process material is out by the crane from a process equipment. Fig. 2 shows the monitoring result. As shown in the figure, it is possible to determine when process material was injected into the UTRU ingot casting process and when it was out from the equipment.

3. Conclusion

The study was performed on the development of algorithms to identify the movement of process material containing nuclear material in hypothetical video camera. The CNN techniques based on deep learning were used to check these conditions and showed good performance. It was confirmed that the developed algorithms were almost completely traceable to process material movement by the crane, except for some minor error. Although these algorithms cannot be applied directly in real facility, if algorithms are developed in the same way, it is expected that they will show good performance in surveillance camera of actual electro-refining cell.

ACKNOWLEDGEMENT

This work was supported by a National Research Foundation of Korea (NRF) grant funded by the Korean government (MSIP) (No. NRF-2017M2A8A5015084).

REFERENCES

[1] Byung Hee WON, et al., “Algorithm Development for Detecting a Crane on Surveillance Camera in Pyroprocessing based on Machine Learning Technique.”, KRS Fall 2018.

[2] Girshick, R., “Faster R-CNN.” Proceedings of the 2015 IEEE International Conference on Computer Vision (2015).

Nuclear Material Diversion Detection Using Intelligent Surveillance Based on Deep Learning

Se-Hwan Park[a,*], Byung-Hee Won[a], Hee-Sung Shin[a], Seong-Kyu Ahn[a], and Shin-Dong Kang[b]

[a] Korea Atomic Energy Research Institute, 111, Daedeok-daero 989beon-gil, Yuseong-gu, Daejeon, Republic of Korea

[b] IDOSI, 44, Seongsuil-ro 12-gil, Seongdong-gu, Seoul, Republic of Korea

[*]ex-spark@kaeri.re.kr-mail

1. Introduction

Deep learning is developed very quickly and it shows remarkable performance in many fields. Especially, the deep learning is applied to anomaly detection using surveillance video. Here, the anomaly is something that deviates from normal or is unexpected. In this application, a deep learning model is trained only with normal video sequence, and the anomaly can be detected if the abnormal sequence is mixed with the normal sequence in the video.

The surveillance is important to detect the diversion in a nuclear facility, and a complementary safeguards measure to the nuclear material accountancy. If an intelligent surveillance is developed to detect the diversion automatically without post analysis, the surveillance will play more important role in the safeguards.

Korea Atomic Energy Research Institute (KAERI) is developing safeguards techniques and safeguards system of a pyroprocessing to enhance the non-proliferation acceptability of the pyroprocessing. In the present work, our progress on the development of the intelligent surveillance in the pyroprocessing facility is presented.

2. Methods and Results

Since it is very difficult to obtain enough surveillance video data inside a pyroprocessing hot cell, virtual video data were produced. The model facility is an electro recovery cell (ER cell) of a pyroprocessing facility.

The virtual video data were produced with WITNESS Visionary Render (WITNESS VR). The process instruments inside the hot cell were reduced metal storage, U&UCl_3 storage, Electro Recovery (ER) instrument, sample storage, U ingot casting furnace, Liquid Cadmium Cathode (LCC) crucible storage, Trans Uranic ingot casting furnace (TICF), salt purifier, waste storage, U ingot storage, and TRU ingot storage. Two process lines with equal instrument arrangement were in the ER cell. A small crane transported the process material in the ER cell. A surveillance video camera was installed obliquely near the ER instrument. Fig. 1 is an image taken by the surveillance camera.

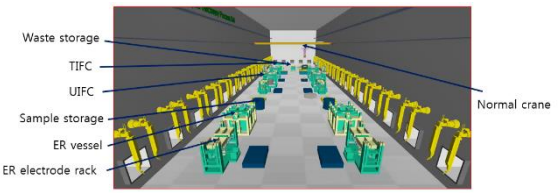

Fig. 1. Image taken with surveillance camera in the virtual ER cell.

One campaign was composed of 2 times U recovery, 2 times U/TRU recovery, 2 times TRU Draw Down (DD), 2 times Rare Earth (RE) DD. Two process lines proceeded independently. The start time difference between the two process lines was changed to make various normal surveillance video data. Also the process operation time and the process material position were slightly changed.

Three type of abnormal surveillance video data were produced; large crane movement, diversion in the sample storage, and diversion of U/TRU product at the ER instrument or before the TICF. All the abnormal data were not included to the normal data.

Autoencoder is one of the deep learning model. In the autoencoder, the input layer is compressed into short code, and then the shot code is decompressed into output, which is almost identical to the original input layer. After training the autoencoder only with the normal data, the trained autoencoder can reproduce the output almost same to the original input if the characteristics of the input is similar to the normal data. However, if the characteristics of the input is very different from the normal data; anomaly, the trained autoencoder cannot reproduce the output. Based on this characteristics of the autoencoder, the anomaly; diversion can be detected with an autoencoder mode trained only with the normal data.

An autoencoder model was developed and trained using the normal data of the virtual video data in pyroprocessing cell. Ten sequence surveillance images were used simultaneously in the training.

Loss is the sum of difference between the input pixel data and the output pixel data. If the autoencoder reproduces the input well, the loss is small, and if the autoencoder cannot reproduce the input, the loss gets larger. The loss of the autoencoder got larger when the anomaly video sequence was included to the test video.

3. Summary

KAERI is developing intelligent surveillance, which can be applied to detect the nuclear material diversion in a pyroprocessing facility. The virtual video data in the pyroprocessing hot cell were produced, and the autoencoder model was developed. The model can detect the diversion sequence in the virtual video data quite successfully. The following effort will be continued to implement this technique to the pyroprocessing safeguards

Our effort will help the effective and efficient safeguards implementation in future pyroprocessing facility.

ACKNOWLEDGEMENT

This work was supported by a National Research Foundation of Korea (NRF) grant funded by the Korean government's Ministry of Science and ICT (MSIT) (No. NRF-2017M2A8A5015084).

REFERENCES

[1] M. Hasan et al., Learning Temporal Regularity in Video Sequences, CVPR, p. 733, 2016.

Laser-induced Breakdown Spectroscopy Analysis for Addressing Copycat Crime of Alexander Litvinenko (Polonium-laced Tea)

Yunu Lee and Sungyeol Choi*

Korea Advanced Institute of Science and Technology, 291, Daehak-ro, Yuseong-gu, Daejeon, Republic of Korea

*sungyeolchoi@kaist.ac.kr

1. Introduction

According to the international atomic energy agency (IAEA) incident and trafficking database (ITDB), unauthorized access to radioactive materials for malicious use is getting easier [1]. One of the most shocking accident is murdering a person named Alexander Litvinenko using radioactive materials. The cause of death was poisoned by radionuclide polonium-210 in tea. In his body, significant amounts of the rare and toxic element were founded by Health Protection Agency. Through the Alexander Litvinenko poisoning with polonium-210, the era of nuclear terrorism started [2].

2. Experimental and Results

2.1 Experimental

To address the radiological threat of food poisoning rapidly, the laser-induced breakdown spectroscopy (LIBS) was considered. LIBS is a type of atomic spectroscopy. The atomic spectra were emitted through the returning to the ground state. In this process, a laser is used as excitation source the samples by forming a plasma. The emitted spectra were transmitted to a spectrograph and recorded to intensified-CCD that can control a few ns time gate.

For excitation the sample, a compact Nd:YAG laser (Quentel Q-smart 450 with the 2nd harmonic module, 532 nm, 5.5 ns, 220 mJ, 20 Hz) was used. For acquiring the spectra, two plano-convex lenses were used and the emissions were analyzed by a spectrograph (Andor, ME5000) with nano-scale of time resolution (Andor, iStar DH334T).

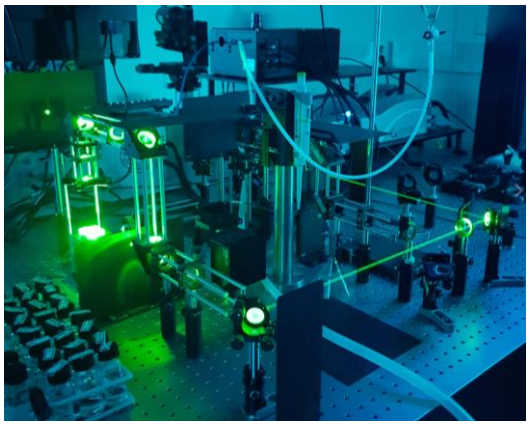

Fig. 1. Experimental setup for aqueous form of samples.

The target material was selected as $SrCl_2$ which is typically used as a radiation source. Since it has high solubility in water (53.8 g/100 mL), easy to use in terrorism such as diluting radionuclides in water tank installing rooftop of buildings and copycat crime of Alexander Litvinenko as known for polonium-laced tea. To calculate the limit of detection for the LIBS technique, numerous concentration was used. In addition, only 4 μL of the sample was investigated by a single laser pulse and it takes only 30 μs for each experiment.

2.2 Optimization

To find a trace of radionuclides in something aqueous form as much as LIBS can, the optimization process was conducted by finding the most signal-to-noise ratio point of LIBS condition. The three parameters of delay time, laser power, and gate width were investigated. As shown in Fig. 2, the time delay of 180 ns, the laser power of 40.4 mJ, and the gate width of 30 μs were obtained as an optimization condition. Fig. 2 depicts an average of wavelength including 338.07, 346.44, 407.77, 421.55, 430.55, 460.73, and 481.18 nm of Sr persistent emission.

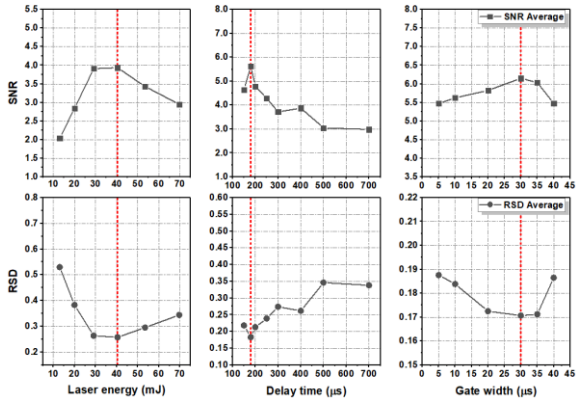

Fig. 2. Optimization points for energy, time, and width.

2.3 Results

Among seven emission line of Sr which is used to find optimization process, the three emissions of 407.77, 421.55, and 460.73 nm were used to calculate the limit of detection (LOD) because these exist clearly in the spectra. Fig. 3 depicts the calibration curves fitted by LIBS. For each point, 30 times of investigation were conducted with numerous concentration. The calibration curve was well fitted with good linearity (R^2=0.9889 for 407.77 nm, R^2=0.9933 for 421.55 nm, R^2=0.9834 for 460.73 nm) as shown in Fig. 3.

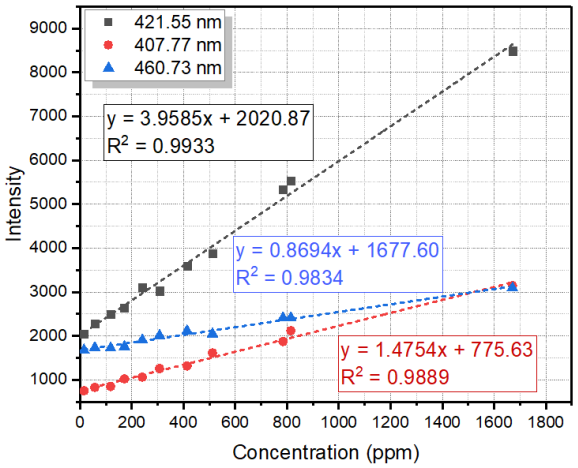

Fig. 3. Calibration curve of $SrCl_2$ in water.

The calculated LODs for each emission line was 197.805 ppm for 407.77 nm, 285.579 ppm for 421.55 nm, 862.108 ppm for 460.73 nm. The lowest LOD was obtained at 407.77 nm due to the highly stable emission for blank measurements overcome.

3. Conclusion

This preliminary result shows the LIBS can be used for analyzing the presence of radionuclides in aqueous medium rapidly. The LODs look like quite high to analyze the trace amount of radioactive materials. However, this limitation can be overcome by accumulating the laser pulse certain times because the LOD can be enhanced by integrating laser pulse can enhance the LOD exponentially.

ACKNOWLEDGEMENT

This work was supported by the Nuclear Safety Research Program through the Korea Foundation of Nuclear Safety (KOFONS), granted financial resource from the Nuclear Safety and Security Commission (NSSC), Republic of Korea (Grant No.1703008-0117-SB110).

REFERENCES

[1] Incidents of nuclear and other radioactive material out of regulatory control 2018 Fact Sheet, in, IAEA INCIDENT AND TRAFFICKING DATABASE (ITDB), 2018.

[2] A.J. Patterson, Ushering in the era of nuclear terrorism*, Critical Care Medicine, 35 (2007) 953-954.

Measurement of Uranium in LiCl-KCl Salt Using LIBS

Seul-Ki Han, Se-Hwan Park*, and Seong-Kyu Ahn

Korea Atomic Energy Research Institute, 111, Daedeok-daero 989beon-gil, Yuseong-gu, Daejeon, Republic of Korea

*ex-spark@kaeri.re.kr

1. Introduction

The Korea Atomic Energy Research Institue (KAERI) has explored Laser Induced Breakdown Spectroscopy (LIBS) as a promising technique for pyroprocessing safeguards measures because a remote, in-situ analysis of a material is possible.[1] LIBS is based on the optical analysis of the plasma generated by concentrating a strong laser beam on the surface of the sample. LIBS has characteristic such as real-time analysis, multi elements analysis and no sample preparation before the analysis.[2-5] In this study, U and lanthanide element in LiCl - KCl salt are measured as electrorefining process material of pyroprocessing via LIBS.

2. Methods and Results

In this experiment, simulated electro-refining salt samples were made by adding $LaCl_3$, $CeCl_3$, $BaCl_2$, $PrCl_3$, $NdCl_3$, YCl_3 , $SmCl_3$ and UCl_3 to LiCl-KCl salt. Five LiCl-KCl samples containing UCl_3 were fabricated. The concentration of U in the samples were from 1.5wt% to 6.8wt%. Composition materials of the samples were placed in the glassy carbon crucible, and they were heated up to 650℃ to melt. This temperature was maintained for two hours, after which the samples were slowly cooled to a solid form in a furnace. Experiments were conducted in a glove box with an atmosphere of Ar gas with moisture and oxygen content of 100 ppm or less for samples with high deliquescence. A laser beam was injected through the port of the glove box and the optical fiber cable was inserted I received it. The sample surface was somewhat irregular and the distance between the sample and the focusing lens was corrected each time the sample surface was changed by interlocking the XYZ moving sample table with a high precision distance meter to match the same focal length. A beam of Q-switched Nd: YAG pulse laser (Brilliant B, Quantel) with a wavelength of 532 nm is focused on the sample surface to generate plasma and Echelle spectroscopy with 20,000($\lambda/\Delta\lambda$) resolution to detect plasma emission line and ICCD camera was used. The emission lines of U and other emission line were selected in the wavelength region of 200 to 410 nm where spectroscopy is permitted. The number of laser pulses in the measurement was 100 shot. After collecting of LIBS spectrum at a position, the sample was moved horizontally to obtain the scan data of the sample surface. The measured U spectrum in the wavelength 357.005 nm, 294.189 nm, 297.101 nm, 304.403 nm and 385.952 nm were analyzed. The U peak intensity is normalized with peak intensity of the K 399.180 nm line.

The U 385.952 nm line had the smallest LOD, 0.0576wt%, and the 304.413 nm line had the highest LOD, 0.1820wt%. For better analysis of the performances, Partial least-squares (PLS) regression modeling was also conducted to obtain a multivariate calibration curve.

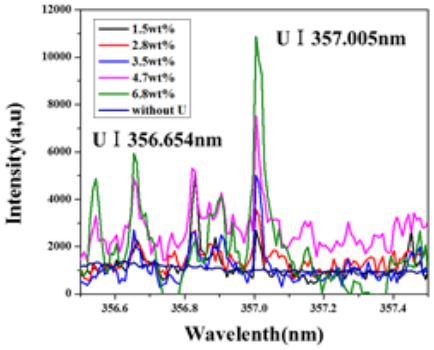

Fig. 1. U spectrum in a sample containing from 1.5 wt% to 6.8 wt% UCl_3 in LiCl-KCl.

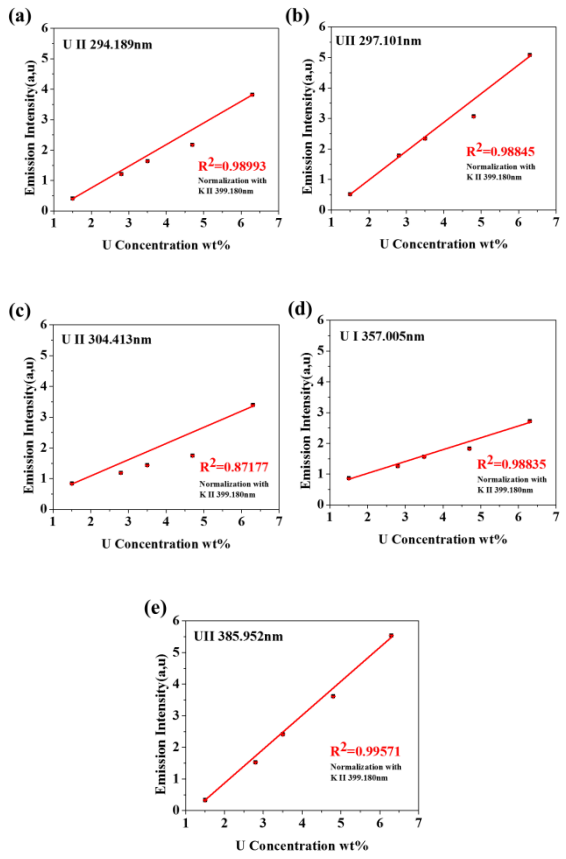

Fig. 2. Univariate calibration curves for U: (a) 294.189 nm line, (b) 297.101 nm line, (c) 304.413 nm line, (d) 357.005 nm line, and (e) 385.952 nm line.

3. Summary

LIBS is a promising technology as the process monitoring technology applicable to the pyroprocessing safeguards. The uranium concentration in LiCl-KCl salt were measured using LIBS system, and the quantitative analysis performance of LIBS. U concentrations in the samples ranged from 1.5wt% to 6.8wt%, the limits of detection (LOD) was 0.0576wt% and R^2 was 0.99 at the 385.952 nm. Our result is promising for application of the LIBS to the safeguards.

ACKNOWLEDGEMENT

This work was supported by a National Research Foundation of Korea (NRF) grant funded by the Korean government's Ministry of Science and ICT (MSIT) (No. NRF-2017M2A8A5015084).

REFERENCES

[1] B.Y. Han et al., Analysis of the applicability of LIBS to address safeguards needs with respect to pyroprocessing, KAERI/TR-6607/2016, 2016.

[2] Ammon N. Williams at el., Elemental Detection of Cerium and Gadolinium in Aqueous Aerosol via LIBS, Appl. spectrosc, Vol 70, pp.1700-1708, 2016.

[3] Cremers. D.A at el., Remote elemental analysis by laser-induced breakdown spectroscopy using a fiber optic cable", Appl. Spectrosc, Vol 49, pp. 857-860, 1995.

[4] Davies. C.M at el.t, Quantitative analysis using remote laser-induced breakdown spectroscopy, Spectrochim. Acta Part B, Vol 50, pp. 1059-1075, 1995.

[5] Andrew I. Whitehouse, Laser-induced breakdown spectroscopy and its application to the remote characterisation of hazardous materials, Spectroscopy Asia, Vol 2, No. 2, pp. 13-18, 2006.

1분과

핵주기정책·규제 및 비확산(Poster)

Analyzing and Suggesting on the Practical Measures to Prevent Illicit Activities on Nuclear Materials and Radioactive Sources

Jae San Kim*

Korea Institute of Nuclear Nonproliferation and Control, 1534, Yuseong-daero, Yuseong-gu, Daejeon, Republic of Korea

*jaesan@kinac.re.kr

1. Introduction

Illicit activities of Nuclear Materials and Radioactive Sources are likely to occur continuously in around the world. Typical illicit activities can be described as follows:

- Accidents following loss of control over, improper use or disposal of nuclear materials and radioactive sources
- Malevolent use ranging from theft over illicit trafficking to the potential misuse

It is difficult to pinpoint the specific intent, type, the number of years, and acquisition material, etc. because such activities are conducted very accidentally and meticulously. The IAEA has collected and analyzed annual illicit activities through its database; Incident and Trafficking Database (ITDB) since 1995. ROK has also participated in the ITDB since 2002, and voluntarily reported the relevant information.

In this paper, it was analyzed to information on recent incident and trafficking activities related to of nuclear materials and radioactive sources. And it also presented the current issues and recommendations for strengthening the practical measures for protecting the illicit activities.

2. Outcomes of Incident and Trafficking Activities 2013-2017

Between 2013 and 2017, 52 incidents (or approximately 6 percent of total reported incidents), involved nuclear material—defined as various forms (or isotopes) of uranium, plutonium, and thorium. [1]

Table 1. Reported Incidents Involving Nuclear Materials

Nuclear Materials	Incidents, 2017	Incidents, 2013-2017
Uranium, total cases:	6	48
Depleted	1	17
Natural	1	8
Low-enriched uranium (LEU)	0	1
Highly-enriched uranium (HEU)	2	3
Unknown enrichment	2	19
U-233	0	0
Plutonium, total cases:	3	7
Plutonium-238 (Pu-238)	0	2
Plutonium-239 (Pu-239)	2	2
Plutonium-241 (Pu-241)	1	1
Unknown plutonium isotope	0	2
Thorium (Th), total cases:	5	12
Subtotal, all nuclear materials:	14	67
Total Unique Cases:	8	52

Most reported activities are incidents involving radioactive materials rather than those involving nuclear materials.

Table 2. Reported Incidents Involving Radioactive Materials

Radioactive Materials	Incidents, 2017	Incidents, 2013-2017
Cesium-137 (Cs-137)	51	245
Americium (Am-241)	42	201
Iridium-192 (Ir-192)	10	52
Radium-226 (Ra-226)	7	43
Cobalt-60 (Co-60)	3	29
Strontium-90 (Sr-90) and its decay product, Yttrium-90 (Y-90)	3	24
Californium-252 (Cf-252)	1	5
Selenium-75 (Se-75)	0	3
Ytterbium-169 (Yb-169)	0	1
Thulium-170 (Tm-170)	0	0
Subtotal	117	603

Large parts of illicit activities are targeted at radioactive sources that are easier to access and seize than nuclear materials.

3. The Domestic Measures to Prevent Illicit Activities on Related Materials

Nuclear materials used in nuclear facilities in ROK are placed within the scope of regulations to prevent illegal transfer and sabotage activities under the Act on Physical Protection and Radiological Emergency (APPRE). Therefore, there has been performed the physical protection regulations like routine inspection, nuclear material control and accounting (MC&A) and transport inspection, etc.

ROK has supported for implementing IAEA's Code of Conduct on the Safety/Security of Radioactive Sources and Supplementary Guidance on April 2004 and September 2012, respectively. And the legal and administrative regulatory framework for the security of Category 1 and 2 radioactive sources (Nuclear Safety Act (NSA) and Notice of the Nuclear Safety and Security Commission on "Regulation on the Security Management of Radioactive Sources) has been established and enforced as of April 2015. "Regulation on the Security Management of Radioactive Sources" stipulate the requirements of security measures and import/export controls of Category 1 and 2 radioactive sources and security management of disused radioactive sources. Licensee should report on production, acquisition, use, sale, possession, storage and disposal of radioactive sources within a month after each quarter online using web-based integrated management system of radiation safety called RASIS (Radiation Safety Information System).

4. Conclusion

If even a minor incident occurs related nuclear materials, the influence can be very large domestically and internationally. There should be needed to strengthen the physical protection regulation of nuclear materials. Especially, when transporting the nuclear material, regulatory and management measures should be consolidated.

Meanwhile, the documents of international regulations on preventing illicit activities of radioactive sources are mostly recommended forms rather than legally binding. So, it is required to strengthen the international regulations to prevent illegal transactions of radioactive sources and needed to keep the voluntary and active compliance by each country.

Also, it is required that the participating countries have to actively discuss various ways to cooperate on preventing illicit activities through the Code of Conduct Review Meeting, etc.

Facilities dealing with related materials need to strengthen the management capacity (site level security measure, rapid response and notification, physical access control, monitor and trace life cycle of nuclear materials, category 1, 2 radioactive sources, etc.) to prevent illicit activities and to facilitate education/training.

REFERENCE

[1] CNS Global Incidents and Trafficking Database, Annual Report, January, July 2018

The Current Status and Prospects of INPRO and GIF Proliferation Resistance Evaluation Methodology

Ji-song Jeong[a,b], Ho-Dong Kim[a,*], and Seung-kyu Ahn[a]

[a] Korea Atomic Energy Research Institute, 111, Daedeok-daero 989beon-gil, Yuseong-gu, Daejeon, Republic of Korea

[b] University of Science & Technology, 217 Gajeong-Ro, Yuseong-gu, Daejeon, Republic of Korea

[*]khd@kaeri.re.kr

1. Introduction

INPRO (International Project on innovative Nuclear Reactors and Fuel Cycles) is an international cooperation project which aims to ensure that nuclear energy is available to contribute to meeting the energy needs of the 21st century in a sustainable manner. GIF (Generation Ⅳ International Forum) is an international cooperation for development of next generation reactor. Both of them are representative projects that developing Proliferation Resistance (PR) evaluation methodology. The evaluation methodology to quantify the PR on a nuclear system is being developed. However, each nuclear system has so many different processes and characteristics that it is difficult to evaluate PR quantitatively and qualitatively. The evaluation methodology which can evaluate safeguardability will be drawn through the development of various methodologies. They were refined over the years through several case studies. Also, Korea actively participates in GIF and INPRO for development of PR evaluation methodology. This paper reviews the current status and prospects of INPRO and GEN-Ⅳ 's PR methodology.

2. Framework of INPRO and GIF Proliferation Resistance Evaluation Methodology

2.1 INPRO PREM

The INPRO Nuclear Proliferation Resistance Evaluation Methodology (PREM) has been developed through numerous IAEA reports. The Evaluation Methodology was divided into basic principle (BP), user requirement (UR), indicator in consideration of international, regional, trends, and technical achievements. BP has included the necessary conditions for satisfying PR over the full life cycle of the future Nuclear Energy System (NES), and UR has identified the items required to satisfy BP. Finally, criteria and indicators for evaluating PR are defined.

2.2 GIF PREM

In GEN Ⅳ, all possible strategies for proliferation are classified as concealed diversion, overt diversion, concealed facility misuse, overt facility misuse and independent clandestine facility use. The Evaluation Methodology is divided into a challenge, a system response to a challenge, and outcomes. Specially, in the evaluation of GEN Ⅳ, scenarios for diversion methodology are set up in the system to evaluate PR of each scenario. Evaluation of PR is highly critical for GEN Ⅳ methodology.

3. Current Status of INPRO and GIF PREM

3.1 Current Status of INPRO PREM and the Related Activities ROK Has Done

INPRO was initiated for purpose of jointly considering the international actions required to achieve the desired innovations in nuclear reactors and fuel cycles. Korea has participated in several INPRO collaborative projects such as RISC, PRADA, PROSA and so on. Especially, PROSA (Proliferation Resistance and Safeguardability Assessment) process has been applied to a SFR Fuel Manufacturing Facility (SFMF) by KAERI. The case study demonstrated that the proposed PROSA process is simpler to perform than the original INPRO methodology and can be applied from the early stage of design showing the relationship of PR assessment to the Safeguards-by-Design process. The ROK is currently making a Technical Document related to PROSA SFMF.

3.2 Current Status of GIF PREM and the Related Activities ROK Has Done

KAERI has contributed to development of the PRPPEM by taking a leading role in GIF Proliferation Resistance and Physical Protection Working Group (PRPPWG). The ROK is actively participating in GIF PRPPWG and planning to increase the effectiveness by sharing the results of nuclear nonproliferation studies. The PRPP Methodology was applied to evaluate a proliferation resistance for a Pyro-processing facility design. The study identified new metrics and a pathway analysis algorithm based on GIF PRPP measures and analysis approach. KAERI used Reference Engineering-scale Pyro-processing Facility (REPF) model in this study. KAERI recently translated “Evaluation Methodology for Proliferation Resistance and Physical Protection of Gen.Ⅳ Nuclear Energy Systems – Revision 6”, which is a technical report by GIF PRPPWG in 2011, into Korean. Also, “System White Papers : PR&PP of the Six Generation Ⅳ Nuclear Energy Systems” is now under revision by GIF PRPPWG.

4. The Prospects and Outlook

The ROK is continuing its nonproliferation research such as the development of PR evaluation methodology in an international initiatives like GIF and INPRO. Nuclear technology needs international cooperation in order to minimize the risks, could be occurred during a long-term investment. Therefore, we have to grasp the constant changes in the international joint study and try to keep participating in it actively.

5. Conclusion

By applying an evaluation system from the initial stage of design of the NES, problems on proliferation threat can be solved early and nuclear system design that reflecting PR can be realized. The INPRO and GEN Ⅳ Proliferation Resistance Evaluation Methodologies will be used as an assessment tool to evaluate PR for future NES. These activities will shed light on PR advancements of the current system designs.

REFERENCES

[1] Generation IV International Forum (GIF), “A Technology Roadmap for Generation IV Nuclear Energy Systems.” Tech. rep, (2002).

[2] Generation IV International Forum (GIF) PRPP Working Group, “Evaluation Methodology for Proliferation Resistance and Physical Protection of Generation IV Nuclear Energy Systems — Revision 6.” Tech. rep, (2011).

[3] S.K. Ahn et al., “A Proliferation Resistance Evaluation for a Pyroprocessing Facility Design”, INMM 55th Annual Meeting (2014)

IAEA Concept for Exemption and Clearance

Jeong-Guk Kim*, Won Hyuk Jang, MalGoBalGaeBitNaLa Yoo, Yujeong Choi, Jongjin Kim, Seeun Chang, Hee-Seoung Park, and Dae-Seok Hong
Korea Atomic Energy Research Institute, 111, Daedeok-daero 989beon-gil, Yuseong-gu, Daejeon, Republic of Korea
*jungkim@kaeri.re.kr

1. Introduction

Exemption and Clearance are very important concepts for reduction of very low-level radioactive materials, thereby ultimately reduce the cost during decommissioning and remediation and determine when decommissioning is finished (decommissioning endpoint). Korea also accepted these concept, recommendations, and guides [1-4], and has established laws and regulations and controlled now.

In this article, IAEA concepts for clearance and exemption, which are needed to integrate with waste classification by IAEA recommendation, have been reviewed.

2. Basic Safety Standards

IAEA's basic safety standards (BSS) for radiation protection system are in accordance with three exposure groups (workers, patients, and general public), three exposure situations (planned situation, emergency situation, and existing situation) and three radiation protection principles (justification, limitation and optimization) [1]. Those safety standards are described as exemption and clearance for controlling radioactive materials. The detail levels for both of exemption and clearance were derived on the basis of trivial dose (de-minimis), e.g. 10 μSv in a year.

3. Exemption

The general criteria for exemption are 1) that radiation risks are sufficiently low as not to warrant regulatory control, or 2) that regulatory control of radioactive materials would be yield no net benefit. Therefore, IAEA suggested that the radioactive materials such as moderate amount (at the most of the order of a ton) of materials below level given in Table I-1 of Schedule I in Ref. [1], bulk amount of materials below level given in Table I-2 of Schedule I in Ref. [1], and radiation generator, which does not cause a directional dose equivalent rate exceeding 1mSv/h at a distance of 0.1 m from surface or with the maximum energy not greater than 5keV, are automatically exempted without further consideration [1].

4. Clearance

'Clearance' is defined, by IAEA, as the removal of regulatory control by the regulatory body from radioactive materials within notified or authorized practices. Therefore, if the materials have been cleared once, they do not again become subject to requirements for notification, registration and licensing, unless otherwise specified by the regulatory body. Usually this clearance is applied with exemption. IAEA describes that clearance level can be applied to all material types, management options and volumes. Namely, the clearance level given in Table I-2 of Schedule I in Ref. [1] is 'general clearance levels', which was derived without any assumptions on material type and management option.

IAEA is now preparing a new safety report series with a title of derivation of 'specific clearance levels' in material being suitable recycling, reuse, or for disposal in landfills, which can be applied to a particular material type and/or management option but independent of material volumes and specific conditions. And moreover, IAEA will have a plan to develop a 'case specific clearance levels, which could be applied to a specific clearance level derived for a particular situation taking into account assumptions on material type, management option, material volume, and specific conditions of material management. Those clearance levels are obviously higher than the general clearance levels.

The activity concentration of an artificial nuclide in solid form does not exceed the level in Table I-2 of Schedule I in Ref. [1], whereas, for natural nuclide, its activity concentration does not exceed the level in Table I-3 of Schedule I in Ref. [1]. For mixture of more than one nuclides, the clearance level is that the sum of the individual nuclide activity concentrations is less than the sum of fraction for each derived level [1].

The IAEA exemption and clearance levels for typical nuclide are shown in Table 1, compared with Korean clearance levels.

Table 1. IAEA exemption and clearance levels for typical nuclides [1]

Radionuclide	Activity concentration (Bq/g)	
	Exemption level of moderate amounts	Exemption level of bulk amounts / Clearance level
H-3	$1x10^6$	100
C-14	$1x10^4$	1
Co-60	$1x10^1$	0.1
Ni-59	$1x10^4$	100
Ni-63	$1x10^5$	100
Sr-90	$1x10^2$	1
Nb-94	$1x10^1$	0.1
Tc-99	$1x10^4$	1
I-129	$1x10^2$	0.01
Cs-137	$1x10^1$	0.1

5. Conclusion

IAEA suggested exemption and clearance concepts to reduce the amount of material disposed as waste, thereby reducing cost. This policy impacts hugely on operator at the waste management point of view. Specific or case specific clearance levels with much higher values are needed to be derived and applied to reduce the amount of very low-level radioactive waste.

REFERENCES

[1] IAEA Safety Standards No. GSR Part 3, "Radiation Protection and Safety of Radiation Sources: International Basic Safety Standards," International Atomic Energy Agency, Vienna, 2014.

[2] IAEA Safety Standards Series No. RS-G-1.7, "Application of the Concepts of Exclusion, Exemption and Clearance," International Atomic Energy Agency, Vienna, 2004.

[3] IAEA Safety Report Series No. 44, "Derivation of Activity Concentration Values for Exclusion, Exemption and Clearance," International Atomic Energy Agency, Vienna, 2005.

[4] IAEA General Safety Guide No. GSG-1, "Classification of Radioactive Waste," International Atomic Energy Agency, Vienna, 2009.

Identifying Radioactive Materials in Dirty Bomb Terror Scene Using Laser-Induced Breakdown Spectroscopy

Hyeongbin Kim, Yunu Lee, and Sungyeol Choi*
Korea Advanced Institute of Science and Technology, 291, Daehak-ro, Yuseong-gu, Daejeon, Republic of Korea
*sungyeolchoi@kaist.ac.kr

1. Introduction

According to Incident and Trafficking Database (ITDB), a total of 1174 incidents that indicate the intent to acquire radioactive material for trafficking or malicious usage are confirmed until 2016 [1]. Recently, terrorist groups such as ISIS and Al-Qaeda have shown more interest in obtaining these hazardous materials. Their goals are to make radiological dispersal devices (RDDs) which are also called dirty bombs. If dirty bombs explode, the surrounding areas will be contaminated with radioactive materials. Those terrorism induces significant health effects with panic.

To minimize the damage caused by dirty bomb terrors, rapid and precise identification of the radioactive materials in early phase is required. The most conventional radiation detector is the Geiger-Muller counter (GM counter). It is portable, however, it cannot distinguish the types of radiation. Secondary-Ion Mass Spectroscopy (SIMS) or Thermal Ionization Mass Spectroscopy (TIMS) is used for isotopic analysis, but it takes at least a day. To overcome these limitations, Laser-Induced Breakdown Spectroscopy (LIBS) has been studied. Previous studies show that LIBS can be used for nuclear forensics with its ability of prompt and accurate nuclear materials analysis [2, 3]

The aim of the present work is to assess the feasibility of identifying radioactive materials by LIBS. Moreover, the best matrix to detect radioactive materials were found by comparing LODs of each matrix.

2. Methodology

2.1 Sample Preparation

Argonne National Laboratory suggested 9 attractive isotopes of interest in RDDs, based on not only portability of the isotopes, but the level of radioactivity they emit [4]. Among them, $SrCl_2$, CsCl, Co, and Ir that were chemical forms of radioactive materials often found in sealed source were chosen as target materials. Since terrorism is highly likely to occur in crowded cities, matrix was chosen as common substances in the city such as aluminum, stainless steel, polyester, and PET.

To simulate the terror scene, target materials are dissolved into highly purified water that ranges from 0.2 ppm to 20 ppm, and sprayed 80 times onto matrix homogeneously using a sprayer. The matrix was heated to 130 ℃ by a heating plate to make sprayed water evaporated continuously without lumping which prevented the coffee-ring effect.

2.2 Experimental Setup

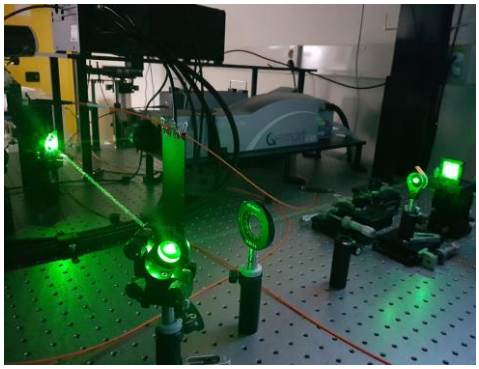

Fig. 1. LIBS System.

To perform LIBS, a compact Q-switched Nd:YAG laser (20 Hz, 532 nm, 220 mJ per pulse, 5 ns pulse width) was used to ablate targets. After ablated material is dissociated into excited ionic and atomic species, the plasma quickly cools down, and then the excited ions and atoms emit characteristic emissions as they return to ground states. Since continuum and

characteristic emissions produced by plasma light are superimposed, light must be separated to analyze each substance. To obtain spectra of targets, an Echelle spectrograph (195 mm focal length, f/7, 200 – 975 nm of operating range) combined with intensified-CCD (13 × 13 μm^2 pixel size) was used.

3. Results

Fig. 2 shows a spectrum of aluminum as a matrix with strontium chloride as a target material among several samples. As shown in the figure, when strontium was sprayed on aluminum, the persistent emission lines of strontium were newly observed while those of the aluminum were constantly observed.

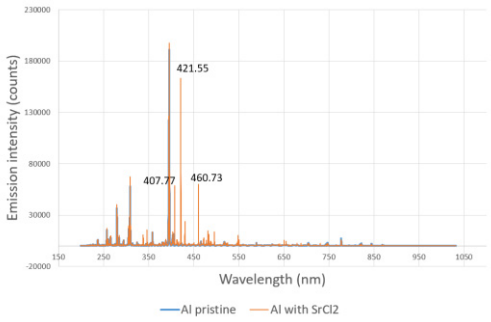

Fig. 2. LIBS spectrum comparison of pristine aluminum and aluminum sprayed with strontium.

In order to calculate limit of detection (LOD) values, the calibration graphs of concentrations of the strontium chloride were obtained. As shown in fig. 3, R^2 of each calibration line exceeded 0.94, indicating that the intensity of the emission line is well fitted to the concentration of the strontium.

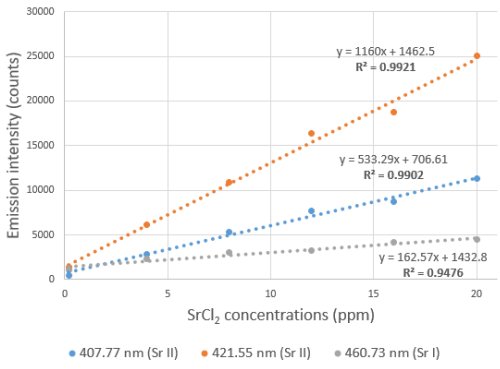

Fig. 3. Calibration graphs for aluminum with strontium sample at 407.77 nm, 421.55 nm, and 460.73 nm.

4. Conclusion

The results of the experiment show that all radioactive materials were identified with low LODs. Therefore, the present work not only establishes LIBS database but demonstrates the feasibility of identifying radioactive materials in urban areas when a dirty bomb terror occurs. This technique is anticipated to provide roadmap of in-situ analysis in a dirty bomb terror scene as handheld and telescope LIBS are developed which makes portable and remote detection by LIBS possible.

ACKNOWLEDGEMENT

This work was supported by the Nuclear Safety Research Program through the Korea Foundation of Nuclear Safety (KOFONS), granted financial resource from the Nuclear Safety and Security Commission (NSSC), Republic of Korea (Grant No.1703008).

REFERENCES

[1] IAEA, (2017). Trafficking Database (ITDB) Incidents of nuclear and other radioactive material out of regulatory control. 2017 Fact Sheet, International Atomic Energy Agency.

[2] Martin, M. Z., Allman, S., Brice, D. J., Martin, R. C., & Andre, N. O. (2012). Exploring laser-induced breakdown spectroscopy for nuclear materials analysis and in-situ applications. Spectrochimica Acta Part B: Atomic Spectroscopy, 74, 177-183.

[3] Bhatt, B., Angeyo, K. H., & Dehayem-Kamadjeu, A. (2018). LIBS development methodology for forensic nuclear materials analysis. Analytical Methods, 10(7), 791-798.

[4] Peterson, J., MacDonell, M., Haroun, L., Monette, F., Hildebrand, R. D., & Taboas, A. (2007). Radiological and chemical fact sheets to support health risk analyses for contaminated areas. Argonne National Laboratory Environmental Science Division, 133.

An Analysis of the Contributions of KAERI's Operation to the Daejeon Regional Economy

Dong Hoon Lee*, Jieun Joo, Man-Ki Lee, and Chae Young Lim
Korea Atomic Energy Research Institute, 111, Daedeok-daero 989beon-gil, Yuseong-gu, Daejeon, Republic of Korea
*dhlee@kaeri.re.kr

1. Introduction

Social acceptance by local residents is very important for the use of sustainable nuclear energy including nuclear R&D activities. This public acceptance of nuclear-related activities includes a variety of factors: social, economic and environmental impact. Among these factors, economic contributions to the regional economy are considered very important factors by local people.

This study examines the economic contribution of the Korea Atomic Energy Research Institute (KAERI)'s operation to the Daejeon regional economy securing local acceptance of the research activities of KAERI.

2. Background

2.1 Overview of KAERI' s Operation

The KAERI is a government-funded research institute established in 1959 and has been the only research institute in Korea dedicated to nuclear energy. As the first research institute of science and technology in Korea and the second largest research institute, KAERI has a total of about 1,580 full-time employees and spends about 544 billion won in annual R&D budget as of the end of 2018, headquartered in Daejeon, and has two branch offices in Jeongeup and Gyeongju.

2.2 Economic Contribution Approach

The scope of this analysis is limited to estimating the contribution from the operations by KAERI's headquarter to Daejeon regional economy in terms of direct effect. The direct economic contribution to the region is made both from the expenditure incurred in the operation of the KAERI and from the expenditure of the workers employed by the KAERI. The local taxes paid by the KAERI and workers contribute to the increase of the local government revenue. In other words, various consumption activities in the region made by workers, and the expenditure in the operation process of the KAERI in the region including the purchase in the local area and the contract with the local company can contribute to the improvement of the local economy.

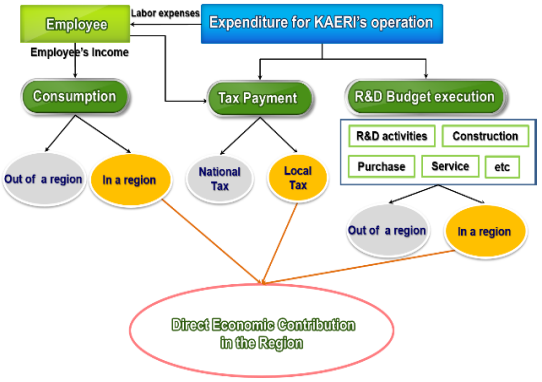

Fig. 1. Mechanism of the economic contribution to the region.

3. Contribution of KAERI's Operations to Daejeon Regional Economy

The direct economic contribution of KAERI's operations to the Daejeon is analyzed by the increase of the local government's tax revenue, the expenditure of the institution in the region, and the expenditure of the workers in the region.

3.1 The Increase of the Local Government's Tax Revenue

The local taxes paid by KAERI are acquisition tax and property tax, and it is analyzed to be about 240 million won per year. The local taxes paid by KAERI's workers are resident tax, income tax, automobile tax, property tax, and tobacco consumption tax and it is analyzed that employees working at the Daejeon pay a local tax of about 2.7 billion won annually.

3.2 The Expenditure of the Institution in the Region

In the process of institutional operation and R&D activities, KAERI spends considerable amounts of a budget in the region by purchasing goods & service from local companies, signing contracts for construction or research with local companies and using corporation card in Daejeon. As a result of analyzing the regional expenditure of the KAERI from 2016 to 2018, it is estimated that the purchase amount from local companies is about 40 billion won per year, the contract amount with local companies for construction, service and R&D is 31 billion won per year, and the expenditure by using corporation card in Daejeon is about 5 billion won per year.

3.3 The Expenditure of the Workers in the Region

KAERI headquarter in Daejeon has a total of about 1,600 full-time and part-time employees with annual expenditure of about 150 billion won[1]. Because the expenditure behavior to region is different according to the residential area of the employees, we analyzed the employees' residential areas, worker type, average wages, etc, and estimated the total amount of consumption by employees in the region based on the consumption propensity scenario and the result are shown in table 1.

Table 1. the expenditure of the workers in the region

Section		Annual expenditure of employees		
		Number of employees	Scenario	Amount (million won)
Full-time	Resident in Daejeon	1,210	high	62,512
			low	41,674
	Resident outside Daejeon	232	high	3,995
			low	1,331
Part-time	Resident in Daejeon	160	high	4,419
			low	2,946
Total		1,602	high	70,926
			low	45,952

4. Conclusion

We estimated the direct contribution to the regional economy and tax revenue generated by KAERI's R&D activities in Daejeon. KAERI's current annual economic impact is estimated to be 3 billion won in tax and 120~150 billion won in expenditure. It is realized during the operation of the institute located in Daejeon.

REFERENCES

[1] www.alio.go.kr

A Study of Training and Qualification of Security Personnel at Nuclear Facilities

Hyun-Kyung Lee*
Korea Institute of Nuclear Nonproliferation and Control, 1534, Yuseong-daero, Yuseong-gu, Daejeon, Republic of Korea
*hklee@kinac.re.kr

1. Introduction

With the increasing global threats of international terrorism and nuclear terrorism, there is a spotlight on the education and qualifications of nuclear power plant protection workers.

In accordance with Article 9-2 of the Protection of Nuclear Facilities and Nuclear Emergency Preparedness Act, the Korea Institute of Nuclear Nonproliferation and Control (KINAC) implements the legal education for the protection workers of nuclear facilities and draws out the job capability based education system through job analysis of the protection workers.

In this paper, we will discuss the education and qualification standards for security personnel at U.S Nuclear Regulatory Commission and discuss the educational development plan for the security personnel of nuclear power plants in Korea.

2. Individual Training and Qualification of Security Personnel for duty

The outline of the US Nuclear Regulatory Commission's (NRC) Regulatory Guide (RG) 5.75 'Training and Qualification of Security Personnel at Nuclear Power Reactor Facilities' is Individual Training and Qualification for Duty, On-the-Job Training (OJT), Performance Evaluation Program, Duty Qualification and Re-certification, Weapons Training, Weapons Qualifications and Re-qualifications, Weapons, Personal Equipment and Maintenance. The active human maintenance for the security personnel at nuclear facilities is based on analysis of Individual Training and Qualification for Duty. Based on this analysis, Nuclear operators in Korea will consist of Duty & Weapons Qualification and Re-certification.

This paper will focus on the element; Individual Training and Qualification for Duty.

2.1 Critical Function Job Tasks

In a security organization, security personnel must be trained and qualified to perform their duties prior to performing security tasks.

In addition, the security education program should have a list of trainings that can complement the job, knowledge, skills, and abilities to acquire set qualifications. In US RG 5.75, the security organizations are divided into detailed duties (divided into 28 categories) according to the security personnel, and the qualifications for these duties are listed as follows.

Table 1. Critical Functions Job Tasks Qualification Table [1 of 28 categories]

Tasks	Watchperson	Armed Security Officer (A)	Armed Responder (AR)	Alarm Station Operator (ASO)	Response Team Leader (RTL)	Security Shift Supervisor (SSS)	Frequency*	Performance Method
1. Perform Critical Administrative Items: Perform administrative tasks associated with the conduct of security operations consistent with station procedures.								
• Identify the role of security personnel in supporting safe operation of the facility	X	X	X	X	X	X		D
• Identify the 10 CFR 73.21 requirements for the protection of Safeguards Information	X	X	X	X	X	X		D
• Identify security chain of command	X	X	X	X	X	X		D
• Conduct shift turnover				X	X	X		P/S/D
• Conduct post turnover	X	X	X	X	X	X		P/S/D
• Prepare duty roster				X	X	X		P/S/D
• Verify inventory of security keys		X	X	X	X	X		P
• Verify inventory of security equipment		X	X	X	X	X		P
• Perform pre-job briefing				X	X	X		P/S
• Inspect security posts				X	X	X		P/D
• Issue vital area keys		X	X	X	X	X		P/S/D
• Identify/perform reportability		X	X	X	X	X		P/S/D
• Change vital area keys and cores/safeguards combinations		X	X	X	X	X		P/S

[Performance Method - M: Must Perform, P: Perform, S: Simulate, D: Discuss]

2.2 Security personnel Training

Nuclear operators should provide physical protection programs to security personnel for training, qualification and periodical revalidation to perform their assigned tasks. According to the NRC RG 5.75, physical protection programs should be designed to include the following list 66 elements: the mainly important elements are NRC requirements and guidance for physical security at nuclear facilities, NRC requirements and guidance for physical security at nuclear facilities, NRC requirements and guidance for physical security at nuclear facilities including 53 elements.

3. Improving Task-based Training for Security Personnel at Nuclear Facilities in Korea

KINAC was designated as a physical protection education institution in 2011 and is carrying out compulsory physical protection training for nuclear

facility security personnel. In order to escape the limitation of time-consuming education, the education courses have been improved to focus on the development of educational contents such as practice-oriented training, visiting training, and improvement of curriculum.

In particular, the following results were derived for establishing a job competency - based education system. The guards are divided into three groups: General Security Personnel (including Security Officer), Cyber security personnel, Security Guides. In order to establish the education reform plan based on job competency, job analysis is developed through focus group interviews (Table 2), Competencies (Knowledge, Skill) are defined by subject (Table 3), and feedback (Table 4) through an education needs survey.

Table 2. Task and Duty for General Security Personnel
< Task: General Security Personnel >

Field	Duty			
Physical Protection training exercise and management	Annual exercise planning	Force on Force/Table top Exercise planning	Writing of exercise planning	Meeting for pre-exercise
	Implementing of exercise	Evaluation & Follow up	Management of trainee target	
Management of security equipment	Review of blind area	CCTV operation and maintenance	Operation and Maintenance of Unmanned Security, Access Control system	Equipment update of Central Alarm Station
	X-Ray detection operation and maintenance	Operation and Maintenance of Fence and sensor		

Table 3. Essential Capability for general security personnel by each subject

Subject	Main contents	Knowledge	Skill
General details and Law of Physical protection	- Act on Measures for the Protection of Nuclear Facilities, etc. and Prevention of radiation disasters - United Defense Act - Introduction to Nuclear Security - General PPS Elements	- Law of National Physical protection - Requirements of Physical protection(Sabotage) - Categorization of physical protection of Nuclear Material - Design Basis Threat	- Use of Physical protectio n system
Regulations of Physical protection, Regulation of security operations	- Regulation of PP & Operation - Instruction of technical standard - Regulation of security tasks - Regulation of Documentary supply - Cooperation with organization of Regulation request - Preparation of amendment	- Regulation of PP - Guidelines of technical standards - Regulation of security tasks - Regulation of Documentary supply - Knowledge about background of amendment	- Ability of making document

Table 4. The subjects based on Competency for General Security Personnel

Subject \ Career	Trainees	
	Initial Training Course (within 1 year)	Continuing Training Course (Annually)
Optional	-	· Exercise for physical protection and management for training · Access Control · Advanced for Physical Protection Inspection · Advanced Management of security equipment · Advanced Vital Area operation · Principle of Physical Protection Sensor
Required	· General Matters concerning Physical Protection; · Physical Protection Regulations & Security Regulations · Physical Protection Inspection · Management and Operation of Security Equipment · Management and Operation of Vital Area · International & National Trends of Threat	

By establishing the basic elements based on the above-mentioned job competencies, we will establish a basic plan based on job competency, develop and improve course-specific curriculum, and ultimately establish job competency-based education within the next five years.

4. Conclusions

The policies of the current government is promoting the regularization of security personnel in the safety and risk fields in order to establish social safety nets. Also, we need not only safe employment but also systematical advanced human resource development program at nuclear facilities in Korea. Therefore it is necessary to improve and develop a customized training program for the security personnel training and qualification in Korea based on NRC RG 5.75.

It contributes to strengthening the national nuclear security culture by establishing a more advanced system for national security personnel, including organizing and providing a task-oriented comprehensive program.

REFERENCES

[1] Nuclear Regulatory Commission Regulatory Guide 5.75 Training and Qualification of Security Personnel at Nuclear Power Reactor Facilities
[2] Report of Job Competence Modeling and Training System Development /KINAC INSA, 2018.12

A Literature Study on Simulation Methods With Respect to Denuclearization

Jinyoung Lee*
Korea Institute of Nuclear Nonproliferation and Control, 1534, Yuseong-daero, Yuseong-gu, Daejeon, Republic of Korea
*jylee86@kinac.re.kr

1. Introduction

Since the PyeongChang Olympics in 2018, the situation around the Korean Peninsula has rapidly changed from decades-long strained relations. Based on these environments, the ROK government launched a new R&D program to develop ROK's technical capability which can be applied in DPRK's denuclearization process.

One of the subjects in the program is development of physical model of DPRK's nuclear facilities. In this paper, for proceeding this research on the prediction methods of unknown variables based on limited information, several literatures which were studied on general simulation researches, and its applications in nuclear non-proliferations were reviewed.

2. Main Subjects

2.1 Simulation Methods in General

In terms of utilized simulation methods in technical and political researches, there are well-known three kinds of techniques as follows; Agent Based Modeling (ABM), System Dynamics (SD) [1], and Bayesian Network (BN).

In a chronical point of view, the BN (or Bayes probability concept) was first developed by Thomas Bayes. The Bayes theorem is known as a theory which can provides a mathematical framework for inference using probability. Secondly, the SD is a widely used for simulation method in the field of factory design, political simulation, decision making, marketing and so on. Basically it is a kind of network analysis among nodes and variables. Thirdly, the ABM, somewhat opposing to top-down mechanism of SD methodology, is a bottom-up methodology which gathers all the phenomena from agent(an agent is defined as a smallest behavioral actor of the subject system). These three techniques are very useful to analyze the unknown phenomena or to find out an unclear mechanism with limited information.

2.2 Precedent Simulation Research in Nuclear Nonproliferation

The first research was conducted by Dr. Hacker's team [2]. John E. Bistline et al. suggest several parts which are critical to make the centrifuge are restricted by China's black market situation. The probability was given to the stockpile of the parts and a Monte Carlo sampling was carried out to optimize the centrifuges for the enrichment [2].

The second one was studied by G.A. Coles, which shows the BN technique that how to evaluate a state level proliferation resistance. The variables are in a very abstract level such as technical factors, international security factors, domestic politics factors, and national identify & Psychology factors [3].

The third one was conducted by C.R. Freeman, which is focused on material acquisition path. He

composed the pathways of each nuclear facilities in an entire nuclear cycle from a U enrichment to a recycling process by BN method, and then combined them all to a state level pathway [4].

The fourth one was studied by R.A. Elmore, which was started from G.A. Cole's previous study [4] to his own research topics. He suggested a multidisciplinary methodology combining the BN and the ABM. In his work, a nation is playing a role of agent as a player of a game theory.

3. Conclusion

Based on the review of previous literatures, several research topics and questions were derived as follows. Firstly, which way of simulation can provide the most confident inference on the total amount of DPRK's nuclear materials? Secondly, how can we evaluate the performance of each methodology? As shown in this paper, there have been many simulation methodologies including the already mentioned the BN, the ABM and the SD. Thus before we select a specific method, it is necessary to find a way of evaluation on those methods very carefully. In the near future, not only the validity of these simulation methods and their combination but also the answer of these questions are necessary to be studied in more detail.

REFERENCES

[1] Andrei Borshchev & Alexei Filippov, "From System Dynamics and Discrete Event to Practical Agent Based Modeling: Reasons, Techniques, Tools", XJ Technologies www.xjtek.com and St. Petersburg Technical University.

[2] John E. Bistline, David M. Blum, et. al., "A Bayesian Model to Assess the Size of North Korea's Uranium Enrichment Program", Science & Global Security, 23:71-100, 2015.

[3] G.A. Coles, A.J. Brothers, J. Olson, P.D. Whitney, "Assessing State Nuclear Weapons Proliferation: Using Bayesian Network Analysis of Social Factors", Conference Proceedings from Pacific Northwest International Conference on Global Nuclear Security - The Decade Ahead, 2010.

[4] Corey Ross Freeman, "Bayesian Network Analysis of Nuclear Acquisitions", a mater degree thesis, Texas A&M University, August 2008.

[5] Royal Albert Elmore, "Dynamic Agent Based Modeling using Bayesian Framework for Addressing Intelligence Adaptive Nuclear Nonproliferation Analysis", a Dissertation for Doctor of Philosophy, Texas A&M University, December 2014.

2분과

사용후핵연료 처분전관리 (Oral)

Calibration of Effective Material Properties of Spent Nuclear Fuel Rod

Sanghoon Lee*
Keimyung University, 1095, Dalgubeol-daero, Dalseo-gu, Daegu, Republic of Korea
*shlee1222@kmu.ac.kr

1. Introduction

In this paper, a procedure for material property calibration to develop a simplified beam model of spent nuclear fuel rod is described. To evaluate the structural integrity of spent nuclear fuel under vibratory or shock loading, a detailed finite element analysis is necessary including spent fuel assemblies and cask. But due to the complicated shape and uncertain material properties of spent fuel rods, the usage of simplified model is inevitable. The procedure introduced in this paper focuses on the treatment of interfacial condition between the pellets and cladding of fuel rod, which is known to have a significant influence to the load resistance of spent fuel rods.

2. Material Properties of Spent Fuel Rod

2.1 Cladding Material Property

The material property of irradiated cladding depends on many variables, such as temperature, neutron fluence, burnup, strain rate and so on. Geelhood et al.[1] developed a sophisticated material model of high burnup fuel cladding from hot cell test data and the model for the Zircaloy-4 cladding under 573 K is adopted in this work. The stress-strain curve for this cladding is as shown in Fig. 1.

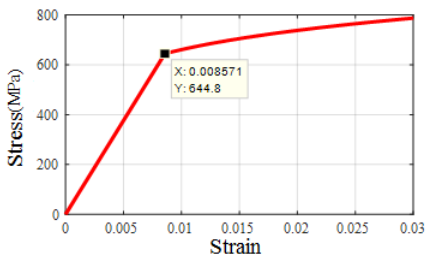

Fig. 1. Stress vs Strain curve of Zircaloy-4 cladding.

The uniform elongation of the cladding is calculated as 1.2% and this value is considered as failure criteria of cladding under impact load in this work.

3. Finite Element Analyses of Detailed Model

3.1 Finite Element Modeling

The finite element model is constructed using solid elements in ABAQUS as shown in Fig. 2. The shape of pellets and cladding are from literature and to account for the stress concentration in the pellet-cladding interface, enough degrees of freedom are assigned.

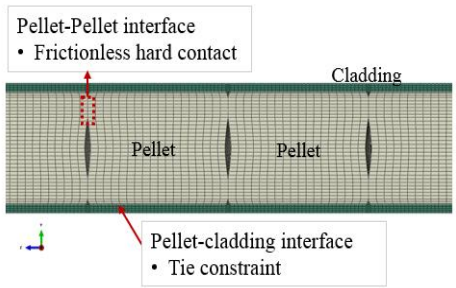

(a) Fully bonded pellet-clad interface

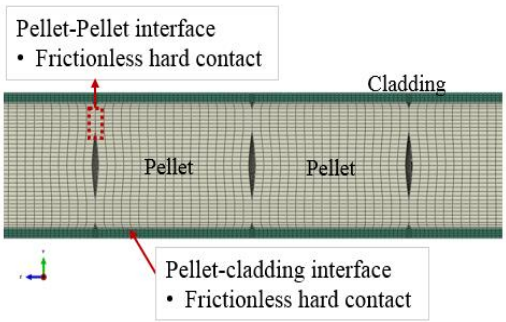

(b) Fully de-bonded pellet-clad interface

Fig. 2. Finite element models of fuel rods.

The fully bonded interface between the pellet and cladding is modeled using the tie constraint between the adjacent surfaces while the fully de-bonded interface is modeled using the frictionless hard contact.

3.2 Analyses Results

In the static analyses, the critical bending moment which produce the critical plastic strain of 1.2% in the cladding is calculated for both models. For bonded interface, the critical moment is 12,690 N·mm while it is 20,410 N·mm for de-bonded case.

4. Material Calibration for Simplified Model

4.1 Strategy of Model Simplification

In this work, the spent nuclear fuel rod is simplified into a beam made of an isotropic material of which the property is formulated with Hook's law and power law. The cross section of the beam has the same diameter with the fuel rod while it can be a hollow tube. Two points in the load-displacement curve of the detailed fuel rod model are chosen and an optimization is performed with this formula:

Find K, n, t such that

$$\text{Minimize } f(K,n,t)= (U_{b1}-U_{s1})^2+(U_{b2}-U_{s2})^2 \quad (1)$$

Where U_b is the displacement calculated with beam model, U_s is the displacement calculated with detailed solid model. The number 1, 2 denote two points at the load-displacement curve.

The solution was found by using an advanced optimization algorithm, the Adaptive Simulated Annealing and the results are shown in Fig. 3.

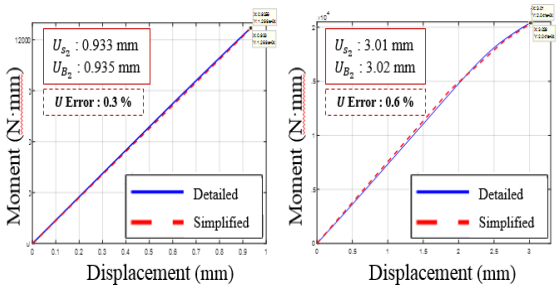

Fig. 3. Comparison the loading curve of detailed model and simplified model.

5. Conclusions

Simplified beam models of spent nuclear fuel rods are successfully developed using a sophisticated optimization procedure. The developed model will be tested considering various types of loadings such as vibration, and impacts. It was also shown that the behavior of fuel rods are significantly different according to the pellet-clad interfacial condition.

REFERENCE

[1] Geelhood, K. J., Beyer, C. E., Lusher, W. G., 2008, "PNNL Stress/Strain Correlation for Zrcaloy," U.S. Department of energy, PNNL-1770.

Thermal Analysis of HISTORM-100 Dry Storage Cask With Oxidation Considered Heterogeneous WH14X14 Fuel Assembly Using COMSOL MULTIPHYSICS Program

SunWoo Park and KwangHeon Park*
Kyung Hee University, 1732, Deogyeong-daero, Giheung-gu, Yongin-si, Gyeonggi-do, Republic of Korea
*kpark@khu.ac.kr

1. Introduction

The use of cask type dry storage systems is inevitable as the wet storage pool becomes saturated. In a typical dry storage cask thermal analysis, homogeneous fuel assembly condition is applied, and thermal properties of a fresh cladding are used. Homogeneous fuel assembly condition makes it difficult to apply detailed conditions to the fuel rods. Oxide film formed on the fuel rods has an effect of reducing thermal conductivity. Therefore, the use of thermal properties of fresh cladding is a non-conservative evaluation method. In this study, thermal analysis of dry storage cask with oxidation considered heterogeneous assembly condition was performed.

2. Procedure and Result

In this study, thermal analysis of the HISTORM-100 dry storage cask with oxidation-considered WH14X14 heterogeneous fuel assemblies was performed using COMSOL MULTIPHYSICS 5.4 program.

2.1 Geometry and Mesh Setting

The specifications of HISTORM-100 CASK, MPC-24, and WH14X14 refer to HOLTEC INTERNATIONAL's FSAR. Geometry is composed of 4,021,868 meshes in total. The average quality of the mesh is 0.3707. Geometry and mesh are shown in Fig.1 below.

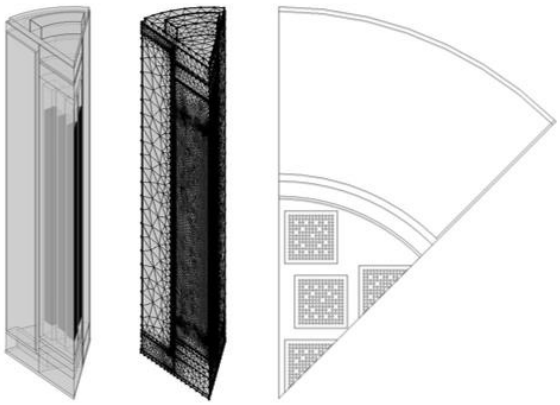

Fig. 1. Geometry and mesh of HISTORM-100 cask with WH14X14 heterogeneous fuel assembly.

2.2 Oxidation Considered Material Property

140um oxide thickness condition was used. Thermal conductivity and thermal transmittance were used to calculate oxidation considered conductivity. Specific heat and density were calculated to reflect the volume ratio. Oxidation-considered conductivity is shown in Fig. 2.

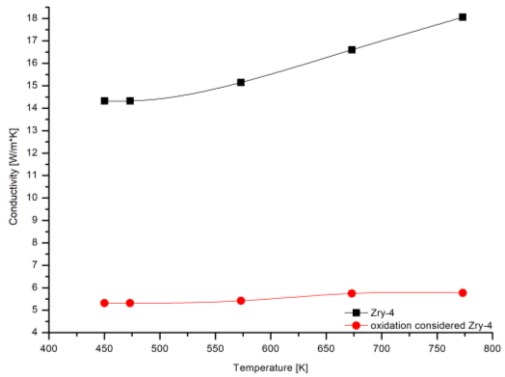

Fig. 2. Thermal conductivity of Zircaloy-4 and oxidation considered Zircaloy-4.

2.3 Computing Result

The difference between the FSAR result and the COMSOL MULTIPHYSICS program result is about 10℃. The difference in PCT (Peak Cladding Temperature) is about 3.1%. The results are shown in Fig. 3.

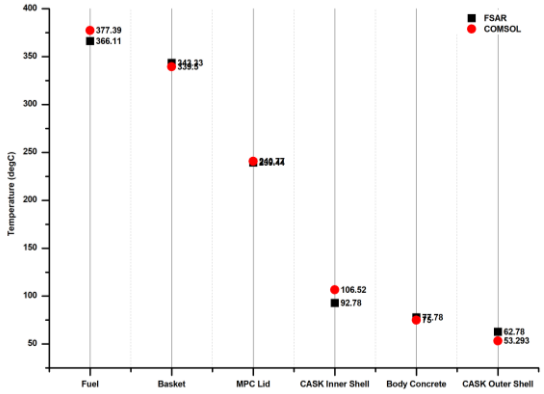

Fig. 3. Comparison of FSAR and COMSOL MULTIPHYSICS results.

Based on the above model, calculation using the oxidation considered thermal properties was performed. The PCT difference between oxidation considered model and oxidation not considered model is about 2℃. The calculation results are shown in Fig. 4.

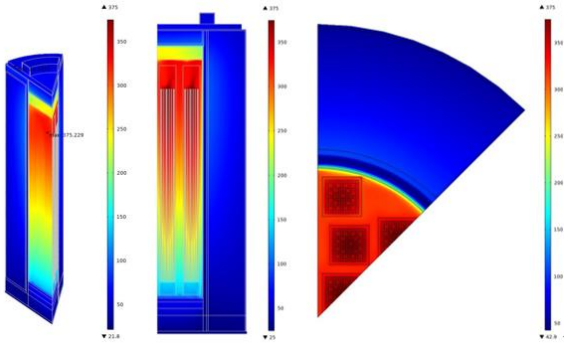

Fig. 4. 3D temperature profile, 2D temperature profile of 45° cutting plane, and 2D temperature profile of PCT height region.

3. Conclusion

According to the reference[2] data, up to 140um oxide can be formed under high burnup condition. PCT value of 140um oxide cladding was higher than the PCT value of fresh cladding by 2℃. In the case of spent fuel with high burnup condition, consideration of the changed thermal properties due to oxide will be more realistic and conservative evaluation.

REFERENCES

[1] Wu Yongjia, Klein Jackson, Zhou Hanchen, Zuo Lei, “Thermal and fluid analysis of dry cask storage containers over multiple years of service”, Annals of Nuclear energy, Vol.112, 132-142 (2018).

[2] T. Motta, Adrien Couet, Robert J.Comstock, “Corrosion of Zirconium Alloys Used for Nuclear Fuel Cladding”, Annual Review of Materials Research, Vol.45, 311-343 (2015).

Cutoff Frequency for Rigid Body Acceleration of KORAD21 Cask in Drop Accidents

Sang Soon Cho[a,*], Yun Young Yang[a], Jaehoon Lim[a], Ki-Seog Seo[a], Woo-Seok Choi[a], Sang-Hwan Lee[b], Chang-Min Shin[b], and Chang-Yeal Baeg[b]

[a] Korea Atomic Energy Research Institute, 111, Daedeok-daero 989beon-gil, Yuseong-gu, Daejeon, Republic of Korea

[b] Korea Radioactive Waste Agency, 174, Gajeong-ro, Yuseong-gu, Daejeon, Republic of Korea

[*]sscho96@kaeri.re.kr

1. Introduction

The purpose of this paper is to investigate the cutoff frequency for rigid body acceleration in KORAD21 drop test. The acceleration of the spent nuclear fuel cask was measured by using three IEPE accelerometers and the cutoff frequency for the rigid body acceleration was determined by obtaining the first natural frequency from the 1-m side puncture test.

2. Cutoff Frequency and Rigid Body Acceleration

9-m free drop test and 1-m puncture test were performed using KORAD21 1/3 scaled model in order to demonstrate the structural performance of KORAD21 spent nuclear fuel cask. In 9-m free drop test, 5-kinds of postures including vertical, lid vertical, horizontal, inclination, center of gravity were considered, and 1-m puncture tests included a side-puncture test and a lid-vertical-puncture test.

One important characteristic of the drop test is that the stress wave propagates through the cask, resulting in very large vibratory motion or stress components in the acceleration data due to rigid body mode, shell mode, and contact between internal components. In order to remove such vibratory components, the raw acceleration data should be filtered with low pass filter at a lowest natural frequency maintaining the acceleration component due to rigid body motion [1-3].

During the drop test of various postures, the 1-m side puncture test is that the cask freely drops over the rupture bar while keeping the cask horizontal. Therefore, this paper used 1-m side puncture test to determine the first bending mode and first order natural frequency of the cask.

3. Test Results for Cutoff Frequency

Accelerometers and strain gauges are attached to the test model to evaluate the behavior characteristics before and after impact due to the drop. Acceleration data were stored at a rate of 100,000 samples/s and the acceleration was measured at a frequency of 10 kHz.

Fig. 1 shows the photographs after the 1-m side puncture test and the raw acceleration data measured from three accelerometers. Fig. 2 shows the result of PSD (power spectral density) using three raw acceleration data. The natural frequency of the first bending mode was calculated as 490Hz.

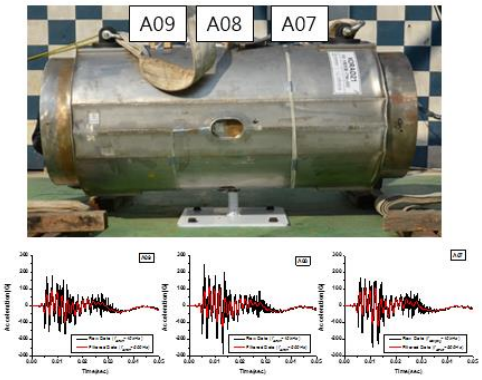

Fig. 1. Side puncture test result and the raw acceleration data.

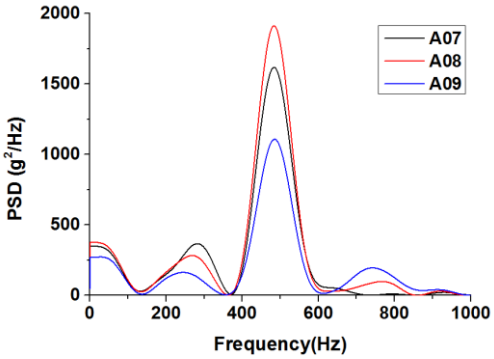

Fig. 2. PSD results obtained from the acceleration data.

Fig. 3 shows an example of the filtered acceleration data in the 9-m vertical drop test using the cutoff frequency obtained in this study. An 8th order Butterworth filter was applied and the cut-off frequency was 500 Hz. For both the drop test and the burst test. The filtered acceleration data means the rigid body deceleration acting on the cask when it was dropped.

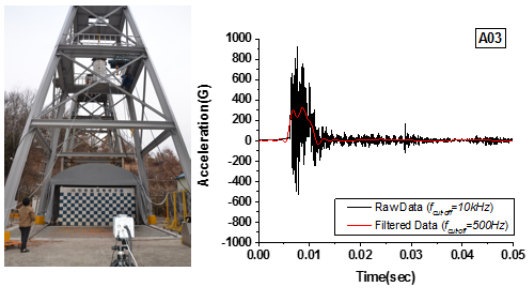

Fig. 3. Vertical drop test and the filtered acceleration data.

4. Conclusions

We presented the cutoff frequency to calculate the rigid body acceleration acting on the cask during drop test of KORAD21. The cutoff frequency for obtaining the rigid body acceleration was obtained as the natural frequency for the first bending mode from the 1-m side puncture test, and it was 490Hz. The cut-off frequency was determined as 500 Hz for both the drop and the puncture tests. The raw acceleration data was applied to the 8th order Butterworth low pass filter with the determined cutoff frequency to check rigid body deceleration acting on the cask. The cutoff frequency presented in this paper should be applied equally to the post-processing of the drop analysis [4].

REFERENCES

[1] IAEA Safety Standards Series No. SSG-26, “Advisory Material for the IAEA Regulations for the Safe Transport of Radioactive Material (2102 Edition)”, International Atomic Energy Agency, 2014.

[2] J.R. Stokley, D.H. Williamson, “Structural Integrity of Spent Nuclear Fuel Storage Casks subjected to Drop”, Nuclear Technology, Vol. 114, pp. 112-121, 1996.

[3] M.C. Witte, J. Hovingh, G.C. Mok, S.S. Murty, T.F. Chen, L.E. Fischer, “Summary and Evaluation of Low-Velocity Impact Tests of Solid Steel Billet onto Concrete Pads”, NUREG/CR-6608, UCRL-ID-129211, 1997.

[4] S.S. Cho, K.C. Park, H. Huh, “A method for multidimensional wave propagation analysis via component-wise partition of longitudinal and shear waves”, International Journal for Numerical Methods in Engineering, Vol. 95, pp. 212-237, 2013.

Development of a Reinforcement Device, SAFER, to Ensure the Handling Integrity of PWR Spent Nuclear Fuel for Dry Storage in Korea

Hyeong Koo Kim*, Jae Jun Lee, Dong Geun Ha, Gyu Cheol Sin, Sung Ki Lee, and Jong Sung Yoo
KEPCO Nuclear Fuel, 242, Daedeok-daero 989beon-gil, Yuseong-gu, Daejeon, Republic of Korea
*hkkim@knfc.co.kr

1. Introduction

As reported at Nuclear Regulatory Commission (NRC) Information Notice 2002-09, the North Anna power plant and some power plants including a Korean plant experienced top nozzle separation of a certain type of Westinghouse type fuel. The top nozzle separation had occurred at the bulge joints connecting the stainless steel grid sleeves to the Zircaloy-4 guide tubes. The root cause was known as Intergranular stress-corrosion cracking accelerated by the presence of chlorides, fluorides, and sulfates [1].

In this study, we have developed SAFER (Safe Adapting FastenER), which is a reinforcement device connecting the top nozzle and guide tube of the Westinghouse type fuel assembly, in order to prevent top nozzle separation during fuel handling.

2. Development of SAFER

2.1 General Description

The SAFER has been developed through the procedure shown in Fig.1. That is, the related patents have been investigated to avoid patent infringement, the finite element analysis model and the prototype model have been developed and modified, and finally, the performance of the optimized reinforcement device has been evaluated through the verification tests.

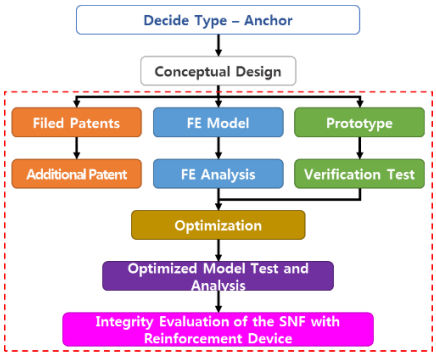

Fig. 1. Procedure of SAFER Development.

The SAFER is an anchor type reinforcement device as shown in Fig. 2. The SAFER consists of three parts, which are clamping outer sleeve, fastening inner rod and adjustable nut. The fastening mechanism of the SAFER uses contour of bulge deformation in the inner surface of the guide tube. The clamping method of SAFER is to adjust the length of the clamping outer sleeve with the adjustable nut to match the outer sleeve tip into the bulge groove in the guide tube of fuel assembly, and then tighten the fastening inner rod to be fastened the clamping outer sleeve tip against the guide tube bulge groove.

2.2 Finite Element Analysis

A finite element model has been developed considering the connection part of the representative fuel using the ABAQUS which is the multi-purpose commercial finite element analysis software. Fig. 3 shows a representative FE analysis result of the 17x17 fuel assembly with bulge connections.

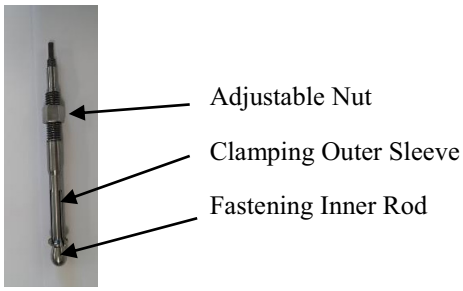

Fig. 2. Prototype of SAFER.

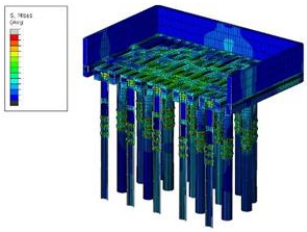

Fig. 3. Stress distribution of the bulge connection.

2.3 Verification Test

To evaluate the fastening force of the device, the fastening strength tests have been performed as shown in Fig.4. In this test, 4 SAFERs were installed at the outer corners of the 17x17 fuel assembly top nozzle and guide tubes. The other guide tubes were free from connection with the top nozzle. Fig. 5 shows typical normalized test results of the verification tests. In this test, one SAFER has been shown to withstand a load close to the weight of a fuel assembly, and even with only four SAFERs installed in a fuel assembly with top nozzle separation concern, it is expected to get additional fastening force more than 3 times the weight of fuel assembly.

3. Conclusion

The SAFER developed in this study is expected to provide a very strong fastening force in the fuel assembly with top nozzle separation concern, and it is considered that SAFER will guarantee the integrity when handling the fuel assembly for dry storage in the future.

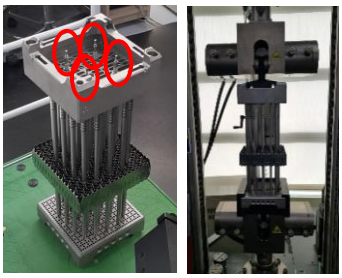

Fig. 4. Test specimen and setup with 4 SAFERs.

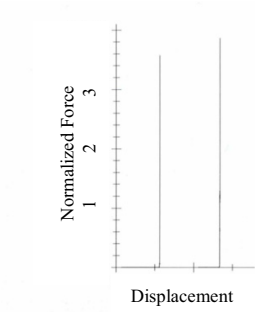

Fig. 5. Normalized Test Results with 4 SAFERs.

ACKNOWLEDGEMENT

This work was supported by the Korea Institute of Energy Technology Evaluation and Planning (KETEP) and the Ministry of Trade, Industry & Energy (MOTIE) of the Republic of Korea (No. 2014171020166C).

REFERENCES

[1] NRC Information Notice 2002-09, “Potential for Top Nozzle Separation and Dropping of a Certain Type of Westinghouse Fuel Assembly”, NRC, (2002).

Fatigue Life Characterization of Simulated Fuel Cladding to Hydride Contents for Normal Transportation Integrity

Kang-Hee Lee*, Heung-Seok Kang, Jae-Yong Kim, Yong-Sik Yang, and Donghak Kook
Korea Atomic Energy Research Institute, 111, Daedeok-daero 989beon-gil, Yuseong-gu, Daejeon, Republic of Korea
*leekh@kaeri.re.kr

1. Introduction

After the interim or long-term dry storage, the spent nuclear fuel should be transported into the central storage site for further extended storage or final disposal, through a certain type and designated route of normal transportation. Degraded spent fuel was known to be brittle from seasoned hydride in in-reactor burnup and storage environment [1, 2], whose integrity was significantly vulnerable against impacts and repeated loads such as transportation or external impact accidents. Fig. 1 showed influential parameters to affect spent fuel fatigue failure. Herein, spent fuel fatigue life characterization was carried out using a rotary bending test machine and non-irradiated cladding tube section with controlled hydride contents. Overall test setup and some insights from test results will be discussed.

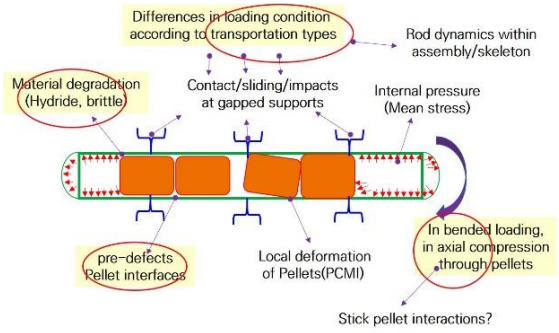

Fig. 1. Influential factors to spent fuel fatigue failure.

2. Experiment

Non-irradiated Zircaloy-4 cladding tube section with 120 mm length was charged 200 ppm and 400 ppm hydrogen and heated to promote a gas penetration into a metal surface for 24 hours in the 410℃ furnace. Table 1 summarized test matrix, test parameters and those test ranges for whole test program of simulated fuel cladding tube fatigue life characterization [3].

Table 1. Test matrix for simulated fuel cladding fatigue test

Moment loading	Excitation Frequency	Hydrogen Contents	Pellet gap effect
2.5~10* Nm by 2.5 Nm Step	25 Hz (1500 rpm), 50 Hz (3000 rpm)	Fresh, 200 ppm, 400 ppm, 600 ppm	No pellet, 30 μm (OD8.917), 50 μm (OD8.877)

The rotary bending fatigue test machine (YAMAMOTO, model GIGA QUAD YRB200, Fig. 2) and straight tube section without grooved cut-out were used for the whole test program. The pure moment loading was applied to rotating tube specimen with certain amount of end mass. Excitation frequencies used were 25 Hz and 50 Hz which is selected for stable operation of the test machine. Rotation rpm and weight of end mass were calibrated for reliability of the test quality program.

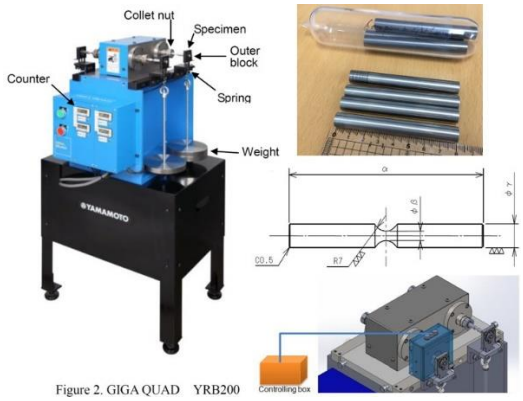

Fig. 2. Rotary bending test machine and non-standard tube specimen to be tested.

3. Test Results

Fig. 3 showed the result comparison of measured fatigue life (cycle to failure) of simulated fuel cladding tube according to the hydride contents up to 400 ppm, for two different frequencies of moment excitation. The slight lines over the dots in the Fig. 3 helped rough grouping and the identification of the

trend; fatigue life became smaller as the hydride contents increase, in particular, for high cycle region above 5.0E5 cycles. There were also somewhat slightly different failure behaviors to the excitation frequency corresponding to the speed of rotation. Results also showed large scatter even in the same moment and excitation frequency, especially in fresh cladding. Fig. 4 showed typical photos of the broken section of failed specimen, which now doesn't show meaningful interpretation, thus the SEM (Scanning Electron Microscopy) will be needed for further investigation. If the more test data would be added up to this diagram, we could map the fatigue life of spent nuclear fuel in a quantitative way for normal transportation integrity.

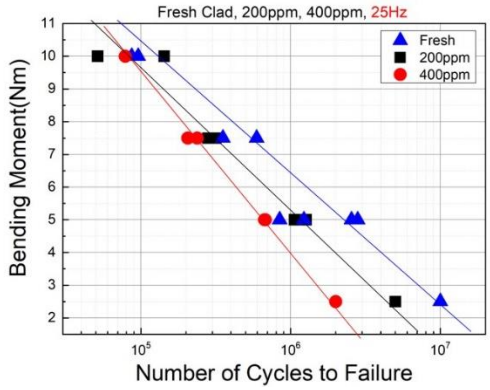

(a) 25 Hz (1500 rpm)

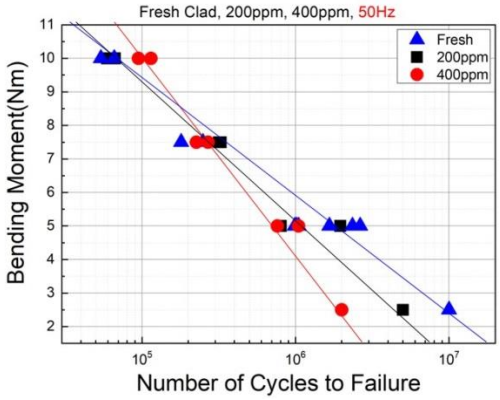

(b) 50 Hz (3000 rpm)

Fig. 3. Typical fatigue test results of simulated fuel cladding according to the hydride contents.

4. Conclusion

Spent fuel fatigue life characterization was carried out using a rotary bending test machine and non-irradiated cladding tube section with controlled hydride contents. Overall test setup and some insights from test results were discussed. The results showed that the hydride contents affected to reduce fatigue life of simulated fuel cladding in somewhat different way to the different frequency of excitation. Further investigation on the broken section of failed specimen and the additional test operation for higher hydride contents were needed to get a solid finding and verify the test results in the near future.

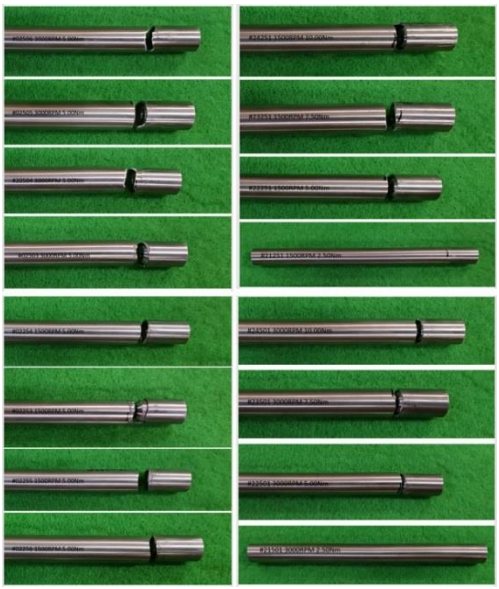

Fig. 4. Typical broken sections of the failed specimen.

ACKNOWLEDGEMENT

This work was supported by the Korea Institute of Energy Technology Evaluation and Planning (KETEP) granted financial resource from the Ministry of Trade, Industry and Energy, Republic of Korea (No. 2014171020166A).

REFERENCES

[1] U.S. NRC, 2014, "Mechanical fatigue Testing of high-burnup fuel for transportation applications", NUREG/CR-7198. ORNL/TM-2014/214.

[2] Dong-Hak Kook et al, 2012, Review of spent fuel integrity evaluation for dry storage, Nuclear Engineering and Technology, Vol. 45, No. 1, 2013.

[3] Kang-Hee Lee, et al, 2018, Spent Fuel Structural Integrity Evaluation Test Plan to Repeated Bending and Impact Loading: Test Matrix, KAERI/TR-7222/2018.

Reduction of Metal Oxides Compounds by Lithium Metal as a Reductant in Molten LiCl Salt

Eun-Young Choi*, Min Ku Jeon, and Sung-Wook Kim
Korea Atomic Energy Research Institute, 111, Daedeok-daero 989beon-gil, Yuseong-gu, Daejeon, Republic of Korea
*eychoi@kaeri.re.kr

1. Introduction

The lithium (Li) reduction process is a technique for chemically reducing actinide oxides to their metals using Li metal as a reductant in molten LiCl. The reaction of the actinide oxides with the Li metal as follows:

$$M_xO_y + 2yLi \rightarrow xM + yLi_2O \quad (1)$$

This technique has been developed to apply pyroprocessing for oxide fuels; the metallic products obtained through the Li reduction process are transferred to an integrated process, electrorefining and uranium and transuranic elements are recovered from the product [1-4].

The reduction of the actinide oxides through the Li reduction process was experimentally proven in the early 2000s. Nonetheless, electrolytic reduction process using Li_2O-LiCl salt as an electrolyte [5] has been actively researched to replace the Li reduction process due to some technical problems; the tricky handling of the Li metal, the continuous accumulation of Li_2O in LiCl salt by the reaction 1, the requirement of micro-size fuel, and the breakage of porous magnesia basket used as a material to contain the micro-size fuel etc. In this presentation, we introduce that the Li reduction process can be still usefully used to reduce the metal oxides to their metals under certain conditions where the electrolytic reduction is difficult.

2. Reduction of Zirconium Oxide Compounds

Pyroprocessing can be adopted for treatment of damaged fuel debris (mainly composed of (U,Zr) O_2) generated by nuclear accidents such as Fukushima. Originally, the Zr in the Zr alloy-based cladding was present in the metal state but oxidized during the accident process and existed in the form of ZrO_2 in the damaged fuel. The reduction of the damaged oxide to metallic form can enable the recovery of uranium, cladding, and fission products through electrorefining, which can allow its long-term storage or final disposal [1,6]. However, the complete reduction of ZrO_2 to Zr metal using the electrolytic reduction is difficult due to the reaction of Li_2O with ZrO_2.

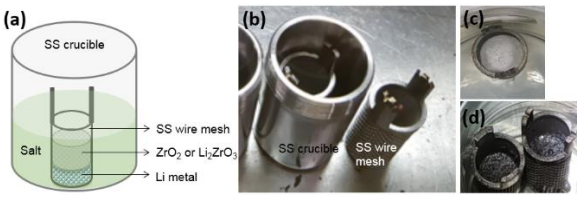

Fig. 1. Schematics and photos of the tests conducted in this study: (a) schematics of the reduction tests, (b) SS crucible and SS wire mesh basket, (c) Zr compound loaded in the basket, and (d) product in the basket after the reduction tests were completed.

It was experimentally demonstrated that ZrO_2 was reduced to Zr metal by Li metal in LiCl salt at 650°C without formation of Li_2ZrO_3 according to the following reaction:

$$ZrO_2 + 4Li \rightarrow Zr + 2Li_2O \quad (2)$$

Also, the reduction of Li_2ZrO_3 to Zr metal by reaction of Li was observed as follows:

$$Li_2ZrO_3 + 4Li \rightarrow Zr + 3Li_2O \quad (3)$$

The detailed experimental conditions and procedures were described elsewhere [7].

3. Reduction of Rare Earth Oxides

Unlike the actinide and noble metal oxides, rare earth oxides are reduced only partially and remain in their oxide form in the cathode after the electrolytic reduction. The standard Gibbs free energies of formation of rare earth oxides are more negative than that of Li_2O. We demonstrated that the low level of the rare earth oxides in the reduction product can be significantly increased by the extra Li reduction. Also, the long-term behavior of the Li metal in salt was monitored. The detailed experimental conditions and results were reported elsewhere [8].

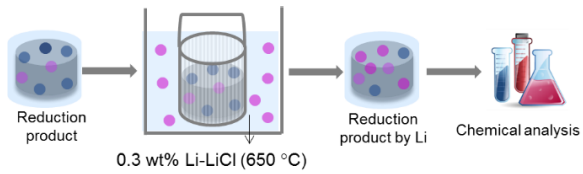

Fig. 2. Schematics: the Li reduction to increase the metal extents of rare earth oxides.

Fig. 3. The changes in Li-LiCl salt as a function of time.

REFERENCES

[1] E.J. Karell, R.D. Pierce, T.P. Mulcahey, DOE Spent Nuclear Fuel and Fissile Material Management presented at ANS, 1996.6.16-20, Reno, NV, 352.

[2] T. Usami, M. Kurata, T. Inoue, H.E. Sims, S.A. Beetham, J.A. Jenkins, J. Nucl. Mater. 300 , 15–26 (2002).

[3] T. Usami, T. Kato, M. Kurata, T. Inoue, H.E. Sims, S.A. Beetham, J.A. Jenkins, J. Nucl. Mater. 304, 50–55 (2002).

[4] T. Kato, T. Usami, M. Kurata, T. Inoue, H. E. Sims, Jan A. Jenkins, in: Proc. of EUCHEM Conference on Molten Salts and Ionic Liquids, Hammamet, Tunisia, 2006.

[5] E.-Y. Choi, S.M. Jeong, Prog. Electrochemical processing of spent nuclear fuels: an overview of oxide reduction in pyroprocessing technologyNat. Sci.: Met. Mater. Int. 25, 572–582 (2015).

[6] Y. Sakamura, M. Iizuka, S. Kitawaki, A. Nakayoshi, H. Kofuji, Formation and reduction behaviors of zirconium oxide compounds in LiCl-Li_2O melt at 923 K, J. Nucl. Mater. 466, 269–279 (2015).

[7] E.-Y. Choi, D. H. Heo, Reduction of zirconium oxide compounds by lithium metal as a reductant in molten LiCl salt, J. Nucl. Mater. 512, 193–198 (2018).

[8] E.-Y. Choi, J. Lee, Highly enhanced reduction of rare earth oxides in simulated oxide fuel in Li_2O-LiCl salt using lithium metal, J. Nucl. Mater. 511, 367–374 (2018).

Micro-cantilever Tests on Hydride Blister and Zirconium Matrix of Zircaloy-4 Cladding Tube

Ho-a Kim[a, b, *], Jae-soo Noh[b], Ju-seong Kim[c], and Yong-soo Kim[a]
[a] Hanyang University, 222, Wangsimni-ro, Seongdong-gu, Seoul, Republic of Korea
[b] Atomic Creative Technology Co. Ltd., 1434, Yuseong-daero, Yuseong-gu, Daejeon, Republic of Korea
[c] Korea Atomic Energy Research Institute, 111, Daedeok-daero 989beon-gil, Yuseong-gu, Daejeon, Republic of Korea
[*]pissan@hanyang.ac.kr

1. Introduction

During nuclear reactor operation, claddings shall be suffered corrosion. Owing to the temperature gradient between cladding inner wall and outer wall, it can cause hydride blister in outer surface of the cladding. It is reported that hydride blister is critical to integrity of fuel cladding due to its fragility. The integrity of spent nuclear fuel (SNF) should be maintained against potential shocks and vibrations during handling, storage and transportation. Most of experiments evaluating cladding integrity do not specifically consider the effect of hydride blister because it is difficult to measure the mechanical property of itself, but it is important to know how hydride blister can erode the ductility of claddings. In this study, micro-cantilever tests were introduced to evaluate the fracture toughness of local hydride blister and zirconium matrix of the cladding.

2. Experimental

2.1 Specimen Preparation

Recrystallized annealed (RXA) Zircaloy-4 cladding tube was used in this study. Two specimens were used: one is as-received (AR) and the other is hydride blister (HB) specimen. HB specimen was charged with hydrogen using a Sievert type apparatus, and hydride blister can occur through the excessive hydrogen charging process. Scanning electron microscope (SEM) image of the HB specimen is shown in Fig. 1.

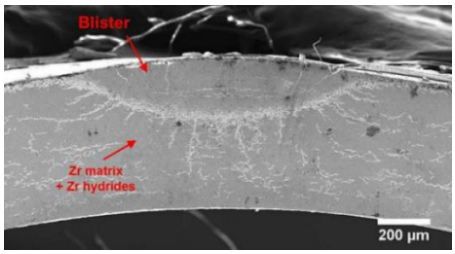

Fig. 1. Scanning electron microscope image of the specimen.

2.2 Micro-cantilever Test

Micro-cantilever tests were conducted using PI 85 pico-indenter (HYSITRON) with four-sided conductive diamond flat tip (1 μm × 1 μm) at a speed of 5 nm/sec. Micro-cantilevers and pre-cracks were ion-milled with Ga^+ ion beam of FEI Helios 600 at 30 kV acceleration voltage from hydride blister region and zirconium matrix region in Fig. 1. Dimension of the micro-cantilever and test images are shown in Fig. 2 and Fig. 3.

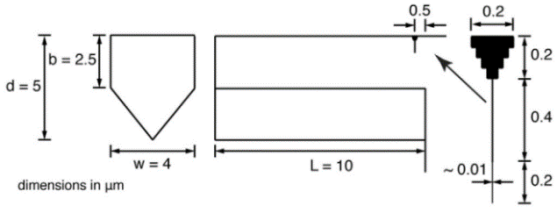

Fig. 2. Dimension of the micro-cantilever [1].

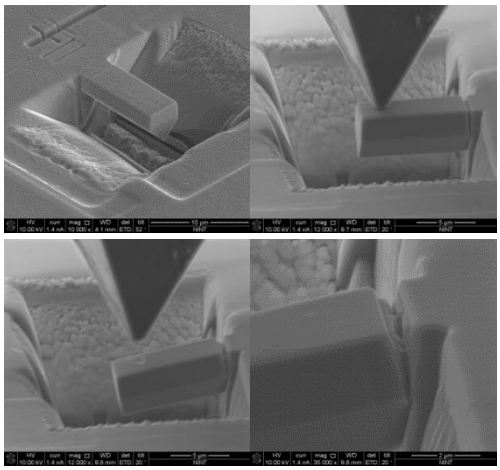

Fig. 3. Images of micro-cantilever test procedure.

3. Results and Discussions

3.1 Micro-cantilever Tests Results

Fig. 4 shows a load-displacement curve of the micro-cantilever tests. A black line indicates as-received specimen, and red and blue lines indicate the hydride blister specimens. Fracture of the as-received specimen occurred in plastic deformation region, but that of the hydride blister specimen occurred in elastic deformation region.

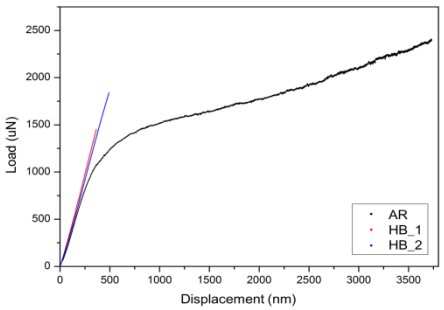

Fig. 4. A load-displacement curve of the test results.

3.2 Fracture Toughness Calculation

$$K_C = \sigma_0 \sqrt{\pi a}\, \mathrm{F}\left(\frac{a}{2\bar{y}}\right) \quad (1)$$

$$\sigma_0 = \frac{P_0 L_0 \bar{y}}{I} \quad (2)$$

Where σ_0 is the fracture stress, a is the crack length, and $\bar{y}$ is the vertical distance between the upper surface and the centroid of the cross-section. $\mathrm{F}(\mathrm{a}/2\bar{y})$ is the dimensionless shape factor determined by finite element analysis [1-3]. P_0 is the fracture load, L_0 is the longitudinal distance between the pre-crack and the indenter tip loading point, and I is the second moment of area. Table 1 shows the calculated fracture toughness of the specimens. The results show that fracture toughness of the hydride blister specimen could drop up to 60% of fracture toughness of the as-received specimen.

Table 1. Fracture toughness of the specimens

Specimen	AR	HB_1	HB_2
Fracture toughness (MPa$\sqrt{m}$)	2.91	2.11	1.76

4. Conclusions

To evaluate the fracture toughness of local hydride blister and zirconium matrix of cladding on a microscale, micro-cantilever tests were introduced and well performed. The hydride blister specimen could be fractured in elastic deformation region, and fracture toughness of the hydride blister specimen could drop up to 60% of fracture toughness of the as-received specimen. Thus, the effects of hydride blister on the mechanical integrity of claddings should be taken into account when evaluating failure criteria of claddings during handling, storage and transportation of SNF.

ACKNOWLEDGEMENT

This research was supported by the Radioactive Waste Management Technology Program of the Korea Institute of Energy Technology Evaluation and Planning (KETEP), funded by the Ministry of Trade, Industry & Energy (MOTIE), Republic of Korea (No. 20181710201770)

REFERENCES

[1] H. Chan, S.G. Roberts, J. Gong, J. Nucl. Mat., 475, 105-112 (2016).

[2] K. Matoy, H. Schonherr, T. Detzel, T. Scho berl, R. Pippan, C. Motz, G. Dehm, Thin Solid Films, 518(1), 247-256 (2009).

[3] D. Di Maio, S.G. Roberts, J. Mater. Res., 20(2), 299-302 (2005).

2분과

사용후핵연료 처분전관리 (Poster)

Effect of the Crucible Cover on the Distillation of Cadmium

S.W.Kwon*, J.H.Jung, and S.J.Lee

Korea Atomic Energy Research Institute, 111, Daedeok-daero 989beon-gil, Yuseong-gu, Daejeon, Republic of Korea

*swkwon@kaeri.re.kr

Abstract

The distillation of liquid cathode is necessary to separate cadmium from the actinide elements in the pyroprocessing since the actinide deposits are dissolved or precipitated in a liquid cathode. It is very important to avoid a splattering of cadmium during evaporation due to the high vapor pressure. Several methods have been proposed to lower the splattering of cadmium during distillation. One of the important methods is an installation of crucible cover on the distillation crucible. A multi-layer porous round cover was proposed to avoid a cadmium splattering in our previous study. In this study, the effect of crucible cover on the cadmium distillation was examined to develop a splatter shield. Various surrogates were used for the actinides in the cadmium. The surrogates such as bismuth, zirconia, and tungsten don't evaporate at the operational temperature of the Cd distiller due to their low vapor pressures. The distillation experiments were carried out in a crucible equipped with cover and in a crucible without cover. About 40 grams of Cd was distilled at a reduced pressure for two hours at various temperatures. The mixture of the cadmium and the surrogate was heated at 470 ~ 620°C. Most of the bismuth remained in the crucible equipped with cover after distillation under 580°C for two hours, whereas small amount of bismuth decreased in the crucible without cover above 580°C. The liquid bismuth escaped with liquid cadmium drop from the crucible without cover. It seems that the crucible cover played a role to prevent the splash of the liquid cadmium drop. The effect of the cover was not clear for the tungsten or zirconia surrogate since the surrogates remained as a solid powder at the experimental temperature. From the results of this work, it can be concluded that the crucible cover can be used to minimize the deposit loss by prevention of escape of liquid drop from the crucible during distillation of liquid cathode.

ACKNOWLEDGEMENT

This work was supported by a National Research Foundation of Korea (NRF) grant funded by the Korean Government (MSIP) (No. 2017M2A8A5015079).

Review of Design Requirements for SNF Dry Storage System

Sunghwan Chung*, Taehyeon Kim, and Yunchang Jeong

KHNP Central Research Institute, 70, Yuseong-daero 1312beon-gil, Yuseong-gu, Daejeon, Republic of Korea

*sunghchung@khnp.co.kr

1. Introduction

Spent nuclear fuel (SNF) dry storage systems (SDSS) including casks and modules (Fig.1) to store SNF under inert gas atmosphere must be designed in compliance with the applicable requirements of related regulations such as Korea Nuclear Safety Act and US 10 CFR Part 72 (10CFR72). But the direct and quantitative requirements for SDSS are not explicitly specified in the related regulations, and so the design requirements for SDSS based on the US regulatory requirements were reviewed.

Fig. 1. SNF dry storage systems.

2. Regulatory Requirements

According to 10CFR72, SDSS must be so designed to maintain the safe storage conditions of SNF, prevent damage to SNF, assure SNF recovery and withstand the effects of design-basis conditions such as normal, off-normal and accident conditions and natural phenomena. Normal conditions are considered as intended operations, planned events and environmental conditions to be expected to routinely occur including ambient temperatures, fuel loading and unloading, 1% failure of fuel rods, handling of SDSS, etc. Off-normal conditions are considered as conditions to be expected to occur with moderate frequency including temperatures beyond normal conditions, 10% failure of fuel rods, failure of confinement boundaries, partial air flow blockage, human error, out-of-tolerance equipment performance, equipment failure, or faulty calibration, etc. Accident conditions are considered as conditions to exceed off-normal conditions including drop, tip-over, fire, 100% fuel rod rupture, leakage of confinement boundary, explosive overpressure, 100% air flow blockage, accidents resulting from operational error, etc. Natural phenomena are considered as events to be expected to occur during normal operations including flood, typhoon, tornado, earthquake, burial, lightning, tsunami, etc.

Design-basis fuel to be stored in SDSS must be specified such as fuel type, max. enrichment, max. burnup, min. cooling time of 1 year or more, max. decay heat, max. SNF mass loading limit, SNF conditions, inert atmosphere requirements, etc.

SDSS must ensure that SNF remains subcritical under all credible conditions. SDSS must provide adequate heat removal capacity with passive cooling systems, suitable shielding features for radiation protection under normal and accident conditions, and confinement systems of radioactive material. 10CFR 72 establishes the potential dose equivalent or committed dose equivalent to any individual on or beyond the controlled area boundary of storage facilities (Fig.2) from accidents or direct radiation from normal. SDSS must have sufficient structural capacity so that the structure can withstand the worst-case loads under normal, off-normal, accident conditions and for natural phenomena events. Design earthquake must be equivalent to the safe shutdown earthquake (SSE) for NPPs. SNF cladding must be

protected that leads to gross rupture or confined such that degradation of fuel will not pose operational safety problems.

Fig. 2. SNF dry storage facility.

3. Design Requirements

Design-basis fuel with max. initial enrichment, max. average fuel assembly burnup and min. cooling time, max. heat load and without any leakage will be specified. And type, weight and dimension of the fuel and max. fuel loading limit in SDSS will also be specified.

SDSS will be so designed that it maintains sub-criticality, confinement, radiation shielding, decay heat removal, structural integrity and physical protection of SNF under design-basis conditions in accordance with the related regulations, thus preventing release of radioactive material and providing protection against radiation exposure. In case of a canister-based SDSS, a fuel-loaded canister will meet the requirements of storage and transport regulations to be transferable within NPP sites.

Design earthquake will be equivalent to safe shutdown earthquake (SSE) for NPP of a horizontal ground motion of min. 0.3 g with appropriate response spectrum. For SSE events, the structural safety of SDSS on the storage pad, on suspending from the crane, during operation in the storage pool, etc. will be verified.

SDSS will provide adequate heat removal capacity with natural convection cooling system, and will be so designed that max. cladding temperature does not exceed 400^{o}C and max. cladding hoop stress is less than 90 MPa for fuel loading operation and normal conditions.

SDSS will be so designed that it reasonably maintains confinement of radioactive material under the design-basis conditions.

SNF loaded in SDSS will be packaged, transported and stored in such a manner that sub-criticality is maintained under the design-basis conditions. Effective multiplication factor (k_{eff}) including all biases and uncertainties with a 95% probability at a 95% confidence level will not exceed 0.95.

Radiation dose rates on SDSS surfaces to comply with the radiation requirements of 10CFR72 depend on the radiation dose rate limits of storage facility including SDSS arrangement on the pad. Since dry storage facility are designated as a radiation control area, the storage facility will meet the radiation dose rate limit for the radiation control area in accordance with Korea regulations on technical standards for radiation safety control. Radiation dose rate limit outside SNF dry storage facility will not exceed 0.4 mSv/week, which is based on annual worker exposure dose limit of 20 mSv. Radiation dose rate limit on SDSS surfaces will not exceed 1 mSv/week, which is based on annual individual exposure dose limit of 50 mSv. And operational limit conditions for SDSS will be established to meet ALARA principles and radiation limits for radioactive materials in effluents and direct radiation levels associated with the storage facility operation.

4. Conclusion

SDSS will be designed to accommodate the effects of site characteristics and environmental conditions associated with normal operations, and withstand accidents and natural phenomena events. It will be designed to ensure adequate safety and withstand the effects of design-basis conditions without impairing its capability to perform safety functions. SDSS will store safely SNF for the design life and be compatible with wet or dry SNF loading and unloading facilities. And SDSS will allow ready retrieval of SNF for further processing such as transport after long-term storage to centralized interim storage facility and final depository.

REFERENCES

[1] Korea Act No.14839, Nuclear Safety Act

[2] US 10 CFR Part 72, Licensing Requirements for the Independent Storage of Spent Nuclear Fuel

[3] Korea NSSC Regulation No.19, Regulations on Technical standards for Radiation Safety Control

An Applicable Study on the Fast Neutron Detection for Nuclear Material Accountancy

Seonkwang Yoon[a,b], Hee Seo[c], Chaehun Lee[a], Byung Hee Won[a], Seong-Kyu Ahn[a], and Ho-Dong Kim[a,*]
[a]Korea Atomic Energy Research Institute, 111, Daedeok-daero 989beon-gil, Yuseong-gu, Daejeon, Republic of Korea
[b] University of Science & Technology, 217 Gajeong-Ro, Yuseong-gu, Daejeon, Republic of Korea
[c] Chonbuk National University, 567 Baekje-daero, Deokjin-Gu, Jeonju, Jeollabuk-Do, Republic of Korea
[*]khd@kaeri.re.kr

1. Introduction

Nuclear Material Accountancy (NMA) is essentially important in nuclear safeguards. Last 50 years, thermal neutron measurement system has been used as representative method. However, He-3 that is needed for detection of thermal neutrons became an uneconomical as demand increased. As a result, fast neutron detection has been focused as a substitutive technique. In this research, we compared relative assay uncertainty between thermal and fast system according to ^{240}Pu mass and measurement time. Also fission informative characteristics of prompt neutrons were investigated by using Monte Carlo simulation with an advanced fission generators.

2. Comparison of Relative Assay Uncertainty

2.1 ASNC vs. Fast Neutron Detector

ACP Safeguards Neutron Counter (ASNC) is a He-3 gas proportional counters for thermal neutron detection developed by KAERI in 2016 [1]. In case of ASNC, neutron moderation mechanism is necessary prior to detection, so that high neutron detection efficiency can be achieved. However useful information of fission; such as emission angle of correlated neutrons, initial energy, contained in prompt neutrons is not available because of thermalisation.

On the other hand, fast neutron detection is based on organic scintillators that enable detection of heavy charged particles produced with neutron elastic scattering. Fast system has two major advantages, for example, fission information acquisition from prompt neutrons and low random uncertainty in coincidence counting. However, there is no commercialized model to which fast system is completely applied. The reason is that lower detection efficiency and high gamma sensitivity are intrinsic challenges in fast neutron measurement.

2.2 Relative Assay Uncertainty

It is substantial to verify and decrease measurement uncertainty in NMA, because it is a key parameter through which reliability can be evaluated. The relative assay uncertainty is described below [1].

$$\sigma_S = \sqrt{\frac{S}{t}}\ ,\ \sigma_D = \sqrt{\frac{D+2S^2G}{t}} \quad (1)$$

$$\sigma_{S(rel)} = \frac{\sigma_S}{S}\ ,\ \sigma_{D(rel)} = \frac{\sigma_D}{D} \quad (2)$$

2.3 Simulated Results

Relative assay uncertainty according to ^{240}Pu mass and measurement time is estimated for ASNC and a fast neutron detector which KAERI has been currently developing. Time bin for coincidence is assumed as 64 μs and 50 ns for both system respectively. The result is shown in Fig. 1.

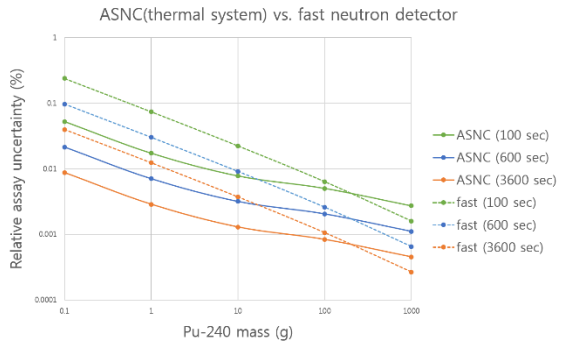

Fig. 1. Relative assay uncertainty of ASNC and the fast neutron detector.

It is confirmed that the fast system showed lower relative assay uncertainty compared to ASNC for ^{240}Pu mass over several hundred grams. This is because, in case of sufficiently high neutron rate of source, statistical uncertainty relevant to detection efficiency is increasingly negligible but random uncertainty corresponding to the time bin of coincidence becomes significant.

3. Angular Characteristics of Fission Neutrons.

The angular characteristics of fission neutrons are fundamentally dependent on angular momentum of fission fragments and species of radioactive isotopes [2]. We simulated angular distribution of prompt neutrons from six special nuclear materials (SNMs), e.g., ^{238}U, ^{238}Pu, ^{240}Pu, ^{242}Pu, ^{244}Cm, ^{252}Cf, and dependence on neutron energy thresholds as well.

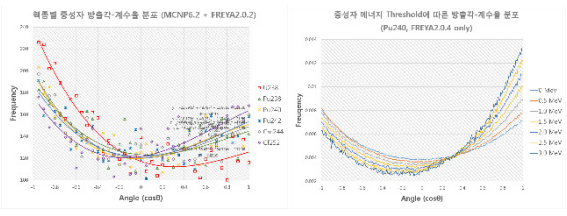

Fig. 2. Prompt neutron angular distributions according to the 6 SNMs and neutron energy thresholds.

It is confirmed that neutrons of same fission generation tend to be emitted into identical or opposite direction. Also the tendency is dependent on radioactive isotopes, and neutron energy thresholds.

Fission Reaction Event Yield Algorithm (FREYA 2.0.4) is compiled independently, and FREYA-integrated MCNP6.2 is used with PTRAC option.

4. Conclusion

Nuclear material accounting and verification of its reliability have critical importance in nuclear safeguards. In this research, relative assay uncertainty of both thermal and fast neutron detectors are calculated and compared. The fast system showed overall comparable performance to the conventional system, even better precision for larger sample mass. Also the angular characteristics of fission neutrons are confirmed by using Monte Carlo simulation with FREYA fission generator. Experimental comparison and mathematical approaches will be investigated to design a prototype and to verify practical applicability of the angular characteristics on NMA model in the future research. Consequently this will be contributive to IAEA safeguards impregnability.

REFERENCES

[1] Hee Seo et al., “Development of ACP Safeguards Neutron Counter (ASNC)”, KAERI/TR-6594/2016 (2016).

[2] J.M. Mueller, J. Mattingly, “Using anisotropies in prompt fission neutron coincidences to assess the neutron multiplication of highly multiplying subcritical plutonium assemblies”, Nuclear Instruments and Methods in Physics Research A, 825, 87-92 (2016).

Measurement of Threshold Stress Intensity Factor of Delayed Hydride Cracking for Unirradiated Zircaloy-4 Cladding

Jong-Dae Hong*, Euijung Kim, and Donghak Kook
Korea Atomic Energy Research Institute, 111, Daedeok-daero 989beon-gil, Yuseong-gu, Daejeon, Republic of Korea
*jongd@kaeri.re.kr

1. Introduction

During dry storage, the spent fuel claddings could degrade through delayed hydride cracking (DHC), which is a time dependent crack growth process resulting from stress assisted hydrogen diffusion to the crack tip. In particular, DHC could be activated within a relatively low temperature range, creep-free range. Because the estimated crack growth rate by DHC is quite high, the methodology using threshold stress intensity factor criteria is appropriate [1,2]. Nevertheless, most of the DHC study were focused on crack growth rate measurement due to pressure tube of pressurized heavy water reactor (PHWR). In this regards, the temperature dependency on DHC of Zircaloy-4 cladding were investigated by measuring threshold stress intensity factor (K_{IH}) according to International Atomic Energy Agency Cooperative Research Project (IAEA CRP) method [3].

2. Experimental

2.1 Test Material

The test material used in this study was unirradiated CWSR Zircaloy-4 cladding, which has been widely used in PWR fuel cladding. The initial cladding thickness (t) and outer diameter (OD) are 0.57 mm and 9.5 mm (Westinghouse 17X17 type). In addition, 200 ppm of hydrogen is charged using the gaseous method under mixed argon/hydrogen condition at 400°C, then heat-treated at 410°C for 24 h for a uniform hydride distribution (Fig. 1).

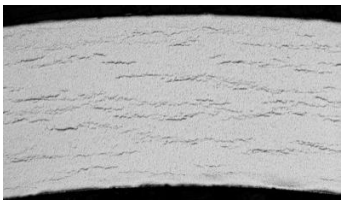

Fig. 1. Hydrided Zircaloy-4 cladding for DHC test.

2.2 Test Method

DHC test to measure K_{IH} was performed using a pin-loaded-tension (PLT) technique and an unloading method (Fig. 2) at 150°C to 300°C, as shown in Table 1. Test specimens were prepared as PLT-13 type with fatigue pre-cracking at RT. A linear variable differential transformer (LVDT) on the crack mouth was used for crack growth monitoring (Fig. 3). Upon detection of a certain amount of crack growth, the load was reduced by 0.5 kgf and the process repeated until no further cracking was detected for 24 h. After the DHC test, scanning electron microscope (SEM) analysis was performed to measure crack length. In addition, the applied stress intensity factor (K_I) and threshold stress intensity factor (K_{IH}) were calculated according to the previous research [3].

Table 1. Materials and temperature for DHC test.

Material	Temp. (°C)
Unirradiated Zry-4 cladding (CWSR) ~200 ppm H	300
	275
	250
	225
	200
	175
	150

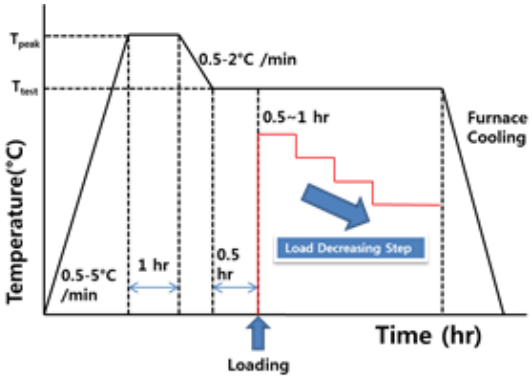

Fig. 2. Test procedures using unloading method [4].

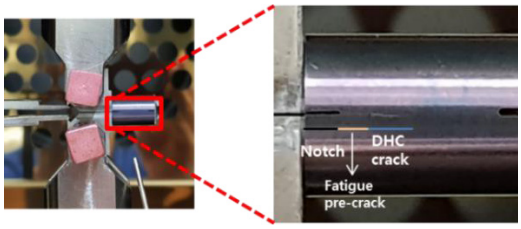

Fig. 3. DHC test setup using LVDT.

3. Results and Discussion

After tests, the area identification and crack length measurements using 9-point method were performed by scanning electron microscope (SEM) analysis, as described in Fig, 4. A clear chevron pattern without striation in the DHC region was observed along the crack growth direction.

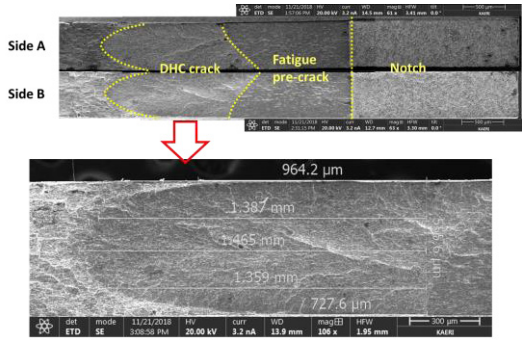

Fig. 4. Area identification and measurement of crack growth by SEM analysis.

The resulting values of K_{IH} from tests using unirradiated specimen are described in Fig. 5. Considering the data of the IAEA CRP and of this study, K_{IH} increases with a significant increase around 300°C as the temperature increases [4]. This tendency shows good agreement to a prediction based on Shi and Puls model [5].

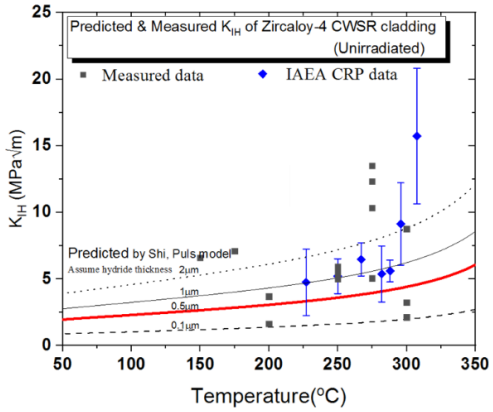

Fig. 5. Temperature dependency of threshold stress intensity factor for unirradiated Zircaloy-4 cladding.

They are highly scattered, similar to IAEA CRP, although all of data meets crack uniformity criteria. The high values of K_{IH} could be contributed to over-night unloading procedure. During over-night, the applied load was reduced to 30 N due to an impracticability of in-situ monitoring. For this reason, a crack could be blunted, then much load is needed to restart crack propagation. Therefore, some of data could be excluded according to an additional acceptance criterion.

4. Conclusion

K_{IH} for unirradiated Zircaloy-4 cladding were measured using a PLT technique and an unloading method. K_{IH} increases with a significant increase around 300°C as the temperature increases, although they are highly scattered.

ACKNOWLEGMENTS

This work was supported by the Radioactive Waste Management Technology Program of the Korea Institute of Energy Technology Evaluation and Planning (KETEP), granted financial resource from the Ministry of Trade, Industry & Energy, Republic of Korea. (No. 2014171020166A)

REFERENCES

[1] J.D. Hong, E. Kim, Y.S. Yang, D. Kook, “Methodology of Delayed Hydride Cracking Assessment of Spent Fuel Cladding”, KRS Spring Meeting, Busan, May 24-26, 2017.

[2] J.D. Hong et al, “Delayed Hydride Cracking Assessment of PWR Spent Fuel during Dry Storage”, Nucl. Eng. Des. 322 (2017), 324-330.

[3] “Evaluation of Conditions for Hydrogen Induced Degradation of Zirconium Alloys During Fuel Operation and Storage”, IAEA-TECDOC-1781, Vienna (2015).

[4] J.D. Hong et al, Zircaloy-4 Cladding Degradation Tests under Simulated Dry Storage Conditions-Creep and Delayed Hydride Cracking, IHLRWM 2019, Paper ID. 27369.

[5] S.Q. Shi, M.P. Puls, “Criteria for fracture initiation at hydrides in zirconium alloys-I. Sharp crack tip”, J. Nucl. Mater. 208 (1994) 232-242.

Characteristics of Vacuum Drying for Canister

Seung-hwan Yu*, Ju-chan Lee, Kyung-sik Bang, and Woo-seok Choi
Korea Atomic Energy Research Institute, 111, Daedeok-daero 989beon-gil, Yuseong-gu, Daejeon, Republic of Korea
*shyu80@kaeri.re.kr

1. Introduction

Drying process of spent nuclear fuel must be required when spent nuclear fuel is transferred from wet storage to dry storage because oxidation composition could be bad effect of fuel cladding and long-term integrity of fuel cladding could not be guaranteed. Vacuum drying method is widely used in nuclear industry. In vacuum drying process, dryness criteria is that internal pressure is less than 3 Torr for 30 min without vacuum pump operation.

Characteristics of vacuum drying were analyzed. Analytic approach to simulate vacuum drying was performed. Simulation results are compared to characteristics of vacuum drying.

2. Concept of Analytic Calculation

2.1 Vacuum Drying Procedure

Vacuum drying process is divided into 3 steps. Fig. 1 shows pressure change during vacuum drying. First step is evacuation phase. Pressure decreases rapidly due to vacuum pump. Second step is evaporation phase. Generally pumping speed of vacuum pump is getting slower as the pressure decreases. In this phase, speed evacuation by vacuum pump is almost same as speed of evaporation of residual water. The duration of this phase is much longer than other phase. Almost residual water is eliminated in this phase. Last step is final drying phase. Only few water remained and speed of water evaporation is less than speed of vacuum pumping. Final drying process continues until dryness criteria is met.

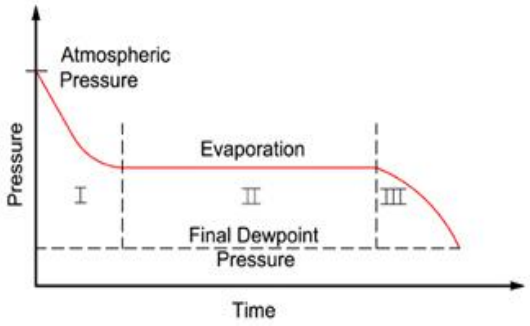

Fig. 1. Pressure change during vacuum drying.

3. Results and Discussion

Assumptions of calculation are below as

- Temperature inside canister was constant.
- Residual water only naturally evaporated.
- Initial pressure is 101.325 kPa.
- Initial residual water at bottom was 50 g.

3.1 Simple Drying Process

To check the effect of residual water, case with residual water and case without water were compared in Fig. 2, 3. Required time until pressure was less than 0.4 kPa (3 Torr) is 111 s for result without water and is 35907 s for result with water. It took much longer time for vacuum drying of case with residual water.

Three phases of vacuum drying were found in Fig. 3. Duration of evacuation phase is for 120 s. Pressure drops from 100 kPa to 3 kPa. Evaporation phase is

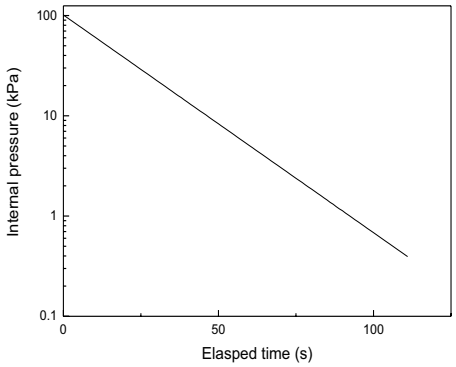

Fig. 2. Result of pressure change without residual water.

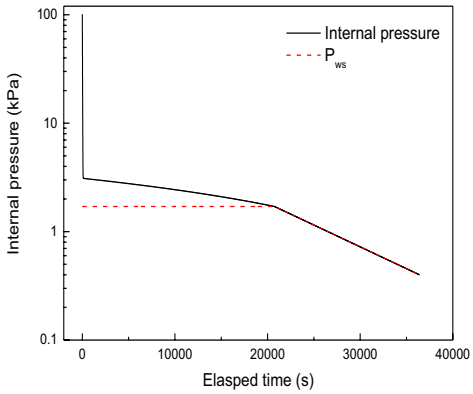

Fig. 3. Result of pressure change with residual water.

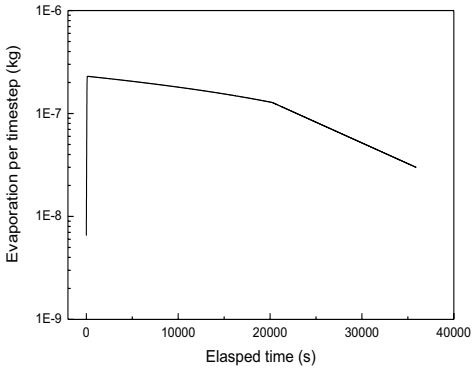

Fig. 4. Result of evaporation rate (kg/s).

from 121 s to 20250 s. Fig. 4 shows that evaporation rate increased in this phase. Pressure drops slowly from 3 kPa to 2 kPa. Most residual water is eliminated. Final drying phase is for 15657 s. Duration of final drying depends on dryness criteria.

4. Conclusion

The calculation program of vacuum drying was developed to analyze analytically vacuum drying process. The effect of residual water on vacuum drying was compared. Three vacuum drying phases were found in the simulation result.

ACKNOWLEDGEMENT

This work was supported by the Korean Ministry of Trade, Industry, and Energy (MOTIE) as a part of the Radioactive Waste Management Technology Development Project (20181720201020).

REFERENCES

[1] USNRC, 2010, Standard Review Plan for Spent Fuel Dry Storage Systems at a General License Facility, NUREG-1536.

The Direction of Extension of the AMORES Code Capability

Daesik Yook, Ara Go, Gyeong-uk Kang, and Haiyong Jung
Korea Institute of Nuclear Safety, 62, Gwahak-ro, Yuseong-gu, Daejeon, Republic of Korea
dsyook@kins.re.kr

1. Introduction

Whereas the current AMORES computer code focuses on the evaluation of the source term of spent fuel [1,2], the Used Nuclear Fuel-Storage, Transportation & Disposal Analysis Resource and Data System (UNF-ST&DARDS) which is a comprehensive integrated data and analysis tool being developed for the US Department of Energy (DOE) can provides cask-specific as-loaded safety analysis, including criticality, thermal and dose evaluations. [3]

In compliance with the nuclear safety act and the notice of NSSC (Nuclear Safety and Security Commission), transport cask or storage cask for spent fuel shall be evaluated the criticality, shielding, heat removal function, etc. Furthermore, KINS (Korea Institute of Nuclear Safety) has in charge of the safety review and inspection of this transport cask or storage cask. There are 5 transport casks which were approved by the regulatory body in Korea. And KORAD-21 dual purpose cask is under review for the design approval by the KINS. The owner of spent fuel transport cask who has intention to use it continuously shall be inspected periodically in every 5 years by the KINS. Spent fuel transport cask has to be confirmed on each safety like as criticality, radiation shielding, containment, heat removal ability, etc. in both review process and periodic inspection.

2. The Direction of Extension of the AMORES Code Capability

2.1 Computer Code Development Direction

The capability of AMORES computer code shall be extended as shown in Fig. 1. First of all, the approved spent fuel transport cask characteristic information will be stored in AMORES code as database. These data can be converted the input file of KENO VI for criticality, the input file of STARBUCS for burnup credit, the input file of MAVRIC for radiation shielding, respectively. For the evaluation of burnup credit and radiation shielding, neutron spectra and gamma spectra from specific spent fuel assemblies are necessary. These spectra can be obtained from AMORES code as shown in Fig. 3, then AMORES code merge neutron, gamma spectra and transport cask configuration data into the input file of STARBUCS or MAVRIC.

Finally, these computer codes for each purpose in SCALE 6.1 can be executed by AMORES automatically. The assumption that fresh fuel will be loaded in the transport cask is applied for the criticality evaluation so that it is not necessary additional information from spent fuel database of AMORES. In case of thermal evaluation of transport cask, both KINS and the applicant for the design approval of spent fuel transport cask use the FLUENT code or CFX code. AMORES code can evaluate the decay heat of specific spent fuel and provide this data to these computer codes as the thermal source input parameter. However AMORES can't make input file of FLUET or CFX code directly and it can provide some parameter merely. In the study, in order to AMORES code validation, criticality evaluation of KORAD 21 dual purpose cask was performed using the cask specification and material information of this cask that was developed to KORAD as parts of the development of the expansion of AMORES code function.

2.2 Preliminary Evaluation Results of Criticality of Transport Cask

Whereas the source term information of spent fuel is necessary for the burnup credit, radiation shielding, and thermal evaluation, in case of the criticality, it is not necessary because the assumption that fresh fuel will be loaded in the transport cask is applied. As shown in Fig. 1, AMORES code can contain the cask specification and material information as a database in advance. This data can be modified as an input file of MCNP code or KENO VI for calculating radiation shielding and criticality automatically by AMORES code, respectively. In the study, in order to AMORES code validation, criticality evaluation of KORAD 21 dual purpose cask was performed using the cask specification and material information of this cask that was developed to KORAD. Cross

section library was used the ENDF-B VII of SCALE 6.1 and it was assumed that the transport cask was arrayed at intervals of 60cm infinitely and surrounded by water. The effective neutron multiplication factor, keff including all biases and uncertainties at a 95 percent confidence level, should not exceed 0.95 under all credible normal, off-normal, and accident-level conditions. keff of KORAD 21 was evaluated as 0.32803(0.34265 by KORAD) and 0.94132(0.94112 by KORAD) under the normal condition and accident condition, respectively.

3. Conclusion

The AMORES was very useful to evaluate inventory, radioactivity, and thermal power from real spent fuel data in Korea. However it is limited the applicability for the evaluation of the safety of transport or storage cask. In order to overcome this limitation, various functions of AMORES code will be developed and will be added to it. Regulatory position and confirmatory procedures will be applied to the development of review guidelines for spent fuel safety information in the future. As the first step to confirm the validation of this code, the criticality evaluation of KORAD 21 was performed and compared to the applicant's calculation result. As a result, the difference range between the two calculations is from 0.02% to 4.27% in the case of normal and accident condition.

ACKNOLEDGEMENT

This work was supported by the Nuclear Safety Research Program through the Korea Radiation Safety Foundation (KORSAFe), granted financial resource from the Nuclear Safety and Security Commission (NSSC), Republic of Korea (No. 1803015).

REFERENCES

[1] Ara Go, Daesik Yook, etc al. "Analysis of Korea's PWR Spent Nuclear Fuel (SNF) Characteristics Evaluated from Existing SNF Inventories (1979–2015) and Projected SNF Inventories (2016–2089)", Nuclear Technology, August, 2018, online : https://doi.org/10.1080/00295450.2018.1500795

[2] GyeongMi Kim, Geon Hee Jung, Dae Sik Yook, et al., " Analysis of Detailed Operational History Effects on the Spent Fuel Characteristics for Hanbit Unit 3", ANUP 2014, 9-12 November 201, Republic of Korea', Transactions of the Korean Nuclear Society Autumn Meeting, Yeosu, Korea, October 25-26, 2018.

[3] Josh Peterson, Bret van den Akker, et al. "UNF-ST&DARDS Unified Database and the Automatic Document Generator", NUCLEAR TECHNOLOGY · VOLUME 199 · 310–319 · SEPTEMBER 2017.

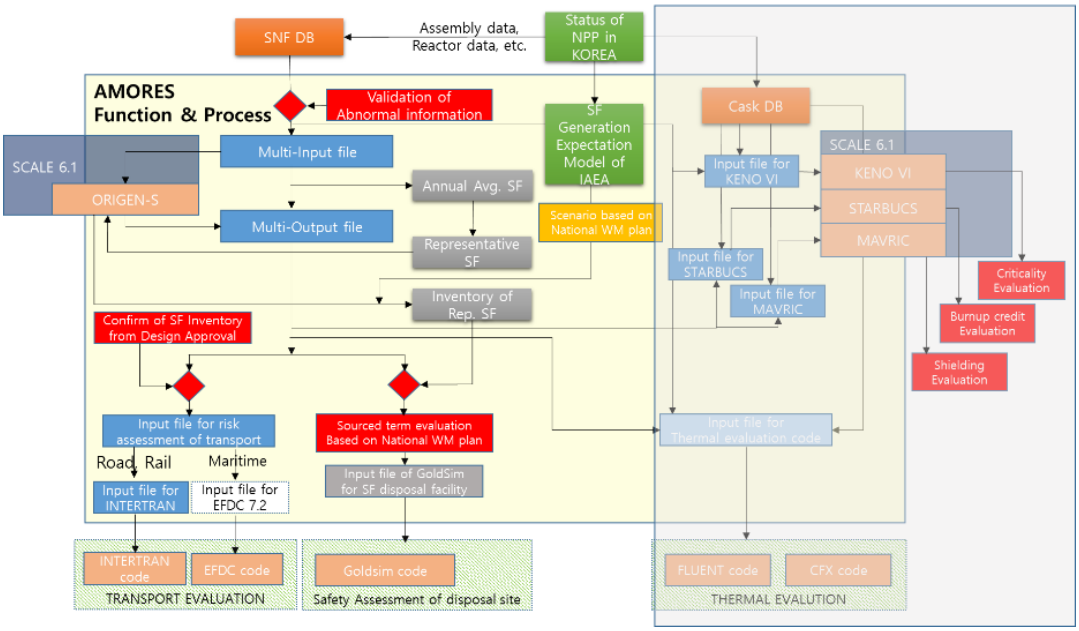

Fig. 1. The direction of extension of the AMORES code capability.

Review on the Control of the Direction of Hydride in Zirconium Clad Tube in Terms of Manufacturing Process

Tae-Sik Jung* and Seong-Ki Lee

KEPCO Nuclear Fuel, 242, Daedeok-daero 989beon-gil, Yuseong-gu, Daejeon, Republic of Korea

*taesik@knfc.co.kr

1. Introduction

Coolant serves as an oxidant and the zirconium cladding corrodes and absorb hydrogen atoms at the same time in nuclear reactors. The absorbed hydrogen atoms precipitate as hydrogen compounds (zirconium hydride) in the region below the solubility [1]. The deterioration of robustness of the cladding due to precipitated zirconium hydride is a major issue in the dry storage [2,3], accident conditions [4], and high burnup fuel [5,6].

Specifically, zirconium hydride differs not only in its precipitation fraction, but also in the mechanical performance deterioration along its direction of in the cladding tube [7]. The tensile stress in the circumferential direction is generated not only by the internal pressure but also by the action of UO_2 pellets pushing out of the cladding tube. Therefore, hydrogen compounds precipitated in the radial direction are of greatest interest [3,7].

In this study, we review the factors that can control the directionality of zirconium hydride which are inevitably formed in a zirconium cladding tube during burnup from the perspective of cladding manufacturing.

2. Clad Tube Manufacturing Factor

2.1 Pilgering Factor

Tube reduced extrusion (TREX) is subjected to three times cold pilgering to reach the final product dimensions and to be able to reach basal pole within 30 to 40^o from the radial direction as shown in the Fig. 1 (a1). Therefore, the preferential formation and growth of the hydride can be achieved on the plane 10-17 which is inclined by 15^o on the 0002 plane.

However, without proper adjustment of the tube reducing ratio (R_w / R_d, R_w: Reduction length of wall thickness, R_d: Reduction length of diameter) in the process of cold pilgering, perpendicular texture is formed as shown in the Fig. 1 (a3). The reason for this is that the change in texture is determined by the ratio (c/a) in crystallography of hexagonal crystal structures.

The cladding composed of zirconium atoms has an aspect ratio of 1.593, which is smaller than 1.633 of the hard sphere model [9]. Therefore, it is necessary to perform cold working at a ratio of R_w/R_d over 1 to develop the desired texture [8,9]. In practice, nuclear fuel manufacturers adjust the ratio using the Q factor.

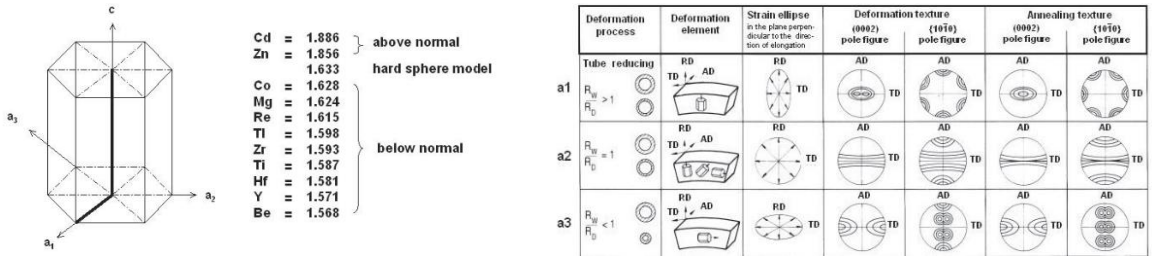

Fig. 1. c/a axial ratio for hcp metals (left) and deformation process for cold deformed and annealed conditions (right) [8].

2.2 Heat Treatment Factor

After the cold pilgering, the strongly formed texture is slightly changed by the heat treatment, but the angle of the basal pole does not change. As shown in the Fig. 2 which is the result of measuring zirconium alloy cladding tube annealed for 8 hours on 520°C, only (10-10), the primary prism plane, perpendicular to the basal pole rotates about 30° around the basal pole. The measurement was performed using electron backscattered diffraction (EBSD) technique.

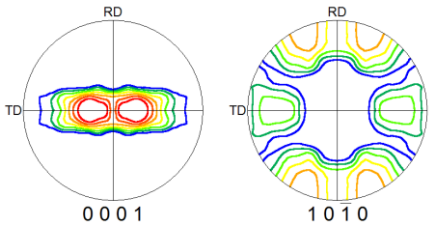

Fig. 2. Inverse pole figure (IPF) in zirconium alloy.

3. Conclusions

In order to control the precipitation direction of the hydride precipitated in zirconium cladding, R_w/R_d ratio is set over 1 in the cold pilgering step. In addition the heat treatment does not cause a large change in the texture. As a result, it is possible to suppress the embrittlement of the cladding due to the formation of hydrogen compounds in circumferential direction by forming the texture of zirconium clad tube at 30 ~ 40° in the direction of the radial direction from the production stage.

ACKNOWLEDGMENT

This work was supported KETEP and MOTIE (No. 20141710201660).

REFERENCES

[1] J. Bair et al., J. Nucl. Mater, 466, (2015).
[2] EPRI-1003416 (2002).
[3] M. Billone et al., J. Nucl. Mater, 466, (2015).
[4] SRP 4.2 App. B, NUREG-0800 Rev. 3.
[5] S. Shimada et al., 327, 97 (2004).
[6] H. Hayashi et al., Proc. Topfuel 2003, (2003).
[7] Q. Auzoux et al., J. Nucl. Mater, 494 (2017).
[8] E. Tenchhoff, ASTM STP 1467, 25-50 (2005).
[9] E. Tenchhoff, ASTM STP 966 (1988).

Benefits of the ISA Application to Pyroprocessing Facilities

Gilsung You*, Seokjun Seo, Woojin Jo, Siwan Noh, Hyojik Lee, Hohee Lee, Seungnam Yu, and Jeonghoe Ku
Korea Atomic Energy Research Institute, 111, Daedeok-daero 989beon-gil, Yuseong-gu, Daejeon, Republic of Korea
*yougil@kaeri.re.kr

1. Introduction

KAERI has been developing pyroprocessing technology for a safe and an effective disposal of spent fuel. For verification of this technology, it is necessary to develop the experimental facility with hot cells and auxiliary systems in the future [1]. In this paper, safety analysis methodologies for fuel cycle facilities in the United States and Korea are introduced, and benefits of the application of the ISA (Integrated Safety Analysis, US NRC) to pyroprocessing facilities are studied.

2. Present and Future of the ISA

NUREG-1520 is a guidance of US NRC for reviewing and evaluating the health, safety, and environmental protection aspects of applications for fuel cycle facility licenses. This guidance addresses the longstanding health, safety, and environmental-protection requirements of 10 CFR Part 20 and 10 CFR Part 70, as well as the accident safety requirements reflected in Subpart H, "Additional requirements for certain licensees authorized to possess a critical mass of special nuclear material," of 10 CFR Part 70. Subpart H of 10 CFR Part 70 identifies risk-informed performance requirements and requires applicants and existing licensees to conduct an Integrated Safety Analysis (ISA) [2].

The ISA is a systematic, risk-informed and performance-based analysis. The NRC considers an ISA method required by 10 CFR Part 70 to be appropriate to address the types of hazards and accident sequences associated with existing fuel cycle facilities.

However, the presence and processing of large quantities of fission products and TRU isotopes at spent fuel processing facilities have the potential to greatly increase consequences far above the 10 CFR Part 70 high-consequence thresholds for some accident sequences (e.g., fires, explosions), and, therefore, 10 CFR Part 70 is not appropriate for spent fuel processing facilities. The NRC concludes approaches that incorporate more quantitative risk assessment, including PRA, are needed to adequately address safety and risk at spent fuel processing facilities. Recently the NRC is considering two basic approaches—a hybrid ISA-PRA approach and a PRA approach. The NRC considers the hybrid approach is a reasonable starting point at this preliminary stage of the NRC's efforts in support of potential future rulemaking activities [3-7].

3. Present Korean Safety Regulations for Pyroprocessing Facilities

The Korean Nuclear Safety Act requires applicants to conduct a standard safety analysis methodology similar to that of nuclear power reactor, such as deterministic and defense-in-depth safety methodologies. The Paragraph (3) of Korean Nuclear Safety Act article 35 requires that a person, who intends to carry on the spent fuel processing business, shall submit to the competent minister an application for the permit or the designation together with radiation environmental report, safety control regulations, explanatory statement of design and work methods, quality assurance program for the operation of the business and other documents as prescribed by the Ordinance of the Prime Minister [8].

In Korea the pyroprocessing facilities are regulated as one of fuel cycle facilities under the Korean Nuclear Safety Act. The act describes the safety requirements for the license and operation of fuel cycle facilities. Although the safety requirements for fuel cycle facilities show small differences compared to those of nuclear power plants, but a large parts of the requirements use the same technical criteria with nuclear power plants.

4. Benefits of the ISA Application to Pyroprocessing Facilities

Pyroprocessing is inherently a batch process which means that materials must be moved as solid physical objects among most of the various steps. The size of the batches is limited by criticality considerations. The maximum throughput of a single electrorefiner is about 50 MTIHM/yr. On this basis, a pyroprocessing plant would require the operation of 16 electrorefiners in parallel to achieve the 800 MTIHM/yr throughput of the French UP3 aqueous spent fuel processing facility. The large number of movements of highly radioactive objects containing fissile materials in this manner is likely to require high equipment reliability, low accident likelihood, and a greater need for nuclear material accountability [9].

The ISA is a systematic, risk-informed and performance-based analysis. The ISA provides the framework and establishes the needed safety basis to assure that the handling of nuclear material is within the programmatic requirements, that the safety program is appropriate for the risk, and that the measures for carrying out the safety program are appropriately monitored.

For development of safer pyroprocessing facilities safety analysis is needed through a better safety analysis methodology that can reflect the properties of pyroprocessing. Applying the ISA to pyroprocessing facilities would benefit for developing a safer and more reliable facility.

5. Conclusions

For development of safer pyroprocessing facilities it is necessary to evaluate the safety through a better analysis methodology that can reflect the properties of pyroprocessing. The ISA is a systematic, risk-informed and performance-based analysis methodology for fuel cycle facilities. Applying the ISA to pyroprocessing facilities would benefit for developing a safer and more reliable facility.

REFERENCES

[1] Gil-Sung You, et al., “Concept and Safety Studies of an Integrated Pyroprocess Facility, Nuclear Engineering Design”, No. 241, pp. 415～424 (2011).

[2] US NRC, NUREG-1520 rev.2, “Standard Review Plan for Fuel Cycle Facilities License Applications” (2015).

[3] US NRC, SECY-0136, “Draft Regulatory Basis for Licensing and Regulating Reprocessing Facilities” (2011).

[4] Gilsung You, et al., “Adaptability Study of Hybrid ISA-PSA Method on Safety of Pyroprocess Facilities”, Proc. of the KRS 2017 Spring Conference, 15(1), May 24-26, 2017, Busan.

[5] Gilsung You, et al., “Enforced Risk Criteria for SF Recycling Facilities in US and Its Availability in Korea”, Proc. of the KRS 2017 Fall Conference, 15(2), Oct 18-20, 2017, Changwon.

[6] Gilsung You, et al., “Applicability of the ANSI/ANS-58.16 on pyroprocessing Facilities”, Proc. of the KRS 2018 Spring Conference, 16(1), May 30-June 1, 2018, Busan.

[7] Gilsung You, et al., “Methodologies and Properties of Safety Analyses for Pyroprocessing Facilities”, Proc. of the KRS 2018 Fall Conference, 16(2), Oct 31-Nov. 2, 2018, Jeju.

[8] Korean Nuclear Safety Act (2018)

[9] US NRC, NUREG-1909, “Background, Status, and Issues Related to the Regulation of Advanced Spent Nuclear Fuel Recycle Facilities” (2008).

Effect of Long-term Cooling on the Hydride Reorientation of Non-irradiated Zircaloy-4 Cladding Tube : 1M, 3M & 6M

DaeHo Kim*, JongDae Hong, Jegeon Bang, IkSung Lim, EuiJung Kim, and Donghak Kook
Korea Atomic Energy Research Institute, 111, Daedeok-daero 989beon-gil, Yuseong-gu, Daejeon, Republic of Korea
*kdh@kaeri.re.kr

1. Introduction

In a dry storage environment, the spent fuel will have a long period of cooling time at high temperatures. At this time, the dissolved circumferential hydride in a cladding is slowly precipitated from the radial hydride, which makes it more brittle and thus degrading the integrity of the cladding tube. The hydride reorientation occurs by internal rod pressure of the fission gas in cladding tube, and the hoop stress is applied to the outer diameter of the cladding, causing hydrogen to flow in a radial direction.[1]

The effects of cooling rate of hydride reorientation, which could occur during long-term dry storage process in the spent fuel cladding, were evaluated.

2. Experiment

2.1 Hydride Reorientation Test Method

Using a non-irradiated Zircaloy-4 cladding tube charged a 200 ppm and 400 ppm hydrogen, the hydride reorientation test (HRT) from 400℃ of maximum temperature to 100℃ on decreasing for a 1 month, 3 month and 6 month were performed at hoop stress 70 MPa, 80 MPa, 90 MPa and 110 MPa respectively. Table 1 is HRT summary of a 1 month, 3 month and 6 month. And the Fig. 1 is test profiles of a temperature.

Table 1. HRT summary

Period	1 Month	3 Month	6 Month
Cooling rate	0.5℃/hr	0.1℃/hr	0.05℃/hr
T_{max}	400℃ → 100℃		
$\sigma_{hoop(MPa)}$	90	70, 80, 90 & 110 (Temperature-dependent hoop stress)	
$C_{H(ppm)}$	200	Each 200 ppm & 400 ppm	

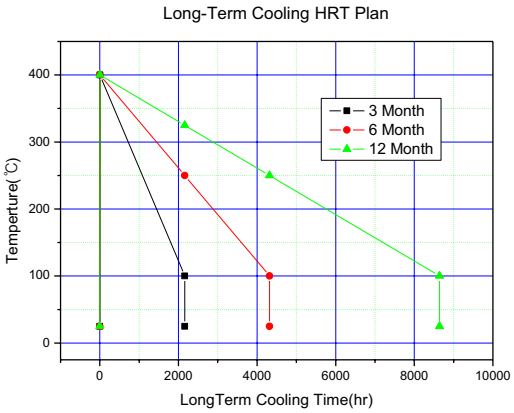

Fig. 1. Temperature profiles of HRT.

2.2 Specimens and Test Condition

The test specimen of non-irradiated Zircaloy-4(cold-worked, stress-relief annealed, CWSRA) cladding were 200 ppm and 400 ppm of the treated homogenization hydrogen respectively, using the injection chamber of the volume of a mass system. And each specimen length is a 150 and 300 mm used fitting at top and bottom. Table 2 lists the specimen and test conditions. Fig. 2 is a long-term cooling HRT specimen.

Table 2. Specimen and Test Condition

Specimen				Condition	
Material	Length (mm)	Hydrogen Concentration (ppm)	Diameter (mm)	Hoop Stress (MPa)	IRP (MPa)
Non Irradiated Zry-4 Tube	150	400	9.5	90	11.53
	300	200	9.5	110	14.09
				90	11.53
		400		80	10.25
				70	8.97

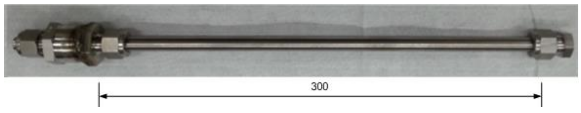

Fig. 2. Long-term cooling HRT specimen.

3. Test Results

After hydride reorientation test of non-irradiated Zircaloy-4 cladding tube, the offset strain was assessed from ring compression test at room temperature, 75℃, 100℃ and 200℃ respectively. And the specimens were reviewed micro-structure of hydride morphology.

3.1 Morphology after HRT

Fig. 3 is a micro-structure of representative 90 MPa hoop stress specimens (200 ppm) after HRT. Through the visualized review, radial hydrides were difficult to observe in 1 month specimens but were easily observed in 3 month specimens.

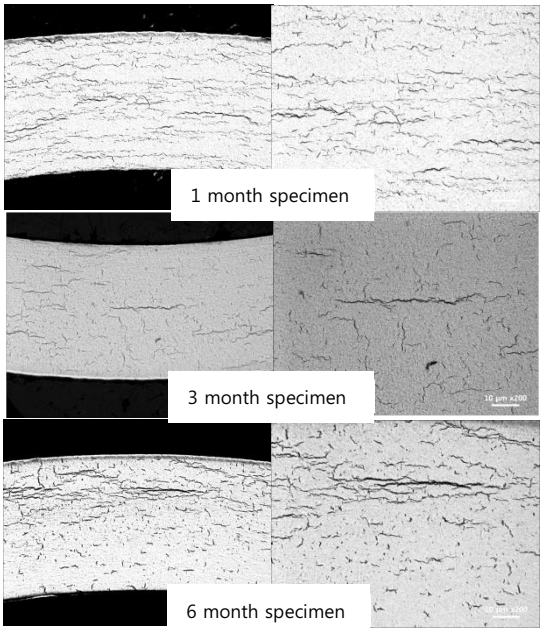

Fig. 3. Morphology after HRT.

3.2 RCT Results at RT

Table 3 and Fig. 4 are ring compression test results at room temperature. At result of offset strain, the brittleness of the long-term cooling specimens of 200 ppm and 90 MPa for 1 month and 3 months was found to be higher, but the ductility was higher in the 6 month specimen.

Table 3. Results of RCT and Offset Strain*

RCT at RT	Hydrogen Concentration (ppm)	Diameter (mm)	Length (mm)	Max. Load(N)	Offset Dis(mm)	Offset strain(%)
1M-HRT	194.6	9.51	10.00	834	2.85	29.9
3M-HRT	200.3	9.55	10.00	655	1.01	10.5
6M-HRT	186.4	9.63	10.00	758	2.17	22.5

*Basis of 90MPa hoop stress specimen

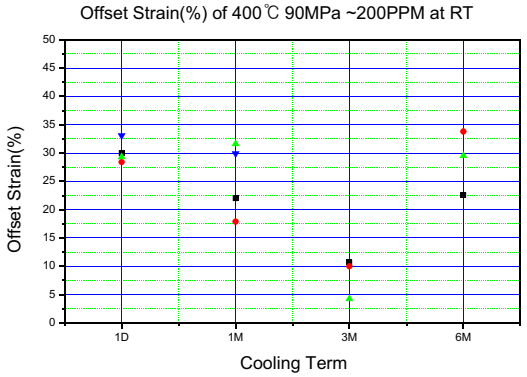

Fig. 4. Results of RCT at RT.

4. Conclusion

Using the non-irradiated Zircaloy-4 cladding tube, was used to conduct long-term cooling hydride reorientation tests (HRT) at 1, 3 and 6 months at various hoop stresses and hydrogen concentrations, respectively. The results showed that the radial hydrides were rearranged by the long-term cooling at 1 month and 3 months, and the brittleness of the specimen increased with time. On the other hand, in the 6 month test specimens, the reversal phenomenon, in which the ductility increased, appeared. In order to evaluate the effect of long-term cooling rate on hydride reorientation, it is necessary to confirm reproducibility through repeated test.

ACKNOWLEDGEMENT

This work was supported by the Korea Institute of Energy Technology Evaluation and Planning (KETEP) granted financial resource from the Ministry of Trade, Industry and Energy, Republic of Korea (No. 2014171020166A)

REFERENCES

[1] Y.J. Kim, “Evaluation of hoop stress on the hydride reorientation and mechanical properties”, Proc. of the KRS 2014 Spring Conference, May 8, 2014, Pyung Chang.

Experimental Investigation of Temperature Profiles in Spent Fuel Model

Dong-seok Oh*, Chang-hwan Shin, and Donghak Kook

Korea Atomic Energy Research Institute, 111, Daedeok-daero 989beon-gil, Yuseong-gu, Daejeon, Republic of Korea

*dsoh1@kaeri.re.kr

1. Introduction

To ensure the integrity of the zirconium-based alloy cladding, standard review plan for spent fuel dry storage systems (SFDSS) at a general license facility limits the maximum calculated cladding temperature to less than 400℃ for normal conditions of storage and short-term loading operations, including cask drying and backfilling. It also requires that the maximum temperature of the SFDSS concrete (ACI 318) does not exceed 200°F [1]. In order for the design temperature to meet these limits, an accurate temperature calculation tool with appropriate design methodology is required. T.E. Michener developed the COBRA-SFS code and calculated the temperature distribution of fuel and the structure of the SFDSS containing 24 fuel assemblies and verified the code reliability by comparing with the test results [2]. In land, code analyses by using a COBRA-SFS [3] and a test facility setup for code verification are being prepared [4]. In this study, the heat transfer of a spent fuel model was examined experimentally.

2. Experiment

Heat transfer experiment for the PWR spent fuel model was conducted using the STEP(Single Fuel Assembly Temperature Experimental Facility) experimental facility designed by KAERI and manufactured by SE & T (Fig. 1). The STEP consists of a mechanical system, an electric system, a gas backfill system, a data acquisition system, and a fuel assembly model. The mechanical system consists of a fuel tube in the form of a duct, which maintains the assembly model at the outer periphery of that and forms an upward flow path, a pipe shaped cask forming a downward flow path from the outside of the fuel tube, a bottom chamber provided with an electric lead wire passage and a gas backfill valve below the cask, and a top flange with Conaxes that forms a thermocouple pressure boundary at the top of the cask. A 50 cm thick ceramic wool blanket cover the cask to minimize heat loss. The electrical system supplies and controls 179 heater rods. The power is divided into five groups and each group can control independently the power. The power supplied to the assembly model can be controlled in units of 0.01 kW from 0.5 to 3 kW. The gas backfill system fills and discharges the gas by a helium gas cylinder and a vacuum pump connected to a valve installed in the lower chamber. The data acquisition system acquires a total of 190 temperatures by k type thermocouples installed in the 13 heater rods, 3 points in the circumferential direction of the fuel tube and 4 points in the circumferential direction of the cask at each 8 different axial location and 30 points in the upper subchannels.

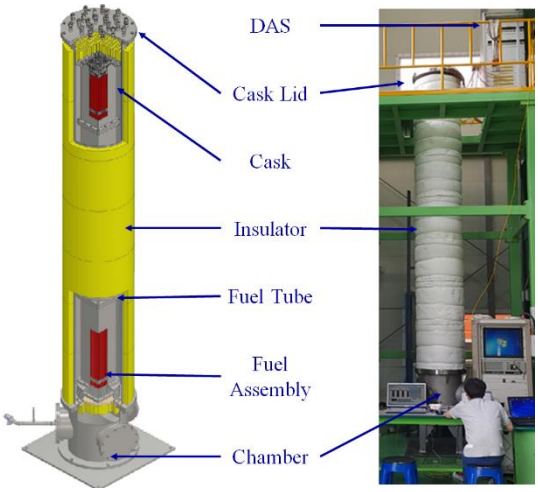

Fig. 1. Test Facility (STEP).

Temperature signals are collected and stored by a laptop equipped with four Keysight 34972a data loggers and Agilent VEE Pro. The fuel assembly model used in the test simulates a spent fuel of Westinghouse 14×14 nuclear fuel assemblies. It consists of 179 heater rods, 16 control rods, and one measuring rod, and consists of seven support grids and upper and lower flow plate simulators. For the heat transfer test at 1 kW power supply condition, the experimental variables are the gas type and the power

distribution type. Vacuum and helium were tested for uniform and non-uniform heat distribution conditions, respectively. For helium backfill, 0.5 kW and 2.0 kW tests are added. The helium pressurization condition is 1.5 bar and the vacuum condition is 75 torr. In case of uniform heat distribution condition, the total 1 kW output was uniformly distributed to the 179 rods. In case of non-uniform heat distribution, 0 output supplied to from rod No. 1 to No. 72, and 1 kW output uniformly distributed for from No. 73 to No. 179.

3. Results and Discussion

Results of 1.0 KW vacuum and helium backfill are presented in Fig. 2. At 1.0 KW uniform distribution, the maximum cladding temperature was 301℃ for vacuum backfill and 233℃ for helium backfill. The temperature distribution varies greatly depending on the backfilled gas. For the vacuum backfill, the peak temperatures are the higher and temperature gradients the steeper than that of the helium, indicating that radiation is the least effective heat transfer mechanism. Helium backfill is evident in enhanced heat transfer due to its high conductivity. The axial profile is flattest. Temperatures of the non-uniform power distribution were larger than those of the uniform distribution, but the difference was not significant.

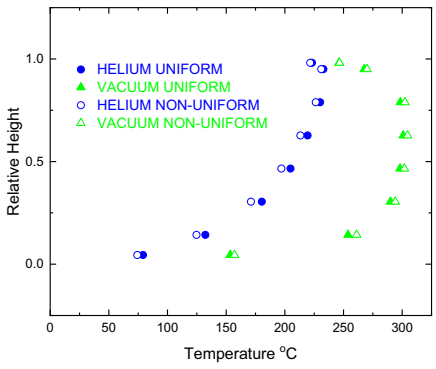

Fig. 2. Temperature Profiles According to Backfill and Power Distribution.

The axial temperature profile at 0.5, 1 and 2 kW output in Helium backfill is shown in Fig. 3. The temperature profiles were similar with the assembly power variation and the maximum temperatures were 143℃, 233℃, and 356℃, respectively.

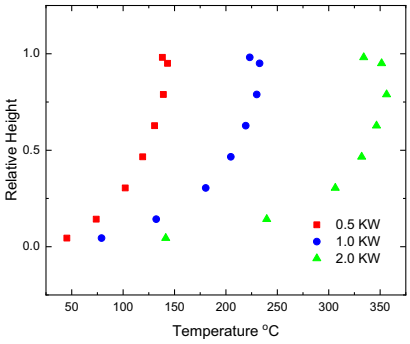

Fig. 3. Temperature Profile According to Power.

4. Conclusions

Temperatures of a 14 × 14 spent fuel model installed in STEP were measured under helium and vacuum backfill. In 1 kW homogeneous power distribution, the maximum cladding temperature was in vacuum backfill. The cladding temperature profile was obviously different according to the backfill gas. Some tests to identify the mechanism of heat transfer under vacuum condition are required as a further work.

ACKNOWLEDGEMENT

This work was supported by the Korea Institute of Energy Technology Evaluation and Planning (KETEP) granted financial resource from the Ministry of Trade, Industry and Energy, Republic of Korea (No. 2014171020166A)

REFERENCES

[1] NRC, “Standard Review Plan for Spent Fuel Dry Storage Systems at a General License Facility,” NUREG-1536 Rev. 1, (2010)

[2] T. E. Micherner, et al., “COBRA-SFS, A Thermal-Hydraulic Analysis Code for Spent Fuel Storage and Transportation Casks, Cycle 4,” PNNL-24841, (2015)

[3] C. H. Shin, K. W. Seo, D. H. Kook, “Sensitivity Analysis of COBRA-SFS for Dry Storage of Spent Fuel.” Proc. of the KRS 2017 Spring Conference, 15(1), May 24-26, 2017, Busan..

[4] D. S. Oh, S, J. Byun, C. H. Shin, D. H. Kook, “Single Fuel Assembly Temperature Experimental Facility (STEP)” Proc. of the KRS 2018 Autumn Conference, 18, October 31- November 2, 2018, Jeju.

Dynamic Buckling Test of Cell Setting Spacer Grid and Normal Spacer Grid

Hong-Ryoul Oh*, Jae-Yong Kim, Kyung-Ho Yoon, Sung-Uk Lee, and Donghak Kook
Korea Atomic Energy Research Institute, 111, Daedeok-daero 989beon-gil, Yuseong-gu, Daejeon, Republic of Korea
*ohr8248@kaeri.re.kr

1. Introduction

As the capacity of spent nuclear fuel storage pool at reactor sites becomes saturates in few years, long term dry storage has been recently discussed as an alternative option in Korea. The Korea Atomic Energy Research Institute have been evaluated the integrity and retrievability of fuel for transportation and long-term dry storage of spent nuclear fuel. Spacer grid is one of the structural parts of the fuel assembly. The studies were focused on buckling behavior of a normal spacer grid and cell setting spacer grid.

2. Method and Results

2.1 Specimen

A test specimen was 14OFA spacer grid fabricated with Zircaloy-4 material as shown in Fig. 1(a). The fuel rods were inserted into every fuel rod slots at a space grid as shown in Fig. 2(b). The fuel rod cell size was expand due to the irradiation effect for operation period. The simulated cell size was increased by 0.07 mm than normal space grid cell size, but all cell size was not uniformly expand.

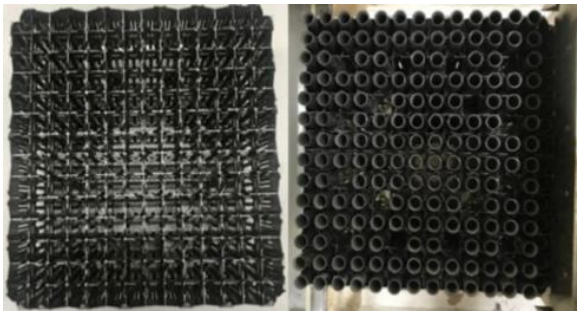

Fig. 1. Photograph of a 14OFA Space Grid (a) and space grid with Fuel Rods (b).

2.2. Pendulum Type Impact Tester and Test Conditions

Fig. 2 shows the schematic drawing of the pendulum type impact tester. The impact hammer was fixed and rotated by the motor. The specimen was fixed with a force of 15.7 kgf using air pressure. Impact energies transmitted to the plate and rod could be controlled. The length of the arm is about 0.88 m and the mass of the hammer is about 38 kg.

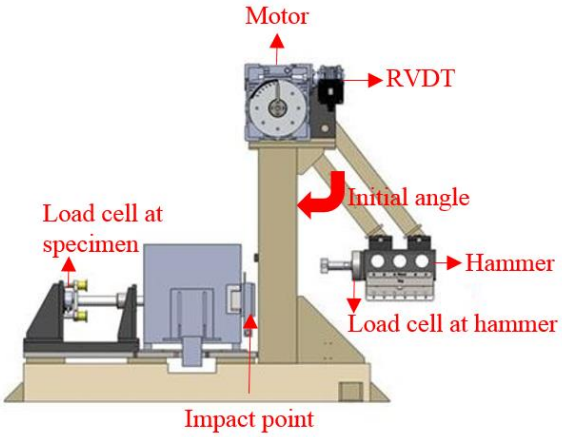

Fig. 2. Pendulum type impact tester.

Pendulum type impact test of the normal and cell setting spacer grid was executed room temperature condition. The initial impact angle was started from 25 degrees. It was increased by 2° until buckling. The number of specimens was three.

2.3 Test Results

The impact test results of normal and cell setting spacer grid specimen were summarized in Table 1 and 2.

Table 1. Impact test results of cell setting spacer grid

	SG no.1		SG no.2		SG no.3	
	H/S	S/S	H/S	S/S	H/S	S/S
25	32,846	36,120	29,460	35,312	32,370	35,604
26	33,826	36,946	32,256	37,007	33,832	37,158
27	34,821	38,150	32,033	36,062	33,482	37,897
28	35,134	39,513	30,802	34,814	35,283	38,594
29	33,240	41,158	22,779	29,216	36,219	38,707
30	31,968	37,292	29,460	35,312	34,888	40,326

Table 2. Impact test results of normal Spacer grid

	SG no.1		SG no.2		SG no.3	
	H/S	S/S	H/S	S/S	H/S	S/S
25	31,908	35,103				
26	33,751	36,375				
27	34,958	37,042	34,600	37,470	32,637	36,412
28	35,751	37,885	36,244	37,875	35,462	38,036
29	37,089	37,844	35,139	38,827	37,011	38,899
30	37,658	38,893	37,056	38,524	38,627	40,131
31	33,866	38,955	37,909	40,316	39,497	40,826
32	28,022	34,636	26,342	34,829	40,468	41,790
33					40,006	42,440
34					28,356	33,755

The average buckling strength and standard deviation of normal spacer grid at the hammer side were 38,478 N and 1,285 N, and average buckling strength and standard deviation of cell setting spacer grid at the hammer side were 34,360 N and 1637 N, respectively. Therefore, the critical buckling strength of the cell setting spacer grid was about 10% smaller than those of the normal spacer grid.

3. Conclusion

The test was carried out to confirm the buckling strength of normal spacer grid and cell setting spacer grid. The simulated spacer grid cell size was increased by 0.05 mm than normal spacer grid cell size, these gaps between the fuel rods and the grid supports eventually caused a reduction in the dynamic impact strength of the spacer grid itself. The critical buckling strength of the cell setting spacer grid was smaller than those of the normal spacer grids. Future works will attempt to identify the effects of hydrogen and use it in the assessment of SNF evaluate the integrity.

ACKNOWLEDGEMENTS

This work was supported by the Korea Institute of Energy Technology Evaluation and Planning(KETEP) and the Ministry of Trade, Industry & Energy(MOTIE) of the Republic of Korea (No. 2014171020166A).

REFERENCES

[1] Jae-yong Kim, Kyung-ho Yoon, Hyung-kyu Kim, Kang-hee Lee and Heung-seok Kang “Drop type impact test to obtain the critical impact strength of structure” KSME spring meeting 2014.

[2] KAERI Document, 2017, Pendulum Impact Tester for Thin Plates Structure, No. KAERI/TR-6942/2017.

[3] Hong-ryoul OH, Sung-Uk Lee, Jae-Yong Kim, Kyung-Ho Yoon, Dong-Hak Kook “Comparison of Strains Measured on Spacer Grid and Fuel Rod Caused by External Load” KNS spring meeting 2018.

Review of Chloride-Induced Stress Corrosion Cracking Issue and Mitigation Technology of Spent Fuel Dry Storage Canister

Donghee Lee* and Yongdeog Kim
KHNP Central Research Institute, 70, Yuseong-daero 1312beon-gil, Yuseong-gu, Daejeon, Republic of Korea
*donghee.lee@khnp.co.kr

1. Introduction

According to the 'basic plan of HLW management' announced by Korean government, a spent fuel(SF) dry storage facility will be construct in NPP sites[1]. In the US, SF dry storage facility has been in operation for a long period of time and many studies have been conducted. In particular, the importance of research on aging management of a dry storage canister has been emerged recently. A typical aging phenomenon of the SF dry storage canister is Chloride-Induced Stress Corrosion Cracking (CISCC). In the case of Korea, the sea is composed of three sides. It is expected that it will be affected by chloride ion during dry storage. Therefore, this paper reviews various mitigation technologies applicable to the CISCC of stainless steel canister on the SF dry storage cask.

2. Pending Issue of the CISCC

In general, a canister made of austenitic stainless steel can cause a CISCC under saline environment with high welding residual stresses present in the canister [3]. Crack growth caused by the CISCC can penetrate the walls of the canister and cause a leakage. Furthermore, crack growth can cause breakage of the canister, which can lead to do harm a containment safety requirement of the canister. To prevent this phenomenon, the CISCC mitigation technology should be studied sufficiently.

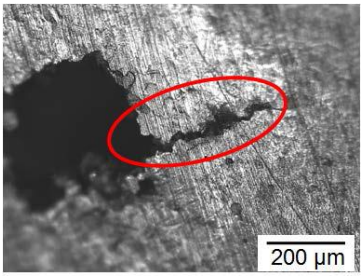

Fig. 1. Pit Serving as Initiation Point for CISCC.

3. Methods of the CISCC mitigation [4]

For CISCC of austenitic stainless steel, there are three components that must be simultaneously present for CISCC degradation to occur as bellows; elevated tensile stress, susceptible material and Corrosive or aggressive environment. In particular, these factors all may be present for the welded regions of the stainless steel canisters. Removing one or more of the components listed above will effectively mitigate the potential for CISCC of the canister external surfaces.

3.1 Applicability for Remediation of Existing Corrosion and Cracks

Some mitigation techniques can also provide remediation or repair of cracked canisters. Examples of such techniques are laser beam overlay/cladding, friction stir welding and encapsulation. In general, techniques which are capable of remediating existing cracks are those which are capable of (1) creating a pressure boundary that does not include the cracked area of material, (2) isolating the crack such that either chemical half-reaction of the corrosion cell cannot occur, or (3) eliminating the crack.

3.2 Surface Stress Improvement Techniques

The surface stress improvement techniques generally work by inducing a plastic strain in a layer of material near the surface of application which results in an elastic relaxation that generates compressive stresses. The potential deleterious effect of the additional cold work is negated by the presence of compressive residual stress, which removes the tensile stress needed for SCC to occur. All of the techniques described below are in-use by the nuclear industry to mitigate the susceptibility to SCC; shock-based (laser & water jet) peening, shot

peening, low plasticity burnishing and ultrasonic-driven surface stress improvement techniques. Each technique is generally known to achieve 1 mm depth of compressive residual stress.

3.3 Use of Corrosion Resistant Materials

The use of materials resistant to CISCC under atmospheric dry storage conditions can prevent the occurrence of SCC in austenitic stainless steels by applying a certain material that CISCC cannot readily initiate and propagate through. The combination of mechanical, thermal, and atmospheric corrosion requirements that a material used in construction of a canister needs to meet significantly narrows the range of appropriate materials. The highly alloyed nature of the materials described below serves to make their implementation less economically viable for many locations; **I**ron-based alloys, nickel-based alloys

3.4 Isolation of Surface from Corrosive Environment

Even if the canister material is susceptible to CISCC in the presence of deliquescent chlorides, susceptibility to CISCC can be reduced or eliminated by ensuring that this corrosive environment does not develop on the surface of the canister. There is the three approaches to isolating surfaces of the welded stainless steel canister from a corrosive environment: addition of material as a barrier between the canister surface and the environment, application of a coating to the canister surface and modification of the environment within the over pack to ensure that a corrosive environment does not develop.

Fig. 2. Laser Beam (left), Ultrasonic Peening (right).

4. Conclusion

This paper reviews the CISCC mitigation technique for a dry storage canister made of austenitic stainless steel. The CISCC occurs caused by elevated tensile stress, susceptible material, or corrosive or aggressive environment. To mitigate the occurrence of CISCC, it is necessary to reduce the tensile residual stresses as well as using of a material resistant to CISCC under dry storage conditions or modifying the canister surrounding environment to sequester corrosive species from CISCC-susceptible material. This paper is expected to help to make a strategy on the CISCC mitigation of dry storage containers in the future.

REFERENCES

[1] Notice of the Ministry of Trade, Industry and Energy, ‘Basic Policy on High Level Radioactive Waste Management’ (2016)

[2] EPRI Report 1003416, “Technical Bases for Extended Dry Storage of Spent Nuclear Fuel”, Palo Alto, CA, 2002.

[3] U.S NRC, “Assessment of Stress Corrosion Cracking Susceptibility for Austenitic Stainless Steels Exposed to Atmospheric Chloride and Non-Chloride Salts”, 2014

[4] EPRI Report 3002008193, “Aging management Guidance to Address Potential Chloride-Induced Stress Corrosion Cracking of Welded Stainless Steel Canisters, 2017.

Preliminary Study of Annular Fuel Fabrication Using Hot Extrusion Method

Sang-Gyu Park*, Kiho Kim, and Jeong-Yong Park
Korea Atomic Energy Research Institute, 111, Daedeok-daero 989beon-gil, Yuseong-gu, Daejeon, Republic of Korea
*sgpark82@kaeri.re.kr

1. Introduction

The innovative fuel fabrication development is the development of the advanced ultra-high burnup sodium-cooled fast reactor metallic fuel concepts. The fabrication experiment seeks to investigate advanced fuel designs with the following features: decreased fuel smeared density (SD), venting of the fission gas to the sodium coolant, reduce the FCCI (Fuel Cladding Chemical Interaction), and an advanced fabrication method that includes consideration of annular fuel and extrusion method. The one of most attractive advantage of extrusion method is save the process waste by omitting the sodium process. From the previous study, annular fuel shows the possibility of the reduction of swelling effect and then prevention of the FCMI (Fuel Cladding Mechanical Interaction) [1]. However, the fabrication technology of the annular fuel has not been developed yet. Hence, KAERI has started to study the annular fuel fabrication method by using hot extrusion method. In this study, the prototype of annular fuel has been fabricated by using Cu billet. The design of billet and annular fuel has been determined, and then and design and material for the mold has been determined by using Deform 3D program. After the mold fabrication, the prototype annular fuel has been fabricated and its texture were examined by us EBSD (Electron Back Scatter Diffraction).

2. Result & Discussion

2.1 Design of Billet & Annular Fuel

The size of the billet and the fuel core specimens for the production of the annular simulated fuel shims were determined. In the case of the fuel padding, the annular shape having a diameter of 5 mm and a smear density of 75% was selected as a ring 10 mm in diameter. In the case of a billet, a diameter of 40 mm was selected by extrusion. The inside of the billet was designed to be easily manufactured into an annular shape by extruding holes of the same size as annular fuel.

2.2 Preliminary Fabrication of Annular Fuel

Based on the analysis results, the jig design was designed, and the mold was manufactured based on the design. In the simulated fuel core extrusion, a press machine capable of extruding a maximum of 200 tons was used, and the extrusion was performed by inserting the billet before extrusion into a mold set at 450°C after heating at 600°C. As a result of the extrusion, it was possible to successfully fabricate the annular fuel. The microstructure distribution of Cu annular fuel after extrusion was analyzed using Electro Back-Scattered Diffraction (EBSD). Cu has a phase centered cubic crystal structure (face centered cubic (FCC)) at room temperature. Cu has a fine grain size of several um to several tens of μm after extrusion. This tendency is different from that of an

general extruded structure exhibiting anisotropy along the machining direction. This is attributed to the fact that the microstructure of the billet formed in the initial machining already has a fine grain size.

Fig. 1. Extrusion equipment.

Fig. 1 shows the result of analyzing the temperature at each part during actual extrusion. The extrusion conditions were selected based on the extrusion of the annular simulated fuel core with Cu at a maximum temperature of 726°C.

2.3 Microstructure Analysis of Billet

In order to analyze the cause of the fine grains of the Cu annular fuel, the microstructure of the billet produced by the conventional machining is analyzed by EBSD. The texture of the treated billet was similar to that of the microstructure after extrusion, but it showed a tendency to have a grain size of at most 100 um or more, which is relatively coarser than that of the extruded fuel core. Therefore, it is considered that the non-anisotropic crystal tendency analyzed after extrusion production is attributed to the fact that the crystal grains used in the processing billet are already small in size. In order to study the anisotropy control in the extrusion process, it is judged to be appropriate. Therefore, in the future extrusion process research, the test will be carried out using the directly melt-cast billets.

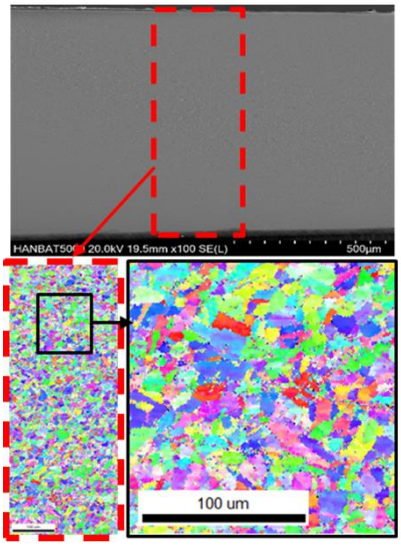

Fig. 2. Texture analysis annular fuel (L direction).

3. Conclusion

In this study, the prototype of annular fuel has been fabricated by using hot extrusion method. The mold for annular fuel was designed using Deform 3D, and the fabrication was successfully done by press extrusion method.

ACKNOWLEDGEMENT

This work was supported by the National Research Foundation of Korea funded by the Ministry of Science and ICT (2017M2A8A5014888).

REFERENCES

[1] K. Marsden, "Report on Development of Concepts for the Advanced casting System in Support of the Deployment of a remotely Operable Research Scale Fuel Fabrication Faculty for Metal Fuel", INL/EXT-07-12469

Speculation on the Boundary Conditions of Spent Fuel Evaluation During Transportation

Donghyo Lee*, Seongki Lee, and Jongsung Yoo

KEPCO Nuclear Fuel, 242, Daedeok-daero 989beon-gil, Yuseong-gu, Daejeon, Republic of Korea

*donghyo@knfc.co.kr

1. Introduction

Integrity of spent fuel (SF) shall be assessed conservatively with general applicability. Characteristics of SF and boundary conditions such as cask properties etc. are necessary to evaluate the integrity of SF. Especially, SF transportation cask shall be designed to meet the regulatory drop accident impact onto unyielding surface. In order to satisfy the requirements, detachable impact limiters which can absorb the kinetic energy are used, but each design is unique and characterized by vendor-proprietary [1]. Using the results of the EPRI [2], impact limiters are replaced by concrete pad with target hardness model. In this paper, we analyzed the target hardness model and the scheme of SF integrity evaluation is to suggest.

2. Methodology of SF Cask Drop

2.1 Target Hardness Model

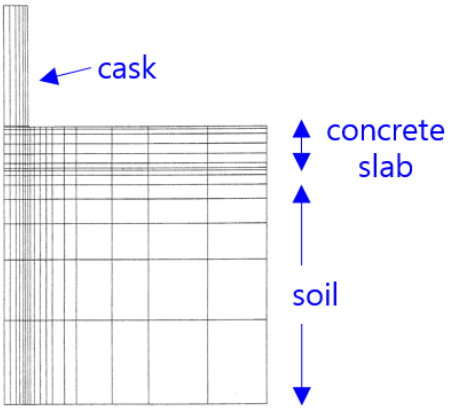

Fig. 1. Finite element model of the cask and the target.

Impact limiter reduces the impact loads on the cask and internal SF. Because of vendor-proprietary, EPRI developed target hardness model. In the model, crushing and cracking of the concrete and deformation of the soil present dissipation of impact energy instead of impact limiter. Target means concrete pad with reinforcements and soil layer. A finite element model of the cask and the target is shown in Fig. 1. Using this model, responses of the target considering complex concrete properties are obtained. In simulation of falling cask onto impact target, coupling between cask and target is complex. To simplify the analysis, assumption that the cask is infinitely rigid is used. Characteristics of target is described by single non-dimensional variable, target hardness number S. S is given below.

$$S = 2rAkM_u\sigma_u/(W^3(1 - e^{-\beta r}cos\beta r)) \quad (1)$$

Parameters are given by:

r: radius of the cask

A: cask footprint area

k: foundation modulus

M_u: ultimate moment capacity of the concrete

σ_u: ultimate strength of the concrete

W: weight of the cask

$\beta = (E_s/4D_c)^{1/4}$

$D_c = E_c h^3/(12(1-\nu_c^2))$

E_s: Elastic modulus of soil

E_c: Elastic modulus of concrete

h: height of concrete

ν_c: Poisson's ration of concrete

Target hardness number is dependent on properties of concrete and soil

2.2 Full-Scale Drop Tests

In order to verify the target hardness model, NRC contracted British Nuclear Fuels Limited (BNFL) to conduct full-scale drop tests. In tests, a 64.5-metric-ton cask was dropped onto a 3-foot reinforced concrete slab at 18-inch, 40-inch, and 60-inch drop heights.

3. Results and Discussion

Table 1. Summary of calculated decelerations with data

Drop Height	Data	Analysis
18 in	48 g	50 g
40 in	56 g	64 g
60 in	73 g	73 g

The experimental steady deceleration was achieved by integrating the first pulse of the acceleration data divided by the time duration of the pulse. Table 1 shows the summary of decelerations. The model has been validated by experimental data [3]. As can be seen from the Table 1, analysis and tests results are in good agreement.

4. Conclusion

Integrity evaluation of SF is essential for transportation and dry storage of SF. To evaluate the integrity of SF, global analysis of cask-SF is required, as shown in Fig. 2. KNF developed indigenous integrity evaluation model for dry storage and transportation. Target hardness model is to be used in integrity evaluation of SF before the design of specific cask and impact limiter is decided.

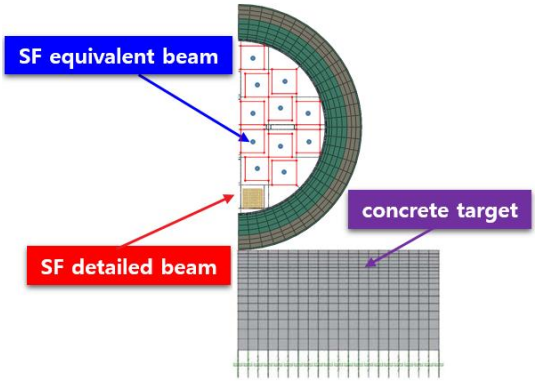

Fig. 2. KNF integrity evaluation model of SF.

ACKNOWLEDGEMENT

This work was supported by the Korea Institute of Energy Technology Evaluation and Planning (KETEP) and the Ministry of Trade, Industry & Energy (MOTIE) of the Republic of Korea (No. 2014171020166C).

REFERENCES

[1] R. James, J. Rashid, R. Dunham and L. Zhang, “Spent Fuel Transportation Applications: Fuel Rod Failure Evaluation under Simulated Cask Side Drop Conditions”, EPRI Technical Report 1009929, June 2005.

[2] Y. R. Rashid, R. E. Nickell, R. J. James and L. Zhang, “Validation of EPRI Methodology of Analysis of Spent-Fuel Cask Drop and Tipover Events”, EPRI Report TR-108760, August 1997.

[3] A. J. Sparkes, J. E. Gillard and P. A. Sims, “Full-Scale Drop Tests for Benchmarking Concrete Pads for Dry Spent Fuel Storage Casks”, AEA Technology, Report No.AEA-D&W-0622, July 1993.

Research Status on Long-term Performance of Seals for Spent Fuel Transport and Storage Casks

Yun-young Yang*, Jongmin Lim, and Woo-seok Choi
Korea Atomic Energy Research Institute, 111, Daedeok-daero 989beon-gil, Yuseong-gu, Daejeon, Republic of Korea
*Yang0124@kaeri.re.kr

1. Introduction

Seals are often used as a main component for the containment of cask for spent fuel transport and storage. Accordingly, various projects have been performed to evaluate the containment performance of seals in the world's leading nuclear power advanced countries.

Therefore, this paper describes the technology trends related to the research on the containment integrity of the seal in Korea and abroad.

2. Research Status

2.1 Domestic

In the "Securement of comprehensive safety verification technology of spent fuel storage and transportation system" project, which was completed in 2016, the proof test was conducted on the metal seal through development of the spent fuel transportation and storage system [1]. In this test, the accelerated method using the Larson-Miller parameter was used to evaluate the containment integrity of the KORAD-21 dual purpose metal cask through two accelerated tests. Accelerated test results have shown that the containment integrity is maintained for 50 years [2].

2.2 United States

In the United States, various tests have been carried out on spent fuel transportation/storage technology since the late 1970s. Recently, R&Ds related to long-term storage have been invested intensively. There has been a growing demand for public interests and regulatory issues on the beyond-design-basis accidents of spent fuel transport and storage systems since 9/11.

The NIST researchers conducted various tests to evaluate the containment integrity of metal and polymer seals under heat exposure conditions that could occur during the beyond-design-basis fire accident, and found that leakages occurred in the metal and polymeric seals under some conditions [3].

SRNL researchers have investigated the aging behavior of elastomer-based Viton GLT and GLT-S O-rings for the purpose of supporting 9975 transport cask for the transportation and storage of Plutonium, and developed a lifetime predictive model [4] . The predictive model based on the compressive stress relaxation test data expected that seals have a life expectancy of about 8 years at a maximum expected temperature of 93°C and decades at a practical operating temperature of 66°C or less. After six years of testing, the package showed only a small compression effect on the O-ring and no significant performance degradation was found.

2.3 Japan

Japan conducted researches on the safety test and the containment integrity evaluation of the transportation cask with the original scale test facility. To evaluate the containment integrity of metal gaskets in the long-term storage, prototype test models including two types of cask lids were developed and used for tests during 19 years [5]. The containment performance proved that the silver jacket gasket showed better results than the aluminum jacket gasket and had a very stable containment performance over 19 years.

In Japan, CRIEP also worked with CEA, TECHNETICS in France and GNS in Germany to study metallic seals. Surface inspection of the metal seal after 100,000 hours at several temperature ranges was carried out, and the behavior of the metallic seal according to change in load were investigated by an analytical method [6,7].

2.4 Germany

Germany conducted a safety evaluation test at

original scale on the transport and storage casks from the end of the 1970s. Various tests have been carried out to show the adequacy of containment evaluation using the reduced model and to obtain the safety factor. The BAM researcher conducted tests to evaluate the behavior of the metallic seal under normal conditions and accident conditions during cask transportation, and evaluated the performance degradation factors of metallic seal for long - term storage under various parameters [8]. Tests of the containment integrity of the seal were carried out to evaluate the effects of axial and radial impact loads and the effects of particles on the seal and flange surface, chemical resistance and corrosion.

In recent years, research has been carried out on elastomeric seals at low and high temperature [9]. In the metallic seals, stress relaxation with respect to time has been researched. In the elastomeric seals, design life has been evaluated by determining the compressibility of the seal with respect to temperature and time.

3. Conclusion

The trends of three countries that study the containment integrity including domestic and abroad are described in this paper. Major advanced countries have already reached leading position by conducting precedent research. Korea needs to make efforts to secure the technology for evaluating the containment performance of the seals. It is also necessary to consider the interaction of flange, bolt, and seal with creep in addition to the study of seal performance.

ACKNOWLEDGMENTS

This work was supported by the KETEP and the MOTIE of the Republic of Korea (no. 2018710201770).

REFERENCES

[1] Woo-seok Choi, “Final Report on Development of Total Safety Tesf Technology for Spent Fuel Transport and Storage System”, Ministry of Trade, Industry and Energy, 2016.

[2] Yun-Young Yang, “Test Report for Containment Integrity of Metallic Seal of spent Nuclear Fuel Metal Storage”, KAERI/TR-6497/2016, 2016.

[3] Jiann C. Yang, Edward J. Hnetkovsky “Performance of Metal and Polymeric O-Ring Seals in Beyond-Design-Basis Temperature Excursions”, NUREG/CR-7115, US NRC, National Institute of Standards and Technology Engineering Laboratory, November 2015.

[4] T. Eric Skidmore, “Aging Behavior of the Viton Fluoro elastomer O-Ring in the 9975 Shipping Package”, SRNL-STI-2015-00017, US DOE, Savannah River Site. Researcher, 2015.

[5] CRIEPI, “Basis and Safety Case of Spent Fuel Storage”, IAEA Work Shop on DPC Safety Case, May 19-21, 2014.

[6] M. wataru, K.shirai, “Summary of recent results from the CEA-GNS-CRIEPI project on metal seals”, ESCP-2016, December 315-327, 2016, Charlotte.

[7] F.Ledrappier, J.F. Juliaa, “Numerical simulation of HELICOFLEX® metallic gasket ageing mechanism for spent fuel”, PATRAM 2016, September 18-23, 2016, Kobe.

[8] S. Schubert, “Behavior of Metallic Seals in CASTOR®-Casks under Normal and Accident Conditions of Transport: Qualification Requirements”, PATRAM 2009, Vol.20 179-182, 2009.

[9] Dietmar Wolff, “METAL AND ELASTOMER SEAL INVESTIGATION”, ESCP 2015, December 153-174, 2015, Charlotte.

Performance of the Reaction of Rare Earth and UCl_3 in the LiCl-KCl Salt

Seungwoo Paek*, Dal-Sung Yoon, Gha-Young Kim, Junhyuk Jang, and Sung-Jai Lee
Korea Atomic Energy Research Institute, 111, Daedeok-daero 989beon-gil, Yuseong-gu, Daejeon, Republic of Korea
*swpaek@kaeri.re.kr

1. Introduction

KAERI (Korea Atomic Energy Research Institute) has developed pyroprocessing technology to resolve a limited storage capacity of the accumulated used nuclear fuel (UNF) in Korea [1]. Uranium and transuranic (TRU) elements from UNF can be recovered by electrochemical method in the molten salt. TRU products recovered from pyroprocessing can be supplied to sodium-fast reactor (SFR) as a metal fuel, and may affect the burning of nuclear fuel and the integrity of the fuel claddings if the rare earth (RE) content is high [2]. Therefore, it is necessary to keep the RE content of TRU product for use as SFR fuel as low as possible. In this study, we investigated the performance of the reaction of RE elements and UCl_3 in the LiCl-KCl molten salt.

2. Experimental

U/RE metal alloy containing U, Nd, and Ce was prepared by heating the metals up to 1474 K using an induction furnace. The prepared U/RE ingot was cut to a certain size for the experiments of the reaction between U/RE and UCl_3. All experiments were conducted in a glove box filled with purified argon and the concentration of oxygen and water were maintained to be below 5 ppm. The concentrations of each element in the salt were determined by ICP-OES. The cyclic voltammetry (CV) measurements were also performed to monitor the concentration of uranium and RE chlorides in the salt. The surface of metal specimen was investigated by XRD and SEM-EDX.

3. Results and Discussion

3.1 Gibbs Free Energy for the Reaction of RE Metals with UCl_3

The reaction between RE elements and UCl_3 proceeds as shown in the following equation.

$$RE(Nd/Ce) + UCl_3 = RE(Nd/Ce)Cl_3 + U \quad (1)$$

This reaction is based on the difference in Gibbs free energy of chloride formation between uranium and RE elements. Using this reaction, the uranium remains in a metal form and the RE elements are converted into a chloride form and dissolved into a molten salt.

3.2 Preparation of U/RE Ingot

Fig. 1 shows schematic diagram of a furnace for the U/RE ingot production and the prepared U/RE specimen for the reaction. The prepared U/RE specimen was visually identified as being separated into two areas and is assumed to be due to the difference of the specific gravity between the U and RE elements.

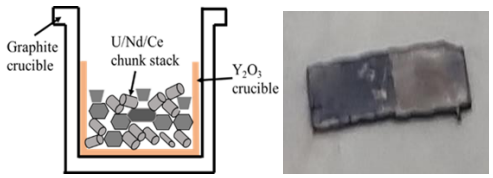

Fig. 1. Preparation of U/RE ingot.

3.3 RE Removal Reaction

Fig. 2 shows the concentration changes of the UCl_3, $CeCl_3$, and $NdCl_3$ in the salt by the reaction of U/RE ingot with UCl_3. Uranium concentration decreased to a near zero about an hour after reaction. On the other hand, the concentration of Ce and Nd increased rapidly to about an hour after reaction, and then to a very small amount, maintaining a nearly constant concentration.

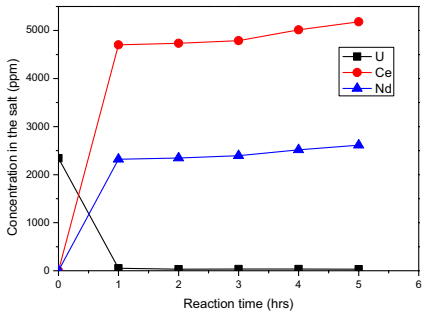

Fig. 2. Concentration change of the reaction salt.

Fig. 3 shows the U/RE specimen after the reaction experiment and results of SEM-EDX analysis. These results shows that RE part of U/RE specimen has been completely removed and only U part remains.

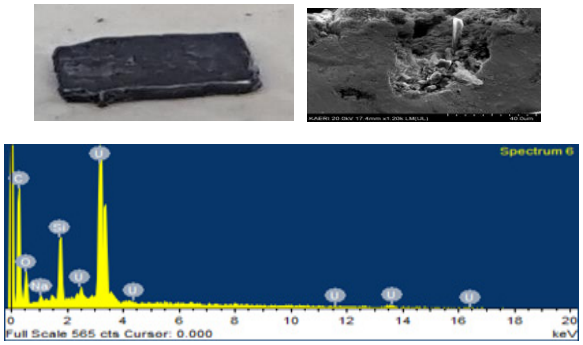

Fig. 3. SEM-EDX results of the surfaces of the U/RE specimen after the reaction.

4. Conclusions

The performance test of the reaction between U/RE ingot and UCl_3 was investigated and it was shown that the RE elements from U/RE ingot was effectively removed using UCl_3 as an oxidant.

ACKNOWLEDGEMENT

This work was supported by a National Research Foundation (NRF) grant funded by the Korean government (MSIP) (No.2017M2A8A5015079).

REFERENCES

[1] K. C. Song, et al., “Status of Pyroprocessing Development in Korea”, Nuclear Engineering and Technology, 42, 131-144 (2010).

[2] Y. I. Kim et al, “SFR Development Strategy for the Re-use of Spent Fuel in Korea”, Nuclear Engineering and Technology, 40(6), 517-526 (2008).

Concentration Change of Electro-refining Salt With the Conditions of a Reduced Fuel

Seungwoo Paek*, Chang Hwa Lee, and Sung-Jai Lee

Korea Atomic Energy Research Institute, 111, Daedeok-daero 989beon-gil, Yuseong-gu, Daejeon, Republic of Korea

*swpaek@kaeri.re.kr

1. Introduction

Electrolytic reduction is a unit process of pyroprocessing to convert the spent oxide fuel into metallic form in Li_2O-LiCl salt at 650℃. KAERI is using a technology that combines the metal reduction by Li and the reductive reaction of Li_2O to Li to occur simultaneously in an electrolytic cell [1]. The electro-refining is the process of recovering uranium by the electrochemical reaction from the reduced metal by the electrolytic reduction [2]. The composition of the reduced metal product produced in the electrolytic reduction process of pyroprocessing affect the concentration of UCl_3 in the molten salt of the electro-refining process and this concentration of UCl_3 is an important operating parameter for the electro-refining process. Therefore this study aims to contribute to improve the efficiency of electro-refining operation by evaluating the concentration of UCl_3 and the amount of TRU accumulation in the electro-refiner.

2. Design for the prediction of UCl_3 concentration

The conditions of the standard spent nuclear fuel (SNF) are set to 55,000 MWD/MTU and 10 years cooling of 10 MTU for U-235 4.5wt%. The capacity of the electro-refiner was based on 50 kg/batch and the amount of the major radionuclide groups are shown in Table 1.

Table 1. The amount of major radionuclide group for the standard SNF based on 50 kg/batch

Radionuclide groups	Contents (g)
U	46,470
TRU	682
(Pu)	(582.3)
RE	856

In this study, it is assumed that the total TRU and RE elements of the reduced metal supplied to the electro-refining are dissolved in reaction with UCl_3. Based on the 10wt% salt accompanied with the reduced metal, the concentration change of UCl_3 was calculated on the assumption that concentration of Li_2O varies from 1 ~ 10wt%.

3. Results and Discussion

3.1 UCl_3 Concentration by the Operation of Electro-refiner

Fig. 1 shows the concentration changes of the chloride elements for the electro-refiner salt according to electro-refining operation. Starting with the initial UCl_3 concentration of 9wt%, UCl_3 concentration was decreased as batch operation progresses. TRU and RE elements of the reduced metal dissolved in the chloride form, resulting in an increase in the concentration. The TRU/U ratio in the salt also increased with the recovery of uranium and the accumulation of TRU elements under electro-refining operation.

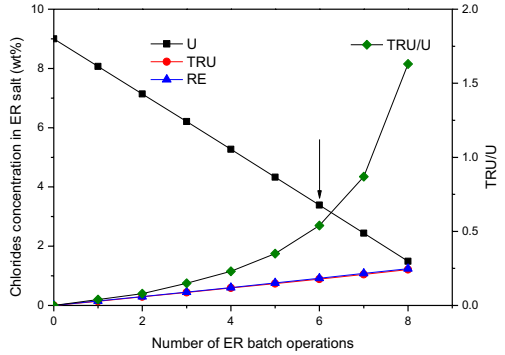

Fig. 1. Concentration change of chlorides by electro-refining operation.

3.2 UCl_3 Concentration in the Electro-refiner by the Residual Li_2O

Fig. 2 shows a change in UCl_3 concentration in the electro-refiner compared to the absence of Li_2O when Li_2O of 1wt% accompanied by the reduced metal transferred to the electro-refiner and the change in the ratio of TRU/U for salt in the electro-refiner also shown. If there was no effect of Li_2O, it was allowed to operate 6 batches to maintain UCl_3 concentration above 3wt%, but if Li_2O 1wt% is introduced to electro-refiner, only 5 batches can be operated.

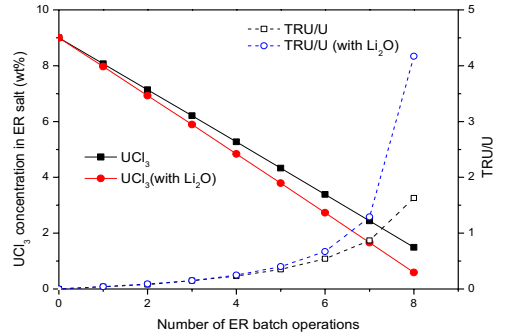

Fig. 2. UCl_3 concentration changes with Li_2O 1wt%.

4. Conclusions

The evaluation of the concentration change of UCl_3 and the accumulation of TRU and RE elements in the electro-refiner according to the conditions of the reduced fuel (especially Li_2O concentration) are expected to improve the efficiency of electro-refining operation.

ACKNOWLEDGEMENT

This work was supported by a National Research Foundation (NRF) grant funded by the Korean government (MSIP) (No.2017M2A8A5015079).

REFERENCES

[1] E. Y. Choi, et al., “Reoxidation of Uranium in Electrolytically Reduced Simulated oxide fuel during Residual Salt Distillation”, JRNC, 314, 207-213 (2017).

[2] J. J. Laidler et al, “Development of Pyroprocessing Technology”, Progressive of Nuclear Energy, 30, 131-141 (1997).

Mass Transfer Analysis on a Rotating Cylinder Electrode in the Molten-salt Electrolyte

Kwang-Rag Kim*, Sung-Ki Kim, and Hyo-On Nam

Korea Atomic Energy Research Institute, 111, Daedeok-daero 989beon-gil, Yuseong-gu, Daejeon, Republic of Korea

*krkim1@kaeri.re.kr

1. Introduction

Pyrochemical processing for the treatment of spent nuclear fuel consists of a series of molten-salt electrochemical reactors as the main processes [1]. This process typically involves the dissolution of spent fuel into a molten-salt media and selective deposition on the electrode.

A successful design of the electrochemical reactors is desirable for a product attainment at the planed throughput, at the projected performance and with the desired quality standards. Its throughput depends exclusively on the mass transfer kinetics in a commercial-scaled system.

The rotating cylinder electrode (RCE) has found a wide variety of applications in the investigation for the commercial-scaled system. This investigation is of industrial importance and allow modeling and quantification of electrode reaction rates, when the process limited by the rate of mass transfer.

In this study, a CFD (Computational Fluid Dynamics) modeling approach was used and simulated to compare with a typical mass transfer correlation for RCE in the molten-salt electrodeposition system.

2. Theory

2.1 Mass Transport Correlation

The electrolyte turbulent flow at the RCE can bring ionic solute from the solution to the surface of the electrode. The mass transport to and from the electrode surface is often the factor which governs the rate of electrode reactions.

Early investigations by Eisenberg [2] provide the most commonly accepted description for RCE mass transport.

The Sherwood number (*Sh*) correlation for rotating cylinder electrode is given by [2]

$$Sh = \frac{k_i d_e}{D_i} = 0.079 Re^{0.7} Sc^{0.356} \quad (1)$$

where, k_i (cm/s) is the mass transfer coefficient to a rotating cylinder, *S*c is the Schmidt number ($= \frac{\mu}{D_i \rho} = \frac{\nu}{D_i}$), d_e is the equivalent diameter (cm), ρ is the electrolyte density (g/cm^3), μ is the absolute viscosity of the solution (g/cm s), and D_i is the diffusion coefficient (cm^2/s).

The electrolyte turbulent flow is often characterized using the Reynolds number (*Re*) to quantify the ratio between inertial forces and viscous forces in an electrolyte solution. For a rotating cylinder electrode with outer diameter, d_{cyl} (cm), and radius, $r_{cyl}=d_{cyl}/2$, the linear velocity, U_{cyl} (cm/s), at the outer surface of the cylinder is given by

$$U_{cyl} = \omega r_{cyl} = \frac{\pi d_{cyl}\, rpm}{60} \quad (2)$$

where, the rate can either be expressed as angular rotation, ω (rad/s), or as revolution rate, rpm.

Accordingly, the *Re* is

$$Re = U_{cyl} d_{cyl} \frac{\rho}{\mu} = \frac{\pi d_{cyl}^2 \, rpm}{60} \times \frac{\rho}{\mu} \qquad (3)$$

2.2 CFD Model

The mass transfer rate (j_w) per unit area from the bulk electrolyte to the cathode surface may be related with mass transfer coefficient (k_i) and described as:

$$j_w = -D_i \frac{\partial C}{\partial r}\Big|_w = -k_i (C_{bulk} - C_w) \qquad (4)$$

The first term indicates that the concentration gradient in the radial direction can be evaluated at the electrode surface in the CFD platform (fig.1). The local Sh_x can be obtained from the precedent mass flux in the spatial domain:

$$Sh_x = \frac{-d_{cyl} \frac{\partial C}{\partial r}\Big|_w}{C_{bulk} - C_w} \qquad (5)$$

3. Results and Discussion

The polarization concentration under a range of turbulent flow has been analyzed in terms of rotating speed of RCE. A CFD model developed here makes it easy to predict the quantitative mass transfer rate from any concentration profiles caused by electrochemical polarization. The Sherwood numbers based on the simulated values of the solute concentration profiles were compared with the Eisenberg correlation. Those are reasonably similar to each other at the mass transfer limited regions.

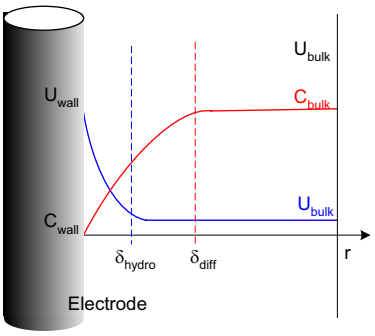

Fig. 1. Schematic of the concentration and velocity profiles for the RCE near the hydrodynamic boundary layer (δ_{hydro}) and diffusion boundary layer (δ_{diff}).

4. Conclusion

This study demonstrated an approach of the coupled solution of electrochemical and mass transport kinetics in the cell employing a rotating cylinder electrode. The model implemented here can be useful to scale-up the RCE system for practical applications.

REFERENCES

[1] OECD NEA, "Spent Nuclear Fuel Reprocessing Flowsheet," NEA/NSC/ WPFC/DOC, Paris, 15 (2012).

[2] M. Eisenberg, C.W. Tobias and C.R. Wilke, "Ionic Mass Transfer and Concentration Polarization at Rotating Electrodes," J. Electrochem. Soc., 101, 306 (1954).

[3] J. Lee and J.B. Talbot, "A Model of Electrocodeposition on a Rotating Cylinder Electrode," J. Electrochem. Soc., 154(2), D70-D77 (2007).

Determination of Alkali and Alkaline Earth Metal Oxide Solubility in Molten LiCl Salt at 923 K

Dokyu Kang[a], Seokjoo Yoon[a], Byung Heung Park[b], and Sungyeol Choi[a,*]

[a] Korea Advanced Institute of Science and Technology, 291, Daehak-ro, Yuseong-gu, Daejeon, Republic of Korea

[b] Korea National University of Transportation, 50, Daehak-ro, Daesowon-myeon, Chungju-si, Chungcheongbuk-do, Republic of Korea

[*]sungyeolchoi@kaist.ac.kr

1. Introduction

The behaviors of alkali and alkaline earth metal oxides in molten LiCl salt are known that they dissolve into the molten salt and react with LiCl and form metal chlorides. Because of their stability in chloride form, they are accumulated in the molten salt after repeated usage of the molten salt during electrolytic reduction process [1].

However, the dissolution mechanisms and kinetics of alkali and alkaline earth metal oxide in LiCl are still not clear. Therefore, mechanisms of metal oxide dissolution into molten salt and the determination method for metal oxide solubility were described in this paper.

2. Definition of Solubility of Metal Oxides in Chloride Molten Salt

Dissolution of metal oxides in molten salt can be described as solvation, interactions between the molten salt and dissolved metal oxides. This solvation consist of the following four reactions [2].

$$Me_xO_y\,(s) \Leftrightarrow Me_xO_y\,(l) \quad (1)$$

$$Me_xO_y\,(l) \Leftrightarrow xMe^{\frac{2y+}{x}} + yO^{2-} \quad (2)$$

$$Me^{\frac{2y+}{x}} + \frac{2y}{x}Cl^- \Leftrightarrow MeCl_{\frac{2y}{x}} \quad (3)$$

$$O^{2-} + 2M^+ \Leftrightarrow M_2O \quad (4)$$

Equation (1) describes solvation of the metal oxide without dissociation and Equation (2) is dissociation of metal cation ($Me^{\frac{2y+}{x}}$) and oxide ion (O^{2-}). Equation (3) and (4) describe fixation of metal cation by constituent anion (Cl^-) and that of oxide ion by constituent cation(M^+), respectively.

Therefore the solubility of metal oxides in molten salt is defined as sum of the saturated activities of metal cations ($a_{s,Me}$) and that of saturated non-dissociated oxide ($a_{s,\,Me_xO_y}$):

$$\sum s_{Me_xO_y} = a_{s,Me} + a_{s,\,Me_xO_y} \quad (5)$$

In this paper, the activities were treated simply as concentration.

3. Determination of Solubility of Metal Oxides in Chloride Molten Salt

The solubility of metal oxides in LiCl at 923 K can be determined by Isothermal Saturation Method (ISM) and Sequential Addition Method (SAM). First,

excessive amount of metal oxides were added into LiCl and heated up to 923 K. After enough time for the molten LiCl salt to be saturated with metal oxide, the molten salt was sampled by quartz samplers. This method is called Isothermal Saturation Method (ISM). The samples were analyzed by titration with 0.01 N of HCl and phenolphthalein indicator to determine the concentration of metal oxide in LiCl.

On contrary to ISM, Sequential Addition Method (SAM) does not require additional sampling of the molten salt. Instead, SAM is in-situ techniques to determine solubility of metal oxides in the molten salt. Because SAM measures changes in electromotive force, potential, result from the amount of dissolved metal oxide in the molten salt. The metal oxide was sequentially added to the molten salt and therefore the potential continuously decrease to more negative value.

However, after certain amount of addition of metal oxide, the potential dose not decrease further and the point can be thought as saturated amount of metal oxide in the molten salt. An oxide ion reversible indicator electrode and Ag^{+}/Ag reference electrode were used to measure potential changes caused by the concentration of oxide ions in molten salt. All experiment should be conducted in a glovebox-furnace combined system which maintain oxygen and moisture concentration below 1 ppm.

4. Conclusion

In this paper, mechanisms of metal oxide dissolution into molten LiCl salt were described and two methods (ISM and SAM) for determination of metal oxide solubility in LiCl salt at 923 K were suggested.

ACKNOWLEDGEMENT

This work was supported by the National Research Foundation of Korea (NRF) funded by the Ministry of Science and ICT (The grant number: NRF-2016M2B2B1945249).

REFERENCES

[1] B.H. Park, “Residual Liquid Behavior Calculation for Vacuum Distillation of Multi-component Chloride System”, Journal of the Korean Radioactive Waste Society, 12 (2014) 179-189.

[2] V.L. Cherginets, “Oxoacidity: Reactions of Oxo-compounds in Ionic Solvents”, Elsevier Science, 41 (2005).

[3] V.L. Cherginets, T.G. Deineka, O.V. Demirskaya, T.P. Rebrova, “Potentiometric investigation of oxide solubilities in molten KCl–NaCl eutectic.: The effect of surface area of solid particles on the solubilities”, Journal of Electroanalytical Chemistry, 531 (2002) 171-178.

Characterization of U-10wt.%Zr-5wt.%RE Fuel Remelt Residue for Recycle of Metallic Fuel Scrap

Ki-Hwan Kim[1,*], Seong-Jun Ha[1, 2], Seung-Uk Mun[1,3], Seok-Jin Oh[1], Seoung-Woo Kuk[1], and Jeong-Yong Park[1]

[1] Korea Atomic Energy Research Institute, 111, Daedeok-daero 989beon-gil, Yuseong-gu, Daejeon, Republic of Korea

[2] Yonsei University, 50, Yonsei-ro, Seodaemun-gu, Seoul, Republic of Korea

[3] Chungnam National University, 99, Daehak-ro, Yuseong-gu, Daejeon, Republic of Korea

[*]khkim2@kaeri.re.kr

1. Introduction

The conventional injection casting method of metallic fuel slugs for Gen-IV nuclear power system has the advantages of high productivity and excellent remote control, but shows a considerably low fabrication yield of about 50%, resulting in considerable amount of metallic fuel scraps containing a residue and fuel slug butts [1-3]. Hence, the recycling technology of the metallic fuel residue has been studied using chemical and mechanical surface treatment method in KAERI since 2016. KAERI could re-fabricate sound U-10wt.%Zr-5wt.%RE fuel slugs recycling initial metallic fuel residue, met with the quality criterion of metallic fuel.

In this study, the characteristics of the 2nd melt residue have been examined, and compared with the initial melt residue formed after re-fabrication of metallic fuel slugs so that the melt residue may be consecutively recycled in order to reduce the radioactive wastes in minimum and increase the fabrication yield of the metallic fuel in maximum.

2. Methods and Results

2.1 Experimental Methods

U-10wt.%Zr-5wt.%RE fuel slugs have been fabricated using pure depleted uranium and zirconium metal, and RE mother alloy with injection casting method. RE is a rare-earth alloy consisting of 53wt% Nd, 25wt% Ce, 16wt% Pr, and 6wt% La. Metallic fuel slugs have been obtained with initial melt residue after the injection casting. Metallic fuel slugs has been re-fabricated with the 2nd melt residue after injection casting with the recycle of initial melt residue. The characteristics of the remelt residue formed after injection casting have been examined, and compared with the initial melt residue. The microstructure and the composition of the melt residues were analyzed using scanning electron microscopy (SEM) and energy-dispersive spectroscopy (EDS).

2.2 Experimental Results

(a) (b)

Fig. 1. The surface states of the he 2nd melt residue of U-10wt.%Zr-5wt.%RE metallic fuel; (a) with plane view, (b) with front view.

The typical surface states of remelt residue of U-10wt.%Zr-5wt.%RE metallic fuel are shown in Fig. 1. Scanning electron micrographs and point analysis results by energy-dispersive X-ray spectroscopy showing the surface layer of U-10wt.%Zr-5wt.%RE remelt residue with as-cast state have been shown in

Fig. 2 and Table 1~2. The U-10wt.%Zr-5wt.%RE remelt residue showed RE-compounds of about 50 μm in thickness in the top surface with as-cast state, according to the integrated results of SEM and EDS analyses. The U-10wt.%Zr-5wt.%RE remelt residue in the bottom surface showed Y_2O_3 plasma-spray coating layer of about 50 μm in thickness as the first impurity layer on the bottom surface and RE-rich layer of about 40 μm in thickness as the second impurity layer. Thus, the surface impurity layers of the 2nd U-10wt.%Zr-5wt.%RE melt residue are similar with those of U-10wt.%Zr-5wt.%RE melt residue.

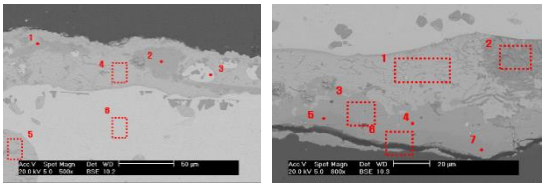

(a) (b)

Fig. 2. Scanning electron micrographs showing the surface layer of U-10Zr-5RE remelt residue with as-cast state; (a) top surface, (b) bottom surface.

Table 1. Point analysis results by energy-dispersive X-ray spectroscopy showing the top surface layer of U-10Zr-5RE remelt residue with as-cast state

Element (wt.%)	C	O	Y	Nd	Ce	Pr	La	Zr	U
#1	3.8	-	18.1	45.0	9.4	9.5	4.7	-	-
#2	3.9	-	16.9	45.2	9.7	10.0	4.6	-	-
#3	1.7	3.6	-	-	-	-	-	9.1	85.5
#4	3.6	2.2	-	49.6	20.2	16.3	8.2	-	-
#5	4.0	3.0	-	41.9	18.7	13.1	6.6	11.3	-
#6	1.7	4.0	-	-	-	-	-	11.5	82.8

3. Conclusion

The characteristics on the remelt residue of U-10wt.%Zr-5wt.%RE metallic fuel have been examined, and compared with the initial melt residue formed after re-fabrication of metallic fuel slugs for the consecutive recycle of the melt residue. The surface impurity layers of the 2nd melt residue are similar with those of the initial melt residue. Thus, the feasibility of the consecutive recycle of the fuel residues has been investigated by the characterization of the remelt residue of U-10wt.%Zr-5wt.%RE metallic fuel.

Table 2. Point analysis results by energy-dispersive X-ray spectroscopy showing the bottom surface layer of U-10Zr-5RE remelt residue with as-cast state

Element (wt.%)	C	O	Y	Nd	Ce	Pr	La	Zr
#1	2.5	2.6	-	49.8	21.3	15.5	8.3	-
#2	4.6	17.1	-	42.8	16.5	13.2	5.8	-
#3	3.3	11.0	20.3	41.7	8.7	9.1	4.1	1.8
#4	4.2	11.7	19.8	42.3	8.5	9.3	4.2	-
#5	7.4	12.9	48.8	20.6	4.2	4.5	1.6	-
#6	-	12.8	42.3	28.5	6.5	6.2	2.4	1.3
#7	7.3	12.7	50.0	19.9	4.0	4.3	1.8	-

ACKNOWLEDGEMENT

This work has been carried out under the Nuclear Research and Development Program supported by the Ministry of Science and Technology in the Republic of Korea.

REFERENCES

[1] L. C. Walters, B. R. Seidel, J.H. Kittel, “Performance of Metallic Fuels and Blankets in Liquid-Metal Fast Breeder Reactors. Nuclear Technology”, 65, 179-231 (1984).

[2] G. L. Hofman, L. C. Walters, T. H. Bauer, “Metallic Fast Reactor fuels”. Progress in Nuclear Energy, 31, 83–110 (1997).

[3] Crawford DC, Porter DL, Hayes SL. “Fuels for Sodium-cooled Fast Reactors: US Perspective”, Journal of Nuclear Materials, 371, 202–231 (2007).

Purification of LiCl Salt Waste Using Enhanced Melt-crystallization Method

Jung-Hoon Choi*, Ki-Rak Lee, Seung-Youb Han, Hyun-Woo Kang, and Hwan-Seo Park
Korea Atomic Energy Research Institute, 111, Daedeok-daero 989beon-gil, Yuseong-gu, Daejeon, Republic of Korea
*mrchoijh@kaeri.re.kr

1. Introduction

Korea Atomic Energy Research Institute (KAERI) is developing pyrochemical process for the recycling of PWR spent nuclear fuels using electrochemical method to achieve the volume reduction of radioactive waste [1-3]. During the process, LiCl salt wastes are planned to be recycled using melt-crystallization process. In this study, modified crystallization monitoring system has been developed to prevent over-growing of LiCl crystal on the crystallization plate during melt-crystallization process. Also, elimination method of corrosion products from reaction vessel has been investigated.

2. Experimental

Melt-crystallization tests were conducted using engineering-scale melt-crystallization system capable of 20kg/batch treatment. In this study, the tests were conducted using 10 kg of surrogate LiCl salt waste. The surrogate LiCl salt waste having 0.03wt% CsCl, 1.11wt% $SrCl_2$ and 2.31wt% $BaCl_2$ were charged in the crystallization vessel and melted at 700°C in the crystallization furnace. Then, crystallizer having 6 crystallization plates were immersed in the molten LiCl salt waste and the LiCl crystals were recovered on the 6 crystallization plates by cooling the plates using Ar coolant gas. Melt-crystallization process was terminated using modified crystallization monitoring system by measuring temperatures at each characteristic points. Nuclide separation efficiencies (%) were calculated by the relationship of $(C_{before}-C_{after})/C_{before} \times 100$, where C_{before} and C_{after} are nuclides concentration in the LiCl salt waste before and after crystallization process.

3. Results and Discussion

Fig. 1 shows the recovered LiCl crystal on the crystallization plates after melt-crystallization test. As shown in the Fig. 1 (a), when used previous monitoring system, over-grown LiCl crystal was found at the center part of crystallization plate owing to the temperature gradients. Meanwhile, modified crystallization monitoring system has been developed in consideration of temperature gradients within the reaction vessel, where the crystallization process of center part of crystallization plate is first terminated owing to the relatively high temperature. Therefore, as shown in the Fig. 1 (a), when used the modified crystallization monitoring system, we could obtain pure LiCl crystals on the crystallization plates with uniform distribution in terms of LiCl quantity. Also, the nuclide separation efficiencies were found to be enhanced as over 90% relative to that of purified LiCl crystal recovered using previous monitoring system.

Meanwhile, the crystal on the crystallizer shows some colors owing to the corrosion product generated from reaction vessel. To eliminate the corrosion product from crystal, the precipitation

method has been applied and clear LiCl crystal has been obtained after crystallization test.

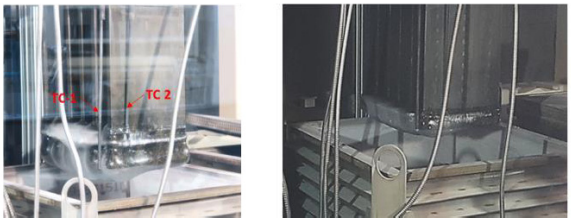

(a) (b)

Fig. 1. (a) Over-grown crystal grown by previous monitoring system, (b) Recovered LiCl crystal without over-growing using modified crystallization monitoring system.

4. Conclusion

In the present study, melt-crystallization monitoring system has been modified to prevent over-growing of LiCl salt on the crystallization plates by considering temperature gradient within the reaction vessel. Using the modified crystallization monitoring system, high nuclide separation efficiency was obtained with uniform distribution of LiCl salt on the crystallization plates. Also, clear LiCl crystal has been obtained using precipitation method eliminating the corrosion products.

REFERENCES

[1] H.S. Lee, J.M. Hur, J.G. Kim, D.H. Ahn, Y.Z. Cho, and S.W. Paek, “Korean Pyrochemical Process R&D activities”, Energy Procedia, 7, 391-395 (2011).

[2] H.S. Lee, G.I. Park, K.H. Kang, J.M. Hur, J.G. Kim, D.H. Ahn, Y.Z. Cho, and E.H. Kim, “Pyroprocessing technology development at KAERI”, Nucl. Eng. Technol., 43, 317-328 (2011).

[3] H.S. Lee, G.I. Park, J.W. Lee, K.H. Kang, J.M. Hur, J.G. Kim, S.W. Paek, I.T. Kim, and I.J. Cho, “Current Status of Pyroprocessing Development at KAERI”, Sci. Tech. Nucl. Install., 2013, 1-11 (2013).

Numerical Method to Estimate Uncertainties Associated With Positioning Error of Stain Measurement in Drop Test of Radioactive Waste Transport Casks

Jongmin Lim* and Woo-seok Choi

Korea Atomic Energy Research Institute, 111, Daedeok-daero 989beon-gil, Yuseong-gu, Daejeon, Republic of Korea

*jmlim86@kaeri.re.kr

1. Introduction

In this paper, a numerical analysis for the estimation of strain measurement uncertainties in a drop test of the radioactive waste transport casks is described. The numerical method is introduced to quantitatively estimate the uncertainty of the positioning error.

2. Sources of uncertainties in stain measurements

2.1 Sources of Uncertainties

There are various types of uncertainties that can be induced in strain measurements. Typical sources of such uncertainties are as follows:

- Sensitivity of stain gauge
- Temperature induced strain
- Location and alignment of strain gauge
- Signal processing unit error
- Data acquisition system error

In this paper, the uncertainty of location and alignment of strain gauge is considered

2.2 Uncertainties due to Location and Alignment of Strain Gauge

In attaching strain gauges on the surface of the specimen, errors can be introduced in the planar or angular directions from the intended position, thereby introducing uncertainty in the measured strain. Uncertainties due to this positioning error include manufacturing tolerances and errors of length measurement tool. These errors are statistically distributed around the intended nominal dimension and can be expressed as Table 1 in consideration of the manufacturing tolerances of the ISO standard [1] and the uncertainties of the rulers used in attaching the gauge. The uncertainties considered assume a uniform distribution.

Table 1. Uncertainties due to positioning error of stain gage

Uncertainty	Distribution	Range
Location error (L_1, L_2) [mm]	Uniform	[-10,10]
Misalignment angle (θ) [∘]	Uniform	[-5,5]

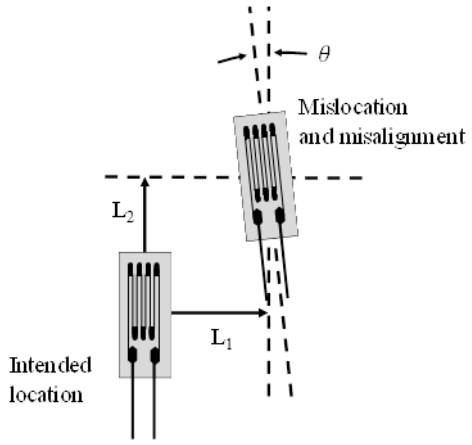

Fig. 1. Mislocation and Misalignment of Strain Gauge.

3. Numerical method to estimate the uncertainties due to mislocation and misalignment of strain gauge

3.1 Numerical Method

It is very difficult to obtain the uncertainty of the positioning error of the strain gauge through experimental methods. Therefore, the Monte Carlo simulation is performed to obtain the statistical distribution of the strain using the displacement field obtained from computational analysis.

3.2 Numerical Example

In order to verify the effectiveness of the method, a drop analysis is performed on a virtual metal rectangular cask as shown in Fig. 2. The strain uncertainties are measured at 6 points. The results of the estimated strain uncertainty are shown in Fig. 3. From the results, it can be seen that the uncertainty is signigicantly affected by the strain gradient. Therefore, it is desirable to attach the strain gauge to a point with low uncertainty as well as high magnitude of strain that can represent physical phenomena.

4. Conclusion

In order to estimate the uncertainties of positioning error of strain gauge, the numerical method is introduced. Using the drop analysis of the metal rectangular cask, the considered uncertainties can be quantitatively obtained.

ACKNOWLEDGMENTS

This work was supported by the KETEP and the MOTIE of the Republic of Korea (no. 20187102017770).

REFERENCES

[1] ISO 2768, “General Tolerances for Linear and Angular Dimensions”.

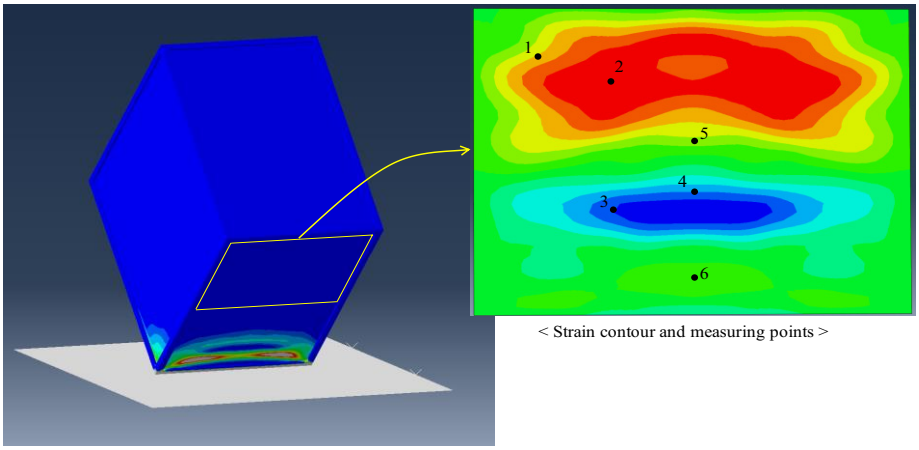

Fig. 2. Drop analysis of the metal rectangular cask.

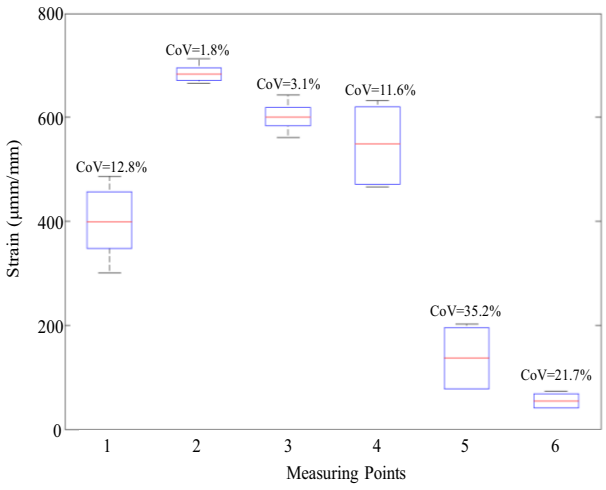

Fig. 3. Quantitatively estimated strain uncertainties.

Development of Si-Al-P Composites for Immobilization of Radioactive Waste Salt

Ki Rak Lee*, Hwan-Seo Park, Jung-Hoon Choi, Seung Youb Han, Hyun Woo Kang, Daegwon Eun, and Seona Jung

Korea Atomic Energy Research Institute, 111, Daedeok-daero 989beon-gil, Yuseong-gu, Daejeon, Republic of Korea

*kirakki@kaeri.re.kr

Pyroprocessing is of considerable technology for advanced recycling of spent fuel as no water is involved. Argonne National Laboratory (ANL) conducted the integral fast reactor (IFR) program and developed electrochemical and pyrometallurgical methods for the treatment of spent metallic fuel. At present, Korea Atomic Energy Research Institute (KAERI) is developing pyroprocessing to safely treat the nuclear spent fuel from pressurized water reactors (PWR). This technology has the advantage of proliferation resistance because the plutonium (Pu) is recovered with other minor actinides rather than as pure Pu. Several kinds of electrochemical processes such as electro-reduction, electro-refining, and electro-winning are included in pyroprocessing. Various kinds of salts such as LiCl, NaCl, KCl, and eutectic salts are used as electrolytes and hence waste salt, which is one of the more problematic wastes generated from pyroprocessing, is produced. At KAERI, LiCl and LiCl-KCl salt wastes are expected to be generated during pyroprocessing efforts. Therefore, it is very important to develop a proper method of waste salt treatment with disposal volume reduction as well as stable isolation from the biosphere.

The SAP (SiO_2-Al_2O_3-P_2O_5) process has been demonstrated to convert the metal chloride salt waste into manageable products at relatively low temperature to avoid evaporation of metal chlorides. The products can be fabricated as a monolithic waste form by adding a glassy material after the dechlorination process. Remarkable chemical durability and high waste loading for LiCl salt waste up to 40 mass% (prior to dechlorination) were achieved with the SAP waste form process. Compatibility between silicate and phosphate phase was generally very low because of immiscibility between the two phases. For the SAP waste form, silicate and phosphate phases were mixed with an intermediate micro-scale phase. Based on previous study, upgraded-SAP (U-SAP) was developed by controlling the composition of the glass phase, including the addition of B_2O_3, and then U-SAP waste forms were consolidated after the dechlorination process without chemical binder such as glassy material. The microstructure of the U-SAP waste form was very different from that of the SAP waste form, where the micro-sized phases were not present in the U-SAP waste form. In this study, U-SAP waste forms were prepared with LiCl salt including simulant radionuclides (CsCl, $BaCl_2$, $SrCl_2$) as a surrogate. Basic properties of dechlorinated products and waste forms were characterized with a variety of physical and chemical analyses. The structure of U-SAP waste form was investigated X-ray diffraction (XRD), transmission, scanning transmission, and scanning electron microscopies (i.e., TEM, STEM, and SEM, respectively), energy dispersive spectroscopy (EDS), secondary ion mass spectrometry (SIMS), and atom-probe tomography (APT).

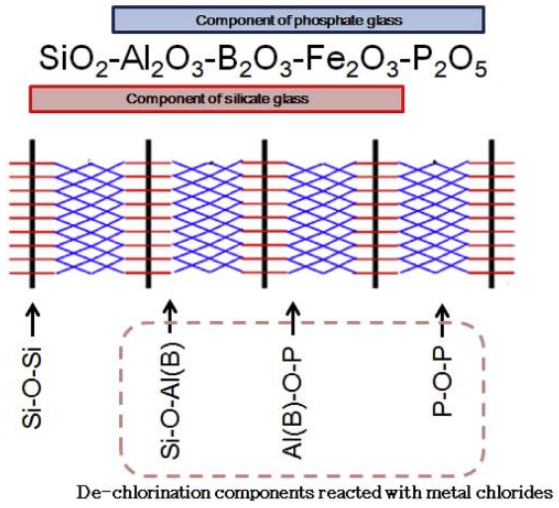

Fig. 1. Conceptual description of U-SAP composite.

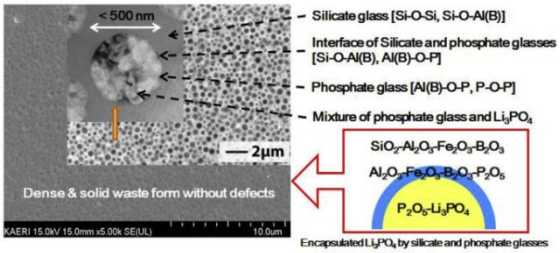

Fig. 2. Schematic image for structural concept of U-SAP waste form.

REFERENCES

[1] H.-S. Park, I.-T. Kim, Y.-Z. Cho, H.-C. Eun, H.-S. Lee, Environ. Sci. Technol. 42 (2008) 9357-9362.

[2] H.-S. Park, I.-H. Cho, H.-C. Eun, I.-T. Kim, Y.-Z. Cho, H.-S. Lee, Environ. Sci. Technol. 45 (2011) 1932-1939.

[3] K.R. Lee, H.S. Park, I.H. Cho, J.H. Choi, H.C. Eun, T.K. Lee, S.Y. Han, D.H. Ahn, Kor. J.Chem. Eng. 34 (2017) 2390-2396.

Development of Spent Fuel Nuclear Characteristic Evaluation System

Jae-Han Kim[1], Hyung-Moon Kwon[1,*], Young-Suk Jung[2], Young-Il Oh[2], and Eun-Kyung Lee[2]

[1] Korea Atomic Energy Research Institute, 111, Daedeok-daero 989beon-gil, Yuseong-gu, Daejeon, Republic of Korea

[2] ACT Co., Ltd. 1434, Yuseong-daero, Yuseong-gu, Daejeon, Republic of Korea

[*]django@kaeri.re.kr

1. Introduction

A research project aimed at safely transporting spent fuel (SF) stored at a post irradiation examination facility (PIEF) at KAERI to nuclear power plants (NPPs) has been performed. To achieve the safe transportation of SF from KAERI to NPPs, it is required to evaluate the accurate nuclear characteristics of SF. In this paper, we introduce a nuclear characteristic evaluation and inventory management system for SF stored at a PIEF. KAERI and Atomic Creative Technology (ACT) have developed an automated evaluation system for the nuclear characteristics of SF, which is to surpass the manual evaluation of nuclear characteristics using a code, ORNL SCALE: ORIGEN-S [1]. The system will lead to an increase in work efficiency and a reduction in human error regarding evaluations of nuclear characteristics.

2. SF Database Construction

An SF information database containing fuel design and operation histories has been created. It holds the following types of information:

- plant information and SF operation cycles;
- fuel type and model;
- fuel specification, including total uranium weight per assembly and rod, U-235 enrichment, zirconium alloy of cladding, and total weight of zirconium alloy per assembly and rod;
- nuclear core design information for each plant and cycle;
- fuel operation information including power history, cooling period and discharged data for each loading cycle.

3. SF Nuclear Characteristic Evaluation System

The developed SF nuclear characteristic evaluation system is designed to:

- manage SF information (C/R/U/D),
- evaluate nuclear characteristics of SF
- evaluate nuclear characteristics of SF container in transportation cask,
- generate an evaluation report, and
- manage system information.

3.1 Design of SF Nuclear Characteristic Evaluation System

The functional structure of the SF nuclear characteristic evaluation system is shown in Fig. 1. The system is configured to enable multiple users (clients) to share a DB server on a local network. Each user can perform information management, evaluation code execution, and result view.

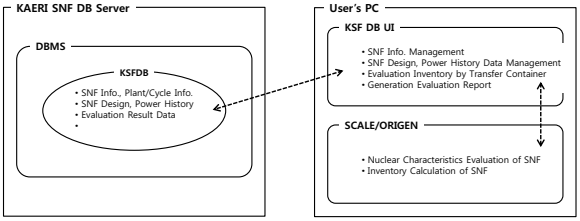

Fig. 1. Functional structure of SF nuclear characteristic evaluation system.

3.2 Implementation of SF Nuclear Characteristic Evaluation System

A menu structure for the implemented functions of the SF nuclear characteristic evaluation system is shown Fig. 2. The system provides the following functions:

- SF Information Management
  - SF assembly and rod information
  - Loading plant and cycle NDR information
  - SF core power history
  - Nuclear core design information for each plant and cycle
- SF Characteristics Evaluation
  - Characteristic evaluation code operation
  - Result view (Table/Graph)
  - Evaluation report generation for SF rod
- Sf Transfer Package Evaluation
  - SF selection for transfer package (with same evaluation reference date)
  - SF package characteristics calculation
  - result view (Table/Graph)
  - Evaluation report for SF package

Fig. 3 shows an example of the system's user interface for nuclear characteristic evaluation of SF rods. Fig. 4 shows a graph of radioactivity (linear scale) for a given SF nuclear characteristic evaluation result. Fig. 5 shows an example of the system's user interface for the construction of a transfer package by means of a combination of evaluated SF rods and a radioactivity (log scale) graph of SF nuclear characteristic evaluation results.

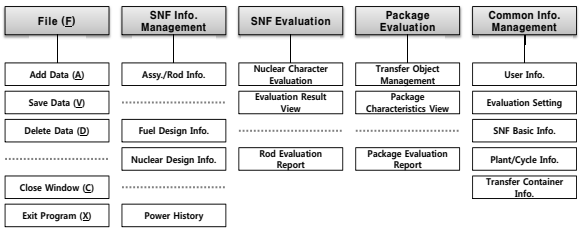

Fig. 2. Menu structure of SF nuclear characteristic evaluation system.

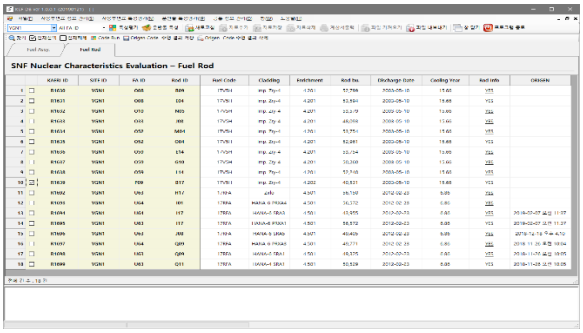

Fig. 3. Example of nuclear characteristic evaluation of SF rods.

Fig. 4. Example SF nuclear characteristic evaluation results.

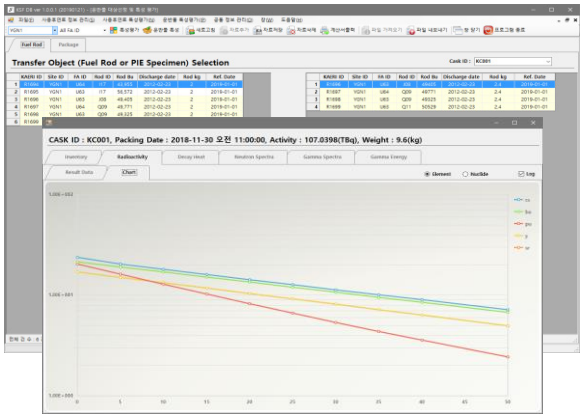

Fig. 5. Example of SF transportation package evaluation results.

4. Conclusion

KAERI and ACT have developed a network-based SF nuclear characteristic evaluation system. The system is convenient to use and is designed to increase the work efficiency of its users. In addition, it provides accurate SF nuclear characteristic evaluations. It will be used to evaluate the nuclear characteristics of SF stored at KAERI for the safe transportation of SF.

REFERENCES

[1] I. C. Gauld, "ORIGEN-S: Depletion Module to Calculate Neutron Activation, Actinide Transmutation, Fussion Product Generation, and Radiation Source Terms", ORNL/TM-2005/39 Version 6.1 Sect. F7, (2011).

Collection of Uranium Metal From the Salt Mixture Using Yttrium Metal

Joon-Bo Shim*, Dal-Sung Yoon, Si-Hyung Kim, and Sung-Jai Lee
Korea Atomic Energy Research Institute, 111, Daedeok-daero 989beon-gil, Yuseong-gu, Daejeon, Republic of Korea
*njbshim@kaeri.re.kr

1. Introduction

The objective of pyroprocessing technology is to reduce a volume of the high level waste (HLW) by recycling the long lived actinide elements in spent nuclear fuel (SNF) into the sodium fast reactor. KAERI has carried out a study to develop unique drawdown method to recover most of the actinide elements remained in a spent molten salt by introducing the rare earth metal. [1, 2] The previous tests on this drawdown method in the uranium chloride salt have shown promising results from the viewpoint of minimizing actinides concentration. In this study, bench scale tests were conducted using the Yttrium metal to examine the collection behavior of uranium metal into an inner crucible from a simulated LiCl-KCl salt.

2. Experimental

A simulated LiCl-KCl molten salt mixture containing the uranium and three rare earth metal such as Nd, Ce and La chlorides was prepared in outer crucible, and two Yttrium metal rods basket was introduced into an inner small crucible to collect recovered uranium metal as shown in Fig. 1. A simulated LiCl-KCl salt mixture (400 g) was composed of the U (1.16wt%), Nd (1.43wt%), Ce (0.96wt%) and La (0.57wt%) metal chlorides for the bench scale test. Yttrium metal basket was introduced into an inner crucible to start collection reaction of uranium with stirring the salt at 40 rpm using the Yttrium rods basket. The ICP quantitative chemical analysis of the salt samples and the on-line cyclic voltammetry (CV) monitoring of a salt phase were used to examine the changes of the salt composition.

Fig. 1. Experimental apparatus for collection of uranium using the Yttrium metal in a LiCl-KCl salt mixture.

3. Results and Discussion

The concentration of the uranium ions contained in a simulated salt mixture was reduced from a value more than one weight percent (1.16wt.%) to low value around 0.28wt.% at 60 minutes due to the chemical reduction of uranium ions with the Yttrium metal in a salt mixture. After 90 minutes the concentrations of uranium in two salt samples (at 90 and 180 minutes) decreased to a very low value less than 50 ppm. The on-line cyclic voltammetry (CV) monitoring results of a salt phase are shown in Fig. 2(a).

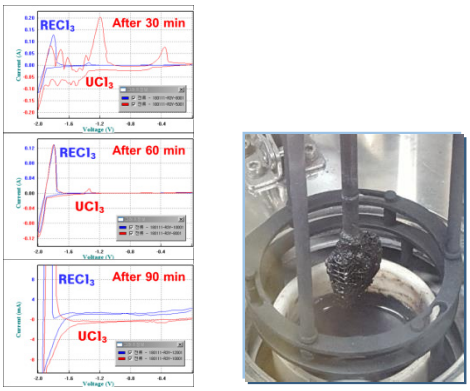

(a) (b)

Fig. 2. (a) CV monitoring of UCl_3 after 30 min. in a salt mixture and (b) U metal covered on Y metal basket.

The recovery reaction of the uranium with Y metal is as follows.

$$Y(s) + UCl_3 + REsCl_3 \rightarrow U(s) + YCl_3 + REsCl_3 \quad (1)$$

The uranium ions in a salt were converted to U metals which covered on the surface of Yttrium rods basket (Fig. 2,b). These uranium metal particles were easily detached from the basket and collected into the inner crucible by an up-down vibrating force. After removing the inner crucible from the salt $CdCl_2$ oxidant were added into the remaining salt. The ICP analysis result of this remaining salt sample shows that the uranium concentration is a very low value less than 50 ppm.

4. Conclusions

The concentration of uranium ions in a simulated salt mixture can be decreased to a very low value less than 50 ppm by introducing the Yttrium metal into a salt.

The converted uranium metals are covered on the surface of Yttrium rods basket, and these uranium metal particles can be easily detached from the basket by an up-down vibrating force for collecting uranium into the inner crucible.

ACKNOWLEDGEMENT

This work was supported by a National Research Foundation of Korea (NRF) grant funded by the Korean government (MSIP) (No. 2017M2A8A5015079).

REFERENCES

[1] J. B. SHIM, et al., “Recovery Method of the Residual Actinide Elements in a Chloride Molten Salt”, Korean Patent No. 10-1576612 (2015).

[2] J. B. SHIM, et al., “Recovery of the Actinides and Content Analysis in the Recovered Product Using Rare Earth Metal Equipped in a Stirring Mesh Basket from a Simulated LiCl-KCl Molten Salt,” Proceedings of the Korean Radioactive Waste Society SPRING 2016, p.0240 (2016).

Preparation of the Pin-loading Tension Test for Evaluation of Fracture Toughness in PWR Cladding Tubes

Myungchul Park*, Jae-Yong Kim, Dosik Kim, and Sangbok Ahn

Korea Atomic Energy Research Institute, 111, Daedeok-daero 989beon-gil, Yuseong-gu, Daejeon, Republic of Korea

*mcpark@kaeri.re.kr

1. Introduction

In Zr cladding tubes, one of the reasons for the phenomenon of hydrogen pick-up in the tube is the surface oxidation. The hydrogen as a by-product of the oxidation leads to formation of hydride and these hydrides cause the embrittlement in the material. Understandably, mechanical properties regarding the embrittlement are required to evaluate for safety management of spent fuel. However, the standardization of fracture toughness in cladding tube is not easy due to thin-wall geometry of that. One suggestion to evaluate the fracture toughness was pin loading tension (PLT) technique and the details of the test was described in the references [1-2]. Recently the PLT testing equipment was set up in PIE facility of KAERI to perform the test for investigating delayed hydride cracking (DHC) property of Zr cladding tube. The purpose of this study is to utilize this equipment for the PLT test to evaluate fracture toughness of Zircaloy tube.

2. Methods and Results

2.1 Specimen Preparation

The PLT-specimens used in the test is identical with that for the DHC test [2] and the nominal length of 13 mm have been manufactured from hydrogen charged Zircaloy-4 cladding. Hydrogen was charged in the conditions of 300 torr H_2 and 400˚C. The notches were machined in the specimen at the front edge (loading position) and back edge.

2.2 Test Equipment Set-up

The PLT test is divided by two steps. The first step is fatigue pre-cracking to minimize the plastic zone size in front of the crack tip. The second step is tensile test with constant strain rate control (in here, 0.1 mm/min). Accordingly, the equipment, which has the function of dynamic force control, was proper for the test. For the reason above, MTS Acumen3 was chosen and the picture of the equipment is shown in Fig. 1.

Fig. 1. PLT testing equipment.

2.3 Test Results

The tensile test result of the PLT-specimen of Zr cladding tube after fatigue test is shown in Fig. 2. In the fatigue test, the target length of pre-crack was 2 mm. The test was finished at the point of peak load. In this point, maximum load was 1.1 kN and the load-line displacement was 1.01 mm.

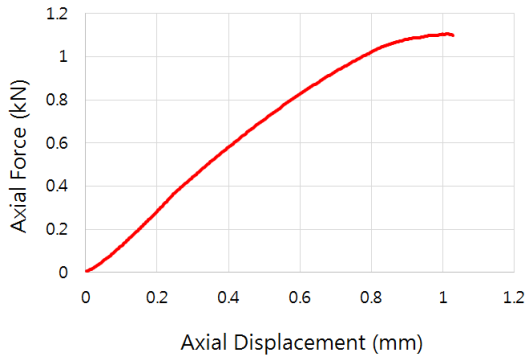

Fig. 2. Axial force as a function of axial displacement.

After the test, the sample was heated up to 300℃ for marking the cracked region. Then, the sample was cooled to RT and fully opened by normal tensile test. Fig. 3 shows the fracture surface of the splitted PLT sample. The notch and pre-crack region was even and clear. Although the main cracked region was not distinct well, the crack length was measured using 9-point measurement method.

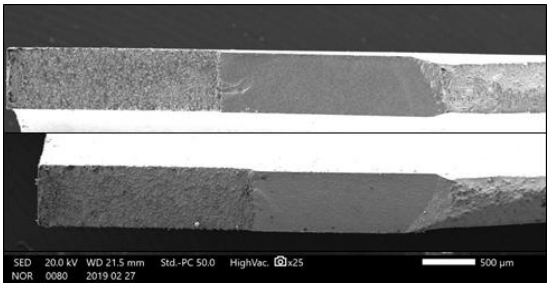

Fig. 3. Fracture surface of the PLT sample.

In that measurement, the crack length at the peak load was 700 µm and the value of "a" (total length between crack tip and load axis) was 12.5 mm. Using the results, COD value can be converted to the crack length, as shown in Fig. 4.

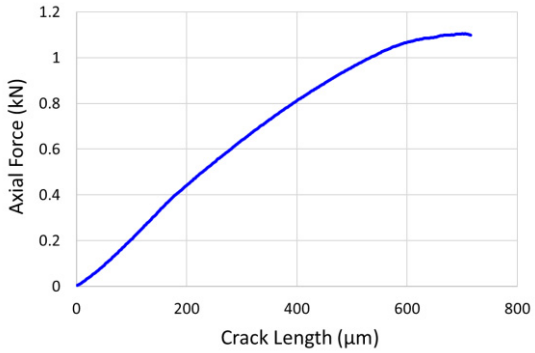

Fig. 4. Axial force as a function of crack length.

The equation below [1] was used to calculate J value at maximum load.

$$J_I = \beta A_T / B b_0 \quad (1)$$

A_T = the total area under the load vs load-line displacement curve

B = specimen thickness

B_0 = the ligament length

The calculation shows that the J_{max} was 72 kN/m. Because it is the approximated result of the pre-test, further study and test to process the data will be performed in the future.

3. Conclusions

The PLT test for fracture toughness of Zircaloy tube was performed to check the availability of new equipment in PIE facility of KAERI. Further tests like compliance test, calibration of crack length for DCPD measurement and so on will be performed for the future demand on the PLT test.

REFERENCES

[1] V. Grigoriev, "Fracture Toughness of Zircaloy Cladding Tubes," 11th symposium ASTM STP 1295(1996).

[2] V. Grigoriev, R. Jakobsson, SKI Report 00:57 (2000).

Dry Atmosphere Test of Pyroprocess Automation Mockup Using Dried Air Supply and Drying System Operation

Jonghui Han*, Byungsuk Park, and Seungnam Yu

Korea Atomic Energy Research Institute, 111, Daedeok-daero 989beon-gil, Yuseong-gu, Daejeon, Republic of Korea

*jhan@kaeri.re.kr

1. Introduction

To evaluate durability and operability of automated pyroprocess equipment in a high temperature salt environment, pyroprocess automation mockup has been constructed [1]. Then to achieve an ultra-low humid atmosphere, a zeolite based drying system has been installed and connected with this mockup [2] as shown in Fig. 1.

Besides the drying system, the dry air (under -40℃) supply can be used to control the dry atmosphere to reduce energy consumption. For this purpose, the leak rate according to pressure of the dry room was measured and it was observed that dew point (DP) in the room was achieved and maintained under -40℃ only by the supply of dry air [3]. These results showed the dry air can be also utilized for lowering and keeping moisture level. Hence the atmosphere control method can combine the supply of dry air and the operation of drying system, depending on the situation.

To build an operation method using two methods, this paper presents test results about dry atmosphere of pyroprocess automation mockup when dry air is supplied and when the drying equipment is operated.

(a) Dry room

(b) Drying system

Fig. 1. Pyroprocess automation mockup.

2. Atmosphere by Dried Air Purge

Park *et al*. measured the leak rate of the dry room according to the pressure before the drying system was built [3]. However the leak rate could be worse because of new holes on the wall of the dry room for duct connections. Hence several experiments were conducted to verify the atmosphere control performance of the dried air supply.

Fig. 2 shows the trends of DP in the dry room during the dried air purge with 10 ㎥/h (CMH). After about 5 days, DP was achieved under -40℃, and so the dry room has still acceptable leak rate. This means that the purge of dry air can be used to control humidity of the mockup.

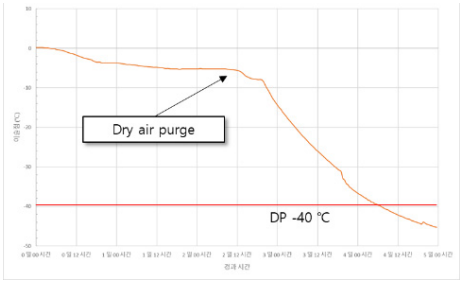

Fig. 2. Dewpoint in the dry room during dry air purge.

3. Atmosphere by the Drying System

Prior to the full operation of the constructed drying system, T.A.B. (Testing, Adjusting, and Balancing) were made to the operating conditions of equipment in the system. In order to adjust the pressure and circulating air volume, the opening angle of duct dampers and the rotation rate of fans were adjusted. Fig. 3 shows the operation screen of the drying system, where it is possible to set the operation conditions.

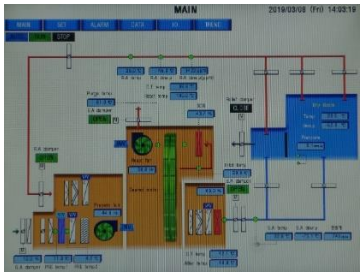

Fig. 3. Graphical user interface of drying system.

Fig. 4 shows the dew point change inside the mock-up during the drying system operation. The main operating parameters of the drying system were 10% outside air damper opening angle, 45 Hz speed for process fan and 40 Hz for react fan. It was confirmed that the target dew point reached within about 30 minutes after the start of operation. Hence the drying system can be actively utilized when it is necessary to make the inside atmosphere of the room quickly dry when the moisture inside the dry room increases rapidly due to worker access or the like.

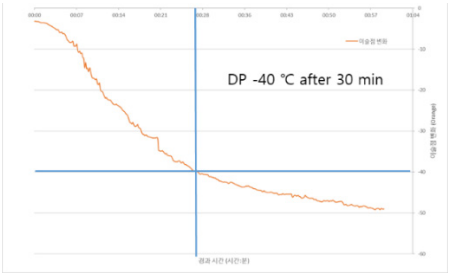

Fig. 4. DP during drying system operation.

4. Conclusion

In this paper, the performance test for drying atmosphere of pyroprocess automation mockup through dry air supply and drying system operation is described. A drying system operation plan will be established to reduce power consumption using these two methods.

REFERENCES

[1] J. Han, et al., “Construction of Dry Room for Pyroprocessing Automation Verification Mock-up”, Proc. of the KRS 2018 Spring Conference, May 30-June 27, 2018, Busan.

[2] J. Han, et al., “Construction of a Drying System for Salt Environment Dry Room”, 2018 Sarek winter annual conference, 11, 2018, Seoul.

[3] B. Park, et al., “Preliminary Evaluation of Process Equipment Test Mock-up for Construction of Drying System”, Proc. of the KRS 2018 Spring Conference, 14(1), May 30-June 27, 2018, Busan.

Design of Modular Electrolytic Reduction Equipment

Jong Kwang Lee*, Sung-Wook Kim, Dong-Seok Ryu, Sun Seok Hong, and Eun-Young Choi
Korea Atomic Energy Research Institute, 111, Daedeok-daero 989beon-gil, Yuseong-gu, Daejeon, Republic of Korea
*leejk@kaeri.re.kr

1. Introduction

The electrolytic reduction process reduces oxide fuel to metal for feedstock to the electrorefiner. To increase remote operation efficiency and explore cost-effective electrochemical process, we are developing a conceptual design of the automated workflow and its related process equipment. In this work, novel equipment consisting of modules with self-assembly concept and automation components has been designed for successful electrochemical processing and convenient remote operation.

2. Design of Equipment Modules

2.1 Flange Module

The flange module shown in Fig. 1 is an integrated structure, providing several interface services: installing anode module, cathode module, reference electrode and sensors, supplying electrical power and argon gas, and exhausting off-gas. It also needs to prevent heat loss from the reactor vessel while maintaining the temperature of the top surface as low as possible. On the center of the flange module, three rectangular slots are formed to install one cathode module and two anode modules. In addition, it is equipped with gas inlet and outlet tubes for supplying pure argon gas to reactor vessel and exhausting off-gas from the inside of the anode shroud to scrubbing system installed outside of the processing cell. Electrical busbar systems are installed on the top surface of the flange and extended to facility feedthrough.

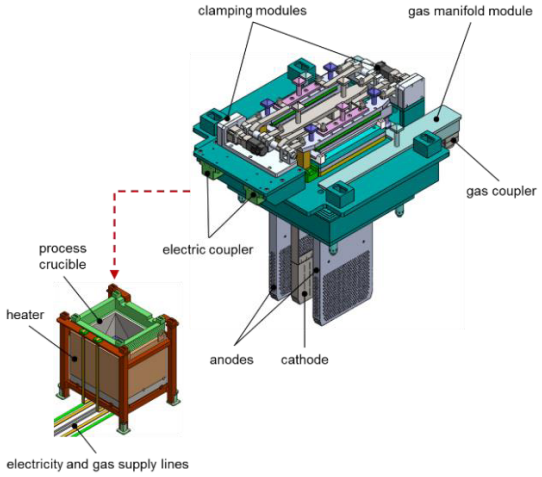

Fig. 1. Heater and process crucible (left) and flange module (right) of the electrolytic reduction equipment.

2.2 Gas Manifold Module

High-temperature corrosion of the off-gas tube is one of the most critical concerns in maintaining the structural integrity of the processing equipment because various corrosive gases are produced in the electrolytic reduction process with a consumable carbon anode. Therefore, the interchangeable gas manifold module has been designed for easy maintenance or repair. It has a similar configuration with the shell and tube heat exchanger: hot off-gas flows through the inner tube while pure argon gas with room temperature or below flows outside of the off-gas tube. This concept helps to cool down the off-gas, therefore less high-temperature corrosion may be expected. In addition, four equally spaced inflow tubes could play an important role in proper positioning of the gas manifold during the assembling step, as shown in Fig. 2(c).

2.3 Clamping Module

Reducing electrical contact resistance is an important factor for increasing current efficiency. In this work, the clamped joint method is used for connection between the anode/cathode module and the main busbar system and its contact should be tightly maintained during the process operation. To provide a proper clamping force, we designed a spring-loaded clamping module. As the torsion bar coupled with driving unit rotates, spring-loaded clamping arms with different length simultaneously push anode/cathode conductor plates tightening them to the main busbar system. The initial compressed lengths of springs are adjusted in advance to have desired clamping force or contact resistance.

3. Analysis on Remote Assembly Operation

Assembly simulation using 3D design model has been conducted to find mechanical interferences and to establish proper remote operation procedure as shown in Fig. 2. With a plug and play concept, as soon as the frame module consisting of a heater and process crucibles is installed on the feed-through of the cell floor, electrical and gas services are provided to the assembled module. Similarly, when the flange module is assembled on to the frame module, those services are ready to use for the process operation. This could dramatically improve the work efficiency comparing with the conventional labor-intensive remote operation. In addition, once the lower part of the anode or cathode module is inserted into the rectangular slot of the flange module, each module can also be accurately aligned and positioned with the aid of the V-shape guide.

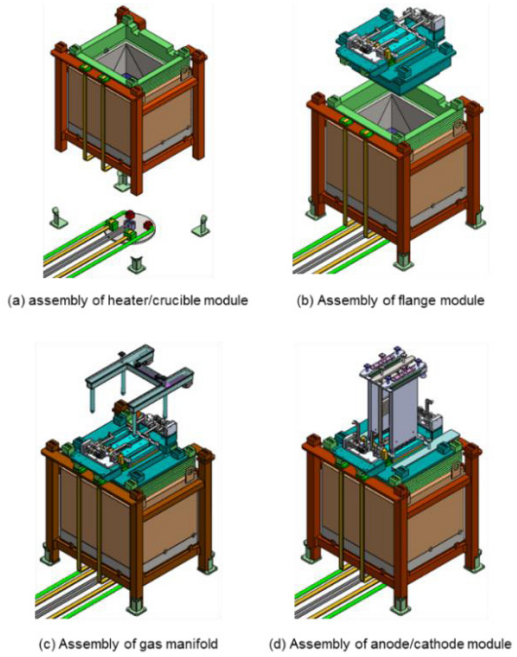

Fig. 2. Assembly simulation of equipment modules.

4. Conclusion

In this work, novel electrolytic reduction equipment consisting of the heater, process crucible, flange, anode, cathode, gas manifold, and clamping device has been designed with the modular concept to increase remote operation efficiency. Key design concepts and remote operation procedures have been evaluated by means of 3D modeling simulation of the assembly operations. We are performing design optimization, especially of the heat exchanger in the gas manifold module.

ACKNOWLEDGEMENTS

This work was supported by the Nuclear Research & Development Program of National Research Foundation of Korea (NRF) funded by the Ministry of Science and ICT (MSIT).

Evaluation of the Accident Frequency Analysis for the Integrated Safety Analysis in Nuclear Fuel Cycle Facility

Woo Jin Jo*, Seok-Jun Seo, Siwan Noh, Hyo Jik Lee, and Seung Nam Yu

Korea Atomic Energy Research Institute, 111, Daedeok-daero 989beon-gil, Yuseong-gu, Daejeon, Republic of Korea

*wjjo@kaeri.re.kr

1. Introduction

Safety Analysis is as important as nuclear power plants in nuclear fuel cycle facilities that handling various chemicals and nuclear materials. However, it is not easy to conduct a consistent safety analysis for the nuclear fuel cycle facilities with different structures, functions and specifications compared to standardized nuclear power plants. In this regards, the US NRC introduced the Integrated Safety Analysis (ISA), a procedure for comprehensive safety analysis of the nuclear fuel cycle facilities by NUREG-1520 [1].

In this paper, an evaluation method for the frequency of the expected accidents can be occurred in the nuclear fuel cycle facilities, which is one of the ISA procedures, is introduced and an example is shown using reference literature.

2. Frequency Analysis in ISA

Frequency analysis is conducted to verify safety by evaluating impacts and frequency of occurrence, in accordance with the degree of hazard, based on the past accident data and experiences of the relevant or similar facilities.

The frequency category can be determined on the basis of various methods including; accident records, items relied on for safety (IROFS) functional failure records, accident records on similar or applicable systems, objectively qualitative criteria controlling system failure rates and availability, or other methods which are objectively verifiable. It is also required to consider duration of accident and common cause failure, as needed. The procedure is shown in the flowchart below.

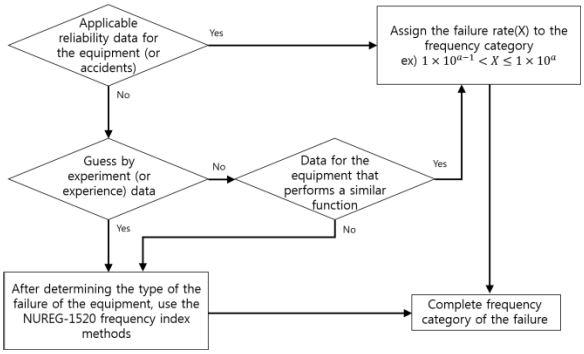

Fig. 1. Flow chart of assigning the frequency category by frequency analysis.

3. Calculation of the Failure Rates

3.1 Failure Rates of SSCs

The frequency of failure and the failure rate of the equipment shall be used if they can be proved according to the past experiment or experience data. Failure rates of structures, systems, components (SSCs) can be obtained by the following procedure. (1) the SSCs failure rate data should be collected according to the failure mode. (2) If there is no failure rate data, the index is assigned by referring to the operation experience or failure experience of the similar SSCs. (3) If data cannot be obtained by the method of (2), an index is assigned according to the management level of the SSCs. (4) If data cannot be obtained also by the method of (3), the index is given according to the redundancy, passive and active of SSCs.

3.2 Failure Rates of Human Errors

The accidents caused by human error are evaluated using the data compared with the past literature[2] or the following procedure when there is no data. (1) Depending on the frequency of the tasks (2) The correction according to the skill of the worker and work environment (3) using the factors from (1) to (3), calculate the human error index.

4. Results of the Failure rates

Table 1. Failure rates of SSCs [3]

Name	Failure mode	Failure rate	Frequency index	Frequency Category (ISA)
HEPA filter	Blockage	3.00E-06/h	-2	Not Unlikely
	Leak	3.00E-06/h	-2	Not Unlikely
	Rupture	5.00E-07/h	-3	Not Unlikely
Rupture disk	Open Failure	1.00E-04/d	-2	Not Unlikely
	Out Leakage	5.00E-07/h	-3	Not Unlikely
	In Leakage	1.00E-06/h	-3	Not Unlikely
	Out Rupture	3.00E-08/h	-4	Unlikely
	In Rupture	5.00E-08/h	-4	Unlikely

Table 2. Failure rates of human errors [2]

Name	Outline	Failure rate	Reason	Frequency index	Frequency Category (ISA)
Label mounting errors	Labeled with the wrong information	5.0E-03 /d	Judge by the scope of the operation that is usually performed	-2	Not Unlikely
Tank overflow	Fill the tank beyond the physical or management level.	5.0E-06 /tank•h	Some margin for the transfer operation (Assumed 17520 tank•h per year)	-1	Not Unlikely

5. Conclusion

In this paper, the frequency of accidents that could be applied in the safety analysis for the nuclear fuel cycle facilities was evaluated using some references. Based on these results, it is expected that ISA for the nuclear fuel cycle facilities with high accuracy can be performed.

ACKNOWLEDGEMENT

This work was supported by Nuclear Research & Development Program of National Research Foundation of Korea (NRF) funded by Minister of Science, ICT and Future Planning (MSIP).

REFERENCES

[1] US NRC, “Standard Review Plan for Fuel Cycle Facilities License Applications”, NUREG-1520 (2015).

[2] US DOE, “Savannah River Site Human Error Data Base Development for Nonreactor Nuclear facilities (U)”, WSRC-TR-93-581 (1994).

[3] US DOE, “Savannah River Site Generic Data Base Development (U)”, WSRC-TR-93-262 (1993).

Current Status of ACPF Argon Cell System

Byungsuk Park*, Jongkwang Lee, and Eunyoung Choi
Korea Atomic Energy Research Institute, 111, Daedeok-daero 989beon-gil, Yuseong-gu, Daejeon, Republic of Korea
*nbspark@kaeri.re.kr

1. Introduction

The advanced spent fuel conditioning process facility (ACPF), which was constructed with air cell, was modified to consist of an air cell and an argon cell. The argon cell was constructed in July 2016, and it has been conducting test operations so far while maintaining the argon environment. This paper introduces the current status of the construction of the argon cell system.

2. Argon Cell System

2.1 Overview

The argon cell system consists of an argon cell, a gastight door, a material transfer system, a lighting device, a remote handling system, a purifier, a cooler, a measuring sensor, a safety device, a control system, an emergency and cleaning device, etc. The argon cell was designed to minimize leakage and was constructed by isolating the first window area with the boundary between the first window and the second window to the right side of the existing ACPF air cell. Fig. 1 shows the front view of the air cell and the argon cell seen in the operating area.

Fig. 1. Modified ACPF.

2.2 Argon cell and remote handling system

Fig. 2 shows the inside of the air cell and the argon cell. An electrolytic reduction (ER) equipment was placed on the working table of the argon cell. The internal dimensions of the argon cell are 1,728 (L) x 1,990 (D) x 2,740 (H) mm (480 mm in working table height). A gastight door with an internal size of 600 (L) x 1,000 (H) mm was installed for situations during the construction and emergency operation of the argon cell. A material transfer system with internal dimensions of 600 (L) x 600 (D) x 600 (H) mm was installed between the cells as a means of transferring material between the air cell and the argon cell. A lighting device was equipped with one metal halide 250W lamp (B type) and one three-wavelength 100W lamp. A pair of master-slave manipulators (MSM) was installed on the left and right side of the shield window, respectively, and a crane was installed in the ceiling inside the argon cell.

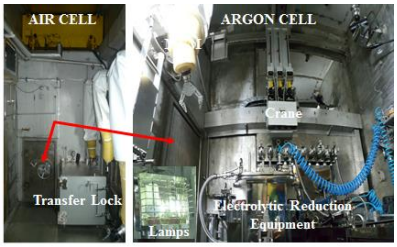

Fig. 2. Inside view of the air cell and the argon cell.

2.3 Purification and Cooling System

The purification system consists of a circulation blower, a dry trap (purifier), a cooling system, etc. Its appearance is shown in Fig. 3. The blower forcibly circulates the argon gas, and in the purifier, Cu

removes oxygen and molecular sieve removes moisture. The heating of the heater of the ER equipment causes the temperature of the argon cell to rise. When the blower frequency increases, the temperature inside the case in which the blower is placed rises. The cooling system cools its rising temperature.

Fig. 3. Purification and cooling system.

2.4 Measuring and Safety System

In order to measure the temperature inside the argon cell, temperature sensor was installed at the middle and the top. The mid-point temperature sensor has a function to block radiated heat directly from the lamp. A differential pressure gauge was installed to measure the pressure of the argon cell and the HEPA Filter. The seal pot was also installed as a pressure safety device so that the pressure in the argon cell would be reduced automatically when the pressure was exceeded. These are shown in Fig. 4.

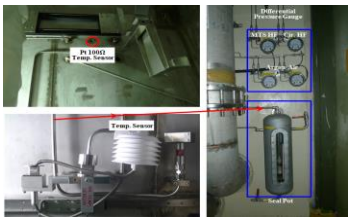

Fig. 4. Measuring sensor and seal pot.

2.5 Control and Monitoring System

The oxygen/hydrogen concentration, pressure and cooler are controlled by PLC and touch PC. In addition, various measurement signals are displayed on the PC and these data are stored in an Excel file.

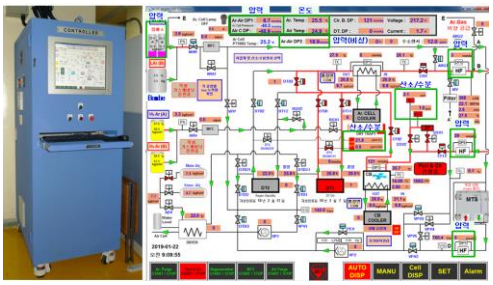

Fig. 5. Control and monitoring system.

2.6 Emergency and Cleaning System

In emergency situations, the valve can be operated manually to supply argon gas to the argon cell. After maintenance of the purification system, it can be cleaned with argon gas.

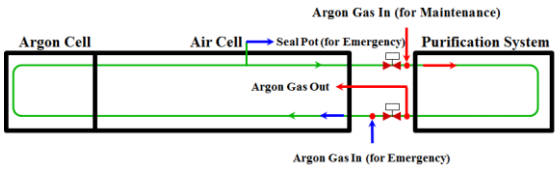

Fig. 6. Emergency and cleaning scheme.

3. Conclusion

The argon cell system for demonstrating the technology of converting the spent fuel into metal by the electrolytic reduction process has been verified by repetitive test operation for more than 2 years.

ACKNOWLEDGEMENT

This work was supported by the Nuclear Research and Development Program of the National Research Foundation of Korea (NRF) funded by the Ministry of Science and ICT.

REFERENCES

[1] B.S. Park, “Construction of ACPF Argon Cell System”, KAERI/TR-6242/2015, 2015.

Studies on the Chlorination Reaction of Uranium Using Zinc Dichloride

Chang Hwa Lee*, Tack Jin Kim, Dalsung Yoon, and Sungjai Lee
Korea Atomic Energy Research Institute, 111, Daedeok-daero 989beon-gil, Yuseong-gu, Daejeon, Republic of Korea
*chwalee@kaeri.re.kr

1. Introduction

Electrorefining process is a key technologies for recovering U and transuranic elements from used nuclear fuels for recycling them as fuel components applicable to sodium fast reactors (SFRs) as well as the minimization of high level nuclear waste [1].

Typical U electrorefining process is proceeded through the following reactions (1, 2) in high temperature LiCl-KCl-UCl_3 molten salts by applying a potential or a current in an appropriate range between the anode baskets filled with used fuels and the cathodic materials where highly pure U metal is recovered.

$$\text{Anode: } U \rightarrow U^{3+} + 3e^- \quad (1)$$

$$\text{Cathode: } U^{3+} + 3e^- \rightarrow U \quad (2)$$

Generally, UCl_3 is added as an initiator to support the electrotransport of U ions to be sustained at a high recovery rate [2]. Among various methods for synthesizing UCl_3, U chlorination using $ZnCl_2$ in LiCl-KCl molten salts is described in this paper.

2. Experimental

An anhydrous LiCl-KCl eutectic salt (99.99wt.%, Sigma-Aldrich) was used as a base electrolyte for the chlorination reaction of U. The concentration of $ZnCl_2$ added into the base electrolyte was 3.8wt.%, which corresponds to 4.3wt.% UCl_3 in LiCl-KCl base salts when 100% of $ZnCl_2$ was assumed to be reacted with U metal. All the experiments were performed at 500°C in an Ar-purging glove box, where the concentrations of oxygen and moisture are maintained below 5 ppm. For the electrochemical measurements, a tungsten (W) wire and depleted U metal were used as a working and a counter electrode, respectively, with a Ag/AgCl reference electrode. Chronoamperometries (CA) were performed at -0.9 V for various times to dissolve Zn and/or U-Zn alloys from the U metal surface at the anode and to monitor the chlorination reaction of U. To examine the electrochemical behavior of Zn and U, cyclic voltammetries (CV) were also measured from the open circuit potential to -1.6 V followed by scanning down to -0.1 V vs. Ag/AgCl at a scan rate of 100 mV/s. ICP-OES was used to analyze the concentration of U and Zn in the salt after the reaction.

3. Results and Discussion

Fig. 1. Shows a summary of cyclic voltammetric curves measured after three runs of chronoamperometry at -0.9 V for 2 to 3.5 hrs at each time. After initially immersing a U metal wound up with a stainless steel in LiCl-KCl-$ZnCl_2$ salt (not shown), the reduction peak corresponding to Zn gradually decreased and an additional reduction peak associated with U-Zn began to appear at about ~ -1.2 V. In order to induce a spontaneous chlorination reaction of U, a constant potential of -0.9 V was

applied to the cell to dissolve Zn formed on the U metallic surface at the anode. After the 1st CA run, the reduction/oxidation peaks for U became obvious at ~ -1.5 V and - 1.4 V with the peaks for U-Zn alloys. However, as the CA runs proceeded, the peaks for U gradually increased, while the peak intensities for the reduction/oxidation of U-Zn and Zn were declined.

After completion of U chlorination reaction, the separation of the final product, liquid Zn, from LiCl-KCl-UCl_3 salt is greatly important for further use for U electrorefining process. In the preliminary quantitative measurement using ICP-OES, the concentration of Zn in the bulk solution was ~0.03wt.%, whereas the concentration of U appeared to be ~4.2wt.%, which is in good agreement with the U concentration that is able to react with the added $ZnCl_2$.

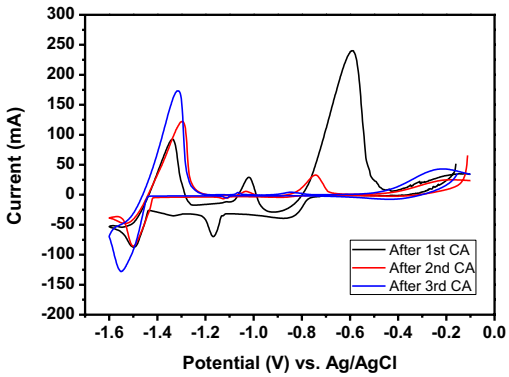

Fig. 1. Cyclic voltammetric curves sequentially measured on W electrode after chronoamperometries at -0.9 V vs. Ag/AgCl in 500℃ LiCl-KCl salts.

4. Conclusion

The UCl_3 production using $ZnCl_2$ was demonstrated and the reaction was monitored by electrochemical measurements in this study. $ZnCl_2$ is expected to be a good candidate as a chlorinating agent to produce UCl_3 for U electrorefining process.

REFERENCES

[1] Z. Tomczuk, J. P. Ackerman, R. D. Wolson, W. E. Miller, Uranium transport to solid electrodes in pyrochemical reprocessing of nuclear fuel, J. Electrochem. Soc. 139, 3523-3528 (1992).

[2] J. J. Laidler, J. E. Battles, W. E. Miller, J. P. Ackerman, E. L. Carls, “Development of pyroprocessing technology”, Prog. Nucl. Energ. 31, 131-140 (1997).

Demonstration of Basket Transportation Between a Station and Equipment Using Automation System in PAVM

Dongseok Ryu*, Jongkwang Lee, Jonghui Han, and Seungnam Yu
Korea Atomic Energy Research Institute, 111, Daedeok-daero 989beon-gil, Yuseong-gu, Daejeon, Republic of Korea
*sayryu@kaeri.re.kr

1. Introduction

Pyroprocessing Automation Verifying Mockup (PAVM) has been constructed at Korea Atomic Energy Research Institute (KAERI) for investigating mechanical durability of equipment in molten salt environment and for demonstrating automation of hotcell works [1]. PAVM has a dry room (4 m × 6 m × 2 m) which can regulate its dew point under -40 degree Celsius, and overhead gantry system was installed for basket handling between equipment [2-4]. To see if the gantry system properly installed and how accurate the system is, a basic demonstration was planned. A station mockup to hold a test basket and dummy equipment was located in the PAVM. This paper shows transportation automation between a station and equipment.

Fig. 1. Inside of PAVM and overhead gantry system.

The needs for the non-radiation experimental space were demanded only for molten salt test.

2. Demonstration Setups

A station to hold a test basket is located a side in PAVM. The station has two different slots, and the one is conceptually for the new basket and the other for the used one. Each slot has 5mm margins in each direction so that the overhead gantry system inserts the basket in the proper accuracy without interference.

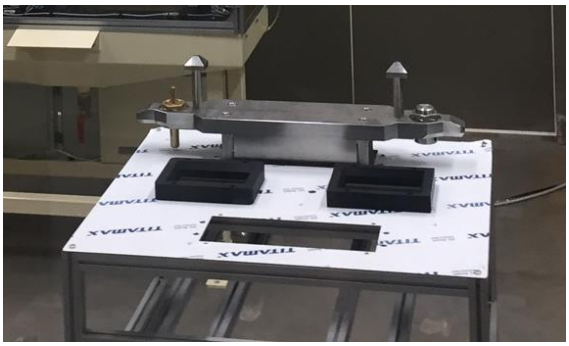

Fig. 2. Station to hold a test basket.

Dummy equipment was prepared in PAVM. A rectangular flange is covered on the top of the dummy equipment, and a slot to insert a test basket is located in the middle of the flange. The test basket has electric connector and a pneumatic coupler at each side, and the top flange has the mate parts for couple it together. A lift module attached side of the equipment to elevate the basket from unload position to load position and vice versa.

Fig. 3. Dummy equipment and lift module.

3. Automation System in the PAVM

In the beginning, the lift is up position to wait the basket. The overhead gantry picks up the basket from the station to the equipment, and install it on the lift module. The lift module moves the transferred basket down, and insert to the slot. When the basket motorized down, not only the mechanical connection but also the electrical and pneumatic connection is made at the same time.

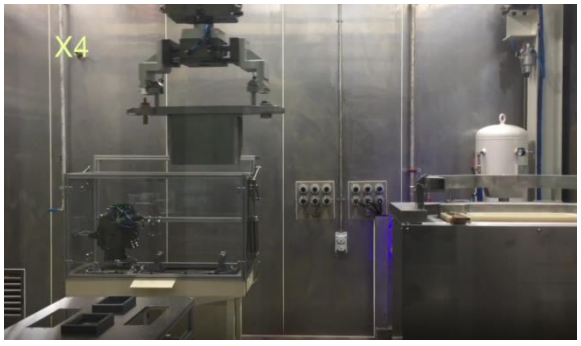

Fig. 4. Automatic transportation of basket by using the overhead gantry system.

After treatment of basket in the equipment, the basket lifted up again, and call the overhead gantry system to extract the basket. The overhead gantry approaches to the equipment and snap the basket out. The used basket transported back to the station.

Fig. 5. Basket installation in the station.

4. Conclusion

The PAVM was successfully constructed including overhead gantry system. By using the gantry system, a demonstration to automatically transport a test basket was conducted. Accurate motion of gantry system shows the possibility of automation in nuclear application. Further experiments were under progress in PAVM.

REFERENCES

[1] Dongseok Ryu, et al. "Needs and Goals of the Pyroprocessing Automation Verifying Mockup," Proc. of KRWS 2017 Fall, pp. 53-4 (2017).

[2] Dongseok Ryu, et al. "Example Operating Procedure for an Automation Concept of Electrochemical Process," Proc. of KRWS 2017 Spring, pp. 151-2 (2017).

[3] Dongseok Ryu, et al. "Design of a Basket Lifting Mechanism for Pyroprocessing Automation Verifying Mockup," Proc. of KRWS 2018 Spring, pp. 84-5 (2018).

[4] Dongseok Ryu, et al. "Automation System for the Pyroprocessing Automation Verifying Mockup," Proc. of KRWS 2018 Fall, pp. 185-6 (2018).

Storage and Decommission of Obsolete Cask

Woo-Seok Choi*, Sang soon Cho, Seung-hwan Yoo, Jongmin Lim, Ju-chan Lee, Ki-seog Seo,
Kyong-Sik Bang, Yun-young Yang, Gileon Jung, and Jaehoon Lim
Korea Atomic Energy Research Institute, 111, Daedeok-daero 989beon-gil, Yuseong-gu, Daejeon, Republic of Korea
*wschoi@kaeri.re.kr

1. Introduction

It has been more than 40 years since the operation of the Kori Unit 1 nuclear power plant in 1978. As of September 2018, we have more than 18 thousand assemblies of PWR SNF inventory and almost 450 thousand assemblies of PHWR SNF inventory. At present, all the spent fuels and stored at reactor sites.

For research purposes and business purposes, transport casks have been used for transporting spent fuel.

As transportation casks of spent nuclear fuels, KSC-1, KSC-4, KN-12, and KN-18, which are PWR transportation casks, and Hi-Star 63, which is a PHWR transportation cask, have been developed and used. In recent years, the KORAD-21 cask is under license review. Of the above mentioned casks, KSC-1 and KSC-4 are not in use at present, while KN-12, KN-18 and Hi-STAR63 are used for internal transportation between units or transportation in nuclear power plant.

We would like to focus on how to manage the obsolete transport casks and whether it is possible to recycle them when the necessity of the transport cask is no longer needed or the life time is exhausted. As Korea has not yet had a case, we would like to investigate based mainly on overseas cases.

2. Management of Obsolete Cask

2.1 Non-decommissioning Storage and Disposal in Non-nuclear Repository of Obsolete Cask

In some cases, when the radionuclide content will be below the regulatory limit for radioactive waste disposal, disposal in non-nuclear repositories could be allowed. In this case, destruction is advisable as it will permit recycling a large part of materials, such as steel, lead, cast iron, aluminum, depleted uranium. The exception would be the presence of prohibited or controlled materials, if its destruction leads to unnecessary exposure to workers or the public.

Storage as-is is recommendable if there are clear disadvantages in taking the cask apart: dispersal of radioactive material or other contaminants, creation of further waste such as tools and consumable, and exposure to workers. Partial destruction may allow reclaiming valuable materials only. There is experience with lead retrieval in France. However, it appears that in most cases, only environmental considerations can outweigh the high cost of using nuclear facilities and workers for little gain.[1]

Fig. 1. Outdoor Storage of obsolete cask (UF6 cask of DAHER-TLI Co.).

Fig. 2. Non-nuclear area storage of obsolete cask (Calvert Cliff NPP).

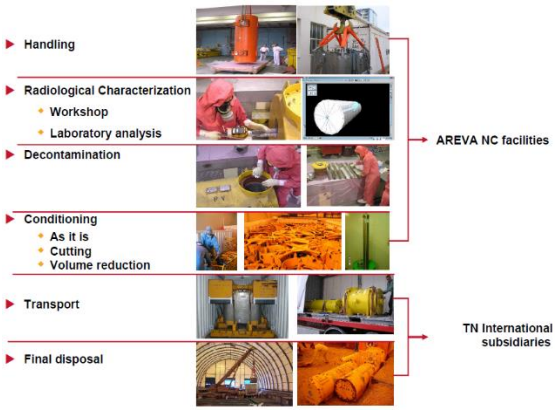

Fig. 3. Decommissioning Process of Obsolete Cask.

2.2 Decommissioning of Obsolete Cask

Decommissioning of the TN1300 transport and storage cask in Germany, including the basket, is feasible in a hotcell with a reasonable transport and crane capacity and tools for remote handling ability. The decommissioning costs were very high and rose in this case to 50% of the cask production costs. In the case of spent fuel contamination of the cask due to cladding failure of fuel rods, a higher level of contamination can be expected.[2]

The decommissioning of the nuclear casks implemented by TN International regarding its own needs and the French regulatory framework is formalized by several processes and is materialized for instance by the final disposal of casks as they are or in ISO container packed with cut-off casks and big bags filled with crushed internal cask equipment, etc.[3].

3. Conclusion

Generally, it is very economical to use an obsolete cask if there is an opportunity for recycling and it is appropriated to modify it for the reuse. When storing the cask, it is advisable to keep the cask without disassembly if there are disadvantages such as dispersion of radioactive materials or other contamination. When there is a need to decommission, the systematic procedure must be well established. The cost, however, is very expensive.

REFERENCES

[1] IAEA-TECDOC-1532, “Operation and Maintenance of Spent Fuel Storage and Transportation Casks/Containers”

[2] IAEA-TECDOC-1081, “Spent fuel storage and transport cask decontamination and modification”

[3] Laurent Blachet, et al., “TN International and its operational feedback regarding the decommissioning of obsolete casks dedicated to the transport and/or storage of nuclear raw materials, fuel and used fuel,” WM’08, Phoenix AR, USA.

Investigation of Trapping Characteristics of Iodine From CsI

Seok-Min Hong*, Do Yeon Lee, Yeoung Soon Lee, and Yung-Zun Cho
Korea Atomic Energy Research Institute, 111, Daedeok-daero 989beon-gil, Yuseong-gu, Daejeon, Republic of Korea
*seokminhong@kaeri.re.kr

1. Introduction

An accumulation of spent fuel has brought a considerable interest due to its energy and environmental issue. Pyroprocessing has been investigated in Korea Atomic Energy Research Institute (KAERI) which reduces the accumulated spent fuel and increases the efficiency of fuel cycle. In head-end process of pyroprocessing, UO_2 pellets are produced from a fuel bundle and various radioactive gases from a spent fuel are released during thermal treatment. Within these gases, I-129 is a harmful semi-volatile gas which had very long half-life with radioactivity, and therefore iodine should be captured using trapping system.

It is well known that iodine highly reacts with silver to form AgI, and these structures are very stable. KAERI had developed iodine trapping process using silver-functionalized zeolite (AgX) as an adsorbent. In this study, iodine trapping process was designed and adsorption behaviors were investigated by using AgX filters.

2. Experimental Section

The CsI as an iodine source and silver-functionalized zeolite (AgX) were prepared from Sigma-Aldrich. The iodine trapping system was consisted of three high temperature regions; CsI vaporization, cesium adsorption, and iodine adsorption zones. CsI was placed in the alumina boat in the center of the vaporization zone and temperature fixed to 1100℃. In the cesium adsorption zone, a Inconel-based cartridge was filled with cylindrical silica-alumina (SA) filters. The temperature of adsorption zone is set at 1000℃ for cesium to react SA filters. The AgX was loaded in the cartridge as shown in Fig. 1, which was placed in cylindrical alumina tube and adsorption temperature was set at 200℃ for iodine capture. For the untrapped cesium and iodine particles, ultra-low particulate air (ULPA) membrane filters and wet-scrubbers were installed at the end of the system.

3. Iodine Trapping Characteristic

Iodine trapping efficiency was measured by comparing mass of iodine vaporized and that of adsorbed on AgX. In addition, wet-scrubber was used to measure iodine concentration of emitted gas from trapping system.

4. Conclusion

Trapping process was designed for iodine capture using trapping system with AgX filters. Iodine trapping performance was investigated and it was confirmed that most of iodine vaporized were effectively captured in the trapping system using AgX filters.

Fig. 1. AgX and AgX filter cartridge.

Transportation Analysis of the 14OFA PWR Fuel Assembly

Sung-Uk Lee*, Jae-Yong Kim, Hong-Ryoul Oh, Kyung-Ho Yoon, Hyo-Chan Kim, and Donghak Kook
Korea Atomic Energy Research Institute, 111, Daedeok-daero 989beon-gil, Yuseong-gu, Daejeon, Republic of Korea
*leesunguk@kaeri.re.kr

1. Introduction

As the amount of Spent Nuclear Fuel (SNF) in KOREA domestic spent fuel pool increases dramatically, the storage capability of the Pressurized Water Reactor (PWR) SNF would be saturated by 2024. [1] The SNFs in the pool must be transferred to the designated wet or dry spent fuel storage facility. In the issues of the SNF treatment, handling and transport of the SNF have been considered as an important factors. In this paper, we tried to develop the dynamic analysis model under transportation and performed the analysis model in the time domain.

2. Transient Dynamic Analysis

2.1 Transient Dynamic Analysis in Time Domain

Generally, dynamic analysis of a vibration system performed in the frequency domain to get data of natural frequencies and mode shapes. These data provide a better understanding of frequency characteristic of the system. However, the modal analysis method is not applicable to systems with various contact constraints such as nuclear fuel assemblies. Therefore, the direct analysis method in time domain should be used to analyze the transportation. The acceleration time history data is typically directly input to the load point. In this paper, we use a displacement control that integrates acceleration of less than 0.2g as shown in Fig. 1.

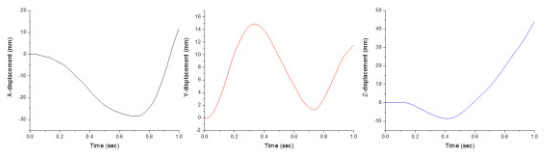

Fig. 1. Time history displacement by each axis direction.

2.2 Dynamic Analysis Model

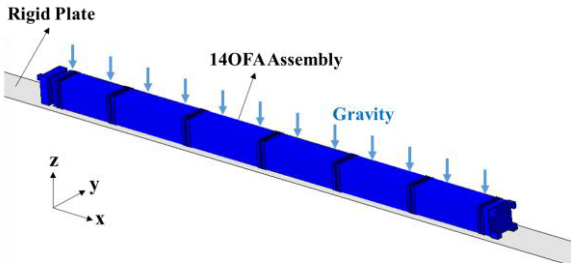

Fig. 2. Dynamic analysis model.

The analysis model consisted of a 14 X 14 full fuel assembly (14OFA) and a basket floor. The time history displacement data is given to the load point (basket floor), and gravity load is applied. Fig. 2 shows the FE model for the dynamic analysis. The specimen was modeled using ABAQUS/explicit, 3D shell element (C3D8R) was used for the fuel assembly, and discrete rigid elements were used for the basket floor. Multi Point Constraints (MPC) was used to represent the spot welding at inner connection of mid-grid for 14OFA. It is assumed that the contact area between each spacer grids and basket floor is a tie condition, because the fuel assembly itself is fixed to the basket during transportation. The material of the guide tube and the fuel rod/spacer grid are SUS304, and Zr-4 at room temperature (from MATPRO) [2].

2.3 Result of Dynamic Analysis

The maximum stress occurs at the contact area between spacer grid and fuel rod as shown in Fig. 3. It was confirmed that a large amount of stress was applied to the portion where the spacer grid and the basket floor contact due to gravity.

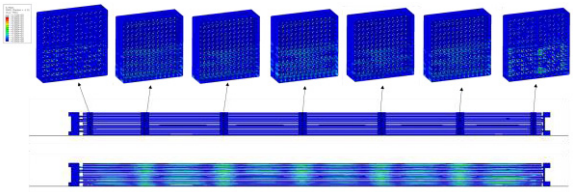

Fig. 3. Analysis result of 14OFA under transportation.

3. Evaluation of Contact Force

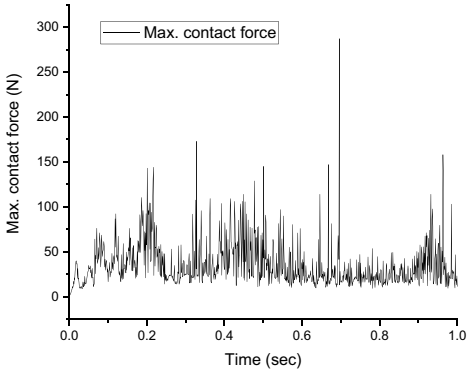

Fig. 4. Max. Contact force between fuel rod and spacer grids under transportation.

Contact interaction occurs between the spacer grid itself and the fuel rod due to vibration during transportation. In order to evaluate the integrity of the fuel rod, it is necessary to analyze the maximum contact force generated at the contact position between each spacer grid and the fuel rod. The results are shown in Fig. 4. The maximum contact load is 300N.

4. Conclusion

The dynamic simulation consists of two boundary condition: (1) gravity, and (2) dynamic loading. Under the vibration of 0.2g acceleration, the maximum stress of the cladding is under material yield strength. Impact forces at outside the fuel rod were analyzed to evaluate the integrity of the fuel rod during transportation. In the future, we will evaluate the safety of the external contact force received by the fuel rod by using the failure criteria according to the burn-up history and the input data considering the normal transportation excitation or shock excitation.

ACKNOWLEDGEMENT

This work was supported by the Korea Institute of Energy Technology Evaluation and Planning (KETEP) and the Ministry of Trade, Industry & Energy (MOTIE) of the Republic of Korea (No. 2014171020166A).

REFERENCES

[1] Ministry of Trade, Industry and Energy, “Roadmap for High-Level Radioactive Waste Management (final version)” (2016).

[2] SCDAP/RELAP5/MOD3.1 code manual volume IV : MATPRO, NUREG/CR-6150, INL (1993).

Round Robin Test Result of Pendulum Impact Testers for Low Burn-up Spacer Grids Operated by Three Different Laboratories

JaeYong Kim[1,*], KyungHo Yoon[1], HongRyoul Oh[1], SungGeun Kim[1], Donghak Kook[1], and YoungIk Yoo[2]
[1] Korea Atomic Energy Research Institute, 111, Daedeok-daero 989beon-gil, Yuseong-gu, Daejeon, Republic of Korea
[2] KEPCO Nuclear Fuel, 240, Daedeok-daero 989beon-gil, Yuseong-gu, Daejeon, Republic of Korea
[*]kjykjy@kaeri.re.kr

1. Introduction

Development of evaluation technology for degradation and mechanical behavior of low burn-up spent fuels (SNFs) during dry storage project has conducted since 2014. Its purposes are developing evaluation technology of SNF characteristics, degradation prediction/evaluation technology, and fuel component/assembly integrity evaluation technology. Four institutions such as KAERI, KHNP, KEPCO-NF, and SE&T, are participating in this project. Each institution has its own specific quantitative technical goals. KAERI has five goals, and this paper is about confirming the reliability of hot cell test equipment for SNF components among them.

2. Technical Goal

To evaluate mechanical integrity of low burn-up SNFs, several types of hot cell tests are planned. Because SNFs during dry storage in low temperature could become more brittle, they are vulnerable to external impact force. The dynamic buckling strength (P_{cr}) of a spacer grid (SG) obtained by pendulum impact test is important characteristics to determine whether it is possible to handle SNFs experienced external loads or not [1]. To confirm the reliability of the pendulum impact test in hot cell, round robin test (RRT) was performed. The technical goal is that the dynamic buckling strengths measured by three different laboratories are all within ±15 kN.

3. KAERI

3.1 Post-Irradiation Examination Facility (PIEF)

PIEF is the only laboratory which has hot cells to evaluate the irradiation performances as well as the fuel integrities in Korea [2]. The pendulum impact tester in hot cell at PIEF is shown in Fig. 1. It is composed of a tester, a controller, a lead (Pb) wall, and a manipulator.

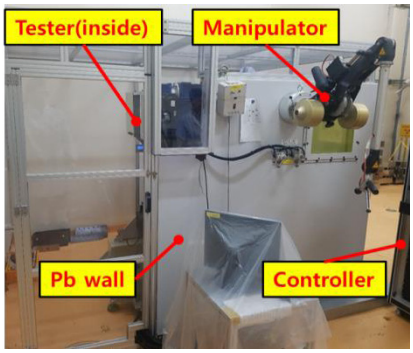

Fig. 1. The pendulum impact tester in hot cell at PIEF.

Research QA for this test is being applied from January 31, 2019. Impact tests were performed with low burn-up SNF representative SGs, 14 KNF-OFA SGs, three times. Test results are summarized in Table 1. Since the impact test result measured at PIEF is most important, the test results at other laboratories are normalized based on that value.

Table 1. Summary of RRT results

Laboratory	PIEF	NFSRD	KEPCO-NF
Normalized avg. P_{cr}	1	0.91	1.24
SD [kN]	1.524	1.746	3.493

3.2 Nuclear Fuel Safety Research Division (NFSRD)

Even though the spent SGs are extracted from the same SNF, their status such as deformed shape, included hydride contents, experienced temperature, etc. are completely different. But impact test in hot cell is very limited and difficult. It is the reason that manipulators should be used to prepare spent SGs for the pendulum impact test in hot cell due to high radioactive. So, the same equipment was installed in cold cell at NFSRD to increase the analytical skills of impact results performed in hot cell [3]. All tests are being conducted according to research QA from April 5, 2018. Test results performed at NFSRD are summarized in Table 1.

4. KEPCO-NF

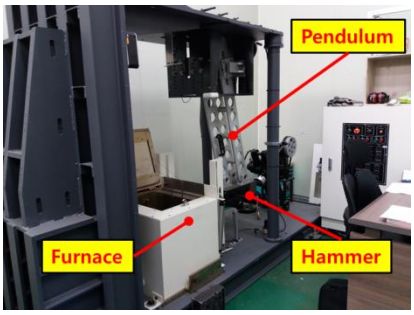

Fig. 2. The pendulum impact tester at KEPCO-NF.

KEPCO-NF is the only nuclear fuel manufacturer in Korea. They have a lot of interpretation/test skills and know-how about nuclear fuels. The hammer within the pendulum impact tester at KEPCO-NF is positioned at desired initial angle by the magnet. The pendulum impact test at KEPCO-NF is a KOLAS certification test. Test results performed at KEPCO-NF are summarized in Table 1.

5. Conclusions

The RRT of pendulum impact testers was conducted by PIEF, NFSRD and KEPCO-NF. In conclusion, the reliability of hot cell test equipment was confirmed through the facts that the measured dynamic buckling strengths are all within the technical goal and the standard deviation (SD) of the impact test results in PIEF is smallest.

ACKNOWLEDGEMENT

This work was supported by the Korea Institute of Energy Technology Evaluation and Planning (KETEP) and the Ministry of Trade, Industry & Energy (MOTIE) of the Republic of Korea (No. 2014171020166A).

REFERENCES

[1] J.Y. Kim et al., “Simplified Geometric Model Development to Evaluate Spent Fuel Integrity of Representative in Long-term Dry Storage”, Proc. of the KRS 2018 Autumn Conference, Oct. 31-Nov. 02, 2018, Jeju.

[2] Y.B. Chun et al., “Underwater Fuel Inspection for Irradiated LWR Fuels in Korea”, IAEA-TECDOC-1635 (2009).

[3] JaeYong Kim et al., “Analysis of Mechanical Integrity of Low Burnup Nuclear Fuel Assembly”, Proc. of IHLRWM 2019, Apr. 14-18, 2019, Knoxville, TN, USA.

Analysis on Remoteness of Spent Nuclear Fuel Assembly for Disassembling

Younghwan Kim*, Yungzon Cho, and Youngsoon Lee

Korea Atomic Energy Research Institute, 111, Daedeok-daero 989beon-gil, Yuseong-gu, Daejeon, Republic of Korea

*Yhkim3@kaeri.re.kr

1. Introduction

Because of harmful toxicity in the ambient environment, there are many situations that the human cannot access directly to the working area. Men cannot access to high radiation area, area with toxicity or explosive chemical, area where breathing is difficult, and area with severe temperature and pressure. The facility or situation with harmful environment includes nuclear fuel recycling and waste related nuclear energy facility, chemical and munitions factory, nuclear fusion reactor, and aerospace industry, etc. The process device operation in such environment shall be remotely done or additional facility shall be equipped to protect the worker. This study compares and analyzes the method of remotely disassembling spent fuel (SF) assembly using servo manipulator or robotic equipment, crane, and control device for the head-end process with radiation environment where human cannot access even with protective facility. The disassembling purpose of SF assembly of is to remove top and bottom nozzle for easy extraction of SF rods. This evaluation method classifies by referencing to the existing disassembly technologies to select the evaluation target, and evaluates the remote operability and efficiency of the disassembly.

2. Evaluation Method of Disassembling

To classify and evaluate the disassembling method on the assembly, a weight considering the effect on the post process such as relative comparison and decladding processing, etc. were reflected. The evaluation method classified the evaluation targets into 5 types and had relative values given to each target. That is, in the relative evaluation, the highest rank was 0.4, and the values were given in the order of 0.3, 0.2, 0.2, and 0, and if it is very important to the post process, which is the decladding process, 2 is given, if it is important, 1.5 is given, and if it is normal, 1 is given. Here, to secure maximum objectivity, the composition elements, number of modules, assembly property related to the number of modules, and complexity graph, etc. [Formula 1] were utilized. The final value is as in formula 2.

$$H_l(S) = H_l(M)+H_l(A) \quad (1)$$

($H_l(S)$: average complexity, $H_l(M)$: manufacturing complexity, $H_l(A)$: assembly complexity)

$$C = P_i*V_i*W_i \quad (2)$$

(C: final value, P: priority=1, V_i: relative value, W_i: weight)

3. Classification of Evaluation Target

The classification of the head-end process assembly disassembly method was done by referencing to the existing classification method, and it is as follows. 5 methods: 1) extracting the rods after shearing the top and bottom nozzle, 2) extracting the rods after saw cutting the top and bottom nozzle, 3) extracting the rods after removing top/bottom nozzle nut and top/bottom nozzle, 4) extracting the rods after laser cutting of the top/bottom nozzle, and 5) decladding after chopping the assembly including the top/bottom nozzle were selected. Here, the assembly disassembling technology for the rods array concentration process for the intermediate storage of SF in the later half of 1980's was referenced as the existing technology. (Westinghouse, General electric, NuTech, NUS, etc.)

The evaluation targets were analyzed with focus on the remote operability and the efficiency of the remote operation. The specific evaluation criteria of the remote operability were operation hours, tool/equipment size, size of the power, tool/equipment position control, maintenance, tool lifespan, equipment failure ratio, post process efficiency, accessibility, and the utilization of the space. Also, the specific evaluation criteria of the

efficiency of the remote operation were accessibility, remote operation of the tool, operation of the top/bottom nozzle removal, utilization of the space, module interference, number of modules, securing the visibility, handling, tool/equipment position control, and tool size. Table 1 is an example of the module interference evaluation in the efficiency of remote operation.

Table 1. Module interference at remote operability and efficiency

module interference																				
item	1 suggestion extraction after shearing of T/B nozzle				2 suggestion extraction after saw cutting of T/B nozzle				3 suggestion extraction after removing cutting of nut and T/B nozzle				4 suggestion extraction after laser cutting of T/B nozzle				5 suggestion decladding after chopping cutting of T/B nozzle and assembly			
module	- Transfer System - Punch Holder - Die Holder - Punch - Die - Clamper - Disassembly Table				- Saw Holder - Transfer System - Saw - Disassembly Table				- Motor - Rotation System - Nozzle Remover				- Laser Holder(4) - Transfer System - Laser Nozzle(4) - Motor - Rotation System - Disassembly Table				- Transfer System - Punch Holder - Die Holder - Punch - Die - Clamper - Pusher - Transfer System			
evaluation	▪ As shown in Figure 1, the larger the number of modules, the larger the assembly complexity and the larger the module interference, ▪ Module interference is the most important because there are 8 modules in Chopping mode. ▪ Module interferences are severe because the number of modules in the shearing system is 7. ▪ Since the number of laser modules is 6, the degree of module interference is normal. ▪ There is no module interference because of the number of modules in the saw mode. ▪ Module interference is minimized because of the number of modules of the nut removal method is three. ▪ All weights=1																			
results (priority, value, weights, total)	p	v	w	t	p	v	w	t	p	v	w	t	p	v	w	t	p	v	w	t
	4	0.1	1	0.1	2	0.3	1	0.3	1	0.4	1	0.4	3	0.2	1	0.2	5	0	1	0

4. Remote Operability and Efficiency Analysis

As a result of the analysis on the efficiency of the remote operation and the remote operability for SF assembly disassembling, the nut removal method had superior efficiency of the remote operation of SF assembly disassembly (relative value of 4.0 compare to the average value of 2.6), and the cutting method had superior remote operability for SF assembly disassembling (relative value of 3.5 compared to the average value of 2.4). In Fig. 1, comprehensively comparing the efficiency of remote operation and the remote operability, the cutting method was found to be suitable.

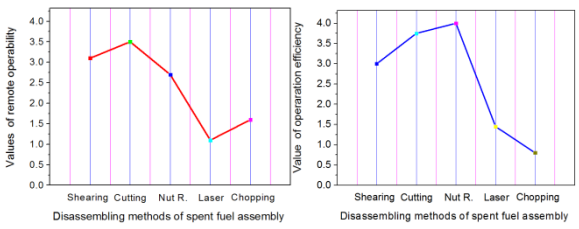

a) efficiency b) operability

Fig. 1. Analysis results related to SF disassembling methods.

5. Conclusion

To compare and analyze the method of disassembling SF assembly, the evaluation targets were classified and selected by referencing to the existing disassembly technologies, and the remote operability and the efficiency of remote operation were evaluated. The evaluation targets were classified to 5 types, and relative values were given to the targets. Also, considering the effect on the post process such as decladding process, weight was considered. Comprehensively considering the efficiency of remote operation and the remote operability, cutting method was found to be suitable for disassembly of SF assembly. But, if there is a variable in the post process, for example, whether mechanical decladding is used, or considering the decladding ration of the oxidation decladding, etc., another disassembling method may be an alternative.

ACKNOWLEDGEMENTS

This paper is the study carried out with the 2013 funding of the Ministry of Education, Science and Technology and the support from National Research Foundation of Korea (Nuclear Energy Technology Development Project, No. 2012M2A8A5025 696).

REFERENCES

[1] H. Chun-Ch “Overview of modular productd development,” Proc. Natl. Sci. Counc. ROC (A) vol. 24, no. 3, pp. 149-165, 2000.

3분과

고준위폐기물처분 (Oral)

Interpretation of Geological Deformation History by Integrated Analysis of Field and Borehole Survey Around KURT Area

Soolim Jung*, Kyung-Woo Park, Sung-Hoon Ji, and Kyung-Su Kim
Korea Atomic Energy Research Institute, 111, Daedeok-daero 989beon-gil, Yuseong-gu, Daejeon, Republic of Korea
*sljung@kaeri.re.kr

1. Introduction

In order to evaluate safety of disposal facilities for radioactive waste, it is necessary to understand the long-term evolution history of the disposal site. Tectonic deformation of geological environment, especially abrupt brittle deformation such as earthquake, can cause serious disturbances to the facility. Tectonic deformation processes are often considered to be less relevant due to the enormous time scale of geological events compared with the relatively short disposal period. However, it is still important to investigate the geological deformation history as a fundamental survey in order to understand the geochemical and hydrogeological environment of the site. In this study, the deformation history was interpreted by integrated analysis of field and borehole survey of the targeted area.

2. Methods

2.1 Study Area

The regional scale area around KURT(KAERI Underground Research Tunnel) is called Yuseong area, which is located in the boundary between Okcheon Belt and Kyunggi Massif. The area is mostly composed of Mesozoic intrusive body. The major rock type consisting KURT area is two-mica granite [1].

2.2 Geological Survey

In a previous study, a regional scale field survey and geological observation were performed along outcrops, exposed in the KURT. Different types of rocks were sampled and underwent chemical and microscopic analysis to interpret the intrusive and ductile deformation history of the site. Faults and joint systems were also observed and measured to interpret the brittle deformation history [2].

In this study, borehole data was gathered to supplement the history and to verify the potential to interpolation of the history into deep underground. Sampled core rocks were observed and logging data were applied to understand the brittle structure of the site.

3. Results

The major deformation history of the area revealed by the previous study was that the Paleozoic metamorphosed basement rock was intruded by magma in the Jurassic and the magma had cooled down until the Cretaceous. During the cooling, the hardened intrusive body started to uplift and fracture, and then mafic dykes intruded along the fractures after cooling in late Cretaceous [2].

Observation of cored rock showed similar petrogenesis to that of the outcrops. The Brittle structures were recognized more clearly in core logging data. Most of distinctive joint sets were

corresponded to approximately 6 sets of joints recognized in the outcrop of KURT, including three major sets of joints measured from the regional scale field survey. Detailed observation using relatively fresh cored rock suggested further classification of fractures with regard to fracture-filling minerals and associated evolution history.

4. Conclusion

According to the results so far, the regional area around KURT site had remained stable at least during the Quaternary period. The classification of fractures indicates that earlier hydrothermal alteration and later low temperature precipitation of calcite occurred during the uplifting and cooling of intrusive body. To clarify the alteration-related geological history, further chemical and microstructural analyses are necessary.

ACKNOWLEDGEMENT

This work was supported by the Ministry of Science, ICT and Future Planning within the framework of the national long-term nuclear R&D program (NRF-2017M2A8A5014858)

REFERENCES

[1] H.-I. Park, J.-D. Lee, and J.G. Jeong, “Geological map of Korea: Yuseong sheet”, Korea Institute of Geoscience and Mineral Resources (1977).

[2] S. Jung, S.-H. Ji, and K.-S. Kim, “Interpretation of geological deformation history using flat-cutting surfaces of the inner wall of KURT”, Proc. of the KRS 2018 Autumn Conference, 16(2), October 31-November 27, 2018, Jeju.

Hydrogeochemical Approaches on the Evaluation of Redox Environments in Granitic Bedrock Through New Borehole Drilling in the KURT

Jihye Jeong*, Jang-Soon Kwon, Yong-Kwon Koh, and Jae-Kwang Lee

Korea Atomic Energy Research Institute, 111, Daedeok-daero 989beon-gil, Yuseong-gu, Daejeon, Republic of Korea

*yz0201@kaeri.re.kr

1. Introduction

A new borehole (DB-3, 350 m) was drilled in the KURT (KAERI Underground Research Tunnel) by 2018, which was established as a study for the disposal of high-level radioactive waste, in order understand the redox environments in granitic bedrock. The specific purpose of this study is 1) to analysis of joints from the investigated core samples, and 2) to evaluate hydrogeochemical characteristics of groundwater with a depth.

2. Study Area

KURT (KAERI Underground Research Tunnel) is located at a mountainous area at the site of the Korea Atomic Energy Research Institute (KAERI) at a northern part of Daejeon city. The topography of the study site is well characterized as rolling hills surrounded by upland of EL. The geology of the study area is mainly composed of Mesozoic plutonic rock, Precambrian metamorphic rock, and a dike (Fig. 1).

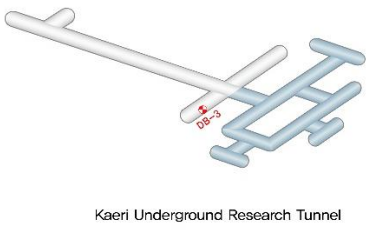

Fig. 1. Schematic diagram of the KURT and location of the investigated borehole (DB-3).

3. Results

3.1 Fracture and Hydraulic Conductivity

The detail core logging (fracture density study) was concurrently carried out with the hydraulic tests by applying a single/double packer system. As a result, we divided A (19 ~ 80 m), B (190 ~ 223 m), C (226 ~ 255 m) and D (275 ~ 350 m) sections with low fracture density (Fig. 2). The section A is considered to be difficult to preserve reduced groundwater because it is close to the surface. The number of fracture in section B is 9 ~ 19, with an average of 12. The number of fracture in the section C is 3 to 16, which is an average of 9. The D section with the lowest fracture distribution is fresh and not altered. This section is expected to be have reduced water because of the low fracture density, hydraulic conductivity and withdrawal rate.

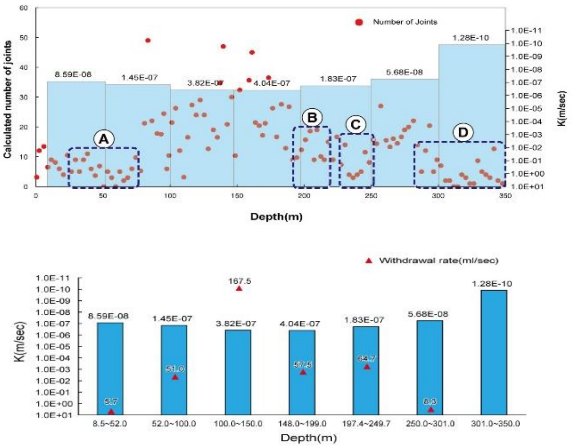

Fig. 2. (a) Hydraulic conductivity and fracture density, (b) Hydraulic conductivity and withdrawal rate of the DB-3 borehole with a depth interval.

3.2 Hydrogeochmical Characteristics

As the depth increases, the water quality evolves from the Ca-HCO_3 type to the Na-HCO_3 type. The geochemical behavior of uranium shows a positive correlation with DO, Eh and NO_3^- ion. Ca^{2+}, Mg^{2+}, SO_4^{2-}, and U-containing ions predominate in the upper section (0-100 m), but the concentrations of HCO_3^-, F^-, Na^+, and SiO_2 ions are higher in the lower

section (200 m or deeper) (Fig. 3).

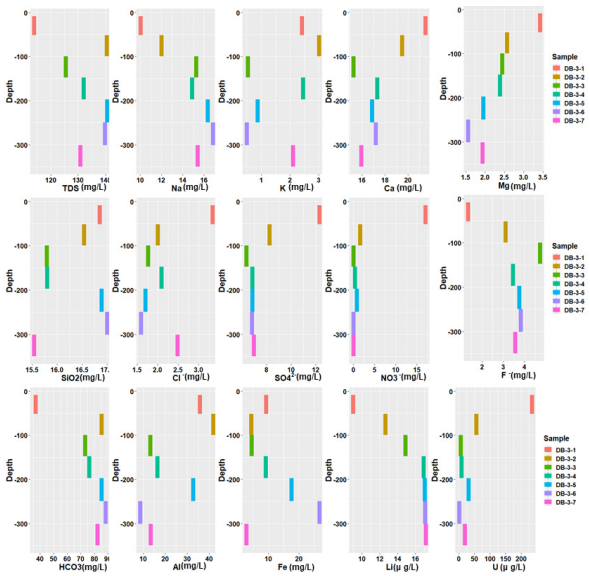

Fig. 3. Geochemical distribution of chemical constituents in DB-3 groundwater by depth interval.

3.3 Long-term Monitoring

Long-term monitoring was performed in D section of DB-3 to understand the redox characteristics in a low fractured area, and the result shows the reduced condition around -500 mV in redox potential (Fig. 4).

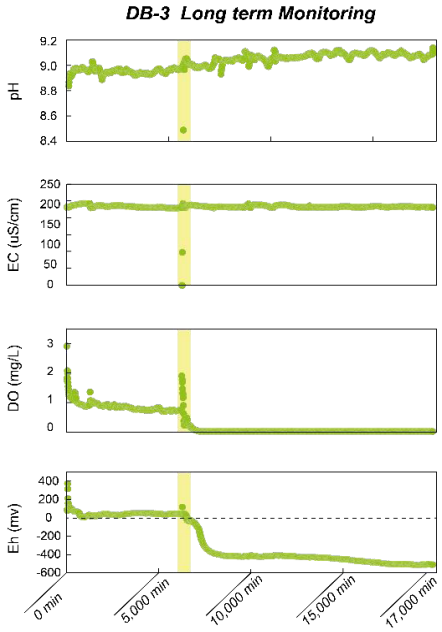

Fig. 4. Long term monitoring result (pH, EC, DO and Eh) of DB-3 borehole, yellow boxes indicates the moment of valve replacement.

4. Conclusion

In order to evaluate the geochemical environments of the granitic bedrock, core logging and on-site hydrogeochemical analyses were carried out at the new borehole in KURT. Homogeneous rocks and partially basic dykes are found in the lower section of deeper than 200 m. Particularly, the 300-350 m section disclosed the extremely reduction state (<-500 mV), and low hydraulic conductivity and flow rate. The changes Ca-HCO_3 type to Na-HCO_3 type with a depth shows the typical evolution in the granitic bedrock. Due to the weathering progress at the low section, concentrations of HCO_3^-, F^-, Na^+, and SiO_2 are increased. Long-term monitoring has been installed in the D section (deepest part) of DB-3 for continued management and characterization of reduced water.

ACKNOWLEDGEMENT

This work was supported by the Ministry of Science and ICT within the framework of the national long-term nuclear R&D program (NRF-2017M2A8A5014859).

Buffer Retardation Experiment for Radionuclides Under the Elevated Temperature Conditions: In-situ Synchrotron X-ray Powder Diffraction Study for the Korean Bentonite Under the Dry Conditions

Tae-Jin Park[1,*], Ji-Hun Ryu[1], Jae-Kwang Lee[1], and Donghoon Seoung[2,**]
[1] Korea Atomic Energy Research Institute, 111, Daedeok-daero 989beon-gil, Yuseong-gu, Daejeon, Republic of Korea
[2] Chonnam National University, 77, Yongbong-ro, Buk-gu, Gwangju, Republic of Korea
[*]etjpark@kaeri.re.kr, [**]dseoung@jnu.ac.kr

1. Introduction

The radioactive wastes including the spent nuclear fuels generate decay heats for a very long time. Thus, to host such wastes, the thermal criteria for the hosting buffer materials for the engineered barrier system must be set for the disposal repository. In most countries, it is set to below 100°C, due to the possible transformation of the smectite to illite which will result in the loss of the properties requested for the buffer.

If the thermal criteria for the maximum temperature for the hosting buffer system increases, the disposal density for the high-level radioactive wastes will increase dramatically [1]. This will certainly help certain nations with a high population density and a small area available for the disposal. Thus, understanding of the performance of the buffer system under the elevated temperatures are of central interest. We have developed a strategy and methodology for the Korean bentonite retardation experiments to validate the performance of the buffer materials under the elevated temperatures, especially from a viewpoint of a buffer retardation of radionuclides [2]. This includes (i) set up a rational condition for the Korean bentonite as a buffer material with time (Fig. 1), (ii) the characterization of the buffer in the absence and/or presence of the groundwater under the elevated temperatures, and (iii) the testing of the buffer retardation for the radionuclides of interest.

Here, we have investigated the hydration and dehydration reactions of the Korean bentonite to provide the characteristics of the buffer under the the elevated temperature conditions. More specifically, we have conducted in-situ X-ray powder diffraction experiments as a function of increasing temperature for the Korean bentonite (e.g., the Gyeongju bentonite).

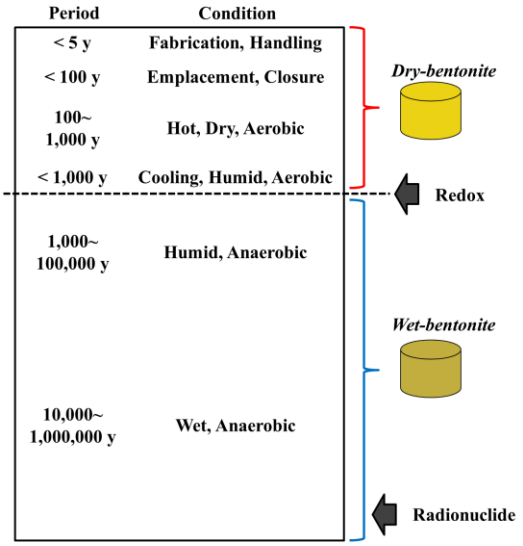

Fig. 1. Illustration of the conditions for the Korean buffer system with time (modified from Peter Keech's work) [2].

2. In-situ Synchrotron X-ray Powder Diffraction

2.1 Method

In-situ synchrotron X-ray powder diffraction on montmorillonite was performed at beamline 3D at Pohang light source (PLS-II) at Pohang accelerator laboratory (PAL). At beamline 3D, approximate 100 ㎛ beam of monochromatized X-rays with a wavelength of 0.6888 Å and MAR345 image plate detector was used to collect powder diffraction data.

For the in-situ sample heating environments, a

sealed capillary with a diameter of 700 ㎛ surrounded by nickel-chrome resistance heating coils was heated from RT to 250℃ as a function of temperature (Fig. 2). Temperature was raised for 30 minutes to each targeted steps, and was stabilized for 30 minutes.

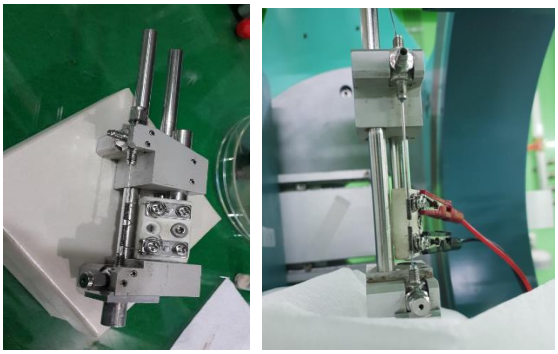

(a) (b)

Fig. 2. Setup for in-situ synchrotron XRD experiments under the elevated temperatures for the Korean bentonite (a) front view and (b) side view with heating linseed.

2.2 Montmorillonite under Dry Condition

Under dry condition, the Gyeongju bentonite shows thermal expansion after first dehydration sequence with 35.4% volume contraction at 120°C. Such hydration and/or dehydration reactions of montmorillonite are of significance in geological processes and also the waste disposal [3,4]. At cooling sequence, (001) reflection remains with 10 Å d-spacing without any hydration expiation. After air contact for a week, however, (001) d-spacing showed complete recovery (15.12 Å) to initial state (Fig. 3).

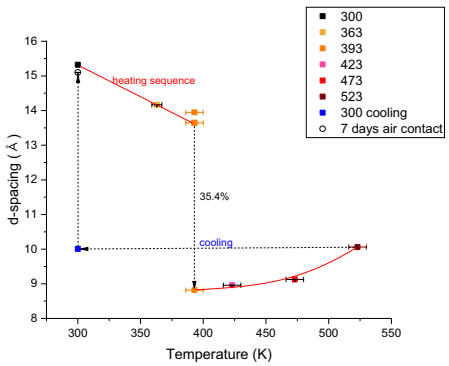

Fig. 3. Changes in the d-spacing (Å) of montmorillonite (001) reflections under dry condition as a function of temperatures.

3. Conclusions

We have experimentally established the characterization methodology for the Korean buffer under the elevated temperature employing a setup especially for the in-situ synchrotron XRD measurements. The montmorillonite (001) d-spacing of the Korean bentonite changes under the elevated temperature conditions show particular contraction at 120℃ with dehydration sequence. Gradual volume expansion of montmorillonite up to 250℃ implies its thermal expansion is anticipated after the dehydration of the buffer.

ACKNOWLEDGEMENT

We acknowledge the Korean government, Ministry of Science and ICT, for support (No. 2017M2A8A5014859).

REFERENCES

[1] Cho, W.-J. and Kim, G. Y., “Reconsideration of thermal criteria for Korean spent fuel repository,” Annals Nucl. Ener. 88, 73-82 (2016).

[2] Park, T.-J., Ryu, J.-H., Cho, W. H., and Lee, J.-K., "Buffer retardation experiments for radionuclides under the elevated temperature conditions: Strategy and methodology development for the Korean bentonite," Proc. Kor. Rad. Waste Soc., 16(2), 203-204 (2018).

[3] Ewing, R.C., "Long-term storage of spent nuclear fuel," Nature Materials, 14(3): p. 252-257 (2015).

[4] Sellin, P. and O.X. Leupin, "The use of caly as an engineered barrier in radioactive-waste management - A review," Clays and Clay Minerals, 61(6): p. 477-498 (2013).

Buffer Retardation Experiment for Radionuclides Under the Elevated Temperature Conditions: In-situ Synchrotron X-ray Powder Diffraction Study for the Korean Bentonite Under the KURT Groundwater Saturated Conditions

Donghoon Seoung[1,*] and Tae-Jin Park[2,**]
[1] Chonnam National University, 77, Yongbong-ro, Buk-gu, Gwangju, Republic of Korea
[2] Korea Atomic Energy Research Institute, 111, Daedeok-daero 989beon-gil, Yuseong-gu, Daejeon, Republic of Korea
*dseoung@jnu.ac.kr , **etjpark@kaeri.re.kr

1. Introduction

Bentonites are to be used as buffer materials in a geological repository designed to host high-level radioactive wastes. The radioactive wastes including the spent nuclear fuels generate decay heats for a very long time. Although, most of the criteria is set to below 100°C for the bentonites, some efforts have been started to reconsider the thermal criteria for the buffer [1]. Thus, the hydration and dehydration reactions under the elevated temperatures of the bentonite, especially the montmorillonite as the main mineral component responsible for the performance of the buffer system, are of crucial importance in geological processes and the radioactive wastes disposal [2, 3].

The hydration and dehydration procedures concomitant with volume expansion and contraction of clay inside bentonite provide important information related with interstratified layers configuration, since the hydration and dehydration process depend on the composition of metal cations and water layers in interstratified layers [4]. We have conducted in-situ X-ray powder diffraction experiments as a function of increasing temperature for the Korean bentonite (e.g., the Gyeongju bentonite) under the dry as well as the KURT groundwater saturated conditions. Here, we report the results obtained under the KURT groundwater saturated conditions.

2. In-situ Synchrotron X-ray Powder Diffraction

2.1 Method

In-situ synchrotron X-ray powder diffraction on montmorillonite was performed at beamline 3D at Pohang light source (PLS-II) at Pohang accelerator laboratory (PAL). At beamline 3D, approximate 100 ㎛ beam of monochromatized X-rays with a wavelength of 0.6888 Å and MAR345 image plate detector was used to collect powder diffraction data.

For the in-situ sample heating environments, a sealed capillary with a diameter of 700 ㎛ surrounded by nickel-chrome resistance heating coils was heated from RT to 250℃ as a function of temperature. The temperature was raised for 30 minutes to each targeted steps, and was stabilized for 30 minutes.

2.2 Montmorillonite under the KURT Groundwater Saturated Condition

At heating sequence, (001) d-spacing gradually decreases. At 120℃ it was drastically decreases from 19.02 Å to 16.11 Å concomitant with 14.2% of volume contraction. As temperature increases, it shows gradual decrease until the final step of experiment, 225℃. At cooling sequence with water saturated condition, it shows complete recovery to 19.12 Å of d-spacing (Fig. 1).

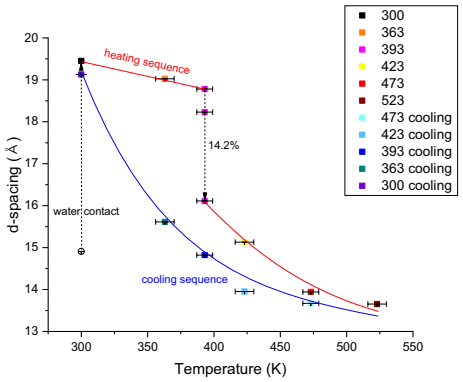

Fig. 1. Changes in the d-spacing (Å) of montmorillonite (001) reflections under water saturated condition as a function of temperature. Black line shows superhydration at initial water contact, red line shows heating sequence, and blue line shows cooling sequence.

2.3 Pretreated-Montmorillonite under the KURT Groundwater Saturated Condition

The Korean bentonite pretreated for longer than 365 days with LAB-TH setup under the elevated temperature conditions was prepared for the comparison.

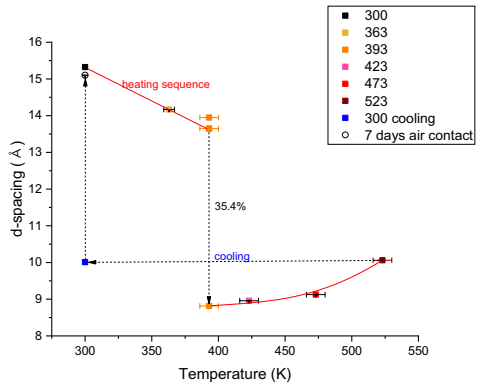

Fig. 2. Changes in the d-spacing (Å) of montmorillonite (001) reflections under dry condition as a function of temperature.

At 120℃, drastic d-spacing decrease from 19.04 Å to 15.36 Å concomitant with about 19.3% of volume contraction was observed. Particularly, it shows additional d-spacing decrease at 200℃ from 13.79 Å to 8.53 Å with ~38.1% volume contraction. After air contact for a week, d-spacing showed minor recovery to 15.75 Å (Fig. 2).

3. Conclusions

We experimentally established that montmorillonite (001) d-spacing changes under the elevated temperature conditions including both hydrothermal and dry conditions show particular contraction at 120℃ with dehydration sequence. Gradual volume contraction of montmorillonite up to 250℃ under water saturated condition implies its second dehydration temperature is anticipated over final stage.

ACKNOWLEDGEMENT

This work was supported by the Korean government, Ministry of Science and ICT, for support No. 2017M2A8A5014859 and NRF-2017R1D1A1B03035418.

REFERENCES

[1] Park, T.-J., Ryu, J.-H., Cho, W. H., and Lee, J.-K., "Buffer retardation experiments for radionuclides under the elevated temperature conditions: Strategy and methodology development for the Korean bentonite," Proc. Kor. Rad. Waste Soc., 16(2), 203-204 (2018).

[2] Ewing, R.C., "Long-term storage of spent nuclear fuel," Nature Materials, 14(3): p. 252-257 (2015).

[3] Sellin, P. and O.X. Leupin, "The use of caly as an engineered barrier in radioactive-waste management - A review," Clays and Clay Minerals, 61(6): p. 477-498 (2013).

[4] Park, T.-J., Ryu, J.-H., Cho, W. H., and Lee, J.-K., "Buffer retardation experiments for radionuclides under the elevated temperature conditions: Strategy and methodology development for the Korean bentonite," Proc. Kor. Rad. Waste Soc., 16(2), 203-204 (2018).

A Prediction on the Behavior of a Multi-layer Repository Using Thermo-Hydro-Mechanical Damage (THM_D) Model for the HLW Disposal

Jin-Seop Kim[1,*], Jun-Seo Jeon[2], and Geon-Young Kim[1]

[1] Korea Atomic Energy Research Institute, 111, Daedeok-daero 989beon-gil, Yuseong-gu, Daejeon, Republic of Korea

[2] Korea Advanced Institute of Science and Technology, 291, Daehak-ro, Yuseong-gu, Daejeon, Republic of Korea

[*]kjs@kaeri.re.kr

1. Introduction

The coupled thermo-hydro-mechanical (THM) behaviors in a geological formation is one of the key issues from the perspective of a nuclear waste disposal. Taking into account the geological condition of Korea, it is necessary to increase the disposal density. Damage evolution in a nuclear waste disposal system is one of the important issues from the perspective of a long-term safety concerns.

The objective of this study is to evaluate the multi-layer repository concept to improve the disposal efficiency in Korea, in which the coupled thermo-hydro-mechanical damage (THM_D) model was applied to simulate the time-dependent long-term behaviors of disposal system.

2. Approach

2.1 General Approach

Mazars damage model was applied to THM_D model development with regard to the damage evolution of rock. A concept of Barcelona Basic Model (BBM) was used to simulate unsaturated and partially saturated bentonite by incorporating an extra state variable for the pore suction. The general approach for THM_D model development is presented in Fig. 1. The primary code in use was Comsol MultiPhysics Ver. 5.4.

2.2 Mass Balance Equations

Solid

$$\frac{(1-n)}{\rho^s}\frac{D^s\rho^s}{Dt}-\frac{D^s n}{Dt}+(1-n)\operatorname{div}\mathbf{v}^s=0 \tag{1}$$

Liquid water

$$\left(\frac{\alpha-n}{K_s}S_w^2+\frac{nS_w}{K_w}\right)\frac{D^s p^w}{Dt}+\frac{\alpha-n}{K_s}S_w S_g\frac{D^s p^g}{Dt}+\alpha S_w\operatorname{div}\mathbf{v}^s-\beta_{sw}\frac{D^s T}{Dt}+\left(\frac{\alpha-n}{K_s}p^w S_w-\frac{\alpha-n}{K_s}p^g S_w+n\right)\frac{D^s S_w}{Dt}+\frac{1}{\rho^w}\operatorname{div}\left\{\rho^w\frac{\mathbf{k}k^{rw}}{\mu^w}\left[-\operatorname{grad}p^w+\rho^w(\mathbf{g}-\mathbf{a}^s-\mathbf{a}^{ws})\right]\right\}=-\frac{n\overset{\&}{\rho}^w}{\rho^w} \tag{2}$$

Gas

$$\frac{\alpha-n}{K_s}S_w S_g\frac{D^s p^w}{Dt}+\frac{\alpha-n}{K_s}S_g^2\frac{D^s p^g}{Dt}-\left(n+\frac{\alpha-n}{K_s}p^c S_g\right)\frac{D^s S_w}{Dt}-\beta_s(\alpha-n)S_g\frac{D^s T}{Dt}+\alpha S_g\operatorname{div}\mathbf{v}^s+\frac{nS_g}{\rho^g}\frac{D^s}{Dt}\left[\frac{1}{\theta R}\left(p^{ga}M_a+p^{gw}M_w\right)\right]+\frac{1}{\rho^g}\operatorname{div}\left\{\rho^g\frac{\mathbf{k}k^{rg}}{\mu^g}\left[-\operatorname{grad}p^g+\rho^g\left(\mathbf{g}-\mathbf{a}^s-\mathbf{a}^{gs}\right)\right]\right\}=\frac{n\overset{\&}{\rho}^g}{\rho^g} \tag{3}$$

2.3 Momentum Balance Equations

$$-\rho\mathbf{a}^s-nS_w\rho^w\left[\mathbf{a}^{ws}+\operatorname{grad}\mathbf{v}^w\cdot\mathbf{v}^{ws}\right]-nS_g\rho^g\left[\mathbf{a}^{gs}+\operatorname{grad}\mathbf{v}^g\cdot\mathbf{v}^{gs}\right]+\operatorname{div}\sigma+\rho\mathbf{g}=0 \tag{4}$$

3. Model Setup

The material properties and model constants used in THM_D modeling are listed in Table 1 below. Fig. 2 shows the model geometry and dimensions used for the developed model application.

Table 1. Material properties used in THM_D model

	Parameter	Bentonite	Rock	plug	Heater
Mechanical	Density of solid particle	2740	2650	2367	7850
	Dry density [kg/m^3]	1600	2650	2367	7850
	Biot's coefficient	0.8	1.0	0.8	1.0
	porosity	0.41	0.01	0.15	0.0001
	Residual porosity	-	0.009	-	-
	Young's modulus [GPa]	-	22.8	20.0	155.0
	Poisson's ratio	0.4	0.2	0.19	0.285

Hydraulic	Intrinsic permeability [m^2]	6e-20	1e-19	1e-19	-
	P_0 [MPa]	3.8	1.5	1.5	-
	m	0.25	0.595	0.595	-
	S_{lr}	0	1	1	-
	S_{ls}	1	0.01	0.01	-
	λ	3	0.595	1	-
Thermal	Thermal conductivity [W/mK]	1.299	3.3	1.2	52.5
	Specific heat capacity [J/kg/K]	1000	1210	964	440
	Thermal expansion Coefficient [1/K]	2.5e-5	7.5e-6	4.3e-6	0

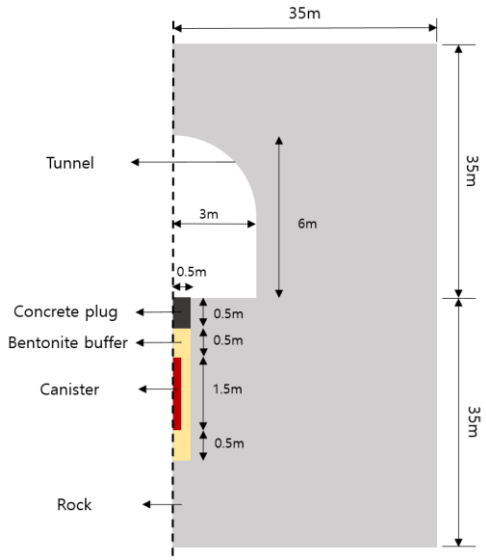

Fig. 1. Model geometry and dimensions of each disposal tunnel.

4. Main Results

The variation of saturation, temperature and pore pressure of bentonite are presented with time in Fig. 3-6.

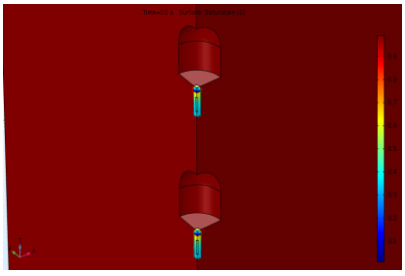

Fig. 2. Saturation profile after 10 years.

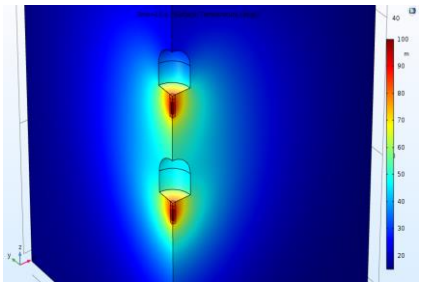

Fig. 3. Temperature profile after 10 years.

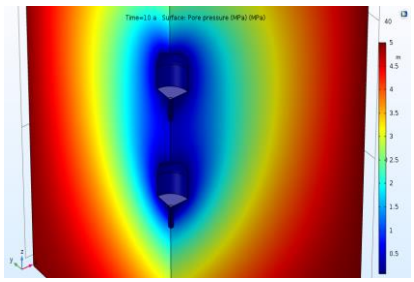

Fig. 4. Pore pressure profile after 10 years.

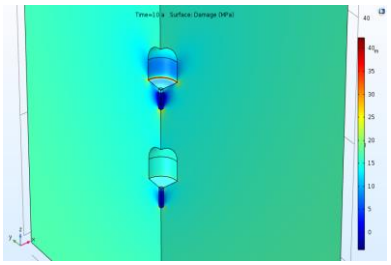

Fig. 5. Stress pressure profile after 10 years.

5. Conclusion

With regard to THM parameters, the interference effects of disposal tunnels can be clearly found under this modeling condition. The results from this study can be utilized to determine the minimum distance of layer-to-layer in the concept of multi-layer repository.

REFERENCES

[1] J. Mazars, “A description of micro-and macroscale damage of concrete structures”, Engineering Fracture Mechanics, 25(5/6), 729-737 (1986).

[2] C. Wei, W. Zhu, S. Chen and P.G. Ranjith, “A coupled Thermal-Hydrological-Mechanical damage model and its numerical simulations of damage evolution in APSE”, Materials, 9(841), 1-19 (2016).

Spherical Gas Migration Modelling Using Mechanical Damage Model

Jaewon Lee*, Changsoo Lee, and Geon Young Kim
Korea Atomic Energy Research Institute, 111, Daedeok-daero 989beon-gil, Yuseong-gu, Daejeon, Republic of Korea
*jwl@kaeri.re.kr

1. Introduction

The flow of repository gases through clay-rich material is usually described by assuming four basic phenomenological models: (1) diffusion; (2) two-phase flow models; (3) models where gas flows along localized dilatant pathways and (4) models where gas fractures the material. Although classic two-phase flow models are highly extended and employed, they are not able to describe the full complexity of gas migration processes, and therefore, new and novel numerical representations for the quantitative description of advective gas flow in clay-based repository systems are required. In this study, we developed a gas migration model using a mechanical damage model, and compared the results of a laboratory gas injection test and numerical analysis for a model validation.

2. Numerical Model

2.1 Mechanical Damage Model

In order to model the gas migration phenomena, we adopted elastic damage model by Tang et al. [1]. In this model, the elastic modulus degrades gradually as damage progresses, and elastic modulus of damaged element is as follows:

$$E = (1 - D)E_0 \quad (1)$$

where D represents the damage variable, and E and E_0 are the elastic moduli of the damaged and undamaged elements, respectively.

2.2 Gas Injection Experiment

The experiment undertaken by the British Geological Survey (BGS) consisted of a spherical gas injection test performed on a pre-compacted bentonite subject to a constant volume boundary condition [2].

2.3 Properties

Table 1 shows properties of bentonite. Elastic modulus, Poisson ratio, porosity, and permeability are given properties. Other mechanical and hydraulic properties are issued by references except damage model properties.

Table 1. Properties of bentonite

Properties	Bentonite	
Elastic model	Elastic modulus (Pa)	3.07E+08
	Poisson ratio	0.4
Damage model	Tensile strength (Pa)	1.00E+06
	Residual tensile strength (Pa)	2.00E+05
	Compressive strength (Pa)	1.20E+6
	Residual compressive strength (Pa)	3.00E+6
	Tensile strain limit	5.00E-03
Biot coefficient		0.86
Porosity (-)		0.44
Intrinsic Permeability (m^2)		3.40E-21

3. Results

Fig. 1 shows injection pressure evolution. Trend of injection pressure has a good fitting with respect to experimental results. However, fluctuation due to the damage is no modelled because damage of bentonite is preserved and outflux is continuous in the numerical model.

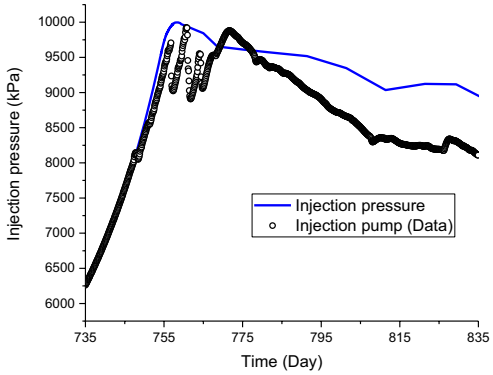

Fig. 1. Injection pressure evolution.

4. Conclusion

For modelling about gas migration, we developed a gas migration model using mechanical damage model and compared the results of laboratory gas injection experiment and numerical analysis. In general, Trend of injection pressure has a good fitting with respect to experimental results. However, fluctuation due to the damage is no modelled because damage of bentonite is preserved and outflux is continuous in the numerical model.

ACKNOWLEDGEMENT

This research was supported by the Nuclear Research and Development Program of the National Research Foundation of Korea (NRF-2017M2A8A5014857) funded by the Minister of Science and ICT.

DECOVALEX is an international research project comprising participants from industry, government and academia, focusing on development of understanding, models and codes in complex coupled problems in sub-surface geological and engineering applications; DECOVALEX-2019 is the current phase of the project. The authors appreciate and thank the DECOVALEX-2019 Funding Organisations Andra, BGR/UFZ, CNSC, US DOE, ENSI, JAEA, IRSN, KAERI, NWMO, RWM, SÚRAO, SSM and Taipower for their financial and technical support of the work described in this paper. The statements made in the paper are, however, solely those of the authors and do not necessarily reflect those of the Funding Organisations.

REFERENCES

[1] C.A. Tang, L.G. Tham, P.K.K. Lee, T.H. Yang, and L.C. Li, “Coupled analysis of flow, stress and damage (FSD) in rock failure”, International Journal of Rock Mechanics & Mining Sciences, 39, 477-489 (2002).

[2] J.F. Harrington, C.C. Graham, R.J. Cuss and S. Norris, “Gas network development in a precompacted bentonite experiment: Evidence of generation and evolution”, Applied Clay Science, 147, 80-89 (2017).

Development of a GoldSim Module for Sequential Bayesian Updating for Better Probabilistic Safety Assessment of an HLW Repository

Youn-Myoung Lee and Dong-Keun Cho

Korea Atomic Energy Research Institute, 111, Daedeok-daero 989beon-gil, Yuseong-gu, Daejeon, Republic of Korea

ymlee@kaeri.re.kr

1. Introduction

During almost the last two decades much effort has been devoted to the development of a safety assessment of a conceptual HLW repository for spent nuclear fuels (SFs) from both PWR and CANDU reactors as templates using the commercial GoldSim [1]. Most representative one, among many similar others, is GSTSPA (GoldSim Total System Performance Assessment) [2] for probabilistic assessment of the repository. This program has been proven to be suitable for such an evaluation of nuclide transports in the near- and far-field of a repository as well as a transition among biosphere compartments under various release scenarios associated with FEPs identified. Although almost all required parameter values associated with the repository system are usually assumed or sometimes overestimated and still far from being highly reliable, such methodology results from the probabilistic models are believed to be reliable and informative not only for safety assessment of the repository, but also for its design feedback. Uncertainties nested in nuclide transport modeling around the repository are mainly dominated by parametric uncertainty, involved in input parameter values, aside from intrinsic model uncertainty. Reliable estimate of the parameter values commonly expressed as probability density functions (PDFs) always require a large amount of measured data. These PDF distributions are used as input to the probabilistic assessment program through Monte Carlo simulation to quantitatively provide possible uncertainty of the results. However, in most cases, especially in the safety assessment of the repository which is typically related with both long time span and wide modeling domain, inefficient observed data from the field measurements are common, making conventional probabilistic calculations rather uncertain. Therefore, in most cases, although estimation of the distributions successfully expressed as PDFs or other types, parametric uncertainty could still remain. Since Bayesian approach is known to be especially powerful and efficient in the case of lacking of available data measured, such short data could be compensated by coupling with a priori belief, reducing uncertainty. By allowing the a priori knowledge for incorporating insufficient observed data, which include expert' elicitation, their beliefs and judgment regarding the parameters as well as recent site-specific measurements, based on the Bayes' theorem, the older parameter distributions, "prior" distribution can be updated to a rather newer and reliable "posterior" distribution. Newer distributions are not necessarily expressed as PDFs for probabilistic calculation. These updates could be done even iteratively as many times as data values are sequentially available, which calls sequential Bayesian updating, making posterior distributions become much more reliable by reducing parametric uncertainty. Through this study the development of the Bayesian updating module implemented to GSTSPA is introduced (Fig. 1.).

2. Sequential Bayesian Updating

Bayesian framework allows us to update our beliefs iteratively every time new data from measurements and observations continuously come in. At time *n*, we may have an updated distribution of parameters to its posterior as

$$p(\vec{\theta}|D_{n+1}) \propto \mathcal{L}(D_{n+1}|\vec{\theta}) \cdot p(\vec{\theta}|D_n). \qquad (1)$$

For Bayesian updating described above, despite of its advantage in buildup of belief for the parameter distribution, practical application is still limited due to difficulty to get a posterior distribution analytically. Markov Chain Monte Carlo (MCMC) sampling algorithm was adopted, by which posterior distribution could be sampled.

3. GoldSim Module

Among several MCMC methods, Hastings-Metropolis (M-H) algorithm has been used in this study for its popularity (Fig. 2). M-H algorithm has been implemented as a GoldSim module into the GSTSPA using a conditional looping container which only activates at time zero on the first realization. Values sampled from either the prior distribution and multiple posterior distributions are then ready to be used as inputs to the GSTSPA model for probabilistic Monte Carlo safety assessments of the repository (Figs. 3 and 4).

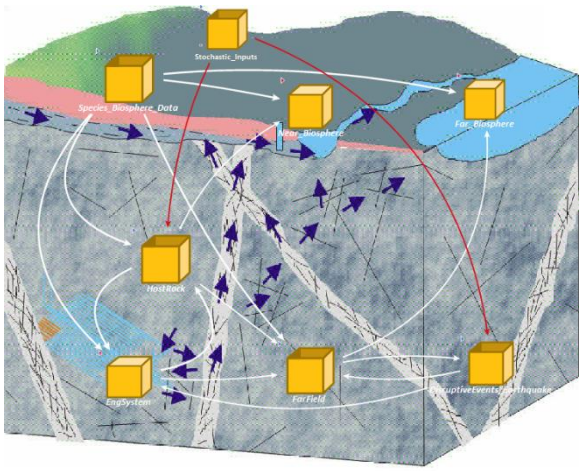

Fig. 1. Banner of GSTSPA program with Bayesian updating module.

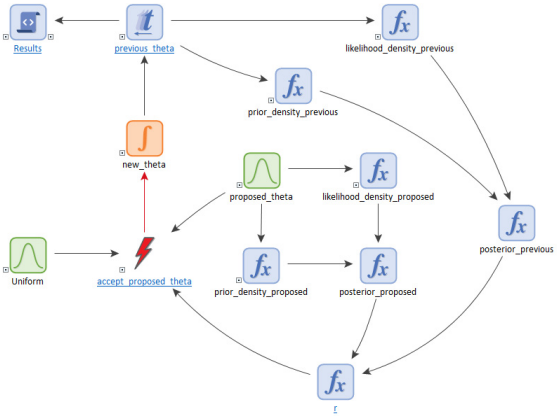

Fig. 2. Implementation of M-H algorithm to GSTSPA.

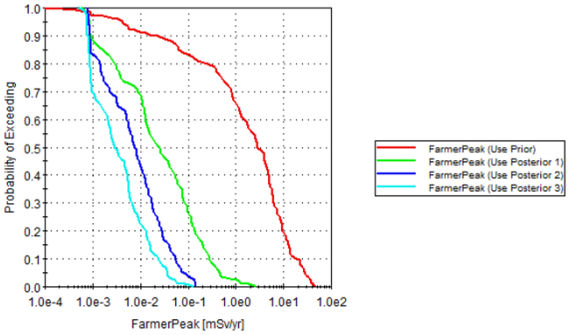

Fig. 3. Annual dose results expressed as CCDFs prior and updated posterior distributions.

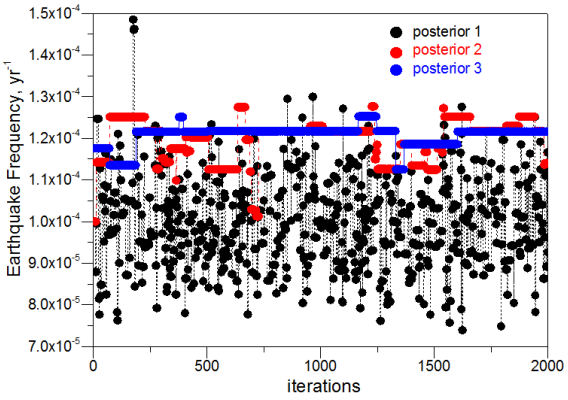

Fig. 4. Realizations of sequential Bayesian updating by MCMC for earthquake frequency.

REFERENCES

[1] GoldSim, GoldSim Contaminant Transport Module, User's Guide, Version 4, GoldSim Technology Group, Seattle, U.S.A. (2006).

[2] Youn-Myoung Lee et al., "An evaluation of an earthquake scenario for a pyroprocessed waste repository," Progress in Nuclear Energy 66, pp.133-145, (2013).

Application of the Adjustment Factor Approach for the Quantification of Model Uncertainty

Jongtae Jeong* and Dong-Keun Cho

Korea Atomic Energy Research Institute, 111, Daedeok-daero 989beon-gil, Yuseong-gu, Daejeon, Republic of Korea

*jtjeong@kaeri.re.kr

1. Introduction

The adjustment factor was suggested by Mosleh and Apostolakis to combine experts' estimate according to Bayes' theorem. They applied it to the quantification of model uncertainty for the problems of groundwater flow and contaminant transport [1]. Combination of predictions by all the models should be considered to quantify model uncertainty. Combination of response predictions by multiple models using adjustment factor approach is carried out by averaging those predictions weighted by model probabilities. In this paper, we applied the additive adjustment factor approach to release rate models for the quantification of model uncertainty.

2. Adjustment Factor Approach

2.1 Adjustment Factor Approach

An adjustment factor can be evaluated by assuming the differences between the prediction by the model with the highest probability and those of alternate models to be normally distributed [2]. Model probabilities are assigned as weights to the models considered. A predictive distribution of a system response is constructed by introducing the evaluated adjustment factor into the prediction by the model with the highest probability.

An additive adjustment factor is added to the prediction by the model with the highest probability to construct a predictive distribution incorporating model uncertainty. When the additive adjustment factor approach is used, the prediction of a system response is represented by

$$\mathrm{y} = y^* + E_a^* \tag{1}$$

where, y^* represents the prediction of the unknown response by the model with the highest model probability among a considered model set, E_a^* represents an additive factor, and y represents an adjusted prediction. An additive adjustment factor E_a^* is assumed to be a normal random variable. If we assume that the predictions and probabilities of a set of models are known, the means and variances of both E_a^* and y can be computed by

$$E(E_a^*) = \sum_{k=1}^{K} \Pr(M_k)\,(y_k - y^*) \tag{2}$$

$$Var(E_a^*) = \sum_{k=1}^{K} \Pr(M_k)(y_k - E(y))^2 \tag{3}$$

$$E(y) = y^* + E(E_a^*) \tag{4}$$

$$Var(y) = Var(E_a^*) \tag{5}$$

where $\mathrm{E}(\cdot)$ is mean of a variable, $\mathrm{Var}(\cdot)$ is variance of a variable, y_k represents the prediction of the response by mode M_k, $\Pr(M_k)$ is the probability of M_k, and K is the number of considered models. The mean and variance of E_a^* are the averaged mean and variance of the differences between the prediction by the model with the highest probability and those by alternate models, using model probabilities as weights.

2.2 Application Adjustment Factor Approach to Release Rates of ^{129}I

We applied the additive adjustment factor approach to the release rate of ^{129}I. The release rates are summarized in Table 1. The model probabilities of each model in Table 1 are assumed values based on the results of Jeong et al. [3]. The Annual release rate model is identified as the best model because it has the highest model probability among three models. Using the additive adjustment factor approach, the mean and variance of the resulting combination of model prediction for release rates of ^{129}I are $2.68x10^{-2}$ and $5.66x10^{-5}$, respectively. The best model prediction is decreased by the amount of $0.29x10^{-2}$. The variance indicates the degree of dispersion in the prediction of models and reflects the degree of model uncertainty.

Table 1. Release rates of I-129 (g/yr)

Release rate model	Release Rate (g/yr)	Model Probability
Annual Release	2.97×10^{-2}	0.5
Congruent Release	2.87×10^{-2}	0.4
Surface Release	4.22×10^{-3}	0.1

3. Conclusions

We adopted the additive adjustment factor approach to incorporate model uncertainty into the composite prediction of a physical system. We applied this approach to the release rates of ^{129}I from the waste package. If deterministic predictions by a model set and experimental data, the approach can be applied to model uncertainty quantification regardless of the numbers of models considered and the observed experimental data.

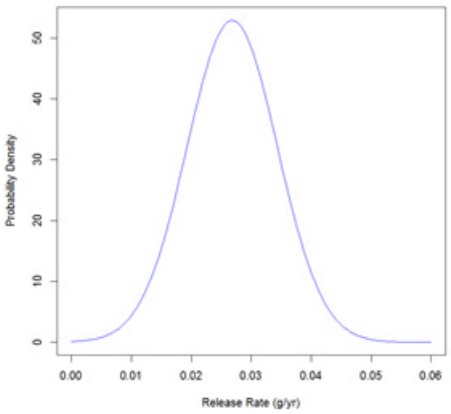

Fig. 1. PDF of release rate of ^{129}I using additive adjustment factor approach.

ACKNOWLEDGEMENT

This work was supported by the National Research Foundation of Korea Nuclear Research and Development Program (2017M2B2B1072407, 2017M2A8A5014856) funded by the Ministry of Science and ICT.

REFERENCES

[1] Zio E, Apostolakis G., "Two methods for the structured assessment of model uncertainty by experts in performance assessments of radioactive waste repositories", Reliability Engineering and System Safety 54, 225–41 (1996).

[2] I. Park et al., "A Bayesian approach for quantification of model uncertainty", Reliability Engineering and System Safety 95, 777-785 (2010).

[3] Jongtae Jeong et al., "Update of model probability for release rates of radionuclides using Bayes' Theorem", Proceedings of 2018 Fall Meeting of the Korean Radioactive Waste Society, 2018.

3분과

고준위폐기물처분 (Poster)

The Methodology for the Decision of Groundwater Monitoring Points Around a Nuclear Facility

Kyung-Woo Park*, Sung-Hoon Ji, and Jang-Soon Kwon

Korea Atomic Energy Research Institute, 111, Daedeok-daero 989beon-gil, Yuseong-gu, Daejeon, Republic of Korea

*woosbest@kaeri.re.kr

1. Introduction

Generally, the radioactive contaminant which is leaked from the nuclear use facility moves to the ecosystem by a run-off through the river or an advective transport through the groundwater flow. Among the two mechanisms, the contaminant plume through the river can be easily detected in surface water monitoring system, but the advective transport of a radioactive contaminant with the groundwater flow is difficult to monitor because of the lack of information for the flow path. To more understand the contaminant flow in groundwater, the description of geo-environment is needed. In this study, we suggest the methodology of the decision of monitoring point from a nuclear use facility by using the results of site characterization.

2. Study Area

The study area is located at a northern part of Daejeon city. The topography of the study site is well characterized as rolling hills surrounded by upland of EL. 300-500 m and the lowland of about EL. 50 m. The geology of the study area is mainly composed of Mesozoic plutonic rock, Precambrian metamorphic rock, and a dike. The geologic formation of the Mesozoic plutonic rock is Jurassic schistose granite and two-mica granite. The Cenozoic alluvium is distributed over a wide area through the surface basin system in the research area with a 3-11 m depth. To make the monitoring system, we imagine the nuclear facility which acts as a contaminant source in the study area (Fig. 1).

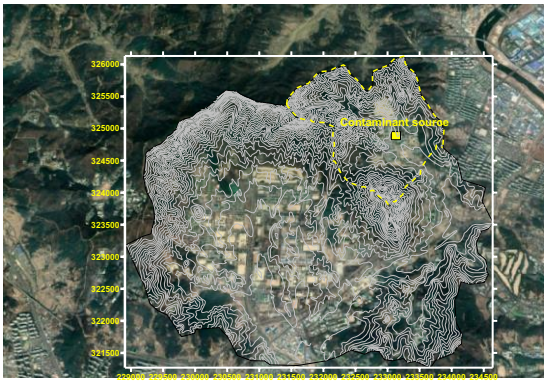

Fig. 1. Location of the imaginary nuclear facility.

3. The Decision of Monitoring Point

3.1 Borehole Location

RM-1 borehole was drilled in 2018 to install the monitoring system. To decide the location of RM-1 borehole, we conducted the groundwater flow modeling based on the site descriptive model. From the result of a groundwater flow simulation, the contaminant transport from the imaginary nuclear facility was simulated by the particle tracking method and RM-1 borehole is located in the middle of the flow path from the imaginary nuclear facility (Fig. 2).

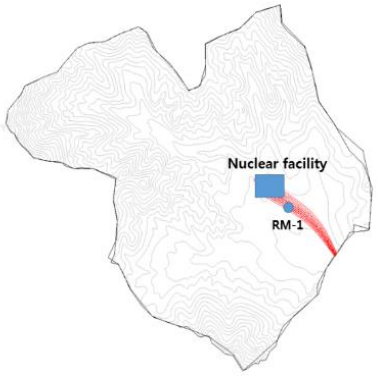

Fig. 2. Location of the RM-1 borehole.

3.2 Field Investigations

To decide the monitoring point in RM-1 borehole, the fracture logging along the borehole, hydro-chemical logging of the groundwater in the borehole and detail hydraulic tests with 30m interval were conducted. From the fracture logging, 4 geological units (weathered zone, upper/lower fracture rock and fracture zone) were defined and total 4 fracture zones were identified in the RM-1 borehole. The Hydro-chemical logging data told that there are 6 hydro-chemical anomalies, which were considered as water-conducting features in RM-1 borehole. And, we could obtain the 3 hydrogeological units (HSD, UHRD, 4 HCDs) from the result of the in-situ hydraulic test.

Table 1. Monitoring points from the result of the geological logging (● : most favorable, ▲:favorable)

Section (GL.-m)	Geological description	Width	Preference
surface~28.0	Weathered zone	28	●
28.0~61.0	Upper fractured rock	33	●
69.0~72.0	Fracture zone1	3	▲
80.0~84.0	Fracture zone2	4	●
100.0~112.0	Fracture zone3	2	▲
143.0~147.0	Fracture zone4	4	●
61.0～150.0	Lower fractured rock		

Table 2. Monitoring points from the hydro-chemical logging (● : most favorable, ▲:favorable)

Section (GL.-m)	Width	Preference
31.0～34.0	3	●
44.0～47.0	3	●
56.0～58.0	2	
63.0～67.0	4	●
69.0～73.0	4	●
143.0～145.0	2	▲

Table 3. Monitoring point from the hydraulic tests (● : most favorable, ▲:favorable)

HG description	Section (GL.-m)	K/T	Preference
HSD	0~28	5.43×10^{-6} m/sec	●
UHRD	28~61	1.52×10^{-6} m/sec	●
HCD	69.0~72.0	1.76×10^{-5} m^2/sec	●
	80.0~84.0	1.64×10^{-7} m^2/sec	▲
	100.0~112.0	8.28×10^{-9} m^2/sec	
	143.0~147.0	4.72×10^{-6} m^2/sec	●

4. Conclusion

When the geological, hydrogeological and hydro-chemical properties were considered, we could suggest that the 4 sections should be monitored in RM-1 borehole. The water table was just a few meters(2～3 m) beneath the surface, so groundwater from the nuclear facility flew to discharge area through the hydraulic soil domain(HSD) and upper hydraulic rock domain(UHRD). We also suggested that the two high permeable fracture zones should be monitored because these fracture zone might act as the preferential flow pathway in deep underground.

Table 4. Suggested monitoring points from the summary of the investigation result

Section (GL.-m)		Geol.	Hydrogeology		Summary
			Chem.	Permea.	
Surface~28.0		●		●	●
28.0 ~61.0	31～34	●	●	●	●
	44～47		●		
	56～58				
63.0～67.0			●		
69.0~72.0		▲	●	●	●
80.0~84.0		●		▲	
100.0~112.0		▲			
143.0~147.0		●	●	●	●

ACKNOWLEDGEMENT

This work was supported by the Nuclear Core Technology of the Korea Institute of Energy Technology Evaluation and Planning (KETEP) grant funded by the Korea government Ministry of Trade, Industry and Energy [No.20171510300670].

Simulations of In-situ Tracer Tests at a Single Borehole With a Wall Having Locally Variable Hydraulic Property

Nak-Youl Ko*, Kyung-Woo Park, and Sung-Hoon Ji
Korea Atomic Energy Research Institute, 111, Daedeok-daero 989beon-gil, Yuseong-gu, Daejeon, Republic of Korea
*nyko@kaeri.re.kr

1. Introduction

When disposal tunnels or deposition holes of a deep geological repository for high-level wastes are excavated, it can be happen to damage walls of the tunnels or holes. It degrades resistance of groundwater flow and radionuclide transport at the near-field. In this study, numerical simulations for in-situ tracer tests with a double chamber (dipole) structure in single borehole was conducted in order to identify effects by the damaged structures and design effective field tests.

2. Method

Using field data obtained from boreholes at Research Gallery #6 in KURT, numerical simulations of tracer tests in a single borehole were conducted. A domain for numerical modeling was constructed and hydraulic properties of each layer were assigned according to field tests performed at the boreholes. A local structure with variable hydraulic conductivity, which represents damaged structures by excavation, was assumed to be located between the upper and lower chamber.

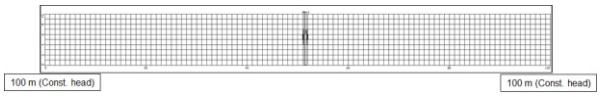

Fig. 1. Discretized modeling domain.

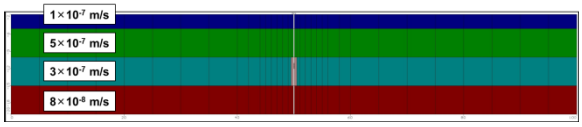

Fig. 2. Distribution of Hydraulic conductivity in the modeling domain.

3. Results

3.1 Transport of Tracer

When a local structure with a variable hydraulic property in a borehole wall was assumed, short-cut flow through the structure occurred during dipole flow tests [1] (Fig. 3). Tracers injected in the lower chamber moved from the lower to the upper chambers, along the groundwater flow field (Fig. 4). Some of tracers transported along the local structures.

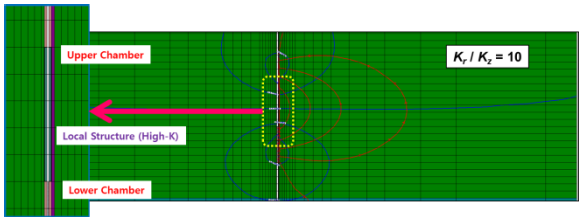

Fig. 3. Groundwater flow path by local structure.

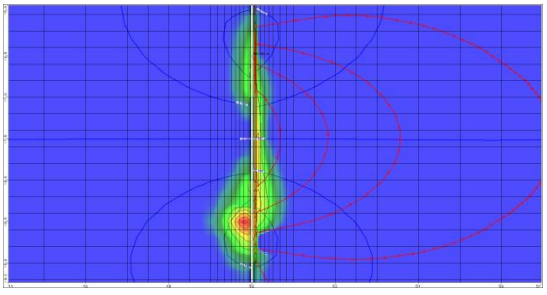

Fig. 4. Tracer transport in a dipole flow test.

3.2 Effect of Local Hydraulic Property

In simulations of tracer tests using dipole flow tests, the local structure behaved as a short-cut of groundwater flow from the lower to the upper chambers when the local structure had more hydraulic conductivity than the surrounding hydrogeological layer. From the simulation results, if the hydraulic conductivity of the local structure was larger than a certain level, 20 times that of the surrounding layer in this study, most of tracers moved through the local structure and the peak time of tracer concentration became shorter (Fig. 5).

4. Conclusions

To investigate an effect of local structure on a borehole wall with variable hydraulic conductivity, numerical simulations of tracer tests using dipole flow tests were conducted. The hydraulic conductivity had influence on a peak time of a tracer breakthrough curve. So, analysis of tracer breakthrough curves may give an implication of local structures caused by excavation. The results of this study can be applied to design effective in-situ test of a dipole flow tracer test.

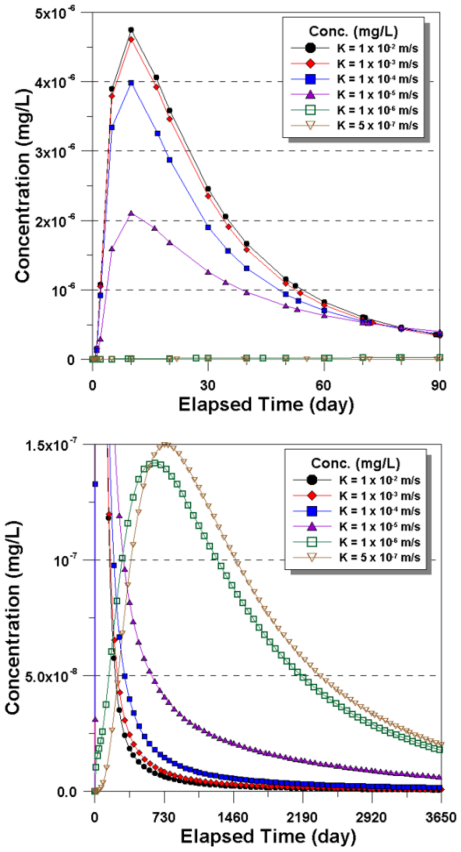

Fig. 5. Breakthrough curves of tracer concentrations for each case of hydraulic conductivities at the local structure.

ACKNOWLEDGEMENT

This work was supported by the Ministry of Science, ICT and Future Planning within the framework of the national long-term nuclear R&D program (NRF-2017M2A8A5014858).

REFERENCES

[1] Z.J. Kabala, “The dipole-flow test: a new single-borehole tests for aquifer characterization“, Water Resources Research, 29(1), 99–107 (1993).

Training Course on Geological Disposal of Radioactive Waste at Mizunami URL
Part I. Introduction to MIU and Practical Training in MIU

Yongheum Jo[a], Naon Chang[b], Sangsu Park[c], HyungJin Byun[d], JiHwan Boo[e], Wonjae Lee[f], Jiwoo Lee[g], Hyunseok Lee[h], Han Young Joo[i], Sol-Chan Han[a], and Chang-Lak Kim[f,*]

[a] Korea Advanced Institute of Science and Technology, 291, Daehak-ro, Yuseong-gu, Daejeon, Republic of Korea

[b] Hanyang University, 222, Wangsimni-ro, Seongdong-gu, Seoul, Republic of Korea

[c] Pohang University of Science and Technology, 77, Cheongam-ro, Nam-gu, Pohang-si, Gyeongsangbuk-do, Republic of Korea

[d] Ulsan National Institute of Science and Technology, 50, UNIST-gil, Eonyang-eup, Ulju-gun, Ulsan, Republic of Korea

[e] Jeju National University, 102, Jejudaehak-ro, Jeju-si, Jeju-do, Republic of Korea

[f] KEPCO International Nuclear Graduate School, 658-91, Haemaji-ro, Seosaeng-myeon, Ulju-gun, Ulsan, Republic of Korea

[g] Kyung Hee University, 1732, Deogyeong-daero, Giheung-gu, Yongin-si, Gyeonggi-do, Republic of Korea

[h] Seoul National University, 1, Gwanak-ro, Gwanak-gu, Seoul, Republic of Korea

[i] Dongguk University, 123, Dongdae-ro, Gyeongju-si, Gyeongsangbuk-do, Republic of Korea

[*] clkim@kings.ac.kr

1. Introduction

Disposal in deep geological repositories is internationally considered as the most preferred option for the long-term management of high-level radioactive wastes. Underground research laboratories (URLs) is facilities that are constructed or developed to provide realistic environmental information and test technical issues and materials. URLs play an essential role in the development of the repository systems and assessment of disposal concepts [1].

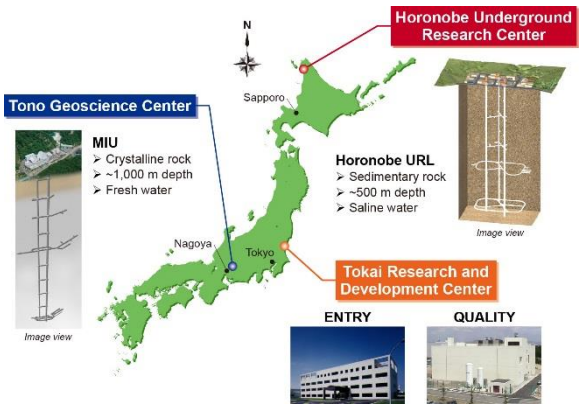

Fig. 1. Research Facilities of JAEA for Geological Isolation Research and Development [2].

Japan has two URLs in Mizunami and Horonobe with different types of host rock. JAEA has been performing geoscientific research on granite rock at the Mizunami site. In this report on the training course on geological disposal or radioactive waste at the Mizunami URL (MIU), the technical and scientific facts of MIU and the lessons from the course and the practical issues during the development and operation of the facility are introduced.

2. Brief Description on MIU

The URL project of Japan in two different sites are based on the recommendation by the Japan Atomic Energy Commission that URLs should be constructed at several places [3]. JAEA started MIU project in 1996. MIU locates at Mizunami city, Gifu prefecture. The host rock of MIU is ca. 70 million years-old granite and fresh groundwater flow. Underground facility mainly consists of main and ventilation shafts. The depth of the shafts are 500 m and the distance between shafts is 40 m. Two shafts are connected by the sub-stage at every 100 m depth. Research galleries for experiments are placed at 300 m and 500 m depth. Surface facilities are operating for auxiliary purposes. For example, the drainage water treatment facility manages groundwater discharge due to the high concentration of fluoride.

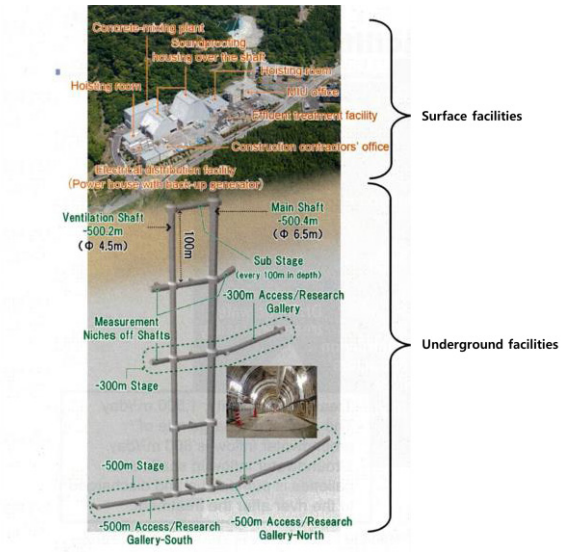

Fig. 2. Surface and Underground Facilities in MIU.

Geological investigation in MIU has been carrying out in three phases. Phase I is a surface-based investigation on the purpose of the understanding the initial condition of the geological environment by borehole and reflection seismic wave. Investigation of Phase II was conducted to understand the short-term evolution and recovery of the geological environment during construction. Geological mapping and sampling are important parts of phase II. Phase III aimed to investigate long-term geological behavior in drifts by monitoring boreholes and in-situ experiments.

3. Practical Training at MIU site

This training course mainly consisted of lectures from researchers working in MIU and the field experiments. The lectures were focused on the procedures, approaches, and results of the geological investigations held in MIU. Geologic, hydrogeologic, hydrogeochemical, and rock mechanical studies in MIU were introduced through a sequence of three phases. In the field experiment, borehole core samples from the underground in MIU were investigated and the borehole logging for finding the fractured zone was performed. Microscopic observation enabled to characterize the filling material and alteration features of the fault zone. In addition, a site visit on the experimental gallery at 300 m provided the insight of understanding the deep geological environment. Groundwater samples obtained in the gallery at 300 m were used for the measurement of pH, Eh, and ion concentrations.

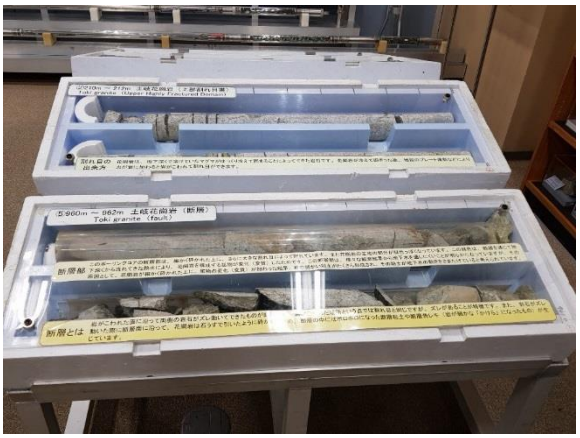

Fig. 3. Borehole Samples for Geological Mapping.

Fig. 4. Groundwater Monitoring System.

ACKNOWLEDGEMENT

This work was supported by a grant from by the Korea Nuclear International Cooperation Foundation.

REFERENCES

[1] IAEA, “The use of scientific and technical results from underground research laboratory investigation for the geological disposal of radioactive waste”, IAEA-TECDOC-1243 (2001).
[2] JAEA, “Geological Isolation Research and Development”, JAEA website
[3] Japanese Atomic Energy Commission, “Long-Term Program for Research, Development and Utilization of Nuclear Energy, 1994.

Sensitivity Analysis of Thermal Conductivity on Thermal Dimensioning of SNF Direct Disposal System

In-Young Kim*, Heui-Joo Choi, and Dong-Keun Cho
Korea Atomic Energy Research Institute, 111, Daedeok-daero 989beon-gil, Yuseong-gu, Daejeon, Republic of Korea
*iykim@kaeri.re.kr

1. Introduction

For safe disposal of SNFs in Korea, the KRS system had been developed. Since then, the KJ-II bentonite was adopted and several important THM properties of bentonite and rock are evaluated and revised. However, these results are not applied to the design of KRS system because of interruption of research on direct disposal. In this study, sensitivity of thermal conductivity on thermal dimensioning is studied by calculating temperature difference between base case and thermal properties variation case.

2. Methods and Results

2.1 Thermal Analysis Model

To evaluate sensitivity of thermal conductivity, the KRS direct disposal system depicted in Fig. 1 is adopted [1]. The plus7 type fuel which has 4.5wt.% of initial enrichment, 55 GWd/MtU of discharge burnup, 40 years of cooling time is selected as a reference fuel [2]. Decay heat of reference fuel is calculated using ORIGEN-ARP. Quarter region FEM model for thermal analyses is developed using ABAUS considering symmetry condition. 40 m of tunnel spacing and 9 m of hole pitch are considered [2]. Geothermal gradient is assumed to be 30℃/km based on KURT data.

Thermal properties of the repository materials used in this study are listed in Table 1. Thermal conductivity of bentonite is assumed to be varying between 0.6 W/mK to 1.3 W/mK based on research of KJ-II bentonite [3]. Thermal conductivity of KURT granite is assumed to be between 2.0 W/mK and 3.5 W/mK according to KURT rock measurement data [4].

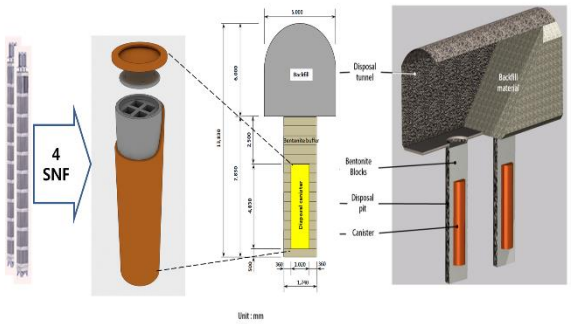

Fig. 1. EBS of the KRS PWR SNF disposal system [1].

Table 1. Thermal properties of system materials [1~4]

	Density [kg/m^3]	Thermal conductivity [W/mK]	Specific Heat [J/kgK]
Cast Iron	7,200	52	504
Copper	8,900	386	383
Ca-bentonite	1,970	base case: 0.8 this study: 0.6 – 1.3 [3]	1,380
Backfill	2,270	2.0	1,190
Rock	2,600	Base case: 3.0 this study: 2.0 – 3.5 [4]	900

2.2 Results

Thermal dimensioning of disposal system is

determined to maintain bentonite peak temperature under 100℃. Bentonite peak temperature is highly affected by thermal conductivity as shown in Fig. 2 and Fig. 3, though thermal conductivity assumed in this study are extensive than expected ones in real disposal system. Therefore, peak bentonite temperature criteria or thermal loading criteria for canister should be modified to consider thermal conductivity changes in accordance with thermal evolution of repository.

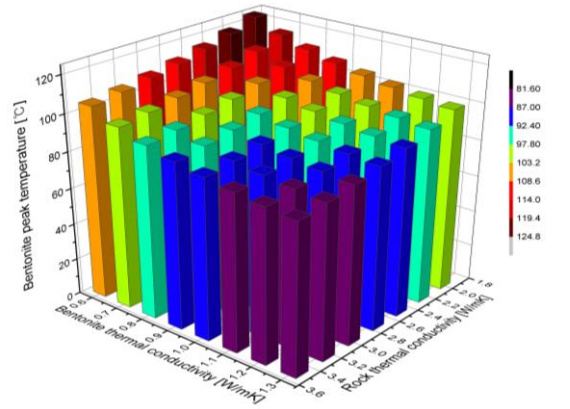

Fig. 2. Bentonite peak temperatures depending on bentonite and rock conductivity.

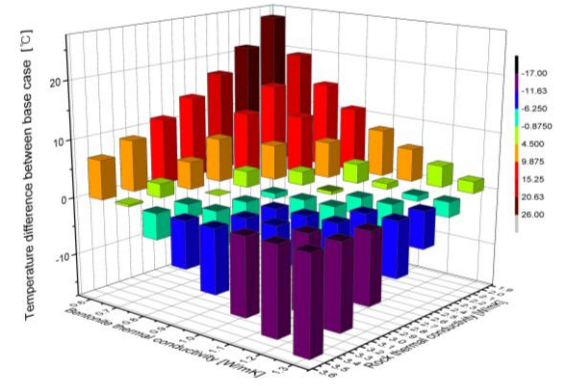

Fig. 3. Bentonite peak temperature differences between base case and thermal conductivity change case.

3. Conclusions

In this study, sensitivity of thermal conductivity on thermal dimensioning is analyzed by calculating temperature difference between base case and thermal property variation case. Thermal properties are assumed based on measurements ranges for KJ-II and KURT granite. From sensitivity analyses, it is clarified that bentonite peak temperature is strongly affected by thermal conductivity. To consider thermal evolution of repository and uncertainty in material properties, criteria on bentonite peak temperature or canister maximum thermal loading criteria should be modified.

ACKNOWLEDGEMENT

This work was supported by the Ministry of Science, ICT within the framework of the national long-term nuclear R&D program (NRF- 2017M2A8A5014856).

REFERENCES

[1] Jongyoul Lee, An Engineered Barrier Concept of Reference Deep Geological Disposal System for High Burn-up Spent Fuels, KAERI/TR-7405/2018, KAERI, 2018.

[2] In-Young Kim et. al., Evaluation on Thermal Performance and Thermal Dimensioning of Direct Deep Geological Disposal System for High Burn-up Spent Nuclear Feul, KAERI/TR-5230/2013, KAERI, 2013.

[3] Seok Yoon et. al., Investigation of the Thermal Conductivity for Compacted Bentonite Buffer, KAERI/TR-6877/2017, KAERI, 2017.

[4] Changsoo Lee et. al., Characterization of thermal and mechanical properties of granite at KURT, KAERI/TR-5566/2014, KAERI, 2014.

Training Course on Geological Disposal of Radioactive Waste at Mizunami URL
Part II. Study About the Geological Environment and HLW Disposal in Korea

Naon Chang[a], Yongheum Jo[b], Sangsu Park[c], HyungJin Byun[d], JiHwan Boo[e], Wonjae Lee[f], Jiwoo Lee[g], Hyunseok Lee[h], Han Young Joo[i], Sol-Chan Han[b], and Chang-Lak Kim[f,*]

[a] Hanyang University, 222, Wangsimni-ro, Seongdong-gu, Seoul, Republic of Korea

[b] Korea Advanced Institute of Science and Technology, 291, Daehak-ro, Yuseong-gu, Daejeon, Republic of Korea

[c] Pohang University of Science and Technology, 77, Cheongam-ro, Nam-gu, Pohang-si, Gyeongsangbuk-do, Republic of Korea

[d] Ulsan National Institute of Science and Technology, 50, UNIST-gil, Eonyang-eup, Ulju-gun, Ulsan, Republic of Korea

[e] Jeju National University, 102, Jejudaehak-ro, Jeju-si, Jeju-do, Republic of Korea

[f] KEPCO International Nuclear Graduate School, 658-91, Haemaji-ro, Seosaeng-myeon, Ulju-gun, Ulsan, Republic of Korea

[g] Kyung Hee University, 1732, Deogyeong-daero, Giheung-gu, Yongin-si, Gyeonggi-do, Republic of Korea

[h] Seoul National University, 1, Gwanak-ro, Gwanak-gu, Seoul, Republic of Korea

[i] Dongguk University, 123, Dongdae-ro, Gyeongju-si, Gyeongsangbuk-do, Republic of Korea

[*] clkim@kings.ac.kr

1. Introduction

It becomes a serious issue that the on-site spent fuel pool of the nuclear power plants is getting saturated. As this reason, it needs the construction of the High Level radioactive Waste (HLW) repository site or interim storage. Therefore, we study about the domestic geological environment for HLW disposal and proposal of the HLW disposal system in South Korea. It was performed as a part of the "Experimentation and practice program of radioactive waste deep geological disposal" supported by KONICOF (Korea Nuclear International Cooperation Foundation). 10 people of students participated the domestic lessons (KINGS, 2019.01.21~2019.01.25) and overseas lessons (JAEA MIU, 2019.01.28 ~2019.02.01) with above program.

2. Geological Environment of Korea

In the HLW repository site, natural barriers play an important role for preventing the releasing of the radionuclides. The geological characteristics (geological distribution, temperature distribution, hydraulic conductivity, earthquake and etc.) effect to the natural barrier and the safety disposal of the HLW directly.

2.1 Geological Distribution

The Geological distribution of Korea is represented in Fig. 1 and Table 1. The plutonic rock painted with an orange in the Fig. 2 occupied largest amount in Korea, about 35.2%. Specially, it is distributed about 25.6% in South Korea. The HLW has to be disposed under the state geological structure. Before construction of the HLW repository site, it needs to estimate the detail volume of the each rock type.

Fig. 1. Geological Distribution Map of Korea [1].

Table 1. Geological Distribution of Korea [1]

Type	Feature	Proportion
Plutonic Rock	Paleozoic & Mesozoic Era	35.2 %
Metamorphic Rock	Crystalline Rock	8.7 %
	Gneiss	21.3 %
Igneous Rock	Intrusion & Eruption	13.6 %
Sedimentary Rock	Paleozoic & Mesozoic Era	16.0 %
Others	Unconsolidated Sediment & Quaternary Deposit	5.2 %

2.2 Temperature Distribution

The temperature distribution in South Korea is shown in Fig 2 according to the various depth. The domestic average heat is 71 MW/m^2 and it decreases to the 69 MW/m^2 at 300 m underground. It needs that total amount of the geothermal heat and heat from the HLW is lower than the regulation limit. Therefore, detail data of the geothermal heat as each area have to be collected before construction of the site.

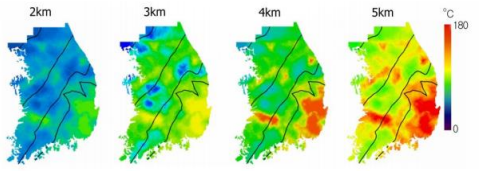

Fig. 2. Estimated temperature distribution at various depth in South Korea [2].

2.3 Hydraulic Conductivity

In the HLW repository site, hydraulic conductivity is considered importantly because the radionuclides leakage follow the groundwater. As shown In South Korea, the hydraulic conductivity with fractured rock aquifers is average 0.076 m/day and with alluvial layers is average 1.26 m/day [3]. However, this result is not suitable for applying HLW disposal due to the depth of the observation hole. The observation is performed about the 200 m underground though HLW repository site is deeper than 200 m. Therefore, it needs to investigate again in the adapt depth.

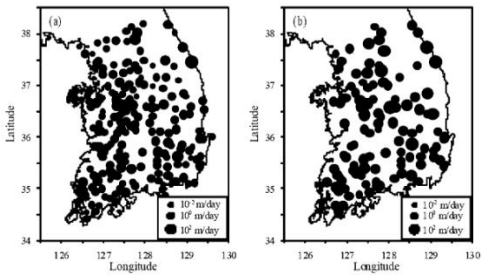

Fig. 3. Hydraulic conductivity distribution in South Korea (a) fractured rock aquifers, (b) Alluvial layers [3].

3. Necessity of URL in Korea

To construct the HLW repository site, it needs to get more information about geological characteristics than now due to above limitation. Also, the geochemical and radiochemical data for getting a licensing process is needed. These investigations can be carried out in the Underground Research Facility (URL) such as MIU in Japan. Therefore, it is suggested that the construction of URL and detail research have to be preceded before construction of HLW repository site.

ACKNOWLEDGEMENT

This work was supported by a grant from by the Korea Nuclear International Cooperation Foundation.

REFERENCES

[1] KIGAM, “TECTONIC MAP OF KOREA”, https://www.kigam.re.kr/modedg/contentsView.do?ucont_id=CTX000152&menu_nix=465k753d, (2019.03.17)

[2] Tae Jong Lee et al., “The First Enhanced Geothermal System Project in Korea”, Proc. Of the 9th Asian Geothermal Symposium, Nov. 7-9, 2011

[3] Byeong Gon Choi et al., “Construction of Basic Evaluation Criteria for Candidate HLW Repository Sites”, KAERI/CM-1192/2009 (2010).

Effect of Temperature on the Interaction of Nuclide With Metal Corrosion Products Under Anaerobic Alkaline Conditions

Hyo-Jin Seo*, Seung Yeop Lee, and Jae-Kwang Lee
Korea Atomic Energy Research Institute, 111, Daedeok-daero 989beon-gil, Yuseong-gu, Daejeon, Republic of Korea
*hjseo@kaeri.re.kr

1. Introduction

High-level radioactive wastes should be considered to be safely disposed with a metal disposal container in a deep underground site to isolate them from ecosystems. Generally, the materials of disposal containers are composed of iron (Fe) and copper (Cu) so that they can maintain geochemical stability. However, corrosion of the disposal canisters can occur due to oxidation-reduction changes, activity of microbes, and radiation effects. When the canisters are corroded, there may form chalcocite (Cu_2S), chalcopyrite ($CuFeS_2$) and mackinawite (FeS) as corrosion products [1]. These corrosion products may affect the chemical behavior of radionuclides that are leaching through them.

In this study, we investigated the effects of high temperature on the interaction between metal corrosion products and nuclides under anaerobic alkaline environment.

2. Materials and Methods

2.1 Heating Treatment of Metal Corrosion Products

Reagents of FeS and Cu_2S used in this study are purchased from Sigma-Aldrich.

The corrosion products are heated at high temperature to later investigate the temperature effects on the interaction between metal corrosion products and nuclides. Both solids of FeS and Cu_2S were heated with dry or wet state in aerobic conditions. In a case of dry-heating, 10 g of each corrosion product was placed in 125 ml-FED bottles and heated to 150°C for 5 days. In a case of wet-heating, H_2O_2 was used as an oxidizing agent and it was added with 0.35 ppm in a 125 ml-serum bottle containing the solids. The bottle was heat-treated at 90°C for 5 days. Finally, the supernatant was removed after centrifugation (5,000 rpm, 5 minutes) and the precipitated solids were freeze-dried.

2.2 Sorption of Nuclides

To investigate the sorption of nuclides on the corrosion products, raw and (dry and wet) heat-treated solids of FeS and Cu_2S were prepared. Three types of those solids were added to each 125 ml-serum bottles in an amount of 100 mg. 100 ml of distilled water was added to the bottles, and they were purged with N_2 gas for 40 minutes to remove oxygen in the solution. Cesium (Cs) and iodine (I) were selected as main nuclides, and they were injected to the solution to be 10 ppm. To know the sorption amount of the nuclides under alkaline conditions, 1.0 N NaOH solution was used to adjust the media as pH 7, 9, and 11. The solution was placed in an incubator shaker for 24 hours (100 rpm at 30°C). During the reaction, the supernatant was sampled after 1, 2, 4, and 24 hours and analyzed by ICP-MS to determine the sorption concentrations of the nuclides and dissolution of metal corrosion products over time. After the experiment, the solid samples were obtained from the centrifugation (5,000 rpm and 5 minutes) and freeze-dried. They were investigated by SEM-EDS to analyze nuclide sorption characteristics.

3. Results and Discussion

The wet-heated FeS sample became reddish unlike Cu_2S. It appears to have oxide-type secondary minerals that combined with the dissolved oxygen

present in the water.

Adsorption of iodine was observed in all types of Cu_2S, and it was significant at pH 7 (Fig. 1). At the same pH 7 condition, the iodine sorption gradually increased with time in the raw- and dry-heated solids of Cu_2S, but decreased for a wet-heated solid after 4 hours. It is presumed that iodine sorption on the oxidized solid is not strong. In addition, iodine was predominantly adsorbed onto the surface of Cu_2S rather than FeS.

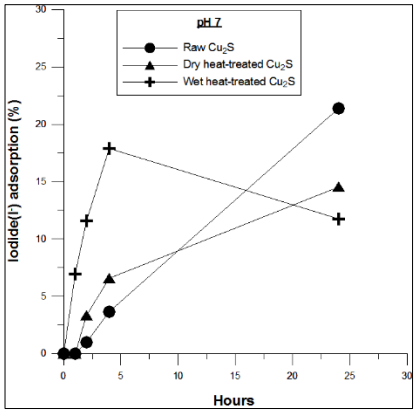

Fig. 1. Characteristic iodide adsorption curves by three solid types of Cu_2S at pH 7.

The FeS was highly sensitive to pH changes. The dissolution of FeS was active at neutral pH. However, at pH 11 the FeS dissolution became weak with increase of cesium sorption over time (Fig. 2).

By SEM-EDS, we confirmed nuclides such as iodine and cesium present on the surface of corrosion products (Cu_2S and FeS).

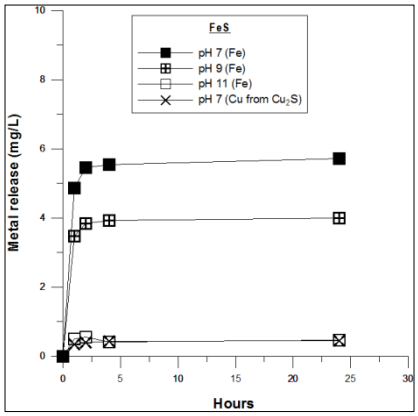

Fig. 2. Metal release from the corrosion products under various pHs.

4. Conclusion

The effect of high temperature on the interaction between corrosion products and nuclides was investigated under anaerobic alkaline conditions. It was found that the sorption of radionuclides was affected by heat-treated sample types and pHs. We confirmed that the change of corroded products by high temperature may delay or accelerate the migration of radionuclides in anaerobic disposal environments. Therefore, it is needed to further study the effect of high temperature on the sorption behaviors of radionuclides onto the metal corrosion products in anaerobic conditions.

ACKNOWLEDGEMENT

This research was supported by National Research Foundation of Korea (NRF) funded by the Ministry of Science, ICT and Future Planning (The nuclear research and development program No. 2017M2A8A5014859).

REFERENCE

[1] J.K. Lee et al., Complex Behavior of Radionuclides in a Deep Geological Environment, KAERI/TR-6547/2016, 2016.

Review of Finnish Posiva Methodology for the Canister Lifetime Assessment

Heui-Joo Choi*, Dong-Keun Cho, and Sung-Hoon Ji
Korea Atomic Energy Research Institute, 111, Daedeok-daero 989beon-gil, Yuseong-gu, Daejeon, Republic of Korea
*HJCHOI@kaeri.re.kr

1. Introduction

The spent nuclear fuels generated from the nuclear reactors should be managed safely. The geological disposal using a disposal tunnel located at the 500 meter depth is one of the promising methods. Sweden and Finland proposed a KBS-3 type repository for the spent nuclear fuels several tens ago. The safety of this concept relies on a copper canister. The most important challenge in KBS-3 concept lies in how to estimate and prove the very long-term lifetime of the canister. Finnish Posiva published the Safety Case report for a construction license [1].

A disposal canister which is the most important engineered barrier in a repository for high-level radioactive waste should maintain its lifetime for a long period (at least several thousand years in Korea) after the closure of the repository. It is very difficult to confirm the long lifetime of a disposal canister through an experiment. Thus, it is predicted by the numerical modeling work in most cases.

In this paper, the methodologies used in a Safety Case report made by the Finnish Posiva that advanced in the construction of the repository were reviewed. And based on the Posiva methodologies a computer program was made and applied to the Korean disposal concepts. Also, some research items were recommended for the further study.

2. FEPs and Requirements

2.1 Climate Change

Generally, the safety assessment including the estimation of lifetime of a canister requires long-term prediction of repository environment. One of the most important conditions is the climate change since it may influence the boundary conditions for groundwater flows.

The future climate was derived from the past records, and it was assumed that the climate change might repeat for one million years in Posiva Safety Case. Fig. 1 briefly showed the past records and the future climate used by Posiva. That is, one glacial cycle of climate was assumed from the construction of a repository to 170,000 years after present as shown in Fig. 1. After 170,000 years, seven cycles are assumed to occur repeatedly for one million years.

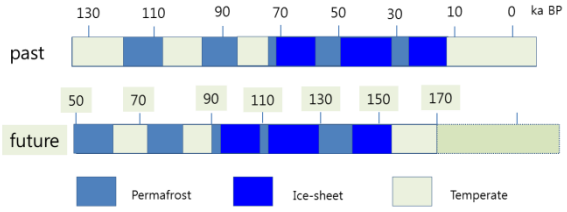

Fig. 1. Climate evolution for Posiva Safety Case.

2.2 Performance Requirements

The performance requirements for a final disposal are described by Government Decree 736/2008 in Finland. Posiva developed a VAHA requirement management system, which covers all requirements in levels 1 – 4. They are classified by performance targets and design requirements. Some important targets related to the canister are as follows:

- In the expected repository conditions the canister shall remain intact for hundreds of thousands of years except for incidental deviations.
- The canister shall withstand corrosion in the expected repository conditions
- The canister shall not impair the safety functions of other barriers.

3. Posiva Methodologies

3.1 Excavation and Operational Phase

In Posiva Safety Case report the safety assessment including the prediction of canister lifetime was carried out at four phases. The excavation and operational phase was expected to continue around 100 years. During this period, the most important corroding agent was oxygen trapped in buffer and backfill.

Posiva calculated the corrosion depth due to oxygen based on the assumption that all the oxygen in buffer and backfill was consumed by reaction with copper. According to the Posiva approach, the corrosion depth of a KAERI disposal canister due to oxygen in buffer was calculated to be around 0.062 mm.

3.2 Post-closure Evolution

After the oxygen in the repository is consumed, the main corroding agent is sulphide. Two kinds of buffer conditions were considered in Posiva Safety Case: intact buffer and eroded buffer. In all the corrosion calculations, a steady state mass transport of corroding agents was assumed [2].

In the case of an intact buffer, two cases were considered, one for the corroding agent from the groundwater and the other from the backfill. The relevant equations were derived respectively.

The first case of intact buffer is the corrosion due to sulphide from groundwater, which might be converted from sulphate. The sulphide in groundwater flowing fracture (see Fig. 2) will diffuse through the buffer, and be consumed by the reaction with copper. The canister failure time (t_f) by this reaction was calculated using the following equations:

$$\int_{t=0}^{t=t_f} \left(2\frac{N_c}{\rho N_s}\right)\frac{F}{A}dt = d \quad (1)$$

$$\frac{F}{A} = \frac{\pi D_e C_b}{2(r_t - r_c) ln[2(r_t - r_c)/b]} \quad (2)$$

$$C_b = \frac{Q_f}{Q_f + Q_b} \quad (3)$$

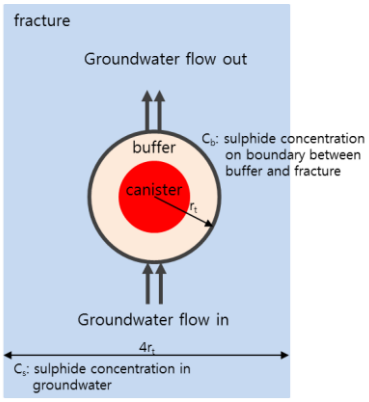

Fig. 2. Schematic view of groundwater flow around the buffer.

The second case of intact buffer is the corrosion due to sulphide from backfill. The reaction rate equivalent to equation (2) was obtained as follows:

$$\frac{F}{A} = \frac{C_s}{\pi r_c^2}\begin{cases} 2\frac{\pi r_t^2}{L} D_e \sqrt{\frac{2D_{et}q}{r_t}} \Big/ \left(2\sqrt{\frac{2D_{et}q}{r_t}} + \frac{\pi}{L}D_e\right) \\ qA_s \end{cases} \quad (4)$$

Finally, the corrosion due to a partially eroded buffer was calculated using the following equation:

$$\frac{F}{A} = \frac{C_s}{\pi r_c (r_t - r_c)}\begin{cases} \sqrt{Q_A Q_{lim}} \\ Q_A \end{cases} \quad (5)$$

A sample calculation for the eroded buffer was illustrated with data used by Posiva. With a sulphide concentration of 3 mg/L, the corrosion depth of a copper canister was 6.24 mm for KAERI and 7.5 mm for Posiva for 1 million years. These differences were caused by the buffer thickness.

4. Conclusion

A computer program was developed using MS Excel to calculate the lifetime of a copper disposal canister based on Posiva methodologies. Steady state mass transport was assumed. The results of the calculation for a disposal canister developed for Korean spent fuels under the Posiva geological conditions showed that no canister failures were expected due to the corrosion for one million years.

The following research items were identified for the further study related to the corrosion of a disposal canister. A study on the erosion of buffer is needed. The groundwater velocities in the fractures intersecting the deposition hole were obtained for the whole repository site in the Posiva project, but the similar results were not available in Korea. So far, the study on the backfill material in a repository has not yet been carried out. We used the data used for the Posiva repository. The reactive transport modeling should be included to estimate the geochemistry of groundwater for one million years after the closure of the repository.

ACKNOWLEDGEMENT

This work was supported by the Ministry of Science and ICT within the framework of the national long-term nuclear R&D program (NRF-2017M2A8A5014856). The first author would like to express his special thanks to Professor Mari Lundström and Aalto University. Most of this study was carried out during his sabbatical stay at Aalto University.

REFERENCES

[1] Posiva, Safety Case for the disposal of spent nuclear fuel at Olkiluoto-performance assessment 2012, Posiva 2012-04, 2012.

[2] Paul Smith, Lawrence Johnson, Margit Snellman, Barbara Pastine, Peter Gribi, Safety Assessment for a KBS-3H Spent Nuclear Fuel Repository at Olkiluoto-Evolution Report, Posiva 2007-08. 2007.

Corrosion Behavior of SKB Copper in KURT Environment

Minsoo Lee* and Sung-Hoon Ji

Korea Atomic Energy Research Institute, 111, Daedeok-daero 989beon-gil, Yuseong-gu, Daejeon, Republic of Korea

*minm@kaeri.re.kr

1. Introduction

SKB (Svensk Kärnbränslehantering AB) has been conducting the corrosion evaluation of forged copper as for the corrosion resistant barrier of a disposal canister in early years [1]. KAERI has also been conducting long-term corrosion studies of cold spray coating copper at KURT since 2010 [2]. And recently KAERI obtained the forged and extruded copper of SKB, and tried to verify their corrosion behavior in the KURT environment. The purpose of the KURT corrosion test was to confirm the applicability of SKB copper in domestic disposal environment and to estimate the difference in corrosion resistance compared with the cold spray coating copper of KAERI. By the way, two vacant tests without bentonite buffer were added in the KURT corrosion test of cold spray coating copper and SKB forged copper.

In this paper, the corrosion experiment for SKB coppers at KURT in progress was introduced, and the first dismantling results of 6 month old specimens were reported. This experiment was started in July 2018, and planned to finish in July 2028.

2. Experiment

Test specimens were ChangSung cold sprayed coating Cu (purity 99.5%), SKB forged Cu (Purity 99.99%, Cast No.05-230-3-1), and SKB extruded Cu (Purity 99.99%, Cast No.O14). A test specimen (D 15.0 × t 1.0 mm) was inserted between two compact bentonite blocks (D 30.0 mm × t 10.0 mm), and then the combination was stored in a small corrosion cell allowing water permeation. Many cells were kept in environmental chambers at 70 ^{o}C at KURT, and fresh underground water was passing through the chamber continuously at 10~20 cc/min.

Two kinds of bentonite buffer were used in the experiment. One is Ca-type GJ bentonite and the other is Na-type Wyoming bentonite which were compacted to 1.6 g/cm^3 in dry density.

In vacant tests, test specimens were loosely wrapped with a porous paper towel (Yuhan Kimberly, KIMECH Science Wipers), and stored in the same corrosion cell.

3. Result

3.1 First Dismantling

The corrosion cells of 209 days old were dismantled in March 2019. The extracted specimens were shown in Fig. 1.

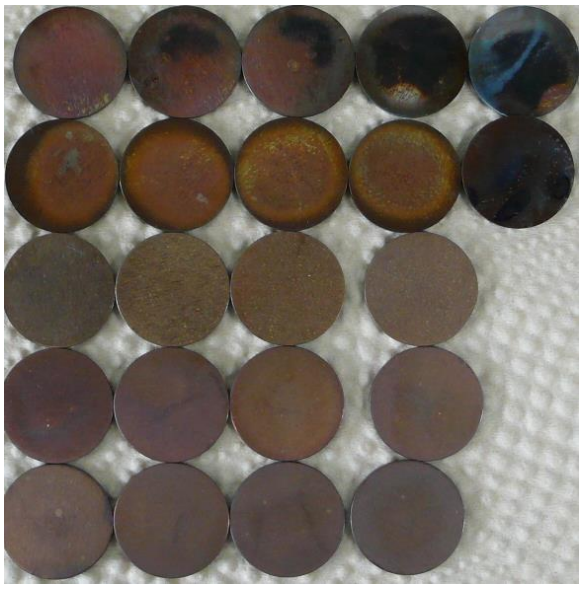

Fig. 1. The 209 days old test specimens after dismantling and surface cleaning (from top; Vacant-cold sprayed Cu, Vacant-SKB forged Cu, Ca bentonite-SKB forged Cu, Na bentonite-SKB forged Cu, Na bentonite-SKB extruded Cu).

3.2 Corrosion Depth

The corrosion depth was determined by weight loss measurement. Vacant specimens showed 2-3 fold higher corrosion depth than the specimens surrounded by compact bentonite blocks (Table 1).

Table 1. Corrosion depths of 209 days old-Cu specimens

Materials	Buffer	Avg.	Std. D.
CSC Cu	Vacant	0.707	0.132
SKB F-Cu		0.400	0.091
SKB-F-Cu	Ca-GJ	0.249	0.071
SKB-F-Cu	Na-Wy	0.225	0.011
SKB-E-Cu	Na-Wy	0.243	0.012

The main corrosion product was cuprite (Cu_2O) in all Cu specimens as a result of XRD analysis. And tenorite (CuO) was also found in vacant specimens unlike others.

4. Conclusion

High pure-SKB Cu specimens showed similar corrosion depth of around 0.2~0.3 ㎛ with KAERI cold sprayed coating Cu. The compact bentonite was very helpful for the corrosion resistance of copper in KURT underground condition.

ACKNOWLEDGEMENT

This work was supported by the Ministry of Science, ICT and Future Planning within the framework of the national long-term nuclear R&D program (NRF-2017M2A8A5014858).

REFERENCES

[1] F. KING, L. AHONEN, C. TAXÉN, U. VUORINEN and L. WERME, “Copper Corrosion under Expected Conditions in a Deep Geologic Repository” SKB TR-01-23 (2001).

[2] M.S. Lee, H. J. Choi, J. W. Choi, and H. J. Kim, “Properties of Copper Coatings from a Cold Spray Technique for an Underground Disposal Canister”, Nuclear Eng. and Tech., Vol.43 No.6, pp. 557-566 (2011).

Coupling Multi Scaled Components of Geological Disposal System in APro (Advanced Process-based Total System Performance Assessment Framework for a Geological Disposal System)

Jung-Woo Kim*, Jaewon Lee, Kyung Woo Park, and Dong-Keun Cho

Korea Atomic Energy Research Institute, 111, Daedeok-daero 989beon-gil, Yuseong-gu, Daejeon, Republic of Korea

*jw_kim@kaeri.re.kr

1. Introduction

For the safety assessment of a geological disposal system of radioactive waste, two types of approaches are generally considered. The one is the system-level safety assessment model which is a kind of conservative approach and has the advantage of short computation time. The other is the process-based total system performance assessment model which is basically able to simulate all the processes that can be occurred in a geological disposal system including thermal, hydraulic, mechanical, chemical, and radiological processes.

Recently, KAERI has been developing a process-based total system performance assessment model for a geological disposal system, which is named as APro. In the previous study, the modeling interface was designed[1], and engineered barrier system (EBS)-related modules were developed and embedded into APro[2].

For the next step, APro will be embedded with the natural barrier system (NBS)-related modules, such as hydrogeology in the far-field. The space scale of NBS or far-field, which is several kilometers, is different from that of EBS or near-field, which is several hundred meters, in the geological disposal system. In this study, therefore, the component coupling technique, in which the near-field and far-field components are separately simulated, and the components are simultaneously coupled, was suggested to be applied into APro to improve the computational efficiency.

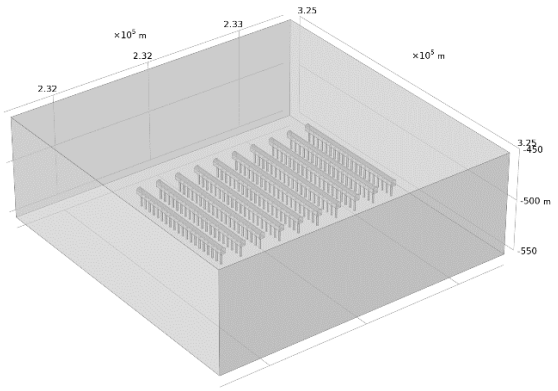

Fig. 1. Near-field of the disposal system.

2. Component Coupling in APro

2.1 Near-field Component

The near-field of the disposal system includes EBS and the host rock nearby the EBS (Fig. 1). The main processes which need to be considered in the performance assessment are radioactive decay heat and thermal transfer, hydraulic saturation, mechanical property change, canister failure, geochemical reaction, radionuclide release and migration, and so on. The typical size of the near-field is several hundred meters based on the repository size.

2.2 Far-field Component

The far-field of the disposal system indicates the host rock within the radionuclide migration impact radius (Fig. 2). The main processes are groundwater flow, geochemical reaction, radionuclide migration,

and so on. The typical size of the far-field is several kilometers based on the radionuclide migration pathway.

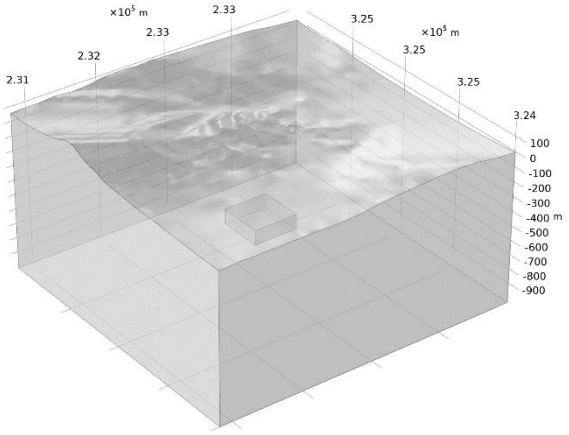

Fig. 2. Far-field of the disposal system.

2.3 Component Coupling

The near-field and far-field components can be coupled by sharing their outer boundary and inner boundary, respectively. That is, the boundary conditions for each component would be the constant boundary condition by using the values computed in the other component:

$$p|_{NF} = p|_{FF} \quad (1)$$

$$p|_{FF} = p|_{NF} \quad (2)$$

3. Conclusion

In this study, the new modeling technique, in which near-field and far-field components are separated and simultaneously coupled, was proposed in order to consider the NBS-related processes in APro. Later, it should be answered to the questions like; how the size of near-field will be determined, how the near-field and far-field will be represented (homogeneous or heterogeneous, and EPM or DFN), and so on.

ACKNOWLEDGEMENT

This work was supported by the National Research Foundation of Korea Nuclear Research and Development Program (2017M2A8A5014856) funded by the Ministry of Science and ICT.

REFERENCES

[1] J.-W. Kim, J. Lee, and D.-K. Cho, “Development of Modeling Interface for a Process-Based Total System Performance Assessment of a Geological Disposal System”, Proc. of the KRS 2018 Spring Conference, May 30 - June 1, 2018, Busan.

[2] J.-W. Kim, J. Lee, I. Kim, and D.-K. Cho, “Development of EBS Modules for a Process-Based Total System Performance Assessment of a Geological Disposal System”, Proc. of the KRS 2018 Fall Conference, October 31 - November 2, 2018, Jeju.

Preliminary Study on the Development of a Horizontal Disposal Concept for PWR Spent Fuels

Jong-youl LEE*, Heui-joo CHOI, In-young Kim, Hyun-a KIM, and Dong-keun CHO

Korea Atomic Energy Research Institute, 111, Daedeok-daero 989beon-gil, Yuseong-gu, Daejeon, Republic of Korea

*njylee@kaeri.re.kr

1. Introduction

A deep geological disposal (DGD) - careful engineered emplacement of HLW(High Level Radioactive wastes) in stable rock formations hundreds of meters below ground - is considered as the most appropriate solution for the long-term management of HLW including spent fuels. And there are several options for DGD. Generally, the KBS-3V (Vertical) type disposal in DGD options has been considered as a reference concept and currently under the stage of licensing. However, there are many methods as alternative concepts to the reference concept. The horizontal disposal concept can be one of the alternative concepts.

In this study, a reference disposal concept for PWR spent fuels was reviewed and preliminary study on the development of a horizontal disposal concept including super container concept as an alternative method was described. In addition, thermal analysis for a horizontal disposal concept was carried out.

2. Reference Disposal Concept

In Korea, there is no site-specific activity for HLW disposal. Therefore, Fig. 1 showed a generic reference disposal concept that was vertical disposal type called KBS-3V. This reference concept has multiple barrier. They are natural barrier that is host rock and engineered barrier that are disposal canister and buffer block. Because the KBS-3 concept has a thermal requirement, the thermal analysis was carried out to check the design requirement. Fig. 2 showed the model for the thermal analysis and the results. As shown in the figure, the disposal system met the thermal requirement.

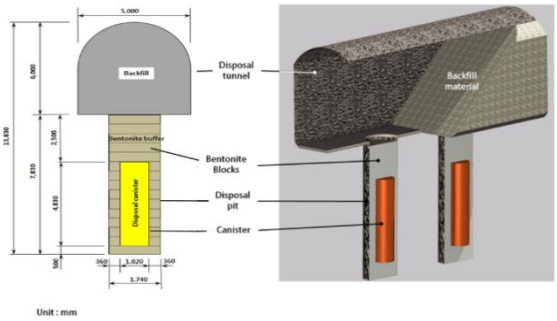

Fig. 1. Reference disposal concepts for SNF.

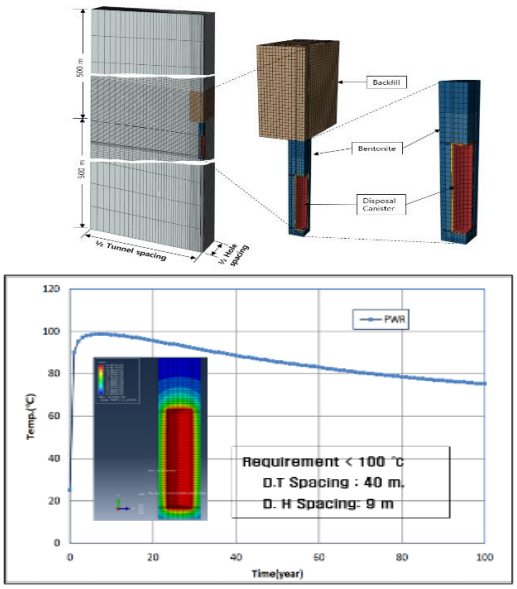

Fig. 2. Thermal analyses model and results for reference concepts.

3. Alternative Disposal Concept: KBS-3H

Development of alternative disposal concepts to improve the efficiency and safety of the reference concept suitable for various environments in each country is necessary. To do this, alternative disposal concepts were analyzed by reviewing the status of disposal concept in various countries (Fig. 3). In this

paper, the KBS-3 type horizontal disposal concept was studied preliminarily based on the results of the review results.

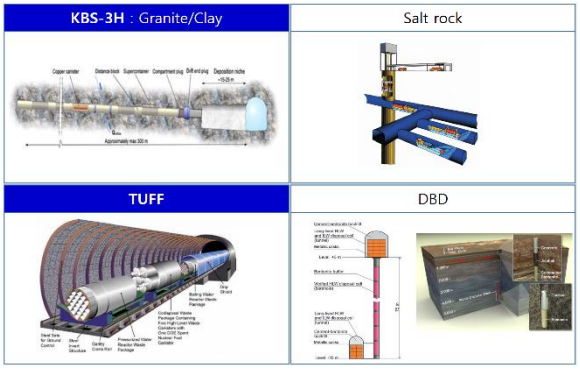

Fig. 3. Alternative concepts.

A KBS-3H type disposal concept is a horizontal type disposal concept. In this concept, a super container concept that integrated the disposal container and buffer blocks was adopted. Fig. 4 showed the concept of super container and Fig. 5 showed the disposal tunnel concept with super-container.

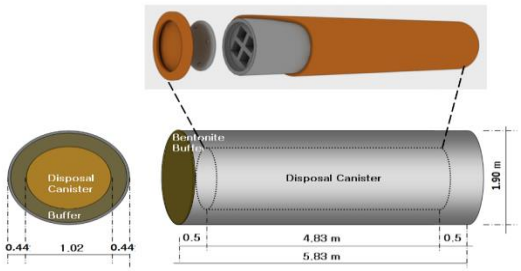

Fig. 4. Super-container concept.

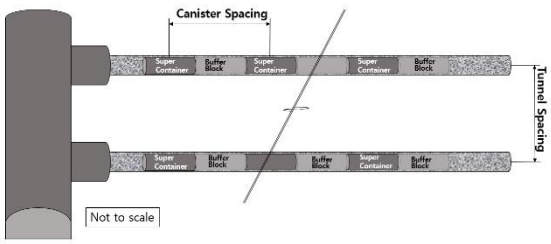

Fig. 5. KBS-3H type disposal concept.

To check the thermal requirement of the disposal concept, the thermal analysis was carried out preliminarily. Fig. 6 showed the model and the result of the analysis.

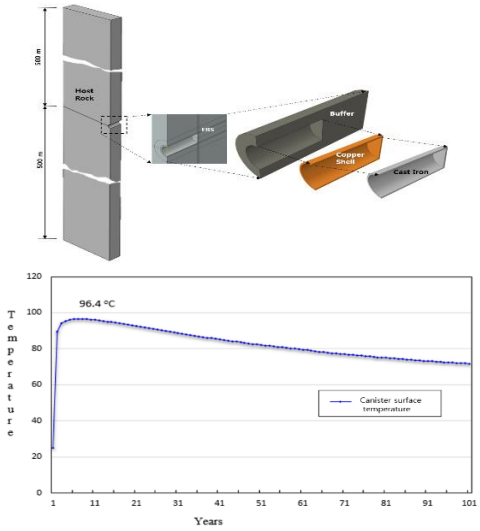

Fig. 6. Analysis model and result for KBS-3H.

4. Conclusion

There are many concepts as alternatives to the reference disposal concept such as KBS-3V (Vertical) type. In this paper, a KBS-3H (Horizontal) type disposal concept for spent fuels including super-container concept was studied preliminary. In addition, the thermal analysis to check the design requirement was carried out.

The results of this study can be used as an input data for the next step of alternative disposal concept development and for establishment of national policy on spent fuel management.

ACKNOWLEDGEMENT

This work was supported by the Ministry of Science and ICT within the framework of the national long-term nuclear R&D program (NRF-2017M2A8A5014856).

REFERENCES

[1] N. Chapman and F. Neall, Geological Disposal Option for High-Level Waste and Spent Fuel, NDA (2008).

[2] SKB, Horizontal emplacement technique of super container and distance blocks, Sweden SKB R-08-43 (2008).

[3] J. LEE, EBS Concepts of Alternative Disposal Systems for Hi-Burnup Spent Fuels, KAERI (2018).

4분과

중저준위폐기물관리 (Oral)

Modification of Granular-Sized Natural Zeolite for Enhancing Practical Use

Seok-ju Hong and Wooyong Um*

Pohang University of Science and Technology, 77, Cheongam-ro, Nam-gu, Pohang-si, Gyeongsangbuk-do, Republic of Korea

*wooyongum@postech.ac.kr

1. Introduction

Nowadays, a lot of synthetic sorbents have been developed with high radionuclide removal efficiency. However, they are still difficult to apply into the real industrial field as practical use, because they usually exist as fine powder.

Fine powder-sized sorbent is difficult to handle, because it can cause micro-dust that can be blown and harmful to workers. Furthermore, when we use the powder sorbent as backfilling material, an enormous amount of sorbent would be required. It means that powder-sized sorbents need to be pelletized for practical use. However, pelletizing process needs additional costs and some sorbents even cannot be pelletized. In addition, removal efficiency may be deteriorated when the sorbents are pelletized.

In this reason, we modified natural zeolite in granular size (2~5 mm), for higher radionuclide removal efficiency and practical use. In addition, modification mechanism from natural zeolite to NaP zeolite as well as radionuclide removal efficiency were also investigated in this study.

2. Experimental

2.1 Materials

Natural zeolite was obtained from guryongpo, Pohang, Korea. Sodium hydroxide (NaOH) was used for hydrothermal modification. Strontium nitrate ($SrNO_3$), Cesium nitrate ($CsNO_3$), Nickel nitrate hexa-hydrate ($Ni(NO_3)_2 \cdot 6H_2O$) were used as surrogates for target radionuclides (Sr-90, Cs-137, and Ni-63) in batch sorption experiment.

2.2 Hydrothermal Modification Method

NaOH solution (250 mL, 3M) was mixed with 10g of natural zeolites, powder size (200~500 um) and granular size (2~5 mm) in High density polyethylene (HDPE) bottle. Then, the bottle was sealed and put in the oven at 96°C with various reaction times. After the reaction, modified zeolites were washed with deionized water for several times until the pH became neutral (~7), and then dried at 50°C for 12 hours.

2.3 Characterization Method

X-ray diffraction (XRD) and Fourier Transformed infrared spectroscopy (FT-IR) were used to identify the type of zeolite and observe the mineral phase changes in zeolites during the modification process. Scanning electron microscope (SEM) was used to observe the surface morphology of zeolites. Brunauer-Emmett-Teller (BET) was used to measure the specific surface area and pore volume.

3. Results

3.1 Characterization

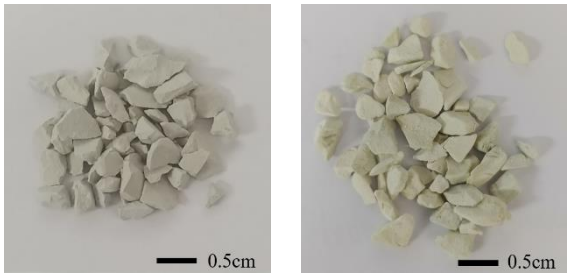

Fig. 1. Granular natural zeolite (left), NaP zeolite (right).

Granular-sized natural zeolite and NaP zeolite are shown in Fig. 1. Natural zeolite mainly consists of clinoptilolite and mordenite. After the thermal modification natural zeolite turned into NaP zeolite, and it formed spherical clusters (Fig. 2). Specific surface area of natural zeolite is 31 m^2/g, and of NaP

zeolite is 92 m^2/g, consistent with increased surface area after the modification.

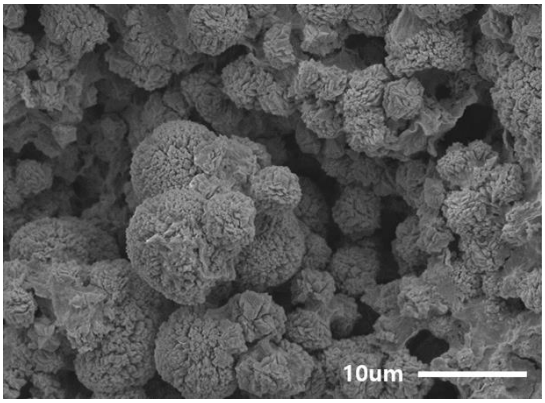

Fig. 2. Spherical clusters of granular-sized NaP zeolite.

3.2 Sorption Experiment Results

Both powder and granular natural zeolites removed Cs very well (> 97%), however, they showed low Sr and Ni removal efficiency (< 30%) in Fig. 3. As pervious paper's results [1], NaP zeolite showed slightly decreased Cs removal efficiency. But, NaP zeolite showed that the removal efficiency of Sr and Ni has reached almost 100%, irrespective of size.

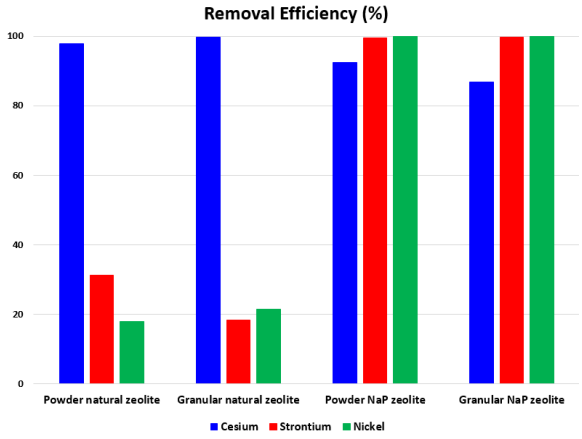

Fig. 3. Removal efficiency of natural and NaP zeolites.

3.3 Modification Mechanism

Dissolution and re-assembling processes are considered for the main mechanism of recrystallization [2], as our natural zeolite also underwent recrystallization during the modification process as shown in Fig. 4.

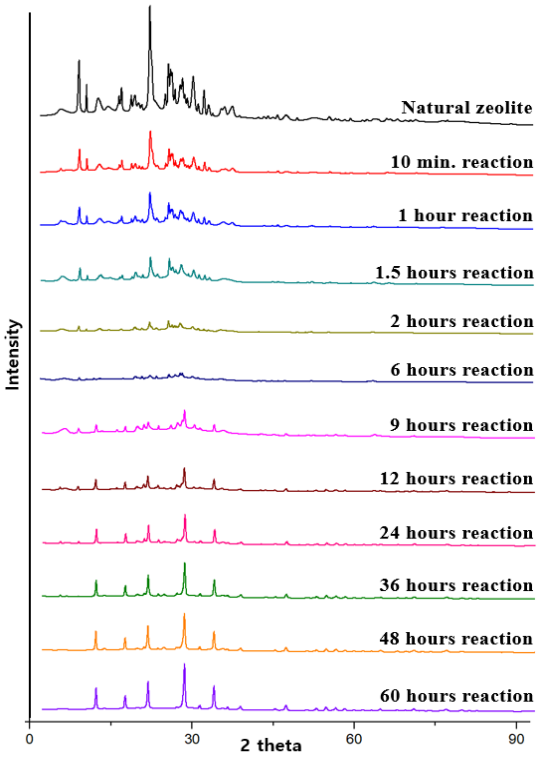

Fig. 4. XRD changes during modification process.

4. Conclusion

Granular zeolite was easier to prepare with cost less than powder zeolite. Furthermore, removal efficiency of granular zeolite and powder zeolite was not significantly different. Both granular sized natural and NaP zeolites are expected to be used for removal of three target radionuclides and practical use in the real field conditions.

REFERENCES

[1] H. Himura, K. Akiba, "Adsorption behavior of cesium and strontium on synthetic zeolite P", Journal of Nuclear Science and Technology (1993), 30:5, 436-443.

[2] Irina I. Ivanova, Elena E. Knyazeva "Micro-mesoporous materials obtained by zeolite recrystallization: synthesis, characterization and catalytic applications", Chemical Society Review (2013), 42, 3671.

The Applicability of New Biological and Chemical Decontamination Technology to Nuclear Power Plant and Economic Analysis

YoungJu Son[1),*], Yongbaek Kim[1)], Seung Yeop Lee[2)], Junggyu Nam[3)], JaeYeon Jung[4)], and Chang-Lak Kim[5)]

[1)] KEPCO Engineering & Construction Company, 269, Hyeoksin-ro, Gimcheon-si, Gyeongsangbuk-do, Republic of Korea

[2)] Korea Atomic Energy Research Institute, 111, Daedeok-daero 989beon-gil, Yuseong-gu, Daejeon, Republic of Korea

[3)] Korea Electric Power Company, 55, Jeollyeok-ro, Naju-si, Jeollanam-do, Republic of Korea

[4)] Korea Hydro and Nuclear Power, 1655, Bulguk-ro, Yangbuk-myeon, Gyeongju-si, Gyeongsangbuk-do, Republic of Korea

[5)] KEPCO International Nuclear Graduate School, 658-91, Haemaji-ro, Seosaeng-myeon, Ulju-gun, Ulsan, Republic of Korea

[*]yjson@kepco-enc.com

1. Introduction

The liquid waste management system (LWMS) in the APR 1400 mainly consists of reverse osmosis (R/O) and ion-exchange processes to meet the discharge criteria. When the radioactive liquid wastes are treated by the ion-exchange process, the byproduct, which is a spent ion-exchange resin, can be classified as intermediate or low level waste. Due to the wide use of ion-exchange process in nuclear power plants (NPPs), the spent ion-exchange resins are annually produced in large volume. In this study, we developed new biological and chemical decontamination techniques to reduce the volume of spent ion-exchange resin in the NPP and conducted their economic analysis.

2. Experimental Results

The basic principle of the developed technology is to convert major radionuclide ions into inorganic crystal minerals (Fig. 1) via chemical or biological techniques.

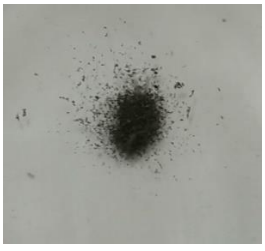

Fig. 1. Solid precipitates from liquid wastes by the biological method.

In a batch experiment, the biological method selectively removed more than 80% of cesium within 24 hours, and the chemical method removed more than 95% of cesium. Other major nuclides (Co, Ni, Fe, Cr, Mn, Eu), which are commonly present in nuclear radioactive liquid wastes, were effectively scavenged by more than 99%.

3. Applicability to Nuclear Power Plant

In the current LWMS of APR1400, radioactive liquid wastes are sequentially passed through a charcoal bed, filter, R/O package and ion-exchanger. Recirculation is frequently required because of the excess presence of ^{58}Co, ^{134}Cs, and ^{137}Cs radionuclides that are incompletely removed by the current ion-exchanger. Therefore, if the chemical or biological decontamination process is available in the current LWMS, recirculation may not be necessary. The newly designed decontamination module with chemical or biological technology is virtually placed between the R/O package and the ion-exchanger.

The operational concept of the chemical or biological decontamination process is shown in Fig. 2.

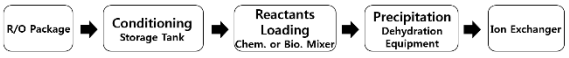

Fig. 2. Conceptual process for the chemical or biological decontamination.

The new process mainly consists of two storage tanks (including level sensors, temperature control, pH control), one columnar chemical or biological reaction mixer (including reagent & reagent

injectors), dehydration equipment, and other pumps and piping lines.

If the chemical or biological decontamination process is very effective to remove radionuclides in LWMS, no recirculation of liquid waste in the LWMS would be required. In addition, it is expected that the spent resin generation rate would be greatly reduced by a large replacement cycle extension.

4. Economic Analysis

Since Shin Kori 3 only started the commercial operation in December 2016, it is impossible to collect long term reliable data on the annual resin consumption in LWMS. For the reason, based on the amount of spent resins being reported from the FSAR document of Shin Kori 3&4 [1], we evaluated the validity and feasibility of the new technology in a modified LWMS process. Considering the waste acceptance criteria (WAC) of the nuclear waste disposal facility [2] and more than one year of half-life, we selected some specific radionuclides, such as ^{55}Fe, ^{60}Co, ^{63}Ni, and ^{137}Cs, which will be target radionuclides of our chemical decontamination process.

We have estimated the emission radioactivity for the five chosen major radionuclides at the end of the R/O package based on the Annual Liquid Release Source Terms of FSAR [1]. By the estimation, the chemical decontamination rate in the modified LWMS was 94.98%. Considering the conservative engineering margin, we reduced the chemical decontamination rate to 90%.

Table 1 shows the results of disposal cost for the two options (only LWMS & LWMS + chemical process). It presumes that the chemical decontamination process achieves a decontamination rate of 90% and thus reduces the burden of post-stage resin process by a factor of 10. Based on this result, it is calculated that the resin life increases 10 times and the amount of spent resin generated per year is reduced by a factor of 10. As a result of comparing Option 1 with Option 2, the annual amount of spent resins decreased from 3 to 2 for HICs and from 36 to 4 for 200 L drums. Based on the MOTIE Notice [3], waste disposal costs are ₩15,804,300 for single 200 L drum and ₩87,177,200 for single high-integrity container (HIC). If the number of disposal containers is converted to disposal costs, it is estimated that the annual disposal cost would decrease from about ₩800 million to ₩200 million (about 71% reduction) per year.

In addition, if the chemical decontamination process is operated for 40 years for Shin Kori 3&4, the total spent resin management cost is estimated to be lessen as follows: -79.74% for material cost, -88.89 % for polymerization cost, -71.39% for disposal cost.

Table 1. Estimated annual costs to dispose the spent resin wastes via two options in Shin Kori 3&4

Unit: ₩ 1,000,000

	Option 1*		Option 2**		
Spent Resin Waste Streams	**High Activity Spent Resin**	**Low Activity Spent Resin**	**High Activity Spent Resin**	**Low Activity Spent Resin**	**Waste from Chemical Process**
Volume from FSAR ($L \cdot yr^{-1}$)	17,060	54,300	1,706	5,430	-
Projected Volume ($L \cdot yr^{-1}$)	2,075	6,600	207.5	660	605.90
Processing Capacity per Unit HIC/Drum	818L	187L	818L	187L	818L
No. of Containers /Drums	3	36	1	4	1
Disposal Cost per Containers/ Drums (₩)	87.18	15.80	87.18	15.80	87.18
Disposal Cost (₩)	261.54	568.80	87.18	63.20	87.18
Total Disposal Cost (₩)	**830.34**		**237.56**		

*Only LWMS [4]
**LWMS + chemical decontamination process

REFERENCES

[1] Korea Hydro & Nuclear Power Co. Final Safety Analysis Report for Shin Kori 3&4 (2010).

[2] Nuclear Safety and Security Commission (NSSC), Regulation in Delivery of Intermediate Level and Low Level Radioactive Waste, NSSC Notice No. 2017-60 (2017).

[3] Ministry of Trade, Industry and Energy (MOTIE), Regulation on Calculation Criteria for Radioactive Waste Management Costs and Spent Fuel Management Fees, MOTIE Notice No. 2017-195 (2017).

[4] N.S. Kamaruzaman, D.S. Kessel, and C.L. Kim, "Management of Spent Ion-Exchange Resins from Nuclear Power Plant by Blending Method", Journal of the Nuclear Fuel Cycle and Waste Technology, 16(1), 65-82 (2018).

Revisit of Recycling of Disposed Radioactive Metal Waste as a Potential Inadvertent Human Intrusion Scenario at a Near-Surface Repository

Wang Hyeon Lee and Jae Hak Cheong*

Kyung Hee University, 1732, Deogyeong-daero, Giheung-gu, Yongin-si, Gyeonggi-do, Republic of Korea

*jhcheong@khu.ac.kr

1. Introduction

The International Atomic Energy Agency (IAEA) has conducted a co-ordinated research project on improvement of Safety Assessment Methodologies for Near Surface Disposal (ISAM) and the final report was published in 2003. In the final report, the vault test case is assumed that there are no valuable resources in or near site [1]. However, globally, the amount of recycled steel using scrap metal accounts for about 30% of steel production every year and the price of many scrap metals increases compared to historical averages [2]. That is, the disposed metal itself can be considered as a valuable resource and the potential of recycling cannot be excluded if the material is drilled or excavated by inadvertent human intrusion (IHI). Therefore, this study aims at reviewing if the practice to screen the disposed metal recycling out of the potential IHI scenarios can be justified.

2. International Human Intrusion Scenario

Table 1 shows the human intrusion scenarios considered in the post-closure safety assessment of previous studies or actual disposal facilities.

Table 1. IHI Scenarios considered in safety cases for LILW disposal facilities

Disposal facility (Organization or nation)	Human intrusion Scenarios
Hypothetical (IAEA)	Dwelling construction, Dwelling residence, Road construction
Hypothetical (OECD/NEA)	House construction, Road construction, Residential, Agricultural
Hanford (US)	Drilling, Post-drilling, Excavation, Post-excavation, Residential garden, Farming
Barnwell (US)	Construction, Agriculture
Drigg (UK)	Borehole drilling, Trial pit excavation, Laboratory analysis, Construction, Occupancy, Smallholding, Informal scavenging, Organized material recovery
L'Aube (FR)	Road works, Homes, Children's playgrounds
El Cabril (ES)	Construction, Residential, Residential Agriculture
Wolsung (KR)	Drilling, Residence, Well development

The IAEA has suggested that the recycling of disposed materials is a phenomena relevant to safety assessment of near surface disposal facilities and that introducing additional metal to potentially 'divert' a drill bit may entice future human intrusion. However, as shown in Table 1, most of the IHI scenarios that have been considered in safety assessments of previous studies and actual disposal facilities do not include the possibility of recycling metal waste.

For Drigg disposal facilities in the UK, 'organized material recovery' scenario was considered to be included in occupancy events because recovered metals could be sent to a foundry for smelting, which would lead to dilution of the contamination prior to re-use and contamination may be discovered on receipt of recovered metals at a foundry, in which case appropriate protective measures would be taken. However, exclusion of the could not be justified because the effectiveness of modern monitoring system for smelting facilities would not be guaranteed in the future.

3. Assessment Framework for Metal Recycling

The IAEA has conducted research for determining internationally agreed principles for exemption can be applied in the case of recycle and reuse. To permit a more detailed assessment of the potential radiation doses from the recycle of contaminated or activated steel, the general recycle steps is shown in Fig. 1 [3].

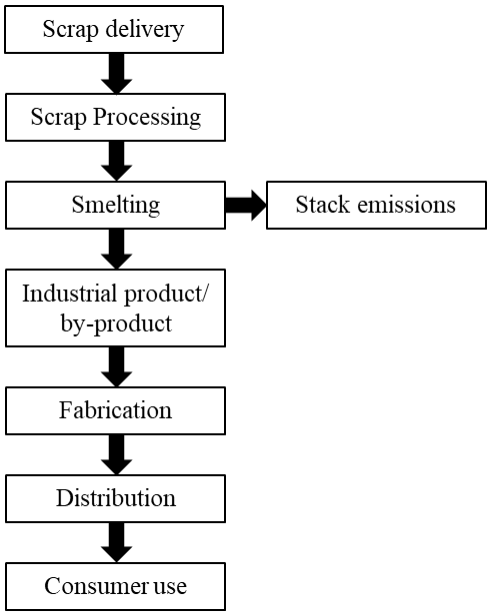

Fig. 1. The metal recycling step proposed by the IAEA.

There are 30 scenarios for each worker and public at each step of metal waste recycling considered in the study. However, the following items are excluded, so additional consideration is required.

- Consideration should be given to the radiation effects about drilling or excavation worker and on-site resident.
- Partitioning of elements occurs by ingot, slag, dust, and volatile during smelting process and the partitioning factor for each by-product differs by element. Therefore, consideration should be given to distribution to determine the concentration of radionuclides.
- The range of elements distributed to the dust presented in previous studies is from 0% to 100%, so the radioactivity concentration can be increased up to 90.91 times [4]. Therefore, additional consideration should be given to the baghouse processor excluded from the IAEA study.

4. Conclusion

It was shown that exclusion of recycling of disposed metal wastes by IHI without appropriate deliberation would not be justified through literature review. Therefore, more detailed and quantitative studies are to be conducted in order to determine the need for additional consideration of potential recycling of disposed metal waste in IHI safety assessment and devise optimized measures for minimizing the likelihood and potential consequence from the scenario.

ACKNOWLEDGEMENT

This work was supported by the Nuclear Safety Research Program through the Korea Foundation Of Nuclear Safety (KOFONS), granted financial resource from the Nuclear Safety and Security Commission (NSSC), Republic of Korea (No. 1605008).

REFERENCES

[1] International Atomic Energy Agency, Safety Assessment Methodologies for Near Surface Disposal Facilities, Volume 2 (2004).

[2] Worldsteel Assosiation, Global steel industry: outlook, challenges and opportunities, International Steel Industry & Sector Relations Conference (2017).

[3] International Atomic Energy Agency, Application of Exemption Principles to the Recycle and Reuse of Materials from Nuclear Facilities, IAEA Safety Series No. 111-P-1.1 (1992).

[4] U.S. Nuclear Regulatory Commission, Radiological Assessments for Clearance of Materials from Nuclear Facilities, NUREG-1640 Vol. 1 (2003).

Identification of Redox Reactions of Nb in Molten LiCl-KCl Eutectic for Pyrochemical Decontamination

Gwan Yoon Jeong, Younghwan Jeon, Jungho Hur, Hyeongjin Byeon, and Jaeyeong Park*

Ulsan National Institute of Science and Technology, 50, UNIST-gil, Eonyang-eup, Ulju-gun, Ulsan, Republic of Korea

*jypark@unist.ac.kr

1. Introduction

Niobium (Nb) is one of the refractory metals, which is widely used as a minor alloying element in the nuclear materials including fuel cladding and reactor structure components. ^{93}Nb is the single stable isotope, but the small amount of ^{94}Nb forms by the neutron-induced activation during the irradiation period. ^{94}Nb has the long half-life of 20,000 years, and its decay generates two high-energy gamma rays with 700 and 870 keV, indicating that ^{94}Nb becomes the major source of radioactivity of hardware wastes from nuclear power plants after the disintegration of short-lived radionuclides, and it can affect their classification for the hierarchy of the radioactive waste into low-level or intermediate level waste [1].

Pyrochemical decontamination processes with a molten salt system for radioactive wastes have been developed to reduce and manage their radioactivity by separating long-lived radioisotopes and recycling valuable elements such as Zr, Fe, or Ni. Their electrochemical behaviors in the molten salt are actively investigated [2], particularly in LiCl-KCl eutectic thanks to its low practicable temperature and low corrosivity. However, few data are available for the electrochemical redox reactions involving Nb in molten LiCl-KCl. Hence, it is necessary to investigate the electrochemical behaviors of Nb in LiCl-KCl to confirm the applicability of pyrochemical process for the decontamination of Nb-containing wastes.

In this study, cyclic voltammetry (CV) was performed to identify all possible redox reactions of Nb in LiCl-KCl-$NbCl_5$. In addition, pyrochemical decontamination processes for each different type of Nb-containing waste are suggested with the consideration of reduction potentials of elements of concern.

2. Experiment

Fig. 1 shows the configuration of setup for the electrochemical experiment. Two Pyrex tubes were placed at the same axial position inside of a furnace; one containing LiCl-KCl-1.0wt.% $NbCl_5$ (99.99%, Alfa Aesar) for CV, and the other for temperature measurement by a type-K thermocouple. A tungsten (W) wire with a diameter of 1.0 mm (99.99%, Alfa Aesar) was used as a working and counter electrode. All potentials were recorded with referenced to Ag/AgCl in which Ag wire (99.99%, Alfa Aesar) is immersed in LiCl-KCl-1.0wt%. AgCl.

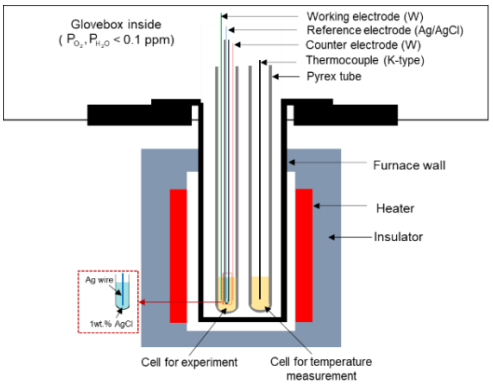

Fig. 1. Configuration of the experiment for cyclic voltammetry.

CV was performed with a scan range from -1.0 to -1.1V at different scan rates (30 ~ 1500 mV/sec) at 450°C by using VersaSTAT3 potentiometer.

3. Results

Fig. 2 shows the voltammogram by CV with identified redox reactions. Peak current density and peak potentials were analyzed to confirm the reversibility of each reaction with the literature data available in [3][4][5].

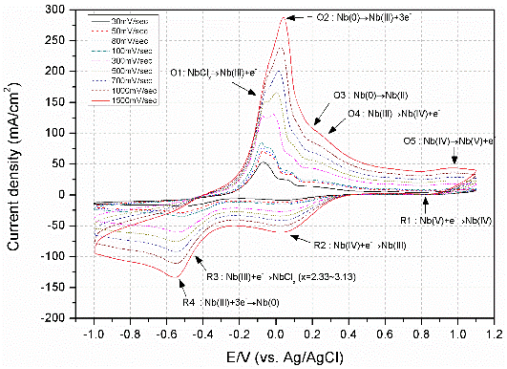

Fig. 2. A voltammograms with a scan range from -1.0 to 1.1V at different scan rates (surface area of electrode = 0.419 cm^2).

Formal potentials of each redox couple were obtained by using cathodic peak potentials as a function of the scan rate, as summarized in Table 1.

Table 1. Comparison of formal potentials for identified redox reaction

Formal potential (E^{0*}) for redox reactions (E/V vs Cl^-/Cl_2) at 450°C					Ref
Nb(Ⅱ) /Nb	Nb(Ⅲ) /Nb	Nb(Ⅲ)/ $NbCl_x$	Nb(Ⅳ) /Nb(Ⅲ)	Nb(Ⅴ) /Nb(Ⅳ)	
-1.54	-1.42				[3]
	-1.44		-1.12	-0.32	[4]
	-1.48		-1.09	-0.32	[5]
-1.61	-1.55	-1.50	-1.11	-0.32	P*

* Present study

It can be noticed that the deposition of metallic Nb (peak R4) competed to that of insoluble nonstoichiometric Nb chloride compounds (peak R3). Thus, it is necessary to apply the potential more negative than -0.6 V (vs. Ag/AgCl) to obtain the metallic Nb deposit during potentiostatic separation of Nb during pyrochemical decontamination processes.

4. Pyrochemical Decontamination Process for Nb-Containing Wastes

Fig. 3 shows schematics of pyrochemical decontamination processes for the different type of Nb-containing waste. Depending on the reduction potentials of elements involved in the process, Nb can be extracted from the residual at the anode or molten electrolytes after the first stage of electrorefining (ER) process; for Zr-Nb waste, Nb remains at the anode and can be separated in the sequential ER process; for Fe-Cr-Nb and Ni-Cr-Nb wastes, Nb can be separated from the residual molten salt by the electrodeposition to purify the salt containing dissolved Cr which can be recycled.

Although multiple-step processes are required to separate Nb from the waste, Nb separation via pyrochemical processes is advantageous because all valuable elements can be recycled and the volume of intermediate waste can be reduced significantly. A further investigation would be necessary to optimize the performance of ER process in terms of Nb concentration as well as the applied potential on the electrode.

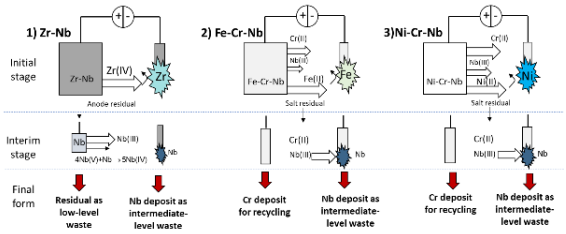

Fig. 3. Electrochemical behaviors of Nb during different pyrochemical decontamination processes.

REFERENCES

[1] K. Noh, C. J. Hah, J. Nucl. Fuel Cycle Waste Technol., 13(1), 21-34 (2015).

[2] Jaeyeong Park, Sungyeol Choi, Sungjune Sohn, Il Soon Hwang, J. Electrochem. Soc., 164(12), D744-D751 (2017).

[3] F. Lantelme, Y. Berghoute, A. Salmi, J. Appl. Electrochem., 24, 361 (1994).

[4] G.S. Picard, P. Bocage, Proc. Electrochem. Soc., 16, 622 (1992).

[5] F. Lantelme, J. Electrochem. Soc., 31, 324 (1993).

Studies on ANS 16.1 Leaching Test of Vitrified Forms for the Korean Low-level Radioactive Solid Wastes and Their Leaching Mechanisms

Miae Kim[1,*], Mihyun Lee[2], Min-Ji Kang[1], Kyong-Soo Hong[1], and Cheonwoo Kim[2]

[1] Korea Basic Science Institute, 30, Gwahaksandan 1-ro 60beon-gil, Gangseo-gu, Busan, Republic of Korea

[2] KHNP Central Research Institute, 70, Yuseong-daero 1312beon-gil, Yuseong-gu, Daejeon, Republic of Korea

[*]miaekim@kbsi.re.kr

1. Introduction

Korea Hydro & Nuclear Power Co. Ltd (KHNP) has developed a SG glass for spent resin and a DG-2 glass for dry active waste [1]. In this study, we conducted leaching experiments by following the American Nuclear Society (ANS) standard 16.1 [2] for two commercialized glass wasteforms, SG and DG-2, and analyzed the morphology of the surfaces of these glasses using a scanning electron microscope (SEM) and the compositional depth profiles and 3-dimensional (3D) mappings using a glow discharge optical emission spectrometer (GD-OES) and a time of flight – secondary ion mass spectrometer (ToF-SIMS). Finally, based on all these results, we suggested the leaching mechanisms for the two glasses.

2. Results and Discussion

2.1 Leaching Tests

Table 1 shows the leachability indices of the target nuclides such as Co, Cs, and Sr obtained from the ANS 16.1 test for the SG and the DG-2 glasses, respectively. All the leachability indices satisfy the requirements (> 6) of the US-Nuclear Regulatory Commission.

Table 1. Leachabilities of the SG and the DG-2 wasteforms

	Co	Cs	Sr
SG	18.00	16.93	16.00
DG-2	∞	14.14	14.76

2.2 GD-OES Depth Profiles

2.2.1 SG.

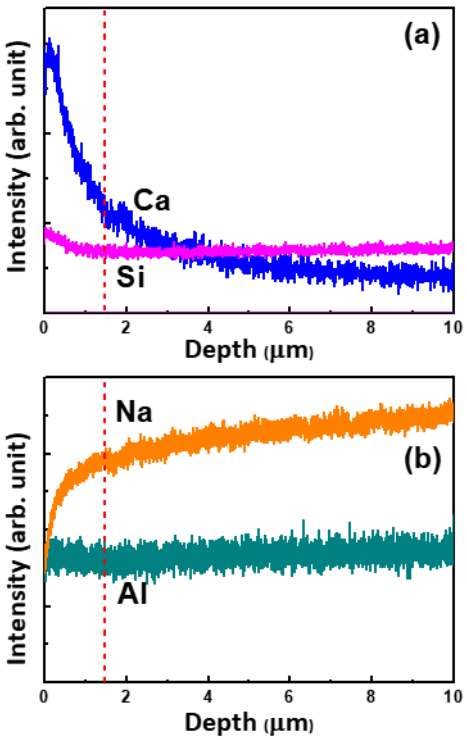

Fig. 1. GD-OES depth profiles of (a) Si and Ca, and (b) Na and Al of the SG.

We found the boundary around 1.5 μm (the vertical lines in Fig 1). Si and Al are accumulated

(Figs. 1a-b) and Na is depleted (Fig. 1b) up to nearly 1.5 μm compared to an internal glass. Especially, Ca is highly accumulated in the alteration layer of the SG. Relatively high Ca concentration of 21% in the SG glass could make the behavior more remarkable.

2.2.2 DG-2.

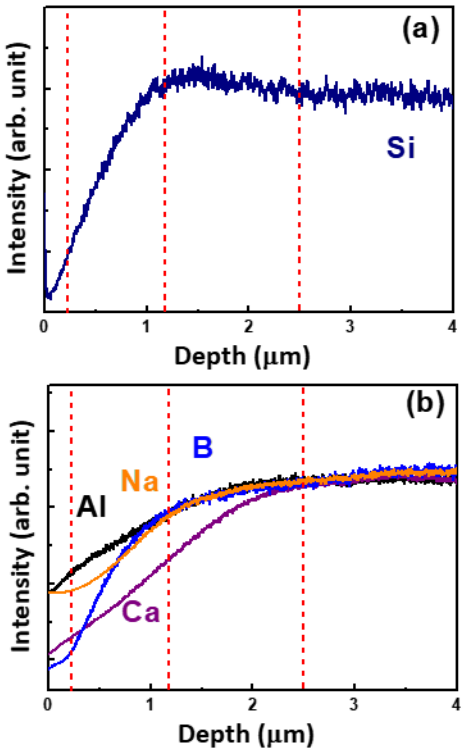

Fig. 2. GD-OES depth profiles of (a) Si and (b) B, Na, Ca, and Al of the DG-2.

The concentrations of all elements in the deeper-depth than 2.5 μm remain constant as the same level as an internal glass. In 1.2 – 2.5 μm, only Si slightly enriched in this section (Fig. 2a). Most major elements including B, Na, Ca, and Al gradually or linearly leached out from the certain depth of the glass to the solution (Fig. 2b). Particularly, Ca starts to decrease rapidly from around 2.5 μm compared to other elements.

2.2.3 Comparisons of the SG and the DG-2. Behaviors of whole elements in the DG-2 generally different from those from the SG. Especially, highly enriched constituents such as Ca and Al at the surface of the SG are not accumulated at the DG-2 surface.

3. Conclusions

We performed leaching experiments, ANS 16.1 test, to two commercialized glass wasteforms, the SG and the DG-2. The leachability values of target nuclides such as Co, Cs, and Sr from the SG and the DG-2 are all more than 14, which satisfy the requirements of the US-Nuclear Regulatory Commission. We analyzed the compositional depth profiles and 3D mappings by a GD-OES and a ToF-SIMS. Based on these results, we suggested the leaching mechanisms of the SG and the DG-2 wasteforms.

REFERENCES

[1] Kim, CW et al. “Glass Formulations for Vitrification of Low- and Intermediate-level Waste” Journal of the Korean Ceramic Society 40(10) (2003).

[2] Measurement of the Leachability of Solidified Low-level Radioactive Wastes by a Short-term Test Procedure, ANSI/ANS-16.1-1986, American National Society, La Grande Park, IL, (1986).

The Activity Calculation Based on Operation History Comparing With Effective Full Power Operation for Decommissioning Plant

YoungJae Maeng*, HyunChul Lee, KyungSik Kim, SungHoon Yoo, and ChoonSung Yoo

Korea Reactor Integrity Surveillance Technology, 324-8, Techno 2-ro, Yuseong-gu, Daejeon, Republic of Korea

*maeng@krist.co.kr

1. Introduction

The evaluation of radioactivity distribution for decommissioning plant recently became important concern in Korea. This can make it possible to reduce the radioactive waste volume produced from the decommissioning plant.

To calculate the activity from activation, various information that interest reaction, cross-section, irradiation time, neutron flux level and so on is required. Especially, neutron flux level is very changeable during the plant life due to fuel loading pattern and irradiation time is perturbative due to plant overhaul, emergence reactor trip. These non-operation periods could contribute to decay product nuclide.

This paper introduces more precise activity calculation method by considering operation history. The introduced method will be compared with the activity calculated from effective full power and measurement data from the neutron dosimeter.

2. Method and Results

2.1 Neutron Activation Based on Effective Full Power

The neutron activation phenomenon is well known and the activity of the product nuclide when product nuclide is produced at the constant rate of R [atoms/sec] due to neutron irradiation can be written as, [1]

$$A = R\,(1 - e^{-\lambda t}) \tag{1}$$

Where A is activity [Bq], and λ is decay constant [sec^{-1}] of the product nuclide. In Eq. (1) R can be written as,

$$R = N_0 \int_0^{\infty} \sigma(E)\phi(E)dE \tag{2}$$

Where N_0 is number of target nuclide irradiated by neutron flux $\phi(E)$, and $\sigma(E)$ is microscopic cross section for the interested activation reaction. And Eq. (2) can be written as a summation form defining reaction rate RR as below,

$$RR = \int_0^{\infty} \sigma(E)\phi(E)dE = \sum_{j=1}^{n} \sigma_j \phi_j \tag{3}$$

In this case, we can calculate the activity by using multi group cross-section and neutron spectrum.

2.2 Neutron Activation Based on Operation History

If the neutron flux of Eq. (3) is changed, the RR will be also changed. Assuming that the neutron flux is constant during the period i, we can get the RR of period i as follow,

$$RR_i = \sum_{j=1}^{n} \sigma_j \phi_j^i \tag{4}$$

The specific activity of the product nuclide during the first time period will become,

$$A_1 = N_0\, RR_1\, (1 - e^{-\lambda t_1}) \tag{5}$$

During the next time period the specific activity A_1 will be decayed with its own decay constant and new product nuclide will be created and then the specific activity will become,

$$A_2 = A_1\, e^{-\lambda t_2} + N_0\, RR_2\, (1 - e^{-\lambda t_2}) \tag{6}$$

And thus, for the i^{th} time period the specific activity becomes,

$$A_i = A_{i-1}\, e^{-\lambda t_i} + N_0\, RR_i\, (1 - e^{-\lambda t_i}) \tag{7}$$

By defining that period i is a month, we can calculate the activity based on operation history as a month.

For decommissioning plant, the plant has its own monthly operation history. In this paper, operation history of Kori Unit 1 from cycle1 to cycle 17 was applied. From the first startup to cycle 17, total irradiation time was 268.5 month which is corresponding to 186.9 effective full power month. In order to get neutron flux data, RAPTOR-M3G [2] and BUGLE-96 [3] code were employed.

Table 1 shows the radiological characteristics of dosimeter used in this paper.

Table 1. Radiological Characteristics of Dosimeters

Sensor Material	Reaction of Interest	Target Atom Fraction	Product Half-Life
Copper	$^{63}Cu(n,\alpha)^{60}Co$	0.6917	5.271 year
Iron	$^{54}Fe(n,p)^{54}Mn$	0.0585	312.1 day
Nickel	$^{58}Ni(n,p)^{58}Co$	0.6808	70.82 day
Coblat	$^{59}Co(n,g)^{60}Co$	0.0015	5.271 year

2.3 Results of Comparison the activity between Operation History and Effective Full Power

Fig. 1 shows the comparison of activity when considering operation history and effective full power. The maximum relative error is up to 5 times for short lived nuclide Co-58, although the relative error is ~ 30% for long lived nuclide Co-60.

The comparisons between calculated activity according to operating history and measured activity from the dosimeter are shown as Table 2. The calculation considering operation history has very good agreement with measured activity.

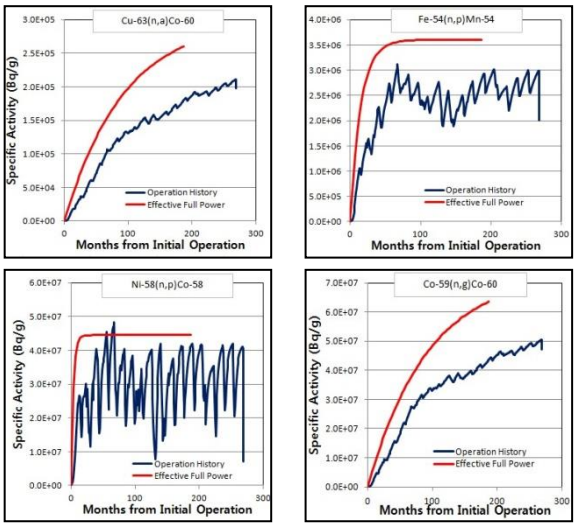

Fig. 1. Activity trends between operation history and effective full power.

Table 2. Comparisons between calculated and measured activity

	Calc. Act. [Bq/g]		Meas. Act. [Bq/g]
	Effec.Full Power	Opertaion History	
$^{63}Cu(n,\alpha)^{60}Co$	2.60E+5	1.98E+5	1.99E+5
$^{54}Fe(n,p)^{54}Mn$	3.60E+6	2.01E+6	1.94E+6
$^{58}Ni(n,p)^{58}Co$	4.45E+7	7.10E+6	7.14E+6
$^{59}Co(n,g)^{60}Co$	6.35E+7	4.88E+7	3.98E+7

3. Conclusion

The activity calculation considering effective full power operation shows significant differences against the activity considering operation history as a month. When it is compared with the measured activity, the method according to operation history is very good agreement. Therefore, this method can be used for the precise evaluation of the radioactivity for decommission plant.

REFERENCES

[1] John R. Lamarsh, Introduction to Nuclear Engineering, 3rd ed. Pearson, 2001, Chapter 2.

[2] Westinghouse, LTR-REA-11-65, Rev. 0 “RAPTOR-M3G Version 2.0 User Manual”, November 3, 2011.

[3] RSIC Data Library Collection DLC-185, “BUGLE-96, Coupled 47 Neutron, 20 Gamma-Ray Group Cross-Section Library Derived from ENDF/B-VI for LWR shielding and Pressure Vessel Dosimetry Applications,” March 1996.

Revisit of the Feasibility of Controlling the Limit of Gross Alpha Activity and Corresponding Definition of Source Terms in Safety Assessment of Near-Surface LILW Repository in Korea

Ki Nam Kwon and Jae Hak Cheong*
Kyung Hee University, 1732, Deogyeong-daero, Giheung-gu, Yongin-si, Gyeonggi-do, Republic of Korea
*jhcheong@khu.ac.kr

1. Introduction

A radioactive waste disposal facility should be under a series of control activities for a specified period even after closure. The International Atomic Energy Agency (IAEA) recommends that the possibility of inadvertent human intrusion (IHI) into the repository after active institutional control period for a limited time (up to a few hundred years) should be considered in safety assessment of a near-surface disposal facility [1]. If an IHI into the disposal facility occurs after the active institutional control period, workers involving in activities such as drilling or excavation into the facility could receive high radiation dose and residents on the closed disposal site could be exposed from radiation.

Therefore, many studies related to the safety assessment of IHI for the near-surface disposal facility has been carried out, and the result of IHI assessment has been used to set a national radioactive waste classification standard and Waste Acceptance Criteria (WAC) of a disposal facility. Additionally, it is used to criteria as making a decision the safety of the repository at after closure. And those studies considered various alpha-emitters as source term (e.g. isotopes of U, Pu, Am, and Cm) [2].

Meanwhile, in Korea, the Low-and Intermediate-Level radioactive Waste (LILW) classification standards specify the limits of activity for 11 radionuclides (i.e. ^{3}H, ^{14}C, ^{59}Ni, ^{60}Co, ^{63}Ni, ^{90}Sr, ^{94}Nb, ^{129}I, ^{137}Cs, and Gross alpha). Likewise, the WAC for Korean LILW near-surface repositories (i.e. Gyeongju Phase I and Phase II) are applied the same limits as the LILW classification standards. In the safety assessment of Gyeongju Phase I and Phase II disposal facilities, ^{239}Pu is assumed as the representative radionuclide of the alpha-emitters. This assumption is differing from the practice of considering various alpha-emitters in the safety assessment of foreign studies. Thus, in this study, various alpha-emitters are set as source term considering domestic radioactive waste streams. And through the assessment of IHI scenarios for the Gyeongju Phase II repository, would like to verifying what difference is with the result of related domestic studies.

For the IHI assessment, this study proposes the source term of alpha-emitters that can be disposed to the Korean planned LILW near-surface repository in accordance with the domestic radioactive waste stream. And this study assesses the radiological impacts of IHI scenarios using GENII Version 2 considering design features of the Gyeongju Phase II repository in Korea. Through this assessment, this study revisits the feasibility of controlling the limits of activity of alpha-emitters which is disposed to LILW near-surface repositories.

2. Materials and Methods

The six human intrusion scenarios are proposed through re-categorization of past cases reported in public literature (i.e. IHI assessment studies of United State Nuclear Regulatory Commission, United State Department Of Energy, Waste Control Specialists LLC, Low Level Waste Repository Ltd., IAEA, Korea Hydro and Nuclear Power Co., Ltd, and Korea Radioactive Waste Agency). The total six scenarios such as Drilling-Worker (DW), Drilling-Resident (DR), Excavation-Worker (EW), Excavation-Resident (ER), Agriculture-Gardener (AG), and Agriculture-Farmer (AF). Fig. 1 shows the assessment model for human intrusion scenarios proposed in this study.

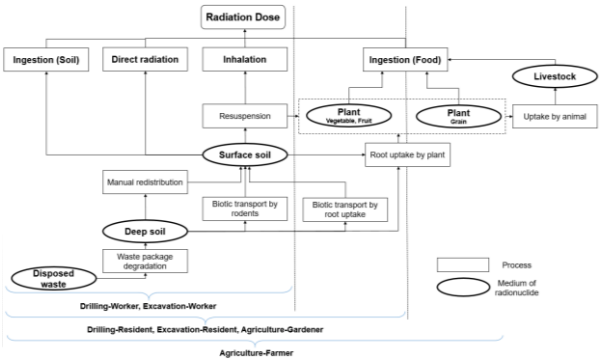

Fig. 1. Schematic diagram of the assessment model for human intrusion scenarios.

The radioactive wastes generated from nuclear power plants (NPPs), Korea Atomic Energy Research Institute (KAERI), and Korea Electric Power COrporation Nuclear Fuel (KEPCO-NF) are planned to be disposed at the Gyeongju Phase II repository. In this study, the source term of alpha-emitters is calculated through Equation 1 which is established in consideration of radioactive waste streams generated from each organization.

$$A_{tot,i} = \sum_{k=NPPs,KAERI,KEPCO-NF} A_{k,i} \cdot D_k \quad (1)$$

where, $A_{tot,i}$ is the activity ratio of alpha-emitter i to

gross alpha in total radioactive waste, $A_{k,i}$ is the activity ratio of the alpha-emitter i to gross alpha in the radioactive waste generated from organization k (i.e. NPPs, KAERI and KEPCO-NF), and D_k is the volume ratio of radioactive waste generated from the organization k to the total radioactive waste.

The radioactive wastes generated from NPPs and KAERI have assumed that the radionuclides included in radioactive wastes are generated from the fission reaction of nuclear fuel is dominantly. Therefore, the activity ratios of the alpha-emitters included in radioactive wastes generated from NPPs and KAERI are calculated through ORIGEN-ARP code (Input parameters are as follows, the enrichment of ^{235}U is 4.5wt %, burn-up is 52,500 MWD/MTU, 3 times of irradiate cycle, and the fuel assembly type is Westinghouse 17×17). And the activity ratios of alpha-emitters included in the radioactive waste generated from KEPCO-NF is referred to related study. Based on the above assumptions, the activity ratios of the alpha-emitters included in total radioactive waste to be disposed at the Gyeongju phase II disposal facility are calculated as shown in Table 1.

Table 1. The activity ratios of alpha-emitters to gross alpha and the activity of alpha emitters included in total radioactive waste to be disposed at the Gyeongju phase II repository

Alpha-emitter	Activity ratio of alpha-emitter to gross alpha (%)	Activity of alpha-emitter (Bq/g)
^{234}U	8.79	2.44×10^{0}
^{235}U	0.34	9.47×10^{-2}
^{238}U	1.13	3.15×10^{-1}
^{238}Pu	1.99	5.52×10^{-1}
^{239}Pu	0.11	3.14×10^{-2}
^{240}Pu	0.20	5.53×10^{-2}
^{241}Pu	56.75	1.58×10^{1}
^{241}Am	0.06	1.80×10^{-2}
^{243}Am	0.02	4.75×10^{-3}
^{242}Cm	27.52	7.65×10^{0}
^{243}Cm	0.02	4.37×10^{-3}
^{244}Cm	3.06	8.52×10^{-1}
Total	99.99	2.78×10^{1}

* Alpha-emitters with an activity ratio of less than 0.01% are cut-off.
** The total activity of the alpha-emitters is referred to the activity of gross alpha assumed in the IHI assessment study for the Gyeongju phase II disposal facility [3].

3. Results and Discussions

As a result of IHI scenario assessment for unit concentration (1 Bq/g), the radiation dose of ^{243}Am in alpha-emitters was calculated to be the highest as shown in Fig. 2. In addition, the highest radiation dose of ^{235}U was calculated for the results of IHI scenario assessment for considering activity ratio of each alpha-emitter as shown in Fig. 3. The couple of results indicate that ^{239}Pu, which is assumed to be a representative radionuclide in the safety assessment of LILW disposal facilities in Korea, is not the most conservative assumption in terms of IHI assessment.

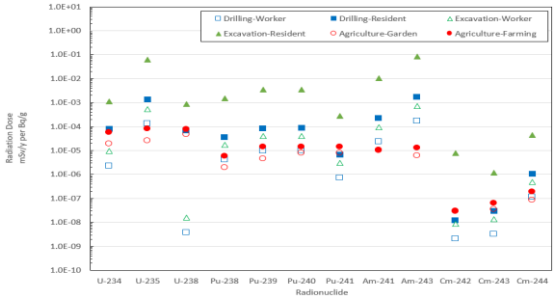

Fig. 2. The radiation doses of IHIs for unit concentration of alpha-emitters.

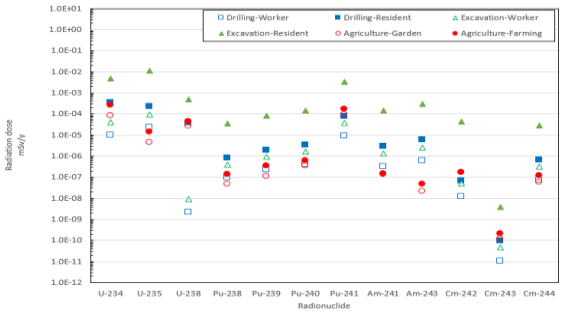

Fig. 3. The radiation doses of IHIs for considering the activity ratios of alpha-emitters.

4. Conclusion

This study assessed the radiological impacts of IHI scenarios considering twelve alpha-emitters which may be included in radioactive waste to be disposed at the Gyeongju Phase II repository. Considering the domestic radioactive waste stream, it is necessary that the revisit of the safety assessment or establishing WAC for the Korean LILW near-surface disposal facilities considering various alpha-emitters as source term.

ACKNOWLEDGEMENT

This work was supported by the Nuclear Safety Research Program through the Korea Foundation Of Nuclear Safety (KOFONS), granted financial resource from the Nuclear Safety and Security Commission (NSSC), Republic of Korea (No. 1605008).

REFERENCES

[1] IAEA, Near surface disposal facilities for radioactive waste, IAEA Safety Standards Series No. SSG-29, IAEA, Vienna, (2014).
[2] IAEA, Derivation of activity limits for the disposal of radioactive waste in near surface disposal facilities, IAEA-TECDOC-1380, IAEA, Vienna, (2003).
[3] S.W. Hong, S.H. Park, J.B. Park, Safety Assessment on the Human Intrusion Scenarios of Near Surface Disposal Facility for Low and Very Low Level Radioactive Waste, JNFCWT. 14(1) (2016) 79-90.

Review on the Possibility of Distinguishing Between "Packaging Container" and "Transport Container" in Domestic Nuclear Regulations

Moonoh Kim[1,*], Jihoon Lee[2], and Nakhoon Sung[1]
[1] Korea Nuclear Engineering & Service, 65, Myeongdal-ro, Seocho-gu, Seoul, Republic of Korea
[2] KHNP Central Research Institute, 70, Yuseong-daero 1312beon-gil, Yuseong-gu, Daejeon, Republic of Korea
*mokim@kones21.com

1. Introduction

After permanent shutdown of the Kori unit 1, the transportation of mass-produced decommissioning waste has been being a pending issue. In Korea, the process of disposal of nuclear decommissioning or radioactive waste from the generator to the Gyeongju radioactive waste disposal facility has been classified into three stages of "packaging", "transportation" and "disposal", and the containers required for each stage are being developed. In this paper, "packaging" is distinguished from packaging of IAEA SSR-6 [1].

In Nuclear Safety Act [2], Enforcement Decree [3], Enforcement Regulations [4] and NSSC (Nuclear Safety and Security Commission) notices [5-6], there are no clear codes & standards for "packaging container", while code & standard for the "transport container" exist. For this reason, there has been confusion about design criteria or requirements for the design of "packaging container" used in the field.

The authors investigated the nuclear regulations or design requirements for the design of "packaging container" and found that "packaging container" and "transport container" were not considered as separate concepts in domestic laws and notices. It was concluded that "the packaging container" and the "transport container" could not be distinguished in domestic codes and standards.

The purpose of this paper is to review the possibility of distinguishing between "packaging" and "transport" container based on domestic laws and notices. Therefore, in order to understand the meaning of the original text as it is, the domestic law and notices were captured via following website: http//www.law.go.kr and presented without being translated into English. In this paper, the provisions of Refs. [2-6] have been reviewed from the legal perspective and those of Regulations on the Technical Standards for Radiation Safety Control [7] were classified into technical aspects.

2. Review of Nuclear Regulations

2.1 Definition

In SSR-6 of IAEA and 10 CFR 71 [8] of NRC, package and packaging are similarly defined as follows: Package is defined as the product consisting of the packaging and its contents prepared for transport, and packaging is defined as one or more receptacles or the assembly of components to perform containment and other safety functions.

The meanings of those defined in domestic NSSC notice No. 2017-56[5] are also similar with those in IAEA and NRC. As shown in Fig. 1, however, the terms that were intended to mean packaging (Hereinafter Clause 2 of Article 2 in [5] is referred as "transport container") and package (Hereinafter Clause 3 of Article 2 in [5] is referred as "transport package"), but could be misinterpreted as meaning only for transport, were used. That is, the container for packaging radioactive contents is defined as a "transport container".

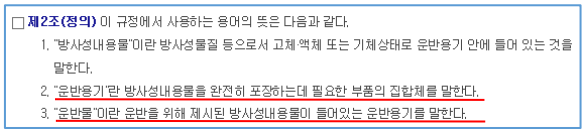
□ 제2조(정의) 이 규정에서 사용하는 용어의 뜻은 다음과 같다.
1. "방사성내용물"이란 방사성물질 등으로서 고체·액체 또는 기체상태로 운반용기 안에 들어 있는 것을 말한다.
2. "운반용기"란 방사성내용물을 완전히 포장하는데 필요한 부품의 집합체를 말한다.
3. "운반물"이란 운반을 위해 제시된 방사성내용물이 들어있는 운반용기를 말한다.

Fig. 1. Article 2 of NSSC notice No. 2017-56.

NSSC notice No. 2017-60 [6] defines "package" as containers containing waste to be delivered to operators of disposal facility. Although "HIC (High-Integrity Container)" is considered as one of "packaging container", no definition of "packaging container" was found in not only Ref. [6] but also other domestic law and regulations.

In the meantime, the US NRC TC [9] regulated that HIC must meet the requirements of Type A containers. In other words, it was stated that the HIC, which is "the packaging container" in Ref. [6], must satisfy the transportation requirement of type A.

2.2 Review on the Legal Aspects

As shown in Fig. 2 and Fig. 3, Article 76 of the Atomic Energy Act, Article 112 of the Enforcement Decree, Article 98 and 104 of the Enforcement Regulations referred to the container for packaging or transporting radioactive materials as "transport container". In other words, "the transport container" is not a container for only "transport", but for both "packaging" and "transportation".

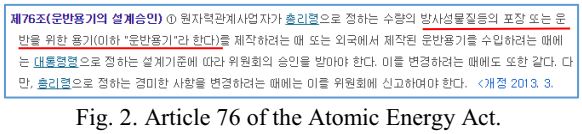
제76조(운반용기의 설계승인) ① 원자력관계사업자가 총리령으로 정하는 수량의 방사성물질등의 포장 또는 운반을 위한 용기(이하 "운반용기"라 한다)를 제작하려는 때 또는 외국에서 제작된 운반용기를 수입하려는 때에는 대통령령으로 정하는 설계기준에 따라 위원회의 승인을 받아야 한다. 이를 변경하려는 때에도 또한 같다. 다만, 총리령으로 정하는 경미한 사항을 변경하려는 때에는 이를 위원회에 신고하여야 한다. <개정 2013. 3.

Fig. 2. Article 76 of the Atomic Energy Act.

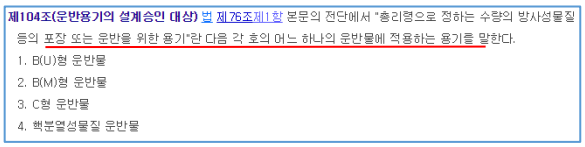
제104조(운반용기의 설계승인 대상) 법 제76조제1항 본문의 전단에서 "총리령으로 정하는 수량의 방사성물질 등의 포장 또는 운반을 위한 용기"란 다음 각 호의 어느 하나의 운반물에 적용하는 용기를 말한다.
1. B(U)형 운반물
2. B(M)형 운반물
3. C형 운반물
4. 핵분열성물질 운반물

Fig. 3. Article 112 of the Enforcement Decree.

2.3 Review on the Technical Aspects

As shown in Fig. 4, Article 90 of Ref. [7] refers to "the radioactive materials and its package" as "transport package" (Clause 3 of Article 2 in [5]) and classifies the type of package as L-type, IP type and A type "transport package".

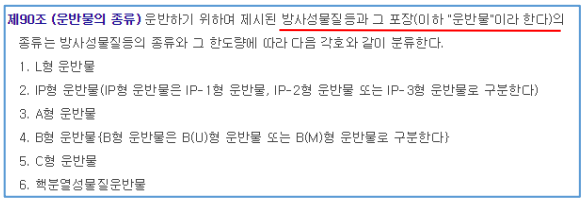
제90조 (운반물의 종류) 운반하기 위하여 제시된 방사성물질등과 그 포장(이하 "운반물"이라 한다)의 종류는 방사성물질등의 종류와 그 한도량에 따라 다음 각호와 같이 분류한다.
1. L형 운반물
2. IP형 운반물(IP형 운반물은 IP-1형 운반물, IP-2형 운반물 또는 IP-3형 운반물로 구분한다)
3. A형 운반물
4. B형 운반물(B형 운반물은 B(U)형 운반물 또는 B(M)형 운반물로 구분한다)
5. C형 운반물
6. 핵분열성물질운반물

Fig. 4. Article 90 of Ref [7].

As shown in Fig. 5, Article 96 of Ref. [7] regulates that the "package" should conform to the design standards of "transport package" (same as package in SSR-6). That is, the design requirements of the "package" is the same as that of "transport package".

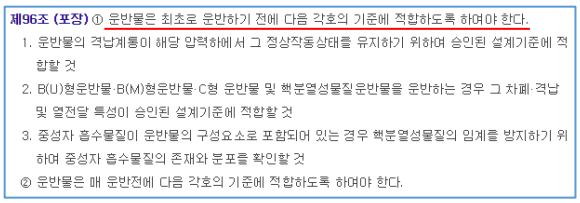
제96조 (포장) ① 운반물은 최초로 운반하기 전에 다음 각호의 기준에 적합하도록 하여야 한다.
1. 운반물의 격납계통이 해당 압력하에서 그 정상작동상태를 유지하기 위하여 승인된 설계기준에 적합할 것
2. B(U)형운반물·B(M)형운반물·C형 운반물 및 핵분열성물질운반물을 운반하는 경우 그 차폐·격납 및 열전달 특성이 승인된 설계기준에 적합할 것
3. 중성자 흡수물질이 운반물의 구성요소로 포함되어 있는 경우 핵분열성물질의 임계를 방지하기 위하여 중성자 흡수물질의 존재와 분포를 확인할 것
② 운반물은 매 운반전에 다음 각호의 기준에 적합하도록 하여야 한다.

Fig. 5. Article 96 of Ref [7].

As shown in Fig. 6, Article 115 of Ref. [7] stipulates that the type L - "transport package" (type L package) should conform to "the packaging standard", but the corresponding "packaging standard" is identical to the technical standard of "the transport container". That is, the regulatory standard for "packaging" and "transportation" are the same.

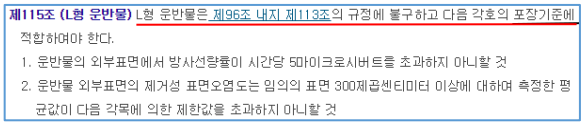
제115조 (L형 운반물) L형 운반물은 제96조 내지 제113조의 규정에 불구하고 다음 각호의 포장기준에 적합하여야 한다.
1. 운반물의 외부표면에서 방사선량률이 시간당 5마이크로시버트를 초과하지 아니할 것
2. 운반물 외부표면의 제거성 표면오염도는 임의의 표면 300제곱센티미터 이상에 대하여 측정한 평균값이 다음 각목에 의한 제한값을 초과하지 아니할 것

Fig. 6. Article 115 of Ref [7].

3. Conclusion

In this study, the provisions of the Korean Nuclear Regulatory Act (Safety Act, Enforcement Decree, and Enforcement Regulations) and NSSC Notices were reviewed.

In the domestic code & standard system, "packaging container" was not defined separately, and no legal or technical basis was found to distinguish between "packaging" and "transportation".

Rather, it was confirmed that the same technical standards were applied to "packaging" and "transportation" in Ref. [5].

Internationally, containers for the purpose of packing and transporting radioactive materials were defined as packaging, and no distinguishing difference between "transport container" and "packaging container" was found separately.

Intrinsically, "packages" and "transport package" in domestic law and regulations have the same concept. Both of them mean package of IAEA and NRC and "transport container" means packaging of IAEA and NRC.

If the separation between "packaging container" and "transport container" is needed, new technical standard for "packaging container" should be required.

ACKNOWLEDGEMENT

This work was supported by the Korea Institute of Energy Technology Evaluation and Planning (KETEP) granted fund by MOTIE, Republic of Korea (No.20181510300870).

REFERENCES

[1] IAEA, "Regulations for the Safe Transportation Materials, IAEA SSR-6, Rev. 1, (2018).
[2] Nuclear Safety Act, Act No. 15281, June.20,2018.
[3] Enforcement Decree for Nuclear Safety Act, Presidential Decree No.28987, June.20, 2018.
[4] Enforcement Regulations for Nuclear Safety Act, Prime Minister Regulation No.1459, June.20, 2018.
[5] NSSC, "Regulations for Packaging and Transportation of Radioactive Material", No. 2017-56 (2017).
[6] NSSC, "Regulations for the delivery of Low and Intermediate Level Radioactive Waste" No. 2017-60 (2017).
[7] NSSC, "Regulations on the Technical Standards for Radiation Safety Control", No-20 (2018).
[8] 10 CFR 71, "Packaging and Transportation of Radioactive Material", NRC, Jan. 2017.
[9] US NRC Waste Form TP, Jan. 1991.

4분과

중저준위폐기물관리 (Poster)

Development of Low-contaminated Sludge Radioactive Nuclides Separation Technology

HeeJin Ahn*, MiHyun Lee, and KangOk Cho

KHNP Central Research Institute, 70, Yuseong-daero 1312beon-gil, Yuseong-gu, Daejeon, Republic of Korea

*cowahn61@khnp.co.kr

1. Introduction

When nuclear power plants are dismantled, radioactive waste of various kinds and levels such as metal, concrete, and soil is generated in a very short period of time. If the appropriate waste management plan is not applied from the beginning of the decommissioning project, it will cause enormous hindrance to the decommissioning business such as increase of the disposal cost. In particular, disposal alternatives are not available due to insufficient treatment technology for disposal unsuitable wastes generated during decommissioning of nuclear power plants such as sludge wastes.

As a part of the development of radioactive waste disposal technology and special waste treatment technology, we conducted a survey on the status of low-contaminated sludge and the case of sludge separation technology and equipment at Hanbit 3 power plant. In addition, samples of low-contaminated sludge from Hanbit 3 power plant, radionuclide analysis and chemical characteristics analysis were performed.

2. Survey of Low-contaminated Sludge and Sludge Separation Technology

2.1 Survey on the Status of Low-contaminated Sludge

A large amount of radioactive waste was generated at the sewage treatment plant due to the contamination of demineralized water supply system of Hanbit Unit 5. It was collected and stored in 220 pieces of 1 ton reinforced plastic cylinders. The contaminants on the upper part of the slurry were dried and stored in a bag of 40 kg. The sludge on the floor is stored in a 689 sack bag of 40 kg capacity and is located 147 feet from the radioactive waste disposal facility. It is expected that the pollution degree of the sludge and the filter material collected at the wastewater treatment plant is very low. Therefore, it is necessary to take measures to properly dispose of these radioactive wastes below the disposal limit in accordance with legal procedures, rather than drum-disposing them.

2.2 Sludge Separation Technology Case Study

The main purpose of the sludge separation technology is to minimize the radiation effects. The key to the treatment technology is separation and concentration. Radioactive waste, which has become very low in concentration through separation, is disposed of itself, and enriched is isolated from the living environment through solidification treatment after volume reduction for efficient storage and management. The method of treatment of radioactive waste should be selected according to the radioactive level of radioactive waste, physical and chemical conditions, kinds of radionuclides contained in radioactive waste, and so on. As a result of the survey, the radioactive sludge generated from the nuclear power plant was partially treated for solidification, but no radioactive material was removed through the separation of nuclides. However, related research is ongoing in the United States and Japan [1].

3. Sampling of Low-contaminated Sludge, Analysis of Radionuclides and Chemical Characterization

3.1 Results of Low-contaminated Sludge Analysis

Radionuclides of the sludge were analyzed. The radionuclides above the reference concentration were Mn-54, Co-58, Co-60, Cs-137 and Nb-94.

The Concentrations of nuclides in waste types were up to 0.5 times higher than that of Co-60, but other nuclides were 0.1 ~ 0.2 times higher than self-disposal concentration or slightly higher than the reference value.

4. Nuclide Removal Experiment of Low-contaminated Sludge

4.1 Washing Treatment and Ultrasonic Treatment

Experiments were conducted to remove the nuclides above self-disposal standards.

As a method of removing nuclides, a washing treatment method and an ultrasonic treatment method were used. In the washing process, 250 cc sample was placed in a 500 cc sample bottle, and 250 cc of deionized water was filled in the sample bottle, followed by washing and ultrasonic treatment. As a result of the nuclides removal treatment, Cs-137 was completely removed. Co-60 was removed to about 1/2 to 1/5 level. This suggests that it was moved to a pH alkaline area by OH- ions present on the surface of sludge. And radioactive cobalt that must be leached are present as sediment in $Co(OH)_2$ and were not leached.

4.2 Chemical Elution and Substitution

4.2.1 Radiochemical Properties of Co-60. Cobalt has oxidation states of 0, +2 and +3, and Co^{2+} & Co^{3+} coexist in a stable state as Co^{2+} ion in aqueous solution. The Cobalt chemical species are absorbed into small particles in the water, settled down to rocks or sand, or are directly absorbed into materials such as sand and gravel [2].

This degree of adsorption depends on the pH, the oxidation-reduction atmosphere, and the concentration of dissolved organic matter. When a strong oxidizing agent is present in the aqueous solution, the cobalt ions are present in the oxidized state of Co^{3+} and exist in the form of a precipitate of $Co(OH)_3$ over the acidic and alkaline regions. In the absence of oxidant, cobalt ions exist in the form of Co^{2+}, and exist in the form of precipitates of $Co(OH)_2$ from alkaline near neutral to strongly alkaline.

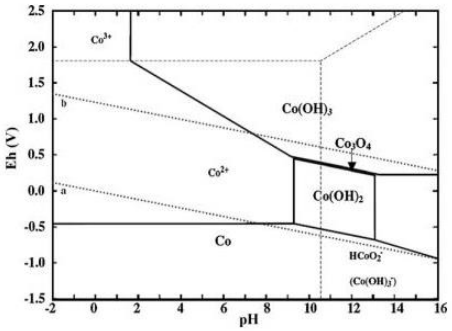

Fig. 1. Eh-pH Diagram for Cobalt Ion.

4.2.2 Co-60 Elution Experiment using Strong Acid. It is believed that the Co-60 are absorbed onto their surfaces due to the presence of large amounts of iron and manganese in the sludge contents, to remove the Co-60 that is absorbed on the surface, use acid solutions such as HCl, HCl+HNO_3, HCl+H_2SO_4, HCl+$HClO_4$ to dissolve iron or manganese[3]. In this experiment, HCI was used, and three kinds of reducing agent such as oxalic acid ($C_2H_2O_4$), chloride tin ($SnCl_2$), and hydroxyl amine ($NH_2OH{\cdot}HC$) were used for elution of Co-60 [4].

$$Co^{2+}(aq) + 3Ox^{2-}(aq) \rightleftharpoons [Co(Ox)_3]^{4-}(aq) \quad (1)$$

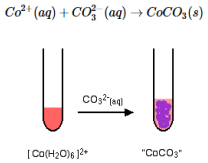

Fig. 2. The reaction of hexaaquacobalt(II) ions with carbonate ions.

In particular, chloride annotations ($SnCl_2$) were used to replace eluted Co-60 with Sn. To check the time effect of elution and substitution, stirred it for 10 minutes, 1 hour, 6 hour and 24 hours, respectively.

5. Conclusion

In order to reduce the amount of radioactive waste generated due to contamination of the desalination water supply system of Hanbit Unit 5, a self-disposal plan was sought. The types of wastes were ground sludge of sedimentation tank, gravel used as filtration media, sand, activated carbon anthracite. As a result of the analysis of radionuclides in low-contaminated radioactive wastes, radionuclides exceeding the self-disposal standard values were analyzed as Mn-54, Co-58, Co-60, Cs-137 and Nb-94. Concentrations of nuclides in waste types were up to 17 times higher than that of Co-60, but other nuclides were 2 ~ 3 times higher than self-disposal concentration or slightly higher than the reference value. In order to confirm the possibility of self-disposal of radioactive waste, a nuclide elimination experiment in radioactive waste was conducted.

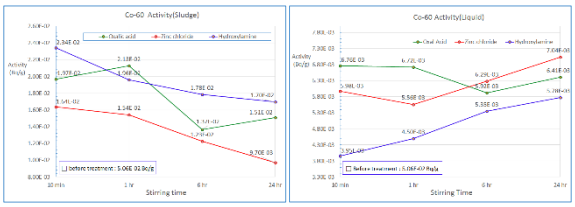

Fig. 3. Co-60 activity in Sludge and Liquid after treating nuclide removal.

The biggest effect of removing nuclide was in case of chloride annotations were treated as reductants when the analysis of sludge nuclides after treating nuclide removal.

The elimination rate of nuclide was treated up to about 20 %, which is equivalent to 1/10 of the criteria for self-disposal and, it is sufficient level self-disposal.

We will build a nuclide removal facility.

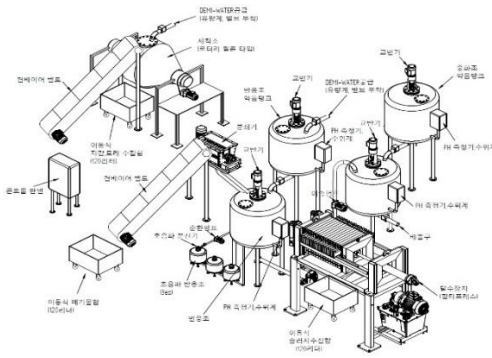

Fig. 4. Nuclide removal facility conceptual diagram.

REFERENCES

[1] ANDRA, "National Inventory of Radioactive Materials and Waste", 2012.

[2] M. Pourbaix, "Atlas of Electrochemical Equilibria in Aqueous Solutions", National Association of Corrosion Engineers, Houston, Texas, USA, p. 325. 1974

[3] Sahuquillo et al, Analytica Chimica Acta, 382(3), 317 ~ 327, 1999

[4] McLaren et al., Journal of Soil Science, 37(2), 223 ~ 234, 1986

Construction of a Plasma Melting Facility for Developing the Treatment & Disposal Technology of Radioactive Waste

Hyun-Je Cho [a,*], Mi-Hyun Lee [a], and Jun-Ho Seo [b]
[a] KHNP Central Research Institute, 70, Yuseong-daero 1312beon-gil, Yuseong-gu, Daejeon, Republic of Korea
[b] Chonbuk National University, 567 Baekje-daero, Jeonju, Republic of Korea
*chohyunje@khnp.co.kr

1. Introduction

In general, radioactive wastes generated in nuclear power plants are stored in a closed 200 L drum container. The wastes stored in drums are collected and stored in various forms, and the wastes comprise a variety of components having characteristic such as flammable, inorganic, etc. Therefore, it is difficult to separate and treat the radioactive waste stored in the 200 L drum separately because of the concern on secondary contamination. Therefore, it is very important that a series of stabilization treatments such as waste input, crushing, combustion and melting, etc. should be continuously made in a melter.

For developing volume reduction method and securing treatment & disposal technology of radioactive waste generated during NPP operation, plasma torch melter technology has been proceed research to treat directly 200 L drum using plasma melting from 2014.

2. Plasma Melting Facility

2.1 Status of Worldwide

The plasma melter melts non-combustible materials such as metals, concrete, and so on, thereby reducing the volume. A large-sized melter for directly processing a 200 L drum scale is used to increase the throughput of a target material, and a megawatt (MW) scale plasma torch is applied in consideration of the heat loss in the melter and the torch. Recently, the plasma torch melter facility in the Kozloduy Nuclear Power Plant in Bulgaria was finished the pre-operation test in July, 2018 and commercial operation from August started for volume reduction of radioactive waste generated during NPP operation. This melter is discharging molten material with a method by tilting like as plasma facility at Zwilag in Switzerland. In case of Tsuruga nuclear power plant, the pouring of molten is using heating method with an induction heating device on around an outlet of the plasma melter.

2.2 KHNP Facility

Fig. 1 shows a schematic diagram of the constricted plasma melting facility constructed at KHNP/CRI. As shown in this figure, the constructed plasma melting facility primarily consists of a 1.5 MVA class DC power supply (750 A x 2 kV), a convertible plasma torch, a utility system for supplying the various gases and water-coolant, a robot arm for transporting the plasma torch, a high-capacity melter, a drum transportation system and an off-gas treatment system. In a plasma melter developed from present research, the upper surface on which the plasma torch is installed is provided with a constant inclined surface. Accordingly, the torch in melter is smoothly operated, and plasma heat source generated by the torch can easily keep balanced up to the upper portion of the melter. The waste input on upper portion of melter is provided by a small-diameter (approx. 20 cm) inlet pipe and non-drum-shaped combustible waste can be input. The large-scale inlet apparatus is installed at the lateral inlet formed through the side of melter such that the waste drum of 200 L is directly introduced.

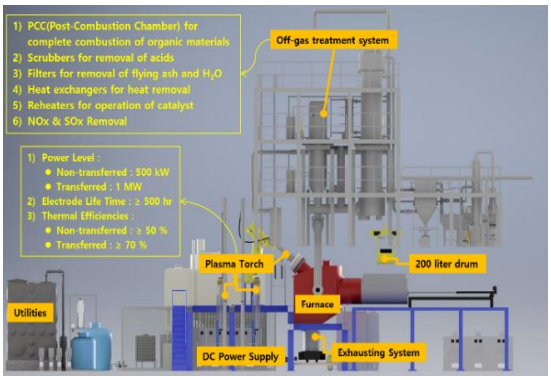

Fig. 1. A schematic diagram of the MW scale plasma melting facility constructed by KHNP/CRI.

The melter was designed to take in a 200 liter drum through the drum gate with the melting pool of 200 liter, and built by using the C-MgO composite blocks. Once a 200 liter drum entrained, the plasma torch melts the drum head in non-transferred mode, pouring the wastes contained in the drum. The wastes are layered on the bottom of the melter and heated up by the plasma torch, resulting in the formation of melting pool on the top parts of the layered wastes. If the electrical conductivity of the waste pool is increased enough for passing the arc currents, the operation mode of the torch can be changed into transferred one. Then, the electrical power is elevated for fast and complete melting of the wastes. In addition, the wastes melt is exhausted into the vessel and transported outside the melter as presented in Fig. 1. Finally, these operation processes were shown briefly in Fig. 2 with four pictures, which are taken by operation sequence of a plasma torch, i.e., ignition, non-transferred, hybrid and transferred modes

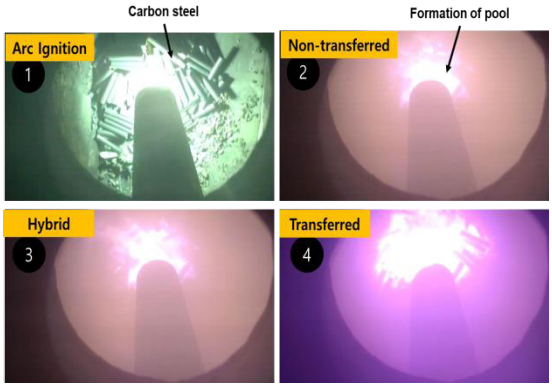

Fig. 2. Pictures taken during the operation of plasma melting facility for carbon steel melting.

3. Conclusions

A plasma melting facility with electrical output of MW scale was constructed at Central Research Institute of KHNP (Korea Hydro & Nuclear Power Co., Ltd) for producing the produce data and testing the volume reduction of low and intermediate level radioactive waste. The plasma melter was developed with direct processing the 200 L drum, the treatment-possible internal capacity is 2 drums/hr for combustible and 1 drum/hr for non-combustible. The melter was designed with section type on top plate as cylindrical type, which has a width 2 m, length 2.2 m and height 2.4 m on internal size. In particular, this facility employed a convertible plasma torch system, which is capable of operation mode change from non-transferred to transferred modes depending on radioactive wastes such as combustible or non-combustible. By converting the operation mode depending on the electrical conductivity of the radioactive waste, the constructed facility was designed to melt not only the soil and concrete blocks in non-transferred mode but also carbon steels in hybrid or transferred modes. In addition, off-gas treatment system was also designed and connected to the plasma melter, allowing the constructed system to treat the radioactive wastes regardless of whether or not they are combustible within the power level of 1.5 MW.

Study on Radiological Inventory Assessment of K 1 Reactor Vessel

Young Hwan Hwang*, Seok-Ju Hwang, and Ju-Young Yoon
KHNP Central Research Institute, 70, Yuseong-daero 1312beon-gil, Yuseong-gu, Daejeon, Republic of Korea
*yhhwang7@khnp.co.kr

1. Introduction

During decommissioning of nuclear power plant (NPP), it is generally understood that large amount of radioactive wastes are generated. The carefully planned waste management strategy, including packaging, transportation, and disposal, is one of the most important prerequisite for the decommissioning to prevent delay or impede of the process [1]. The accurate radiological inventory assessment comes first to construct the waste management plan.

The radiological inventory assessment of activated component usually involves computer codes (Fig. 1.). The monte-carlo based computer code, MCNP, is used to understand the neutron behavior and evaluates the neutron flux and fluence over operation. The ORIGEN calculates the inventory of activated materials by neutron. It is generally accepted that accurate and detailed input of operation history, geometry of component, and materials composition should be provided to achieve accurate radiological inventory of the components.

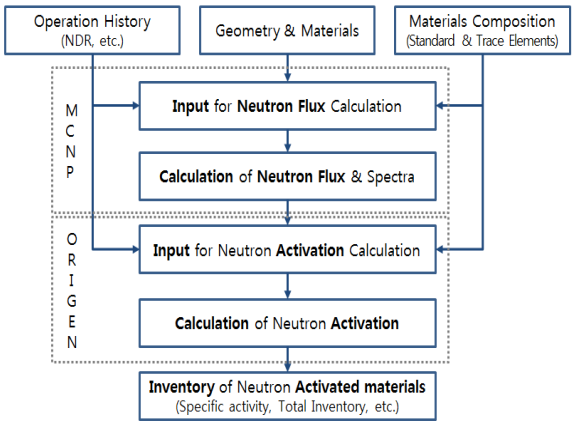

Fig. 1. Activation Analysis Procedure [2].

2. Results and Discussions

The reactor vessel (RV), which is a representative component of NPP, is massive and relatively highly activated. The RV consists of shell, HOT/COLD legs, head, etc. The RV is covered with several layers of crumpled STS304 foil. The detailed geometry and neighboring structures are shown in Fig. 2. Since the small gap between sub-components can be a path for neutron transportation, the geometry is carefully described and confirmed, according to several walkdowns and investigations.

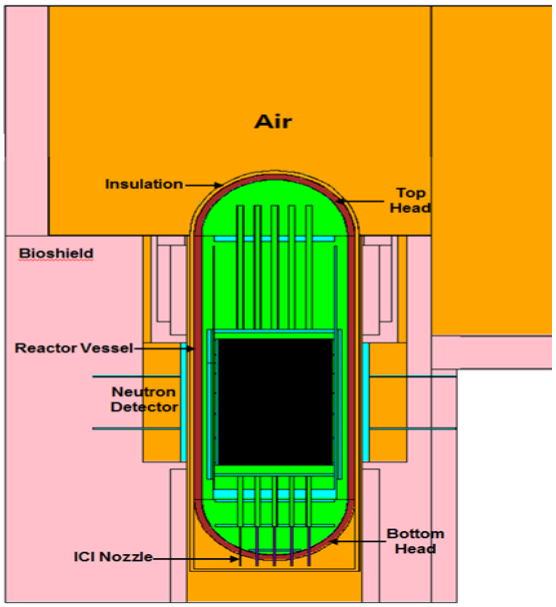

Fig. 2. Geometry of K1 RV and RVI.

The material composition is also an important input for analysis. As it is noted in previous analysis, the trace elements in the component significantly affects the analysis result [3]. The majority elements of the RV, which is made of carbon steel, are Fe, Mn, Cr, and Ni. (Table 1)

Table 1. Material Composition of RV (Selected)

Element	Weight Fraction	Unit	Element	Weight Fraction	Unit
Cr	0.17	%	Cu	1274	ppm
Mn	1.02	%	Zn	100	ppm
Fe	98	%	Ga	80	ppm
Ni	0.66	%	As	532	ppm
Li	0.3	ppm	Se	0.7	ppm
N	84	ppm	Br	0.85	ppm
Na	23	ppm	Rb	48	ppm
Al	330	ppm	Sr	0.15	ppm
Cl	40	ppm	Y	20	ppm
K	12	ppm	Zr	10	ppm
Ca	14	ppm	Nb	18.8	ppm
Sc	0.26	ppm	Mo	0.56	ppm
Ti	2	ppm	Ag	2	ppm
V	80	ppm	Sb	11	ppm
Co	122	ppm	Cs	0.2	ppm

The calculated specific activity of the K1 RV is shown in Table 2. At a standpoint of direct exposure to worker, the primary concern comes from the isotopes emitting energetic gammas [3]. The ^{60}Co, produced from ^{59}Co, emits 1.173 and 1.332 MeV gamma rays and attracts large attention. Although pure beta emitters are not as harmful as gamma emitter due to their low penetration characteristics in direct exposure, their potential hazard should be taken into account for disposal. The low beta energy from tritium results in a low hazard from direct exposure. However, the high mobility of ^{3}H requires careful treatment. The ^{63}Ni is a second most abundant nuclide in the RV. The long half-life of ^{63}Ni requires continuous attention when considering disposal of the RV. Also the vapor of Ni, which could be evaporated and become mobile during thermal segmentation, is harmful to workers and attracts large attention during segmentation process. It means that the sufficient local ventilation system and emergency plans should be equipped to protect workers and prevent the proliferation of contaminants.

Table 2. Specific Activity of RV (Selected)

(Unit: Bq/g)

Nuclide	RV (Active fuel)	RV (upper)	Insulation (Active Fuel)	RV Head
^{55}Fe	6.33E+06	1.16E+05	1.46E+02	3.24E+01
^{63}Ni	4.09E+05	6.84E+03	1.87E-02	3.56E-01
^{60}Co	2.03E+04	3.20E+02	7.44E-01	4.77E-02
^{54}Mn	3.28E+03	4.34E+01	3.34E-02	2.45E-02
^{59}Ni	4.15E+03	6.90E+01	1.78E-04	3.23E-03
^{3}H	5.61E+02	9.38E+00	2.49E+01	8.75E-04
^{14}C	1.99E+01	3.30E-01	2.12E-02	1.50E-05
^{93m}Nb	7.76E+00	1.35E-01	1.29E-03	8.25E-06
^{154}Eu	1.12E+01	2.14E-01	1.51E-02	2.15E-05
^{93}Mo	1.52E-03	2.52E-05	2.09E-05	9.18E-10
^{134}Cs	2.36E+00	4.26E-02	8.30E-03	1.40E-05
^{94}Nb	5.25E-01	8.73E-03	8.98E-05	3.29E-07
^{36}Cl	1.04E+00	1.73E-02	3.02E-02	8.16E-07
^{155}Eu	3.42E-01	1.00E-03	3.06E-04	1.36E-07
^{99}Tc	2.14E-04	3.60E-06	2.98E-06	1.30E-10
^{152}Eu	6.02E+01	1.59E+00	1.19E-01	1.42E-04
^{151}Sm	3.26E-01	2.87E-03	1.19E-03	1.26E-07
^{110m}Ag	2.98E-03	3.41E-05	3.49E-08	3.12E-08

3. Conclusion

The radiological inventory assessment is performed to understand and classify the K1 RV. The majority nuclides of activated RV are ^{55}Fe, ^{63}Ni, ^{60}Co, etc. The active fuel region of the RV is classified as LLW. The specific activity of the RV head, which is replaced several years ago, is much lower than other components.

REFERENCES

[1] EPRI, Review of Waste Management Best Practices During Nuclear Plant Decommissioning, 3002005252 (2015).

[2] IAEA, Radiological Characterization of Shut-Down Nuclear Reactors for Decommissioning Purposes, TRS No.389, (1998).

[3] PNNL, Long-Lived Activation Products in Reactor Materials, NUREG/CR-3474 (1984).

Development Status of Radioactive Waste Container Package for Decommissioning Nuclear Power Plant

Mi-Hyun Lee* and Hee-Jin Ahn
KHNP Central Research Institute, 70, Yuseong-daero 1312beon-gil, Yuseong-gu, Daejeon, Republic of Korea
*mihyun.lee@khnp.co.kr

1. Introduction

The decommissioning of nuclear power plants in Korea was decided due to the permanent suspension of the Kori Unit 1. A large amount of radioactive waste may be generated when decommissioning nuclear power plants. In particular, high-activated reactor vessel internal(RVI) is evaluated as Intermediate-level radioactive waste, and there is a risk of radiation exposure to the treatment.

In this paper, it describes the low and intermediate-level radioactive waste container that occurs during decommissioning at nuclear power plants.

2. Main Subject

2.1 Classification of Decommissioning Waste

Most of the radioactive waste generated by decommissioning the nuclear power plant is metal and debris type soil and concrete. Most are low-level or very low-level radioactive wastes, and high-activated RVI which is classified as intermediate-level radioactive wastes. The radioactive waste generated in decommissioning is classified as Table 1.

Table 1. Waste Categories [1]

Waste Classes	Typical Characteristics	Disposal Options
High Level Waste (HLW)	4,000 Bq/g for alpha-emitting radionuclide having a Half-life longer than 20 years	-Deep geo.
Intermediate Level Waste (ILW)	Less than HLW, More than concentration Limit of LLW	-Deep geo. -Silo
Low Level Waste (LLW)	More than 100 times of CW level, Less than concentration limit of LLW	-Deep geo. -Silo -Eng. barrier
Very Low Level Waste (VLLW)	More than concentration limit of CW, Less than 100 times of CW level	-Deep geo. -Silo -Eng. barrier, -Landfill

2.2 Disposal of Oversea Waste Best Practice [2]

US : The BUD(Beneficial Use Determination) release criterion for foundations and slabs, as well as for materials used as backfill(i.e., concrete, asphalt, soil). Reactor vessel and internal were cut off in the water and high-activated structures were removed while operating a purge system capable of removing nuclides in the air. In addition, the use of reusable containers (Fig. 1) has reduced costs.

Fig. 1. Inter-Modal, Reactor Head and Pressurizer.

Spain : The standard of disposable waste containers was diversified to facilitate disposal. Plastic bag, metal drum and metal box etc. were used (Fig. 2).

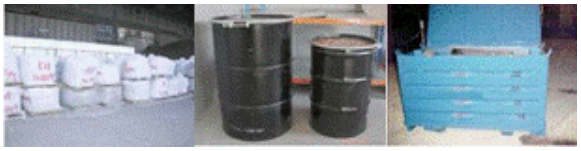

Fig. 2. Packages at E1 Cabri Disposal site.

Germany : Volume 1.32 m^3 to 10.8 m^3 waste containers used, small volume containers(MOSAIK II) were packed with high-activated waste, and large volume containers were packed with low-level radioactive waste (Fig. 3).

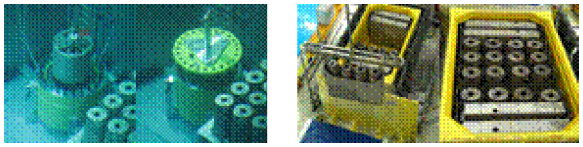

Fig. 3. MOSAIK II and Steel Container.

Sweden : Reactor vessel internal, which are highly radioactive wastes exceeding the disposal standard, were packed and stored in BFA box (Fig. 4). The BFA box is metal container with 3.4 x 1.5 x 2.3 m, thickness 10 cm. The container can pack 23 tons of waste.

Fig. 4. BFA Boxes for High Activity Waste in Sweden.

3. Conclusion

The intermediate-level radioactive wastes generated when decommissioning the nuclear power plants have high radiation dose and are difficult to pack. The large amount of radioactive waste treatment and disposal has a large impact on the cost of decommissioning. Considering the limited radioactive waste disposal volume and considering the disposal stability such as employee radiation exposure, more efficient waste disposal is needed.

REFERENCES

[1] International Atomic Energy Agency, Classification of Radioactive Waste, IAEA Safety Standards Series No. GSG-1(2009).

[2] EPRI, “Review of Waste Management Best Practices During Nuclear Plant Decommissioning”, Final Report (2015).

Manufacture of RWTF Cement Waste Form Including Low-level Liquid Waste for Final Disposal

Gi Yong Kim, Junhyuck Im, Jong Sik Shon, and Dae Seok Hong*

Korea Atomic Energy Research Institute, 111, Daedeok-daero 989beon-gil, Yuseong-gu, Daejeon, Republic of Korea

*dshong@kaeri.re.kr

1. Introduction

Radioactive waste at Korea Atomic Energy Research Institute (KAERI) are generated from the research reactor, Radio Isotope (RI) production facility and laboratories using RI. Therefore, it is essential to operate the Radioactive Waste Treatment Facility (RWTF) that can safely manage all radioactive waste at KAERI. One of the efficient way to treat radioactive waste is cement solidification. The cement solidification method is efficient and simple than other solidification method. Hence, this study is focused on the development of cement solidification for final disposal facility. We used zeolite to improve the radioactive nuclide leaching resistance of RWTF cement waste form containing low-level liquid waste (LLLW). All RWTF cement waste form should meet the waste acceptance criteria for final disposal in several tests such as thermal cycling, immersion, and compressive strength test.

2. Methods and Results

2.1 Materials

Portland cement (Type I) and Zeolite were purchased from SSangyong, Zeobuilder. All other chemicals used are of analytical or research grade**.** Table 1 shows the Radioactivity level of the LLLW from RWTF.

Table 1. Radioactivity level of LLLW

Radionuclide	Radioactivity (Bq/mL)
^{60}Co	20.3
^{134}Cs	26.6
^{137}Cs	2,460

2.2 Fabrication of RWTF Cement Waste Form

The RWTF cement waste form were fabricated in accordance with the Korean Industrial Standard (KS-L-5109) [1]. The mechanical mixer (Jl-206) was purchased from Jeil Precision [2]. The RWTF cement waste forms were made at W/C 0.6 considering the result of the free standing water test (Fig 1a).

We added zeolite to improve the radioactive nuclide leaching resistance of RWTF cement waste form(S/C S; zeolite, C; cement) from 0 and 10wt.% (Fig. 1b-c). RWTF cement was solidified while curing at room temperature with relative humidity of 40 to 60% for 28 days [3].

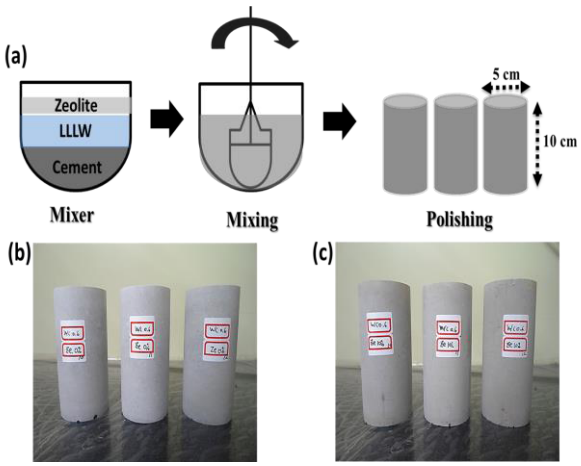

Fig. 1. (a) Schematic diagram showing a RWTF cement waste form including LLLW, (b) RWTF cement waste form (control) (c) RWTF cement waste form zeolite with 10%.

2.3 Acceptance Criteria of Final Disposal Facility

2.3.1 Thermal Cycling Test. The thermal cycling test is performed to confirm heat resistance of the cement waste form. RWTF cement waste form is tested by changing from -40 to 60 degree for one day (1 cycle) and the procedure were repeated 30 times (30 cycle). Fig. 2 shows real images of RWTF cement waste form after thermal cycling test. RWTF cement waste form did not show crumbling and cracking during thermal cycling test.

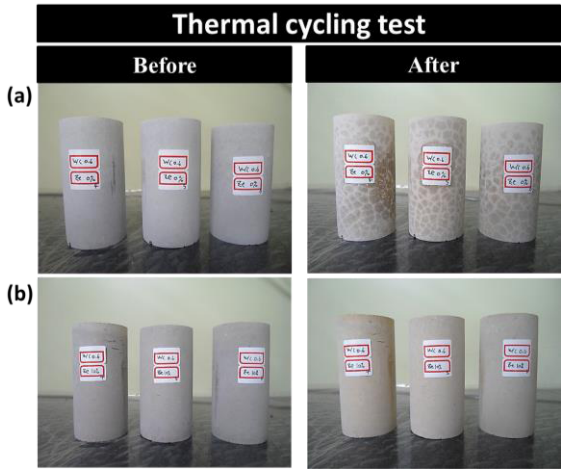

Fig. 2. Real images of RWTF cement waste form after thermal cycling test. (a) control, (b) RWTF cement waste form zeolite with 10%.

2.3.2 Immersion Test of RWTF Cement Waste Form. In order to evaluate the durability of the RWTF cement waste form containing zeolite, the immersion test for 90 days was performed (Fig. 3). RWTF cement waste form did not show any cracking.

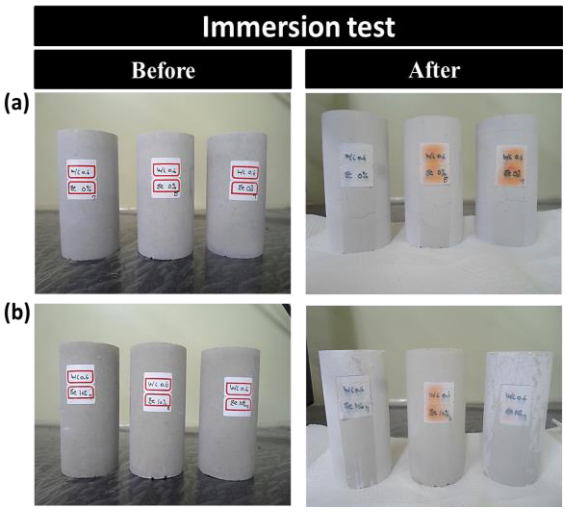

Fig. 3. Images of RWTF cement waste form after immersion test. (a) control, (b) RWTF cement waste form zeolite with 10%.

We measured pH and electronic conductivity(Eh) of RWTF cement waste form during the leaching test (Fig.4). pH and Eh show a continuous increase with leaching time. After 47 days, pH and Eh of leachate were not changed. It was showed that the pH and Eh decreased with zeolite content of RWTF cement waste form. It is likely that zeolite adsorbed such as component of cement metal ions and Cs, Co in the leachate.

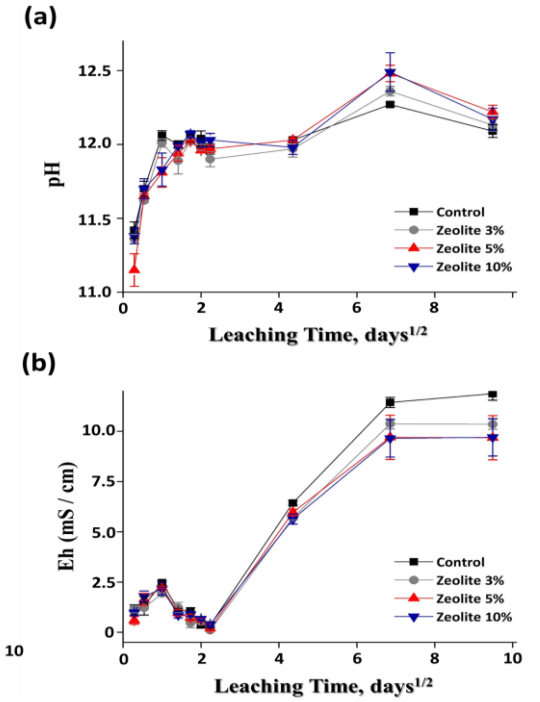

Fig. 4. pH and electronic conductivity with a leaching time of RWTF cement waste form (a) pH, (b) Eh.

3. Conclusions

In this study, we made RWTF cement waste form with low-level liquid waste. RWTF cement waste form was made at W/C 0.6 considering the result from a free standing water test. In addition, we used zeolite to improve the radioactive nuclide leaching resistance of KJRR cement waste form. We demonstrated that RWTF cement waste form had water and heat resistance based on immersion and thermal cycling test.

REFERENCES

[1] J.S. Shon, et al., “Treatment and Disposability of Intermediate Level Liquid Radwastes generated by Fisson Moly Production”, Proc. of the Korean Radioactive Waste Society, 15 (2017)

[2] W.H. Jang, et al., "A Study on Operating Range of Cement Solidification for Final Disposal of Radioactive Soil”, Journal of Korea Society of Waste Management, 34 (2017)

[3] G.Y. Kim, et al., “Characterization of cement solidification for enhancement of cesium leaching resistance”, Journal of Nuclear Fuel Cycle and Waste Technology, 16(2), 189-193 (2018)

Evaluation of Measurement Uncertainty in the Determination of ^{59}Ni in Radioactive Wastes Using Low Energy Photon Spectrometry

ChangHeon Lee*, SeChul Sohn, KeChun Choi, Preun Kim, and SeungMin You
Nuclear Decommissioning Research Institute, 20-13, Yulliyeonghae 2-gil, Cheongnyang-myeon, Uljin-gun, Ulsan, Republic of Korea
*Chang4076@hanmail.net

1. Introduction

There is only a few presentations for evaluating measurement uncertainty in the field of radiochemical analysis although quality assurance is more emphasized than ever before. In general, the reliability of the analysis results in most studies are still defined by the standard deviation of only repeated measurements obtained through the final instrumental analysis with no regard for source of uncertainty such as sample collection, carrier concentration, chemical yield and detector efficiency, etc. The purpose of this work was to demonstrate a procedure to evaluate sources of uncertainty in the determination of ^{59}Ni in a radioactive waste sample by low energy photon spectrometry (LEPS).

2. Experimental

2.1 Dissolution of Radioactive Waste Samples

Thirty grams of a dry active waste sample was heated at 450℃ for 12 h and then 0.6~0.8 g of the resulting ash was transferred to a 100 mL Teflon bomb vessel. 6 mL of 70% HNO_3, 3 mL of 37% HCl and 1 mL of 48% HF were added. Sample dissolution was performed using a microwave acid digestion system. The acidic sample solution was transferred to a 20 mL volumetric flask and diluted with deionized water.

2.2 Preparation of a Loading Solution

After 8 mL of the acidic sample solution, 0.2 mL of a Ni carrier solution (10 mg/mL) and an aliquot mL of Re, Sr, Nb and Fe carrier solutions and conc. 0.5 mL HF were pipetted to a 50 mL beaker, the mixture was evaporated on a hot plate. The resulting residue was dissolved in 10 mL of conc. HCl with stirring. After pipetting 0.5 mL of saturated boric acid, followed by evaporation. Ten milliliters of 0.5 M HNO_3 was added to the beaker, and the residue was dissolved.

2.3 Separation of Nickel from a Sample Matrix

The loading solution was injected on the anion exchange resin column for separation of Re as a surrogate of ^{99}Tc. Effluents containing Sr, Fe Nb and Ni was collected in a 50 mL centrifugation tube. According to the separation procedure shown in Fig. 1, Sr was separated by extraction chromatography and Fe and Nb by anion exchange chromatography. Finally, Ni was recovered by pipetting 9 M HCl on the Ni-resin column stacked in series with the anion exchange resin column and its recovery was measured by Inductively Coupled Plasma Atomic Emission Spectrophotometry (ICP-AES).

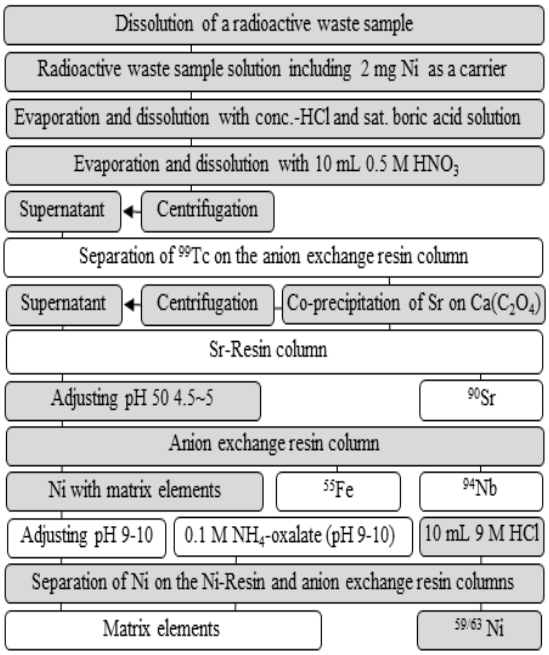

Fig. 1. Separation procedure of ^{59}Ni in radioactive waste samples.

3. Result

3.1 Reliability of the Nickel Separation

The effluent was collected to prepare a ^{59}Ni source, and Ni-recovery measured by ICP-AES was 92.6%±0.6% (n=5) [1].

3.2 Chemical Yield of ^{59}Ni Sources

$Ni(DMG)_2$ precipitates as a ^{59}Ni source was obtained at pH 9~10, and their chemical yield of measured gravimetrically was 88.5%±1.3% (n=5) [1] .

3.3 Radioactivity Analysis of ^{59}Ni

Radioactivity ^{59}Ni was measured with low energy spectrometer which was composed with Ge detector, HV Supply and Pulse analyzer [2].

3.4 Evaluating of Measurement Uncertainty

Uncertainty produced in the chemical process from weighing of the radioactive waste sample to radioactivity analysis of ^{59}Ni in the $Ni(DMG)_2$ precipitate were evaluated according to the following steps: Specification of measurand, identify uncertainty components, quantify uncertainty components, calculate combined uncertainty [3].

3.4.1 Specification of Measurand. The equation for the calculation of activities of ^{59}Ni in radioactive wastes is expressed as follows.

$$A = \frac{1}{W} \times \frac{V_t}{V_s} \times \frac{Ni_{Carrier}}{Ni_{PPT}} \times \frac{N_{Ni}}{\epsilon} \quad (1)$$

where A: ^{59}Ni radioactivity of sample (Bq/g), W: weight of sample, V_t : total sample volume, V_s: sampling volume, $Ni_{Carrier}$: weight of Ni carrier plus weight of Ni in sample, Ni_{PPT}: weight of $Ni(DMG)_2$ precipitate, N_{Ni}: net count of ^{59}Ni in $Ni(DMG)_2$ precipitates and ε: counting efficiency.

3.4.2 Identify Uncertainty Components. The components to evaluate measurement uncertainty were as follows; sample weight uncertainty: [$u(W_t)$], sample volume uncertainty: [$u(V_t)$], sampling volume uncertainty: [$u(V_s)$] weight uncertainty of nickel in carrier and in the sample: [$u(Ni_{carrier})$], weight uncertainty of $Ni(DMG)_2$ precipitate: [$u(Ni_{ppt})$], ^{59}Ni activity uncertainty for ^{59}Ni in $Ni(DMG)_2$ precipitate: [$u(N_{Ni})$] and counting efficiency uncertainty: [$u(\varepsilon)$].

4. Conclusion

The uncertainty arising from each individual source evaluated as the standard uncertainty is either of type A or type B. Combined relative uncertainty calculated by using results obtained through evaluation of source measurement uncertainty was 2~3%. Expanded uncertainty calculated on the basis of the component measurement uncertainty was 4~6% (at confidence interval of 95%, k = 2). The major uncertainty contributions were found to be the repeatability of the chemical yield determination and the counting efficiency of ^{59}Ni.

REFERENCES

[1] Chang Heon Lee, HongJoo Ahn, Jeong-Mook Lee, Yeong-Keong Ha, and Jong-Yun Kim, “Rapid separation of ^{99}Tc, ^{90}Sr, ^{55}Fe, ^{94}Nb and ^{59,63}Ni in radioactive waste samples” Journal of Radioanalytical Nuclear chemistry, 308 809-816 (2016).

[2] Byoung Chul Song, Young Bok Kim, Chang Heon Lee, SunHo Han, Sechul Sohn, “Measurement of ^{59}Ni and ^{63}Ni in the radioactive wastes”, Proc. of the KRS 2008 Spring Conference, 6(1), May 22-23, 2008 Seoul.

[3] Sechul Sohn, Hong Joo Ahn, SunHo Han, KwangYong Jee, “Measurement uncertainty of the analysis method for the radionuclide in the radioactive wastes samples”, Proc. of the KRS 2006 Autumn Conference, 4(2), Autumn 16-17, 2006, Jeju.

Analysis on US NRC Regulatory Position for Blending Radioactive Waste

Jungjin Kim*, Jeheon Bang, Chan Woo Jeong, and Jinyong Park
Korea Institute of Nuclear Safety, 62, Gwahak-ro, Yuseong-gu, Daejeon, Republic of Korea
*jjkim@kins.re.kr

1. Introduction

South Korea didn't have any regulatory requirements related with permission or prohibition about blending radioactive waste for reducing radioactive waste level. Recently, radioactive waste generators asked regulatory positions about blending. Therefore, this paper discussed and identified the main considerations for making technical guidelines through analyzing the Concentration Averaging and Encapsulation Branch Technical Position of US NRC.

2. US NRC Position for Blending Low-level Radioactive Waste

2.1 Background

The US NRC(United States Nuclear Regulatory Commission) reviewed blending about mixing wastes of different concentrations to create a product with more uniform radionuclide concentrations. The different concentrations wastes mean high concentration LLW(Low Level radioactive Waste) and low concentration LLW. The blending was conducting for several reasons;

1) The integration of radioactive waste which is generated from a variety of sources in a NPP(Nuclear Power Plant) for operational efficiency
2) Reducing radiation exposure dose of radiation workers
3) To make lower waste class by averaging radioactive concentration.

Similarly, the blending in South Korea may be needed because lots of LLW and ILW(Intermediate Level radioactive Waste) were generating from same waste stream.

2.2 Blending policy

SECY-10-0043 report provided a variety options about blending policy. In those options, US NRC selected Risk-informed and Performance-based. In the two options, the regulatory agency position was based on the public health, safety, security and environmental protection. The main performance indicator was safe disposal of blended waste and additional details were considered;

1) Safely managing radioactive waste from human intrusion based on the 10 CFR 61.42
2) In accordance with 10 CFR 61.42, ensuring public protection with site-specific performance analysis
3) Clarifying the regulatory position to all operators including radioactive waste generator

Therefore, regulatory staffs in South Korea need to consider similar principles as above.

3. Technical Basis for Blending Low-level Radioactive Waste of US NRC

The US NRC allowed blending after conducting a review for the mixed waste in 2010. In the CA BTP (Concentration Averaging and Encapsulation Branch Technical Position, Rev1, the technical basis for blending was explained. The NRC staff evaluated results of intrusion into blendable waste using "Exposed Cuttings Scenario". In the exposed cuttings scenario, intrusion occurred at 100, 300 and 500 years after site closure for Class A, B and C, respectively. In addition, a variety detail exposure pathways (direct exposure from cuttings, vegetable/grain/fruit consumption from gardening and etc.) were considered. The most effective radionuclides for Class A and B waste were Cs-137. In case of Class C, the main radionuclides were C-14, Pu-241 and Am-241. Through these results, the revised CA BTP Table 1 values were calculated as below.

Table 1. Thresholds for demonstrating adequate blending [1]

Characteristics of Most Concentrated Influent Waste Stream	Volume of Mixture in m^3 (ft^3)		
	Class A Mixture	Class B Mixture	Class C Mixture
Sum of fractions less than 10	No limit	No limit	No limit
Sum of fractions less than 10 and 20	No limit	No limit	50(1800)
Sum of fractions less than 20 and 30	60(2100)	No limit	20(700)
Sum of fractions less than 30 and 50	20(700)	No limit	6(210)
Sum of fractions less than 50 and 100	6(210)	40(1400)	2(70)

4. Conclusion

Currently, there is no certain regulatory requirements about blending radioactive waste in South Korea. Therefore, blending can only be permitted if pre-disposal management is properly conducted and proved justification of blending. Based on the US NRC's CA BTP, the specific blending technical guidelines of South Korea will be developed.

ACKNOWLEDGEMENT

This work was supported by the Nuclear Safety Research Program through the Korea Foundation of Nuclear Safety(KoFONS), granted financial resource from the Nuclear Safety and Security Commission(NSSC), Republic of Korea (No.1703005). Regulatory points discussed here are the authors' opinion in the process of research.

REFERENCES

[1] US NRC, "Concentration Averaging and Encapsulation Branch Technical Position, Revision 1" (2015).

[2] US NRC, "Blending of Low-Level Radioactive Waste", SECY-10-0043 (2010).

A Study on the Comparison of WTS for Establishment of Radioactive Waste Management

Ki Tae Yang, Sun Il Kim, and Jong Soon Song*

Chosun University, 309, Pilmun-daero, Dong-gu, Gwangju, Republic of Korea

*jssong@chosun.ac.kr

1. Introduction

Domestic radioactive waste is generated by nuclear power plants, the Korea Atomic Energy Research Institute and KEPCO Nuclear Fuel Company. Each organization has different waste classification criteria. There is also no established integrated waste classification standard.

2. Classification of Domestic Agency

2.1 Korea Atomic Energy Research Institute

As for the Korea Atomic Energy Research Institute, the decommissioning waste due to decommissioning of research reactors NO. 1&2, and the low and intermediate-level radioactive waste, generated by the operation of High Flux Advanced Neutron Application Reactor (HANARO), account for the most. Korea Atomic Energy Research Institute Radioactive waste classification standards (Table 1) are classified into combustible, non-combustible, organic waste, and inorganic waste.

Table 1. Korea Atomic Energy Research Institute Radioactive waste classification standards

Large Category	Middle Category	Type
Combustible	Vinyl	Vinyl Sheet, Vinyl Glove, Disposable Gowns
	Cotton	Cotton Gloves, Cotton Mask, Cloth, Bandage,
	Plastic	Acrylic, PVC Cask, PVC Bottle, PE Container
	Timbers	Timbers
	Paper	Paper, Decontamination Paper
Non-Combustible	Concrete	Concrete, Cement
	Glass	Glass Bottle, Glass Vial, Glass Fiber
	Metal	Hoyle, Alloy, Aluminum
	Filter	Charcoal Filter, Air Purification Filter, Liquid Purification Filter
	Sludge	Sludge
Organic Waste	Organic Waste	Alcohol, Acetone
Inorganic Waste	Inorganic Waste	Water in which various salts are dissolved

2.2 KEPCO Nuclear Fuel Company

KEPCO Nuclear Fuel produces the nuclear fuel used in nuclear power plants, and the nuclear production process generates radioactive waste. It is classified into 8 types of waste according to the solid waste management procedure as shown in Table 2.

Table 2. KEPCO Nuclear Fuel Radioactive waste classification standards

Categorize	Type
Dry Active Waste	Glove, Mask, Decontamination Paper
Composite	Plastic, Rubber, cable sheath
Metallic materials	Pipe, Duct, Vessel
Calcific Deposit	Calcific Deposit in the form of sludge during liquid waste

Concrete	Sinter furnace, Concrete waste
Timbers	Wood, Plywood, Equipment packaging
Glass	Reagent bottle , fluorescent lamp, A variety of light bulbs
Sodium fluoride	By-product waste generated after disposal of waste liquid

2.3 Korea Hydro & Nuclear Power Company

The miscellaneous solids, generated in the Hanbit NPP of Korea Hydro & Nuclear Power Co., Ltd., are classified as shown in Table 3 in consideration of the physical properties, density and amount of the waste, and substances subject to restricted disposal.

Table 3. Hanbit Nuclear Power Plant Radioactive waste classification standards

Categorize	Large Category	Type
Combustibility	Cotton	Experiment Gown, Glove, Socks
	Paper	Decontamination Paper, Other Papers
	vinyl	Tape, vinyl
	Plastic	PVC, Bottle
	Timbers	walk plate, paving, Wood
	Other combustibles	Rubber, nylon, other combustibles
Non-combustibility	Iron	Metal plate, Pipe, Grating, Wire, Spray Can, H-beam, S/S
	Aluminum	Aluminum, foil
	Activated carbon	HVAC internals
	HVAC waste filter	HVAC Pre-filter, HEPA-filter
	Other Non-combustibility	sludge, asbestos , plaster, glass

3. Conclusion

This paper investigated the classification standards and treatment methods according to the characteristics of the radioactive substances handled by each agency. These classification and treatment methods can be applied to the database when the radioactive waste tracking system is implemented in the future. It is expected that more efficient and safe WTS can be constructed by integrating the radioactive waste generated by each institution into the integrated WTS database input and field application.

ACKNOWLEDGEMENTS

This work was supported by Korea Institute of Energy Technology Evaluation and Planning (KETEP Project no.20171510300710) and Ministry of Trade, Industry and Energy, Republic of Korea.

REFERENCES

[1] “Establishment Of Database System for the Management of KAERI Wastes”, KAERI.

[2] “Establishment of an Integrated Information Management System for Safe Management of Radioactive Waste”, KINS.

[3] 10CFR61(Waste Classification and Waste Form Requirements).

Development of Pretreatment Technology of Radioactive HVAC Filter Waste

NakJeom Kim*, MinHwan Mo, YongHo Cho, and HeeCheol Yoon
KEPCO KPS, 211, Munhwa-ro, Naju-si, Jeollanam-do, Republic of Korea
*k1n2j3@naver.com

1. Introduction

A large amount of radioactive filter wastes spent in HVAC of commercial nuclear power plants and dismantled nuclear power plants should be separated by materials for disposal according to the regulation of medium and low level radioactive waste disposal.

If this works are done manually, there are problems that a lot of manpower should be input and a large amount of dust is generated during the works. Particularly, it is difficult and time-consuming to remove the adhesive of poly urethane material that sealed with filter media on filter frame because of hardening after use. This paper introduces automatic filter separation system as pretreatment technology of HVAC filter waste for treating filters by materials.

2. Methods and Results

2.1 Development Background

A HEPA filter consists of metal frame, glass fiber media, aluminum separator, poly urethane sealant etc as shown in Fig. 1 and Table 1. Therefore, in order to disposal contaminated filter wastes, the filter wastes should be separated by materials according to regulation on the disposal of low-level radioactive waste.

Fig. 1. HVAC System and Filters in NPP.

Table 1. HEPA Filter Materials

Parts	Material
Frame	Stainless Steel
Media	Glass Fiber
Separator	Aluminum
Sealant	Poly Urethane
Gasket	Neoprene rubber

Fig. 2 shows manual separation process of the spent filter. There are 8 stages for separating the spent filter and manpower for the process requires 0.8MD per a filter by manual. Especially cutting sealant stage which separates the filter media on the frame is most difficult and time consuming work.

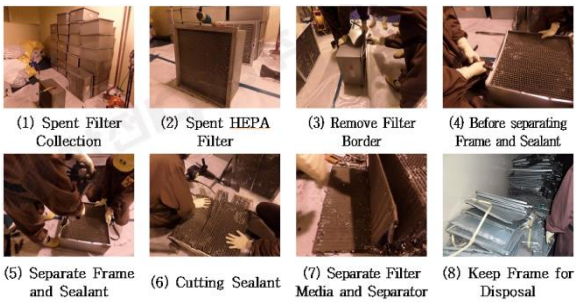

Fig. 2. Manual Waste Filter Separation Process.

So we developed automatic filter separation system that can reduce manpower and exposure time of workers and minimize dust during operation as shown Fig. 3.

Fig. 3. Filter Separation System.

2.2 Principle of Equipment

Automatic filter separation system equipped the sizing mechanism and cutting mechanism to force the filter width to be constant because there is no clear standard about the width and tolerance of the filter frame which makes it difficult to develop standardized equipment.

Fig. 4 shows sizing and cutting device. Sizing device fix left side of the filter frame and press right side of the frame inward for making filter width uniform as shown fig 4. In case of cutting mechanism, the cutter moves up and down in the vertical direction to separate the sealant and filter frame. These devices make inside width of filters which have various size uniform.

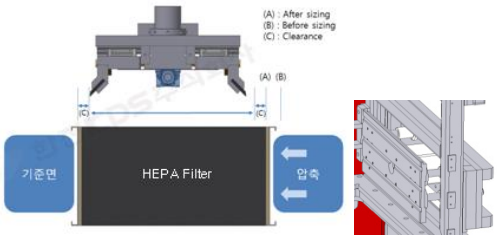

Fig. 4. Flexible Cutting and sizing Device.

2.3 Performance Test

The performance test for the developed system was performed with the filters (HEPA filter 8ea, Medium filter 1ea) which used in the Han-ul #5 and #6. Test results showed good performance of separating sealant on the filter frame as shown Fig. 5. As a result, one worker could separate seven filters using system in a day. That is, it is possible to improve 7 times of working efficiency compared with manual work that one worker could separate two filters in a day.

Table 2. Spent filter Specification and test condition

Test Filter	Size(mm)	Sealant	Load	Cutting speed
HEPA Filter	610×610×292	Urethane	14ton	7mm/s
Medium Filter	610×610×292	Urethane	14ton	7mm/s

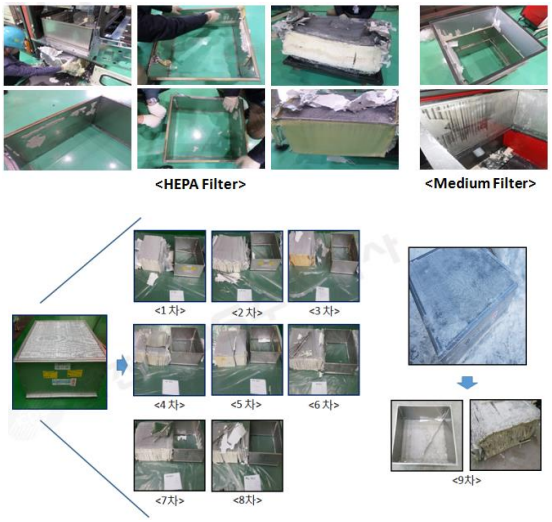

Fig. 5. Performance Test Results using HEPA Filters.

3. Conclusion

We have developed automatic filter separation system for the separation of contaminated HVAC waste filters, which have been separated by manual work. And also on-site performance tests of the system have been performed. Developed systems are expected to be widely used as pretreatment technology for radioactive filter wastes generated from operating NPP and dismantled NPP in the future.

Review on the Potential Measure for Inadvertent Human Intrusion into LILW Disposal Facility

Sangho Lee*, Hayan Lim, Yohan Kim, and Jinyong Park
Korea Institute of Nuclear Safety, 62, Gwahak-ro, Yuseong-gu, Daejeon, Republic of Korea
*sh.lee@kins.re.kr

1. Introduction

The risk prevention criteria for inadvertent intruders at the disposal facility are specified in NSSC Notice No.2017-62 (Prevention Criteria) [1]. But domestic regulations are not classified considering the type of disposal facility (near surface, geological). This paper reviews the internationally agreed potential measure through the analysis of the status of international joint research projects, and discusses possible intruder protection measures applicable to domestic disposal facilities.

2. Assessment for Human Intrusion into LILW Disposal Facility

2.1 HIDRA Project

In order to assess the safety of disposal facility, international organizations have consistently conducted research. The Human Intrusion in the context of Disposal of Radioactive Waste (HIDRA) Project addressed Inadvertent Human Intrusion (IHI) involving a disruption of the disposal facility, occurring after closure and following the loss of institutional control for a properly closed facility [2].

2.2 Key Factors for Human Intrusion

The HIDRA has considered several factors for developing a safety case related to human intrusion. Fig. 1 shows the human intrusion in the components of the safety case. It also covered social factors. It distinguishes inadvertent from deliberate intrusions, and discusses how to set the period of knowledge preservation.

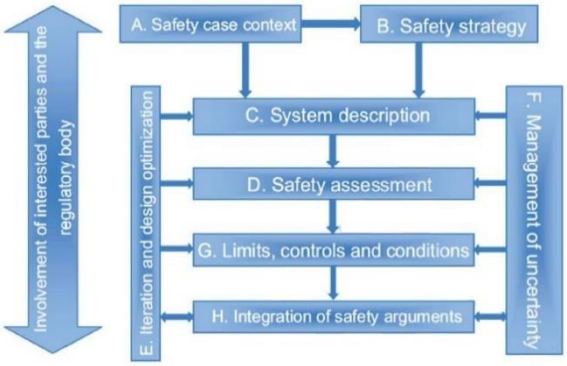

Fig. 1. Safety Case Components.

Because it is impossible to predict specific human action in the future, HIDRA considers potential scenarios that could affect the disposal facility. Drilling, excavation (residential) and excavation (road) scenario for near-surface disposal, and drilling, subsurface mining, solution mining scenario for geological disposal scenarios are considered.

3. Potential Measures

3.1 Definition of Potential Measures

There are various approaches to reduce the

likelihood of IHI, and this approach is called Potential Measure in the HIDRA Project.

The potential measures approach of HIDRA consists of four steps. First step is defining the framework. This step identifies potential actions and then derivation protective actions in the context of optimizing the disposal facility. Step 2 is compilation of general measures. This step studies database development and existing literature and projects about IHI. Step 3 is defining the identification of potential inherent measures. Potential actions, those measures identified as relevant to a specific disposal system are analyzed. The last step is the derivation of protective measures. The potential measures identified in previous step are analyzed using qualitative and, if possible, appropriate and quantitative assessments. The main purpose of the analysis is to assess whether potential measures conflict with key safety objectives.

3.2 Potential Measures by Disposal Type

In HIDRA Project, potential measures are considered differently depending on the disposal type. The period of institutional control differs according to the policy of each country, and it is usually several hundred years. With respect to timescales and the safety case, the main issues of concern are: a) How long should institutional controls be maintained including monitoring?

And it also considers about the design of disposal facilities and engineering barriers, knowledge management, siting, waste types and characteristics.

4. Conclusion

This paper reviewed research on the potential measures for radioactive waste disposal types performed in international studies. The International recommendation manages type of the disposal facilities by near-surface and geological. In the near future, we need to review the necessity of incorporating it into the domestic regulation standards by referring to the human intrusion safety case.

ACKNOWLEDGEMENT

This work was supported by the Nuclear Safety Research Program through the Korea Foundation of Nuclear Safety (KoFONS), granted financial resource from the Nuclear Safety and Security Commission (NSSC), Republic of Korea (No.1703005). Regulatory points discussed here are the authors' opinion in the process of study.

REFERENCES

[1] Nuclear Safety and Security Commission, "Radiological Protection Criteria for Long term Safety on Low and Intermediate Level Radioactive Waste Disposal", Notice No.2017-62 (2017).

[2] International Atomic Energy Agency, The International Project on Inadvertent Human Intrusion in the context of Disposal of Radioactive Waste (2017).

Evaluation of Shielding Performance Effect of Liner Attenuation Coefficient During Radiation Shielding

Jin Koh* and Eun-duk Han
Korea Radioactive Waste Agency, 111, Daedeok-daero 989beon-gil, Yuseong-gu, Daejeon, Republic of Korea
*Kj1496@korad.or.kr

1. Introduction

Korea Radioactive Waste Agency radioisotope Waste Management Facility is a facility licensed under Article 63 of the Nuclear Safety Law (construction and operation permit for radioactive waste management facilities, etc.) [1]. It storages and management unsealed and sealed source wastes generated after use by domestic radioisotope use organizations, and about 60 nuclides, including ^{3}H and ^{14}C, have been acquired.

The radioisotope wastes was acquired by the radioisotope management facility in Daejeon before July 2015, but it is now acquired at the Gyeongju disposal facility. The wastes stored in Daejeon radioisotope management facility are processed and transported sequentially to the Gyeongju disposal facility.

2. Influence of Spplication of HVL and TVL in Evaluating Shielding Performance

2.1 Shielding Status of Waste Sealed Source

When disposing of sealed source The package surface radiation dose rate should be less than 0.5 mSv per hour in accordance with paragraph 1 (5) of the Guidance on the Acquisition of Radioisotope Waste 3.1 (Sealed source Classification and Packaging). If the weight increases due to unnecessary shielding, the burden of the management cost may increase, and handling and transportation may be difficult. Also, in the case of incorrect shield assessment, there may be an increase in radiation exposure and costs associated with additional fabrication. In this paper, we investigated the influence of the HVL and TVL additive in evaluating the shielding performance.

2.2 Basic Information of Shielding Performance Evaluation

The basic information for the evaluation of the shielding performance of the disused source is as follows.

- Nuclide : Cobalt–58
- Half-life : 70.8 days
- Emission energy : 511 keV (30%), 811 keV (99%), 1675 keV (<1%)
- Source form : Point source
- External Exposure (mSv/h) for an activity of 1MBq, Point source (30 cm) : Gammas, X rays 1.7 E-0.3 mSv/h
- HVL : Lead 10 mm, Steel 31 mm
- TVL : Lead 31 mm, Steel 76 mm

$$I = I_0 e^{-\mu t} \quad (1)$$

- I : Radiation dose rate after shielding
- I_0 : Radiation dose rate before shielding
- t : Shield thickness
- μ : Linear attenuation coefficient
  (mass attenuation coefficient * density)

In this paper, the linear attenuation coefficients for the HVL and TVL are used to investigate the effect of the linear attenuation coefficients on the radiation shielding performance [2], [3].

2.3 Variation of Linear Attenuation Coefficient Between HVL and TVL

In order to obtain the linear attenuation coefficient in equation (1), equation (2) is derived, I = 1 mSv/h and I_0 = 2 mSv/h were applied for HVL of ^{58}Co lead, and I = 1 mSv/h and I_0 = 10 mSv/h were applied for the lead TVL for ^{58}Co application.

$$\mu = \frac{[\ln\frac{I_0}{I}]}{t} \quad (2)$$

The linear attenuation coefficient (1/2) obtained by the HVL is 0.069 mm^{-1}, The linear attenuation coefficient (1/10) obtained by the TVL is 0.074 mm^{-1}, which is different from each other, This is an issue that needs to be taken into account when assessing radiation shielding performance.

2.4 Evaluation of Shielding Performance by Applying Linear Attenuation Coefficient

10 msv/h based on radiation dose rate value corresponding to the linear attenuation coefficient (1/2) 0.069 mm^{-1} for the dose applied to the shield thickness change and the linear attenuation coefficient(1/10) 0.074 mm^{-1} was applied for the reference dose of 10 msv/h Table 1 shows the radiation dose rate value according to the thickness change of the shield.

Table 1. μ Change in dose rate value for linear attenuation coefficient (1/2) and linear attenuation coefficient (1/10)

Shield thickness	HVL μ	TVL μ
	Dose rate	Dose rate
5 mm	**7.082 mSv/h**	6.907 mSv/h
10 mm	**5.016 mSv/h**	4.771 mSv/h
15mm	3.552 mSv/h	**3.296 mSv/h**
20 mm	2.516 mSv/h	**2.276 mSv/h**
25 mm	1.782 mSv/h	**1.572 mSv/h**
30 mm	1.262 mSv/h	**1.086 mSv/h**
35 mm	0.894 mSv/h	**0.750 mSv/h**

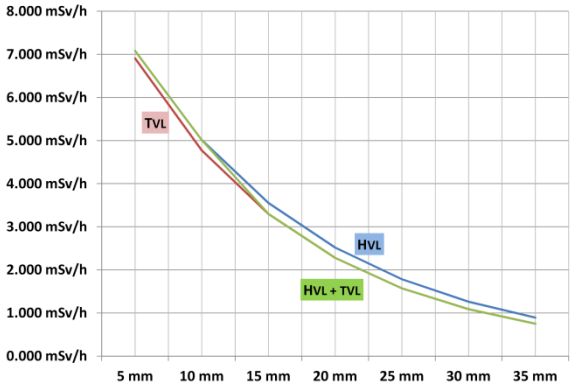

Fig. 1. Changes in dose rate according to the application of HVL and TVL.

3. Application of Linear Attenuation Coefficient

The thickness of the shielding box is determined according to the shielding performance evaluation during radiation shielding. If the shielding performance is overestimated, it increases the thickness of the shielding box, which affects the economical efficiency. On the other hand, underestimation of the shielding performance will increase the radiation exposure and affect safety.

Therefore, the evaluation of the shielding performance should be accurately performed. In the case of using a shielding material having a half value or less in which the linear attenuation coefficient (μ) value derived from the semi-active layer and the innermost layer is different, the linear attenuation coefficient (μ) value derived from the semi-active layer is used. Apply linear attenuation coefficient (μ) value derived from the ten-layer and half-price layer to ensure both economic and safety.

REFERENCES

[1] Nuclear Safety Law (2019.02.15)
[2] KINS, Cyber Radiation Safety Information Center (https://rasis.kins.re.kr).
[3] JOHN R. LAMARSHA. “INTRODUCTION TO NUCLEAR ENGINEERING, 1982.

Adsorption of Krypton on Porous Carbon at Low Temperature

Ju Ho Lee*, Seok-Min Hong, Jae-Won Lee, and Yung-Zun Cho
Korea Atomic Energy Research Institute, 111, Daedeok-daero 989beon-gil, Yuseong-gu, Daejeon, Republic of Korea
*jhlee835@kaeri.re.kr

1. Introduction

In pyro-processing of spent-fuel, volatile fission products such as Krypton-85 and Xenon are released during high-temperature treatment in head-end processes. As Krypton-85 exhibits a half-life of 11 years, it should be trapped and stored until it reduces to non-radioactive species. Several trapping strategies [1] were developed and in KAERI, the process based on solid adsorption has been considered and tested [2]. In this study, the adsorbent based on porous carbon developed for CO_2 adsorption are tested for low-temperature Krypton trapping.

2. Experimental Procedure

Porous carbon were prepared by carbonizing poly (vinylidene fluoride) powders. The powers of 13 to 15 g were contained in crucible and heated to 1000^{o}C in argon environment at heating rate of 5^{o}C/min and maintained during 1 hr. As demonstrated in Fig 1, the prepared porous carbon were found to shrink due to the release of hydrogen and polymer attached to polymer backbone during heat treatment and its final weight were found to be approximately 34% of original powder weight implying complete carbonization, less than the yield of theoretically complete carbonization of 37.5%.

Fig. 1. Prepared porous carbon.

The prepared porous carbons were fragmented to the particles of 1 – 3.35 mm through sieving for increasing packing fraction in adsorbent container and the employed mass was 17.7 g. The packing density for the fragmented porous carbon was found to 0.2 g/ml

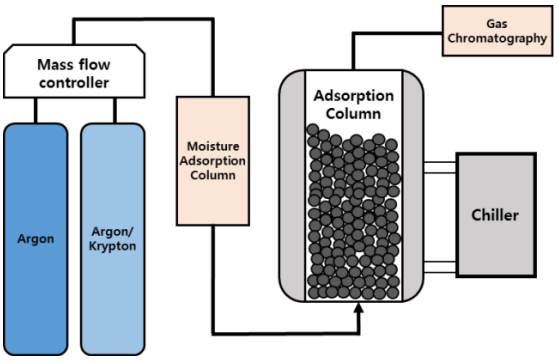

Fig. 2. Schematic Diagram of Kr adsorption process.

3. Results

As shown in Fig. 2, Kr adsorption process is composed of gas supplying unit, adsorption column and concentration analyzer. By adjusting flow rates of gases and mixing, the gas of the desired concentration are fed to adsorption column filled by porous carbon and its breakthrough curve are measured by gas chromatography. The adsorption test was carried at -74^{o}C and 500 ppm Kr/Ar for 17.8 g porous carbon. The breakthrough adsorption time is considered at the condition that the concentration of Krypton in effluent corresponds to 5% of inlet concentration. Fig. 3 shows that the breakthrough of Krypton begins at 165 min.

4. Conclusion

In this study, we prepared porous carbon for

Krypton adsorption by carbonizing poly(vinylidene fluoride) and implemented the adsorption test at -74°C. Further study is in progress for the evaluation of the adsorption capacity for porous carbon at different condition and the derived data is expected to design Krypton adsorption process for pyro-processing.

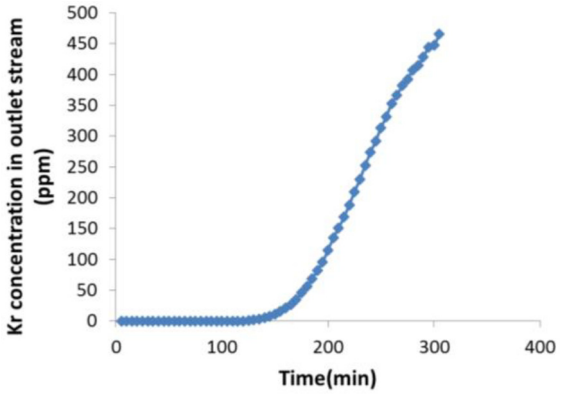

Fig. 3. Breakthrough curve for porous carbon (-74°C, 126 ml/min, Kr 500 ppm).

REFERENCES

[1] W.R. A. Goossens, G.G. Eichholz and D.W. Tedder, “Treatment of Gaseous Effluents at Nuclear Facilities”, Harwood academic publishers (1991).

[2] S.M.Hong, G.Lim, S.H.Kim, J.H.Kim, K.B.Lee, and H.C.Ham “Preparation of porous carbons based on polyvinylidene fluoride for CO_2 adsorption: A combined experimental and computational study”, Micropor. Mesopor. Mat, 15, 59-65 (2016).

A Study on the Applicability of Foreign Test Requirements for Type IP-2 Soft Bag Container

Hyosub Kim [1,*], Moonoh Kim [1], Jaewoo Park [1], Jihoon Lee [2], Dong-gyu Lee [1], and Nakhoon Sung [1]
[1] Korea Nuclear Engineering & Service, 65, Myeongdal-ro, Seocho-gu, Seoul, Republic of Korea
[2] KHNP Central Research Institute, 70, Yuseong-daero 1312beon-gil, Yuseong-gu, Daejeon, Republic of Korea
[*]hyosubk@kones21.com

1. Introduction

Recently, decommissioning of nuclear power plants is being emerged as a main issue since Kori unit 1 was shut down on June 18, 2017. In the process of dismantlement of nuclear facilities, huge amounts of radioactive wastes will be produced over a short period of time. Since VLLW are expected to be generated in the largest volumes during decommissioning, the management of VLLW should be given as one of the top priority.

In this paper, the soft bag container as Type IP-2 package is mainly considered. The soft bag is now widely utilized in many countries [1] because this container is regarded as one of the most economical way to deal with VLLW. However, unfortunately, there are no regulatory requirements for the soft-sided bag in Korea yet.

Hence, the principal foreign test requirements [2][3][4] of the soft bag container in comparison with those of NSSC notice No. 2017-56 [5] are reviewed for an applicability of the international regulatory standards.

2. Review of Foreign Test Requirements

The soft bag container has become popular in recent years. Globally, several countries such as US and UK have already lots of experience in utilizing the soft-sided bag for the management of decommissioning waste [1]. In Korea, KONES corp. designed various radioactive waste packagings including an IP-2 soft bag container in 2016 [6].

The key advantages of this soft bag are two things: 1) applicability for a variety of waste form; 2) utilization for both transportation and disposal [7]. For instance, the soft-sided package is possible for storing, transporting and disposing of D&D wastes (e.g. concrete rubble, contaminated soils and construction debris, etc.). Therefore, these efficiencies facilitates for the immediate and safe decommissioning work.

2.1 Comparison of Test Requirements

In general, the soft bag container is intended for the packaging and transportation of VLLW. Thus, if the soft bag meets the requirements of Type IP-2 container, then it is considered to be sufficient to achieve this objective. In this study, we mainly compare the test requirements in association with IP-2 standards of the several domestic and foreign popular specifications: 1) NSSC notice No. 2017-56 [5]; 2) IAEA SSR-6 [2]; 3) US DOT 49 CFR Part 173 [3]; 4) US DOT 49 CFR Part 178 [4].

As for NSSC notice No. 2017-56, IAEA SSR-6 and US DOT 49 CFR 173, they provide the regulations for the transport of radioactive materials. On the other hand, US DOT 49 CFR 178 contains the requirements of FIBC (Flexible Intermediate Bulk Container) since this code literally provides the specific requirements of the packaging in the form of the soft bag, which is the primary research subject of this paper.

Table 1 below shows the comparison of the test requirements for the soft bag container regarding the domestic and foreign various codes.

Table 1. Comparison of Test Requirements for Soft Bag

Test Type	NSSC 2017-56 (IP-2)	IAEA SSR-6 (IP-2)	US DOT 49CFR173 (IP-2)	US DOT 49CFR178 (FIBC)
Drop Test	O	O	O	O
Top Lift Test	–	–	–	O
Stacking Test	O	O	O	O
Topple Test	-	-	-	O
Righting Test	-	-	-	O
Tear Test	-	-	-	O

(Type IP-2 is applied except for 49 CFR 178)

As shown in Table 1, NSSC notice No. 2017-56, IAEA SSR-6 and 49 CFR 173 are identical for Type IP-2 packaging: drop test, stacking test, whereas four more additional tests (top lift test, topple test, righting test, tear test) for FIBC are required under 49 CFR 178 standard. Actually the reason for this difference is that according to US code, the flexible packaging for hazardous waste needs to be tested and certified to the FIBC standards of 49 CFR 178, as a UN rated package [8]. That is why they have different requirements based on what kind of waste they are designed to contain.

2.2 Applicability Case Study: PacTec Inc.

PacTec Inc. is famous for designing and manufacturing the radioactive waste packaging such as LiftPac and MacroBag. As for LiftPac, this container is a DOT-certified flexible packaging and there are two different types of LiftPac [7]. The characteristics of them are as follows: 1) Type IP-1/2 LiftPac for radioactive waste per 49 CFR 173; 2) UN rated LiftPac for hazardous waste per 49 CFR 178.

However, in some cases, this DOT-certified soft bag per 49 CFR 178 could be also Type IP-2 if it is tested and certified to UN and ADR standards [7].

3. Conclusion

The several foreign test requirements for the flexible Type IP-2 soft bag compared to domestic NSSC standard are reviewed for the future applicability of extra tests on current requirement.

As it turns out, domestic test requirements for the radioactive material is equal to IAEA SSR-6, which is also exactly same as 49 CFR 173. On the other hand, 49 CFR 178 is different since it mainly aims for the hazardous waste. However, this flexible bag per 49 CFR 178 could be also Type IP-2 packaging under UN and ADR standards for other hazardous waste such as asbestos [7].

Hence it is worth considering the test requirements of 49 CFR 178 for Type IP-2 soft bag to secure more safety as a purpose of contingency plan in the future.

ACKNOWLEDGEMENT

This work was supported by the Korea Institute of Energy Technology Evaluation and Planning (KETEP) granted fund by MOTIE, Republic of Korea (No. 20181510300870).

REFERENCES

[1] Jaesol Lee et al., “Development of Multi-Purpose Containers for Managing LLW/VLLW from D&D”, JNFCWT, Vol.14, pp.157-168 (2016).
[2] IAEA, “Regulations for the Safe Transportation Materials, IAEA SSR-6, Rev. 1 (2018).
[3] US DOT, “Shippers-General Requirements for Shipments and Packagings”, 49 CFR Part 173 (2011).
[4] US DOT, “Specifications for Packagings”, 49 CFR Part 178 (2011).
[5] NSSC, “Packaging and Transportation of Radioactive Material”, No. 2017-56 (2017).
[6] KONES Corp., “Development of Standard Packages for Concrete and Steel Waste from NPPs”, KETEP (2016).
[7] PacTec Inc., internet: www.pactecinc.com (2019).
[8] UN, “Recommendations on the Transport of Dangerous Goods”, Orange Book, Vol. II (2019).

Development of the Practical Technology for Thermal-Chemical Treatment of Low-Level Spent Resin

Hyeon-Oh Park[a,*], Kyu-Tae Park[a], Young-Ku Choi[a], and Hee-chul Yang[b]
[a] Sunkwang T&S Co., Ltd, 3, Gongwon-ro, Guro-gu, Seoul, Republic of Korea
[b] Korea Atomic Energy Research Institute, 111, Daedeok-daero 989beon-gil, Yuseong-gu, Daejeon, Republic of Korea
[*]pho1428@daum.net

1. Introduction

About 620,000L of low-level spent resin was generated during NPP operations in 2018, and it is now temporarily stored in 200 L drums. The incineration or vitrification treatment technology may be considered for treatment of this large quantity of low-level spent resin, but they have problems, i.e. generation of large amounts of harmful gases and discharge of radioactive nuclides. Also, as the cement and polymer solidification technology has a low volume reduction effect, it is regarded as inappropriate for treatment of large quantities of spent resin generated by a secondary system.

Meanwhile, among the technologies that can be used for treatment of low-level spent resin of NPPs, the technology for thermo-chemical treatment of spent resin, developed by the Korea Atomic Energy Research Institute, is a technology for coalification of spent resin whose main component is carbon. It is an outstanding volume-reducing technology that evaporates the radioactive nuclides in the spent resin at a high temperature and removes them. It is a practical technology that can be used in domestic NPPs.

2. Process Description

In this study, the authors will try to use the original technology, developed by the Korea Atomic Energy Research Institute, to make a pilot device for thermo-chemical treatment of low-level spent resin generated in NPPs and use mock spent resin to derive practical applicability and a treatment technology.

2.1 Spent Resin Thermo-Chemical Treatment Process

The technology for thermo-chemical treatment of spent resin gasifies only the hydrogen (H), oxygen (O), nitrogen (N) and sulfur (S) component among the organic components (C-H-O-N-S) in the spent resin, and coalifies the carbon (C) component. This technology halogenates, evaporates and separates a very small amount of inorganic matters, including the radioactive nuclides remaining in carbide, at a high temperature. The principles of the spent resin thermo-chemical treatment process are as follows:

1) Removing and recovering the moisture containing tritium (H-3) included in the spent resin
2) Analyzing the functional group by means of pyrolysis
3) Coalification of spent resin containing inorganic nuclides whose functional group is removed
4) Chlorination of nuclides in spent resin carbide, such as Cs and Co, and other inorganic components at a high temperature
5) High-temperature evaporation, separation, and condensation recovery of chlorinated metal nuclides and inorganic matters

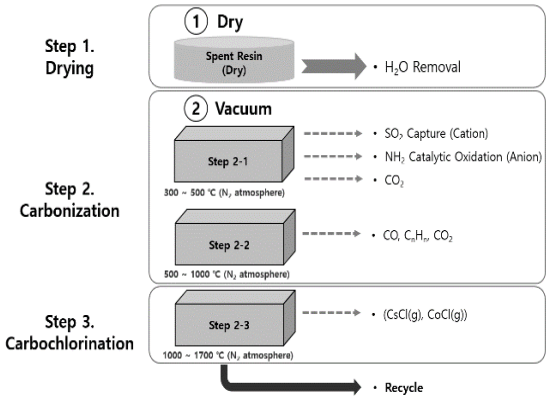

Fig. 1. Thermo-chemical treatment process of spent resin.

[Step 1] is the process of recovering and treating the tritium (H-3) in the spent resin by drying the spent resin at a temperature ranging between 100℃ and 120℃. [Step 2-1] causes the pyrolysis reaction by maintaining the temperature between 150℃ and 500℃. In this pyrolysis reaction temperature range, as styrene divinyl benzene copolymer and the

functional group are separated, SO_2 and NH_2 gas are generated in the spent resin. [Step 2-2 / 2-3] analyzes the styrene divinyl benzene copolymer and coalifies it. To separate the inorganic nuclides in the coalified spent resin, it reacts with Cl_2 of a certain concentration, and evaporated into such chlorides as CsCl(g) and $CoCl_2$(g) at a temperature exceeding 1,000℃.

2.2 Making a Device for Thermo-Chemical Treatment of Spent Resin

Based on the spent resin thermo-chemical treatment process, the authors made a pilot device for batch-type thermo-chemical treatment of spent resin with a capacity of 20 kg that can treat spent resin once. The device is comprised of the high-vacuum thermo-chemical treatment reactor for treating the radioactive nuclides, contained in spent resin, at a high temperature, and the plasma incinerator and wet scrubber for treating the harmful gases and volatile radioactive nuclides, generated in the high-vacuum thermo-chemical treatment device.

Fig. 2. Device for thermo-chemical treatment of spent resin.

2.3 Mock Spent Resin Thermo-Chemical Treatment Experiment

The same numbers as used in NPPs were used to conduct the mock thermo-chemical treatment experiment. To treat mock spent resin thermo-chemically, the holding time for the optimal temperature range of each stage, i.e. intermediate temperature, high temperature and ultra-high temperature, must be derived. In the mock spent resin in the intermediate temperature range, styrene divinyl benzene copolymer and the functional group are separated, and in the high temperature and ultra-high temperature range, it reacts with Cl_2 of a certain concentration, and the mock radioactive nuclides, contained in the mock spent resin, are evaporated. The plasma incineration used to remove the harmful gases and volatile radioactive nuclides generated in the spent resin thermo-chemical treatment reactor essentially generates NOx. As for the N_2 and O_2 doses to minimize NOx generation, optimal conditions must be derived in consideration of the sample dose.

3. Experimental & Result

In this study, the authors used the technology for thermo-chemical treatment of spent resin, developed by the Korea Atomic Energy Research Institute, to make the pilot device for thermo-chemical treatment of spent resin. The mock spent resin was used to conduct the device performance verification experiment for deriving the nuclides separation and recovery process. To treat the mock spent resin thermo-chemically, the temperature ranges were set up, i.e. the intermediate temperature (300 ~ 350℃), high temperature (500 ~ 1,000℃) and ultra-high temperature (1,000℃ or higher), and the pyrolysis reaction in each temperature range was verified. Also, to minimize NOx generated essentially in the plasma incineration method, the optimal N_2 and O_2 doses were derived in consideration of the sample dose.

4. Conclusion

The technology for thermo-chemical treatment of spent resin can address the problems of the existing incineration or vitrification technology, i.e. discharge of harmful gases and low volume reduction. Also, coalified spent resin can be recycled industrially, or self-disposed. Accordingly, based on the result of the experiment using mock spent resin, the authors will verify the practical use of the technology by demonstrating treatment of the spent resin of NPP sites and secure the spent resin treatment technology.

REFERENCES

[1] KAERI/RR-4249, “Study on mineralization of radioactive waste”, 2016.

[2] Hee-Chul Yang, “Thermokinetic analysis of spent ion-exchange resins for optimization of carbonization reactor condition”, Journal of Thermal Analysis and Calorimetry, 2016.

Fabrication and Characterization of New Glass Wasteforms for Radioactive Iodine Immobilization

Min-Ji Kang[1,*], Miae Kim[2], and Kyong-Soo Hong[2]

[1] Western Seoul Center, Korea Basic Science Institute, 150, Bugahyeon-ro, Seodaemun-gu, Seoul, Republic of Korea

[2] Busan Center, Korea Basic Science Institute, 30, Gwahaksandan 1-ro 60beon-gil, Gangseo-gu, Busan, Republic of Korea

[*]mjkang@kbsi.re.kr

1. Introduction

The management and disposal of radioactive waste are important issues that we have to solve, because the nuclear fuel we use contains not only a high levels of radiation but also has a half-life of tens of thousands of years [1]. In particular, ^{129}I is known to be harmful to human body as well as to have a considerably long half-life of 1.57 x 10^7 y [1-2]. The purpose of this study is to fabricate AgI-Ag_2O-B_2O_3 glass to immobilize ^{129}I and characterize the various properties of the glasses.

2. Experiments

Three specimens having different composi-tions were prepared as shown in Table 1.

Table 1. Compositions (mol%) of the specimens

Specimen	AgI	Ag_2O	B_2O_3
30AgI-35Ag_2O-35B_2O_3	30	35	35
40AgI-30Ag_2O-30B_2O_3	40	30	30
50AgI-25Ag_2O-25B_2O_3	50	25	25

The glasses were prepared by using the conventional melt-quenching method [2]. The weighed starting materials were mixed homogeneously by using an agate mortar and a pestle, the mixture were put into alumina crucibles, and then melted at 600^{o}C for 15 min. The melt is poured onto an iron plate for quenching. The prepared glassy pieces were ground into fine powders, and then collected by sieving to 75 ~ 150 μm particles. These powders were analyzed for the surface morphology, the structural analysis, and retention confirmation by using an SEM, XRD, and ICP-OES, respectively.

3. Results

Fig. 1 shows images of the surface after quenching. All three were opaque and brown in color.

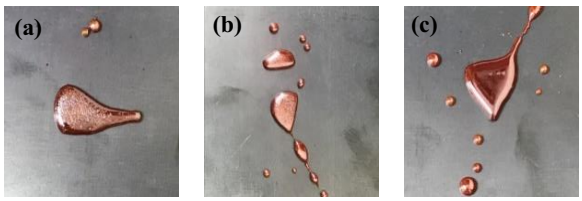

Fig. 1. Images of the AgI-Ag_2O-B_2O_3 specimens after quenching. (a) 30AgI-35Ag_2O-35B_2O_3, (b) 40AgI-30Ag_2O-30B_2O_3, and (c) 50AgI-25Ag_2O-25B_2O_3.

The retention value means the amount of iodine remained in the wasteform and can be confirmed by using an ICP-OES measurement. The obtained retention values in table 2 are 1.5364, 1.9539, and 2.2626 for 30AgI-35Ag_2O-35B_2O_3, 40AgI-30Ag_2O-30B_2O_3, and 50AgI-25Ag_2O-25B_2O_3, respectively.

Table 2. Iodine retention (unit: mg/kg)

Specimen	Retention
30AgI-35Ag_2O-35B_2O_3	1.5364
40AgI-30Ag_2O-30B_2O_3	1.9539
50AgI-25Ag_2O-25B_2O_3	2.2626

Surface morphology of each sample was observed by SEM. Figs. 2(b) and 2(c) are found to be homogeneous while Fig. 2(a) shows white spots.

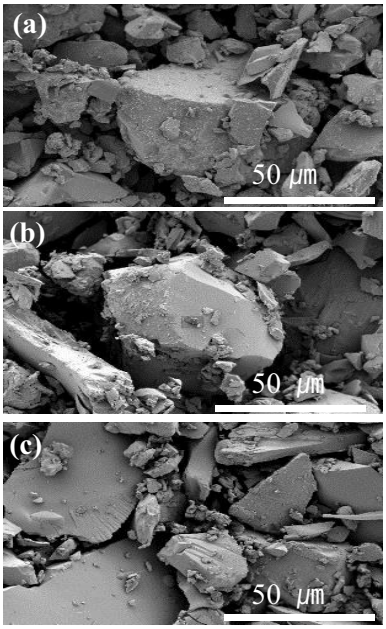

Fig. 2. SEM images of the AgI-Ag_2O-B_2O_3 specimens (a) 30AgI-35Ag_2O-35B_2O_3, (b) 40AgI-30Ag_2O-30B_2O_3, (C) 50AgI-25Ag_2O-25B_2O_3.

XRD patterns were measured to investigate the crystallinities of the specimens. Fig. 3 shows the XRD patterns of the specimens (a) 30AgI-35Ag_2O-35B_2O_3, (b) 40AgI-30Ag_2O-30B_2O_3, and (c) 50AgI-25Ag_2O-25B_2O_3. Specimens (b) and (c) are amorphous but specimen (a) has crystalline phases. Formed crystalline phase (represented by dark green circles) is determined to be $Ag_5B_4IO_8$ (crystal system unknown, JCPDS code 00-036-0761).

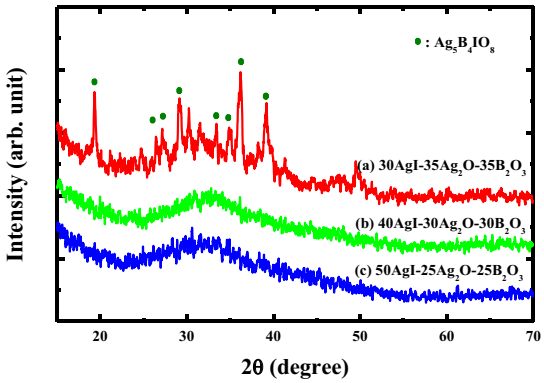

Fig. 3. XRD patterns of the AgI-Ag_2O-B_2O_3 specimens.

4. Summary

We fabricated three AgI-Ag_2O-B_2O_3 glasses with different compositions. As a result, two specimens appeared in amorphous phases and one in a crystalline phase. The prepared glasses in this study are considered as one candidate of immobilizing matrices for ^{129}I.

REFERENCES

[1] J. H. Yang, H. S. Park, and Y. Z. Cho, “Silver phosphate glasses for immobilization of radioactive iodine”, Ann. Nucl. Energy, 110 (2017) 208–214.

[2] A. K. Varshneya, “Fundamentals of Inorganic Glasses”, 2nd Edition, Society of Glass Technology (2014).

Experimental Study of the Analysis Method for Paste Content in the Waste Concrete

Donghee An*, Hyunkook Choi, and Jaeyoung Kim

SungShin Cement Research and Development, 48-37, Bugangoecheon-ro, Bugang-myeon, Sejong-si, Republic of Korea

*anzilda@sscem.com

1. Introduction

The greatest amount of waste that occurs during the dissolution of nuclear power plants is concrete. In the concrete of the radioactive elements of the cement paste is present in most cases, separating the parts of the aggregate, a radioactive concrete waste volume can be greatly reduced.

The purpose of this study is to obtain the basic data necessary for developing a method of effectively Solidifying cement paste separating the aggregate from the waste concrete and finding a method for inferring the paste content of the waste concrete.

2. Experiments

2.1 Materials

The cement paste was made W/C = 0.40 and cured for 3 months in room temperature. After cured, the paste was crushed to several millimeters using jaw-crusher. And they were dried at 100℃ to remove moistures. Dried powers were mixed with three types of sand up to 100wt.% each 20% at a constant ratio(ISO standard sand, Crushed sand, Sea sand).

2.2 Experiment Methods and Items

In order to get the reference guide for a portion of cement paste in a mortar, we use X-ray fluorescence analysis method (XRF, Rigaku, Japan, ZSX Primus II) and measurements of loss on ignition at 600℃ for 90 min. using the electric furnace.

To estimate cement pastes contents in the mortar, we used CaO content which get from XRF analysis results and weight loss of mixtures.

2.3 Result of Paste Content calculation

The results of the XRF analysis for the sand and mixtures are shown in table 1~2. XRF analysis results showed that there is a good relationship between the measure values of CaO with cement pastes contents in mortars (Fig.1).

For three type of sand, ignition loss of mortar at 600℃ showed few differences but the good relationship for cement paste content (Fig.2).

Table 1. XRF analysis of Sand

No	Sand Type	Chemical Composition(%)		
		CaO	SiO_2	Al_2O_3
1	ISO	0.1	97.7	0.6
2	Crushed	0.9	80.5	7.6
3	Sea	2.9	70.4	12.1

Table 2. Test results for mixtures (paste, sand)

No	Type	Mixture ratio(%)		Results(wt.%)	
		Paste	Sand	CaO	Ignition Loss
1	ISO Standard Sand	-	100	0.1	0.1
2		20	80	9.6	2.5
3		40	60	21.7	5.1
4		60	40	36.1	7.7
5		80	20	49.5	10.5
6		100	-	70.8	13.0
7	Crushed Sand	-	100	0.9	0.4
8		20	80	10.8	2.8
9		40	60	23.7	5.4
10		60	40	34.5	7.9
11		80	20	51.0	10.5
12		100	-	70.8	13.2
13	Sea Sand	-	100	2.9	0.6
14		20	80	14.4	3.0
15		40	60	24.1	5.5
16		60	40	39.5	8.0
17		80	20	55.5	10.5
18		100	-	70.8	13.2

The result according to CaO contents of XRF analysis or weight loss of mixtures at 600℃, we found to predict approximate contents of cement paste in the recycled concrete is possible. And this method will be useful to solidifying process concrete

waste from decommissioning a nuclear plant. If we know cement paste contents in concrete waste, solidified concrete waste would be made more safe and durable by control portions of mixtures(waste, solidifying agent and water etc.)

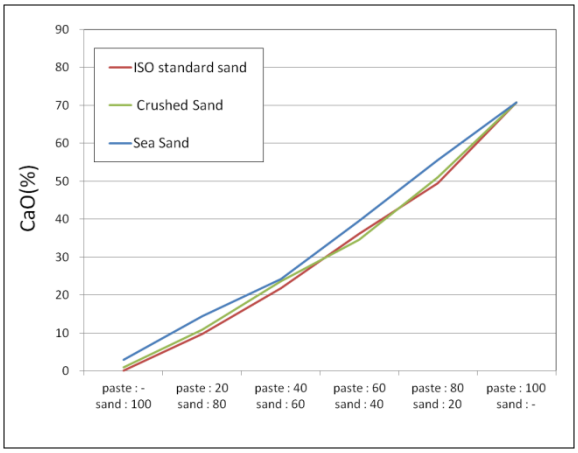

Fig. 1. Analysis of CaO contents of mixtures.

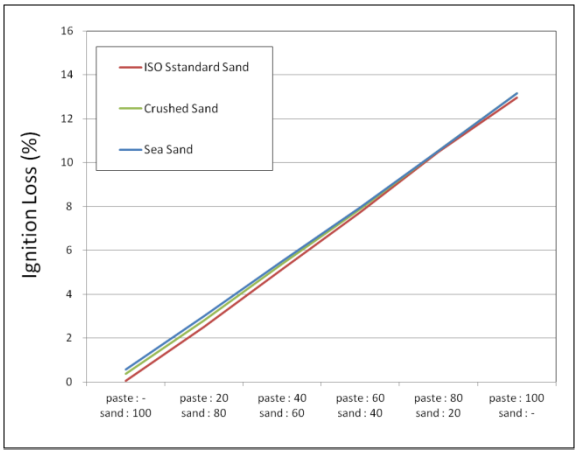

Fig. 2. Analysis of Ignition Loss of mixtures.

3. Discussion and Conclusion

In this study, we used cement paste cured for 3 months and maybe there are some differences in periods of curing time for cement pastes. Therefore it should be considered that periods of curing time could effect on the results of analysis. To make sure this, we prepared specimens cured for 12 months or more, and we will carry same research to get more data.

Fig. 1 and Fig. 2 show there are good relationship CaO contents get from XRF analysis data or weight loss of mortar at 600℃ with cement paste content in the mixtures. Therefore, if we use these analysis methods to estimate approximate cement paste contents in a mortar and apply obtained data in the solidification process for concrete waste that occurs during the dissolution of nuclear power plants, solidifications would be more safe and durable.

ACKNOWLEDGEMENT

This work was supported by the Energy Technology Program of the Korea Institute of Energy Technology Evaluation and Planning(KETEP) granted financial resource from the Ministry of Trade, Industry & Energy, Republic of Korea (No. 20161510300420)

REFERENCES

[1] Jang Jong-Ho, “A Study on the Fundamental Properties and Application as Cementious Admixture by heating Temperature of Recycled Powder”, Proceeding of Korea Concrete Institute, May 12, 635-40 (2001).

[2] Ahn JC, Lee JH, Kang BH, “Properties of Recycle Cement made of Cementitious Powder from Concrete Waste by Conditions of Burning”, Journal of Architectural Institute of Korea, Nov,19(11):109-12 (2013).

[3] Mun YB, Choi HK, “A Fundamental Study for Development of Radioactive Waste Content and Solidifying During the Dissolution of Concrete in Decommissioning Nuclear Power Plant” Journal of the Korean Radioactive Waste Society, Vol.2018 No.05, 295-296.

Criticality Analysis for Washing of the UF_6 Cylinder and Treatment of the Waste Water Facility

Janghwan Lim*, Manseok Do, Seongki Lee, and Jongsung Yoo

KEPCO Nuclear Fuel, 242, Daedeok-daero 989beon-gil, Yuseong-gu, Daejeon, Republic of Korea

*jhlim@knfc.co.kr

1. Introduction

KEPCO NF treats a heel remaining in the UF_6 cylinder after reconversion vaporization process has been completed and the waste water has been generated during the washing process. To improve washing capacity and minimize environmental impact, washing of the UF_6 cylinder and treatment of the waste water facility were improved by vacuum evaporation concentration method and installed in waste management plant. The criticality of the facility was evaluated using KENO-VI code with ENDF/B-VII library.

2. Analysis Results

2.1 Bias and Uncertainty Evaluation

For the criticality bias calculation, criticality experiments with Uranium Oxyfluoride Solution in "International Handbook of Evaluated Criticality Safety Benchmark Experiments"[1] has been selected considering the characteristics of washing of the UF_6 cylinder and treatment of the waste water facility.

2.2 Calculation of Upper Subcritical Limit (USL)

For the verification of the criticality experiments, Goodness of Fit test from ProUCL 5.1 was used. As a result of the verification, data for criticality experiments were shown as a non-normal distribution. According to NUREG/CR-6698[3], Non-parametric statistical treatment can be applied when experimental results do not have normal distribution. In non-parametric statistical treatment method, the reliability of the population can be calculated as follows:

$$\beta = 1 - \sum_{j=0}^{m-1} \frac{n!}{j!(n-j)!}(1-q)^j q^{n-j} \qquad (1)$$

where :

q = the desired population fraction (normally 0.95)

n = the number of data in one data sample

m = the rank order indexing from the smallest sample to the largest

$$\beta = 1 - q^n = 1 - 0.95^n \qquad (2)$$

K_L = Smallest k_{eff} value – Uncert. for smallest k_{eff} – Non parametric Margin (NPM) (3)

where :

K_L = A weighted single-sided lower tolerance limit

The USL value was calculated as shown in Table 1 using the above equation.

Table 1. Calculation results of USL

No. of experiment		22
β		67.65%
NPM (Ref. NUREG/CR-6698 Table 2.2)		0.03(>60%)
K_L		0.96165
USL	Flooding	0.91165
	Optimum	0.94165

2.3 Sensitivity Analysis of the Single UF_6 Cylinder

Most of the UF_6 is used in the reconversion vaporization and the remainder is transferred to the washing process. Sensitivity analysis was performed by modeling as shown in Fig. 1 and Table 2, where the results depend on the condition of UF_6 heel remaining in the cylinder.

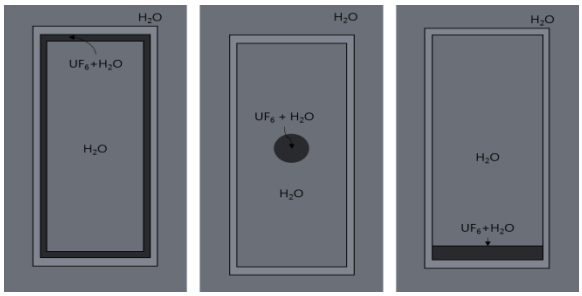

Fig. 1. Criticality Analysis Model of UF_6 cylinder for based on each condition (Left: initial, Center: massed state, Right: sediment).

Table 2. Sensitivity analysis results

Condition	k_{eff}	σ	k_{eff} +2σ
Initial	0.03766	0.00005	0.03776
Massed	0.37620	0.00014	0.37648
Sediment	0.18813	0.00011	0.18835

2.4 Criticality Analysis Results for Facility

As shown in Sec. 2.3, the reactivity of UF_6 cylinder was the highest in massed condition. Therefore, this condition was applied to the criticality analysis model of UF_6 cylinders, and it is assumed that treatment of the waste water facility was filled with waste water.

2.4.1 Flooding Condition. As a calculation result from above condition and assumption, the effective multiplication factor(k_{eff}) of flooding condition is 0.76606 smaller than the USL(0.91165).

2.4.2 Optimum Moderation Condition. The water density of all the flooded volumes was modeled at 0.01g/cm^3 ~ 1.00g/cm^3 to investigate the impact on criticality with changing moderator density. As a result, the maximum effective multiplication factor of optimum moderation condition is 0.76636 smaller than the USL(0.94165).

3. Conclusion

According to the results of sub-section 2.4.1 and 2.4.2, it is confirmed that all nuclear criticality safety assessment for washing of the UF_6 cylinder and treatment of the waste water facility are fully satisfied.

REFERENCES

[1] NEA/NSC/DOC(95)03, “International Hand book of Evaluated Criticality Safety Benchmark Experiments,” NEA Nuclear Science Committee, September 2008 Edition.

[2] J.C. Dean, R.W. Tayloe, Jr, “Guide for Validation of Nuclear Criticality Safety Calculational Methodology,” NUREG/CR-6698, Jan 2001.

A Study on the Clearance Strategy of Surface Contaminated Radioactive Waste Using Mass to Surface Ratio

Ji Young Song*, Ki Baek Shin, Dong-Ju Lee, and Junhyuck Im
Korea Atomic Energy Research Institute, 111, Daedeok-daero 989beon-gil, Yuseong-gu, Daejeon, Republic of Korea
*Jysong1994@kaeri.re.kr

1. Introduction

In most nuclear and radiation facilities, a large amount of radioactive waste is generated. Therefore, many of them are considering clearance of very low level radioactive waste for economic reason. For the clearance of radioactive waste in Korea, it is necessary to satisfy the regulatory requirements of radioactivity concentration by radionuclide or exposure dose. However, clearance regulatory requirements for surface contaminated radwastes are not yet available. In USA, various studies have been carried out for solving similar problems. As a result, the relationship between surface and volume radioactivity, mass to surface ratio, has been defined and can be used to analyze the radioactivity concentration of surface contaminated radwastes. Thus, it is necessary to confirm that mass to surface ratio is applicable to analyze the radioactivity concentration of surface contaminated radwastes in Korea.

In this study, we have demonstrated clearance strategy of surface contaminated radwastes in Korea using mass to surface ratio.

2. Clearance Strategy

2.1 Overview

The schematic diagram of clearance strategy for surface contaminated radwastes is given in Fig. 1. In this paper, we have focused on analysis method of radioactivity concentration.

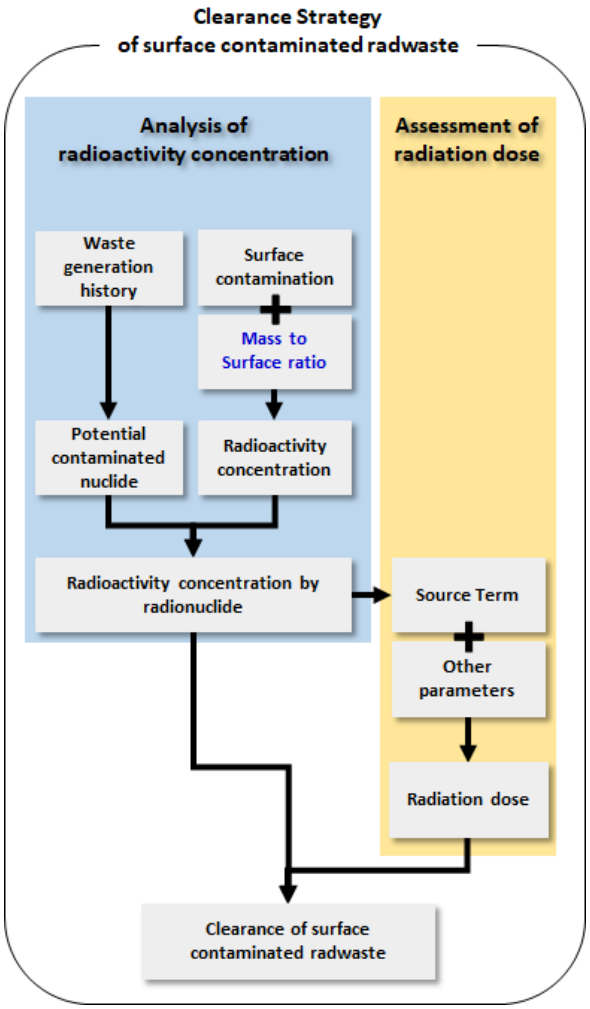

Fig. 1. Clearance strategy of surface contaminated radioactive waste.

2.2 Analysis of Radioactivity Concentration

To determine if surface contaminated radwastes satisfy the clearance level for radioactivity concentration, it is necessary 1) to select potential contaminated nuclide and 2) to analyze radioactivity concentration by radionuclide. At this time, radioactivity concentration is calculated by using

surface contamination (Bq/cm^2) and mass to surface ratio.

2.2.1 Analysis of Radionuclide. Potential contaminated nuclide in radwastes could be identified by reviewing the waste record history. Furthermore, analysis of the origin, radiation field, and surrounding environment of radiowaste should be done together.

2.2.2 Radioactivity Concentration. In order to convert measured surface contamination to radioactivity concentration, specific values are needed. In this study, the mass to surface ratio presented in USNRC has been applied. Some of values are shown in Table 1. The values were derived by analyzing the surface and volume radioactivity of the metal components of reference PWR and reference BWR. Once the mass to surface ratio is derived in USNRC, not only surface contaminated radwastes but also potential clearance radwastes are also included. Therefore, this was deduced to be more conservative than the mass to surface ratio for surface contaminated wastes. If this is applied to convert the surface contamination to the radioactivity concentration for the surface contaminated waste, it can be used as a conservative value. Thus, in this study, the mass to surface ratio was used to determine whether the surface contaminated radwastes satisfy the clearance acceptable radioactivity concentration.

Table 1. A part of mass to surface ratio information from USNRC

Material	Mean value of mass to surface ratio
Ferrous metals	4.53 – 5.34
Aluminum	0.90
Copper	0.52
Concrete	280 [1)]

[1)] Total average of all case considering USNRC studies

3. Conclusion

This study is to establish clearance strategy of surface contaminated radwastes in Korea using mass to surface ratio. In this paper, we have focused on analysis method of radioactivity concentration. We suggest the method to determine whether surface contaminated radwaste satisfies the clearance level for radioactivity concentration. 1) selecting potential contaminated nuclide by analyzing the waste record history. 2) confirming whether the radioactivity concentration satisfy clearance acceptable requirement using surface contamination using mass to surface ratio. This results will be contributed to develop the clearance strategy of surface contaminated radwaste.

REFERENCES

[1] ANSI/HPS N13.12, “Surface and Volume Radioactivity Standards for Clearance” (2003).

[2] K. Shin, D. Hong, I. Kang, W. Jang, “Application of mass to surface ratio for regulatory clearance of VLLW metal radwastes at KAERI”, IAEA-CN-242 (2016).

Structure Stability for Porous Materials to Extract Alkanes From Liquid Radwastes : Preliminary Results

Jongjin Kim[1,*], Junhyuck Im[1], Hyungwoo Kim[2], and Donghoon Seoung[2]
[1] Korea Atomic Energy Research Institute, 111, Daedeok-daero 989beon-gil, Yuseong-gu, Daejeon, Republic of Korea
[2] Chonnam National University, 77, Yongbong-ro, Buk-gu, Gwangju, Republic of Korea
[*] jjkim@kaeri.re.kr

1. Introduction

The organic liquid radwastes that has been generated in the KAERI is temporarily stored and managed in the radioactive waste treatment facility. Approximately 67% of these organic hybrid wastes are comprised of alcohol, acetone, TBP, Dodecane, and etc. The best treatment option to treat the organic liquid waste is incineration but it is not easy to have approval from governments due to the politic issue.

In this study, the candidates of polymer compounds that can selectively adsorb only organic matters in the mixed solution were selected. In order to understand the structure and characteristics of synthesized candidates, Density of State (DOS), band structure and optimized structure were calculated by using Density Functional Theory (DFT) calculation technique and the adsorption energies to TBP and dodecane, which are typical organic materials for organic radioactive wastes, energies to TBP and dodecane, which are typical organic materials for organic radioactive wastes, were calculated by molecular mechanics technique.

The final goal of this research is to develop a technology for separating organic compounds and inorganic materials from organic hybrid waste liquids using microporous polymer polymers- and graphene-sponge materials.

2. Method

2.1 Density Functional Theory

Density functional theory (DFT)[1] is a computational quantum mechanical modelling method used in physics, chemistry and materials science to investigate the electronic structure (or nuclear structure) (principally the ground state) of many-body systems, in particular atoms, molecules, and the condensed phases

All calculations consider the spin-polarization, and the density functional theory (DFT) was used to calculate the total energies, forces, and energy profiles.

2.2 Building Blocks

For the sponge materials, we prepare several types of building blocks. Fig. 1 shows the first building block and we calculated the structure stability and binding energy using DMol3 DFT calculation package.

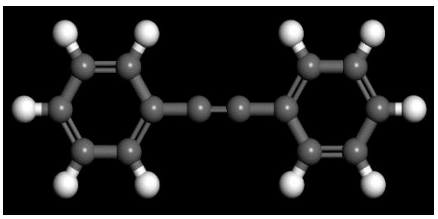

Fig. 1. Building block #1. White balls represents hydrogen and gray balls are carbon.

We performed geometry optimization in order to calculate the structure stability, and we performed binding energy calculation between building blocks and dodecane in order to check the absorption possibility.

Calculation parameters are summarized in Table 1.

Table 1. Parameter values

Parameters	Values
Energy Limit	1.0E-5 Ha
SCF tolerance	1.0E-6
Max. Force	0.002 Ha/Å
Max. SCF Cycles	50
Max. Displacement	0.005 Å
Max. iterations	100

3. Results and Discussion

We performed the geometry optimization and binding energy calculation for the building block and honeycomb structure. And calculate the geometry energy with dodecane.

Table 2. shows the results for each structure

Table 2. Structure optimization results

Structure	Energy (Ha)
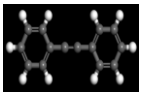	-538.9455
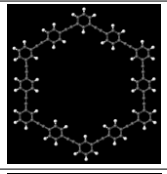	-3683.1248
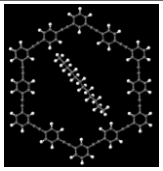	-4628.0137

The results shows that the final geometry energy which has dodecance inside is lower than the predicted energy. The prediction energy is -4155.5703 Ha, which is summation of all energies of building block and dodecane. It means that the structure containing dedecane is stable. And the binding energy between dedecane and the honeycomb structure is -1.05eV.

4. Conclusion

The structure stability with dodecane of building block was calculated and it shows that the structure is stable. And the binding energy between dodecane and honeycomb structure is -1.05eV. It indicate that the dodecane will be absorbed strongly in the honeycomb structure.

3~4 more candidate building blocks will be calculated and compared.

REFERENCES

[1] Hohenberg, P. and Kohn, W: Pysical Review B, 136, pp 864-871 (1964).

Study on the Method to Determine Grouping Analysis Range for KAERI's Radioactive Waste Using Concentration Averaging Method

Dong-Ju Lee, Junhyuck Im*, and Dae Seok Hong

Korea Atomic Energy Research Institute, 111, Daedeok-daero 989beon-gil, Yuseong-gu, Daejeon, Republic of Korea

*jhim@kaeri.re.kr

1. Introduction

Nuclear Chemistry Research Division at the Korea Atomic Energy Research Institute (KAERI) has used the grouping method for efficient radioactive waste analysis during the sampling. However, it is currently not easy to apply the grouping method due to the difficulty of decision on optimum amount of drum for grouping and proving its validity.

In this study, we applied the waste concentration averaging method proposed by US NRC [1] to KAERI's radioactive waste. Through this review, we would like to propose a method to determine the reasonable range for grouping analysis.

2. Background of the Idea

2.1 Review of the Concentration Averaging Method

According to NRC, the radioactive waste can be divided into two categories, one is "blendable waste" and another is "discrete items". If each waste with certain radionuclide concentration is mixed together under the certain threshold (volume or concentration), the total radionuclide activities in the wastes can be averaged by its total volume or mass without additional blending of the wastes. And the averaging method are described in the document of NRC [1].

2.2 Applying the Averaging Method to the Grouping Range Determination

The grouping analysis is based on a fact that radioactive waste packages composed of same material with identical generation history would have same radiological characteristics. So, analysis result for representative sample can be applied to each single package. This method presupposes that a single measurement value for a well-made composite sample will be close to the average concentration value of the individual components of the composite sample. That is, the range of the volume or concentration allowed to average the concentration of the individual measurement values is equivalent to the concept of the grouping range for making a composite sample.

Based on the above information, we have demonstrated that the method of decision on the allowable range of concentration averaging described in CA BTP could be applied to the method of determining the allowable grouping range.

3. Suggestions on the Methodology of Grouping Range Determination

Prior to set the grouping range, it is necessary to classify KAERI's waste according to the classification standards proposed by NRC (blendable waste or discrete items) through reviewing the record history of each waste. Then, the standard value of radionuclide concentration for each type of wastes should be determined.

After the above process, grouping range determination has been performed based on the waste type as follows.

3.1 In case of Blendable Waste

Once the waste is classified as blendable waste, the procedure for decision on grouping range is as shown in Fig. 1.

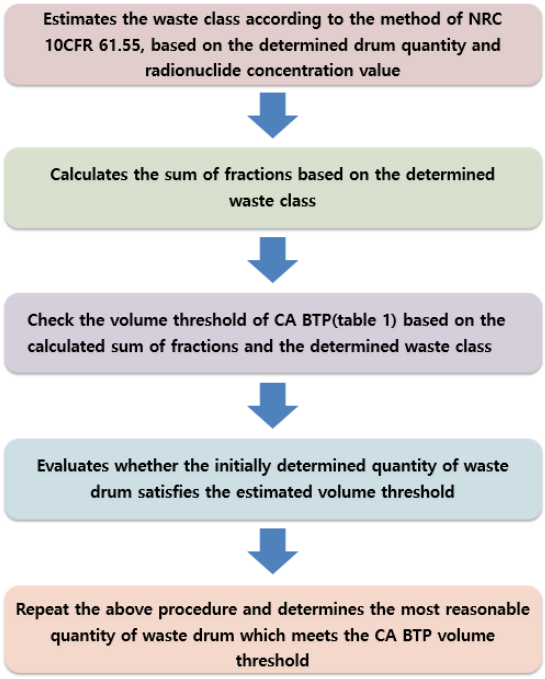

Fig. 1. Method of Determining Grouping Range (In Case of Blendable Waste).

The method to calculate "sum of fractions" and volume threshold shown in Table 1 are described in the document [1].

Table 1. Thresholds for Demonstrating Adequate Blending

Characteristics of most concentrated influent waste stream	Volume of Mixture in m^3 (ft^3)		
	Class A Mixture	Class B Mixture	Class C Mixture
Sum of fractions less than 10	No Limit	No Limit	No Limit
Sum of fractions between 10 and 20	No Limit	No Limit	50 (1800)
Sum of fractions between 20 and 30	60 (2100)	No Limit	20 (700)
Sum of fractions between 30 and 50	20 (700)	No Limit	6 (210)
Sum of fractions between 50 and 100	6 (210)	40 (1400)	2 (70)

3.2 In case of Discrete Items

In case of discrete items, the procedure for determining grouping range is as follows. First, waste class should be estimated in the same way as blendable waste. Then, allowable range of concentration averaging should be estimated for primary gamma-emitting radionuclides and for radionuclides of concern that are not primary gamma-emitter, respectively. The procedure of determining the concentration limit in each case is shown in Fig. 2.

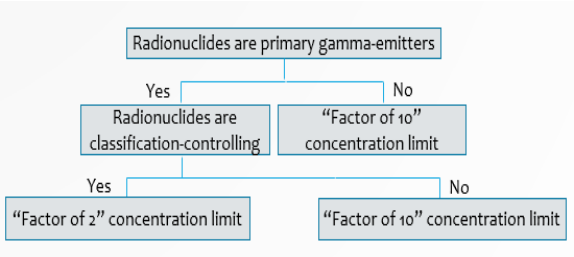

Fig. 2. Procedure of Determining the Concentration Limit for Concentration Averaging.

The concentration limit is the standard value depending on waste class described in NRC 10CFR 61.55 [2].

Through the above procedure, it is possible to determine the maximum allowable concentration standard value that can be averaged. And to estimate the maximum amount of drums that can be grouped for analysis is possible by comparing the initial determined concentration value with allowable concentration standard value.

4. Conclusion

In this study, we proposed a method to determine the range of grouping KAERI's waste using NRC concentration averaging method. By developing this method further, it may help solve the grouping issues. And if this method is established appropriately, the analysis efficiency will increase and also transportation of radioactive waste to the final repository will be promoted. Also, efficient analysis of wastes can be conducted when the large quantities of wastes are generated by dismantling of nuclear power plant in the future.

REFERENCES

[1] U.S. NRC, "Concentration Averaging and Encapsulation Branch Technical Position, Revision 1", Vol.1, February 2015.

[2] U.S. Nuclear Regulatory Commission, 10CFR Part 61.55, "Waste Classification"

Dose Calculation of Landfill Workers Based on the Concrete Landfill Method

ByeongIk Park*, Hun Kim, and Chang-Lak Kim
KEPCO International Nuclear Graduate School, 658-91, Haemaji-ro, Seosaeng-myeon, Ulju-gun, Ulsan, Republic of Korea
*parkx578@gmail.co.kr

1. Introduction

As of June 2017, Kori unit 1 has permanently ceased its operation and phased into permanent shutdown. Since the decommissioning process will produce a large amount of concrete waste, this study suggests the optimized strategy to landfill the concrete wasted produced during the decommissioning process.

2. Experiment

2.1 Background

In this study, existing Kori-1 site underground area was used as a landfill site. The total volume of Kori-1 underground portion is approximately 3807 m^3. If the density of concrete wastes is set to 2.0 g/cm^3, 7,614 tons of concrete wastes can be filled in this area. the landfill work will be performed in three of 15 tons trucks, which operates 5 times a day filling 225 tons per day.

The concentrations of radionuclides in Bioshield concretes were obtained through survey data in very low-level wastes (VLLW) and clearance waste (CW), shown below in Table 1. Then, the concentrations were recalculated with 5 years of decay applied since the decommissioning process does not begin at least 5 years after the permeant shutdown.

A further assumption was made that VLLW can be cleared of regulation in restricted terms to be landfilled in Kori-1 sites, as shown in Table 2.

The radiation dose calculation was performed with RESRAD onsite 7.2 using the above data and other Kori-1 site-specific data [1,.2]. RESRAD onsite 7.2 uses ICRP 60 as the base for external, inhalation, and ingestion dose conversion factors.

Table 1. Bioshield Concrete Concentration

Radionuclides	Concentration (Bq/g)	
	VLLW	CW
Fe55	2.77E+01	2.49E+00
H3	3.51E+01	3.06E-01
Co60	5.16E-01	1.09E-02
Eu152	1.76E-01	1.44E-03
Mn54	1.47E-03	1.44E-03
Cl36	6.17E-02	3.17E-04
C14	4.38E-02	2.22E-04
Ni63	3.72E-02	2.00E-04
Eu154	1.73E-02	1.97E-04
Cs134	8.00E-04	1.55E-04
Nb93m	2.01E-03	1.53E-05
Sm151	2.37E-03	1.27E-05

Table 2. Bioshield Concrete 5 years decay applied

Radionuclides	Concentration (Bq/g)	
	Restricted	Unrestricted
Fe55	4.38E-02	2.22E-04
H3	6.17E-02	3.17E-04
Co60	2.67E-01	5.65E-03
Eu152	1.49E-04	2.89E-05
Mn54	1.36E-01	1.11E-03
Cl36	1.16E-02	1.32E-04
C14	7.81E+00	6.82E-01
Ni63	2.65E+01	2.31E-01
Eu154	1.45E-03	1.42E-03
Cs134	1.62E-03	1.23E-05
Nb93m	3.59E-02	1.93E-04
Sm151	2.28E-03	1.22E-05

For the exposure pathway, external gamma exposure, inhalation, and soil ingestion were selected as normal industrial work scenario, shown in Fig. 1.

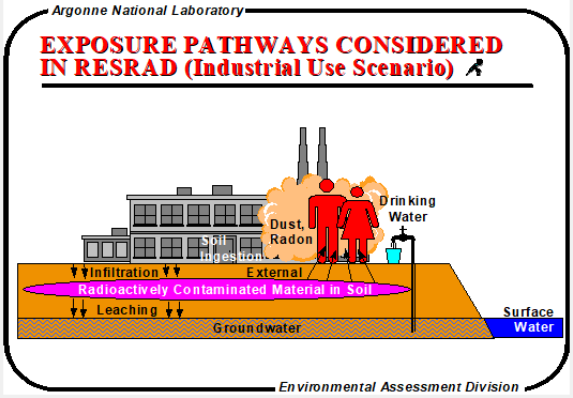

Fig. 1. RESRAD Industrial Scenario.

2.2 Calculation & Result

Three different cases were set to find the method, which gives minimum dose exposure to landfill workers. The total weight of concrete was proportionally increased to meet the capacity of the landfill site, which is 7,614 tons.

The first case, 855 tons of restricted clearance waste were landfilled in the center of 6709 ton of unrestricted clearance wastes. The unrestricted clearance wastes were buried in the area of 56.7 m^2 and 7 m deep. As a result, the total radiation dose is 3.570 μSv/y.

The second case, 855 tons of restricted clearance waste were landfilled on the top of 6709 ton of unrestricted concrete wastes. However, the restricted clearance wastes were buried in the area of 427.45 m^2 in 1 m deep. As a result, the total radiation dose is 4.12 μSv/y.

The third case, 7,614 tons of unrestricted and restricted clearance waste were landfilled on the site in well-mixed form. The result shows that the total radiation dose is 3.91 μSv/y.

3. Conclusion

In this study, radiation doses of landfill workers were calculated based on the individual concrete landfill methods. This result was based on the assumption that Kori-1 site is used as a landfill site and the concentrations of unrestricted and restricted clearance wastes are below the concentrations used in the calculation. (Table 2). As shown in the result, the first case produces the lowest dose exposure for landfill worker. However, it is not a realistic landfill method. Since the depth of total landfill is 10 m and it is almost impossible to fill with leaving center off to fill restricted clearance waste later. The third case has the possibility to violate the regulation, which does not allow to mix different wastes to lower the radiation dose. The second case is the most conservative method, but also very realistic and applicable, thus it would be the most optimized method to landfill the concrete wastes.

ACKNOWLEDGEMENT

This research was supported by the Nuclear Safety Research Program through the Korea Foundation of Nuclear Safety (KOFONS), granted financial resource from the Nuclear Safety and Security Commission (NSSC), Republic of Korea (No.2019-0002).

REFERENCES

[1] KINGS R&D Foundation, Pusan University R&D Foundation, “Final Report of Decommissioning and Site Remediation Research for Nuclear Power Plant”, Nuclear Safety and Security Commission (2018).

[2] KAERI, “The Results of the Assessment for Clearance of Dismantling the Concrete Waste from the Research Reactor Facilities:”, Korean Atomic Energy Research Institute (2006).

A Convertible Plasma Torch System for Treatment of Low and Intermediate Level Radioactive Waste

Jun-Ho Seo*, Junseok Nam, In-Mok Yang, Min-Gyu Choi , Mi-Yeon Lee , Hyo-Jeong Kim,
Ho-Sang Lee , and Shi-Young Yang
Chonbuk National University, 567 Baekje-daero, Deokjin-Gu, Jeonju, Jeollabuk-Do, Republic of Korea
*jhseo@jbnu.ac.kr

1. Introduction

As reported in many other papers [1-4], plasma torch systems are promising for volume reduction of decommissioning wastes of nuclear power plants. By melting the radioactive waste drums directly without complicated processes for sorting or pretreating, plasma torch systems can provide a unified melting process for both of metallic and non-metallic wastes. In addition, the melted slugs can be obtained in non-leachable glass form, which are preferable in LILW disposal facility. Most of all, plasma melting route is expected to produce excellent volume reduction ratio compared with other technologies such as super-compaction.

In this work, we report the development of a convertible plasma torch system applicable to the volume reduction of low and intermediate level radioactive waste. For this purpose, a hollow electrode plasma torch with inter-electrodes was designed and tested in reverse polarity. By forcing the arc column to extend as long as the inter-electrode length, this type of plasma torch can increase plasma power with the arc voltage at fixed arc currents, allowing for high plasma enthalpy. In addition, double cathodes were employed for the designed plasma torch. By reducing the arc current per electrode, we expect that this introduction of double cathodes can help in extending the service life time of the electrodes. Finally, a plasma torch operation system was constructed and the performance test was carried out at the power level of 0.3~1.2 MW

2. Design of Plasma Torch System

Fig. 1 shows a schematic diagram of a plasma torch system used in this study. As shown in this figure, the designed plasma torch system primarily consists of a 1.5 MVA class DC power supply (750 A x 2 kV), a hollow electrode plasma torch, a gas supply system and a water supply system to cool down the plasma torch. For the torch performance test, the flow rates of plasma forming gases and the cooling water were controlled by mass flow meters and a water pump with an inverter controller. In addition, the temperature risings in cooling water were measured by K-type thermocouple installed at inlet and outlet of the coolant line. From these instruments for measurement of the operation parameters, torch efficiency defined as the ratio of exit plasma enthalpy to the input power can be measured together with the V-I characteristics as a basic performance data of the torch.

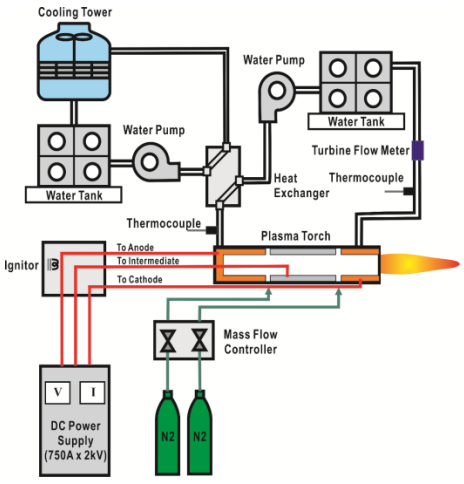

Fig. 1. A Schematic diagram of the hollow electrode plasma torch system with inter-electrode and reversed polarity discharge structure.

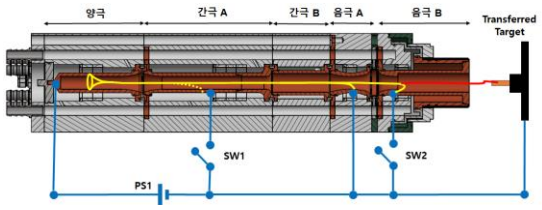

Fig. 2. A cross-sectional view of hollow electrode plasma torch with inter-electrode and reversed polarity discharge structure.

Table 1. Design values of the hollow electrode plasma torch with inter-electrode and reversed polarity discharge structure

Part Name	Design Value [mm]	
	Diameter	Length
Anode	25	180
1st I.E	25	180
2nd I.E	25	120
3rd I.E	25	120
Cathode	25	80

Fig. 2 illustrates the cross-sectional view of the hollow electrode plasma torch with inter-electrodes employed in the plasma torch system of Fig. 1. In this figure, the presented plasma torch has three inter-electrodes, designated as 1st I.E., 2nd I.E. and 3rd I.E., respectively, between hollow cathode and cylindrical anode. In order to investigate the effects of inter-electrodes length, performance tests were conducted with increasing the number of inter-electrodes from 1 to 3. In Fig. 2, the arc column between front and rear electrodes is also presented together with the electrical connection diagram for reversed polarity discharge structure setting the rear and front electrodes as anode and cathode, respectively. For easy ignition, the 1st inter-electrode was used as a pilot cathode in this work. After ignition, the arc column was transferred to the front electrode and the electrical connection to the inter-electrode was disconnected. The number of inter-electrode can be increased by inserting additional one between first inter-electrode and front cathode.

In this work, the performance tests were carried out for the plasma torch with single inter-electrode and two inter-electrodes, respectively, in order to check the effect of inter electrode number. The details on the design parameters of the plasma torch are listed in Table 1.

REFERENCES

[1] D.G. Cacucci (Ed.), Handbook of Nuclear Engineering volume V, 3253-3420 (2010).
[2] S.C. Park, D.U. Kim, M.H. Kim, J.H. Seo, O.B. Yang, J. Kor. Phys. Soc. 63, 1746-1754 (2013).
[3] S.L. Camacho, Pure Appl. Chem. 60, 619 (1988).
[4] G. J. Hanus, T. J. Stahl and S. L. Camacho, US Patent 5,451,740

5분과

제염해체 (Oral)

SACER: A Computer Program for Decommissioning Schedule Analysis and Cost Estimate of Nuclear Power Plants

Tongkyu Park*, Byoungchan Han, and Kibeom Park

FNC Technology Co., Ltd., 32F, 13 Heungdeok 1-ro, Giheung-gu, Yongin-si, Gyeonggi-do, Republic of Korea

*tongkyu@fnctech.com

1. Introduction

In Korea, the decommissioning cost for nuclear power plants should be reviewed and re-estimated every two years to fulfill the Enforcement Decree of the Radioactive Waste Management Act[1]. To estimate the decommissioning cost, lots of efforts have been devoted over decades to develop several computer programs in the world. Most of them are based on UCF (Unit Cost Factor) and WDF (Work Difficulty Factor) introduced in Ref. 2. In Korea, DeCAT (Decommissioning Cost Assessment Tool) [3] is the most popular cost estimate code for decommissioning of nuclear power plants and widely used in KHNP.

This paper introduces a newly user-friendly computer program, SACER (Schedule Analysis and Cost EstimatoR for decommissioning) for decommissioning schedule analysis and cost estimate by adopting the UCF and WDF methodologies.

2. Overview of SACER

The SACER code is designed to run on a Microsoft Windows platform and written in C++ and C#. All the input and output are written in Microsoft Excel format and thus user can easily handle all the given information and results. Area designation data, waste management strategy, basic decommissioning work breakdown, unit cost factor, work difficult factor, contingencies, and general information need to be provided as input to execute the SACER code. Main output consists of cost estimate, work activities, and schedule analysis. This code can also calculate the crew size to satisfy the user-specified removal period for each decommissioning area. The major input of SACER is listed in Table 1 and Fig. 1 shows the flow chart of the SACER code.

Table 1. Major Input of SACER

Input	
File name	Information
General	Contingencies, work schedule
UCF	Unit Cost Factor
Labor	Position, labor Rates, overhead
Material	Materials, tools, and equipment
Techniques	Decommissioning techniques
Strategy	Waste management strategy
Component	List of components to be removed
Area	Area designation, WDF

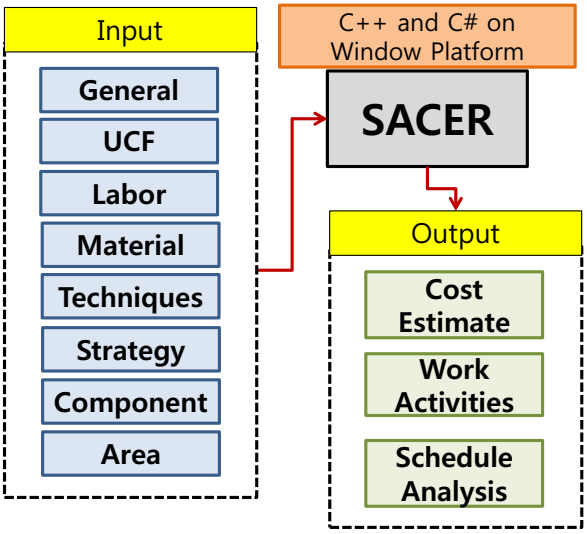

Fig. 1. Flow chart of SACER.

3. Main Capabilities of SACER

3.1 Multiple Waste Classes and Types in an UCF

In a user-specified UCF prepared as one of input, only one waste class and type have been considered to calculate the mass or volume of radioactive waste generated from activities related the corresponding UCF. It means conservative estimate might be performed in the aspect of the volume of radioactive waste generated from whole area, and thus decommissioning cost might be overestimated. To resolve this shortcoming, SACER can handle multiple waste classes and waste types in an UCF.

3.2 Automatic Generation of Number of UCFs

In SACER, the component list and area list are provided as input. The component list includes all the components, the corresponding systems, their volumes, their masses and related data while the area list consists of area designation and its WDF values. Using those input, SACER can automatically generate the number of UCFs to be carried out in each area. Namely, work activities in each user-specified decommissioning room can be generated.

3.3 Schedule Analysis for Removal and Demolition

In SACER, user can initially assume removal or demolition work period of a certain building. By comparing to this user-specified work breakdown for system removal and demolition of building, SACER can generate a proper work schedule for each decommissioning room using the number of UCFs to be performed in the room, the total duration of each UCFs, and the maximum permissible crew size in the room.

3.4 Cost Estimate

One of the main capabilities of the SACER code is to estimate the decommissioning cost of nuclear power plants. It includes additional cost, undistributed cost, staff cost, removal cost, decontamination cost, transportation cost, and disposal cost.

4. Conclusion

In this study, a new computer program for decommissioning schedule analysis and cost estimate of nuclear power plants, SACER, has been developed. It can handle multiple waste classes and waste types in an UCF, and automatically generate the number of UCFs in each user-specified decommissioning area as well. It is expected that the SACER code can be widely used to estimate the decommissioning cost of nuclear power plants because it has several strengths and enhancements compared to the existing programs.

REFERENCES

[1] Radioactive Waste Management Act Enforcement Decree in Korea (2008).

[2] Guidelines for Producing Commercial Nuclear Power Plant Decommissioning Cost Estimates, AIF/NESP-036, 1986.

[3] Hak-Soo Kim and Jong-Kil Park, “Development of Computer Program for Estimating Decommissioning Cost”, Prof. of the ASME 2011 14th International Conference on Environmental Remediation and Radioactive Waste Management, September 25-29, 2011, Reims, France.

Study on the Functional Group Affinity Toward Aqueous Cesium

Il-Kwon Jung[a], Youngho Sihn[b], and Jong-Il Yun[a,*]

[a] Korea Advanced Institute of Science and Technology, 291, Daehak-ro, Yuseong-gu, Daejeon, Republic of Korea

[b] Korea Atomic Energy Research Institute, 111, Daedeok-daero 989beon-gil, Yuseong-gu, Daejeon, Republic of Korea

[*] jiyun@kaist.ac.kr

1. Introduction

Radioactive waste management is a major challenging issue to solve in the nuclear industry. Among the nuclides in the waste, cesium-137 (Cs-137) has become a major concern due to its long half-life and toxicity. Since Cs-137 is soluble in the aqueous phase, the released Cs-137 would readily migrate through groundwater pathways [1].

Silica is a popular material in the field of surface modification studies. Silanol groups on the silica surface can covalently bind with organosilyl functional groups by the condensation reaction. Through the condensation process, various functional groups such as carboxyl (-COOH), phosphonate (-$P=O(OH)_2$), and hydroxyl (-OH) can be attached on the silica surface, i.e., silica surface functionalization. The functionalized ligands would interact with aqueous Cs, improving the sorption performance of the silica [2-3]. In the present study, we have functionalized the silica surface with three different functional groups, e.g., COOH, OH, and $P=O(OH)_2$. Their adsorption capacities of Cs were measured and compared by batch sorption experiments.

2. Materials and Methods

2.1 Preparation of Adsorbents

All functionalization processes were conducted in anhydrous and anoxic conditions (99.999% Ar, H_2O and O_2 < 1 ppm). 300 mg of silica (Sigma-Aldrich, S5130) was added to the borosilicate bottle containing 50 mL of anhydrous toluene. The mixture was magnetically stirred at 400 rpm for 10 minutes. Organosilane reagents, 3-(triethoxysilyl)propyl-succinic anhydride (TESPSA 95%, BOC science), (3-glycidyloxypropyl) trimethoxysilane (GPTMS 98%, Sigma-Aldrich), and (2-diethylphosphatoethyl)triethoxysilane (DPTS 95%, Gelest) were injected into the suspension. The injected amount of organosilane was 0-70% based on the weight of silica and stirred for 12 hours after the injection. Functionalized silica was separated by centrifugation and washed with ethanol and deionized water several times. The product was then subsequently freeze-dried for 48 hours.

2.2 Hydroxylation

After the preparation of adsorbents, each ligand of functionalized silica was hydroxylated by addition of 0.1 M aqueous solution of perchloric acid (diluted $HClO_4$) to form sorption sites. The final product was washed with deionized water and freeze-dried for 24 hours (Fig. 1).

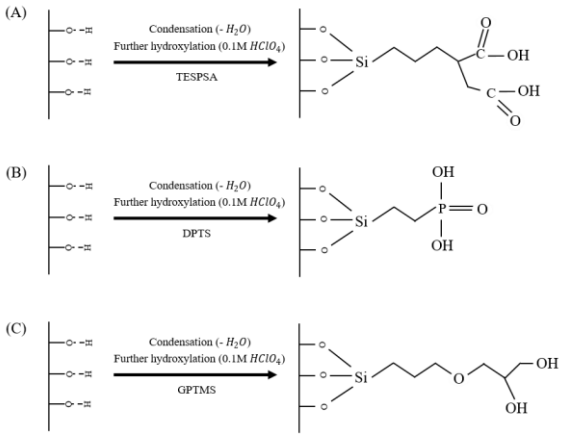

Fig. 1. Schematic illustration of functionalization onto silica surface: (A) carboxylation, (B) phosphonation, and (C) hydroxylation.

2.3 Characterization

To quantitatively evaluate the functional group density, the functionalized silica particles have been analyzed by ATR-FTIR, EA, and TGA analysis.

2.4 Batch Sorption Experiments

Cesium chloride (99.9% CsCl, Sigma-Aldrich) was dissolved in 200 mL of distilled water and 10^{-4} M cesium was prepared. The pH was adjusted by adding 0.1 M $HClO_4$ and 0.1 M NaOH solution. After the injection of functionalized silica, 2 mL of the solution was sampled periodically from the beginning and immediately separated by a membrane filter (Amicon Ultra-centrifuge 10K filter). The cesium concentration in diluted solution was quantitatively analyzed by ICP-MS.

3. Result and Discussion

3.1 Characterization

The functional group density was compared and quantitatively evaluated by two analyzes (EA, TGA). Table 1 shows that the density of each representative organosilane converges within a certain range.

Table 1. Comparison of functional group density

Analysis	TESPSA density (/nm^2)	GPTMS density (/nm^2)	DPTS density (/nm^2)
EA	0.212±0.008	0.233±0.016	0.148±0.020
TGA	0.223±0.015	0.296±0.039	0.168±0.010
Average	0.217±0.008	0.264±0.021	0.158±0.011

From the above results, it was confirmed that a monolayer was formed with a surface ligand density of 0.217 /nm^2 for TESPSA, 0.264 /nm^2 for GPTMS and 0.158 /nm^2 for DPTS.

3.2 Sorption of Cesium onto Functionalized Silica

Batch sorption experiments were conducted under pH 6.8 condition, as shown in Fig. 2. The molar ratio of cesium to the functional group was controlled by the functional group : cesium = 3:1 (mol). Among three oxygen-containing functional groups, carboxyl group (-COOH) showed the highest adsorption capacity (0.14 mol-CS/mol), followed by phosphoric acid (-P=O(OH)$_2$, 0.13 mol-Cs/mol) and then hydroxyl group (-OH, 0.08 mol-Cs/mol).

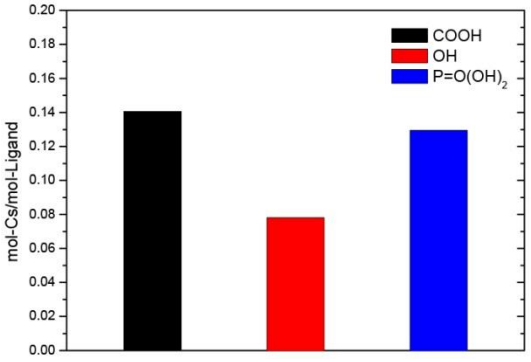

Fig. 2. Cesium sorption capacities of each functional group (functional group : cesium = 3:1 (in molarity), pH 6.8).

4. Conclusion

Functionalized silica with various functional groups was synthesized and compared on a molar scale. Among the three functional groups, the carboxyl group showed the highest adsorption capacity for cesium, suggesting that the functionalization of the carboxyl group might improve the sorption affinity for cesium.

REFERENCES

[1] Bascetin, E., Haznedaroglu, H., and Erkol, A., "The adsorption behavior of cesium on silica gel." Applied radiation and isotopes, 59, (1), 5-9 (2003).

[2] Toworfe, G., Composto, R., Shapiro, I., and Ducheyne, P., "Nucleation and growth of calcium phosphate on amine-, carboxyl-and hydroxyl-silane self-assembled monolayers." Biomaterials, 27, (4), 631-642 (2006).

[3] Wang, X., Yuan, L., Wang, Y., Li, Z., Lan, J., Liu, Y., Feng, Y., Zhao, Y., Chai, Z., and Shi, W., "Mesoporous silica SBA-15 function-alized with phosphonate and amino groups for uranium uptake." Science China Chemistry, 55, (9), 1705-1711. (2012).

Characterization of Ceramicrete Waste Form for Disposal of Concrete Waste of Decommissioned Nuclear Power Plant

Jae-Young Pyo* and Jong Heo

Pohang University of Science and Technology, 77, Cheongam-ro, Nam-gu, Pohang-si, Gyeongsangbuk-do, Republic of Korea

*vywodud@postech.ac.kr

1. Introduction

According to the IAEA report, 900 tons of radioactive concrete wastes are expected to be generated in the decommissioning of one PWR unit [1]. In previous researches, most of the radionuclides are present in porous cement paste and thus the volume of radioactive concrete wastes can be reduced by separating aggregates through heating and grinding process [2]. During the heating and grinding process, 80% of the total waste volume is reduced and powder wastes composed of cement paste and sand of less than 1 mm size are generated. In this study, these powder wastes are solidified with ceramicrete. The principle of ceramicrete formation is that calcined MgO and KH_2PO_4 are dissolved in the aqueous solution to synthesize $MgKPO_4 \cdot 6H_2O$. The objectives of this study are to solidify radioactive concrete wastes with ceramicrete and evaluate the waste acceptance criteria.

2. Experimental Procedures

The simulated concrete was formulated according to the mix proportion used in nuclear power plants constructed by the Korea Hydro & Nuclear Power Co., Ltd [3]. The simulated concrete cured for 28 days were heated at 550°C for 1 hour, pulverized into powder and sieved to 1 mm. The formulation of ceramicrete is shown in Table 1. Cesium and cobalt nitrates were added to evaluate the leaching characteristics of the ceramicrete. The samples of ceramicrete with a diameter of 15 mm and a length of 30 mm were made to evaluate the waste acceptance criteria of the disposal. Compressive strengths were measured using a universal testing machine. The thermal cycling and immersion tests were carried out according to the ASTM B553 and ASN 16.1 method, respectively. Specific details of these evaluation methods are described in the reference literature [4]. Concentrations of Co, Cs, Mg, K and P ions in the leachates were analyzed by inductively coupled plasma atomic emission spectroscopy (ICP-AES). After the thermal cycling and immersion tests, the compressive strengths of ceramicrete specimens were measured.

Table 1. Composition of ceramicrete prepared (wt.%)

Waste	MgO	KH_2PO_4	H_2O	H_3BO_3	$CsNO_3$	$Co(NO_3)_2$
50	10.32	23.24	15.38	0.50	0.29	0.27

3. Results and Discussion

The compressive strengths of ceramicrete specimens cured for 28 days were 56.27 MPa, but decreased to 47.90 and 25.15 MPa after immersion and thermal cycling tests, respectively. Despite the decreases in compressive strengths after immersion and thermal cycling tests, ceramicrete specimens were satisfied with the waste acceptance criteria of >

3.45 MPa. Fig. 1 shows the results of the ceramicrete components leached for 90 days. During immersion, $MgKPO_4 \cdot 6H_2O$ phase was incongruently dissolved and K ion was relatively leached. Fig. 2 shows the cumulative fraction leached and leaching rates of Cs ions evaluated to ANS 16.1 test. The leachability index of Cs was 11.06 and satisfied with the waste acceptance criterion of > 6. On the other hand, the leaching of Co ions hardly occurred below the detection limit of ICP-AES. Therefore, the ceramicrete that solidify radioactive concrete wastes have satisfactorily met the waste acceptance criteria.

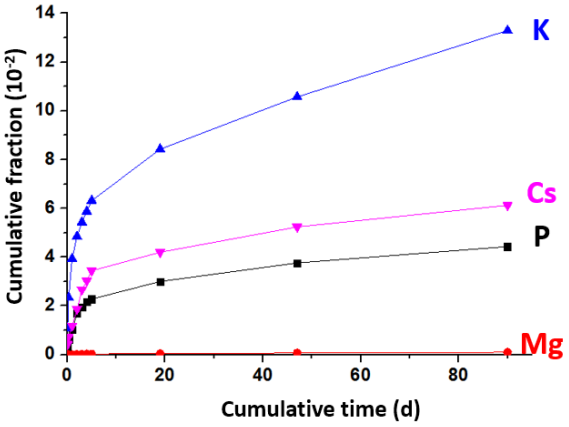

Fig. 1. Cumulative fraction of elements constituting the ceramicrete.

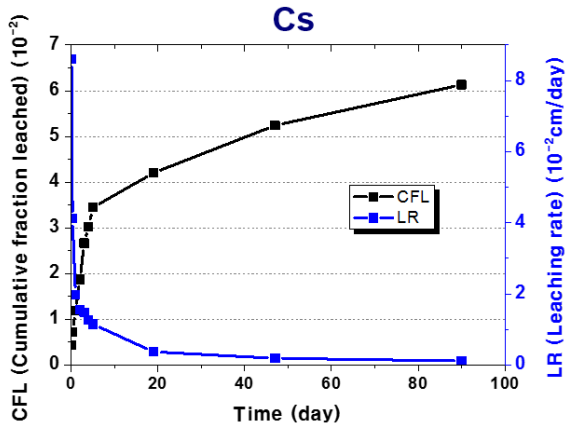

Fig. 2. Cumulative fraction leached and leaching rate of Cs in the ceramicrete.

4. Conclusion

Ceramicretes for the solidification of waste generated in the decontamination process of radioactive concrete were evaluated according to waste acceptance criteria. The Compressive strengths of the ceramicrete before testing were excellent at 56.27 MPa, and were 25.15 and 47.90 MPa after the thermal cycle and immersion test, respectively, which satisfied the regulation of > 3.45 MPa. The leachability index of Cs was 11.06 and satisfied the regulation of > 6.

ACKNOWLEDGMENT

This work was supported by the National Research Foundation (NRF) grant funded by the Ministry of Science & ICT (NRF-2017M2B2B1072405).

REFERENCES

[1] International Atomic Energy Agency, “Methods for the minimization of radioactive waste from decontamination and decommissioning of nuclear facilities”, Technical Reports Series No. 401, IAEA, Vienna (2001).

[2] B. Min, et al., “Separation of radionuclides from dismantled concrete waste”, J. Kor. Rad. Waste Soc., 7(2), 79-86 (2009).

[3] J. Kim. et al., “Influence of sand to coarse aggregate ratio on the interfacial bond strength of steel fibers in concrete for nuclear power plant”, NUCL. ENG. DES. 252, 1-10 (2012).

[4] Y. Lee, et al., “The characterization of cement waste form for final disposal of decommissioning concrete wastes” Ann, Nucl, Energy, 77, 294-299 (2015).

Optimal Scenario Selection Methodology for Treatment Decontamination of Decommissioning Waste

Daehyeon Kim[a, b,*], Jae Hak Cheong[a], Inhye Hahm[b], Daeseo Koo[b], Kwanseong Jeong[b], Jaehyun Ha[b], Seungkook Park[b], Sangbum Hong[b], and Bum Kyoung Seo[b]

[a] Kyung Hee University, 1732, Deogyeong-daero, Giheung-gu, Yongin-si, Gyeonggi-do, Republic of Korea

[b] Korea Atomic Energy Research Institute, 111, Daedeok-daero 989beon-gil, Yuseong-gu, Daejeon, Republic of Korea

[*] rlaeogus5290@khu.ac.kr

1. Introduction

In the decommissioning of nuclear facilities, a large amount of waste with various characteristic information is generated. Decommissioning operators should minimize the amount of radioactive waste and treatment costs while taking into account the characteristics of wastes. Also, safety of workers should be considered. This can be ensured by selecting the optimal treatment process according to various waste characteristics data.

2. Methodology

In order to select process scenarios according to various wastes, evaluation is carried out according to the algorithm as shown in Fig. 1.

Fig. 1. Evaluation Algorithm.

2.1 Evaluation Criteria

OECD/NEA recommend that five criteria (Safety, Efficiency, Cost-Effectiveness, Waste Minimization, Feasibility of industrialization) should be considered to select the optimal decontamination technology [1].

In order to select optimal treatment decontamination, we must define the weight of five evaluation factors. We use the Analytic Hierarchy Process (AHP), which is a method of finding the optimal alternative through a pairwise comparison. Since the largest change in the target wastes through decontamination is the radioactivity level, the weights were selected by dividing the radioactivity levels of the waste.

2.2 Process Evaluation

Process evaluation of decontamination techniques is divided into three steps.

In the first step, the applicability of the technology is screened according to the waste characteristics. For example, Sulfuric acid is suitable rather than nitric acid for decontamination on carbon steel.

In the second step, weights are determined by normalizing the performance comparison between processes.

In the third step, preference of the process is calculated by the sum of the product of the evaluation factor and the performance weight of the corresponding process. It is calculated by the following equation:

$$T_i = \sum_{j=1}^{m} w_j \times p_{ij} \ , (i = 1, 2 \ldots . n) \qquad (1)$$

Where T_i is Preference of i-th technique, w_j is weight of the j-th evaluation criteria, p_{ij} is performance weight of i-th technique corresponding to the j-th evaluation criteria, n is the number of evaluation techniques, m is the number of evaluation criteria.

2.3 Optimal Scenario Selection

First, the decontamination factor required for the target wastes can be determined by determining the end state of the waste. Then, among the various scenarios satisfying the DF, the scenario having the highest average value of the process preferences based on satisfaction of the user's limitation is selected as the optimal scenario.

3. Result

Two assumption is needed before proceeding with the evaluation. One is the assumption that the process performance data is accurate. Another assumption is that the evaluation factor weights only take into account the physical and radiological characteristics. The reason for making assumptions is that the process performance depends on characteristics of waste, but in this study we refer to other literature [2].

We used AHP for virtual low-level contaminated metal waste requiring decontamination factor (DF) = 110 to calculate the weight of the evaluation criteria shown in Table 1. The experts who performed the evaluation were those who had experience of decommissioning or who had researched decommissioning.

Table 1. Weight of Evaluation Criteria for virtual waste

Criteria	Weight (LLW)	Weight (VLLW)
Safety	0.075	0.045
Efficiency	0.150	0.163
Cost-Effectiveness	0.215	0.217
Waste Minimization	0.497	0.477
Feasibility of Industrialization	0.064	0.098

Applying the evaluation algorithm makes the scenario shown in the Fig. 2. Optimal scenarios can achieve up to 35.5% cost savings or up to 45% waste reduction compared to other scenarios.

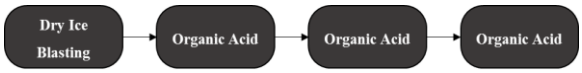

Fig. 2. Optimal Scenario.

4. Conclusion

Although the evaluation was based on virtual waste, the weight of waste minimization among the five evaluation criteria was the highest. As a result, Scenarios that generate a relatively small amount of waste have been selected as the optimal scenarios. This means that optimal scenarios can also change depending on the decision of the decommissioning operator.

By choosing the appropriate treatment process according to the characteristics of the waste, it is possible to minimize the amount of waste and cost while considering the safety of the worker.

In the future, we will compare the results of this study with the processing scenarios applied in domestic and overseas experience. This will be meaningful in terms of ensuring the soundness of the evaluation criteria and process performance data.

ACKNOWLEDGEMENT

This work was supported by a grant from the National Research Foundation of Korea (NRF), funded by the Korean government, Ministry of Science, ICT and Future Planning (No. 2017M2A8A5015143).

REFERENCES

[1] OECD/NEA, “Decontamination Techniques Used in Decommissioning Activities”, Report by the NEA Task Group on Decontamination, 1999.

[2] U.S. Environmental Protection Agency (EPA). Technology Reference Guide for Radiologically Contaminated Surface, EPA-402-R-06-003, 2006.

An Approach to Reconstruct Digital Mockup Based on Three-dimensional Scan Data for Nuclear Dismantling Process Evaluation System

Jonghwan Lee*, Ikjune Kim, Sungmoon Joo, and Dongjun Hyun
Korea Atomic Energy Research Institute, 111, Daedeok-daero 989beon-gil, Yuseong-gu, Daejeon, Republic of Korea
*jhl@kaeri.re.kr

1. Introduction

In order to solve the problem of the difference between the digital mockup of the dismantling facility and the actual field environment, it is necessary to update the digital mock-up of the facility to be cut based on the real-world three-dimensional information. In this study, a methodology for solving these issues was developed and implemented as a unit module of the existing dismantling process simulation and integrated evaluation system.

2. Research Method for Digital Mockup Reconstruction

We examined the digital mockup update methodology that applies the transformation matrix obtained by comparing the difference between two models on the point cloud based on the CAD model composing the digital mockup and the 3D scanned environment information characteristic to the CAD model. In addition, we developed a framework by applying various point cloud processing technologies to improve the accuracy and speed of updating digital mockups, and also tested the system based on real industry data.

3. Two-step Reconstruction for Digital Mockup

In order to compare the digital mockup with the CAD model to the point cloud model of the dismantling site obtained by 3D scanning, point sampling was first performed in the CAD model. The point sampling method applied in the CAD model is to generate a point cloud by performing Poisson Disk Sampling on all faces of the mesh model of each part of the CAD model created using the tessellator provided by the CAD kernel. In addition, in order to improve the matching speed and accuracy, the extended bounding box of the extracted point cloud was cropped in the point cloud of the scan model and the point cloud extracted from the CAD model was matched to the cropped scan model.

Generally, Iterative Closest Point (ICP) is widely used as a method for precise registration, but the ICP method is very sensitive to the initial conditions and ICP cannot be performed if there is no overlap between these two point clouds. To overcome these drawbacks, this study added a first registration procedure to derive the initial conditions of ICP. In the first registration process, key points that best represent the model shape were extracted from each model, and feature values were calculated using Fast Point Feature Histogram (FPFH) method at each keypoint.

Based on these calculated feature values, the first registration was performed using the Sample Consensus Initial Alignment (SAC-IA) method. For secondary registration, the first registration result was applied to the point cloud extracted from the initial CAD model, and then the point cloud was registered with the scanned point cloud using ICP. Finally, the CAD model was updated by applying the transformation matrix for initial registration and the transformation matrix for precise registration to the CAD model.

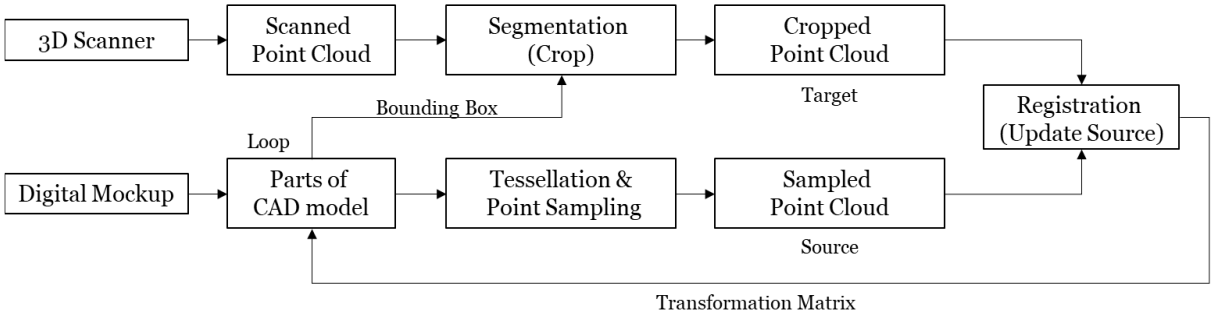

Fig. 1. Overall flow to reconstruct digital mockup based on 3D scan data for nuclear dismantling process evaluation.

Fig. 1 shows the overall framework of the methodology for digital mock-up reconstruction, outlining the process of sampling the point cloud for each part of the CAD model, registering the 3D scanned point clouds, and updating the results back to the CAD model. The scanned point cloud increased registration speed and accuracy by using only the cropped portion of the bounding box area of each part.

4. Conclusion

The digital mockup reconstruction methodology that has been set up was applied to the dismantling process evaluation system through modularization. In the future, we will improve the performance through sufficient test and evaluation. Through this, the technology to reflect the environmental information of the decommissioning site in real time on the dismantling process evaluation system and remote cutting system will be developed.

ACKNOWLEDGEMENT

This work was supported by the nuclear research and development program (2017M2A8A5015146) through the National Research Foundation of Korea, funded by the Ministry of Science and ICT, Republic of Korea.

REFERENCES

[1] I. Kim, B. Choi, D. Hyun, J. Moon, J. Lee, K. Jeong, et al., “A framework for a flexible cutting-process simulation of a nuclear facility decommission”, Annals of Nuclear Energy, 97, 204-207 (2016).

[2] J. Lee, G.-H. Kim, I. Kim, D. Hyun, K.S. Jeong, B.-S. Choi and J. Moon, “Establishment of the framework to visualize the space dose rates on the dismantling simulation system based on a digital manufacturing plat-form”, Annals of Nuclear Energy, 95, 161-167 (2016).

Development of Contaminated Soil Decontamination Technology for NPP's Using Selective Nuclide Adsorption Technique and Micro-bubble Vortex Breakdown Based on High Pressure Cleaning

Woohyeon Rhee*, Dukwon Kang, Seungil Kim, Pilyong Jeon, and Damhyang Kim

Elim-global Inc., 767, Sinsu-ro, Suji-gu, Yongin-si, Gyeonggi-do, Republic of Korea

*woohyeon.rhee@elim-global.com

1. Introduction

In June 2017, the National Energy Committee (N.E.C.) decided to immediately dismantle Kori Unit 1, the country's first nuclear power plant and, 12 out of 25 the nuclear power plant's design like will end by 2030. The nuclear power plant (NPP) dismantlement and decontamination market has begun to form, and the necessary technologies are needed accordingly.

This study is to develop the pilot-scale (1.2 m^3/hr) decontamination technology of soil using high pressure washing and ultrasonic process in the decommissioning NPP.

2. Field Survey and Method

2.1 Field Survey

The system is a technology developed to secure decontamination technology in advance for contaminated soil generated by the Kori #1, NPP, which will be dismantled for the first time in the country. Therefore, the target, which are the basic data of the development of the soil-contaminated process, were collected and analyzed twice for soil near the Kori #1, NPP.

Fig. 1. Sampling point of Kori #1, N.P.P.

2.2 Analysis

The sampled soil was analyzed by commissioning an external testing agency with respect to pH, electrical conductivity, moisture content, organic content, pore rate and cation exchange ability.

Table 1. Analysis data of soil in the NPP

Category		result	
pH		7.2	
Conductivity		0.094 dS/m	
Water %		1.90%	
Organic %		3.21%	
Porosity		36.2%	
C E C	Ca	9.33 cmol /kg	7.80 cmol /kg
	Mg		1.15 cmol /kg
	Na		0.27 cmol /kg
	K		0.11 cmol /kg

3. Pilot-scale Soil Decontamination System

3.1 Selection of the Decontamination Process

Fig. 3 shows a schematic diagram of the soil decontamination process to be developed. The soil is firstly decontaminated by high-pressure vortex washing process, and considering the contamination degree of each soil classified by particle size, the soil with high radioactivity is additionally subjected to the combined process of ultrasonic & degassing membrane process to carry out entire decontamination.

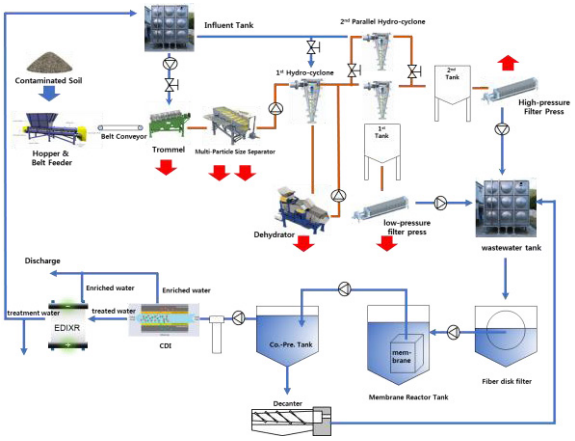

Fig. 2. Schematic Diagram of Pilot-scale Soil Decontamination Process.

3.2 Design the Technology

First, contaminated soil removes large contaminants through the trommel. Next, the particles are separated by particle size through a multi-stage separator and a hydro cyclone. The soils separated from the micro-soil are separated from the soil and water by filter press. The separated water moves through the deconta-mination process to the subsequent water treatment process. The water is cleanly filtered through the disk filter and membrane, and the ionic nuclides are removed through CDI and EDI to finally discharge the reusable water.

4. Conclusion

Pilot-scale Soil decontamination system (1.2 m^3/hr) to prepare for the dismantling of nuclear power plants in Korea can improve their technological capabilities by securing original technologies. In addition, the cost can be expected to be reduced by reducing radioactive waste generated during the dismantling of nuclear power plants, which is expected to grow further if the market is expanded overseas.

ACKNOWLEDGEMENT

This work was supported by the Korea Institute of Energy Technology Evaluation and Planning (KETEP) granted financial resource from the Ministry of Trade, Industry and Energy, Republic of Korea (No. 20181510300800)

REFERENCES

[1] Sang-min Park et al., “Influence of Physico-chemical Properties on Cesium Adsorption onto Soil”, Journal of Soil Groundw. Environ., 22(1), 27-32 (2017).

Study on Activation Evaluation of the Kori unit 1 Bioshield Concrete

Ju-Young Yoon* and Young Hwan Hwang

KHNP Central Research Institute, 70, Yuseong-daero 1312beon-gil, Yuseong-gu, Daejeon, Republic of Korea

*august63@khnp.co.kr

1. Introduction

The first step to prepare for the cutting process for disassembly of the Kori Unit 1 is to evaluate the release.

The focus of this activation evaluation is accurate modeling of the structure and evaluation of the full cycle.

This is because the difference in the small information of the structure may be significantly different from the evaluation result and bioshield concrete of the Kori unit 1 used for 1 to 32 cycles.

2. Structure Modeling

In order to evaluate the correct activation evaluation, we analyzed the structure of the Kori Unit 1.

We analyzed the effects of nuclear fuel, reactor vessel, reactor vessel internals, and surrounding structures on the bioshield concrete.

Structural modeling was performed using the MCNP 6 code. The results are shown in Fig 1.

Critical evaluation was performed using the KCODE option in the MCNP 6 code calculation and the ENDF / B-VII.1 nuclear data library was used.

In the three - dimensional MCNP 6 model for each cycle, only the information of the nuclear fuel assemblies of the inner and outer regions of the core was modified and evaluated.

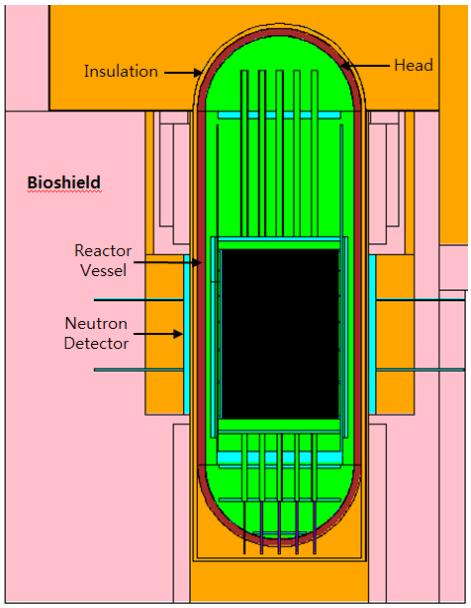

Fig. 1. Modeling of the Kori Unit 1.

3. Activation Evaluation

3.1 Neutron Flux Calculations

During the total of 32 cycles, the neutron irradiation of the Kori Unit 1 resulted in the activation of the surrounding structures of the reactor. So flux was calculated for 1 to 32 cycles.

The neutron flux evaluation was performed with the MCNP 6 code. As a result, the core part is about 1.0E+13 #/cm^{2}·s, and it is decreased to 1.0E+03 #/cm^{2}·s to fall down.

The neutron flux in the upper and lower parts was very low and almost no spinning occurred.

Most neutrons are located in the center of the core, and the distribution of neutrons becomes smaller toward the outside.

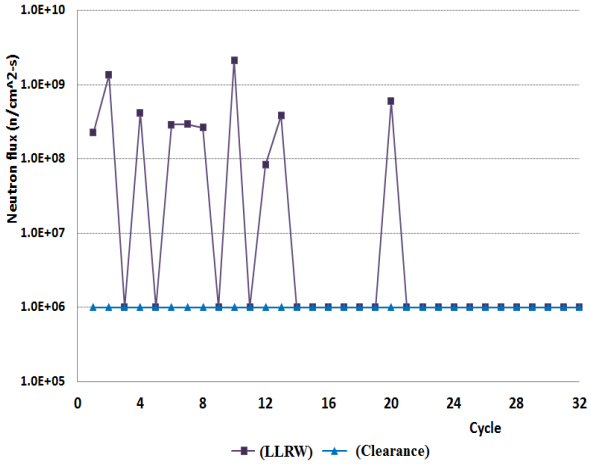

Fig. 2. Neutron Flux Distribution.

3.2 Activation Evaluation of the Bioshield Concrete

Based on the neutron fluxes obtained for a total of 32 cycles, specific activity was calculated by performing ORIGEN-S code of positional activation evaluation.

Activation evaluation was performed at this point in anticipation of decommissioning after a cooling period of 10 years after the shutdown.

The results of the specific activity are shown in the Table 1 below.

Table 1. The results of activation assessment

Structure	Mass(kg)*	Total Activity(Bq)	Classification
Core center part	63,920	6.36E+09	VLLW
the other part	506,080	1.58E+09	Clearance
	570,000	7.94E+09	

* Assuming a total of 570 tons

Based on the neutron flux and specific activity calculated for each structure location, the waste classifications of the bioshield concrete were classified and the mass and total activities were calculated.

4. Conclusion

The computational system for the activation evaluation computes the neutron flux and specific activity using the MCNP 6 and ORIGEN-S codes and classifies the waste classifications.

The calculations show that the concrete adjacent to the center of the reactor core is classified as very low level radioactive waste(VLLW), and the other parts are classified as clearance wastes.

The results of the activation evaluation need to be verified through some sampling performed in the future. For accurate evaluation, it is necessary to perform sample such as coring and to analyze the radioactivity.

REFERENCES

[1] I.C. Gauld, O.W. Hermann, R.W. Westfall, ORIGEN-S: SCALE System Module to Calculate Fuel Depletion, Actinide Transmutation, Fission Product Buildup and Decay, and Associated Radiation Source Terms, ORNL/TM-2005/39, Ver.6, Vol.II, Sect. F7, Oak Ridge National Laboratory (2009).

[2] J.T. Goorley, et al., Initial MCNP6 Release Overview - MCNP6 version 1.0, LA-UR-13-22934, Los Alamos National Laboratory (2013).

[3] J.C.Evans, E.L.Lepel, R.W.Sanders, C.L.Wilkerson, W.Silker, C.W.Thomas, K.H.Abel, D.R.Robertson, Long-Lived Activation Products in Reactor Materials, NUREG/CR-3474 (1984).

A Study for Dismantling Method of Bio-shield in Kori Unit 1 Nuclear Power Plant

Kwang-Soo Park[1,*], Han-Sol Im[1], Hee-Dong Sohn[1], and Ju-Young Yoon[2]

[1]Doosan Heavy Industries & Construction, 22, Doosan volvo-ro, Seongsan-gu, Changwon-si, Gyeongsangnam-do, Republic of Korea

[2] KHNP Central Research Institute, 70, Yuseong-daero 1312beon-gil, Yuseong-gu, Daejeon, Republic of Korea

[*]kwangsoo.park@doosan.com

1. Introduction

In general, after the contaminated components and structures in reactor building are dismantled, the bio-shield concrete will be dismantled. Caused by the activated structures, it is necessary to consider dismantling technology as other activated ones like reactor pressure vessel and internals – from activation evaluation to mockup test using actual size of the bio-shield in nuclear power plant.

Under the above background, the dismantling test was performed using the mockup.

2. Dismantling Test of Bio-shield

2.1 Preparation of Mockup

The shape of the bio-shield is a rectangular parallelepiped having a hollow cylindrical shape in the middle. The typical size is 9 m length, 9 m width and 11 m height as shown in Fig.. 1.

The mockup is designed and manufactured based 1/4 part of the bio-shield and actual one of width and length. Fig. 2 shows the designed and manufactured concrete mockup. The bio-shield was manufactured with concrete having about 3,000 psi compressive strength, and the rebar was installed based on the as built drawing.

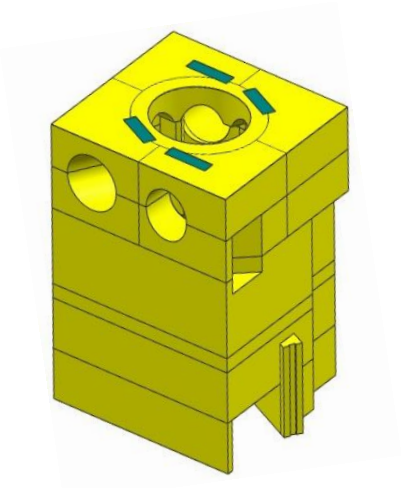

Fig. 1. Bio-shield of Kori unit 1.

Fig. 2. The manufactured bio-shield mockup.

2.2 Dismantling Test Plan

Because the bio-shield is activated by the neutrons, it is necessary to decontaminate and dismantle only the activated area in it. In order to develop the dismantling technology, a test plan should be set-up. Fig. 3 shows the test plan.

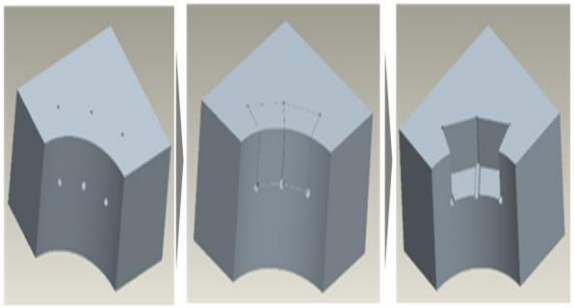

Fig. 3. Mockup test plan.

The activated depth to the radial direction is assumed to be about 1 m. The size of the concrete structure to be removed cutting was set to 1m in width, height and height. And cutting method is coring and wire saw. The coring and wire saw method are known to cut the rebar and concrete structure together. The reason for the need for coring is to create a path through which the wheel for wire saw cutting can be driven. All cutting operations are performed using a dry method because tritium is well soluble in water.

2.3 Test Result

Table 1 shows the result of test.

The horizontal coring is applied by dry method. As a result, the cutting speed is about 8 mm/min. The slow cutting rate is due to the work of crushing the internal core concrete using a breaker after cutting. Therefore, in order to dismantle the bio-shield of the Kori unit 1, it is necessary to develop the customized device.

The wire saw method is applicable to both pulling and pushing methods. The pushing cutting speed is slower than the pulling one. This is thought to be the effect of the shape to be cut during cutting.

Dust is collected more than 90% in total. This means that about 10% of the contaminated dust that is generated is diffused. Therefore, the customized dust collection device and the ventilation device are necessary to dismantle the bio-shield.

Table 1. Result of test

Item	Drilling	Coring	Wire Saw		
method	Vertical	Horizontal	Pushing	Pulling	Pulling
Speed (mm/min)	273.9	7.8	60.2	119.9	75
Dust Recovery Rate (%)	93	100	89	93	93
Work Time(min)	32.2	289.5	90.8	42.2	57.4

3. Conclusion

The dismantling test was performed using the mockup. It is confirmed that coring and wire saw methods can dismantle contaminated concrete structures. Also, in order to dismantle the bio-shield of the Kori unit 1 safely, customized device such as dust collection and ventilation and so on need to be developed.

ACKNOWLEDGEMENT

This research was supported by a grant from Technology Program Funded by KHNP(Korea Hydro & Nuclear Power).

REFERENCES

[1] CPD, “Decontamination and dismantling of radioactive concrete structures”, NEA /RWM/R(2011)1, (2011).

5분과

제염해체 (Poster)

The Implementation Strategy of Stakeholder Involvement Plan for Decommissioning of Nuclear Facilities

KwanSeong Jeong*, DaeSeo Koo, InHye Hahm, JaeHyun Ha, SangBum Hong, and BumKyoung Seo
Korea Atomic Energy Research Institute, 111, Daedeok-daero 989beon-gil, Yuseong-gu, Daejeon, Republic of Korea
*ksjeong1@kaeri.re.kr

1. Introduction

The impacts of closure at the end of a nuclear facility's design life are both national and local, and open dialogue and communication should be established between the operator, regulator and local stakeholders early in the process. Decisions regarding closure of nuclear facilities, particularly reactors, are usually taken as part of national energy policy. Involvement of all stakeholders is therefore essential.

Internal and external communication is equally important. Effective internal communication can help to build a team that clearly understands the different yet equally demanding roles of experts. Effective external communication can present the expertise of the organization to broad external audiences. Good communication cannot guarantee success, as safe nuclear management is the basis on which public confidence is built. Communication can reduce the risk of needless conflict that arises when otherwise acceptable nuclear events are not understood by the public, when they do not see problems being addressed or when people feel their opinions or concerns are not being treated respectfully.

2. Development of a Strategy for Stakeholder Involvement

An important aspect in developing a strategy is knowing the knowledge and opinions of the general public and other stakeholder groups regarding the nuclear facility/program being considered. Thus, the use of opinion polls and surveys should be considered. This also highlights the importance of having the right mix of skills in the team that will be involved in the stakeholder involvement program from the beginning. In the past, nuclear technology professionals have taken the lead in such program, and have underestimated the need for including professionals in social sciences such as communication, opinion surveys and organizational psychology as members of the team. The effectiveness of the program has suffered as a result.

3. Development of a Stakeholder Involvement Plan

Timing is essential to successful integration of stakeholder involvement in a nuclear project's decision making processes. If stakeholders do not have the opportunity to provide early input, they may believe that their participation was superficial or that their interests were ignored or worse, that they were being patronized. The public and other stakeholders need to be provided initial information about a project and its related implications and decisions before their input is sought; otherwise, stakeholder input may fail to address questions that would prove useful to the decision making process. The plan should be updated as necessary but at least annually

to reflect changes in the project, the decision process and evolving stakeholder populations

4. Implementation and Adjustment of the Stakeholder Involvement Plan

Stakeholder involvement should be an integral part of the management of nuclear facilities/program from their conception through final closure and decommissioning. Thus, implementation of the plan will need to include mechanisms to continually monitor the effectiveness of the program and make changes and improvements based upon the results of this evaluation. The most important criteria for this evaluation are whether or not the strategic objectives of the program are being achieved. Where the evaluation steps identify shortcomings in stakeholder satisfaction or process outcomes, it is important to continue development of new tools and involvement techniques. These can often be developed in cooperation with stakeholders, an approach that is highly recommended, wherever feasible, in the nuclear program itself may require a through revision of the communication plan. Regardless of the scope of adjustment, nuclear communication with stakeholders must continue to be implemented even while it is continually adjusted in a disciplined and deliberate manner.

5. Conclusions

Decisions regarding any type of nuclear facility have typically received considerable attention of the public and other stakeholders. Regardless of the stage in the life cycle of the nuclear program properly addressing stakeholder needs and concerns improves the probability of program success. Engaging stakeholders as early as possible and with ongoing attention is essential, including helping stakeholders to understand the extent of their involvement and responsibility in decision making processes regarding these nuclear facilities/program.

There is no one ideal model for stakeholder involvement. The stakeholder involvement strategies and approaches depend on the nature of the nuclear facility, the point in its life cycle, cultural and legal norms and other factors. Continual assessment of the stakeholder involvement program is necessary to ensure that it continues to achieve its goal and objectives, as well as to determine if these objectives continue to be relevant. Active involvement of stakeholders in evaluation of the program is strongly encouraged.

Underwater Laser Cutting for Dismantling Nuclear Facilities

Jae Sung Shin*, Seong Yong Oh, Hyunmin Park, Gwon Lim, Taek-Soo Kim, Lim Lee, Chin-Man Chung, and Jonghwan Lee

Korea Atomic Energy Research Institute, 111, Daedeok-daero 989beon-gil, Yuseong-gu, Daejeon, Republic of Korea

*jsshin12@kaeri.re.kr

1. Introduction

Laser cutting technology has many advantages in dismantling nuclear facilities. For application to this field, it is necessary not only to be able to effectively cut thick steel, but also to be capable of underwater cutting. In our laboratory, the laser cutting technology was developed with a high power fiber laser and a cutting technique capable of cutting about 15 mm thickness per kW was achieved by performing a study of cutting thick stainless steel and carbon steel plates in air [1-4]. Subsequently, an underwater cutting head was developed and cutting studies have been conducted [5]. In this paper, the experimental results of the underwater cutting was summarized. It was obtained with a 6-kW fiber laser as a cutting source.

2. Experimental Procedure

The underwater laser cutting is performed in the following order. First, place the specimen in the water tank and place the cutting head above the water surface. A small assist gas flows out of the nozzle to prevent water from entering the nozzle, then lower the cutting head to the underwater cutting position. Next, a large amount of assist gas is jetted out of the nozzle and the laser is turned on. The head moves and cutting of the specimen begins.

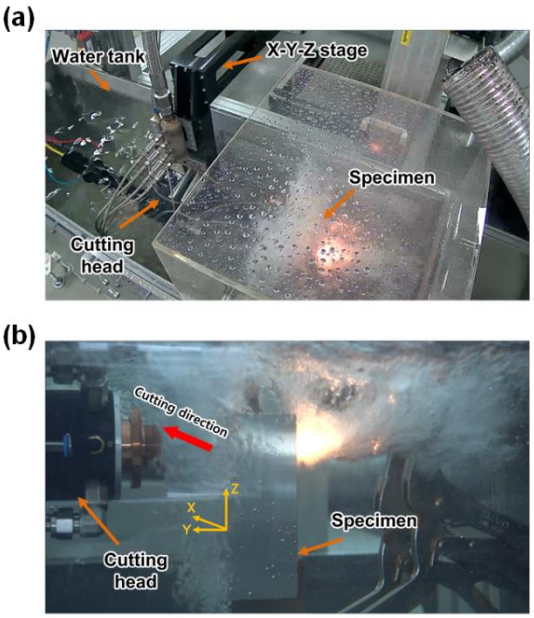

Fig. 1. Views of the underwater laser cutting experiment: (a) whole view, (b) partial side view.

Fig. 1 shows the views of the underwater laser cutting experiment. Fig. 1(a) shows the whole view and Fig. 1(b) shows a partial side view of the cutting progress. The cutting head was completely submerged during the cutting process.

3. Experimental Results

The maximum cutting speeds were measured to be 80 mm/min for the 50 mm thickness and 40 mm/min for the 60 mm thickness. As in ordinary laser cutting, the kerf widths were narrow. For the cutting at each maximum speed, the kerf widths for the 50 mm thickness were 1.6 mm for the front surface and 0.7 mm for the rear surface, and the kerf widths for the

60 mm thickness were 1.5 mm for the front surface and 1.2 mm for the rear surface.

4. Conclusion

Underwater cutting of 50 and 60 mm thick stainless steel plates with a 6-kW fiber laser was performed as a fundamental study for application to dismantling nuclear facilities. It is expected that the results of this study will contribute to the continued development of underwater cutting research for dismantling nuclear facilities.

ACKNOWLEDGEMENT

This research was supported by the Nuclear Research and Development Program through the National Research Foundation of Korea (NRF), funded by the Ministry of Science and ICT (grant no.: NRF-2017M2A8A5015146), Republic of Korea.

REFERENCES

[1] J. S. Shin, S. Y. Oh, H. Park, C.-M. Chung, S. Seon, T.-S. Kim, L. Lee, B.-S. Choi, and J.-K. Moon, “High-speed fiber laser cutting of thick stainless steel for dismantling tasks,” Optics and Laser Technology, 94, 244-247 (2017).

[2] J. S. Shin, S. Y. Oh, H. Park, C.-M. Chung, S. Seon, T.-S. Kim, L. Lee, and J. Lee, “Laser cutting of steel plates up to 100 mm in thickness with a 6-kW fiber laser for application to dismantling of nuclear facilities,” Optics and Lasers in Engineering, 100, 98-104 (2018).

[3] S. Seon, J. S. Shin, S. Y. Oh, H. Park, C.-M. Chung, T.-S. Kim, L. Lee, and J. Lee, “Improvement of cutting performance for thick stainless steel plates by step-like cutting speed increase in high-power fiber laser cutting,” Optics and Laser Technology, 103, 311-317 (2018).

[4] J. S. Shin, S. Y. Oh, H. Park, C.-M. Chung, S. Seon, T.-S. Kim, L. Lee, and J. Lee, “Cutting performance of thick steel plates up to 150 mm in thickness and large size pipes with a 10-kW fiber laser for dismantling of nuclear facilities,” Annals of Nuclear Energy, 122, 62-68 (2018).

[5] J. S. Shin, S. Y. Oh, H. Park, T.-S. Kim, L. Lee, C.-M. Chung, J. Lee, “Underwater cutting of 50 and 60 mm thick stainless steel plates using a 6-kW fiber laser for dismantling nuclear facilities,” Optics and Laser Technology, 115, 1-8 (2019).

Simulation Modeling for Planning a Soil Remediation Process

David Kessel, Chang-Lak Kim, Jihan Jeon, and Eui-taek Lee

KEPCO International Nuclear Graduate School, 658-91, Haemaji-ro, Seosaeng-myeon, Ulju-gun, Ulsan, Republic of Korea

1. Introduction

This paper describes the development of a simulation model that can be used for logistics planning for soil remediation at the Kori 1 reactor site. A FlexSim discrete event simulation model of the site soil remediation and waste management process was developed to support optimization of performance, resources, and time and to minimize nuclear waste.

Operation of a nuclear power plant may result in the release of radioactive materials to the soil and groundwater at the site. Small radioactive releases may not be discovered until the NPP undergoes decommissioning [1].

Nuclear power plant site remediation is performed after site structures have been removed and is the last step in decommissioning. Remediation may be required remove contamination from the site soil to allow the reuse of the site subject to the regulatory requirements for site release.

2. Development of the Simulation Model

In this study we modeled the soil washing process shown as Module 2 Contaminated Soil Treatment (Fig. 1).

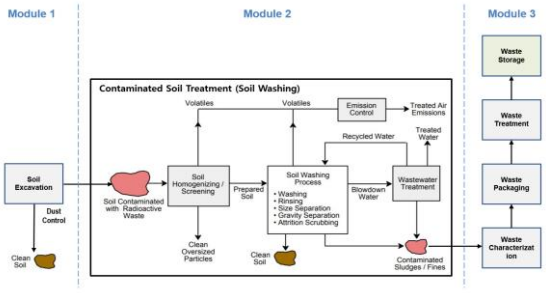

Fig. 1. Soil Washing Process Model [1].

The soil washing process recommended by the US EPA for removal of radionuclides was chosen as the basis for the soil washing process model (Fig. 2) [2]. A simulation model of the soil washing process was developed using Flexsim, a discrete-event simulation modeling application that is widely used in industries such as material handling, manufacturing, logistics, transportation, and mining [3]. The model was operated as a batch process rather than a continuous process because it may be necessary to meet radioactive waste management requirements that prohibit mixing of wastes with different classifications.

Soil particle size distribution data collected by KAERI at the Kori site was used as input data [4]. The simulation model has several simplifying assumptions as follows: Fifteen tons of soil can be treated per a batch. The system has 240 tons/day processing capacity under 8-hour operation a day. The system has enough capacity to operate without bottlenecks and there are no unplanned shutdowns due to equipment failure or maintenance.

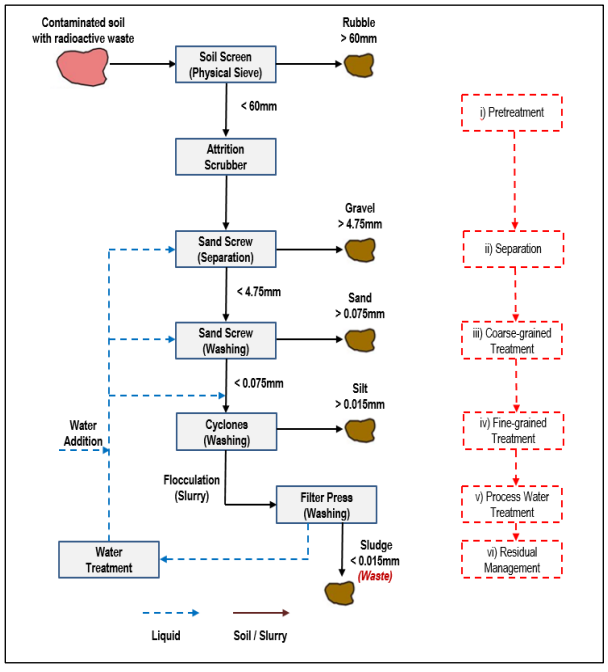

Fig. 2. Detailed Soil Washing Process Model [2].

Fig. 3 shows the soil washing FlexSim model. The excavated soil from the contaminated site is fed to the feed hopper on the left side of the Fig. 3, and the soil that has been cleaned through dry separation is sent to each queue according to the grain size i.e. rubble, gravel, sand, silt and sludge/clay.

In this study, the simulation model was verified by checking the output of the simulation. In the simulation, we can observe the soil washing process and the waste throughput. Once the simulation starts, 30 tons of soil per hour are supplied to the feed hopper and the soil washing system operates at 36 tons per hour. Due to the difference between the soil excavation rate and process rate, this system can be maintained as a 1-hour batch process.

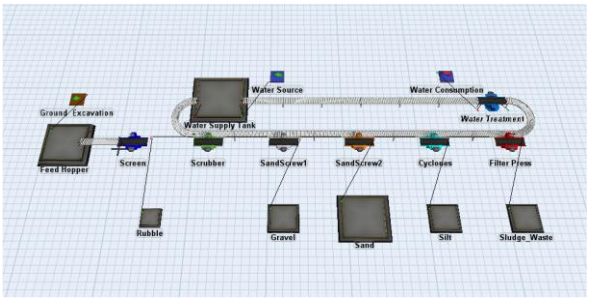

Fig. 3. Logistical Simulation of Soil Washing Process.

Table 1 shows the process results after 2 hours of operation. The results show that the process output is approximately equal to the input meaning the simulation is operating correctly according to the intended logic. The model generates detailed processing data as a numerical table or graphical chart as shown in Table 1 and Fig. 4.

Table 1. Simulation Results at 2 Hours of Operation

Queue	Rubble	Gravel	Sand	Silt	Sludge	Total
Processed Soil (ton)	0.588	3.111	50.031	2.354	3.916	60.000
Ratio (%)	0.98%	5.19%	83.39%	3.92%	6.53%	100.00%
Input Data (%)	1.0%	5.3%	83.4%	3.9%	6.4%	100.00%
Error (%)	-2.00%	-2.08%	-0.01%	0.51%	2.03%	-

The system is shown to be operating in a batch process as seen in Fig. 4 which shows that the soil in the feed hopper accumulates and is emptied repeatedly. The State Pie diagram in Fig. 4 shows utilization of the system equipment elements.

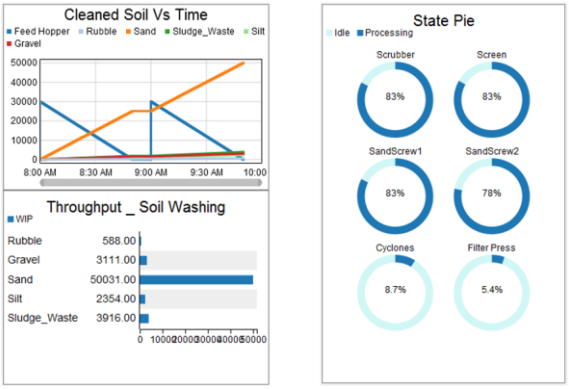

Fig. 4. Graphical Report for Soil Washing (at 2 hours).

3. Conclusions

In this study, we investigated the applicability of discrete event simulation for a soil washing process for planning site remediation. It was shown that a batch process such as soil washing can be effectively modeled as a discrete event process. Efficient allocation of resources and efficient waste management including volume reduction can be achieved by use of the model for planning the soil remediation process. Furthermore, we suggest extending the scope of the simulation model to include excavation and waste management as shown in Fig. 1 (Module 1 and 3).

ACKNOWLEDGEMENT

This research was supported by the Nuclear Safety Research Program through the Korea Foundation of Nuclear Safety (KOFONS), granted financial resource from the Nuclear Safety and Security Commission (NSSC), Republic of Korea (No. 1605008).

REFERENCES

[1] U.S. Environmental Protection Agency, “Technology Reference Guide for Radioactively Contaminated Media,” Oct. 2007.
[2] U.S. Environmental Protection Agency, “Soil Washing/Soil Flushing Volume 3,” U.S. Environmental Protection Agency, EPA 542-B-93-012, Nov. 1993.
[3] “FlexSim User Manual.” Flexsim Software Products, Inc., Apr-2017.
[4] Bumkyeong, Seo, et al., “Development of Site Remediation Technology for Decommissioning and Contaminated Site,” Korea Atomic Energy Research Institute, Daejeon, Korea, KAERI/RR-4233/2016, 2017.

Development of Decommissioning Process of the Kori Unit 1 Reactor Vessel Internal Using Full-scale Mockup

Sunghoon Hong* and Young Hwan Hwang
KHNP Central Research Institute, 70, Yuseong-daero 1312beon-gil, Yuseong-gu, Daejeon, Republic of Korea
*Sunghoon.hong@khnp.co.kr

1. Introduction

Since permanent shutdown of the Kori unit 1 was determined in 2017, the importance of decommissioning technology has been emphasized. Development of segmentation and dismantling process for reactor vessel internals (RVI) is mightily important in comparison with other component of the nuclear power plant. The large component was highly activated by the neutron during the commercial operation. Accordingly, it could be the time-consuming process in the decommissioning. And the decommissioning of the Kori unit 1 is expected to be at least 15 years from the decommissioning preparation to the site remediation [1]. Therefore, the development of decommissioning process using the mockup, which is similar to the actual scale of RVI, is necessary to confirm the applicability of segmentation technology, the minimize worker exposure in the radiation environment and the work efficiency for decommissioning schedule.

In this study, the development of dismantling process for the Kori unit 1 RVI using the full-scale mockup will be discussed.

2. Design of RVI Mockup

The reactor vessel internals, which is a representative component of nuclear power plant, is massive, complicated and significantly activated. The reactor internal consist of thermal shield, core barrel, core flange, baffle plate assembly, core support forging, lower core plate, secondary core support assembly ,and etc. The RVI of the Kori unit 1 is a stainless steel (STS304) structure with an outer diameter of about 3.1 m, a height of about 9.4 m, weight of 120 ton and a maximum thickness of about 340 mm.

To verify the applicability for promising segmentation and dismantling technology, the RVI mockup is being fabricated in a size and material that is similar to that of the Kori unit 1 as shown in Fig.1 and Fig.2.

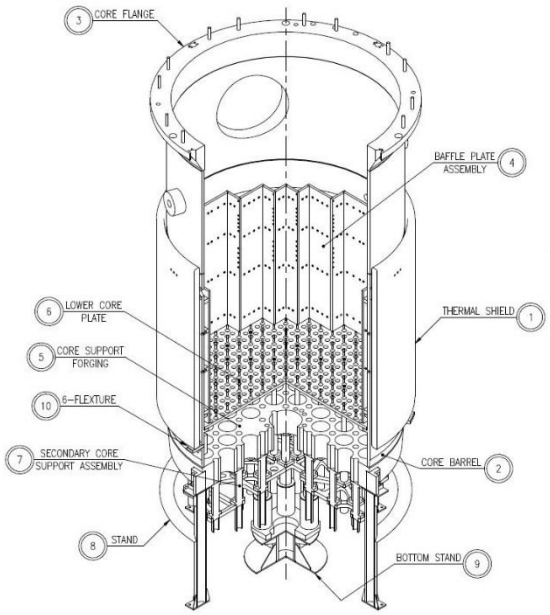

Fig. 1. Design of the Kori unit 1 RVI mockup.

Fig. 2. Mockup of (left) core support forging and (right) secondary core support.

3. Development of Decommission Process

The RVI components of the Kori unit 1 are fastened by bolts and nuts. For efficient cutting process, components are dissembled by removing the fastener. And then, each components will be cut off by promising cutting technology which is considered with respect to the thickness, the design, and degree of activation. The promising cutting technologies and target component for the Kori unit 1 summarized in Table 1 and Fig. 3. Because of high activity caused by neutrons, the dismantling process should be conducted underwater using lower cavity and upper cavity. The decommissioning of the mockup will be performed as following the procedure in Table 2.

Table 1. Promising cutting technologies [2]

Tech.	Advantage	Consideration
Band saw	No gas/Fume	Under water process Short lifetime
Fine plasma	Thick plate available Fast	Filter system Shielding gas Cooling system
CAMC	Various shape cutting Fast	Under water process Long lifetime Thick plate available

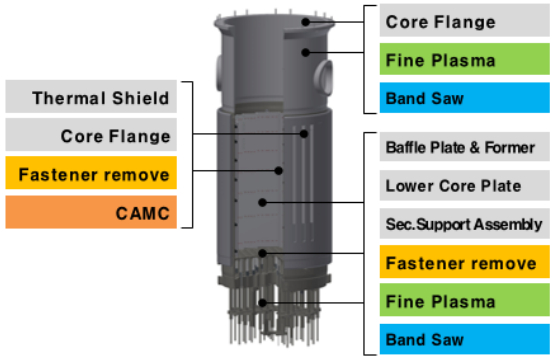

Fig. 3. Applied dismantling technology for RVI.

Table 2. Concept of procedure for RVI decommissioning

Lv. 1	Lv. 2	Process
1		Preparation
	1.1	Document
	1.2	Plan
	1.3	Equipment setup
2		Conduct
	2.1	Upper RVI seg. & dismantling.
	2.2	Lower RVI seg. & dismantling.
	2.3	Capture the sec. waste
	2.4	Check the foreign in cavity
3		Clean up
	3.1	Removal internals
	3.2	Removal workstation
	3.3	Removal equipment
	3.4	Move the container
	3.5	Remover filter system
	3.6	Clean up for etc.

4. Conclusion

To develop the segmentation and dismantling process for the decommissioning of the Kori unit 1, the full size mockup for RVI is being fabricated. The performance of mockup test will be considered with respect to the applicability of promising cutting technologies, the feasibility of the procedure, and the workability underwater.

ACKNOWLEDGEMENT

This work was supported by the Korea Institute of Energy Technology Evaluation and Planning (KETEP) and the Ministry of Trade, Industry & Energy (MOTIE) of the Republic of Korea (20161510300430)

REFERENCES

[1] Y.H. Hwang, “Conceptual Design for Kori Unit 1 Reactor Vessel and Internal Segmentation Process”, Proc. Of the KRS 2017 Fall Conference (2017).

[2] R. Heim, Evaluation of Technologies for Segmentation of Reactor Vessel Internals, EPRI Technical Report (2017).

Radiation Shielding Evaluation for Existing Transport Container Containing Decommissioning Waste of KORI Unit 1

Jae-Hun Ko[1, *], Dong-Gyu Lee[1], Ji-Hoon Lee[2], and Nak-Hoon Sung[1]

[1]Korea Nuclear Engineering & Service, #5, Hyundai Plaza, 798-1 Yuseong-daero, Yuseong-gu, Daejeon, Republic of Korea

[2]KHNP Central Research Institute, 70, Yuseong-daero 1312beon-gil, Yuseong-gu, Daejeon, Republic of Korea

[*]kojh4@kones21.com

1. Introduction

For safe and economic transportation of radioactive wastes generated during decommissioning in the NPP, not only their radiological characteristics but also transportation and conditions of disposal site should be considered. Since most of decommissioning wastes are classified as LLW or VLLW, they can be transported using IP-2 type transport container operating in the NPP. In Korea, radioactive wastes generated from nuclear power plants are mainly packed in 200 or 320 liters drums and then transported to disposal facilities using IP-2 type transport containers. IP-2 type container has the ability to carry eight drums at the same time.

The purpose of this study is to evaluate the feasibility of existing IP-2 container with minor modification for efficient transportation of decommissioning wastes.

2. Shielding Evaluation of IP-2 container

2.1 Dose Rates Criteria

There are several regulations related to radioactive waste transport in the domestic and international laws. Under the Normal transport condition, the dose rate at the surface of the IP-2 transport container is limited to 2 mSv/hr and one at any point 2 m away from the container is limited to 0.1 mSv/hr.

2.2 Source Terms

According to previous evaluation for radioactive nuclide inventory of RV/RVI of the KORI unit 1, LLW/VLLW accounts for about 65% of the activated RV/RVI radioactive waste [1].

The radioactive waste with the highest radioactivity among the low-level wastes generated during decommissioning is the upper core plate of RV/RVI. For conservative evaluation, the upper core plate of RVI is assumed to be the contents of the existing IP-2 type transport container. Since the expected maximum allowable weight of the package used for transportation of decommissioning wastes is 35 tons and the weight of the existing IP-2 container is 3.6 tons, the maximum allowable weight of the contents is 31.4 tons. The calculated radioactivity of the contents in the IP-2 type transport container is shown in Table 1.

Table 1. Radioactivity of Upper Core plate

Nuclides	Specific Activity [TBq/g]	Activity [Bq]
Fe-55	1.91E-06	6.00E+13
Co-60	7.51E-09	2.36E+11
Ni-59	1.78E-08	5.59E+11
Ni-63	1.88E-06	5.90E+13

2.3 LLW Package

External dimensions of the existing IP-2 transport container are 1.6 m (W) × 3.4 m (L) × 1.2 m (H) and thickness of it is 0.012 m. The upper core plate used as the radiation source is assumed to be uniformly distributed inside the transport container. Fig. 1 shows the model of IP-2 transport container with LLW such as upper core plate of RVI for shielding evaluation. The volume inside the transport container is 6.26 m^3 and the upper core plate is made of stainless steel with a density of 8.03 g/cm^3, so the volume corresponding to 31.4 tons is 3.91 m^3. Therefore, 62.5% of the inside of the container is filled as the contents.

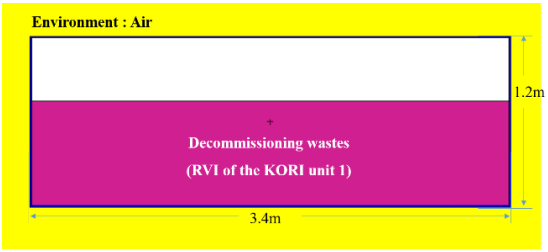

Fig. 1. Shielding Evaluation Model.

2.4 Shielding Evaluation

MCNP5 computer code using the three-dimensional Monte Carlo method has been used to calculate dose rates at the various desired locations of the IP-2 type transport container [2]. The flux-to-dose conversion factor was added to the input data so that it could be expressed as the dose rate at the locations of interest. The dose conversion factors used in this calculation was taken from ICRP-74 (1996) [3].

3. Shielding Evaluation Results

In this MCNP calculation, 15 detectors were placed at the external surface and 2 m position of the IP-2 transport container, respectively. Table 2 shows the maximum dose rates at all positions and Fig. 2 shows dose rates at calculated points for the top and side of the IP-2 transport container. Relative errors of these detectors were 0.01~0.02.

Table 2. Dose Rates Results for IP-2 Container

[Unit : mSv/hr]

Cal. Point	External Surface		2 m from the Surface	
	Results	Limit	Results	Limit
Top	2.113	2.0	0.422	0.1
Side	2.396		0.285	

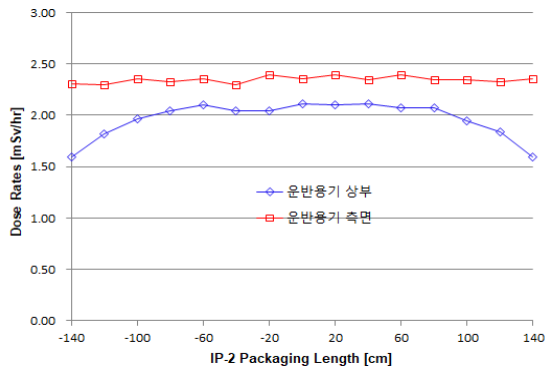

(a) Dose rates at External Surface

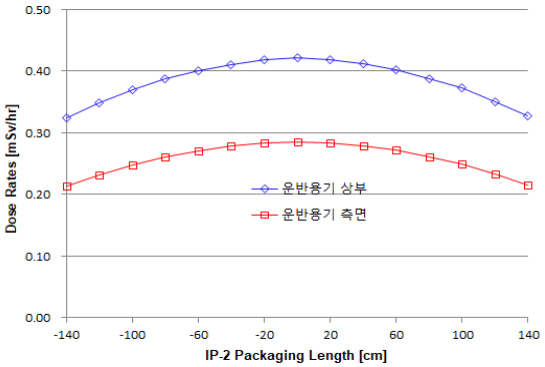

(b) Dose rates at 2 m form the Surface

Fig. 2. Results of Shielding Evaluation.

4. Conclusion

Radiation shielding evaluations for existing IP-2 transport container containing LLW such as RVI of KORI unit 1 were performed. Existing IP-2 transport container containing the upper plates among RVI didn't satisfy the radiation dose limits under normal transport condition. Therefore, in order to use existing containers for efficient transport of bulk decommissioning waste, additional shielding and/or conditioning such as solidification should be reflected.

ACKNOWLEDGEMENT

This work was supported by the Korea Institute of Energy Technology Evaluation and Planning (KETEP) generated financial resource from the MOTIE, Republic of Korea. (No.20181510300870)

REFERENCES

[1] KHNP, Evaluation report on the decommissioning source term and the quantity of radioactive waste of the PWR and CANDU reactor, (2016).

[2] Los Alamos National Laboratory, MCNP –A General Monte Carlo N particle Transport Code, Ver.5, Release 1.40(2005).

[3] ICRP, Conversion Coefficients for Use in Radiological Protection Against External Radiation, ICRP-74(1996).

Event/accident Simulation Model of the Reactor Pressure Vessel Internal Segmentation Activity

Chang-Su Nam* and Byung-Sik Lee

Dankook University, 119, Dandae-ro, Dongnam-gu, Cheonan-si, Chungcheongnam-do, Republic of Korea

*72180291@dankook.ac.kr

1. Introduction

Though the occurrence of accidents caused by technical problems has been reduced due to the development of various technologies, accidents caused by human error still relatively high. Therefore, task analysis and related performance shaping factors were derived in the previous study [1], in order to reduce the human error for the decommissioning activity, such as the reactor pressure vessel internal segmentation. In this paper, the event/accident simulation model on the reactor pressure vessel internal segmentation is described how to make it step by step.

2. Event / Accident Simulation Model

The event/accident simulation model refers to a model of variables for event/ accidents that may occur in the reactor pressure vessel internal segmentation. It is possible to understand the influence relationship between events and accidents that may occur based on the performance shaping factor derived from the eight task analysis of the reactor pressure vessel internal segmentation [1]. In this paper, an event/accident simulation model for "Human" has been developed, which is one of level 1 performance shaping factor for the reactor pressure vessel internal segmentation. The performance shaping factors of Level 2 and Level 3 for "Human" are shown in Table 1. A total of three (3) event/accident simulation models such as stress, fatigue, and safety awareness were been developed by integrating the contents of nine (9) Level 3 performance shaping factors.

Table 1. Level 2 and Level 3 performance shaping factors for "Human"

Level 2	Level 3
Psychological State	Stress
	Emotional State
	Safety Awareness
Physical State	Fatigue
	Physical Capability
	Discomfort
Performance Capability	Task Knowledge and Memory
	Experience
	Personal capability

2.1 Event / Accident Simulation Model for Stress

There are various influencing factors in stresss [2]. But in this paper, these factors are limited to the activity of the reactor pressure vessel internal segmentation as follow;

- Stress due to occupation or responsibility during work
- Stress due to possible safety accidents during work
- Stress due to work shift
- Stress due to environmental factors

Fig. 1 shows the relationship between stress and influencing factors.

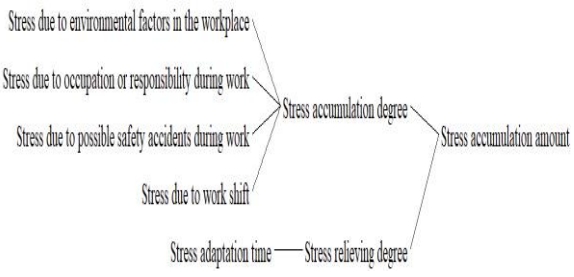

Fig. 1. Relationship between stress and influencing factors.

2.2 Event / Accident Simulation Model for Fatigue

Fatigue also has various influencing factors [3]. But fatigue factors for reactor pressure vessel internal segmentation are selected as follows;

- Fatigue due to Repetitive work
- Fatigue due to work intensity
- Fatigue due to tension during work
- Fatigue due to job accumulation

Fig. 2 shows the relationship between selected fatigue factors.

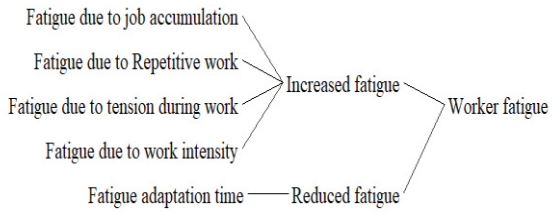

Fig. 2. Relationship between fatigue and influencing factors.

2.3 Event / Accident Simulation Model for Safety Awareness

Safety awareness refers to the cognitive function of the severity of consequences associated with human diagnosis or decision [1]. Therefore, five (5) factors were derived for reduction and increase of safety awareness. Fig. 3 shows the relationship between the five factors.

- Reduced safety awareness
  - About the duration of repetitive tasks
  - Whether the work experience
- Increased safety awareness
  - Safety training for related tasks
  - Compliance with safety regulations and procedures
  - Tension for work

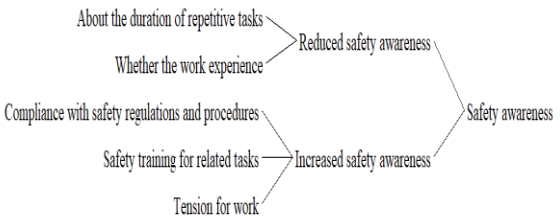

Fig. 3. Relationship between safety awareness and influencing factors.

3. Conclusion

Human error can be caused by various factors. In this paper, the major influencing factors of stress, fatigue, and safety awareness are identified for “Human”, which are the causes of human error. Then an event / accident simulation model is developed based on “Human” factor. Identification of these influencing factors of importance can be used to ascertain which factors are more important to manage due to stress, fatigue, and safety awareness using by VENSIM program [4]. Through further study, an event / accident simulation model will be generated for the entire influencing factors on the reactor pressure vessel internal segmentation.

REFERENCES

[1] Hyun-Jae Yoo, Chang-su Nam, Byung-Sik Lee, “Task Analysis for Decommissioning Activities in Nuclear Power Plants”, Korean Radioactive Waste Society Fall Meeting (2018).

[2] Chang-Il Ahn, Gwi-Yeo-Roo Ahn, Seon-AhYoon, “A Study of Development of Stress Inventory for the Nuclear Power Plant’s Operator” (2008).

[3] Sei-Jin Chang, Sang-Baek Koh, “Correlates of Self rated Fatigue in Korean Employees” J Prev Med Public Health (2005).

[4] Korea Atomic Energy Research Institute, Development of Human Error Countermeasures for Nuclear Safety (2016).

Consideration Factors for Public Dose Assessment During Decommissioning of Nuclear Power Plant

Kwang-Ho Jo* and Su-Hee Lee
KHNP Central Research Institute, 70, Yuseong-daero 1312beon-gil, Yuseong-gu, Daejeon, Republic of Korea
*kwangho.jo@khnp.co.kr

1. Introduction

Kori unit 1, the Korean oldest commercial NPP, was permanently shut down in 2017 and decommissioning activities will be conducted five years later. Also the Wolsong unit 1 is expected to be in decommissioning stage in the near future. KHNP, the licensee, should arrange the full-scale stage plan in order to safely carry out the power plant decommissioning.

A final decommissioning plan (FDP) should be submitted to the regulator with incorporating the results of the public hearings in order to get approval for decommissioning. The safety assessment is one of essential part of the FDP because it describes how exposures of the public are kept as low as reasonably achievable (ALARA) below the relevant limits during decommissioning [1]. However, there is no useful assessment methodology for the public dose assessment in decommissioning stage.

For this sake, we have carried out the review IAEA safety assessment methodology and developed a conceptual diagram that be applicable to the chapter 6. safety assessment part in FDP. Based on this concept, we have analyzed the normal events and abnormal events during the decommissioning, which assessed public dose for each exposure scenario. This paper is to propose considering factors for public dose assessment not only the normal decommissioning activities but also the abnormal events.

2. Considering Factors

Decommissioning stage is different from the operation phase of nuclear facilities in that decommissioning has cutting activities of radioactively contaminated and/or activated components and structures, where radioactive dusts and gas are dispersed into atmosphere.

It is necessary for public dose assessment to estimate the amount of radionuclides released into the atmosphere and the ocean during decommissioning operation. Therefore, it should be assumed in consideration of dismantling activities, residual radioactive inventory, and decommissioning schedule, etc. Fig. 1 shows the conceptual diagram to assess the doses to public in the normal situations and abnormal situations. Each consideration is presented in the Fig.1 as alphabet (a), (b), (c), (d) and described details in the below.

2.1 Amount of Radionuclides Discharged (a)

Two types of waste (gaseous, liquid) are generated and released into atmosphere and ocean according to the dismantling activities. Amount of radionuclides discharged waste are assumed based on the quantity of generating waste and filtration efficiency. The gaseous wastes are only considered in this study.

The amount of gaseous wastes depends on cutting technology, number of cutting pieces, cutting length, etc. Especially, each cutting methods such as plasma arc, thermal cutting, mechanical cutting has respectively different kerf width and dispersion ratio during cutting activities. And the kerf length depends on the type of the container in which the component will be stored. Shapes of components such as piping and ducts also affect the kerf lengths. Therefore these factors need to be considered for the evaluating the amount of gaseous wastes. To calculate the quantity of generating aerosol, the following information is required and total amount of generating wastes (G_{ij}) is simply expressed in the below equation (1) [2].

- G_{ij} of radionuclide i and cutting tool j
- Concentration of radionuclide : C_i (Bq/cm^3 or Bq/cm_2)
- Kerf volume / surface : K_j (cm^3 or cm^2)
- Dispersion ratio of each cutting tool : D_{ij}

$$G_{ij}(Bq) = \sum(C_i \times K_j \times D_{ij}) \quad (1)$$

2.2 Filtration Efficiency (b)

To minimize the radiological hazards, the ventilation systems are installed to prevent the aerosols that are generating from the cutting activities. Also the evaporator systems and resin systems are equipped in the facility to prevent radionuclide release to the ocean. In order to calculate the amount of radioactive material deposited on the filters, the filtration efficiency should be considered.

2.3 Radiological Environment Analysis (c)

If the radionuclide inventory discharged into the environment is calculated, the next step is to assess the public dose that is the same as the existing methodology for the operate phase. Based on the values such as diffusion factor, site characteristics factor, and amount of intake, etc., the public exposure dose can be evaluated.

2.4 Accident Scenario (d)

To draw the potential accident scenario that could occur during the decommissioning activities, the HAZOP process should be performed [2] and it is in progress by an expert group. The typical accidents during decommissioning can be caused by drop, fire, explosion, loss of containment and liquid spill.

The scenario that could lead to the biggest accident is an accident in which all the radioactive material deposited on the filter is released to the atmosphere due to the filter fire. Based on the mentioned factor (b), the amount of radioactive material can be assumed and accident scenario should be conservatively approached to evaluate.

3. Conclusion

In this paper, we reviewed the considerations to assume the radioactive discharge rate. Reasonable assumptions for the sake of safe decommissioning are very important to evaluate the dose of the public. In most cases, for conventional estimation of public exposure dose, the quantity of radionuclides that disperse or migrate over an entire period of decommissioning were assigned to the first year of dismantling work to evaluate public exposure dose [3]. Assuming that all dismantling activities are carried out in one year, we have evaluated the public dose considering the aforementioned factors. And in order to obtain reliable results, actual power plant characteristic data will be applied.

REFERENCES

[1] Nuclear Safety and Security Commission, Regulations of Nuclear Facilities Decommissioning Plan, Notice 2018-10.

[2] Safety Assessment for Decommissioning, IAEA Safety Report Series No.77.

[3] Decommissioning plan of Tokai power station, Japan Atomic Power Company, 2006.

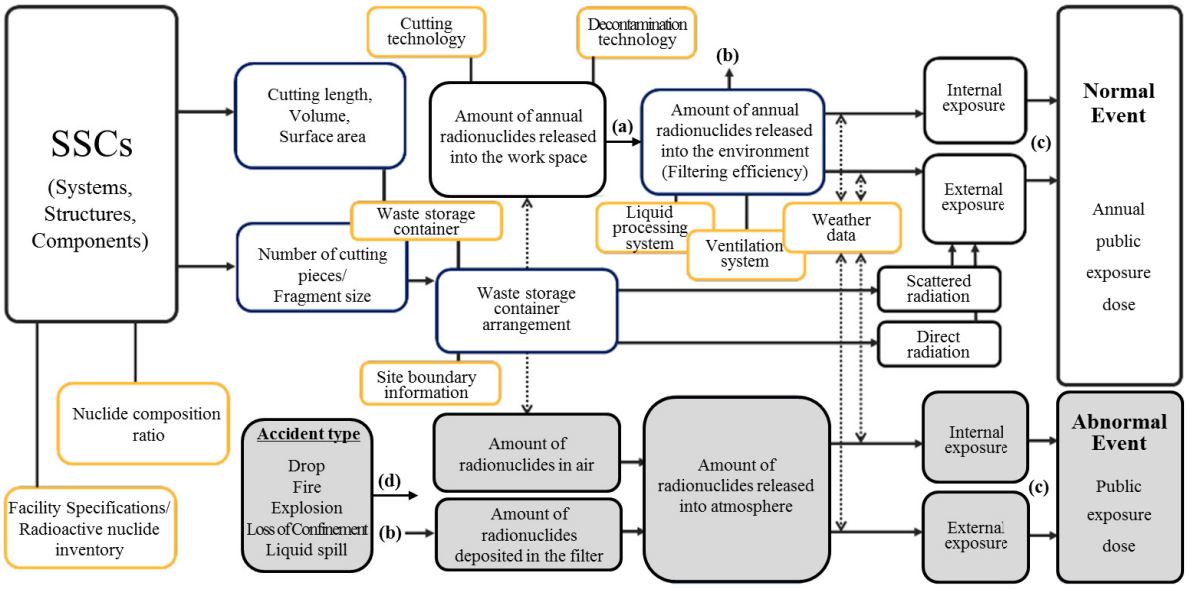

Fig. 1. Conceptual diagram for public dose assessment during decommissioning.

Analyzes the Status of Patents and Utility Models Related to Domestic Self-Disposal

ByeongMok-Park, JeongMi-Lee, AhRan-Cha, CheolWan-Park, Sang Hwan-Jun, DoYeong-Jung, and JaeSeok-Park
SAE-AN ENERTECH CORP, #923, 184, Gasan digital 2-ro, Geumcheon-gu, Seoul, Republic of Korea
pbm@sae-tec.com

1. Introduction

The fields where self-disposal takes place can be divided into nuclear power plant sector and non-nuclear power plants sector.

First, in nuclear power plant sector 23 nuclear power plants are currently operating commercially, and Wolsung Unit 1 is proceeding with the procedure to Reactor shutdown by taking out the fuel rod, and applied to the Nuclear Safety And Security Commission for a change of operation for permanent shutdown on February 28, 2019. In addition, Kori Unit 1 was permanently shutdown on June 18, 2017 and is already undergoing a decommissioning process.[1] The quantity of self-disposal at nuclear power plants will be generated in large quantities during commercial operation and during the decommissioning of nuclear power plants.

The following are non- nuclear power plant sectors: medical institutions, industries, research institutes, educational institutions, public institutions, and military organizations, In particular, medical institutions periodically apply for their self-disposal, and when permission to use facilities is terminated, unlike nuclear power plants, the radiation controlled area is not wide, so select a method to deregulate the facilities.

In this paper, we have identified and analyzed the trends of domestic self-disposal technologies related to the decommissioning of nuclear power plants that are expected to be self disposed of in large quantities in the future. Increase economic effects by reducing the cost of permanent disposal by increasing the amount of self-disposal according to the establishment of self-disposal technology and the direction of future technology development, through high level, intermediate level, low level and extremely low level radioactive wastes will be disposed of safely through the Korea Radioactive Waste Agency, it is expected social effects through changing the public's perception of nuclear facilities.

2. Main Subject

In this paper, the status of patents·utility models registration related to self - disposal registered in the Korean Intellectual Property Office was examined in Patent Information Net KIPRIS. Search method is free search, and among patents·utility models that include one of the four search words 'Radiation', 'Radioactivity', 'Radioactive', 'Nuclear power plant', and searched for registered patents·utility models containing the words 'self' or 'disposal', and a total of 1,363 patents·utility models were searched, among these were 88 patents·utility models related to self-disposal.[2]

For 88 registered patents·utility models related to self-disposal, based on the year of application, the status by annual patentee, by year, by content, by type of waste subject to disposal are shown in Fig. 1, Fig. 2, Fig. 3.

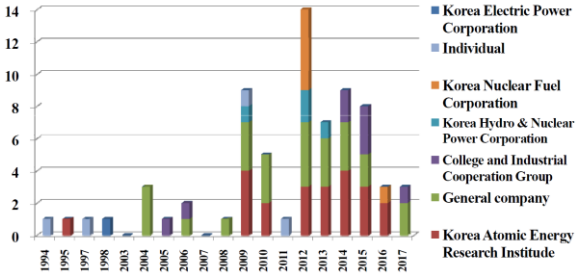

Fig. 1. Application status of patents·utility models by patentee per year caution) If the two organizations have patents together, they are divided by half.

In Fig. 1, shown the status of application by agency from 1994 to the present, general companies that promote self-disposal projects is 32 the number of patents·utility model registration, followed by the Korea Atomic Energy Research Institute (KAERI), which is the research institute, with 28.5, and the university-industry cooperation group with 8.5. In addition, it was confirmed that a total of 12 patents·utility models were registered in 13 years from 1994 to 2007, and 76 cases were registered in 9

years 2008 to 2017. Until 2007, the registration status of patents·utility models related to self-disposal was a low registration rate, but the registration has been steadily carried out since 2008. This is when self-disposal services are ordered from Korea Hydro & Nuclear Power Corporation, companies have begun to develop their self-disposal related technologies in earnest in order to receive their self-disposal service.

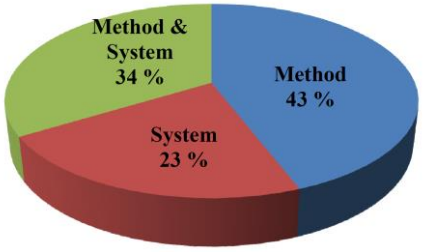

Fig. 2. Application status of patents·utility models by technology content.

Fig. 2. analyzed the technology-specific contents of patents·utility models registered as self-disposal technologies, method (44%) was studied twice as much as the system (23%) and it was found that it was registered as a patent·utility models.

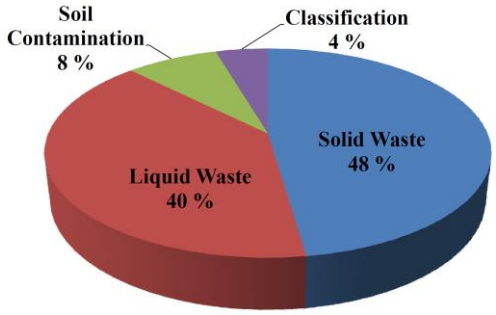

Fig. 3. Application status of patents·utility models by target waste.

Fig. 3. shows that solid waste disposal technology accounts for 48% and liquid waste disposal technology accounts for 40%.

The content covered in this paper is the analysis of the patent and utility model registered in the Korean Intellectual Property Office with the related search terms in the title and text contents.

This method of searching may omit some self-disposal technologies. For example, in case 'A decontamination device inside of pipes contaminated with radioactive material' of the application number (date) 1020150151197 (2015.10.29) developed by SAE-AN ENERTECH CORP., when grinding the inner circumferential surface of the contaminated pipe to a uniform thickness and it is possible to reliably prevent re-contamination due to the by-products of grinding, after decontamination, the piping is self-disposal, which corresponds to its self-disposal technology, but It has been confirmed that omitted from the technical analysis becouse are cases in which the titles and texts do not contain "self" or "disposal"

3. Conclusion

In this paper, it was confirmed that the patent and utility model related to domestic self-disposal are concentrated in the field of decontamination of liquid and solid waste, and the accidents at the Fukushima nuclear power plant increased interest in patent and utility model related to soil contamination.

In addition, there have also been inventions of facilities or devices capable of decontamination using existing technologies and have been many cases where the decontamination method and the apparatus have been registered together.

However, since decontamination methods are registered but the device has not yet been registered, it would be very desirable if the device is developed for the registered patent technology to be actively implemented, and the development of automatic decontamination equipment is also carried out.

In addition, information provided by OPIS(Operational Performance Information System for Nuclear Power Plant) indicates that 168 nuclear reactors went into decommissioning in 38 countries and 454 nuclear reactors in operation (based on 2018.11.07.). Of these 454 reactors, more than 60 percent of them have been operating for more than 30 years, more nuclear power plants will go into decommissioning in the future.

Therefore, it is necessary to secure a favorable position in the overseas decommissioning market in the future by supplementing the insufficient parts of the domestic self-disposal technology when the Kori Unit 1 is decommissioning

REFERENCES

[1] Homepage of Korea Atomic Industrial Forum
http://www.kaif.or.kr
[2] Patent Information Net KIPRIS
http://www.kipris.or.kr

Preliminary Study on HyBRID Chemical Decontamination Demonstration for the Reactor Coolant Pump Shaft

Ki-Chul Kim*, Bum-Chul Seo, Sun-sik Yoon, Jung-Yeop Cha, Nam-Kyun Kim, Kwang-Hee Joo, Do-Yong Kwon, Dong-Yeon Kim, Keun-Woo Kim, and Ju-Hyeon Park
KEPCO KPS, 69-46, Munsan 2sandan 1-ro, Oedong-eup, Gyeongju-si, Gyeongsangbuk-do, Republic of Korea
*KICHKIM@kps.co.kr

1. Introduction

In the previous research, KEPCO KPS performed pilot scale test applying HyBRID chemical decontamination process and confirmed high Decontamination Factor (DF) and low waste generation [1]. Based on previous research, we will demonstrate HyBRID process using contaminated Reactor Coolant Pump (RCP) shaft in Hanul#1. The loop test equipment for HyBRID process demonstration was manufactured and tested by RCP shaft mock-up.

2. Test Equipment and Experiments

In this experiment, we use RCP shaft mock-up and ultrasonic decontamination jacket (15 L). The loop test system (30 L) contains decontamination part and precipitation part. The decontamination part is designed to circulate the process water and control the temperature through the line heater and pump. The precipitation part is consisted of precipitation tank (30 L), diaphragm pump, and membrane filter designed to filter the precipitate.

2.1 Experimental Method

The three STS304 specimens (50×50×2 mm) with simulated corrosion oxide film were mounted on the RCP shaft mock-up and ultrasonic decontamination jacket was fastened. After 30 L of DI water was added to the decontamination part, heat up the DI water to 95℃, and the oxidation/reduction process were carried out for 3 hours each. After the oxidation/reduction process, the process water was cooled to 40℃, and conducted ultrasonic cleaning for 10 minutes, and the process water transferred to the precipitation tank. The concentration of chemicals is same as pilot scale test [1] except for SiO_2. The oxidation, reduction, and precipitation processes were carried out for 3 cycles.

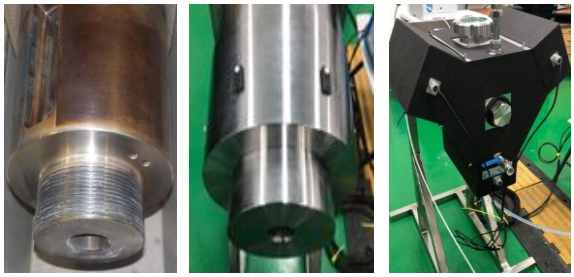

Fig. 1. RCP shaft, mock-up and ultrasonic decontamination jacket.

2.2 Thickness Reduction Calculation of Specimen

The mole of metal for weight loss before and after the HyBRID chemical decontamination process of STS304 specimen is expressed as $x\ mol_{M^{n+}}$, and the thickness reduction formula is as follows:

$$d_{M^{n+}} = x\ mol_{M^{n+}} \times \frac{F.W(g/mol_{M^{n+}})}{Oxide\ layer\ density(g/cm^3)} \quad (1)$$

After the HyBRID chemical decontamination process, the weight loss for each of the three specimens in each cycle was added up and averaged, and the weight of the measured metal was substituted into the above formula to calculate the thickness reduction of the specimen.

2.3 Analysis Method of Precipitated Process Water

In the precipitation process, the filtered process water was sampled and the TSS (Total Suspend Solids), SO_4^{2-} (sulfate ions), and N_2H_4 (hydrazine) concentrations were measured by spectrometer (HACH DR1900, USA).

3. Experiments Result

3.1 HyBRID Chemical Decontamination Result

The HyBRID chemical decontamination results show that an average of 2.0 ~ 2.2 ㎛ oxide film is removed in each cycle and the thickness reduction is shown in Table 1.

Table 1. Measurement results of Average Thickness Reduction by HyBRID decontamination

Average Thickness Reduction [㎛]	
1 Cycle	2.21
2 Cycle	2.01
3 Cycle	2.16

3.2 Analysis Result of Precipitated Process Water

In the precipitation process, TSS was filtered to 1 mg/L and SO_4^{2-} was measured less than 1 mg/L within 1 hour. The N_2H_4 concentration was measured to 0.18 mg/L.

Table 2. Filtrated process water analysis result

Time	TSS [mg/L]	SO_4^{2-} [mg/L]
5 min	5	1
30 min	3	1
60 min	1	0
90 min	0	0

4. Conclusion

The loop test using RCP mock-up and coated specimens showed that 6 ㎛ of oxide film was removed by 3 cycles. In the precipitation process, all SO_4^{2-} was removed by $Ba(OH)_2$, and the removal rate of N_2H_4 was also very high.

Based on these results, we will apply HyBRID chemical decontamination demonstration test to Hanul#1 RCP shaft.

ACKNOWLEDGEMENTS

This work was supported by the National Research Foundation of Korea (NRF) and the Ministry of Science and ICT (MSIT) of the Republic of Korea. (NRF-2017M2A8A5041776)

REFERENCES

[1] K. C. Kim, J. H. Park, J, H. Lee and D. Y. Kim, “Study on HyBRID Chemical Decontamination and Waste Water Treatment By using Pilot Scale Equipment”, Proc. of the KRS 2018 Spring Conference, 16(2), 10.31- 11.02, 2018, Jeju.

Effect of Raw Amount of $CuSO_4$ on Precipitation of Cu_2O in the HyBRID Decontamination of Magnetite

Byung-Chul Lee[1,*], Seon-Byeong Kim[2,*], and Jei-Kwon Moon[2]
[1] Hannam University, 1646, Yuseong-daero, Yuseong-gu, Daejeon, Republic of Korea
[2] Korea Atomic Energy Research Institute, 111, Daedeok-daero 989beon-gil, Yuseong-gu, Daejeon, Republic of Korea
*bclee@hnu.kr; sbkim@kaeri.re.kr

1. Introduction

The removal of radioisotopes from the primary coolant system of a nuclear power plant takes place with the dissolution of corrosion metal oxide layers deposited with the radioisotopes. Chemical decontamination by oxidative and reductive dissolution is considered to be the most effective method to date. KAERI has developed the HyBRID process without using any organic acids or organic chelating agents [1]. The solution containing sulfuric acid (H_2SO_4), hydrazine (N_2H_4), and copper sulfate ($CuSO_4$) provided the acidic and reductive dissolution of transition metal ions from the corrosion metal oxides. Since the HyBRID decontamination process does not use any organic chelates, precipitates of metal ions can be formed as the solution pH changes. Under a reducing condition, Cu^+ ions may form precipitates of Cu_2O or be hydrolyzed into $Cu(OH)_2$ precipitates. Thus it is important to find the reducing conditions at which no precipitation of Cu_2O or $Cu(OH)_2$ is formed.

In this work we studied the effect of the concentration of copper ions in the HyBRID aqueous solution on the formation of Cu_2O or $Cu(OH)_2$ precipitates for the HyBRID dissolution of magnetite. Raw amount of $CuSO_4$ was changed in order to control the concentration of copper ions.

2. Reaction Scheme and Calculation Method

The key reactions of the HyBRID dissolution of magnetite are as follows:

$$Fe_3O_4 + 4H_2SO_4 \rightarrow Fe^{2+} + 2Fe^{3+} + 4SO_4^{2-} + 4H_2O \quad (1)$$

$$2CuSO_4 + \frac{1}{2}N_2H_4 \rightarrow 2Cu^+ + 2SO_4^{2-} + \frac{1}{2}N_2 + 2H^+ \quad (2)$$

$$Fe^{3+} + Cu^+ \rightarrow Fe^{2+} + Cu^{2+} \quad (3)$$

$$Fe_3O_4 + 2CuSO_4 + \frac{1}{2}N_2H_4 + 4H_2SO_4 \rightarrow 3Fe^{2+} + 2Cu^{2+} + 6SO_4^{2-} + \frac{1}{2}N_2 + 2H^+ + 4H_2O \quad (4)$$

Cu^{2+} are reduced by N_2H_4 to produce Cu^+. The resulting Cu^+ are oxidized to Cu^{2+} after reducing the Fe_3O_4 layer, and the Cu^{2+} are rapidly reduced to Cu^+ by N_2H_4, thereby completing redox cycling. N_2H_4 participates in the reaction pathway of reducing Fe^{3+} to Fe^{2+} and simultaneously regenerating oxidized Cu^{2+} into Cu^+. During the cycle of Cu^+ ions to Cu^{2+} ions, the released electrons promote the reduction of Fe^{3+}.

To determine the effect of the concentration of copper ions in the HyBRID dissolution of magnetite, the E-pH (Pourbaix) diagram for Cu was first constructed and then compared with the equilibrium composition and pH of the solution. The E-pH diagram shows the thermodynamic stability areas of different species as functions of pH and potential scales in an aqueous solution. Thus, the E-pH diagram for Cu shows the stability areas where species and ions such as Cu^+, Cu^{2+}, Cu_2O, $Cu(OH)_2$ are present depending on the pH and the redox potential. The Eh-pH module in the HSC Chemistry® version 9 [2] was used to construct the E-pH diagram. The module is based on STABCAL (Stability Calculations for Aqueous Systems) developed by Haung [3].

Calculation of the multicomponent equilibrium compositions in heterogeneous systems like the HyBRID dissolution of magnetite was conducted using the GEM module of the HSC Chemistry® 9. The equilibrium composition was calculated using the GIBBS solver, which used the Gibbs energy minimization method. In aqueous solution, the Pitzer model was used to calculate mean activity coefficients of the aqueous species [4]. Gas is assumed to behave as ideal mixture. The Pitzer parameters were obtained from the HSC AQUA Pitzer database [2].

3. Results and Discussion

Fig. 1 shows the E-pH diagrams for Cu constructed at a constant temperature of 95℃ and at different concentrations of Cu. It gives the pH values at the boundaries between the region where Cu exists in the form of Cu^+ ion exist and the region where Cu exists in the form of Cu_2O solid. The pH values varied depending on the total concentration of Cu. Fig. 2 illustrates the relationship between the pH value and the Cu concentration at two boundaries between stability areas. The pH value decreased linearly with increasing the Cu concentration. Since the species affecting the magnetite dissolution is Cu^+ ions, it is important to adjust so that the Cu^+ ions do not change to Cu^{2+}, Cu_2O(s), or $Cu(OH)_2$(s). To prevent the Cu^+ ions from being oxidized to the Cu^{2+} ions, the redox potential should be lower than 0.2 V by adding N_2H_4. In order to prevent precipitation of Cu^+ ions into Cu_2O(s), the pH of the solution should be made sufficiently low.

The equilibrium calculations were conducted at the experimental conditions given in Table 1. Raw amount of $CuSO_4$ changed from 5×10^{-4} to 1×10^{-1} mol. Raw amounts of Fe_3O_4, N_2H_4, and H_2SO_4 in the feed were kept constant. Fig. 3 shows the effect of the raw amount of $CuSO_4$ on the amount of Cu_2O precipitates produced in the HyBRID dissolution of magnetite. At very low amounts of $CuSO_4$, no precipitation of Cu_2O

occurred. However, precipitation of Cu_2O was apparent at higher amounts of $CuSO_4$. The amount of Cu_2O produced increased with the increase of the raw amount of $CuSO_4$ and decreased with the increase of the temperature.

Table 2 shows the equilibrium amounts of Cu_2O and $Cu(OH)_2$ and the solution pH values calculated at different raw amounts of $CuSO_4$ at 95℃. The pH values at the boundaries between the areas of Cu^+ and Cu_2O obtained from the E-pH diagrams (Fig. 1) are also listed in Table 2. Precipitation of $Cu(OH)_2$ did not occur at any $CuSO_4$ amounts. The solution pH decreased with the increase of the raw amount of $CuSO_4$. When the raw amount of $CuSO_4$ was less than 1×10^{-2}, there was no precipitation of Cu_2O because the solution pH was lower than the pH value obtained from the E-pH diagram. However, at the raw amounts of $CuSO_4$ higher than about 1.6×10^{-2}, the solution pH was higher than the pH value from the E-pH diagram, causing the precipitation of Cu_2O.

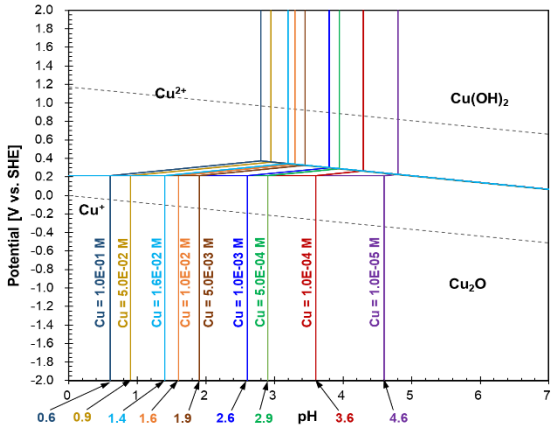

Fig. 1. E-pH diagrams for Cu at 95℃.

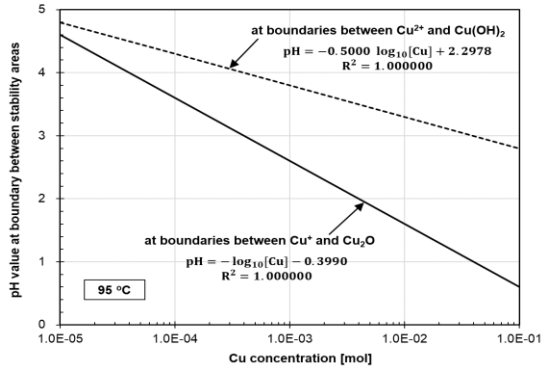

Fig. 2. The pH values at the boundaries between stability area as a function of Cu concentration at 95℃.

Table 1. Recipe of experiments for the HyBRID dissolution of magnetite

Reagent	Phase	Raw amount [mol]
Fe_3O_4	solid	2.16×10^{-4} (0.05 gram)
H_2SO_4	aqueous	0.03377
N_2H_4	aqueous	0.05791
$CuSO_4$	solid	$5 \times 10^{-4} \sim 1 \times 10^{-1}$
H_2O	aqueous	55.5 (1 liter)

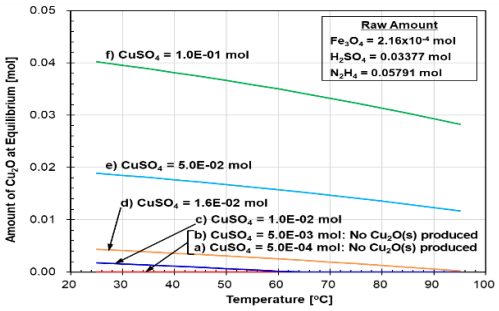

Fig. 3. Equilibrium amount of $Cu_2O(s)$ calculated at different raw amounts of $CuSO_4$ in the HyBRID dissolution of magnetite.

Table 2. Results of equilibrium calculations conducted by the recipe of Table 1 at 95℃ and 1 bar

Raw amount of $CuSO_4$ [mol]	At equilibrium			pH at boundary between Cu^+ and Cu_2O
	Cu_2O [mol]	$Cu(OH)_2$ [mol]	Solution pH	
5.0×10^{-4}	0.0000	0.0000	1.541	2.9
5.0×10^{-3}	0.0000	0.0000	1.539	1.9
1.0×10^{-2}	0.0000	0.0000	1.536	1.6
1.6×10^{-2}	0.0002	0.0000	1.529	1.4
5.0×10^{-2}	0.0117	0.0000	1.324	0.9
1.0×10^{-1}	0.0283	0.0000	1.141	0.6

4. Conclusion

The effect of the concentration of copper ions in the HyBRID solution on the formation of Cu_2O or $Cu(OH)_2$ precipitates was studied in the HyBRID dissolution of magnetite. The pH values at which the coexistence of Cu^+ and $Cu_2O(s)$ occurred were found by preparing the E-pH diagram with varying Cu concentration at a constant temperature (95℃). According to the results of the equilibrium calculations for the aqueous system of the HyBRID dissolution of magnetite, precipitation of Cu_2O occurred at a high amount of $CuSO_4$ added into the solution and there was no precipitation of $Cu(OH)_2$ at any raw amounts of $CuSO_4$. To prevent precipitation of Cu^+ ions into $Cu_2O(s)$, the amount of $CuSO_4$ added into the HyBRID solution should be adjusted so that the pH of the solution is less than the pH value found in the E-pH diagram.

ACKNOWLEDGEMENT

This work has been carried out under the Nuclear R&D Program (NRF-2018M2A8A5024102 & NRF-2017M2A8 A5015144) funded by Ministry of Science and ICT.

REFERENCES

[1] W.K. Choi, Development of Advanced Decontamination Technology for Nuclear Facilities, KAERI Report No. 2012M2A8A5025655 (2017).
[2] HSC Chemistry software, www.outotec.com.
[3] Haung, H., Canadian Metallurgical Quarterly, 28, 225-239 (1989).
[4] Pitzer, K.S., J. Phys. Chem., 77, 268-277 (1973).

Underwater Laser Cutting Using High-Pressure Supersonic Nozzle

Seong Y. Oh*, Jae Sung Shin, Taek Soo Kim, Hyunmin Park, Lim Lee, Chin-Man Chung, and Jonghwan Lee
Korea Atomic Energy Research Institute, 111, Daedeok-daero 989beon-gil, Yuseong-gu, Daejeon, Republic of Korea
*syoh73@kaeri.re.kr

1. Introduction

Underwater laser cutting technology associated with a high-power fiber laser can be suitable candidate as a dismantling tool in nuclear decommissioning site owing to the ability of remote manipulation and the small production of secondary waste. In the view of a technical point, underwater laser cutting intrinsically uses the pressurized gas jet discharging from a small-diameter nozzle to construct the column filled with air in the underwater. The constructed column serves the safe path for a high-powered laser beam to propagate into water environment to minimize possible laser energy loss by the absorption of water. After passing through the column, the laser beam heats up the steel specimen above melting point. The gas jet also contributes to blowing out the melted outside the specimen. Therefore, it is noted that the thrust force of gas jet discharging from the cutting nozzle is significant in safely guiding the laser beam as well as blowing out the laser-produced melt in water environment. [1]

In this study, supersonic nozzle was newly designed to be effectively operated at very high stagnation pressure of 15.0 MPa. [1] The 60-mm-thick stainless steel was cut to examine the cutting performance of newly manufactured nozzle using 6 kW laser beam.

2. Experimental Setup

Fig. 1 shows experimental setup of the laser cutting experiment. [2] The long process fiber (core dia.: 100-μm, length: 25 m) delivers a 6 kW laser beam produced by fiber laser (IPG YLR-6000, λ = 1070 nm) system into cutting head.

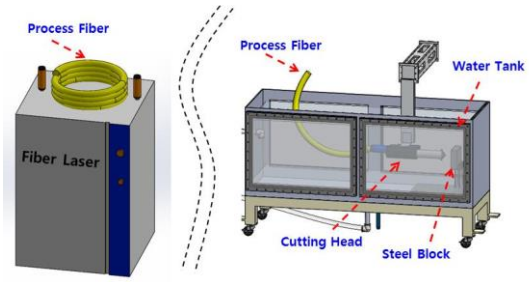

Fig. 1. Experiment setup for underwater laser cutting.

Cutting head is made up of collimation (f = 160 mm) and focusing (f = 600 mm) optics in order to effectively focus the high-powered laser beam toward steel specimen. [2] The flexible pipe lines and supersonic nozzle (See Fig. 2.) is coupled with cutting head to effectively discharge the compressed air toward stainless steel specimen (SUS 304L). Before cutting head immersing in the water tank, the compressed air is continuously discharged from the nozzle to protect the penetration of water inside cutting head. The compressed air with a gauge pressure of approximately 1.5 MPa was used in this experiment. The cutting head is spatially translated by an X-Y-Z stage controlled by computerized numerical control.

3. Result and Discussion

Fig. 2 presents underwater cutting scenes of 60-mm-thick stainless steel captured in time order. Initially, compressible air is discharged from supersonic nozzle with 1310 L/min mass flow rate. The throat diameter of supersonic nozzle was 3.0 mm.

Fig. 2. Underwater cutting scenes in time order.

The stand-off distance (the distance between the nozzle tip and the top surface of the steel plate) was set to be 10 mm. The focal point of laser beam is located inside specimen (F: - 12.3 mm). The entire laser-cut length is 40 mm. Initial cutting speed until 10 mm of the cut was set to be 5 mm/min and then cutting speed was increased for the remainder of 30 mm cut. Complete cut was observed at 50 mm/min cutting speed.

4. Conclusion

The 60-mm-thick stainless steel was successfully cut using designed supersonic nozzle to be effectively operated at high stagnation pressure of 15 MPa.

REFERENCES

[1] H. C. Man, J. Duan, T. M. Yue, “Analysis of the dynamic characteristics of gas flow inside a laser cut kerf under high cut-assist gas pressure”, Journal of Physics D: Applied Physics, 32, 1469-1477(1999).

[2] Jae Sung Shin, Seong Yong Oh, Hyunmin Park, Taek-Soo Kim, Lim Lee, Chin-Man Chung, Jonghwan Lee, “Underwater cutting of 50 and 60 mm thick stainless steel plates using a 6-kW fiber laser for dismantling nuclear facilities”, Optics and Laser Technology, 115, 1-8(2019).

Metal Oxide Solubility in Deep Eutectic Solvents – Applications in Decontamination in Decommissioning

James T. M. Amphlett* and Sungyeol Choi
Korea Advanced Institute of Science and Technology, 291, Daehak-ro, Yuseong-gu, Daejeon, Republic of Korea
*j.amphlett@kaist.ac.kr

1. Introduction

Deep eutectic solvents (DES's) are a new class of solvent, widely regarded as ionic liquid (IL) analogues [1]. The most commonly studied type of these liquids are composed of a quaternary ammonium salt (QAS), and a hydrogen bond donor (HBD). Most published works have focused on choline chloride as the QAS, mixed with either a carboxylic acid, amine or alcohol as the HBD (Fig. 1). Upon mixing the two components at the correct molar ratios, a clear eutectic liquid is formed.

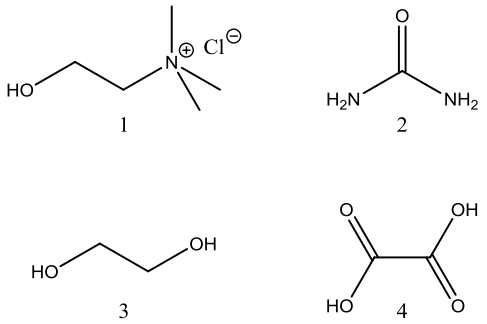

Fig. 1. Chemical structures of common components of DES's (1 = choline chloride, 2 = urea, 3 = ethylene glycol, 4 = oxalic acid).

These DES's have many of the advantages of their analogous IL's, such as low vapour pressure, wide liquid range, non-flammability and good conductivity. However, unlike IL's they are made of inexpensive, common chemicals and are considered non-toxic. These advantageous properties have promoted interest in them in many areas, such as separations, waste recycling, catalysis, and batteries [2], [3].

DES's have been shown to dissolve metal oxides such as CoO, NiO, ZnO and MnO_2 (among others) which are insoluble or barely soluble in most molecular solvents [1]–[3]. Solubilizing these in aqueous systems usually requires harsh conditions such as acid, alkali and high temperatures. In addition to this, aluminate and silicate compounds have been shown to be insoluble in DES's [3]. This ability to dissolve such metal oxides under relatively benign conditions, whilst leaving silicates and aluminates alone may make them appropriate for the decontamination of wastes produced during nuclear decommissioning, such as concrete.

In this work a set of choline chloride based DES's have been studied for their ability to dissolve metal oxides relevant to nuclear decommissioning processes. We have focused on NiO, CoO and lanthanide oxides as they are all present in nuclear wastes.

2. Methods

2.1 DES Production

DES were produced by stirring choline chloride and a hydrogen bond donor at the appropriate molar ratio (Table 1) on a heating mantle at 50°C overnight, whereupon a clear liquid was produced. The DES were stored in glass bottles until they were required for experiments.

Table 1. Ratio of choline chloride (QAS) to selected hydrogen bond donors (HBD) used in this work

HBD	QAS : HBD
Ethylene glycol	1 : 2
Glycerol	1 : 2
Malonic acid	1 : 2

2.2 Metal Oxide Dissolution

Metal oxide (*ca*. 0.1 g) was added to a glass vial, followed by DES (*ca*. 4 g). Vials were left heating for at least 2 weeks at 50°C using a Daihan MaXtable HM dry heating block. Samples were then removed from the heating block and 3 samples of loaded DES (*ca*. 0.5 g) were taken from each. These samples were removed from the glovebox, dissolved in 10 mL of deionized water (> 18 MΩ) and filtered using a Whatman 0.45 μm filter. Aliquots of solution from these samples were then diluted with HNO_3 (10%) for ICP-OES analysis.

3. Results and Discussion

Metal oxide solubilities in three common DES's are shown in table 2. The general trend in solubility based on HBD is MA > EG > G. The higher solubility in the malonic acid DES is thought to be due to the presence of acidic protons acting as good oxygen acceptors and promoting dissolution. Increased solubility with the ethylene glycol HBD when compared to glycerol may be due to complexation stabilizing the dissolved metal cation. Ethylene glycol has been reported to bind to Ni^{2+} in choline chloride based DES's via its oxygen atoms [4]. It is unknown whether this happens with the other metals studied, but it is possible. Another factor may be differences in solvent polarity. However, quantification of this for DES's has proved challenging, and both explicit and relative values remain unknown.

Table 2. Solubilities of metal oxides in DES (ChCl = choline chloride, MA = malonic acid, EG = ethylene glycol, G = glycerol). Errors are reported as one standard deviation

	Solubility / mg kg^{-1}		
	ChCl - MA	**ChCl - EG**	**ChCl - G**
NiO	814 ± 25.7	2.35 ± 0.305	< 1
CoO	23600 ± 1550	150 ± 8.76	59.9 ± 3.92
CeO_2	15.1 ± 0.787	1.16 ± 0.092	< 1
Nd_2O_3	1530 ± 355	101 ± 5.97	43.9 ± 9.15
Eu_2O_3	-	84.0 ± 5.68	39.4 ± 2.88
Dy_2O_3	4760 ± 119	26.6 ± 7.79	10.4 ± 1.07

CoO exhibits the highest solubility in all DES studied. Of particular interest is its much larger solubility than NiO. This has been observed previously in a choline chloride – malonic acid DES [2]. Though the explicit reasons for this are unclear, we believe that the affinity of the metal centre to Cl^- ligands may be important. Co^{2+} readily forms complexes with Cl^- ($[CoCl_2]$, $[CoCl_3]^-$, $[CoCl_4]^{2-}$), unlike Ni^{2+}. However, this is based on aqueous data, so this conclusion must be treated as tentative until further studies can be carried out.

In DES's with an alcohol HBD, the observed solubility series for Ln oxides is Nd > Eu > Dy >> Ce. In aqueous systems, CeO_2 is only soluble in the presence of acid, whereby it is reduced to Ce(III). This reduction requirement may explain why it is more soluble in the acidic than alcoholic DES, and less soluble than the other trivalent Ln oxides tested.

4. Conclusions

Metal oxides are soluble in DES's, but care must be taken when selecting the HBD as this can change solubility behavior. This brings in the idea of selecting a HBD to tailor the properties of the solvent to target processes. This could be especially useful in decommissioning.

The general trend for metal oxide solubility with changing HBD is MA > EG > G. It is hypothesized that this due to the presence of acidic protons and the ability of the HBD to coordinate with the metal ion.

With regards to decommissioning, if a carboxylic acid HBD is used then the solvent will degrade. This means it will need to be replaced more often than an alcohol HBD, having implications for process design and sustainability. Lower solubilities in alcohol DES's may be combated through controlling redox potential, the addition of complex forming ligands, or continuous removal of the metal.

ACKNOWLEDGEMENTS

This work was supported by Korea Research Fellowship Program through the National Research Foundation of Korea (NRF) funded by the Ministry of Science and ICT.

REFERENCES

[1] E. L. Smith, A. P. Abbott, and K. S. Ryder, "Deep Eutectic Solvents (DESs) and Their Applications," *Chem. Rev.*, vol. 114, no. 21, pp. 11060–11082, 2014.

[2] A. P. Abbott, G. Capper, D. L. Davies, K. J. McKenzie, and S. U. Obi, "Solubility of metal oxides in deep eutectic solvents based on choline chloride," *J. Chem. Eng. Data*, vol. 51, no. 4, pp. 1280–1282, 2006.

[3] Q. Zhang, K. De Oliveira Vigier, S. Royer, and F. Jérôme, "Deep eutectic solvents: Syntheses, properties and applications," *Chem. Soc. Rev.*, vol. 41, no. 21, pp. 7108–7146, 2012.

[4] J. M. Hartley *et al.*, "EXAFS study into the speciation of metal salts dissolved in ionic liquids and deep eutectic solvents," *Inorg. Chem.*, vol. 53, no. 12, pp. 6280–6288, 2014.

Consideration About Assessment of Radiation Source Term When Decommissioning of Nuclear Power Utilization Facilities

ByeongMok-Park*, JeongMi-Lee, CheolWan-Park, and AhRan-Cha
SAE-AN ENERTECH CORP, #923, 184, Gasan digital 2-ro, Geumcheon-gu, Seoul, Republic of Korea
*pbm@sae-tec.com

1. Introduction

Among the domestic nuclear power plants, Kori Unit 1 has been permanently shut down on June 18, 2017 and is in the process of decommissioning. Therefore, many organizations such as industry, research institute, educational institution are conducting research and development for decommissioning nuclear power plant, and many contents about radiation source term have been established.

But, when decommissioning nuclear power utilization facilities except for nuclear power plants, it is no certainty about the definition of radiation source term therefore it is necessary to establish

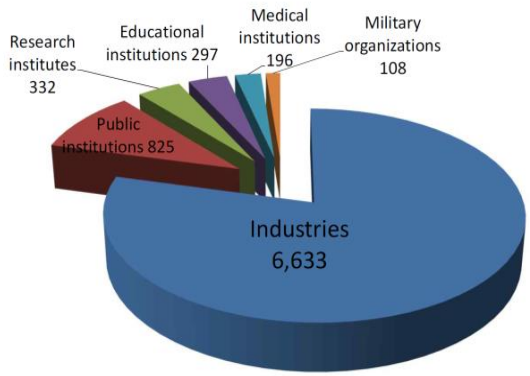

Fig. 1. Status of nuclear power utilization facilities in 2019.

2. Assessment of Radiation Source Term of Nuclear Power Utilization Facilities

Currently, there are 8,391 licensed and reported nuclear power utilization facilities in Korea, and in this paper, when decommissioning nuclear power plants, radioisotope production facilities, opened radioisotope use facilities, neutron source calibration facilities, nuclear fusion research institutes and high energy linear accelerator facilities.

I will describe the considerations for assessment of radiation source term.[1]

2.1 Characteristics of Radiation Source Term by Facility

2.1.1 Nuclear Power Plants. The radiation source term for nuclear power plants is the fission products generated during the fission process and radioactivation material by the neutrons generated during the fission process.

2.1.2 Radioisotopes Production Facilities. When assessing the radiation source term in the case of decommissioning a radioisotope production facility, consideration should be given to radioactivation. And, if the produced radionuclides is a short-lived radionuclides, it can be excluded from the evaluation of the radiation source term.

Recently, cyclotrons are mainly used in the medical field. A typical nuclide production is ^{18}F. Neutrons are generated in the course of producing the desired radioisotope by the reaction of the accelerated protons and target material. Therefore, it is necessary to consider the radioactivation of the surrounding material by the neutron when assessing the radiation source term.

Reaction formula : $^{18}_{8}\mathrm{O} + {}^{1}_{1}\mathrm{p} \rightarrow {}^{18}_{9}\mathrm{F} + {}^{1}_{0}\mathrm{n}$ (1)

2.1.3 Opened Radioisotope Use Facilities. Open radioisotope is less use than sealed radioisotope. But, radioactive contamination occurs in open radioisotope facilities.

When the facilities are divided into a short-lived radionuclides and a long-lived radionuclides facilities, the assessment of the degree of contamination with

the long-lived radionuclides facility must be carried out.

Also, when used in combination, an assessment of contamination is essential.

Table 1. The amount of radioactivity licensed for the last four years [1]

(Unit : TBq)

Classification	2013	2014	2015	2016
Opened RI	19,475	19,848	18,288	19,039
Sealed RI	144,737	145,844	146,531	191,633
Sum	164,212	165,692	164,819	210,672

Table 2. The amount of open radioisotope licensed by agency for the last four years [1]

(Unit : GBq)

Classifi-cation	2013	2014	2015	2016
Industry	3,278,087	3,278,111	28,639	433,396
Public	5,983	1,235	4,787	7,299
Medical attention	4,984,994	5,362,955	5,488,058	5,642,716
Education	1,459	2,084	2,014	175,874
Research	11,204,769	11,203,471	11,203,601	11,218,479
Military affairs	-	-	1,561,000	1,561,000
Sum	19,475,292	19,847,856	18,288,099	19,038,766

2.1.4 Neutron Source Calibration Facilities. When decommissioning of neutron source calibration facilities, the radiation source term should be assessed taking into account the effect of radioactivation by the neutrons.

Radioactivation by neutrons is important for the neutron energy spectrum and the surrounding materials. This is because radioactivation is determined by neutron energy level and the radioactivation absorption cross section of the materials. Especially, the energy level of neutrons is a major factor because it affects the depth of the radioactivation of material.

2.1.5 Fusion Research Institute. The Fusion Research Institute is conducting research to obtain energy using fusion reaction.

At this time, neutrons are generated.

Since these neutrons cause radioactivation, the effects of radioactivation should be considered in assessing of the radiation source term at the decommissioning of the fusion research institute. Typical fusion reactions are as follows.

Reaction formula 1 : $^{2}_{1}\mathrm{H} + {}^{2}_{1}\mathrm{H} \rightarrow {}^{3}_{2}\mathrm{He} + {}^{1}_{0}\mathrm{n}$ (2)

Reaction formula 2 : $^{2}_{1}\mathrm{H} + {}^{3}_{1}\mathrm{H} \rightarrow {}^{4}_{2}\mathrm{He} + {}^{1}_{0}\mathrm{n}$ (3)

2.1.6 High Energy Linear Accelerator Facilities. Photons with high energy generate neutrons through photonuclear reaction with materials, Therefore, the effect of radioactivation by neutrons must be taken into consideration in the decommissioning of high energy linear accelerators.

3. Conclusion

Domestic nuclear power utilization facilities have steadily increased over the past years. So, the number of decommissioning nuclear power utilization facilities is expected to be higher than in the past.

Therefore, procedures related to decommissioning nuclear power utilization facilities should be established. In addition, decommissioning technology should be developed in consideration of facility-specific radiation source term in accordance with the characteristics of various nuclear power utilization facilities.

REFERENCES

[1] Korean Association for Radiation Application http://koara.or.kr/

Effect of Alkyl Chain Length of Ionic Liquids on Extraction Efficiency and Phase Separation in the Ionic Liquids Solid-liquid Cs^+ Extraction System

Jung-Weon Choi*, Hayeon Ryu, Myogwang Kim, Wonzin Oh, and Sang-June Choi
Kyungpook National University, 80, Daehak-ro, Buk-gu, Daegu, Republic of Korea
*jungweon@knu.ac.kr

1. Introduction

From now on, the solid-liquid separation from Cs^+ extraction process using 1-ethyl-3-methy limidazolium bis(trifluoromethylsulfonyl)imide [C_2mim][Tf_2N] were studied [1-3]. It was confirmed the extraction and phase separation depends on solubility of Ionic liquids (ILs). Therefore, the purpose of this study is to investigate the relationship between the solubility of imidazolium based ILs with alkyl groups, extraction efficiency and phase separation.

2. Experimental

2.1 Materials

Cesium nitrate ($CsNO_3$, 99%) and the extractant, dicyclohexano-18-crown-6 (DCH18C6, 98%) were purchased from Sigma-Aldrich Chemical Co. (Germany). The 1-ethyl-3-methylimidazolium/1-butyl-3-methylimidazolium/1-hexyl-3-methylimidazolium/1-othyl-3-methylimidazolium bis(trifluoromethylsulfonyl)imide ([C_2mim/C_4mim/C_6mim/C_8mim][Tf_2N]) were purchased from C-TRI Co. Ltd. (Korea).

2.2 Method

To estimate the ILs' solubility in water and water contents in ILs, water and ILs were conducted for 2 h. Water contents in ILs was estimated by Karl Fisher (899 Coulometer, Metrohm). ILs' solubility in water was confirmed by weighing before and after weight of ILs.

For extraction, 15 mM of $CsNO_3$ simulated waste solution (40 mL) were reacted with 0.6 mM DCH18C6 and 2 mmol ILs for 2 h at 25°C. After extraction, observing the phase separation, and calculate the removal efficiency of Cs^+ (%). The equation removal efficiency of Cs^+ could be written as:

$$R_{Cs}\ (\%) = \frac{(C_o - C_e)}{C_o} \times 100 \qquad (1)$$

where Co and Ce are initial and equilibrium concentration of Cs^+ (mmol/L).

3. Results

3.1 Solubility According to ILs

ILs solubility in water and water content in ILs varied depending on type of ILs (Table 1). It was confirmed that the longer the alkyl group was, the more hydrophobic, and the solubility with water was also smaller. On the other hand, the water content did not show any tendency. C_4mimTf_2N had the largest water content.

Table 1. ILs Solubility in water and water content in ILs according to type of ILs

Ionic Liquids	ILs solubility in water (g/L)	Water content in ILs (g/L)
C_2mimTf_2N	18.00	0.939
C_4mimTf_2N	6.09	2.332
C_6mimTf_2N	2.00	0.269
C_8mimTf_2N	0.86	0.318

3.2 Results of Cs^+ Extraction and Phase Separation

In same mole quantities of ILs, phase separation was differ according to type of ILs. As the hydrophobicity increased, the solubility decreased and the volume of the organic phase became larger. As a result, phase separation was observed from S-L to S-L-L and L-L. However, when the alkyl chain length is longer, the Cs^+ removal efficiency is lowered because the cation exchange is not performed well because of hydrophobicity.

Table 2. Removal efficiency of Cs^+ and phase separation according to type of ILs

Ionic liquids	Removal efficiency of Cs^+ (%)	Phase separation (S-L/S-L-L/L-L)
C_2mimTf_2N	91.21	S-L
C_4mimTf_2N	84.79	S-L-L
C_6mimTf_2N	71.52	S-L-L
C_8mimTf_2N	43.06	L-L

4. Conclusion

Through the studies on the effect of alkyl chain length of ILs on extraction efficiency and Phase separation in the ILs solid-liquid Cs^+ extraction system, we got the two conclusions:

1) The precipitate ($Cs^+Tf_2N^-DCH18C6$) is formed by the supersaturation in ILs phase. Therefore, it is considered that the ILs in the ILs phase is reduced by the ILs solubility in water and the precipitate is formed better.

2) The longer alkyl chain length, the more hydrophobicity, the less distribution coefficient of Cs^+ and the longer range of S-L-L phase separation.

ACKNOWLEDGEMENT

This research was supported by the Nuclear Energy Development Program through the National Research Foundation of Korea (NRF), funded by the Ministry of Science and ICT (2018M2B2B1065631).

REFERENCES

[1] S. Kwon, J. Choi, S. Cho, W. Oh and S.J. Choi, “A novel method for separating Cs^+ from liquid radioactive waste using ionic liquids and a selective extractant”, Journal of Radioanalytical Nuclear Chemistry, 311, 1605–1611 (2017).

[2] S. Choi, J. Choi, W. Oh and S.J. Choi, “Studies on a new solid–liquid Cs separation using the ionic liquid extraction system in comparison with the conventional adsorption”, Journal of Radioanalytical Nuclear Chemistry, 319, 387–392 (2019).

[3] J.W. Choi, H. Ryu, W. Oh and S.J. Choi, “Study of Cs extraction in an ionic liquid system using a common anion in both aqueous and ionic liquid phases”, Journal of Radioanalytical Nuclear Chemistry, DOI. 10.1007/s10967-019-06473-1 (2019).

Molecular Binding Affinity of Aqueous Uranyl Tricarbonate Towards Basic Surface Functional Groups

Youngho Sihn[a,*] and Jong-Il Yun[b]

[a] Korea Atomic Energy Research Institute, 111, Daedeok-daero 989beon-gil, Yuseong-gu, Daejeon, Republic of Korea

[b] Korea Advanced Institute of Science and Technology, 291, Daehak-ro, Yuseong-gu, Daejeon, Republic of Korea

[*]sihnyh@kaeri.re.kr

1. Introduction

Uranium (U) is one of the major raw material in the nuclear power plant and military-weapon industries. The U-handling activities have resulted in the widespread contamination of groundwater [1]. Numerous adsorbents including metal-oxide, inorganic, and organic materials have investigated to separate U from aqueous phase. Silica showed high surface area and good physical stability, however, its limited surface density of U binding sites preclude the effective adsorption performance. Recent studies have functionalized the silica surfaces with N, O-ligands and the functionalization process could enhance the adsorption efficiency.

Various types of the N,O-ligands and its derivatives have been confirmed in the increasing silica sorption behavior, but the binding affinity toward U between ligands cannot be directly compared due to the different experimental conditions that would affect the binding characteristics.

In this study, silica surface was functionalized with basic ligands including amine (NH_2), carboxyl (COOH), hydroxyl (OH), and phosphonate ($P{=}O(OH_2)$) groups as a monolayer structure, i.e., surface functional groups. Previous spectroscopic studies have reported that uranyl tricarbonate ($UO_2(CO_3)_3^{4-}$) is a dominant uranium (U) species in groundwater, therefore, the binding affinity of uranyl carbonate toward surface functional groups were measured and compared in terms of adsorption kinetic/capacity.

2. Materials and Methods

2.1 Preparation of Surface Functional Groups

All the functionalization process was carried out under the anhydrous and anoxic atmosphere (99.999% Ar and $H_2O(g)/O_2$ < 1 ppm) at room temperature. Two hundred mL of anhydrous toluene was injected into the amber glass bottle containing 1.2 g of silica. The suspension was magnetically stirred and appropriate amounts of organosilanes ((3-aminopropyl)triethoxysilane (APTES, Sigma 99%), (3-glycidyloxypropyl)trimethoxysilane (GPTMS, Sigma > 98%), 3-(triethoxysilyl)propylsuccinic anhydride (TESPSA, BOC science 95%), and (2-diethylphosphatoethyl)triethoxysilane (DPTS, Gelest 95%)) were added indicating the functionalization process initiate. The particles in the suspension was separated after 16 h by centrifugation (100,000 g for 10 min.). The particles were washed and dried, respectively.

2.2 Batch Sorption Experiments

Uranyl tricarbonate solution was prepared by adding U stock solution (concentration in the mixture: 1×10^{-4} M) into the 1×10^{-2} M CO_3^{2-} solution pH buffered at 7.5 with 2×10^{-2} M HEPES. The exact amount of functionalized silica was transferred into the 200 mL of uranyl tricarbonate solution and the suspension was magnetically stirred at 300 rpm at room temperature. Three mL of the suspension was periodically taken and immediately filtered by membrane filter (Amicon, Ultra-15). The remaining U concentration in the filtrate was quantified by ICP-OES (Agilent 5110).

2.3 Analysis

The functionalized silica was characterized by Attenuated Total Reflection-Fourier Transform Infra-Red (ATR-FTIR, Nicolet iS 50), Elemental Analysis (EA, FlashEA 1112), ThermoGravicmetric Analysis (TGA, Netzsch), and Nuclear Magnetic Resonance (NMR, Agilent VNMRS600) analysis to verify the formation of monolayer structure oganosilanes on the silica surface. The surface charge of functionalized silica was quantified by zeta potential analyzer (ELS-Z2) before and after the adsorption experiments.

3. Result and Discussion

3.1 Surface Functional Groups Characterization

The surface density of functional group on the silica surface was quantified by EA and TGA as shown in Table 1.

Table 1.

Type	NH_2	COOH	OH	$P=O(OH)_2$
density ($\#/nm^2$)	1.38±0.13	1.45±0.16	2.09±0.02	1.11±0.16

The density was in the range of monolayer value and the presence of the surface ligands were identified from ATR-FTIR analysis (data not shown). NMR analysis revealed that the attached organosilane on the silica surface has monolayer structure indicating the surface functional groups were prepared as similar surface density and geometrical structure.

3.2 Molecular Binding Affinity of Aqueous Uranyl Carbonate

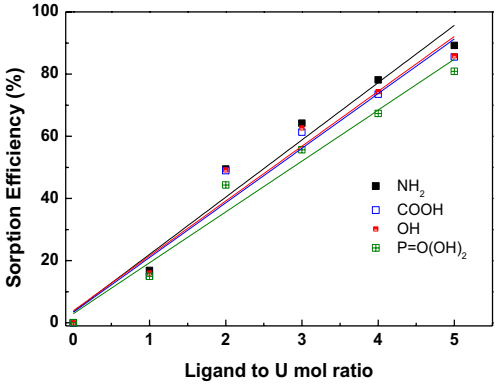

Fig. 1. Uranium adsorption efficiency of the functionalized silica with respect to the molecular ratio of uranium to surface ligand.

Fig. 1 shows the adsorption efficiencies of the functionalized silica for $UO_2(CO_3)_3^{4-}{}_{(aq)}$ at pH 7.5. The efficiencies have linearly increased and complete adsorption were obtained at molecular ratio of 1 to 5 implying that penta-coordinated U-ligand complexes might be formed on the surface. The sorption data have fitted with pseudo-second order kinetic model and the results well followed the model ($R^2 > 0.990$) indicating the calculated adsorption kinetic and capacity values were reliable. In four different basic groups, $\equiv NH_2$ showed the fastest adsorption kinetic (1.67×10^{-2} mmol/(mg·min)) while ≡COOH had the highest adsorption capacity (32.27 $mg/mmol_{ligand}$). The charge of NH_2-surface was the most positively charged (+7.5 mV) and COOH-surface was the most negatively charged one (-25.0 mV). After the interaction with U, the NH_2-surface charge was shifted to the negative region (-13.5 mV) while that of COOH-surface was maintained. From the obtained results, we propose that the complexation of U with ≡N- and ≡O-ligand would occur via ionic- and covalent-bonding, respectively (Fig. 2).

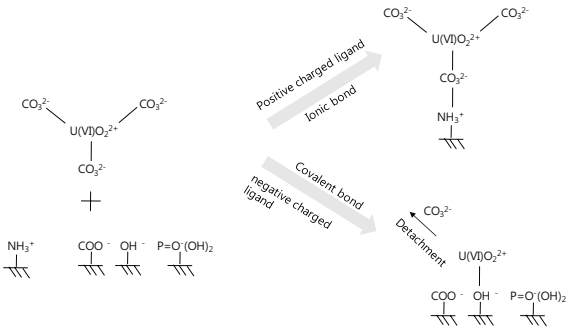

Fig. 2. Proposed binding mechanism of uranyl tricarbonate to the surface ligands.

4. Conclusion

The binding affinity of aqueous uranyl tricarbonate toward basic surface ligands were investigated under the controlled mole ratio of the reactants. Amine group showed the fastest binding kinetic due to its positively charged property in which it could effectively bind with the negatively charged uranyl tricarbonate, i.e., ionic bonding. The highest binding capacity was obtained from the carboxyl group. It might be attributed to the most negatively charged properties of COO^- that could effectively repel the CO_3^{2-} from the $UO_2(CO_3)_3^{4-}$ species during the binding process, i.e., covalent bonding.

REFERENCES

[1] P. D. Bhalara, D.Punetha, K. Balasubramanian, "A review of potential remediation techniques for uranium(VI) ion retrieval from contaminated aqueous environment." Journal of Environmental Chemical Engineering, 2, 1621-1634 (2014).

Planning for Document Management System Setup of Decommissioned Waste

Daeseo Koo*, Kook-Nam Park, Sang Bum Hong, In Hye Hahm, and Bum Kyoung Seo
Korea Atomic Energy Research Institute, 111, Daedeok-daero 989beon-gil, Yuseong-gu, Daejeon, Republic of Korea
*ndskoo@kaeri.re.kr

1. Introduction

Nuclear power plants of 24 units are operating in republic of Korea and Kori 1 unit from 24 units was shutdown. As all the operating nuclear power plants approach design life time of them, they will gradually have a view of shutdown. When a nuclear power plant is decommissioned, a lot of decommissioned waste will be generated. The documents of decommissioned waste information are very important for the strategy of decommissioning of the nuclear power plants. They are to be documents from generation of decommissioned waste to disposal of decommissioned waste. These documents are to be document for optimization of treatment process, document for classification, document for cutting technology, document for decontamination of decommissioned waste, and document of decommissioned design. To conduct setup of document management system which these documents of decommissioned waste is reviewed, approved, registered, referred, searched, and printed is to be considered as essential strategy of decommissioned waste [1-2].

In this study, to do planning for setup of document management system of decommissioned waste, the document lists for decommissioned waste is drawn up. The component document forms are drawn up and the flow sheet of document management is also drawn up. In the future, when completing the setup of document management system of decommissioned waste, the performance tests on document management system of decommissioned waste will be carried out.

2. Document Management System of Decommissioned Waste

2.1 Component Document Management

Table 1 shows component documents management. To do planning for setup of document management system of decommissioned waste, the components of document management for decommissioned waste are to be drawn up. They consist of the document lists, document cover for approving the documents, document distribution for reviewing the documents, document form for waste history management, and document form for confirming waste treatment of decommissioned waste.

Table1. Component Documents Management

Document Name	Use
Document Review & Approval Sheet	Document Drawing
Design Document Cover	Document Approval
Document Distribution for Agreement	Document Review
Radioactive Waste History Management Application	Document Application
Radioactive Waste Treatment Confirmation Application	Document Application

2.2 Flow Sheet of Document Management

Fig. 1 shows the flow sheet of document management of decommissioned waste. At first, the documents of decommissioned waste are drawn up. They are reviewed by project members, independent expert, and ALARA (as low as reasonably achievable). The reviewed documents are approved by decider and they are registered.

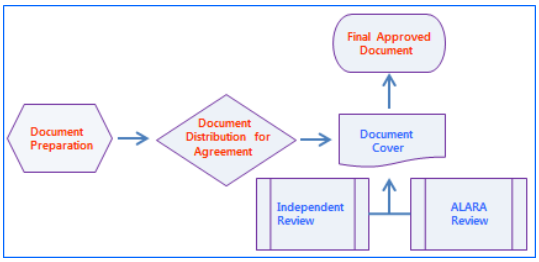

Fig. 1. Flow Sheet of Document Management.

2.3 Organization of Document Management System

2.3.1 Documents management. Documents management is to draw up documents and approve them. Documents management consists of document distribution for agreement (DDA), Inter-office correspondence (IOC), design documents, design drawing, and project manager memo (PM memo). First, document distribution for agreement is to gain agreement from reviewing of technical related division about internal production documents and to approve them. Second, IOC is to co-operate the work of organization and to hold technical information in common. Third, design documents contains document number, title, prepared signature, reviewer's signature, approver's signature on document cover and is to be completed documents through DDA.

2.3.2 Organization management. To conduct decommission project, decommission technology research division has to organize structure, register structure, manage structure, manage business related institutes, give the rights to use document management system, and manage it. Decommission technology research division is now the structure of research and development. When decommissioning nuclear power plants and research reactors, decommission technology research division will change the structure of research and development into the business structure.

2.3.3 Documents keeping. Documents keeping is to store approved documents (DDA, IOC, PM memo, design documents, design drawing), to register approved documents with manuscript, the minutes, test materials, educational training, procurement, quality assurance, and related business data.

3. Conclusion

To draw up, review, approve, register the documents of radiological characteristic information of decommissioned waste, the planning for document management system setup is drawn up. The document sheet is drawn up. Document management system is also organized. In the future, when completing setup of document management system of decommissioned waste, the performance tests on document management system of decommissioned waste will be carried out.

ACKNOWLEDGEMENT

This work was supported by a grant from the National Research Foundation of Korea (NRF), funded by the Korean government, Ministry of Science, ICT and Future Planning (No. 2017M2A8A5015143).

REFERENCES

[1] P. Kook-Nam, H. In-Hye, K. Dae-Seo, H. Sang-Bum, O. Jung-Sup, G. Moon-Joo, "Development of Decommissioning Project Management System Platform", Korean Radioactive Waste Society Spring Meeting, May 31-June 01, 2018, Busan.

[2] P. Kook-Nam, H. In-Hye, K. Dae-Seo, H. Sang-Bum, H. Jea-Hyun, P. Seung-Kook, "Conceptual Design for Development of Decommissioning Project Management System", Korean Nuclear Society Autumn Meeting, October 26-27, 2017, Gyeongju.

Separation of Clay Minerals Using Polyethylenimine-coated Magnetic Nanoparticles

June-Hyun Kim[1,2], Sung-Man Kim[1], In-Ho Yoon[1], Sang-June Choi[2], and Il-Gook Kim[1,*]

[1] Korea Atomic Energy Research Institute, 111, Daedeok-daero 989beon-gil, Yuseong-gu, Daejeon, Republic of Korea

[2] Kyungpook National University, 80, Daehak-ro, Buk-gu, Daegu, Republic of Korea

*ilgook@kaeri.re.kr

1. Introduction

Radioactive Cs released by nuclear accident such as Fukushima Daiichi Nuclear has resulted in severe soil contamination. According to Horie et al. (2017), after Fukushima Daiichi Nuclear accident, the total quantity of contaminated soils discharged through the work is expected to be 16~22 million m^3 [1].

Radioactive Cs was mainly adsorbed on topsoil within 5 cm of the area round due to strong affinity with clay minerals. It was reported that clays account for approximately 7% within the surface 10 cm of the soil near to the Fukushima area [2]. Therefore, separation of clay minerals from soil is necessarily needed for soil waste volume reduction.

Cs is strongly and selectively adsorbed onto especially 2:1 type clay minerals such as illite (ILT) that have high selective adsorption property of Cs, due to their negatively charged surface and frayed edge site.

For selective clay mineral separation, the surface properties of clay minerals are considered for a key role. Therefore, the surface-modified magnetic nanoparticles (MNPs) by polyethylenimine (PEI) which is known for its high density of positive charge, were used to separate clay mineral having a negative charge. PEI-coated magnetic nanoparticles were applied to separate clay mineral. Also, several primary parameters that affect the separation of clay mineral were investigated.

2. Materials and Methods

2.1 Synthesis of Naked MNPs

Naked MNPs were synthesized by co-precipitation method. The concentration of MNPs suspension were represented by the concentration of the total Fe determined by contrAA 700 (F-AAS).

2.2 Synthesis of PEI-coated MNPs

1 mL of 5% (w/w) PEI solution was mixed with different mass ratio (0.01:1, 0.02:1, 0.04:1, 0.05:1, 0.06:1, 0.08:1, 0.1:1) of MNPs solution, and the mixture was sonicated for 30 min. In order to remove residual PEI, PEI-MNPs were separated from the solution by magnetic separation and washed with DI water for seven times.

2.3 Clays Separation

The naked MNPs and PEI-MNPs were mixed with different mass ratio (0.005:1, 0.01:1, 0.05:1, 0.1:1, 0.2:1, 0.4:1, 0.8:1, 1:1) of clay mineral (ILT). Clay separation efficiency (SE%) was calculated using SE% =100% - ($m_f/m_0 \times 100\%$), where m_0 is the initial clay mineral mass in the suspension and m_f is the final clay mineral mass in the suspension.

3. Results and Discussion

3.1 MNPs Physicochemical Properties

Increasing PEI to MNPs mass ratio, zeta potential of PEI-coated MNPs have more and more positive charge, which is maximum level at the 0.1 of PEI to MNPs mass ratio (Fig. 1 (a)). Also, PEI-coated

MNPs (mass ratio 0.1) have positive charge at a wide pH range, whereas naked MNPs have positive charge above pH 6, and clay mineral has negative charge (Fig. 1 (b)). These results imply that PEI-coated MNPs are likely to adsorb on clay mineral because of the electrostatic attraction against naked MNPs.

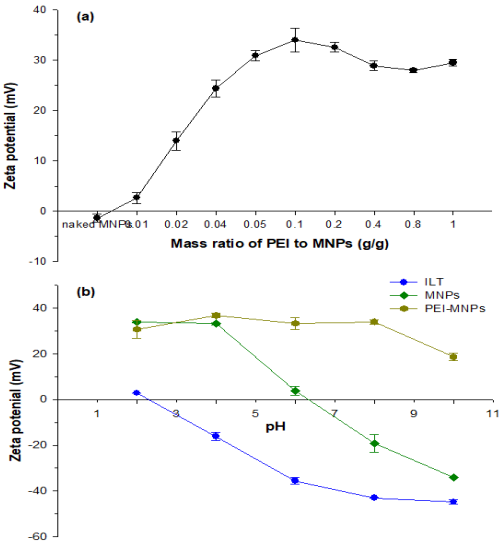

Fig. 1. Zeta potentials of (a) PEI-MNPs at different mass ratio of PEI to MNPs (g/g) at pH 7, (b) naked MNPs, PEI-MNPs (mass ratio 0.1) and clay mineral at different pH.

3.2 Effect of PEI Coating on Clays Separation.

Fig. 2 indicates that the separation efficiency (SE%) of clay minerals increased with the increase of the mass ratio between the both naked MNPs or PEI-MNPs and clay minerals.

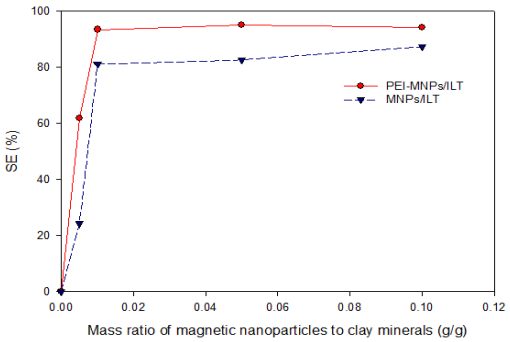

Fig. 2. Clay separation efficiency (SE%) as a function of the mass ratio of magnetic nanoparticles to clay minerals at pH 7. The initial clay mineral mass was 50 mg.

When the mass ratio of naked or PEI-coated MNPs to ILT was 0.01 and 0.1 g/g, the maximum separation efficiency of 94.3% and 87.3% was achieved, respectively. This result shows that the PEI coating significantly reduces the dose demand to separate clay minerals compared to naked MNPs.

4. Conclusion

PEI-coated MNPs which were synthesized at 0.1 of the mass ratio (g/g) PEI to MNPs to separate clay minerals. When the mass ratio PEI-MNPs to clay mineral exceeded 0.1 g/g, maximum separation efficiency was obtained. Hence, the PEI-coated MNPs with magnetic separation provide a promising method for efficient separation of clay minerals.

ACKNOWLEDGEMENT

This work was supported by a National Research Foundation of Korea (NRF) grant funded by the Korean government (Ministry of Science and ICT) (NO.2017 M2A8A5015148)

REFERENCES

[1] Horie, H. et al, Volume reduction of cesium contaminated soil by magnetic separation-Pretreament of organic matters-, J. Phys.: conf. ser 2017, 871, 012102

[2] Zhang, H., et al., Selective separation of cesium contaminated clays from pristine clays by flotation, Chem. Eng. J 2019, 355, 799-804

Removal of Cesium From the Field Soil Using Chemical Extraction

Sung Man Kim[1,2], Chan Woo Park[1], Il-Gook Kim[1], Jun-Hyun Kim[1], So-Jin Park[2], and In-ho Yoon[1,*]

[1] Korea Atomic Energy Research Institute, 111, Daedeok-daero 989beon-gil, Yuseong-gu, Daejeon, Republic of Korea

[2] Chungnam National University, 99, Daehak-ro, Yuseong-gu, Daejeon, Republic of Korea

[*]ihyoon@kaeri.re.kr

1. Introduction

The operation of nuclear facilities can pollute the soil of the facility site by the emitted gas and liquid radioactive materials. Furthermore, decommissioning the nuclear facility requires significant costs for decontamination and disposal of contaminated soil. A trace amount of Cs is well known to be strongly adsorbed by clay minerals. This factor is also one of the reasons for the use of clay as barriers in the disposal of radioactive waste. Cs is specifically adsorbed onto micaceous minerals notably onto the frayed-edge sites on illite, which account for about 1% of their total cation exchange capacity (CEC).

In this study, The sample was collected near the Kori No. 1 nuclear power plant located in Gyesang-gun, Busan, and the composition analysis and desorption experiment using oxalic acid was performed by contaminating non-radiative cesium.

2. Materials and Method

2.1 Materials

The clay used in this study was sieved using a sieve (Mesh Size 20 um, EF-8F020) with particle size (> 20 um) an collected from the soill Kori No. 1 nuclear power plant located in Gyesang-gun, Busan. Oxalic acid dehydrate, NaTPB, Hydrofluoric acid, Ammonium sulfate purchased from Sigma-Aldrich as a desorbent to remove Cs from Cesium chloride and clay. A shaking heating bath (BS-21, JEIO TECH Company, Korea) was used to conduct desorption experiments at 80°C.

2.2 Hydrothermal Desorption of Cs-gori Clay Minerals

We add oxalic acid 0.015, 0.15, 1 and 1.5 mol/L (35 ml) to the illite (0.35 g) contaminated with CsCl in a 60 ml tube (Graduated Bottle Wide neck, PP 60 ml, Azlon®, UK). The reaction was carried out in a shaking heating bath (BS-21, JEIO TECH Company, Korea) for thermal desorption at 80°C for 3 days. After 3 days, the solid / liquid was separated using a centrifuge (Multi-purpose Centrifuge, Combi-514R, Hanil Science Inc., Korea), and only the supernatant was collected and filtered through a polyvinylidene fluoride (PVDF) membrane filter (pore size = 0.45 um) The desorption efficiency of Cs in clay is analyzed by inductively coupled plasma mass spectroscopy (ICP-MS; ELAN DRC II, Perkin-Elmer, USA).

3. Results and Discussion

3.1 Cs Desorption Effect of the Clay on Oxalic Acid and Complex Desorbents

The higher the concentration of oxalic acid desorbent, the increaser the desorption rate. At the

concentration of 1.5 M, the Cs desorption rate was 88.41%. Furthermore, desorption experiments were carried out with various desorbents in a sequential process. It was confirmed that 92% of Cs desorption was achieved with in HF and $(NH_4)_2SO_4$.

Table 1. Cs desorption rate using oxalic acid and complex desorbents in gori-vicinity surface clay at 80℃ for 3day

Clay	Chemical	Concentratin (mol/L)	Cs desorption(%)
Gori	Control	D.W	0.72±0.03
	Oxalic acid (mol/L)	0.015	39.06±0.13
		0.15	69.61±2.25
		1	80.46±0.30
		1.5	88.41±3.83
	Oxalic acid 1.5 (mol/L)	HF	92.22±1.90
		$(NH_4)_2SO_4$	92.27±1.90
		NaTPB	90.51±1.90

3.2 Effects of Oxalic Acid and Complex Desorbents on the Structures of Clay Minerals

Fig. 1 shows the interlayer and structural changes of Clay following treatment with oxalic acid and complex adsorbents using XRD. It was confirmed that the reflection intensity of 2theta – 7.22°, 10.15° peak in oxalic acid were significantly weakened because the structure of clay was changed from crystalline to amorphous structure. Also, the leaching of cations by organic acids causes the making them finer, thinner and weakening the mineral.

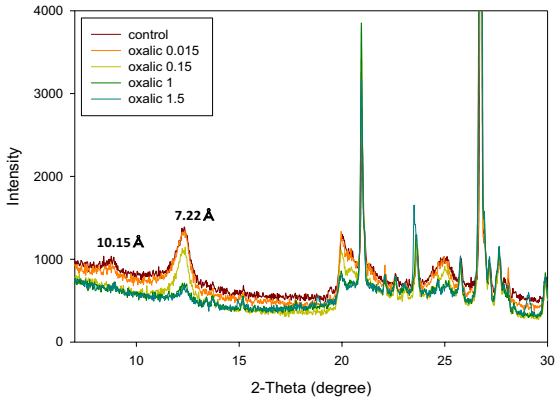

Fig. 1. XRD patterns of Kori-vicinity surface clay with various concentrations of oxalic acid at 80℃ 3day.

4. Conclusion

In conclusion, the oxalic acid proved to be effective in desorbing Cs from clay. The oxalic acid binds to the metal ions forming the crystal of the clay through the chelating mechanism and breaks the interlayer. For that reason, it facilitates Cs desorption. Therefore, it can be effectively used to restore soil in a residential area that has been widely contaminated with radioactive radionuclides such as Fukushima nuclear accident.

ACKNOWLEDGMENTS

This work was supported by a National Research Foundation of Korea (NRF) grant funded by the Korean government (Ministry of Science and ICT) (No. 2017 M2A8A5015148).

REFERENCES

[1] K. mingming, L. Haung, et al, “Effect of oxalic and citric acids on three clay minerals after incubation”, Applied clay Science., 99, 207-214 (2014).

Studies on UVC Photo-Fenton Decomposition of Oxalate Waste Depending on the Reactor Size

Yoon-Ji Park[1,*], Hyun-Kyu Lee[1], Sae-Binna Lee[1], Wonzin Oh[1], Sang-June Choi[1], Hak-Soo Kim[2], Cho-Rong Kim[2], and Ki-Chul Kim[3]

[1] Kyungpook National University, 80, Daehak-ro, Buk-gu, Daegu, Republic of Korea

[2] KHNP Central Research Institute, 70, Yuseong-daero 1312beon-gil, Yuseong-gu, Daejeon, Republic of Korea

[3] KEPCO KPS, 96-1, Gilcheon-gil, Jangan-eup, Gijang-gun, Busan, Republic of Korea

[*]qkrdbswl2@knu.ac.kr

1. Introduction

To remove the oxalic acid used as a reducing agent in the NPP system decontamination, it is necessary to decompose oxalic acid ($H_2C_2O_4$) into CO_2 and H_2O to reduce the amount of waste [1]. Photo-Fenton reaction can be applied to decompose oxalic acid by the combination of H_2O_2, Fe^{2+} and UV [2]. In Photo-Fenton reactions, the type of UV lamp and the irradiance density are important factors in determining the decomposition performance. The amalgam lamp has a short wavelength of 257.3 nm, long life and low energy consumption [3]. In this study, the effect of reactor size on decomposition behavior of $H_2C_2O_4$ was investigated according to energy irradiation density.

2. Experiments

2.1 Materials and Apparatus

Ferrous chloride ($FeCl_2 \cdot 4H_2O$, Min. 99%), oxalic acid ($H_2C_2O_4 \cdot 2H_2O$, Min. 99.5~100.2%), and hydrogen peroxide (H_2O_2, Min. 28%) were purchased from Ducksan company Korea. The size of UV reactor was varied to 3, 46 L, and details are shown in Table 1.

Table 1. Specification of UVC Photo-Fenton reactors

Type	Reactor size (L)	Mixing tank volume (L)	UVC Energy Irradiation	
			Power (W)	Power/Reactor volume (W/L)
KNU	3	6	34	4.4
CRI	46	45.2	204	2.79

2.2 Method

The experimental method was as following. 2 mM $FeCl_2$ and 30 mM $H_2C_2O_4$ were mixed in the UV reactor. Then, 30 mM H_2O_2 was injected into the mixed solution. Residual concentration of $H_2C_2O_4$ with reaction time was confirmed by TOC analyzer (TOC-V CPH, SHIMADZU, JAPAN).

Table 2. Experimental Conditions

Operation conditions	KNU	CRI
Waste volume (L)	9	60
Reactor volume (L)	3	14.8
Circulation rate_Q (L/min)	0.2	0.005
Reactor residence time (min)	15	2960

3. Results

Fig. 1 and, 2 shows the decomposition rate of oxalic acid by reactor size. The experimental results

show that the decomposition rate of oxalic acid depends on the energy irradiation density regardless of reactor size, circulate rate and waste amount.

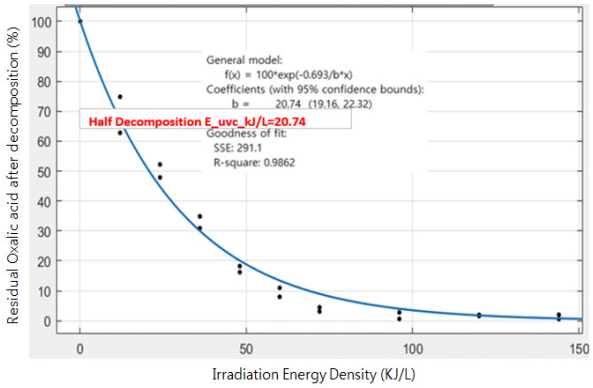

Fig. 1. Fraction of oxalic acid residual depending on energy irradiation density (KNU).

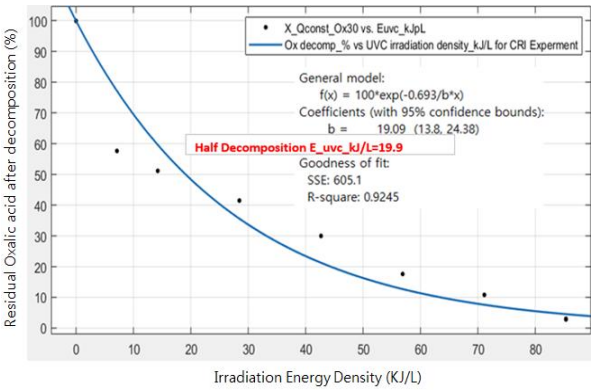

Fig. 2. Fraction of oxalic acid residual depending on energy irradiation density (CRI).

4. Conclusion

The following conclusions were obtained in comparison of the oxalate Photo-Fenton decomposition behavior by using two different size of reactors.

1. The oxalate decomposition behavior by UVC Photo-Fenton depends on the UVC energy irradiation density, regardless of the size of the UVC reactor.
2. The oxalate decomposition reaction depends on the UVC energy irradiation density (KJ/L) regardless of the circulate rate and waste amount.

ACKNOWLEDGEMENT

This work was supported by the Korea Institute of Energy Technology Evaluation and Planning (KETEP) and the Ministry of Trade, Industry & Energy (MOTIE) of the Republic of Korea (No. 20141510300310).

REFERENCES

[1] H.S. Kim, K.C. Kim, W.Z. Oh et.al., “Development of Decontamination Technology of Reactor Coolant System and Dismantled Equipment for NPP Decommissioning.”, Final report (2018).

[2] Y. Zuo, Y. Deng, “Iron (II) catalyzed photochemical decomposition of oxalic acid and generation of H_2O_2 in atmospheric liquid phases.”, Chemosphere, 35(9), 2051-2058 (1997).

[3] S. Schalk, V. Adam, E. Arnold, K. Brieden, A. Voronov, H.D. Witzke, "UV-lamps for disinfection and advanced oxidation-lamp types, technologies and applications.", IUVA news 8.1, 32-37 (2005).

Radioactive Aerosol Modeling in Metal Cutting Process During NPP Decommissioning and Dismantling

Hwa Jeong Han, Woong Ryul Choi, Jae Hong Yim, Yeong Sang Jo, and Byung Gi Park*
Soonchunhyang University, 22, Soonchunhyang-ro, Sinchang-myeon, Asan-si, Chungcheongnam-do, Republic of Korea
*byunggi@sch.ac.kr

1. Introduction

In the decommissioning process of nuclear power plants, cutting is an important process for dismantling radioactive contaminated structures into sizes that can easily handle them. Cutting techniques used to dismantle radioactive contaminated structures are roughly divided into thermal cutting techniques using plasma torches, lasers, arc discharges, and mechanical cutting using saws, grinders, and the like. Aerosols are inevitably generated in the process of cutting structures using these technologies. In particular, cutting of radioactive contaminated structures generates radioactive aerosols, which are emitted not only to the operator but also to the atmosphere when not appropriately sealed. Therefore, in order to secure radiological safety during dismantling of nuclear power plants, it is necessary to evaluate the generation and spread of radioactive aerosols during the cutting process and apply appropriate protection techniques.

Aerosol modeling in nuclear facilities has been developed and used mainly focusing on the diffusion behavior of aerosols generated from accidents, but it is not appropriate to consider the worker environment for work performed in closed spaces. Since the ventilation system is installed to prevent the release of radioactive aerosols into environment generated during the work process such as dismantling work, it is necessary to develop a tool for evaluating the behavior of radioactive aerosols in order to protect workers participating in the work.

2. Radioactive Aerosol Model

The mechanism for removing the base metal in laser cutting is known to be melt breakdown by high pressure gas, evaporation of melt, release of melt by recoil pressure due to evaporation, and the like. The recoil pressure is caused by the reaction force acting on the surface by the vaporizing gas and increasing the surface pressure of the melt, causing the melt to flow in a direction parallel to the evaporation surface. Therefore, the model of the laser cutting process should consider the momentum conservation of the recoil pressure by melting, evaporation, supporting gas flow and evaporation. Evaporation from the melt is modeled by Hertz-Knudsen equation and vapor pressure by Clausius-Clapeyron.

The size distribution and concentration of aerosol particles vary with time and location. Assuming that the cutting for disassembly of the structure is done in a closed space with a ventilation system, the worker's health in the confined space will be greatly influenced by the distribution of radioactive aerosols and will require various protective equipment to protect the workers. Furthermore, even if the radioactive contaminated structure is cut in a closed space having a ventilation system, the radioactive aerosol that has leaked from the protective barrier or the ventilation system is likely to be released into the atmosphere. Therefore, the aerosol model associated with dismantling work should be divided into two parts: the aerosol distribution in confined space and the diffusion path of aerosols emitted into the

atmosphere. This study focuses on the time and space distribution of radioactive aerosols in the work space for the purpose of suppressing radioactive aerosol exposure to workers and preparing for ventilation systems. Evaluation models for aerosols leaked through protective barriers have been developed in many ways, so the priority is dealt with in this study. Since the generation of radioactive aerosols depends on the cutting mechanism, the generation model is constructed as a separate model.

Depending on the time and space in the workspace, the aerosol particles move according to the atmospheric flow, and the particles are removed by flocculation and condensation, particle interactions, immersion, re-floating, (PSD) and the total number of particles. Computing the atmospheric flow using CFD under the assumption that the atmospheric flow and the PSD are independent when modeling the aerosol behavior in a given space, and calculating the PSD change due to the coagulation and condensation phenomenon after the particle moves by convection and diffusion is often used. Simulation of gas phase and particulate multiphase flow in one direction is reasonable when the volume, mass, and mass occupied by the particle are small. Usually this type of simulation is known to be suitable for.

3. Conclusion

Cutting in a closed workspace generates a large amount of dust, so it is likely that there will be a limit to understanding the overall phenomenon when simulating a multiphase flow including particles and gases in one direction. As an alternative to unidirectional simulation, a method of combining and simulating multiphase flows has been developed. The multiphase flow is modelled using Eulerian-Lagrangian methods. The PBMC (Population Balance-Monte Carlo) method has recently been developed as a suitable model for the multiphase flow model that implements the flow-trajectory. The PBMC method is implemented using the constant-number method and the differentially weighted MC method.

ACKNOWLEDGEMENT

This work was supported by a Nuclear Technology & Development Program of the National Research Foundation of Korea (NRF) grant funded by the Ministry of Science and ICT (MSIT) (Grant No. NRF- 2017M2A8A4018593).

Review and Preliminary Application of SADRWMS Methodology to Decommissioning Waste From NPPs

Ji Su Kang, Na Yoon Choi, and Jae Hak Cheong*
Kyung Hee University, 1732, Deogyeong-daero, Giheung-gu, Yongin-si, Gyeonggi-do, Republic of Korea
*jhcheong@khu.ac.kr

1. Introduction

While the radioactive waste management framework at nuclear power plants(NPPs) in operation has been well established in Korea, the regulatory guide considering the characteristics of decommissioning waste has not been developed yet. Therefore, the operator of the NPP may take various options for predisposal management of decommissioning waste generated during the dismantling and decontamination processes.

Each decommissioning waste would be subject to various predisposal management steps such as pretreatment including proper sorting and collection, treatment, conditioning, storage, and transport. In order to systematically identify these management steps, it is essential to develop regulatory technologies that can evaluate and verify the safety of decommissioning waste in various predisposal management phases. The development of authorizations and of limits, conditions and controls for the predisposal management of radioactive waste benefits from close communication and cooperation between the operators, regulatory bodies and other interested parties [1].

The IAEA has provided safety assessment principles and basic approaches in predisposal management of radioactive waste as well as an example of the safety review of the regulatory body in the Safety Guide for the Safety Case and Safety Assessment for Predisposal Management of Radioactive Waste [2]. The authors identify representative decommissioning wastes generated during decommissioning through the Decommissioning Experience Report in other countries and expected amount of Kori Unit 1 permanently shut down [3].

2. Review of SADRWMS Methodology to Decommissioning Waste

In 2004, the IAEA commenced joint research on Safety Assessment Driving Radioactive Waste Management Solutions (SADRWMS) on the safety of radioactive waste management prior to disposal. SADRWMS was carried out for the purpose of establishing the safety assessment methodology for the predisposal and storage facilities of radioactive waste, and the Safety Assessment Framework (SAFRAN) computer code was developed in 2005.

The SAFRAN computer code can be used to perform the predisposal management safety assessment of each decommissioning waste through the algorithm shown in Fig. 1.

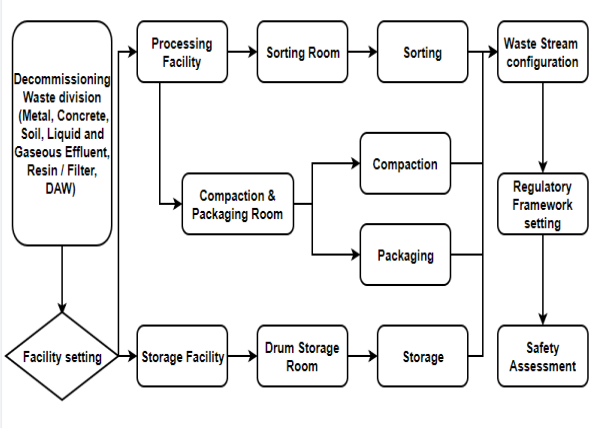

Fig. 1. Algorithm of Safety Assessment evaluated in SAFRAN computer code.

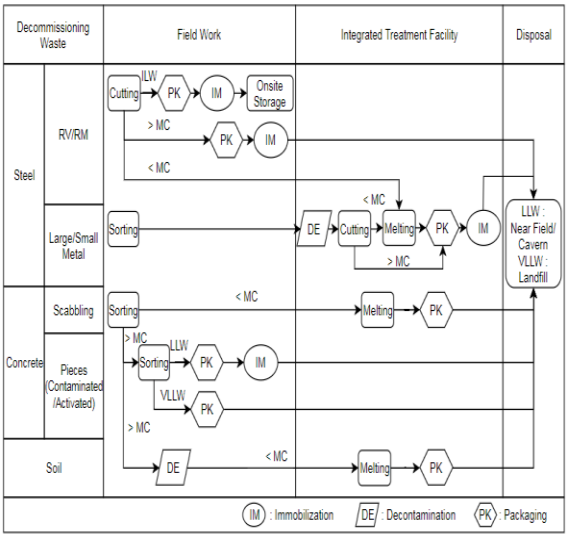

Fig. 2. Example of Predisposal Management of Decommissioning Waste from NPPs [4].

The stages of predisposal management usually include sorting, compaction, sedimentation, packaging, and storage. The steps of the predisposal management of decommissioning waste presented by test case are shown in Fig. 2. To make Waste Stream with SAFRAN computer codes, it should be divided in three parts, Sorting room, Compaction and Packaging room and Storage room. From these results, there is a limit to the representation of 'Decontamination', 'Cutting', 'Melting' and 'Immobilization. Fig. 3 shows waste stream implemented by SAFRAN code.

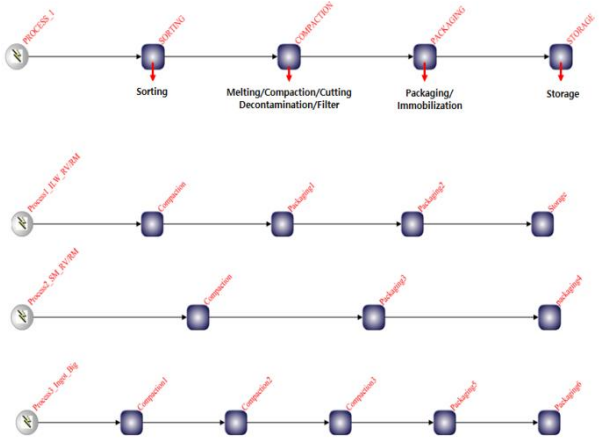

Fig. 3. Waste Stream implemented by SAFRAN computer code.

3. Conclusions

Since the actual decommissioning system differs from the operation, the safety assessment for various stages in predisposal management is required. Through the standard methodology, SADRWMS, its applicability to the predisposal management stage of domestic decommissioning waste was identified. If information on the processing system to be adopted at the actual decommissioning site is available, more detailed practical studies are to be needed.

ACKNOWLEDGEMENT

This work was supported by the Nuclear Safety Research Program through the Korea Foundation Of Nuclear Safety (KOFONS), granted financial resource from the Nuclear Safety and Security Commission (NSSC), Republic of Korea (No. 1605008).

REFERENCES

[1] IAEA Safety Standards Series No. GSR part 5, "Predisposal Management of Radioactive Waste", (2009).

[2] IAEA Safety Standards Series No. GSG-3, "Safety Guide for the Safety Case and Safety Assessment for Predisposal Management of Radioactive Waste", (2013).

[3] Electric Power Research Institute (EPRI), "Review of Waste Management Best Practices during Nuclear Plant Decommissioning", (2015).

[4] Korea Hydro and Nuclear Power Corporation (KHNP), "Decommissioning Waste Management System Using RFID", Workshop of Radioactive Waste Treatment and Disposal, June 26, 2018, Daejeon.

Status of Tritium Permeation Analysis Tool for HCCR TBS

Hyung Gon Jin [a,*], Dong Won Lee [a], Jae Sung Yoon [a], Suk Kwon Kim [a], Eo Hwak Lee [a], Seong Dae Park[a], Chang Wook Shin[a], and Seungyon Cho[b]

[a]Korea Atomic Energy Research Institute, 111, Daedeok-daero 989beon-gil, Yuseong-gu, Daejeon, Republic of Korea

[b]National Fusion Research Institute, 169-148, Gwahak-ro, Yuseong-gu, Daejeon, Republic of Korea

[*]jhg@kaeri.re.kr

1. Introduction

Korea has been developing a Helium Cooled Ceramic Reflector (HCCR) TBM to be tested in the ITER [1]. It consists of two major systems, which are HCS (Helium Cooling System) and TES (Tritium Extraction System) (Fig. 1). Important safety issue is tritium permeation of the system. Tritium is one of the most highly permeable molecules on earth, therefore tritium permeation takes place from TES to HCS in the TBM. Permeated tritium migrates along the system pipes, thus tritium inventory should be considered with respect to entire TBS. Simplified steady state tritium analysis models and codes were developed by KO TBM team (Fig.1), which can accommodate parameter change of each design stage, such as PD-1, -2 and 3 etc. Tritium analysis code has been developed since 2015 and this paper shows current status of the achievement.

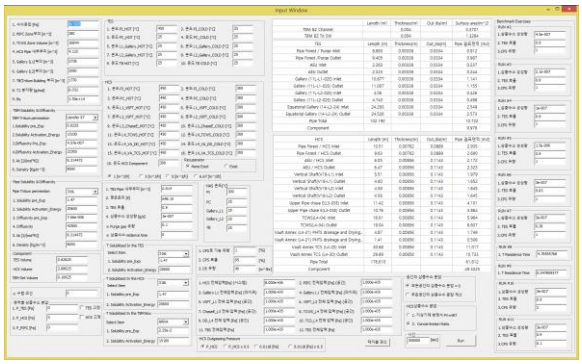

Fig. 1. Schematics of HCCR-TBS.

2. Characteristics of the Code

The simplified tritium permeation model has following characteristics:

TBS sub-systems fully interconnected, the tritium concentration, tritium generation and losses are calculated together for all concerned sub-systems. The tritium mass conservation is ensured. Tritium is assumed in T2 form in all fluid, and tritium transport mechanisms in solid materials limited to the diffusive regime, which means the surface phenomena is not taken into account. The system is modelled as connection networks of volumes. 0-D lumped model is used, which means the interior properties like tritium concentration, temperature, pressure etc. are assumed to be uniform in each volume. Steady state assumption, which means the generation and loss of tritium are in balance, all the parameters do not change by time. No multi-physics phenomena modelled, the flow distribution of main fluid and temperature distribution in structure materials are inputs of the analysis.

3. Input Data Set of the Code

Table 1 is summary of boundary condition which is applied to HCCR TBS calculation and Fig. 2 is pipe length and operational temperature information of each room which HCCR-TBS is allocated. Design of HCCR-TBS is evolving and this data reflects recent update of PD-1 phase. [2]

Table 1. Summary of boundary condition

Tritium Production Rate	25.9 mg/day (continuous back to back with duty 0.25)
PI/PC Volume	280.264 m^3
TCWS VA Volume	500 m^3 (considering occupied by HCCR HCS/CPS)
TES Pipe Thickness	3.68 mm
HCS Pipe Thickness	8.56 mm (Vertical shaft pipe thickness 8.56 mm)
BZ Pipe Thickness	4.0 mm
N-DS at PI/PC	40 m^3/h
HVAC at TCWS	1 Vol/hr, i.e. 500 m^3/h

4. Result Screens

Examples of result screen is given as Fig. 2. IO (ITER Organization) requests various kinds of tritium permeation analysis results and each result screen is optimized for that specific issue, for example, Fig. 2 is the output of tritium analysis for CDR (Conceptual Design Review) of HCCR TBS.

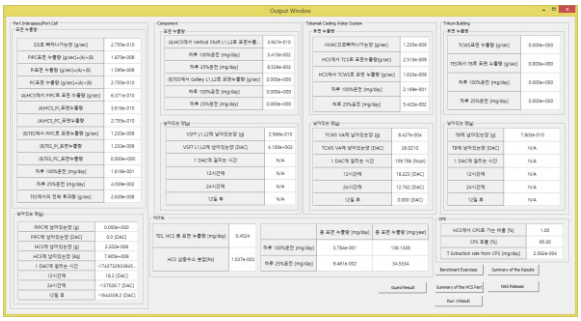

Fig. 2. Tritium release analysis result screen for CDR.

And Fig. 3 is the result screen for the tritium benchmark analysis of each TBS. This result is one of related outcomes of TF-TPSD (Task Force on the TBM Program Safety Demonstration) and sensitivity study had been performed.

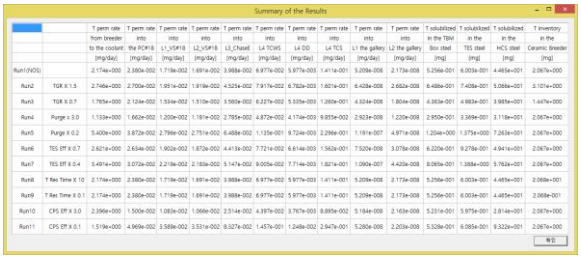

Fig. 3. Tritium release analysis result screen for tritium benchmark analysis for each TBS.

Fig. 4 is based on the given tritium permeation model and boundary conditions, tritium release rate from NAS (Neutron Activation System) of HCCR TBS is presented, which is estimated values after 500 cycles of operations. Continuous operation 500 cycles postulate equivalent load over ten days of 3-shift back to back operation, which is nearly one campaign (11 days operation + 3 short term maintenance). Tritium concentration at the end of 500 cycles is 2.48E-01 Pa, however, it is drastically decreased in real situation. Because service vacuum system of ITER is continuously venting the used driving gas in NAS tubes.

5. Further Works

Developing tritium analysis tool is successfully on going work, which will adopt latest design of the HCCR TBS and estimate tritium release rate at each ITER building room. At this stage of development, using simplified 1D is the most efficient approach to draft tritium release estimation, however, it is expected that multi-D or multi-effect model should be used for precise result.

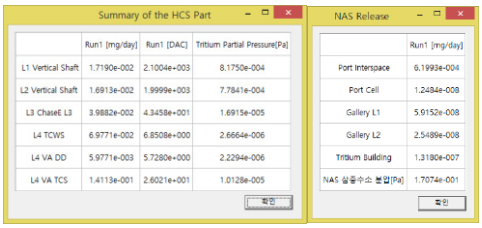

Fig. 4. Tritium release analysis result screen for NAS.

ACKNOWLEDGEMENT

This work was supported by the R&D Program through the National Fusion Research Institute (NFRI) funded by the Ministry of Science and ICT of the Republic of Korea (NFRI-IN1903).

REFERENCES

[1] D.W. Lee, et. al., “Current Status and R&D Plan on ITER TBMs of Korea,” Journal of Korean Physical Society, 49 S340-S344 (2006).

[2] I. Ricapito, TBM Project team, F4E “Guideline for the Benchmark Exercise on Tritium Modelling of TBSs”, TM9J3Q (2016).

Extraction of Radioactive Ions Using Entrainer and Supercritical Decontamination Technic Equipped With Ultrasonic-horn

Jaebin Shin, Kwangheon Park*, and Tae hun Kim
Kyung Hee University, 1732, Deogyeong-daero, Giheung-gu, Yongin-si, Gyeonggi-do, Republic of Korea
*kpark@khu.ac.kr

1. Introduction

Due to the aging of domestic nuclear power plants, the importance of decontamination technology for decommissioning power plants is increasing. However, current decontamination technologies have the problem of generating a large amount of secondary waste. From this point of view, supercritical CO_2 ($scCO_2$) seems to be an alternative solvent to solve this problem. In this study, extraction experiments of radioactive metals were carried out using supercritical decontamination technology with ultrasonic horn.

2. Material and Methods

2.1 Preparation of Metal Specimen

In this study, the SUS bolts were used as specimen. The process of preparation is illustrated in Fig. 1 that used Co-60 (3.7×10^3 Bq/ml) standard solution from KAERI.

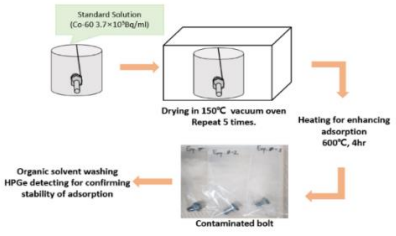

Fig. 1. Procedure of specimen preparation.

2.2 Selection of Surfactant

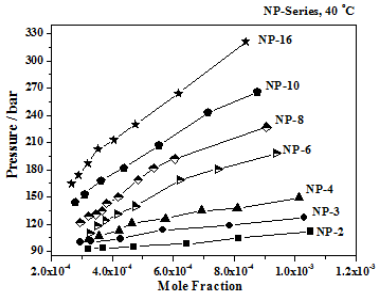

Fig. 2. Solubility of NP-series in $scCO_2$.

NP-series has solubility in $scCO_2$. For this study, surfactant selected as NP-4 that used by our Lab in the past study [1].

2.3 Procedure of Decontamination Experiment

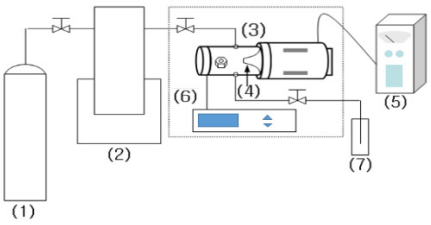

Fig. 3. Experiment of metal surface decontamination using ultrasonic horn (1) CO_2Tank (2) Syringe Pump (3) High pressure vessel equipped with ultrasonic horn (4) Ultrasonic Horn (5) Ultrasonic Wave Generator (6) Temperature Controller (7) Bubbler.

The extraction experiment consisted of 10 cycles for 1 hour, each cycle consisted of generating ultrasonic for 5 minutes and then stabilizing for 1

minute under 200 bar, 40℃. In this way, experiments were performed depending on four entrainers. (LiOH, H_2O, Nitric Acid and Oxalic Acid).

The decontamination efficiency was obtained by comparing the peak (1.17 MeV and 1.33 MeV) counts before and after the experiment of cobalt through HPGe (ORTEC, OR, Tennessee, USA).

3. Results and Discussion

3.1 Extraction Efficiency Depending on pH of Entrainers

Table 1. Variation of extraction efficiency with changing condition

Nuclide	Energy (MeV)	Entrainer	pH	Efficiency (%)
Co-60	1.17	LiOH	11	53
		H_2O	7	55
		Nitric Acid	1	95
		Oxalic Acid	1.2	97
	1.33	LiOH	11	52
		H_2O	7	54
		Nitric Acid	1	95
		Oxalic Acid	1.2	95

Table 1 shown the results of experiments. Relatively high pH such as LiOH and H_2O shown low efficiency. However, Acids that has low pH, shown high efficiency.

3.2 Corrosion Observation

The experiments showed similar efficiencies when the entrainer has the pH value about 1. In the case of inorganic acid test, the corrosion was observed on the surface of specimen after experiment. But the other one was not.

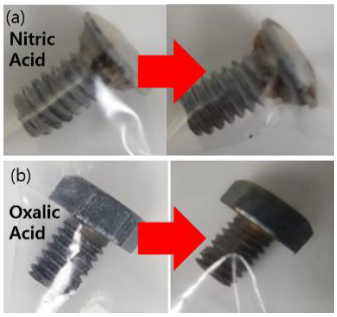

Fig. 4. Surface condition of specimens before and after experiment according to acid type.

4. Conclusion

In this study, experimental results showed that the lower the pH value of the solution forming the reversed micelles, the better the decontamination effect. Moreover, almost the same high extraction efficiency was obtained in solutions with low pH values regardless of acid type. However, the corrosion occurred on the surface of the metal specimen used in inorganic acid condition. Based on all these results, one of the important factors in this technic is the acid concentration of the additive, and it is concluded that the use of organic acids is appropriate to minimize the damage of the specimen.

REFERENCES

[1] Koh, M., et al. "Micro Emulsions in Supercritical Carbon Dioxide Utilizing Nonionic Surfactants." Clean Technol 10.4, 221-228 (2004).

Status of Development of Final Decommissioning Plan for Kori Unit 1

Suk Bon Yoon*, Su Hee Lee, and Jin-Won Son
KHNP Central Research Institute, 70, Yuseong-daero 1312beon-gil, Yuseong-gu, Daejeon, Republic of Korea
*sbyooncri137@khnp.co.kr

1. Introduction

The Final Decommissioning Plan (FDP) is a license document required for approval of the decommissioning of power generating reactors and related facilities in accordance with Article 28 (2) of the Nuclear Safety Act. The FDP is a document that describes all activities to permanently shut down a licensed nuclear power plant and to exclude it from the scope of the law through dismantling of the facility and site or removal of radioactive contamination. In accordance with the recently revised Nuclear Safety Act and the legal requirements for decommissioning such as the Enforcement Regulations of the same Act, the licensee must submit a license document to the regulatory body for the nuclear power plant subject to decommission.

In this work, we briefly introduce the activities such as research projects, decommissioning engineering, and reviewing overseas case on the decommissioning plan that are being carried out to develop the FDP for Kori Unit 1 in accordance with the instructions for the FDP, as specified in Notice No. 2015-8 of the Nuclear Safety Commission [1].

2. Performing Research Projects Related to Decommissioning

We are currently carrying out research projects to secure input data for the FDP of Kori Unit 1 such as decommissioning risk analysis and work difficulty evaluation of decommissioning process. This project aims to develop the technology for the detailed decommissioning cost and process, the program for evaluating decommissioning volume/cost/process, analysis and evaluation of major factors for decommissioning strategy, technology for evaluation of contamination/dose change during decommissioning, and radiological characterization guidelines.

In addition, researches are under way to secure groundwater contamination restoration, groundwater monitoring and contamination evaluation, site release guidelines, and safety evaluation technology.

3. Performing Decommissioning Engineering for Kori Unit 1

Decommissioning engineering is being carried out to promote the decommissioning project of Kori Unit 1. Decommissioning engineering consists of the four fields such as business process design, construction design, radiological characterization, and waste treatment facilities for decommissioning of Kori Unit 1.

The decommissioning project process design includes the development of the integrated process, the detailed process of the decommissioning stage, and the process management system. The decommissioning construction design includes the dismantling of the buildings/structures of the

radiation controlled/non-controlled area and the comprehensive planning for the use of the site/building. Radiological characterization includes the development of radiological characterization procedure and environmental impact assessment. Finally, the decommissioning waste treatment facility includes the basic/implementation design licensing of the waste treatment facility.

4. Reviewing Overseas Cases on the Decommissioning Plan

In order to develop the FDP of Kori Unit 1, the decommissioning plan of Zorita nuclear power plant (NPP) in Spain is secured and the related documents are under review. In addition, decommissioning plan of the Yankee Rowe NPP [2] and the First Nuclear Power Plant in Taiwan were reviewed to examine the scope and depth of the FDP.

5. Conclusion

We developed the Final Decommissioning Plan (FDP) for the decommissioning of Kori Unit 1, the first commercial nuclear power plant in Korea. This FDP will be continuously revised through reflection of results of research and engineering related to decommissioning.

In addition, we intend to enhance the completeness of the FDP for Kori Unit 1 by reflecting the analysis results of the decommissioning plan of the Zorita NPP and the First Nuclear Power Plant in Taiwan.

REFERENCES

[1] Nuclear Safety Commission, “Nuclear Safety Commission Notice No. 2015-8, Regulations on the Preparation of Nuclear Power Plant Decommissioning Plan” (2015).

[2] Yankee Atomic Electric Company, “Yankee Nuclear Power Station Decommissioning Plan, Rev. 0” (1996).

A Review on Generation Characteristics of Sludge Waste During Decommissioning of Nuclear Power Plant

Hang-Rae Cho* and Ji-Hoon Lee
KHNP Central Research Institute, 70, Yuseong-daero 1312beon-gil, Yuseong-gu, Daejeon, Republic of Korea
*hrcho6795@khnp.co.kr

1. Introduction

The decommissioning of unit 1 of Kori nuclear power plant, whose permanent shutdown had been decided in 2017, is expected to begin in 2026. Failure to apply appropriate radioactive waste management measures from the outset of the decommissioning project could cause enormous disruption to the project, including increased disposal costs and early saturation of the disposal sites.

The radioactive sludge wastes generated by nuclear power plant operation include sump sludge, tank sludge, waste oil sludge and other mixed sludge, most of which will be treated in the form of cement solidification and disposed of through securing the disposal suitability of the solids.

In the case of cement solidification, the volume increase due to the low rate of waste loading and the difficulties in securing the disposal suitability will be occur. However, it is expected that there is no significant problem in the application of the technology since the amount of the sludge waste generated is not large.

It is expected that a large amount of various organic and inorganic sludge wastes in the forms of corrosion products, concrete, soil, mixture etc. that are difficult to be processed and disposed of are generated when dismantling NPPs.

Therefore, the origin and physicochemical properties of decommissioning sludge wastes were investigated in order to facilitate the derivation of treatment conditions and technologies for the effective collection, high volume reduction, stabilization of sludge waste and disposal suitability in consideration of the location and physicochemical characteristics of the sludge wastes.

2. Classification of the Sludge

The sludge wastes generated during dismantling of nuclear power plants can be classified as floor sludge, sump sludge and tank sludge, etc. depending on the place of generation. They also can be classified as concrete sludge, soil sludge, organic sludge and mixed sludge depending on the physicochemical properties.

Since decommissioning sludge wastes are incidental wastes generated by the decontamination and dismantling processes carried out at the time of dismantling of NPPs, identifying the types and characteristics of decontamination and dismantling processes first will help to understand the generation characteristics of the decommissioning sludge waste.

2.1 Process-specific Classification

Firstly, corrosion products will be generated by grinding in the process of physical decontamination of piping and equipment, and corrosive sludge will be generated by chemical decontamination with corrosive chemicals.

In the concrete decontamination process, concrete sludge will be generated by scabbling and shaving operations.

Since almost all decontamination processes use water to reduce dust and to dilute chemicals, decontamination sludge will contain a lot of moisture.

2.2 Place-specific Classification

The floor sludge exists at the bottom of the concrete structure in the radiation controlled area and will have a variety of physicochemical properties although it has a small amount of generation.

The sump sludge is a solid that has been deposited into the sump along with waste water, oil, decontamination solution, cleaning water, etc. through the piping of equipment drainage, floor drainage and will include corrosion product, micelle, insoluble compound, dust, etc. as shown in Fig 1.

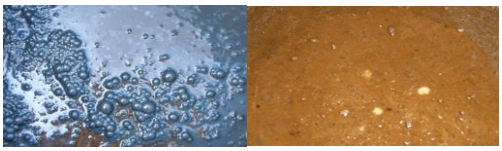

Fig. 1. Shapes of sump sludge [1].

The tank sludge can occur at the bottom of the tanks during dismantling, as the long-term operation of the tanks that collect and store liquid radioactive waste and boric acid water causes deposits of highly dense corrosion products and insoluble compounds produced by micelles and mineral components as shown in Fig. 2. The insoluble compounds may include hydroxides, sulfates, carbonates, phosphates, silica, silicates, borates and the like.

Fig. 2. A shape of tank sludge [1].

3. Characteristics of the Sludge

3.1 Organic Sludge

Since corrosive sludge occurs through chemical agents, there will be a mixture of decontamination and corrosion products with the addition of corrosive chemicals used in the decontamination process.

Organic sludge may occur if a large quantity of organic matter such as chelating agent, antifreeze, lubricant, etc. is leaked during the dismantling and demolition of the primary system equipment and is collected in sumps and mixed with particulate matter. A small amount of leakage can be removed with decontamination paper, so it will be generated as DAW rather than sludge waste.

Oil sludge is a type of organic sludge that occurs when oil such as control oil, fuel oil and lubricating oil contaminated by radioactive materials generated during the dismantling and demolition of the primary system equipment is mixed with a large quantity of corrosion product and particulate matter such as dust as shown in Fig. 3. If the oil alone exists, self-sludge created by oxidation and deterioration of the oil may exit but will not be classified as sludge waste.

Fig. 3. Oil sludge (left) [1] & concrete sludge (right).

3.2 Inorganic Sludge

Corrosion product sludge wastes will occur by mixing dust-reducing water with removed corrosion products during physical grinding of equipment and piping.

Concrete sludge is a concrete powder generated by scabbling and shaving of radioactive materials on the concrete structure in the radiation controlled area for decontamination, and will exit with a mixture of dust-reducing water and concrete powder as shown in Fig. 3. From the source point of view, it may also be classified as floor sludge waste.

Soil sludge occurs as fine soil and clay as shown Fig. 4 except rock and gravel, when radioactive liquid leaks from the buried pipe and soil is contaminated under and around the concrete structure. And depending on the degree of contamination, very large quantities may occur.

Mixed sludge refers to a mixture of two or more of the above mentioned sludge wastes.

Fig. 4. A shape of soil sludge [2].

4. Conclusion

The generation characteristics of decommissioning sludge wastes have been investigated in order to develop a treatment technology that can effectively collect and process and safely dispose of various sludge waste that may occur during dismantling process of NPPs.

First, in terms of generation place, it classified into bottom sludge, sump sludge and tank sludge.

In terms of physicochemical characteristics of decommissioning sludge wastes, they were classified as organic sludge wastes such as corrosive sludge, organic sludge, oil sludge and inorganic sludge wastes such as corrosion product, concrete sludge, soil sludge and mixed sludge waste.

The characteristics of radioactive wastes generated in the nuclear power plant will vary depending on the situation, so it will not be possible to determine the composition or physicochemical characteristics of each type of waste.

Likewise, it is difficult to accurately grasp the physicochemical and radiological characteristics and amounts of decommissioning sludge wastes.

The generation characteristics of sludge wastes may vary depending on the decontamination and dismantling process, and the operation histories of the NPPs.

Therefore, in the basis on general assumptions and forecasts, the generation characteristics of decommissioning sludge wastes have been roughly reviewed in order to capture the concept of development of processing technology such as collection, high volume reduction and stabilization of the sludge waste ensuring the disposal suitability.

REFERENCES

[1] Development of Solidifying Agent of Oily waste Liquid, sludge and Equipment for Solidifying, Final Report, KONEC (2007).

[2] Marek Meciar, Experience with treatment of radioactive waste from NPP of VVER type – Sludge/Resins/Borates, Amec Foster Wheeler Nuclear Slovakia Ltd. (2015).

Radiolysis of Hydrazine in a Reductive Decontamination Solution

Naon Chang[1,2], Huijun Won[2,*], Sangyoon Park[2], Heechul Eun[2], Seonbyeong Kim[2], and Yongsoo Kim[1]
[1] Hanyang University, 222 Wangsimri-ro, Seongdong-gu, Seoul, Republic of Korea
[2] Korea Atomic Energy Research Institute, 111, Daedeok-daero 989beon-gil, Yuseong-gu, Daejeon, Republic of Korea
*nhjwon@kaeri.re.kr

1. Introduction

Before decommissioning of the nuclear power plant, the chemical decontamination process to the reactor coolant system (RCS) is required for reducing the worker exposure. An oxidation and a reductive step are carried out alternately in the chemical decontamination process. Reductive decontamination agent is used for removing oxide layer including Fe by reducing the Fe^{3+} ions to the Fe^{2+}. The HyBRID (Hydrazine Based Reductive metal Ion Decontamination) agent developed by KAERI can be applied in a reductive dissolution step. It is composed of N_2H_4-Cu(I)-H_2SO_4, and hydrazine (N_2H_4) is used as a reductant. However, the hydrazine in HyBRID agent can be decomposed during the decontamination due to an irradiation released from the radionuclide such as Co-60 in the RCS. In this regard, the objective of this study is to investigate the effects of γ-ray irradiation on the radiolytic decomposition of hydrazine. In addition, we compared the results of hydrazine decomposition by varying the solution pH.

2. Methods and Results

2.1 Sample Preparation and ɤ-irradiation

HyBRID-simulated decontamination solution was composed of 0.05 M N_2H_4, 5×10^{-4} M $CuSO_4$. Solution pH was adjusted by adding H_2SO_4 gradually. Tests were carried out at pH 3, 4 and 5. All samples were irradiated with γ-ray and the absorbed doses were 0, 10, 20, and 40 kGy by using a high-dose ɤ-ray irradiator at Jeongeup facility.

2.2 Effect of the Copper Ion

A separate test was carried out for investigating the effect of the copper ion on the radiolysis of N_2H_4. Copper ion increased the decomposed portion of N_2H_4 at same absorbed dose.

2.3 Decomposition of N_2H_4

$[N_2H_4]$ was analyzed by UV spectrometer (DR 5000, Hach Co.). A p-dimethylaminobezaldehyde method was used. Fig. 1 shows the change of $[N_2H_4]$ against the absorbed dose. The concentration of hydrazine decreased with increasing absorbed dose regardless of pH. Even at 40 kGy, however, N_2H_4 remained up to 85% in all pH conditions.

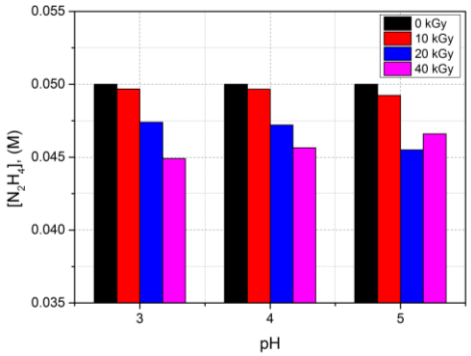

Fig. 1. Change of $[N_2H_4]$.

2.4 Generation of NH_4^+ ion, N_2 and NH_3

NH_4^+ ion, N_2 and NH_3 were produced by radiolytic decomposition of N_2H_4 [1-2]. The concentration of ammonium ions was analyzed by using an ion chromatograph (881 Compact IC pro, Metrohm, Chungnam national university center for research facility). In addition, the produced portion of N_2 and NH_3 was calculated from $[N_2H_4]$ and $[NH_4^+]$. As shown in Fig. 2, the ammonium ion was produced after 40 kGy of γ-ray irradiation in all samples. The amount of NH_4^+, N_2 and NH_3 produced from N_2H_4 decreased with increasing pH.

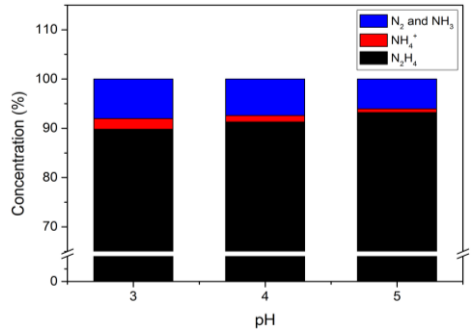

Fig. 2. Concentration of N_2H_4 and products after 40 kGy of ɤ-ray irradiation.

2.5 Decomposition Mechanism

The chemical yield of water radiolysis is $0.27e_{aq}^-$, $0.06H^\bullet$, $0.26OH^\bullet$, 0.045 H_2, 0.08 H_2O_2, and $0.27H_3O^+$. In addition, the e_{aq}^- reacts with H^+ and produces $H^\bullet$ following as Eq. (1).

$$e^-_{aq} + H^+ \rightarrow H^\bullet \quad (1)$$

N_2H_4 exists as a $N_2H_5^+$ in an acidic condition due to the hydrolysis reaction as shown in Fig. 3. $N_2H_5^+$ ion is a dominant species.

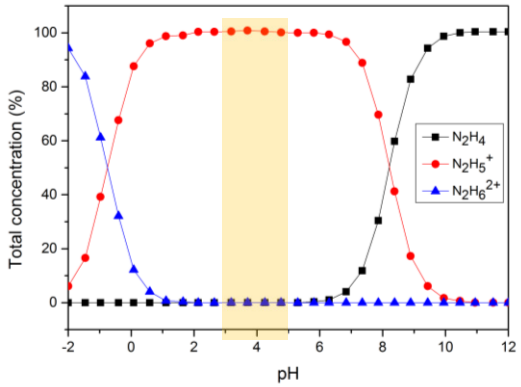

Fig. 3. Hydrolysis of N_2H_4 at different pH condition.

$N_2H_5^+$ ion reacts with radiolysis products of water and produces N_2H_4, $N_2H_4^{\bullet+}$, $^\bullet NH_2$ and NH_4^+ ions as shown in Eq. (2-4). The unit of rate constants is represented with $k/dm^3\ mol^{-1}$.

$$N_2H_5^+ + e^-_{aq} \rightarrow H^\bullet + N_2H_4 \quad (k=1.6\times10^8) \quad (2)$$
$$N_2H_5^+ + OH^\bullet \rightarrow N_2H_4^{\bullet+} + H_2O \quad (k=8.2\times10^7) \quad (3)$$
$$N_2H_5^+ + H^\bullet \rightarrow {}^\bullet NH_2 + NH_4^+ \quad (k=1.3\times10^5) \quad (4)$$

N_2H_4, produced by reaction Eq. (2), hydrolyzed to the $N_2H_5^+$ ion rapidly and it reacts repeatly as Eq. (2-4). Otherwise, it can reacts with $^\bullet NH_2$, $H^\bullet$, and $OH^\bullet$ following as Eq. (5-7).

$$N_2H_4 + {}^\bullet NH_2 \rightarrow {}^\bullet N_2H_3 + NH_3 \quad (k=1.0\times10^7) \quad (5)$$
$$N_2H_4 + OH^\bullet \rightarrow H_2 + {}^\bullet N_2H_3 \quad (k=1.3\times10^5) \quad (6)$$
$$N_2H_4 + H^{\bullet+} \rightarrow {}^\bullet N_2H_3 + H_2O \quad (k=1.3\times10^5) \quad (7)$$

Furthermore, $^\bullet N_2H_3$ reacts with the other $^\bullet N_2H_3$ or $N_2H_5^+$ ion following as Eq. (8) and (9).

$$^\bullet N_2H_3 + {}^\bullet N_2H_3 \rightarrow N_2H_2 + N_2H_4 \quad (k=6.0\times10^8) \quad (8)$$
$$^\bullet N_2H_3 + {}^\bullet N_2H_5^+ \rightarrow N_4H_6\ (\rightarrow N_2 + 2NH_3) \quad (k=4.0\times10^8) \quad (9)$$

$N_2H_4^{\bullet+}$ ion decomposes into H^+ and N_2H_3 or reacts with $N_2H_4^{\bullet+}$ as shown in Eq. (10).

$$N_2H_4^{\bullet+} + N_2H_4^{\bullet+} \rightarrow N_4H_8^{2+}\ (\rightarrow N_2 + NH_3) \quad (k=1.0\times10^8) \quad (10)$$

As a result, hydrazine is decomposed into NH_4^+, N_2 and NH_3.

2.6 Discussions

As the increase of the absorbed dose, the above reactions proceed to further due to the radiolysis products of the water. In this regard, $[N_2H_4]$ decreased according to increasing absorbed dose as shown in Fig. 1.

As shown in Fig. 2, $[N_2H_4]$ at 40 kGy was lower as pH was lower. Low pH means higher concentration of H^+ ions. Therefore, more occurrence of reaction in Eq. (1) could cause more decomposition of hydrazine. This is also the reason that $[NH_4^+]$ increased with decreasing pH.

3. Conclusion

Hydrazine in a reductive decontamination solution can be decomposed due to the ɤ-ray irradiation. The reason of decomposition was explained by reaction the radiolysis product of hydrazine with the radiolysis product of water. This reaction was confirmed by analyzing of ammonium ion. However, it was investigated that decomposed portion of hydrazine was increased when copper ion is contained in a solution. Therefore, it is necessary to study about the effects of copper ions on the radiolytic decomposition of hydrazine. In addition, it needs to analyze N_2 and NH_3 generated during the irradiation.

ACKNOWLEDGEMENT

This work has been carried out under the Nuclear R&D program (NRF-2017-M2A8A5015144) funded by Ministry of Science and ICT.

REFERENCES

[1] G. R. Sunaryo and S. L. Butarbutar, “The effect of hydrazine addition on the formation of oxygen molecule by fast neutron radiolysis”, KnE Energy, 2016 (2015).

[2] George V. Buxton and Howard E. Sims, “On the mechanism of the ɤ-radiolysis of deoxygenated aqueous solutions of hydrazine” Phys. Chem. Chem. Phys., 2, pp. 4941-4946 (2000).

Studies on Precipitation Characteristics of Mn^{2+} and SO_4^{2-} by $Ba(OH)_2$

Hyun-Kyu Lee[1,*], Sae-Binna Lee[1], Yoon-Ji Park[1], Myo-Gwang Kim[1], Wonzin Oh[1], Sang-June Choi[1], Ju-Hyeon Park[2], Bum-Chul Seo[2], and Ki-Chul Kim[2]

[1] Kyungpook National University, 80, Daehak-ro, Buk-gu, Daegu, Republic of Korea

[2] KEPCO KPS, 69-46, Munsan 2sandan 1-ro, Oedong-eup, Gyeongju-si, Gyeongsangbuk-do, Republic of Korea

[*]lhk7933@knu.ac.kr

1. Introduction

One of the important characteristics of the HyBRID chemical decontamination developed by KAERI is a waste treatment method using precipitation of decontamination reagents including potassium permanganate and sulfuric acid and decontaminated ions instead of the conventional method of ion exchange treatment in an effort to reduce the chemical decontamination waste volume and to make the resulted waste more suitable and stable for a final radioactive disposal [1]. In this study, the precipitation characteristics of Mn^{2+} and SO_4^{2-}, the component ions of oxidizing agents, by $Ba(OH)_2$ or NaOH were investigated for optimization of the precipitation process.

2. Experimental

The concentration of $Ba(OH)_2$ or NaOH injected into the 6 mM $MnSO_4$ solution was varied from 0 to 7.2 mM to confirm the precipitation characteristics of Mn^{2+} and SO_4^{2-} by $Ba(OH)_2$. In order to investigate the precipitation characteristics of Mn^{2+} and SO_4^{2-} in the HyBRID conditions containing excess amount of sulfate, 37 mM H_2SO_4 and 6.33 mM Mn^{2+} were mixed in a glass beaker. Then, $Ba(OH)_2$ or NaOH were added to the mixed solution to raise the pH up to 11. To confirm that the precipitated $Mn(OH)_2$ was re-dissolved, $Mn(OH)_2$ was stirred in 37 mM H_2SO_4. The pH value was measured by pH meter (STARA211, Thermo Orion, USA) and residual concentration of Mn(II) was confirmed by Inductively Coupled Plasma-Optical Emission Spectroscopy (Optima 2100DV, PerkinElmer).

3. Results and Discussion

Based on the dissociation constants of $MnSO_4$ ($5.2x10^{-3}$), Mn is predominantly presents as $MnSO_4$ (aq) rather than Mn^{2+} under the condition that SO_4^{2-} coexists. Moreover, as can be seen from Pourbaix diagrams of Mn in Fig. 1, Mn^{2+} is generally precipitated as $Mn(OH)_2$ above pH 7.

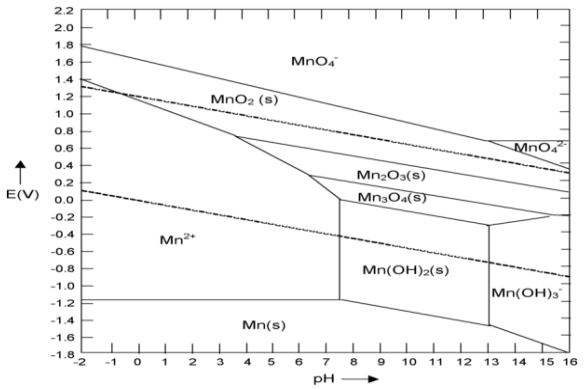

Fig. 1. Potential-pH Pourbaix diagrams of manganese.

However, the residual fraction of Mn(II) was abruptly decreased with increasing pH by $Ba(OH)_2$ or NaOH injection under HyBRID conditions, and around 60% of Mn(II) was precipitated at pH 3. This result suggests that Mn(II) could be precipitated below pH 3 as $Mn(OH)_2$ by OH^- injected to neutralize H_2SO_4 (Fig. 2). Moreover, the added OH^-

is expected to react more favorably in the formation of $Mn(OH)_2$, because $Mn(OH)_2$ has a lower ΔG value than Mn^{2+} and H_2O (Table 1).

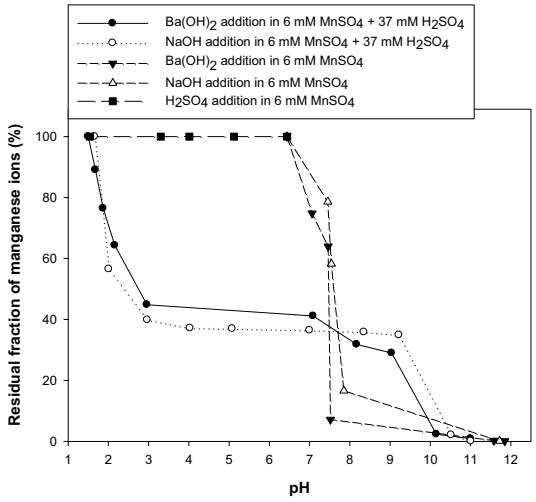

Fig. 2. $Mn(OH)_2$ precipitation behavior by $Ba(OH)_2$ or NaOH addition in the simulated HyBRID Mn^{2+} and sulfate liquid waste and $MnSO_4$ solution.

Table 1. Standard thermodynamic values at 25℃

ΔG	H_2O	Mn^{2+}	$Mn(OH)_2$	$MnSO_4^*$
(KJ/mol)	-237	-228	-615	-957.42

* is not precipitated due to high solubility in water.

On the other hand, when the precipitated $Mn(OH)_2$ was dissolved by 37 mM H_2SO_4, the dissolution rate of Mn was confirmed to be slow.

Table 2. Dissolution rate of precipitated $Mn(OH)_2$ in 37 mM H_2SO_4

Time (min)	pH	Dissolved Mn (%)
30	1.62	37.4
60	1.58	40.1
120	1.57	41.6

4. Conclusion

The manganese precipitation characteristics with the addition of barium hydroxide were compared with the case where there was more sulfuric acid than manganese and the same concentration, and the following conclusions were obtained.

1. The manganese precipitate is a manganese hydroxide and the manganese hydroxide precipitation in excess sulfate condition can be take place even in the low pH far less than 7 unlike the Mn Pourbaix diagram in the water.
2. The precipitation of manganese hydroxide at the low acidity seems to be due to heterogeneous mixing of barium hydroxide in the process of transition from turbulent macro-mixing to molecular diffusional micro-mixing and thereby formation of a local acidity of 7 or more where a manganese hydroxide is precipitated, and the reverse reaction was not took place after uniform mixing of barium hydroxide due to the solid liquid non-equilibrium characteristics.

ACKNOWLEDGEMENT

This work was supported by the National Research Foundation of Korea (NRF) and the Ministry of Science and ICT (MSIT) of the Republic of Korea. (No. 2017M2A8A5041776)

REFERENCES

[1] J.Y. Jung, H.C. Eun, S.Y. Park, N.O. Chang, S.B. Kim, B.K. Seo, and S.J. Park, “A study on the removal of impurities in a SP-HyBRID decontamination wastewater of the primary coolant system in a pressurized water reactor”, Journal of Radioanalytical and Nuclear Chemistry, 318(2), 1339-1345 (2018).

Sampling for Characterizing Radioactive Aerosol From Activated Metal During Cutting With Plasma Arc Torch for Internal Dose Assessment

Wonseok Yang*, Nakkyu Chae, Minho Lee, and Sungyeol Choi
Korea Advanced Institute of Science and Technology, 291, Daehak-ro, Yuseong-gu, Daejeon, Republic of Korea
*abw94@kaist.ac.kr

1. Introduction

Cutting process occurs during decommissioning for radioactive waste management purpose. Decommissioning workers will cut activated materials in the closed workplace. Radioactive aerosols can be inhaled during this process. When the inhalation of radioactive aerosols occurs, the worker's committed effective dose should be evaluated. For accurate estimating committed effective dose by radioactive aerosols, the intake of radionuclide, the absorption parameter, and the aerodynamic diameter have to be defined [1].

The aerosol measurement system in KAIST Nuclear Fuel Cycle (K&FC) laboratory enables to characterize aerosol from metal cutting with plasma arc torch. In the system, less distorted sampling is critical to analysis aerosols. This study focused on aerosol sampling technique which used in the aerosol measurement system in K&FC.

2. The System for the Measurement of Characteristics of Aerosol from Metal Cutting

2.1 The Aerosol Measurement System in K&FC

Fig. 1. The aerosol measurement system in K&FC.

The aerosol measurement system in KAIST Nuclear Fuel Cycle laboratory (Fig. 1) is composed of an aerosol chamber with HEFA filter inlet, a plasma arc torch (powermax125, Hypertherm), an x-stage automatic cutting system, an isokinetic sampling system and a high resolution electrical low-pressure impactor (HR-ELPI+, Dekati).

After the measurement of the aerodynamic distribution of aerosols from cutting experiment, collected and size classified aerosols were analyzed by ICP-OES to measure the chemical element distribution.

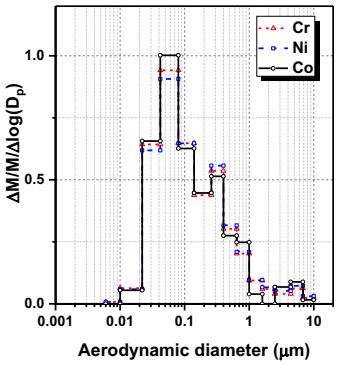

Fig. 2. Particle size distributions of nuclides for plasma cutting of SUS304.

2.2 K&FC Isokinetic Sampler

To minimize distortion aerodynamic diameter distribution and aerosol concentration during the sampling, isokinetic sampling is significant. In order to meet isokinetic sampling, the velocity of carrier gas at the sampling point in the sampling pipe and sample flow velocity must be matched [2].

K&FC isokinetic sampler are composed of sampler body and sampler head. The sampler head has six different diameters from 5 mm to 10 mm, at 1 mm interval. For matching the velocity of air during sampling, we measured velocity at the sampling point with hot wire anemometer (Testo110, Testo). According to the measured velocity, we choose the sampler head diameter depending on the flow rate of the measuring device.

Fig. 3. (Left)K&FC isokinetic sampler, (right) sampler head.

3. Simulation

The K&FC Isokinetic sampler was simulated with COMSOL Multiphysics 5.2a simulation software. The gas flow inside the sampling pipe was calculated by using the Incompressible Navier-Stokes model. The density and dynamic viscosity of air were assumed to be constant. The inlet flow of the sampling pipe is 895.27 l min^{-1} and the sampling rate through isokinetic sampler is fixed to 10 l min^{-1} equal to the ELPI+ sampling rate.

Particle tracing module was used to simulate aerosol particle motion in fluid flow. Stokes drag with slip correction factor is applied for particles which have a relative Reynolds number much less than one.

A ten thousand same diameter(0.01, 0.1, 0.2, 0.5, 1, 2, 5, 10 μm) particles were created at uniform intervals. Thin-wall isokinetic nozzle, K&FC isokinetic sampler and without any sampler case were simulated and calculated number of particles pass through the sampler.

4. Result

The thin-wall nozzle and the K&FC Isokinetic sampler with 8mm sampler head simulated by COMSOL Multiphysics 5.2a. The number of particles which pass through the sampler is similar when the aerodynamic diameter is less than 2 μm. It's not much different from the thin-wall nozzle which was widely used.

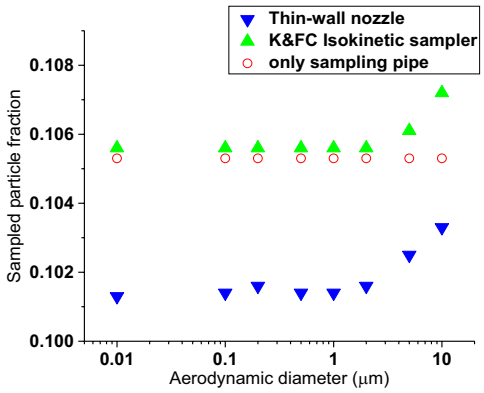

Fig. 4. Sampled particle number with particle diameter simulated with COMSOL Multiphysics 5.2a.

5. Conclusion

The sampled aerosol that is representative is important to know the characteristics of aerosols. The aerosol measurement system in K&FC is used to analysis aerosols from metal cutting with plasma arc torch. In the system, K&FC isokinetic sampler was used. To identify the effect of the sampler, it was simulated with COMSOL Multiphysics 5.2a. The 8 mm diameter thin-wall nozzle and the K&FC Isokinetic sampler with 8 mm diameter sampler head both have an impact on fluid flow than ideal pipe flow. But the impact is not significant, and there was no significant difference between the existing products used and the sampler we made ourselves. Our K&FC isokinetic sampler has six different diameter heads; thus, we can apply our system to various measuring devices without sampling error for characterizing the aerosols from the metal cutting process.

ACKNOWLEDGEMENT

This work was supported by the National Research Foundation of Korea (NRF) funded by the Korea government (MSIT: Ministry of Science and ICT) (Grant No. NRF-2017M2A8A4018596).

REFERENCES

[1] T.E. Johnson, “Introduction to Health Physics”, 5th Edition, McGraw-Hill education, (2018).

[2] Vincent, James H, “Aerosol Sampling. Science and Practice”, JOHN WILEY & SONS LTD., NEW YORK, NY (USA) (1989).

3D Underwater Scanning for Nuclear Decommissioning: Laser Beam Distortion

Sungmoon Joo*, Jonghwan Lee, Ikjune Kim, and Dongjun Hyun
Korea Atomic Energy Research Institute, 111, Daedeok-daero 989beon-gil, Yuseong-gu, Daejeon, Republic of Korea
*smjoo@kaeri.re.kr

1. Introduction

Planning for the safe and controlled deactivation and decommissioning of highly contaminated nuclear facilities requires that engineers and managers fully understand the 3D workspace in which personnel and equipment will operate. 3D information that precisely depicts the work environment can reduce uncertainty, thus expedite the accomplishment of the work with minimum radiation exposure and safety risks.

3D scanning is known to be an effective method for quickly and accurately capturing a structure's actual geometry. 3D scanning is a technique used to capture the shape of an object using a 3D scanner. 3D scanners measure a large number of points on the external surfaces of objects and generate output in the form of data points in space, which is known as a point cloud.

For highly contaminated elements such as reactor pressure vessels or reactor internals, it is a viable option to cool-down and dismantle these elements in submerged state. However, underwater 3D scanning faces technical challenges, making a straightforward application of well-established scanning algorithms in air. Fig. 1 shows an example of underwater 3D scanning; point cloud in purple represents the scanning of a flat plate in air; point cloud in green represents the scanning of the same plate in a water tank, which looks closer and bent. The compensation of the distortions requires elaborate analysis.

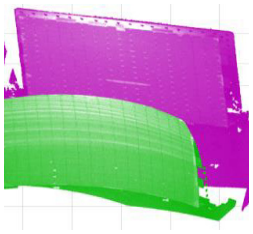

Fig. 1. Example of Distortion.

This study provides modeling of the distortion for underwater 3D laser scanning using a flat viewport. This paper focusses on the laser beam distortion.

2. Laser Scanner

Fig. 2 shows a schematic of a underwater laser scanning system.

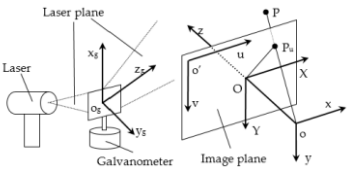

Fig. 2. Schematic of laser scanning system.

The laser projection model describes the laser plane, the mirror, and the air/viewport/water interfaces in order to estimate the laser shape in the underwater environment. Laser planes are created using a laser beam and a lens. One could model the laser plane by introducing the lens and the beam into the overall model. However, for the sake of simplicity, it is assumed that the laser plane is produced by a source of light expanding at a given aperture angle.

From a geometrical point of view, the only two optical processes that take place in the light-emission side of the sensor are: (1) reflection on the mirror and (2) refraction at both the air/viewport and the viewport/water interfaces. Light reflection is the process of light changing its directionwhen it reaches a given surface without crossing it. Light refraction is the change in direction that a light beam suffers when crossing the surface separating two different media. This optical process follows Snell's law described in Eq (1).

$$r_r = \frac{n_1}{n_2}(n \times (-n \times i)) - n\sqrt{1 - \left(\frac{n_1}{n_2}\right)^2 (n \times i) \cdot (n \times i)} \quad (1)$$

This law involves three elements: (1) the index of refraction of the first medium n_1, (2) the index of refraction of the second medium n_2 and (3) the angle α between the incident light i and the normal of the surface separating the two media n.

To produce the underwater laser surface, a number of rays are sampled evenly spread across the laser aperture. For each of them, its reflection by the mirror is computed. Then it is refracted using Eq. (1) first with the air/viewport interface using $n_1 = n_{air}$ and $n_2 = n_{viewport}$, and second with the viewport/water interface using $n_1 = n_{viewport}$ and $n_2 = n_{water}$.

Fig. 3 shows the intersection of the simulated laser rays with a plane parallel to the viewport at a distance of 1.5 m. In geometry, the intersection of two planes is a straight line. However simulation shows that as the incidence angle increases the beam bends. The data obtained with this model suggests that the laser remains planar after passing the viewport only when the normal to the viewport is parallel to the laser plane. Therefore, the laser plane is distorted because of the change in the index of refraction of the different media when such condition is not met.

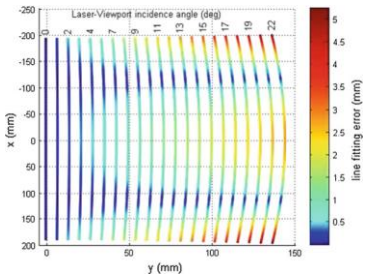

Fig. 3. Projection of the simulated laser beam.

3. Conclusion

This study provides a model for laser beam refraction that occurs at the viewport of 3D underwater laser scanning system. The simulation suggests that the laser beams are distorted due to the refraction. Future work includes the modeling of distortion at camera side and integration of the distortion models.

ACKNOWLEDGEMENT

This work was supported by the nuclear research and development program (2017M2A8A5015146) through the national research foundation of Korea funded by the Ministry of Science and ICT.

REFERENCES

[1] A. Plomer, P. Ridao, D. Ribas, and J. Forest, "Underwater 3D Laser Scanners: The deformation of the Plane", Sensing and Control for Autonomous Vehicles, pp. 73-88, Springer (2017).

A Study on the Volume Reduction of Concrete Waste by Sintering Method

Dasom Yang[1,2,*], Woojung Shon[1], Kwangwook Kim[1], and Keunyoung Lee[1]

[1] Korea Atomic Energy Research Institute, 111, Daedeok-daero 989beon-gil, Yuseong-gu, Daejeon, Republic of Korea

[2] Kyungpook National University, 80, Daehak-ro, Buk-gu, Daegu, Republic of Korea

[*]dsyang@kaeri.re.kr

1. Introduction

A large amount of radioactive waste is generated when nuclear power plants are dismantled. Most radioactive wastes, except for the clearance level waste are deemed to be treated and disposed in various ways according to the waste acceptance criteria. Many of them need to be solidified for that. Methods for solidifying waste include cement solidification, geopolymer, bitmen, ceramic, glass, glass-ceramic solidification method. Among these solidification methods, the glass and ceramic manufacturing method by sintering have the following advantages as shown in Table 1.

Table 1. Characteristics of the manufacturing method by glass and ceramic [1]

	Ceramics	Glass
Waste loading	Up to 50% dry weight	Up to 25% dry weight
Volume	Increase	Reduction
Leach resistance	High for most radionuclides	Very high

Therefore, in this work, the solidification experiment was performed by the sintering method using the glass-ceramic solidification method.

2. Methods and Results

The materials used in the experiment were fine concrete waste powder which was sieved under 1 mm after the aggregate was separated from the concrete waste. The remaining wastes were pulverized after heat treatment at over 500℃. According to the waste acceptance criteria, wastes containing particulate dispersive matter should be treated and packaged to be non- dispersible. To evaluate glass-ceramic waste form, pellets with height of 8 mm were manufactured at a pressure of 30, 60, 120, 150 MPa using a mold in diameter of 13 mm. The sintering temperature was maintained at 1,000℃, 1,050℃ and 1,100℃.

B_2O_3, which is an additive to form glass-ceramic matrix from the concrete waste, was added at certain ratio according to the content of SiO_2 in the waste and solidified. The compositional analysis of the concrete waste by SEM-EDS showed 26.93wt.% of CaO, 26.82wt.% of SiO_2 and others are Al_2O_3, Fe_2O_3 etc. The experiment of sintering with a change of temperature showed that the pellet melted over 1,050℃ and there was no significant large volume reduction below 1,000℃.

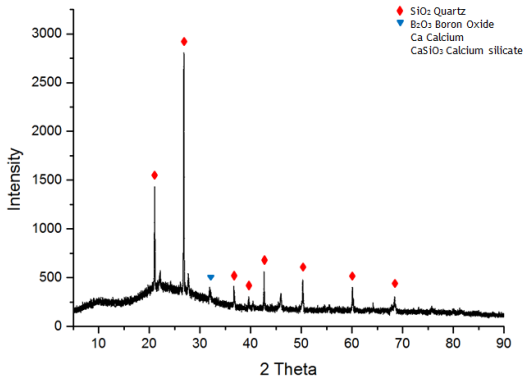

Fig. 1. XRD pattern of material remained after sintering.

The XRD results of the sintered body at 1,050℃ are shown in Fig. 1. It shows generally amorphous phase due to formation of glass phase with partially crystal phase. Such a matrix means that glass-ceramic wasteform can be formed from the concrete waste.

Fig. 2 shows the photos of the sintered body and SEM photo of fractured surface. Fig. 2(a) shows the sintered pellet which is the volume reduced and Fig. 2(b) shows the fractured pellet has non porosity.

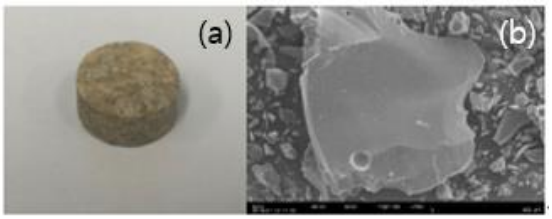

Fig. 2. (a) Sintered pellet, (b) Surface of the fractured pellet after sintering.

3. Conclusion

The concrete waste was confirmed to form the glass-ceramic wasteform with volume reduction. And the shrinkage ratio of sintered body was approximately 40% from the initial concrete waste fine powder.

REFERENCES

[1] Michael I. Ojovan, “Handbook of advanced radioactive waste conditioning technologies”, Woodhead Publishing (2011).

[2] Kwang-wook Kim, Richard I. Foster, Jimin Kim, “Glass-ceramic composite wasteform to immobilize and stabilize a uranium-bearing waste generated form treatment of a spent uranium catalyst”, Journal of Nuclear Materials, 516, 238-246 (2019).

Removal of Cs From Contaminated Aquatic Environments by Water-powered Janus Micromotor Adsorbent

Chan Woo Park[1,*], Juri Hwang[1,2], Inae Lee[3], In-Ho Yoon[1], and Hee-Man Yang[1]

[1] Korea Atomic Energy Research Institute, 111, Daedeok-daero 989beon-gil, Yuseong-gu, Daejeon, Republic of Korea

[2] Chungnam National University, 99, Daehak-ro, Yuseong-gu, Daejeon, Republic of Korea

[3] Sungkyunkwan University, 2066, Seobu-ro, Jangan-gu, Suwon-si, Gyeonggi-do, Republic of Korea

[*]chanwoo@kaeri.re.kr

1. Introduction

The accidental release of radioactive substances from nuclear facilities can induce contamination of the aquatic environment. Among various radionuclides, cesium is considered as one of most hazardous substances because of its long half-life and high gamma radiation energy. Nevertheless, it has been difficult to remediate large aquatic environments on site using the conventional Cs adsorbent. In this presentation, we report the self-propelled micromotor that can move under self-generated propulsion in an aqueous environment using a force generated by water-metal reaction. The Cs selective half-shell of the Janus micromotor enabled removal of Cs from the contaminated water.

2. Experimental

Mg particles (38~45 μm) were deposited on the poly(vinylpyrrolidine)-coated glass substrate, and the humidity was raised until the polymer layer became adhesive to fix Mg particles in the polymer layer. Top surfaces of the Mg particles were coated with Ni and Au layers to prepare half-coated Janus microspheres. The Au layer was cationically modified by reaction of the particles with thiolated polyethyleneimine (PEI). The Cs-selective layer-by-layer film was formed on the half-surface of the particle by sequential treatment of the particles with anionic ferric ferrocyanide particles and cationic PEI.

Self-propulsion of the Mg/ferric ferrocyanide micromotor was observed in aqueous solutions using a stereomicroscope (Leica M250C, Germany) equipped with a high-speed CMOS camera (Lt225, Aegis Electronic, USA).

The radioactivity of ^{137}Cs solution before and after treatment with the micromotor adsorbent was measured using high-resolution gamma spectrometry (CANBERRA Ind.) with a high-purity germanium detector equipped with a multi-channel analyzer.

3. Result & Discussion

The Cs-selective ferric ferrocyanide functionalized Janus micromotor particles were prepared by modifying the surfaces of the Au half-shell on the Mg microspheres with layer-by-layer film of ferric ferrocyanide and PEI. SEM analysis of the particles demonstrated that half of the Mg microsphere surface was coated with cubic ferric ferrocyanide particles.

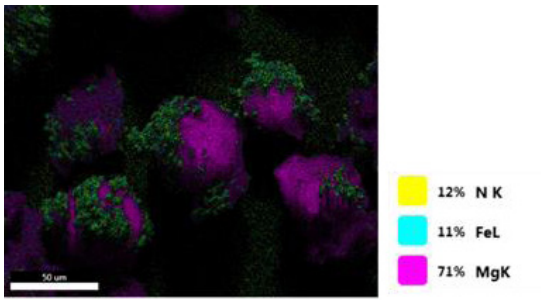

Fig. 1. Janus micromotor adsorbents observed using scanning electron microscopy with elemental mapping using energy dispersive spectroscopy.

The propulsive motions of the Janus micromotors were analyzed in an aqueous solution containing Cl^- or HCO_3^- anions. The reaction between Mg metal and water generated hydrogen gas bubbles. Asymmetrical bubble evolution from the Janus particle produced a net propulsive force on the particle.

Finally, we demonstrated the removal of radioactive ^{137}Cs by the self-propelled Mg/ferric ferrocyanide micromotor. The self-propelled micromotors were able to remove over 99.7% of Cs from ~85 Bq/mL of ^{137}Cs concentrations.

4. Conclusions

We successfully demonstrated the preparation of Mg/ferric-ferrocyanide micromotors by a layer-by-layer technique. The synthesized micromotor could be self-propelled in aqueous solutions via the water-metal reaction. Adsorption of Cs by the micromotor adsorbent enabled the successful removal of radioactive ^{137}Cs from aqueous solutions

REFERENCES

[1] Hwang J, Yang H-M, Lee K-W, Jung Y-I, Lee K J, Park C. W. A remotely steerable Janus micromotor adsorbent for the active remediation of Cs contaminated water, 2019. J Hazard Mater, 2019;369.

Development of Radioactive Waste Tracking System (WATS) for Decommissioning of NPPs

Ji-Hoon Lee* and Kang-Ok Cho
KHNP Central Research Institute, 70, Yuseong-daero 1312beon-gil, Yuseong-gu, Daejeon, Republic of Korea
*leejihoon@khnp.co.kr

1. Introduction

Because large amounts of decommissioning waste will be generated in a short period, radioactive wastes tracking system is required for the efficient management of radioactive waste during decommission of NPPs. In this system, many kinds of radioactive waste information such as waste types, radioactivity and physico-chemical characteristics can be managed during decommissioning activities. This system will be also tracked the waste route from decommissioning site, temporary storage, treatment facility and disposal site. The reasons why tracking the radwaste are efficient monitoring of waste, quality assurance, planning the waste process, package management and sampling minimization. Therefore, radioactive waste tracking system are introduced for the efficient management of wastes during decommissioning of NPPs.

2. Radioactive Waste Tracking System

2.1 Concept of Radioactive Waste Tracking

During decommissioning, various kinds of metal wastes will be generated such as valve (WI002), pipe (WI003) and equipment (WI004). A lot of concrete waste (WI001) will be also generated which has similar radioactive characteristics in a same decommissioning area (ZO1). These kinds of waste should be treated to reduce waste volume and satisfy the waste acceptance criteria for radioactive disposal site. The radioactive waste such as WI002 will be converted WI0021, WI0022 and WI0023 during waste treatment process as shown in Fig. 1.

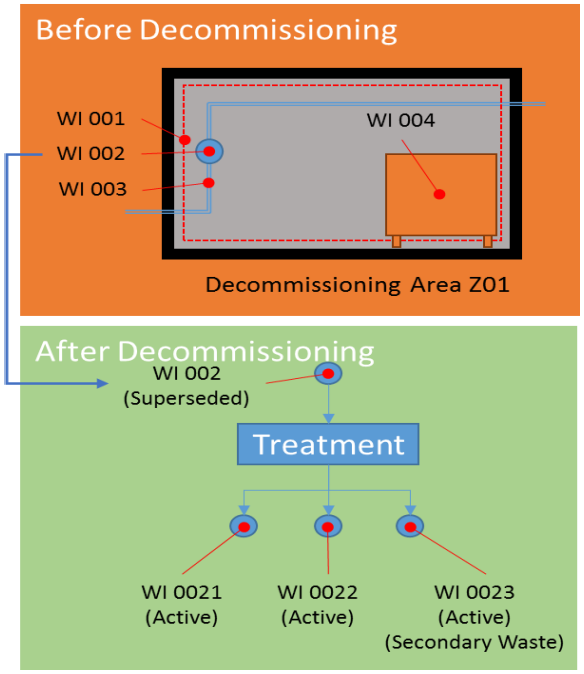

Fig. 1. Concept of radioactive waste tracking system.

2.2 Radioactive Waste Tracking Data Base

Radioactive waste tracking data base consist of various kinds of modules such as radioactive measurement module, package and transportation module and waste conversion module etc. Radioactive measurement module has the information of surface contamination, dose rate and radionuclide analysis data of radioactive wastes. Package and transportation module can provide the waste location in real time by managing the packaging, transportation of waste in dismantle area, storage and treatment facility. Waste conversion module can be showed waste conversion status in real time so that find what kinds of waste treatment processes were performed. After treatment, produced wastes can be tracked for the decommissioning waste management.

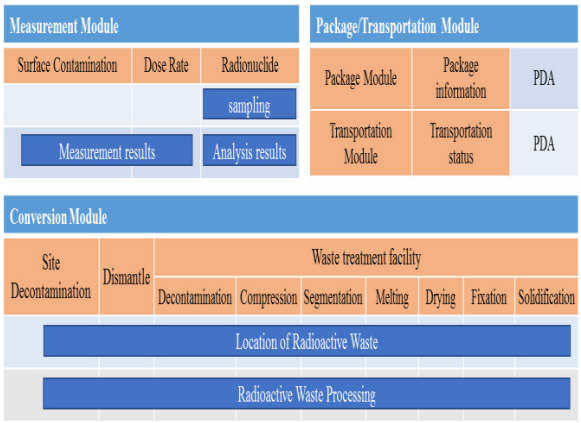

Fig. 2. Radioactive waste tracking data base.

2.3 Radioactive Waste Tracking System

Fig. 3 and 4 show radioactive tracking system which use PDA, RFID and stationary recording system in each waste management area. RFID has various information of radioactive waste such as radioactive characteristics, treatment history, physical and chemical characteristics which will be meet the waste acceptance criteria in disposal site.

PDA

RFID

Physical Characteristics		Electrical Characteristics	
Parameter	Specification	Parameter	Specification
Length(L)	108[㎜]	Chip Feature	Alien Higgs3
Width(W)	108[㎜]	Memory Size(bit)	EPC[96] + USER[512]
Thickness(T)	6.4[㎜]	Write Endurance	10,000 Programming Cycles
Material	PCB/Silicon	Data Retention	10 years
Finish	Silicon	Interface Protocol	ISO/IEC 18000-6C EPC global Class1 GEN2
Adhesive	Silicon tape	Frequency	UHF (917Mhz – 923.5Mhz)
Max. Temperature	-40℃ ~ +200℃	Reading Distance	Up to 2.5m

Fig. 3. Specification of RFID system.

RFID attached on each waste package can recognized by PDA or automatic stationary recording system in each waste management area. This system can be used by smart phone and web site.

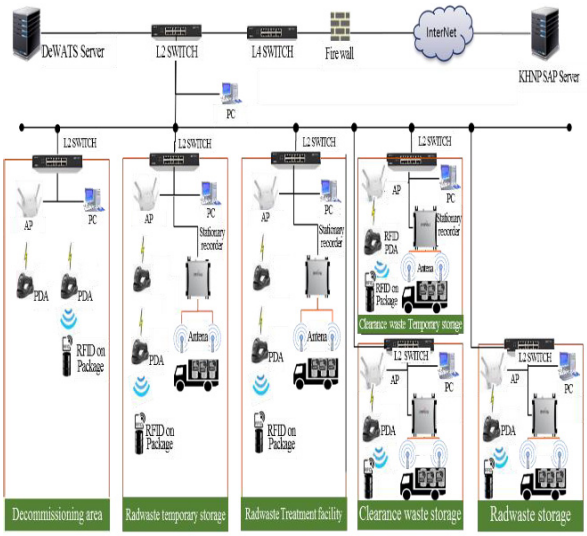

Fig. 4. Schematic diagram of radioactive tracking system.

3. Conclusion

During decommissioning of NPPs, a lot of radioactive waste will be generated simultaneously so that it is very important to track the radioactive waste for volume reduction and efficient management of radioactive wastes. This radioactive tracking system is under developing. When this system will be established, it will be useful to manage the radioactive waste during decommissioning of NPPs.

REFERENCES

[1] IAEA-TECDOC-1222, “Waste inventory record keeping systems (WIRKS) for the management and disposal of radioactive waste” (2001).

[2] EPRI TR3002008169, “Waste Management Tracking Software : Technical Specifications” (2016).

[3] KAERI/RR-2454, Establishment and operation of data base system for radioactive waste in KAERI (2003).

6분과

방사선환경 및 안전 (Oral)

Long Term History of Radiocaesium Activity Concentration in Seawater in the Western North Pacific Ocean and Adjacent Seas Since 1950's Until 2018

Michio AOYAMA
University of Tsukuba, 1 Chome-1-1 Tennodai, Tsukuba, Ibaraki, Japan
michio.aoyama@ied.tsukuba.ac.jp

1. Introduction

The world's oceans act as a sink for artificial radionuclides as well as for other anthropogenic pollutants released into the environment. Owing to physical and biogeochemical processes in the ocean, artificial radionuclides in the ocean are redistributed from their initial entry points which depend on the various sources. The extent of radioactive contamination in the ocean due to atmospheric weapons tests, releases from nuclear fuel reprocessing plants, and accidental releases from nuclear power plants (i.e., the Chernobyl accident in 1986 and the Fukushima accident in 2011) is of global concern. ^{137}Cs has been released to the marine environment as a result of global and local fallout from atmospheric nuclear weapons tests [1], discharges from nuclear reprocessing plants, dumping of nuclear wastes into the global oceans, and fallout from the Chernobyl accident and the Fukushima Accident

The spatial and temporal changes of ^{137}Cs in seawater reflect the flow of seawater such as through advection/diffusion and subduction/obduction , because most of the ^{137}Cs exists in the dissolved form in seawater.

2. Data

Long range transport of radiocaesium derived from local fallout occurred early 1950s, global fallout which occurred mainly late 1950s and early 1960s and the Fukushima accident occurred in 2011 were investigated in ocean surface in the East China Sea (ECS), the Sea of Japan (SOJ) and the western North Pacific Ocean since 1953 to 2018.

After the FNPP1 accident, many radiocaesium measurements were taken in the SOJ, the ECS and the North Pacific Ocean. To elucidate the temporal and spatial distributions of the radiocaesium activity concentrations, we used as many data points as possible. We therefore compiled all available data from the literature and reported studies including our data. Most of the data before the FNPP1 accident are included in the database "Historical Artificial Radionuclides in the Pacific Ocean and its Marginal Seas (HAM database)" by Aoyama and Hirose, 2004 and their updated version [2]. We also included the Japanese government's monitoring data and the Korean government monitoring data in this study. (Marine Ecology Research Institute, 2011, 2012, 2013, 2014, 2015, 2016 and Korea Institute of Nuclear Safety, 2011, 2012, 2013, 2014, 2015, 2016)

3. Results and Discussion

Radiocaesium activity concentration in surface water showed maximums in 2014/2015 in the northern East China Sea and in 2015/2016 in the Sea of Japan [3]. A part of the radiocaesium derived

from the Fukushima accident was transported within several years to the northern ECS and then to the SOJ via Sub Tropical Mode Water (STMW) from the western North Pacific and subduction/obduction processes made systematic delay of timing of maximum. After radiocaesium activity concentration in surface water reached maximum, it has been decreasing slowly until mid of 2018 in the SOJ.

Both ^{134}Cs and ^{137} Cs were observed in the SOJ and northern ECS while ^{134}Cs was not observed in the western and southern ECS where Kuroshio enters from the western North Pacific to the ECS. This indicate that obduction of Fukushima derived radiocaesium from STMW might occur in the just south of STMW formation region.

4. Conclusions

Both the main local/global fallout regions and injection of radiocaesium by Fukushima accident had occurred in the western North Pacific and constrain of surface current systems which governed surface transport processes were subtropical gyre and subarctic gyre. Radiocaesium transport in surface water in the mid latitude was characterized as rapid eastward transport along Kuroshio and Kuroshio Extension while the second largest controlling factor of radiocaesium activity concentration was subduction/obdusction and flow field in the ocean interior. The westward-flowing undercurrent would have transported FNPP1-derived ^{137}Cs in the STMW south-westwards, as reported [4]. The ^{137}Cs entrained in the STMW would have reached the western boundary of the SOJ at lower latitudes and become entrained into the Kuroshio [5] before being transported northwards to the west of Kyushu by the Tsushima Warm Current bifurcation from the Kuroshio.

REFERENCES

[1] M. Aoyama, K. Hirose, Y. Igarashi, Re-construction and updating our understanding on the global weapons tests 137Cs fallout, J. Environ. Monit., 8 (2006) 431-438.

[2] M. Aoyama, K. Hirose, Artificial radionuclides database in the Pacific Ocean: HAM database, ScientificWorldJournal, 4 (2004) 200-215.

[3] Y. Inomata, M. Aoyama, Y. Hamajima, M. Yamada, Transport of FNPP1-derived radiocaesium from subtropical mode water in the western North Pacific Ocean to the Sea of Japan, Ocean Sci., 14 (2018) 813-826.

[4] E. Oka, Seasonal and interannual variation of North Pacific subtropical mode water in 2003–2006, Journal of oceanography, 65 (2009) 151-164.

[5] E. Oka, B. Qiu, Progress of North Pacific mode water research in the past decade, Journal of oceanography, 68 (2012) 5-20

In-Situ Gamma-Ray Spectrometry for Radioactivity Analysis Using the Scintillation Detector

Jun-Ho Lee[1], Jong-In Byun[2,*], and Dong Myung Lee[1,2]

[1] University of Science & Technology, 217 Gajeong-Ro, Yuseong-gu, Daejeon, Republic of Korea

[2] Korea Institute of Nuclear Safety, 62, Gwahak-ro, Yuseong-gu, Daejeon, Republic of Korea

[*]k975bji@kins.re.kr

1. Introduction

Scintillation detectors such as NaI(Tl), $LaBr_3$(Ce) and $CeBr_3$ have been widely used for the measurement of field radiation because they can be used at room temperature and operated with relatively compact electronics. Much research has been done on the applications of these detectors in soil and marine environments [1, 2]. In addition, the study on the quantification of radioactivity in soil and marine environments using these detectors might be required to improve the applications of the detectors for in-situ gamma-ray measurement. This paper presents the in-situ gamma-ray spectrometry for radioactivity analysis in soil and marine environments using the scintillation detectors. In the soil, the NaI(Tl), $LaBr_3$(Ce) and $CeBr_3$ detectors were used to evaluate the applicability of in-situ measurement. In the marine environment, the fractional contribution of radionuclide in both seawater and sediment for marine environment presented using the $CeBr_3$.

2. Methods and Materials

The properties of the NaI(Tl), $LaBr_3$(Ce) and $CeBr_3$ used in this study are shown in Table 1.

Table 1. The properties of the NaI(Tl), $LaBr_3$(Ce) and $CeBr_3$

	NaI(Tl)	$LaBr_3$(Ce)	$CeBr_3$
Density ($g \cdot cm^{-3}$)	3.67	5.29	5.10
Decay time (ns)	230	16	18~20
Energy resolution (% at 661.6 keV)	6.0~8.0	2.0~3.5	4.1
Intrinsic radioactivity	-	^{138}La, ^{227}Ac	^{227}Ac

In the soil, to convert net peak count rate in spectrum for any radionuclide to radioactivity, the NaI(Tl), $LaBr_3$(Ce) and $CeBr_3$ detectors were calibrated using semi-empirical method that takes into account the response and angle of the gamma-rays entering the detector [3]. In-situ gamma-ray spectrometry using the calibrated the NaI(Tl), $LaBr_3$(Ce) and $CeBr_3$ detectors was carried out by measuring the natural radionuclides U, Th-series and ^{40}K in an open field (more than 2.5 km^2) with almost flat surface. The results were compared with those of sampling analysis in the laboratory.

In marine environment, peak of any radionuclide obtained by in-situ gamma-ray spectrometry contributes to the corresponding radionuclide in both seawater and sediment. These contribution can be evaluated using the ratio R_T of two in-situ result with relative measurement points h_1 and h_2, and the ratios R_W and R_S of each efficiency in seawater and sediment, as follows :

$$\frac{N_{S_x,h1}}{N_{W_x,h1}} = \frac{\left(1 - {R_T}/{R_W}\right)}{\left({R_T}/{R_S} - 1\right)} \; or \; \frac{N_{S_x,h2}}{N_{W_x,h2}} = \frac{\left(1 - {R_W}/{R_T}\right)}{\left({R_S}/{R_T} - 1\right)} \quad (1)$$

where $N_{W,h1}$, $N_{S,h1}$, $N_{W,h2}$ and $N_{S,h2}$ mean each count rate of radionuclide in seawater and sediment at detector height h_1 and h_2 from seabed, respectively. To validate this formula, two in-situ measurements with detector height using the $CeBr_3$ were performed by measuring ^{40}K in the marine environment with the tidal phenomenon, and the calibrations for efficiency in seawater and sediment were carried out by the GEANT4 code. The in-situ results were compared with those of seawater and sediment samples analysis.

3. Results and Discussion

In the soil, radioactivity of ^{40}K, ^{208}Tl and ^{214}Bi by in-situ and laboratory measurements agreed well within 5%. The 1460.8 keV (^{40}K), 1764 keV (^{214}Bi) and 2614 keV (^{208}Tl) peaks for the NaI(Tl) and $CeBr_3$, and 583 keV (^{208}Tl), 609 keV (^{214}Bi) and 1460.8 keV (^{40}K) peaks for the $LaBr_3(Ce)$ can be analyzed because of the resolution and internal background. When analyzing ^{40}K in the $LaBr_3(Ce)$ and $CeBr_3$, internal background peak was subtracted because the ^{40}K peak overlaps with the internal background peak by ^{138}La for the $LaBr_3(Ce)$ and ^{227}Ac for the $CeBr_3$, respectively.

In the marine environment, the difference between the in-situ analysis applied by Equation (1) and the sampling analysis showed 3% in seawater and 11% in sediment for the characterization of sediment with depth by the GEANT4 code using the analysis result of sediment samples with depth in the laboratory.

4. Conclusion

We have present the applicability of the NaI(Tl), $LaBr_3(Ce)$ and $CeBr_3$ detector in in-situ measurement for soil, and fractional contribution of radionuclide in both seawater and sediment for marine environment using the $CeBr_3$ detector. The conclusion can be drawn these scintillation detectors can be utilized for the quantification evaluations in in-situ gamma-ray spectrometry in both ground and marine environments.

REFERENCES

[1] Tyler, A.N. “In-situ and airborne gamma-ray spectrometry”, Radioactivity in the Environment 11 407-448 (2008).

[2] Jones. D.G. “Development and application of marine gamma-ray measurements: a review”, J. Environ. Radioactivity 53 313–333 (2001)

[3] Beck, H.L., Gogolak, C., and DeCampo, J, “In situ Ge(Li) and NaI(Tl) gamma-ray spectrometry”, New York: U.S. Department of Energy, Environmental Measurements Laboratory; HASL-258; 1972.

Verification Method for the in Situ Measurement for Decommissioning Characterization

Sang Bum Hong*, Byung Chae Lee, Jun Ha Kim, Young Yong Ji, In Hye Hahm, and Bum Kyoung Seo
Korea Atomic Energy Research Institute, 111, Daedeok-daero 989beon-gil, Yuseong-gu, Daejeon, Republic of Korea
*sbhong@kaeri.re.kr

1. Introduction

The objective of radiological characterization is to provide a reliable data of the physical, chemical and radiological status for preparing the decommissioning nuclear facilities. Three kinds of in situ measurement may be used in relation to characterization: dose rate measurements, radioactive contamination measurements and measurement of relative individual radionuclide activities by spectrometry. In situ gamma spectroscopy has been shown to be cost effective and powerful tool in characterization survey for decommissioning [1-2]. The ISOCS software is capable of establishing an absolute efficiency calibration for a desired energy range based on numerical simulation and adequate knowledge of the sample geometry and chemical composition. The software provides a variety of geometry templates which covers a wide range of possible sample configurations [3].

In this study, verification method was proposed based on the dose comparison between spectrum derived dose rate and MCMP calculation dose from the radionuclide activities from spectrum analysis. The verification method was applied to the characterization survey for the pipe geometries in the Kori unit 1.

2. Verification in Situ Measurement Method for Characterization

2.1 Spectrum Derived Dose Rate Calculation

The dose rate from spectroscopy using a portable HPGe detector (ISOCS, GC4019, Canberra Inc.) was established by calculating a G-factor method through the Monte Carlo simulation. The G-factor is a dose conversion factor used to measure the ambient dose rate from the count rate at the measured energy spectrum, which was calculated using MCNP code. The response function of the detector was calculated for the vertical incident photon to the detector axis by the Monte Carlo simulation. The doe rate could be calculated of multiply the integration of the measure count rate by G-factor for the measured energy range.

$$\dot{X} = \int n(E)G(E)dE \quad (1)$$

where $\dot{X}$ is the ambient dose rate, n(E) is the measure count rate, and E is the photon energy.

2.2 MCNP Simulation of Dose Rate Calculation

The ISOCS system couples previously proven detector hardware with innovative calibration software to produce an integrated instrument capable of quantified analysis in the field comparable to laboratory analysis. The user must fully define the geometries and chemical compositions of the system and then input this information into the ISOCS software.

The source term was measured and calculated using ISOCS system and the results of the radionuclides used for dose calculation using MCNP simulation. The ISOCS system was applied for characterization of pipes geometries in Kori unit 1, the physical characterization of the pipe was consisted of the SUS SA-240 type 316 L stainless steel with density 8.03 g/cm^3.

The measuring condition of the field measurement was adopted the 45-degree shield, so the field of

view of geometry was limited the diameter is 10.2 cm, length is 60 cm. the contaminated layer is assumed 0.1 cm thickness of contamination in the pipe. Fig. 2 shows the geometry of the MCNP simulation.

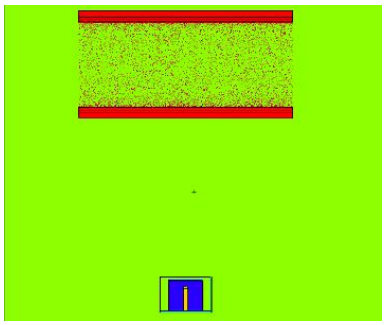

Fig. 1. MCNP simulation for pipe geometry.

2.3 Verification Methods and Results

The dose rate was calculation and compared between the G-factor method from measured spectrum and MCNP simulation from the defined source term of using ISOCS analysis method for validation of in situ measurement results for decommissioning.

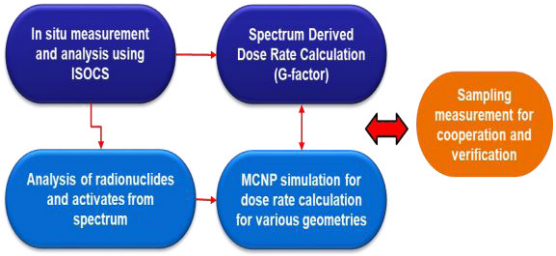

Fig. 2. Flow Sheet of verification process.

Table1. Component Documents Management

	Pipe A	Pipe B
G-factor (Sv/h)	3.31	3.31
MCNP calculation (Sv/h)	3.22	2.61
Relative error (%)	2.7	1.9

Fig. 2 shows the flow sheet of validation process by comparing the dose rate calculation.

The table show the compression results of in situ measurement for validation, the calculation results of dose rate show good agreement.

3. Conclusion

There is no better alternative NDA technique to the high resolution gamma spectrometry method with absolute calibrated such as implemented with ISOCS. In situ measurement has higher uncertainty than sampling analysis in laboratories form the measuring condition such as background of surrounding area, source position, radiation dose etc. In situ measured spectrum based dose rate calculation with compered with ISOCS and MCNP calculation could be the validation for decommissioning characterization

ACKNOWLEDGEMENT

This work was supported by a grant from the National Research Foundation of Korea (NRF), funded by the Korean government, Ministry of Science, ICT and Future Planning (No. 2017M2A8A5015143).

REFERENCES

[1] IAEA, “Radiological Characterization of shut Down Nuclear Reactors for Decommissioning Purpose”, International ATOMIC ENERGY AGENCY Technical Report Series No. 389, 1998, VIENNA.

[2] S. B. Hong, M. J. Kang, K. W. Lee, U. S. Chung, “Development of scaling factor for the activated concrete of the KRR-2," Applied radiation and Isotopes, 67, 1530-1533 (2009).

[3] V. Nizhnik, A. Belian, A. Shephard and A. Lebrun, “In Situ Object Counting System (ISOCSTM) Technique: a Cost-Effective Tool for NDA Verification in IAEA Safeguards, IEEE, 2011.

Environmental Radiation Analysis of Ulsan Metropolitan City Region Around Kori and Wolseong Nuclear Power Plants

UkJae Lee*, Chanki Lee, and Hee Reyoung Kim
Ulsan National Institute of Science and Technology, 50, UNIST-gil, Eonyang-eup, Ulju-gun, Ulsan, Republic of Korea
*dldnrwp@unist.ac.kr

1. Introduction

Ulsan metropolitan city is surrounded by 12 nuclear power plants within an emergency radiation planning area which is 30 km. It is the highest nuclear power plant density in the world. Also, many earthquakes have occurred frequently in active faults located in southeastern South Korea which is near the Ulsan. In order to secure the radiological safety of Ulsan, beta and gamma monitoring was conducted with appropriate pretreatment and radiation detection methods.

2. Methods

2.1 Selection of Sampling Point

The 12 operating NPPs located 30 km from the radiological emergency planning zone of Ulsan are Shin-Wolseong NPP 1-2, Wolseong NPP 1-4, Shin-Kori NPP 1-3, and Kori NPP 2-4. Considering that 24 nuclear power plants are in operation in South Korea, it is the highest density.

In Ulsan, also there are nondestructive testing companies and hospital facilities using radioactive isotopes. Therefore, radiation monitoring is essential for ensuring radiological safety for residents of Ulsan. The sampling points are selected with considering the characteristic of Ulsan. The Fig. 1 shows the location of sampling points for populated area, medical facilities, industrial facilities and nuclear power plant.

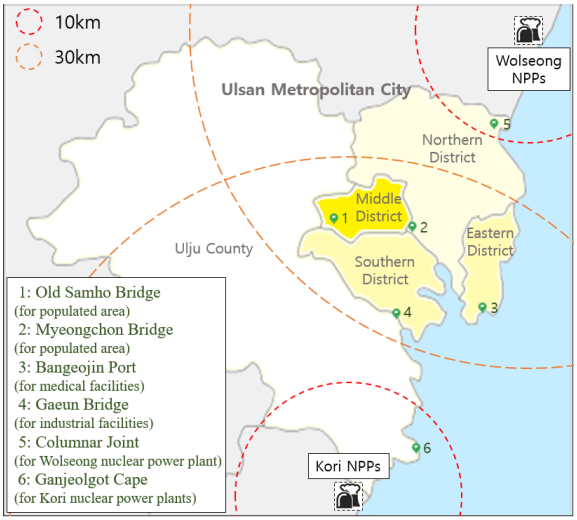

Fig. 1. Location for sampling points considering nuclear power plants (NPPs) near Ulsan Metropolitan City.

2.2 Pretreatment and Radiation Measurement

For pretreatment and measurement of gamma isotopes, 10 L of water sample was placed in a beaker and evaporated to 1 L on a hot plate. Concentrated samples were transferred to a 1 L Marinelli beaker and allowed to cool. The prepared sample was measured for 80,000 seconds per sample using an HPGe detector.

2.3 Gamma Dose Rate Monitoring Methods

The gamma dose rate for overall Ulsan city was

monitored by portable radiation detector based on NaI(Tl) scintillator. The detector was loaded at vehicle and operated continuously. The result of gamma dose rate distribution was shown as contour map with map image of detected area.

3. Results

3.1 Gamma Isotopes Analysis

The samples are analized with considering K-40, Be-7, Te-123m, I-131 and Cs-137. The overall isotopes are under the minimum detectable activity except K-40. The radioactivity value of K-40 is in table 1.

Table 1. The radioactivity value of K-40

Sampling Points	K-40 (Bq/L)
Ganjeolgot Cape	1.07E+01 ± 1.77E-01
Gaeun Bridge	1.45E+00 ± 6.37E-02
Myeongchon Bridge	4.61E+00 ± 1.07E-01
Bangeojin Port	1.07E+01 ± 1.15E-01
Columnar Joint	1.02E+01 ± 1.69E-01
Old Samho Bridge	1.48E-01 ± 4.00E-02

3.2 Gamma Dose Rate Distribution

The highest measured point is the Columnar Joint, and its value is 0.075 $\mu Sv/h$. The point with the lowest average value is the Gaeun Bridge, whose value is 0.0653 $\mu Sv/h$. The highest mean value is 0.0721 $\mu Sv/h$ at the Columnar Joint. The distribution of gamma dose rate of Ulsan with contour map is shown at Fig. 2.

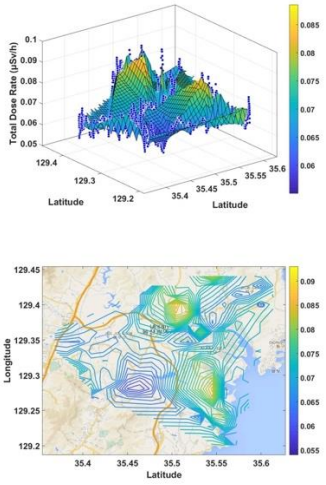

Fig. 2. Gamma dose rate distribution map for the entirety of Ulsan City.

4. Conclusions

The radiological safety of Ulsan area with the highest density of nuclear power plant was confirmed by sampling and monitoring of mobile radiation dose rate. It was confirmed that the radiation levels of populated areas, industrial facilities and medical facilities around nuclear power are not high.

REFERENCES

[1] Rao, D. D., Baburajan, A., Sudheendran, V., Verma, P. C., & Hegde, A. G., Evaluation and assessment of 25 years of environmental radioactivity monitoring data at Tarapur (India) nuclear site, Journal of environmental radioactivity 101(8) (2010) 630-642.

[2] Hemic, G., Environmental radiation monitoring in the context of regulations on dose limits to the public, Journal Office de la Republique Française 4 (1988) 88-521.

Wind Tunnel Performance Test for Shrouded Probes

Ho Young Kim[1,*] , Maria D. King[2], John S. Haglund[2], and Ahmed A. Kalbasi[2]

[1] LabWorks Inc., 19-5, Cheomdan venture so-ro 38beon-gil, Buk-gu, Gwangju, Republic of Korea

[2] Texas A&M AgriLife Research, Suite 512, 600 John Kimbrough Blvd., College Station, TX 77843, United States

[*]labworks@labworks.co.kr

1. Introduction

The ANSI/HPS N13.1-1999 states that at least 50% of the 10μm AD particles present in the stack free stream must be delivered to the sample collector. For this purpose, a sampling nozzle shall have an aerosol transmission ratio within the range of 0.80 to 1.30, and also the aspiration ratio shall be within the range of 0.80 to 1.50 for the anticipated range of normal operating conditions or anticipated accident operational conditions for an aerosol particle size of 10μm AD, or for the range of sizes that could be encountered in normal or accident conditions if those sizes are greater than 10μm AD.[1]

This paper presents wind tunnel performance test for two types of shroud nozzles which designed and incorporated as per ANSI/HPS N13.1-1999.

2. Wind Tunnel Test for Shroud Nozzles

2.1 Shroud Nozzle and Test Facility

Test models were designed for 2 CFM suction flow by LabWorks Inc. and tests were performed at Texas A&M university. To evaluate nozzle Wall Losses, the conservative testing methods with liquid aerosols was applied.

Table 1. The shrouded and isokinetic probes

Probe	RF-2-111	RF-2-112	
U_∞(m/s)	10, 15, 20	5	10, 15
Iso Nozzle	ISO-1	ISO-2	ISO-1

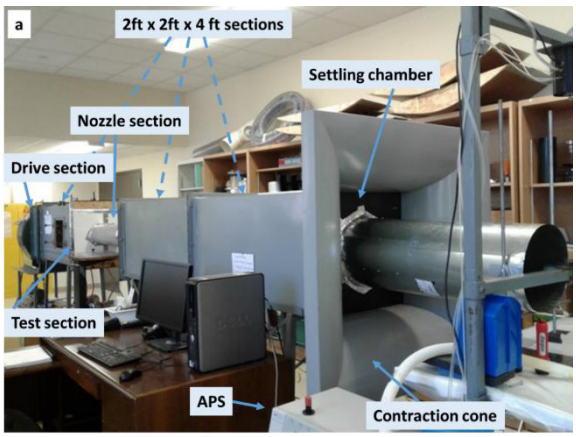

Fig. 1. General layout of the Test Facilities (BAEN, Texas A&M University).

2.2 Definition of Nozzle Performance

There are two basic terms concerning nozzle performances: aspiration ratio(A) and wall losses (WL), are defined as

$$A = \frac{C_i}{C_\infty} \quad (1)$$

$$WL = \frac{C_i - C_e}{C_\infty} \quad (2)$$

where,

C_i is the concentration at the nozzle inlet plane;

C_∞ is the aerosol concentration in the free stream;

C_e is the concentration at the nozzle exit plane.

In evaluating the effectiveness of a sampling nozzle, both the A and WL should be considered. Their effects are manifested in the transmission ratio(T) as such ;

$$T = \frac{C_e}{C_\infty} \quad (3)$$

2.3 Aerosol Generation and Measurements of Free Stream Aerosol Concentration

Experiments were performed with mono-disperse liquid oleic acid aerosol particles with sodium fluorescent tracer generated by the VOAG TSI Model 3450 and introduced into the wind tunnel flow. Flattening effects for aerosols are considered.[2]

Basically free stream aerosol concentration was measured by isokinetic nozzle and the shroud probe test model was mounted isoaxially at the middle section of the wind tunnel(20cm apart in parallel between two test nozzles).

2.4 Calculation of Nozzle Performance Factors

Shroud nozzle performance were calculated using following equations :

$$T = \frac{C_{f,spr}}{C_{f,iso}+C_{w,iso}} \quad (4)$$

$$A = \frac{C_{f,spr}+C_{w,spr}}{C_{f,iso}+C_{w,iso}} \quad (5)$$

$$WL = \frac{C_{w,spr}}{C_{f,spr}+C_{w,spr}} \quad (6)$$

where, subscripts 'spr' and 'iso' are used for shrouded and isokinetic probes respectively.

2.5 Test Results

Fig. 2 show summarized test results for two shroud nozzles. Aspiration ratio and Transmission ratio which incorporated Wall Losses are presented.

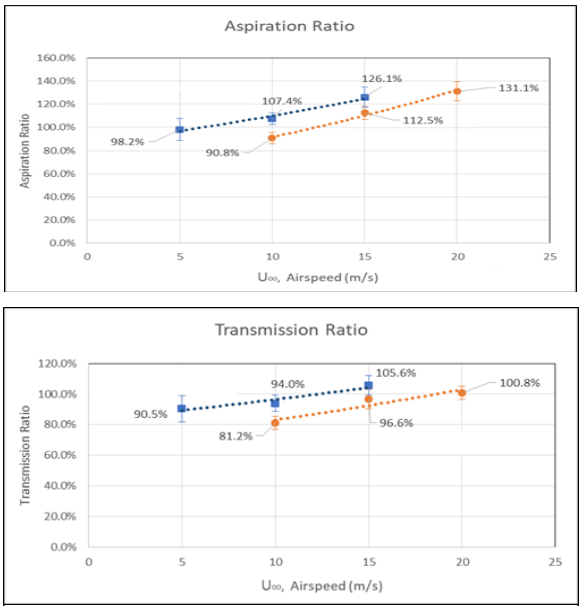

Fig. 2. Summary of the Aspiration and Transmission Ratio values for RF-2-111( ) and RF-2-112 ( ).

3. Conclusion

Test results show that LabWorks Inc's commercial shroud nozzle(RF-2-111 and l12) meet acceptance criteria for the performance in accordance with ANSI/HPS N13.1-1999 requirements. Wall losses are 10.5~23.0% for RF-2-111 and 7.8~16.2% for RF-2-112. The measured whole data shows COV is lower than twenty (20)% of its allowable limits.

REFERENCES

[1] ANSI/HPS N13.1, "Sampling and Monitoring Releases of Airborne Radioactive Substances from the Stacks and Ducts of Nuclear Facilities", HPS (1999).

[2] Faulkner, W.B. and J. S. Haglund, "Flattening Coefficients for Oleic Acid Droplets on Treated Glass Slides", *Aerosol Science and Technology*, 46(7), 828-832 (2012).

Development of Leak Position Detection System Using Noise and Reflected Wave Remove Technique

Minsoo Kim, Yongho Hong, Sooyeun Park*, Hyungmin Park, Heekyung Kim, Taegyu Lee, Youngseok Jung, and Eunseok Choi

Atomic Creative Technology Co., Ltd, 1434, Yuseong-daero, Yuseong-gu, Daejeon, Republic of Korea

*linapark@actbest.com

1. Introduction

Pipeline leakage in a nuclear power plant can cause not only environmental contamination but the public and occupational exposure. It is difficult to inspect damages or corrosion of pipelines because of the deeply and intricately buried construction. With increasing various concern and awareness for the social issues, development of the reliable leakage detection system of buried pipelines in a nuclear power plant is strongly in demand.

In this study, we developed the pipeline leakage detection system which adopts cross-correlation analysis method to provide the leakage locations among underground buried pipelines

2. Materials and Methods

2.1 Design and Construction

Developed system consists of acceleration sensors for detecting signal, data acquisition system (DAQ) for collecting analog signals, analog to digital converters (ADC) for translating analog electrical signals for data processing, cables for connecting sensors and signal acquisition modules, signal transmission module for transferring converted digital signal, analysis module for analyzing and confirming transferred digital signal, a rechargeable batteries for power supplying.

In particular, the developed leakage detection system is designed to resolve the issue with portability so as to be used for underground site where the pipelines are buried. Furthermore, high signal noise ratio (SNR) was established to allow the detection of a slight amount of leakage.

2.2 Development of Software

The measured signal analysis software was programed to graphic user interface (GUI) as it was shown in the Fig. 1. It is configured with information setting function, signal detection function, leakage signal analysis function, and data manage function. When the measured vibration signal is entered to the developed software, the signal analysis algorithm will be applied to assume the leakage location.

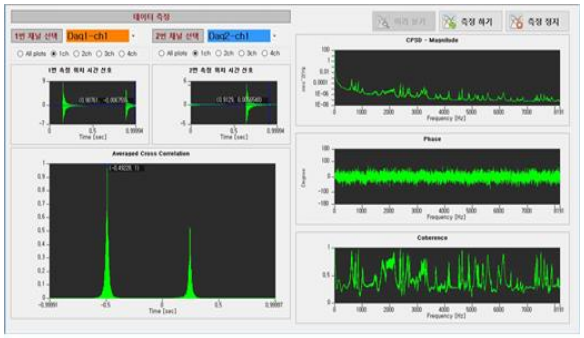

Fig. 1. Signal captured by the developed software under normal working condition.

Fig 2. Signal detection experiment using developed system (Korea Atomic Energy Research Institute, KAERI).

2.3 Leak Detection System Simulation

Practice test is performed using leakage simulation model constructed in Korea Atomic Energy Research Institute (KAERI) for performance evaluation.

3. Result and Discussion

In this study, leakage detection system is developed that can estimate the approximate location of buried pipelines in nuclear power plant.

Table 1. Result of leak detection experiemtn

Nozzle diameter (mm)	Detected location (m)	Difference (m)
2.5	18.48	-0.48
3.0	16.90	1.10
4.0	17.33	0.67
5.0	17.33	0.67
Average (m)	17.51	0.73

Table 1 shows the results of the detected location using developed system and the differences between actual and detected values. The average error in detection distance presented at 0.73 m, which included all the environmental errors and statistical errors due to the electrical noise.

In order to reduce influence of the environmental noise that can be appeared around the nuclear power plant, our group plans to apply the edge detection method into the adopted algorithm. It is expected to enhance the accuracy by applying advanced algorithm.

4. Conclusion

The newly developed leakage detection system based on signal detection technique has been presented. It is clear that ongoing project is successfully implemented by applying the time differences from reached signals to sensors. Thus, to provide accurate leakage location information, it is planned to carry out more practice test in various environment.

The results of this study will be applied to various facilities where safety needs to be secured related to complicated pipelines such as underground pipelines for water or gas.

Reference

[1] Yoon, Doo Byung, Park, Jin Ho, Shin, Sung Hwan. “A Feasibility Study on Leak Detection Technique for Buried Pipes (KAERI/TR--4219/2010)”. Republic of Korea.

[2] Lee. W, Cho. S, “Sensor Network for Pipeline Leakage Detection in Nuclear Power Plant.” IEIE, 54(12), 10-18 (2017)

Review on Revision History of ANSI/ANS-18.1 and PWR-GALE Along With Its Potential Impact to Anticipated Radioactive Source Terms to Environment From PWRs

Ji Woo Lee, Ji Su Kang, Sae Gun Lee, and Jae Hak Cheong*

Kyung Hee University, 1732, Deogyeong-daero, Giheung-gu, Yongin-si, Gyeonggi-do, Republic of Korea

*jhcheong@khu.ac.kr

1. Introduction

In case of Korea, as same as US NRC, uses the PWR-GALE and the concentrations in principal fluid systems of the reference PWRs as given in ANSI / ANS-18.1 to estimate the annual release rate of Nuclear Power Plants(NPPs). After first published in 1976, ANSI / ANS-18.1 has been revised in 1984, 1999 and 2016, but most Korean NPPs use the 1984 version (Table 1). Therefore, it is necessary to verify whether the current evaluation system is suitable.

In this study, release rates of target plant(APR-1400) were estimated by applying concentrations of ANSI / ANS-18.1-1976, 1984, 1999, and 2016 to PWR-GALE86.

Table 1. Current Status of South Korea NPPs

Anticipated Source Term	Nuclear Power Plants
ANSI-N237-1976	Kori 1,2, 3, 4
	Hanbit 1,2 / Hanul 1,2
ANSI/ANS 18.1-1984	Hanbit 3,4,5,6
	Hanul 3,4 5,6
	Shin Kori 1,2,3,4
	Shin Kori 5,6 PSAR
ANSI/ANS 18.1-1999	APR-1400 DCD
ANSI/ANS 18.1-2016	None

2. Methodology

2.1. Analysis of ANSI/ANS-18.1 Revision

ANSI/ANS-18.1 provides coolant concentration of the reference PWR. Also it supplies calculation formula and parameter of Adjustment Factor used for estimating anticipated source term of target plant.

Although there are some differences between the revisions, the overall coolant concentration of the reference PWR has decreased since 1984. For Adjustment factor, all are calculated by the same formula since 1984 except for situations where the natural or depleted zinc have been used. (Table 2).

Table 2. Adjustment Factors of Primary Coolant change

Element Class	1984	1999, 2016
1	$\frac{P \cdot WP_n \cdot (R_{n1} + \lambda)}{WP \cdot P_n \cdot (R_1 + \lambda)}$	
2	$\frac{P \cdot WP_n \cdot (R_{n2} + \lambda)}{WP \cdot P_n \cdot (R_2 + \lambda)}$	
3	$\frac{P \cdot WP_n \cdot (R_{n3} + \lambda)}{WP \cdot P_n \cdot (R_3 + \lambda)}$	
4	1.0	
5	*	
6	$\frac{P \cdot WP_n \cdot (R_{n6} + \lambda)}{WP \cdot P_n \cdot (R_6 + \lambda)}$	
6 (Zn-65)	$\frac{P \cdot WP_n \cdot (R_{n6} + \lambda)}{WP \cdot P_n \cdot (R_6 + \lambda)}$	10
6 (Co-58)	$\frac{P \cdot WP_n \cdot (R_{n6} + \lambda)}{WP \cdot P_n \cdot (R_6 + \lambda)}$	10

2.2 PWR-GALE

PWR-GALE86 calculates the release rate of the target NPP based on the information of reference NPP. Since PWR-GALE86 basically uses the information of ANSI / ANS-18.1-1984, the results were derived by applying the information of 1976,1999,2016 version through the change of hardwired parameters.

3. Results and Discussion

3.1 Noble Gas and Halogens

In this case, the change in release rate was the same as the change in coolant concentration of the reference PWR. Release rates decreased sharply except for ^{133}Xe and ^{131m}Xe (Fig. 1).

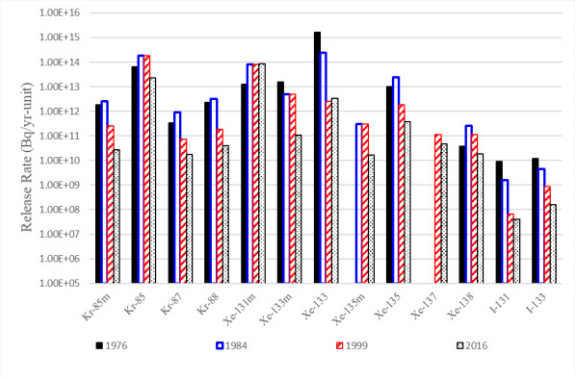

Fig. 1. Release Rate Result for PWR-GALEG.

3.2 Liquid

In the case of PWR-GALEL, 0.16 Ci per NPP is to be adjusted considering the AOO situation. Therefore, the change in release rate is not in perfect agreement with the change in coolant concentrations. However, all nuclides that has big-changed showed the smallest value in the 2016 revision (Fig. 2).

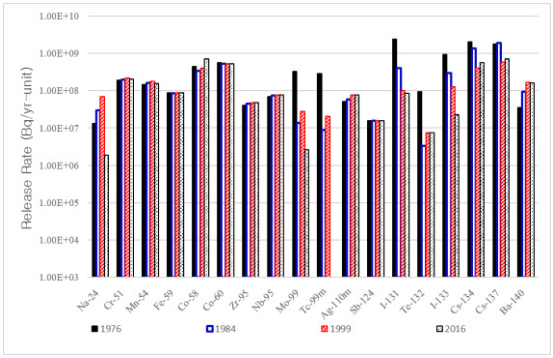

Fig. 2. Release Rate Result for PWR-GALEL.

3.3 Particulates & Specific Nuclides (^{14}C,^{41}Ar,^{3}H)

For particulates and ^{14}C, ^{41}Ar, ^{3}H, PWR-GAEL86 outputs a specified release rate without performing any calculations. This is the average data of the US NPPs in 1970s, so it will need to be additional considered for application to Korea.

4. Conclusion

This study analyzed the expected release rate changes of radioactive effluent from NPP following the ANSI/ANS-18.1 revision.

When the revised version is applied, the estimated release rate is reduced. In order to verify the effectiveness, a comparative analysis with the actual domestic emission data is necessary.

ACKNOWLEDGEMENT

This work was supported by the Nuclear Safety Research Program through the Korea Foundation Of Nuclear Safety (KOFONS), granted financial resource from the Nuclear Safety and Security Commission (NSSC), Republic of Korea (No. 1605008).

REFERENCES

[1] American Nuclear Society, “American National Standard Radioactive Source Term for Normal Operation of Light Water Reactors”, ANSI/ANS-18.1 (1976,1984,1999,2016)

[2] “Calculation of Releases of Radioactive Materials in Gaseous and Liquid Effluents from Pressurized Water Reactors – PWR-GALE Code”, NUREG-0017 Rev. 1, Nuclear Regulatory Commission (1985)

6분과

방사선환경 및 안전 (Poster)

Environmental Radiation Survey Using Airborne Gamma-Ray Spectrometry Based on Manned and Unmanned Aerial Vehicles

Young-Yong Ji[1,*], Taehyung Lim[2], Jang Hee Lee[3], Eun Young Song[3], Kun Ho Chung[1], and Mun Ja Kang[1]

[1] Korea Atomic Energy Research Institute, 111, Daedeok-daero 989beon-gil, Yuseong-gu, Daejeon, Republic of Korea

[2] SI Detection Co. Ltd., 21, Yuseong-daero 1628beon-gil, Yuseong-gu, Daejeon, Republic of Korea

[3] Nuclear Safety Division, Busan Metropolitan City, 1001, Jungang-daero, Yeonje-gu, Busan, Republic of Korea

[*]yyji@kaeri.re.kr

1. Introduction

After the nuclear accident of the Fukushima Daiichi nuclear power plants (FDNPP), the importance of environmental radiation survey has increased to quickly assess radioactive deposits in the ground. In general, the airborne gamma-ray spectrometry is widely used to rapidly estimate the distribution of environmental radiations over wide area for the purpose of the mineral exploration as well as emergency response by surveying natural and anthropogenic radiations [1-3]. Especially, the dose rate map established from the airborne monitoring was used to be the fundamental data for selecting the decontamination areas and evacuation zones in Japan.

Large-volume NaI(Tl) detectors are loaded in the manned aerial vehicle with a large payload. On the other hand, because unmanned aerial vehicles, such as a drone, has a small payload, the weight of detecting system should be limited to be generally about 10 kg. For the purpose of airborne gamma-ray spectrometry, two kinds of aerial measuring system were developed based on a 4”x4”x16” NaI(Tl) detector and two 2”φx2” $LaBr_3$(Ce) detectors, respectively. The total weight including detecting system was below about 20 and 6 kg dedicated manned and unmanned aerial vehicles.

In this study, the performance test was conducted to quickly assess the averaged ambient dose rate at 1 m above the ground over the wide area. First, the airborne survey using a drone was performed at three flight heights in relatively flat land of Jeju Island. Second, the airborne survey using a manned helicopter was conducted at about 300 m height to assess the dose rate by comparing with the results of carborne survey in the same site of Busan, with the help of Busan metropolitan city hall.

2. Method and Results

2.1 Airborne Survey System

Fig. 1 shows the airborne survey system based on a large-volume of NaI(Tl) detector and two 2 inch $LaBr_3$(Ce) detectors. These system can be also applied to the ground-mobile gamma-ray spectrometry, such as the carborne survey. Especially, the airborne system with $LaBr_3$(Ce) detectors is the multipurpose system for environmental radiation survey, which can be used to the ground-based gamma-ray spectrometry using a tripod and ground-mobile system using a backpack and carborne survey. Therefore, the results of airborne survey at diverse heights can be simply corrected to those at 1 m above the ground. In addition, the quality of survey results can be enhanced by comparing two results of airborne and carborne survey in the same site.

Fig. 1. The sites for the environmental radiation survey around the FDNPP.

2.2 Unmanned Aerial Vehicle

Fig. 2 show the result of the airborne survey using a drone in Jeju Island. The survey was then conducted in wide area of above 100x200 m^2 at several flight heights and line spaces. The survey speed was fixed to be about 10 km/h. All results depending on the flight heights were corrected to those at 1 m above the ground by applying the attenuation correction factor, which was obtained from the hovering states at five heights of 3, 9, 20, 30, and 50 m. The airborne survey results were then compared with those of backpack survey and ground-based gamma-ray spectrometry using a tripod at the same site.

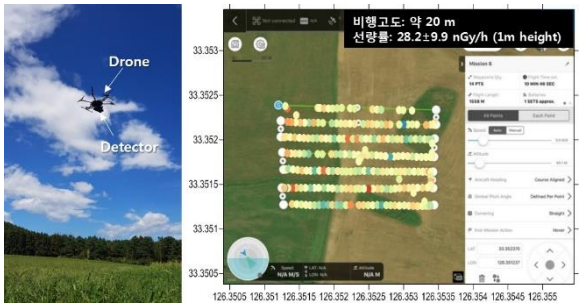

Fig. 2. The airborne survey and an example of the survey result at the flight height of 20 m.

2.3 Manned Aerial Vehicle

The airborne survey using manned helicopter was conducted by loading a large-volume NaI(Tl) detector in a vehicle. The survey height and speed were about 300 m and 100 km/h. The survey site was designated to cover the residence area, beach, and sea of Busan with different dose rate levels. The carborne survey with the same survey system was also conducted around the site of airborne survey. The performance of airborne survey was then evaluated by comparing two survey results.

Fig. 3. The airborne survey using a manned helicopter.

3. Conclusion

The diverse aerial measuring system based on a NaI(Tl) and $LaBr_3$(Ce) gamma-ray spectrometer were developed to calculate the ambient dose rate. Two types of airborne survey system was developed for the purpose of using in manned helicopter and drone, respectively. Finally, the performance of airborne survey was evaluated by comparing with ground mobile gamma-ray spectrometry using a backpack and carborne survey.

ACKNOWLEDGMENTS

This work was performed under the auspices of the Ministry of Science and ICT of Korea, NRF contract No. NRF-2017M2A8A4015256.

REFERENCES

[1] IAEA, Airborne Gamma Ray Spectrometer Surveying, Technical Reports Series No. 323 (1991).

[2] Y. Sanada et al., Temporal variation of dose rate distribution around the Fukushima Daiichi nuclear power station using unmanned helicopter, Appl. Radiat. Isot. 118: 308-316 (2016).

[3] K. Ochi et al., Estimation of the vertical distribution of radiocesium in soil on the basis of the characteristics of gamma-ray spectra obtained via aerial radiation monitoring using an unmanned helicopter, Int. J. Environ. Res. Public Health 14, 926; doi: 10.3390/ijerph14080926 (2017).

Calculation of Effective Dose Coefficient to Workers Due to Inhalation of Radon at Groundwater Treatment Facility

Kwang Pyo Kim[1,*], Jung Hwan Jang[1], Jae Kwon[1], Se Jong Lee[1], Seung Woo Ji[1], and Jae Kook Lee[1, 2]

[1] Kyung Hee University, 1732, Deogyeong-daero, Giheung-gu, Yongin-si, Gyeonggi-do, Republic of Korea

[2] Korea Institute of Nuclear Safety, 62, Gwahak-ro, Yuseong-gu, Daejeon, Republic of Korea

[*]kpkim@khu.ac.kr

1. Introduction

Rn-222 is a radioactive gas produced by the radioactive decay of U-238. Generally, groundwater contains higher concentrations of Rn-222 than surface water. IAEA identified types of workplace which may need priority in any investigation of radon levels [1]. Workplace supplying large amounts of groundwater, such as groundwater treatment facility may give rise to enhanced indoor radon concentration. Therefore, the workers in groundwater treatment facilities are subjected to radon exposure. However, the radon exposure to workers at domestic groundwater treatment facilities has not been adequately addressed. Before evaluating effective dose due to inhalation of radon, it is necessary to calculate effective dose coefficient to workers.

The objective of this study was to calculate effective dose coefficient to workers due to inhalation of radon at groundwater treatment facility. Calculation of effective dose coefficient was based on ICRP 66 Human Respiratory Tract Model (HRTM) using major exposure parameters of ICRP Publication 137.

2. Materials and Methods

Calculation of effective dose coefficient was conducted using IMBA (Integrated Modules for Bioassay Analysis) based on the ICRP 66 HRTM. The breathing rate, aerosol parameters, activity ratios of radon progeny were considered as major exposure parameter to calculate dose coefficient.

Inhalation dose due to radon is mainly caused by alpha particles emitted from radon progeny. However, Po-214 has a very short half-life (160 μs), and the radionuclides of Pb-210 and below have extremely low radioactivity. Therefore, these radionuclides were excluded from target of calculation. In this study, Po-218, Pb-214 and Bi-214 were considered to calculate dose coefficient.

The activity size distribution of the radon progeny can be represented by summing of lognormal distributions. Porstendöfer and Reineking (1999) measured the activity size distribution at a water supply facility [2]. Table 1 shows aerosol parameter values for groundwater treatment facility. The aerosol parameters were difficult to select appropriate data due to lack of data on the domestic environment. In this study, we adopted aerosol parameters based on ICRP 137. The average breathing rate of 1.2 m^3/h was adopted as a reference value for light workers.

Table 1. Aerosol parameter values for groundwater treatment facility

Description of Parameter	Mode [a]		
	u	Attached	
		n	a
Total PAEC fraction (%)	5	15	80
Aerosol size (nm)	0.8	50	300
Dispersion (σ_g)	1.2	1.5	1.8
Particle Density (g/cm^{-3})	1	1.4	1.4
Particle Shape Factor	1	1.1	1.1

[a]: 'u', 'n', and 'a' represent the unattached, nucleation, and accumulation modes, respectively.

The activity concentrations of radon progeny are vary with the particular environmental conditions of exposure. Based on measurements of the activity concentration of Po-218, Pb-214 and Bi-214 carried out indoors, the following activity ratios of radon progeny were assumed for dosimetry in this study [2].

Unattached: Po-218 : Pb-214 : Bi-214 = 1 : 0.1 : 0

Attached: Po-218 : Pb-214 : Bi-214 = 1 : 0.75 : 0.6

3. Results and Discussion

Table 2 shows regional committed equivalent doses and effective dose per working level month (WLM) assuming groundwater treatment facilities conditions.

Table 2. Regional committed equivalent doses and effective dose per WLM assuming groundwater treatment facilities conditions

Region	Committed equivalent dose (mSv/WLM)		
	Unattached (5%)	Attached	
		Nucleation (15%)	Accumulation (80%)
ET	20.0	8.4	60.5
BB	66.2	36.6	82.7
bb	25.3	74.0	104.1
AI	0.01	3.4	5.6
Equivalent dose coefficient	88.9 mSv/WLM (Extra Thoracic) 132.7 mSv/WLM (Thoracic)		
Effective dose coefficient	16.7 mSv/WLM		

Effective dose coefficients was calculated as 16.7 mSv/WLM (around 27 nSv/Bq·h·m^{-3}). Effective dose to extra thoracic and thoracic region contributed more than 99% of the effective dose coefficient. The dose coefficient corresponds to range of 10-20 mSv/WLM for the workplace provided by ICRP Publication 137.

The equivalent dose to the extra thoracic regions is similar to the thoracic region. However, its contribution to the effective dose is generally quite small as it is one of 13 remainder organs [3]. Therefore, effective dose due to inhalation of radon progeny is dominated by the equivalent dose to the thoracic region.

Despite the unattached fraction representing only 5% of the potential alpha energy concentration (PAEC) of radon progeny, the unattached fraction accounts for 23% of effective dose coefficient. Because the dose contribution to BB and bb regions are greater for aerosols with unattached radon progeny. Fig. 1 shows effective dose per WLM as a function of particle size of aerosol [2].

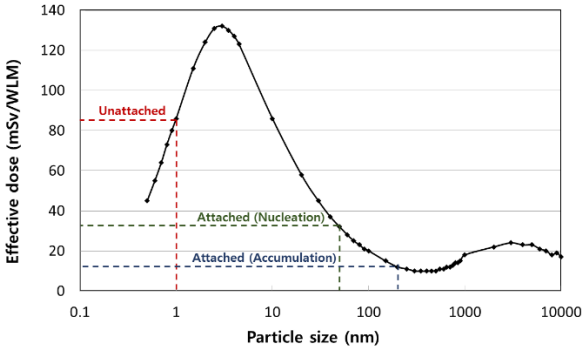

Fig. 1. Effective dose per WLM as a function of particle size of aerosol.

4. Conclusion

We calculated effective dose to workers due to inhalation of radon at groundwater treatment facility. Effective dose coefficients was calculated as 16.7 mSv/WLM (around 27 nSv/Bq·h·m^{-3}). We adopted major exposure parameter based on ICRP Publication 137 due to lack of data on the domestic environment. Therefore, establishment of site-specific data in NORM industry may be necessary. The results of this study can be used for assessment of radiation exposure at Korean NORM industries.

ACKNOWLEDGMENTS

This work was supported by a grant from “Establishment of Technical Basis for Measurement and Assessment for Radiation in the Natural Environment and Resulting Radiation Impact” carried out by Korea Institute of Nuclear Safety.

REFERENCES

[1] IAEA, Assessing the Need for Radiation Protection Measures in Work Involving Minerals and Raw Materials, SRS 49 (2006).

[2] ICRP, Occupational Intakes of Radionuclides: Part 3, ICRP 137 (2017).

[3] ICRP, The 2007 Recommendations of the International Commission on Radiological Protection, ICRP 103 (2007).

Evaluation of CH_3I Removal Performance and Physical Characteristics for New TEDA Impregnated Activated Carbon Stored in Nuclear Power Plants

Hak-Soo Kim* and Cho-Rong Kim

KHNP Central Research Institute, 70, Yuseong-daero 1312beon-gil, Yuseong-gu, Daejeon, Republic of Korea

*Hskim0071@khnp.co.kr

1. Introduction

Air Cleaning Unit (ACU) in Nuclear Power Plant (NPP) is adopted to remove radioactive waste as well as toxic materials from operation and accidents. Absorber in ACU is filled with Tri-Ethylene-Di-Amine impregnated activated carbon (TEDA-AC) and has been chosen as an absorbent to remove the radioiodine during normal operation and accident conditions. The CH_3I removal performance of TEDA-AC is affected by the environment factors such as temperature, humidity and toxic materials and should satisfy Regulatory Guide 1.52 for Safety-Related-System and Regulatory Guide 1.140 for Non-Safety-Related-System. But there are only quality assurance requirements for packaging, storage and handling for new TEDA-AC in storage [1]. The performance of new TEDA-AC may be deteriorated due to the environment conditions in storage areas. In this paper, the analysis results of CH_3I removal performance, physical characteristics and TEDA loss for new TEDA-AC according to the storage period are introduced.

2. Representative Sample Selection and TEDA-AC Storage Conditions

In order to evaluate the CH_3I removal performance, physical characteristics and TEDA loss of new TEDA-AC under storage, representative samples were selected according to storage period. Table 1 shows the storage period for new TEDA-AC.

Table 1. Storage Period for New TEDA-AC

NPP	Purchase Date	Sampling Date	Storage Period
NPP 1	2016-07	2017-06	< 1 year (11 months)
NPP 2	2012-04	2017-03	< 5 year (59 months)
NPP 3	2011-06	2017-07	> 5year (73 months)

The new TEDA-AC in NPP is packed and stored in according with Level 2 requirements of ASME NQA-1-2015, Subpart 2.2 [1]. The new TEDA-AC is sealed in vinyl and then stored in a sealed drum as shown in Fig. 1.

Fig. 1. Packaging Status of New TEDA-AC.

3. Analysis Results of New TEDA-AC

The CH_3I removal performance of new TEDA-AC was tested according to ASTM D3803-91 [2]. The results are shown in Table 2.

Table 2. Analysis Results of CH_3I Removal Performance

NPP	Samples	Results
NPP 1	< 1 year (11 months)	99.785±0.07
NPP 2	< 5 year (59 months)	99.885±0.004
NPP 3	> 5year (73 months)	99.821±0.007

The physical characteristics of new TEDA-AC was analyzed according to ASME AG-1-2015 FF-5120 [3] and its results are shown in Table 3.

Table 3. Analysis Results of Physical Characteristics

Test Items	Method	Criteria	Results		
			< 1 year	< 5 year	> 5 year
Apparent Density	D2854	Min. 0.38 g/mℓ	0.57	0.54	0.57
Particle Size Distribution ASME E-11 Sieves -retained on No.6 -retained on No.8 -No.8 retained on No.12 -No.12 retained on No.16 -through No.16 -through No.18	D2862	 Max. 0.1% Max. 5.0% Max. 60.0% Min. 40.0% Max. 5.0% Max. 1.0%	Passed	Passed	Passed
Moisture Content	D2867	Measured	2.3	2.9	3.8
ball-pan hardness	D3802	Min. 60.0%	99.6	99.7	99.8
pH	D3838	Measured	10.1	10.1	9.7

ACU in NPP use activated carbon with 5% TEDA-AC to remove the radioiodine. It was additionally analyzed whether TEDA loss occurred according to storage period. TEDA loss analysis was performed using a thermal analyzer system and the results of TEDA loss are shown in Fig. 2.

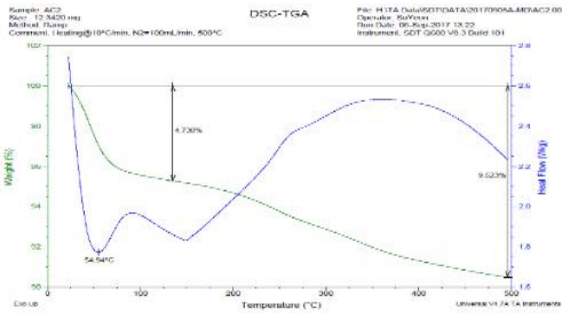

(< 1 year)

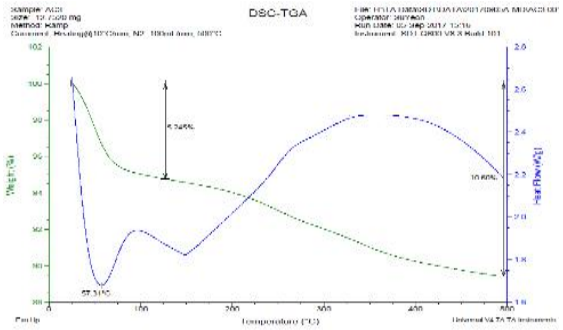

(< 5 year)

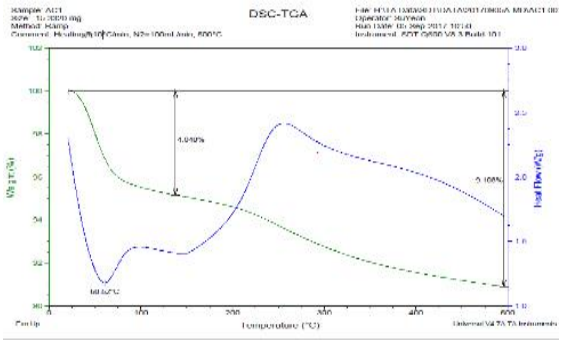

(> 5 year)

Fig. 2. Analysis Results of TEDA Loss.

4. Conclusion

The new TEDA-AC is stored in warehouse for long-term periods before being installed in ACU. The results of the analysis showed that there was no significant change in the CH_3I removal performance and physical characteristics of new TEDA-AC after long-term storage.

REFERENCES

[1] ASME, “Quality Assurance Requirements for Nuclear Facility Applications”, ASME NQA-1-2015, Subpart 2.2, New York, NY.

[2] ASTM, “Standard Test Method for Nuclear-Grade Activated Carbon”, ASTM D3803-91, 2014.

[3] ASME, “Code on Nuclear Air and Gas Treatment, Article FF-5000 Inspection and Testing”, ASME AG-1-2015, 2015.

Laboratory Establishment for Measuring Uranium Radioactivity in Urine

Cheol Hyun Kang* and Jong Il Lee
Korea Atomic Energy Research Institute, 111, Daedeok-daero 989beon-gil, Yuseong-gu, Daejeon, Republic of Korea
*chkang1@kaeri.re.kr

1. Introduction

Recently Korean government's regulatory guideline suggests bioassay of radiation workers who can have annual dose of over 1 mSv [1]. When it comes to radiation workers who deal with Uranium, it is impossible to achieve minimum detectable activity through in-vivo bioassay, like lung counter. In-Vitro bioassay can be a solution for achieving lower MDA. Nowadays, many research groups have been developed a variety of in-vitro bioassay methods for Uranium bioassay. For many of those use the 1-day urine of the radiation workers. However, it is hard to gather 1-day urine of the workers due to cumbersome reasons. The creatinine or volumetric normalization can be alternatives even though there are variation from individual or different urine samples [2]. The urine sample should be acid digested, because organic matters can interrupt measuring the uranium concentration by producing complex compounds. After eliminating organic matters, the solid phase extraction (SPE) process can be executed. Mostly, UTEVA® Resin, Eichrom is used for extracting Uranium. The extracted uranium can be measured either alpha spectroscopy or Ion-Coupled Plasma mass spectroscopy (ICP-MS).

In this study, bioassay laboratory to access the internal dose of workers who deal with Uranium isotopes has been established. The laboratory will carry out bioassay of KAERI's radiation workers who treat Uranium isotopes.

2. Analytical Methods

2.1 Microwave Digestion System

To remove organic matters, KAERI's bioassay laboratory adopted ETHOS EASY Advanced Microwave Digestion system, Milestone srl. It can make high pressure and temperature condition so that the urine samples can be digested faster than hot-plate assisted wet digestion without the loss of volatile materials in the urine samples. The urine samples were kept in the 3℃ refrigerator and 5 g spot urine sample is accurately weighed. The sample is transfer to the PTFE digestion vessel to digest with 8 ml concentrated HNO_3. The sample put into the Microwave system and then digested under the setting program (Table. 1) under the optimal conditions, the clear digestion solution can be obtained. The digestion solution transferred to the glass beaker and evaporation to dryness in 140℃ hot- plate. The residue is dissolved with 2 mL 4M HNO_3 for the solid phase extraction (SPE) process.

Table 1. Microwave digestion program for urine samples

Step 1			Step 2		Step3		
T/℃	R time /min	H time /min	T/℃	R time /min	T/℃	R time /min	H time /min
120	5	3	170	5	200	7	15

Note : R means increasing temperature time
H means holding temperature time

2.2 Solid Phase Extraction

The one-stage ion exchange column chemistry procedure has been used in order to remove interfering elements except Uranium isotopes. The SPE begins with 2 mL empty column (Eichrom), which were packed with 1 mL of UTEVA Resin (Eichrom). The 2 mL of the sample solution is loaded onto the ion exchange column. The complete ion exchange chromatography procedure is presented in Table 2. The eluted solution is evaporated to dryness in 140℃ hot- plate to dissolve the residue 5% HNO_3 for measuring ICP-MS.

Table 2. Procedure used for the ion exchange chromatography

Step	Solution	Concentration (M)	Amount of solution (ml)
Resin Cleaning	DIW	-	10
Conditioning	HNO_3	4	4
Sample loading	HNO_3	4	2
Washing 1	HNO_3	4	4
Washing 2	HCl + Oxalic acid	5 , 0.05	6
U elution	HNO_3	0.1	6

The 2 mL cut of the ion exchange chromatography procedure by using multi-elemental solution is presented Fig. 1. The Recovery of Uranium was measured by ICP-MS (Nexion2000, PerkinElmer)

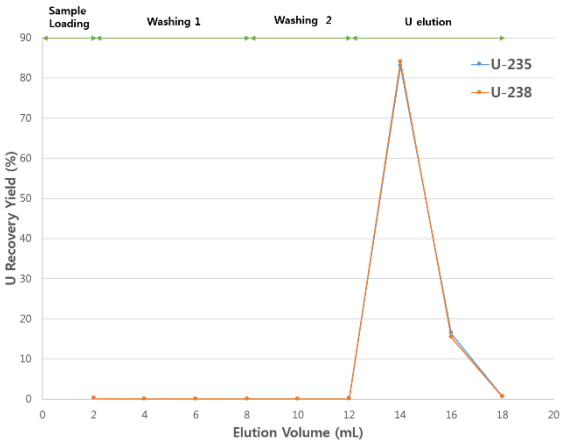

Fig. 1. Ion exchange chromatography elution curve of Uranium measured by ICP-MS.

3. Conclusion

Bioassay laboratory for measuring Uranium in radiation worker's urine of KAERI has been established. By using the microwave digestion method, the analytical time has been shorted and the reagent for analysis can be less consumed.

With this method, this laboratory will analyze radiation worker's urine routinely and occasionally. For further work, the ICP-MS setting for optimal measurement will be proceeded to get the reliable data from human urine.

REFERENCES

[1] Nuclear Safety And Security Commission, "Guidelines for internal dosimetry management of radiation workers" (2017).

[2] Kerpas, Zeev et al., "Uranium in Urine-normalization to Creatinine", Health physics, 74, 86-90 (1998).

Development of Freshwater Foodchain Model for Calculating Tritium Transfer in Aquatic Organisms in Freshwater Following Nuclear Accident

Sora Kim, Kyung-suk Suh*, Byung-Il Min, Kihyun Park, Byung-Mo Yang, and Jiyoon Kim
Korea Atomic Energy Research Institute, 111, Daedeok-daero 989beon-gil, Yuseong-gu, Daejeon, Republic of Korea
*kssuh@kaeri.re.kr

1. Introduction

In the field of radiation protection, tritium was not major concern, because the radiological impact of tritium is not significant comparing with other radionuclides. Interest in tritium has grown after the experience of the release of tritium from the Fukushima Daiichi Nuclear Power Plant accident [1, 2] and the high OBT (Organically bound tritium) level measured in aquatic organisms [3, 4]. Tritium can pose a health hazard due to internal exposure via inhalation or ingestion, but health effect of external exposure could be negligible.

A model has been developed to estimate tritium concentrations in aquatic organisms and the effect on human health. Calculation was performed on the Fukushima accident case.

2. Materials and Methods

2.1 Aquatic Food Chain Model for Tritium

The model calculates the OBT and HTO (tritiated water) transfer through the aquatic food chain following accidental releases of tritium. It is based on a dynamic model for OBT and an equilibrium model for HTO. It considers 4 types of aquatic organisms: phytoplankton, zooplankton, prey fish, and predatory fish.

2.2 Input Data and Assumptions for Calculation

Measurement data of tritium concentration at Hiso River in Iitate village from 2011 to 2014 were taken from Ueda et al. (2015) [5].

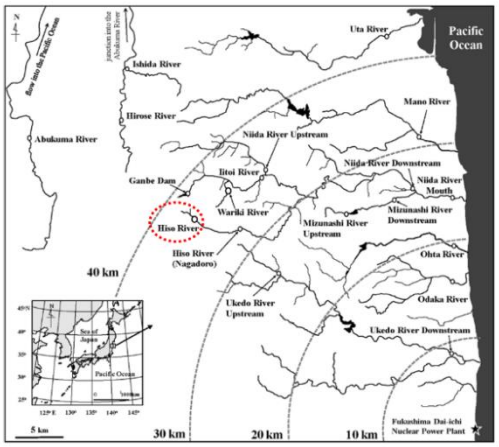

Fig. 1. Sampling location of Rivers in Fukushima prefecture. Figure taken from Ueda et al. (2015) [5].

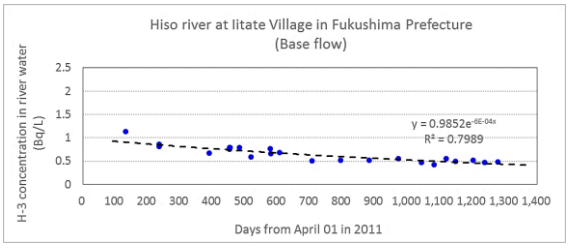

Fig. 2. H-3 concentration in Hiso river water. Data taken from Table 1 of Ueda et al. (2015) [5].

3. Results and Discussion

River water in some regions of Japan have been contaminated with radionuclides released from Fukushima Daiichi nuclear power plant (FDNPP)

accident. We calculated HTO and OBT concentration in aquatic organisms which were inhabited at Hiso River in Iitate village in Fukushima Prefecture from 2011 to 2014. Fig. 3 (a) and (b) show the predicted activity concentrations of H-3 in 4 types of aquatic organisms at Hiso River for two cases: 1) the use of mean background H-3 concentration (0.4 Bq/L) in river water, 2) use of fitting data (contaminated by FDNPP accident) presented in Fig. 2. About 1,200 ~ 1,400 days after the Fukushima accident, concentration levels of H-3 in aquatic organisms inhabited at Hiso River become similar to those aquatic organisms inhabited at rivers with background levels of H-3. OBT concentration was predicted to account for less than about 5% of H-3 concentration in aquatic organism.

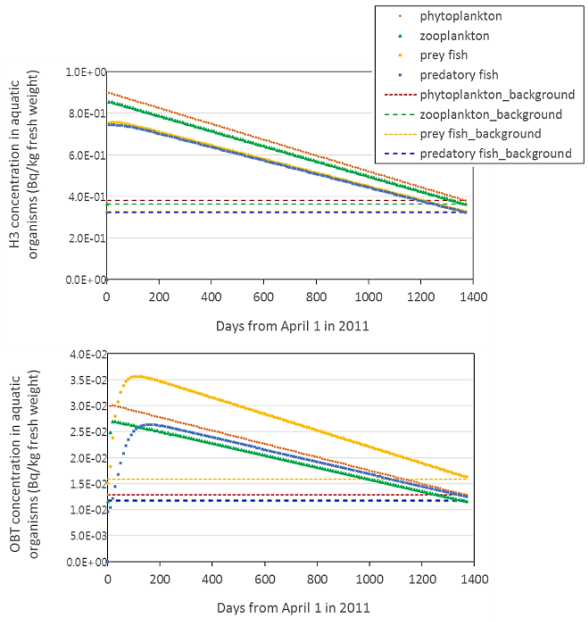

Fig. 3. (a) H-3 (HTO+OBT) and (b) OBT concentration in aquatic organisms in Hiso River from 2011 to 2014.

4. Conclusions

A tritium aquatic food chain model was recently developed to estimate tritium transfer through the aquatic food chain and the resulting radiological impact on the public following accidental releases. Comparative analysis with monitoring data and simulation results from other model will be conducted after collecting sufficient data. The developed tritium aquatic food chain model will be used as a tool to estimate contaminated levels of aquatic food and ingestion doses for accidentally release of tritium.

ACKNOWLEGEMENT

This work was supported by the National Research Foundation of Korea (NRF) and funded by the Korea government (MSIP) (MSIP: NRF-2017M2A8A4015253, NRF-2015M2A2B20342 82).

REFERENCES

[1] H. Kakiuchi et al., “Concentration of ^{3}H in plants around Fukushima Dai-ichi Nuclear Power Station. Scientific Reports”, 2(947). doi: 10.1038/srep00947 (2012).

[2] N. Takahata, et al., “Direct tritium emissions to the ocean from the Fukushima Dai-ichi nuclear accident”, Geochemical Journal, 52. doi:10.2343/ geochemj.2.0499 (2018).

[3] A. Melintescu, D. Galeriu, “Dynamic model for tritium transfer in an aquatic food chain”, Radiat Environ Biophys, 50:459-473 (2011).

[4] F. Eyrolle-Boyer et al., “Apparent enrichment of organically bound tritium in rivers explained by the heritage of our past”, J Environ Radioact. 136:162-168 (2014).

[5] S. Ueda et al., “Nuclear accident-derived 3H in river water of Fukushima Prefecture during 2011-2014”, J Environ Radioact. 146:102-109 (2015).

A Method for Improvement of Operation Efficiency of Chemical Cleaning Liquid Waste Equipment

Kyung-Wook Shin, Jeong-Nam Jeong, Yun-Soon Jeong, Dae-Woo Lee, Gyung-Sun Chae, and Hee-Kon Jang
SAE-AN ENGINEERING CO., 184, Gasan digital 2-ro, Geumcheon-gu, Seoul, Republic of Korea
and9211@sae-an.co.kr

1. Introduction

Maintaining steam generator integrity for stable operation of nuclear power plants is a very important. Nuclear power plants are adhered to the secondary side of the steam generator in the form of sludge as the years of operation increase. The deposits typically consist of a mixture of metal oxides, primarily magnetite(Fe_3O_4), and copper(Cu and CuO). These deposits accumulate on the tube sheet, tube support plates and on the steam generator tube surfaces. The accumulation of corrosion products on heat transfer surfaces and within tubesheet and support regions has been linked with tube corrosion degradation and steam generator secondary side corrosion is an ongoing problem in nuclear power plants with pressurized water reactors. In addition, the accumulation of corrosion products within the support structure has led to severe blocking leading to water level control problems. Blocking and a loss of heat transfer due to tube deposits have led to inability to reach designed power output. As a method for removing such corrosion products, method such as lancing and chemical cleaning are used.

In this study, we have reviewed a method to improve the operation efficiency by improving chemical cleaning liquid waste treatment equipment for the disposal of liquid wastes generated by chemical cleaning.

2. Methodology

Chemical cleaning processes include EPRI SGOG(Electric Power Research Institute Steam Generator Owners Group) process, EdF(Electricite de France) process, and KWU(Kraftwerk Union) process and domestic nuclear power plants use the same process as Table 1.

Table 1. Domestic Chemical cleaning process

	EPEI SGOG process		AREVA process	
	[1)]ASCA	[2)]HTCC	[3)]DMT	HTCC
Chemical	EDTA 2%	EDTA 20%	Oxalic Acid 1%	EDTA 20%
Temperature	82℃	110~121℃	82~90℃	165℃
Cleaning Efficiency	Soft Sludge	Hard Sludge	Soft Sludge	Hard Sludge

2.1 Composition of Equipment Operation

The chemical cleaning waste liquid treatment equipment is designed to decompose the liquid waste containing EDTA generated at the secondary side of the steam generator into high temperature. The main component of the equipment is composed of pyrolysis furnace, an oxidation furnace, a catalytic device, a heat exchanger, and HEPA filter and the main function show.

- Pylolsis Furnace : Pyrolyzing the liquid waste containing EDTA and ammonia (800~1000℃).
- Oxidation Furnace : Oxidation of air pollutants such as NOx and CO (500~900℃).
- Catalytic Device : Converts air pollutants such as NOx and CO into dischargeable gases.
- Heat Exchanger : Device to lower the temperature of the exhaust gas as required.
- HEPA Filter : Removal of particulate matter contained in the exhaust gas

The pyrolysis furnace is an electric furnace with a heater at the top and bottom. The electric furnace bottom is composed of two bodies, two inner chambers and four baskets.

Fig. 1. Inner chamber and basket.

2.2 Problem of Equipment

The bottom of the electric furnace receives the chemical cleaning liquid waste from liquid waste tank and performs pyrolysis. The average operating temperature during pyrolysis is 850℃, and the maximum temperature rises up to 1000℃ and the operation time is about 10 hours. In this case, the problem that arises when the chemical cleaning liquid waste is treated at a high temperature is the deformation and corrosion of the basket made of carbon steel. These problems are caused by various causes, such as the chemicals in the chemical cleaning liquid waste, the operating temperature. And it decreases the soundness and thermal conductivity of the electric furnace heater and reduces the treatment efficiency of the chemical cleaning liquid waste.

Fig. 2. Basket deformation and corrosion.

In addition, 353㎥ of chemical cleaning waste were treated in nuclear power plants, and about 69 basket waste were generated by deformation and corrosion.

2.3 Improvement Plan

In order to prevent problems caused by basket corrosion during the treatment of chemical cleaning liquid waste at high temperature, the basket material was studied as stainless steel which is used at high temperature. Stainless steels are formed from oxides on the surface at high temperature only when they are frequently used at high temperature. The rate of growth of oxides depends on many metallurgical and environmental factors and properties of the oxides themselves. Stainless steel strength corrosion damage caused by high temperature gas is oxidation, which is the most common cause of high temperature corrosion, was examined. Oxidation resistance differs depending on the stability of the oxide, bonding properties, adhesion, etc. The reason why stainless steel has a strong resistance to oxidation is usually related to the formation of Cr_2O_3. In addition, chromium and nickel are the most influential factors influencing the composition more than the cystal structure of the alloy. The chromium content in the alloy must be sufficiently high for the Cr_2O_3 scale to remain stable and the chromium concentration must be high, such as 310 stainless steel, in order to have sufficient resistance in an oxidation environment near the maximum operating temperature of 1000℃. And nickel improves mechanical properties Cr_2O_3 scale and prevents diffusion of metal ions to enhance oxidation resistance and is suitable for environments that must withstand high temperatures and heat.

Table 2. Chemical composition of austenite stainless steel

ASIS	Chemical Composition (wt%)						
	Cr	Ni	C	Mn	S	P	Si
301	17	7	0.15	2	0.03	0.045	1
304	19	9	0.08	2	0.03	0.045	1
310	25	20.5	0.25	2	0.03	0.045	1

3. Conclusion

Oxidation resistance is also improvement in a high temperature oxidizing environment but high temperature mechanical properties of the material itself are also important variables. Since the strength of austenite stainless steel is generally higher than that of ferrite stainless steel at high temperature, austenite stainless steel was used as a base material. Stainless steel has weaknesses in terms of thermal conductivity and manufacturing cost compared to conventional basket material, but it has strengths in continuity of equipment operation, maintenance and waste reduction. The changes in the basket material will continue to be complemented by comparison with existing material at the planned chemical cleaning liquid waste disposal site.

REFERENCES

[1] EPRI “Utility Experience With Steam Generator Chemical Cleaning” TR-104553, 1-1, December 1994.

[2] KOREA HYDRO & NUCLEAR POWER “Steam Generator Management Program”, 16th Nuclear Safety Information Conference April 3-4, 2012.

[3] “The Oxidation Behavior of Sintered STS 316L at High-Temperature in the Air” Journal of Korean Powder Metallurgy Institute Vol.20 No.6 pp. 432-438.

Experience in Lancing Process of Steam Generator at PWR Nuclear Power Plants

Kyung-Wook Shin, Yoon-Ki Min, Young-Suk Choi, Tae-Hwa Kim, Gyung-Sun Chae, and Hee-Kon Jang
SAE-AN ENGINEERING CO., 184, Gasan digital 2-ro, Geumcheon-gu, Seoul, Republic of Korea
and9211@sae-an.co.kr

1. Introduction

Maintaining steam generator integrity for stable operation of nuclear power plants is a very important and spending a lot of money for maintenance and inspection of steam generator. In pressurized water reactor, the generation and transport of corrosion products in the feedwater, drain and condensate systems from deposits on the secondary side of the steam generator. The deposits have problems such as increasing the possibility of corrosion of the tube material and reducing the efficiency of heat transfer. Although it is the best way to prevent such deposits through water quality management, it is very difficult in reality. Therefore, chemical cleaning and mechanical cleaning are performed to remove deposits from the steam generator.

In this study, deposits and cleaning methods of steam generators and lancing processes performed at nuclear power plants are described.

2. Methodology

The steam generator deposits typically consist of a mixture of metal oxides, primarily magnetite (Fe3O4) and copper (Cu, CuO). According to the previous research report, deposits of the steam generator are as follows.

- Deposits contain >85% by weight magnetite.
- Deposits contain ~5% by weight metallic copper.
- Copper can account for as much as 50% by weight of the deposits in some PWR steam generators.
- Copper in deposits is generally found as copper metal, but minor amounts of Cu_2O and CuO have also been found.

There are chemical and mechanical methods for removing such sludge removal from steam generator.

2.1 Chemical Cleaning

The goal of chemical cleaning is to maximize the dissolution of deposits and simultaneously minimize the corrosion of steam generator materials. Chemical cleaning is different depending on each process. However, in case of EPRI method applied in domestic nuclear power plant, the temperature of ASCA is 82℃, EDTA is about 2%, the high temperature is 110~121℃, and EDTA is about 20%. In addition, a small amount of hydrazine reduces ferric ions which decrease corrosion of the base material and simultaneously dissolution of magnetite increase. And corrosion inhibitor in the solution doesn't have effect on the dissolution rate of the magnetite but decrease corrosion rate.

Although chemical cleaning is an effective technique if the steam generator needs to be completely cleaned, there are problems such as the cost of expensive cleaning, generation of undesired waste, and possibility of corrosion of the steam generator during chemical cleaning.

2.2 Mechanical Cleaning

Sludge removal from steam generators is typically uses mechanical cleaning including blowdown, gas pressure and lancing.

The blowdown method removes only sludge that exists as suspended particles and is ineffective at removing hardened sludge. This method is also used only for recirculating steam generators and uses a built-in drainage system in the steam generator.

The other mechanical cleaning processes, pressure pulse and water slap, periodically release pressurized nitrogen at the bottom of the tube bundle. The nitrogen produces upward movement of the water mass in the steam generator, thereby dislodging deposits from the tube surfaces and from the tube sheet and tube support plate regions.

Finally, lancing uses a high-pressure water jets to remove the sludge from the steam generator. This method can insert the water jet through the inspection port into the steam generator and remove the soft and some sticky sludge through high pressure jets.

2.3 Experience of Performing Lancing

At present, lancing of domestic nuclear power plant performs sludge removal the tube sheet top of the secondary side of the steam generator. The lancing equipment used in nuclear power plant depends on the steam generator type. The types are shown in Table 1.

Table 1. Types of Lancing Equipment by NPP

Type	NPP
FOLAS	Kori #2,#3,#4 Hanbit#1,#2
OLAS	ShinKori #1,#2,#3 Hanul #3,#4,#5,#6 Hanbit#3,#4,#5,#6 ShinWolsong #1,#2
CECIL-3	ShinWolsong #2,#3,#4
CECIL-4	Hanul #1,#2

Equipment used to remove deposits can be roughly classified into a robot system, control system, and process system. The schematic layout is shown in Fig. 1.

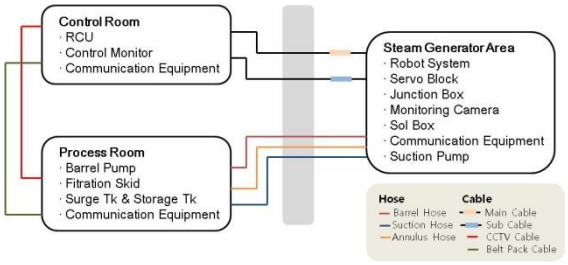

Fig. 1. Schematic of Lancing Equipment Configuration.

The robot system inserts the robot assembly through the steam generator handhold, attaches to the inner wall surface by magnetic force, and is driven and cleaned. The system performs the cleaning operation according to the input of the moving speed, the nozzle angle, the cleaning time, the number of the column to be moved, and the like through the operation program.

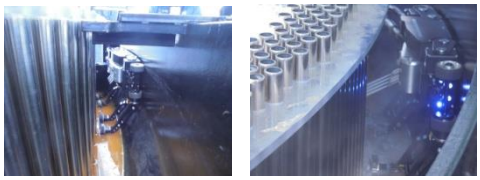

Fig. 2. Lancing Mock-up.

When the cleaning operation is performed, the cleaning waste liquid is collected by the sludge suction pump and the hose into the surge tank of the process room located in the maintenance area. The cleaning waste collected in the surge tank is collected in the storage tank after passing through the filtration system, and the sludge is removed from the filtration system, and then the cleaning operation is repeated while being supplied to the robot system. The weight of the sludge removed is the difference in filter weight generated during the cleaning operation at the initial filter weight and before the filter weight measurement; water is removed from the filter by air blowing for about 3 minutes. Lancing is preformed according to the conditions of the site, but generally, all columns are four times and terminated.

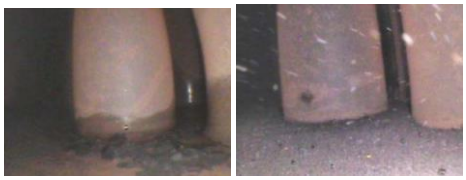

Fig. 3. Before and After performing Lancing.

3. Conclusion

The lancing process is one of important processes to secure the integrity and safety of the steam generator by removing the deposited sludge on the secondary tube sheet. Therefore, understanding of the process for the generation and removal of deposit and sludge in the steam generator is essential for the worker performing the cleaning process.

REFERENCES

[1] Mikko Vepsäläinen “Deposit formation in PWR steam generators” Research Report VTT-R-00135-10

[2] KOREA HYDRO & NUCLEAR POWER “Steam Generator Management Program”, 16th Nuclear Safety Information Conference April 3-4, 2012.

[3] IAEA “Assessment and management of ageing of major nuclear power plant components important to safety: Steam generators” IAEA-TECDOC-981, 1997

[4] SAE-AN ENDINEERING CORPORATION “(Temporarily)[SAE-AN ENDINEERING] Deposition of secondary side of steam generator” Maintenance Procedure HU06G- Temporarily-18-0002, 2018

Development of De-burring Machine in Hot Cell

Y.M. Jung*, G. S. Kim, Y.G. Jin, and G. S. Heo

Korea Atomic Energy Research Institute, 111, Daedeok-daero 989beon-gil, Yuseong-gu, Daejeon, Republic of Korea

*jym@kaeri.re.kr

1. Introduction

The IMEF(Irradiated Material Examinations Facility) has been conducting PIE(Post-Irradiation Examinations) on irradiated materials used in the HANARO research reactor and NPP reactors. The main goal of the facility is to support the PIE data and also the inventory report should be kept for the testing and stored materials in a hot cell. The M5 hot cell in IMEF have carried out many mechanical tests such as impact test, tensile test, and fracture toughness test for irradiated specimens. Prior to the mechanical test, the cutting of the specimens is required, which results in burrs. If these burrs are not removed, they can affect the results of mechanical test and accumulate in hot cell, increasing radiation level in hot cell. Eventually, workers are exposed to more radiation. Therefore, it was necessary to develop the equipment that can remove burrs efficiently and quickly for irradiated specimens.

2. Methods and Results

2.1 Principle

The media pin which has a magnetic material and the specimen are put in the working container, then the electron base under the working container is rotated. As a result, an electromagnetic force is generated in the working container, and the media pin is rotated to grind the specimen. Eventually, the burr on the surface of specimen is removed without change the dimension and shape.

2.2 Results

The de-burring machine is divided to four parts. A body of de-burring device including an electronic base, a control box which can control a setting pint, media pins to remove burr and a working container. At first, the de-burring machine didn't have remote control in the hot cell so we had carried out improving the remote control of the de-burring machine.

First, we set the wheels under the de-burring machine and made it possible to move in the hot cell freely (Fig. 1.). Device which can move freely can help to utilization of space in hot cell.

Second, handles were attached to both side for easy handling with a manipulator.

Third, the controller that was attached to the body of de-burring machine was removed and re-manufactured the new control box (Fig. 2.). All cable (power, communication) were extended by 8m to can be operated outside the hot cell (operating area).

Fourth, we made a working container (Fig. 3.). The existing container was made of plastic so it was not appropriate in the radiological environment. Therefore, the working container was re-manufactured using acrylic which has a radiation resistant relatively.

Fifth, we made a media pin and a collector of media pins (Fig. 4.). The diameter of pin is 0.7 mm and the length is 5 mm. And an apparatus was needed to apparatus to control the radioactive media pins by processing the irradiated materials. We made a collector using a syringe and magnet, this collector can easily collect only the media pins.

Fig. 1. De-burring machine.

Fig. 2. Control box.

Fig. 3. Working container.

Fig. 4. Media pin and a collector.

2.3 Application

Table 1. De-burring condition according to material

Material	Media pin (Φ)	Operating Speed (R.P.M)	Operating time (Min)
Aluminum	0.2 ~ 0.7	600 ~ 1,200	3 ~ 10
Copper, Brass Beryllium	0.2 ~ 0.5	600 ~ 1,300	3 ~ 10
Stainless steel, Titanium	0.2 ~ 1.2	700 ~ 1,300	3 ~ 10
Zinc, Nickel, Chrome steel	0.3 ~ 1.0	600 ~ 1,400	2 ~ 8

Table 2. Operating conditions for de-burring machine.

	Operating conditions	Remarks
Media pin (g)	300	- Depends on type, size, and weight of specimen. - No bunching and sticking of pins. - The height is 0.5~1 cm from the bottom of the working container.
Operating time (Min)	5 ~ 10	- Depends on the size and condition of the initial burr. - Depends on removal amount of the burr and the purpose.
Operating speed (R.P.M)	1,000 ~ 1,500	- The media pin and the specimen rotate together until they are vortex. - Evenly rotate - Depends on the size of specimen

The de-burring machine is suitable for removing the burrs of fine holes, inner corner and small sized specimen. Even after the work, the quality is homogeneous and there is no dimensional change and shape deformation. De-burring machine is capable of dry operation and it can minimize the generation of radioactive waste because there is a wastewater. In addition, the operating time is very short (3~10 min), easy to use and can be operated by even unskilled operator.

Most of specimens to be de-burred in M5 cell are expected to be Zircaloy cladding and PTS tube. The standard operating conditions are shown in Table 2.

4. Conclusion

De-burring machine was introduced to remove the burr of irradiated materials in a hot cell. The burrs of irradiated specimens were successfully removed and result is shown in Fig. 5.

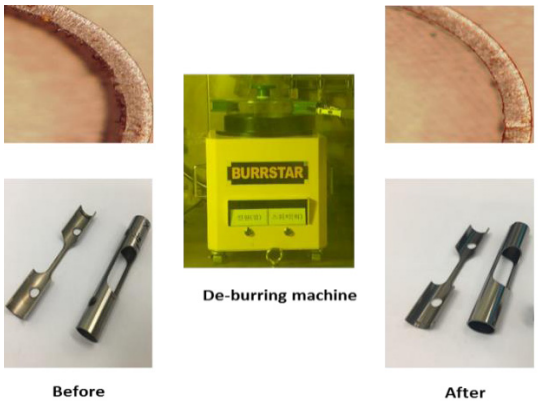

Fig. 5. Comparison between before and after de-burring.

REFERENCES

[1] Peter Sachnik, Sheikh Enamul Hoque, Wolfram Volk, Burr-free cutting edges by notch-shear cutting, Journal of Materials Processing Tech. 249(2017), p.229-245

Comparison of Atmospheric Dispersion Factors Using Different Approaches in Decommission of a Nuclear Power Plant

Seung-hee Lee[1], Won-tae Hwang[2], and Chang-Lak Kim[1]

[1] KEPCO International Nuclear Graduate School, 658-91, Haemaji-ro, Seosaeng-myeon, Ulju-gun, Ulsan, Republic of Korea

[2] Korea Atomic Energy Research Institute, 111, Daedeok-daero 989beon-gil, Yuseong-gu, Daejeon, Republic of Korea

1. Introduction

Decommissioning is a critical issue in Korean nuclear power plant industry. During decommissioning, radioactive materials will be released to the environment, and will affect radiological dose to nearby residents via various pathways. To evaluate off-site radiological dose, the prediction of atmospheric dispersion is required as the first step.

Generally, atmospheric dispersion is predicted under the recommendation of the NRC's Regulatory Guide 1.111 [1] in routine releases of gaseous radioactive materials. This approach would be produced conservative results. It can be applied to protect health detriment during decommissioning process. However, the realistic estimation may be necessary to avoid overestimating results for the optimal decommissioning strategy. In this study, comparison of atmospheric dispersion factors using different approaches in decommission of a nuclear power plant was performed.

2. Comparison of Atmospheric Dispersion

2.1 Calculation of Atmospheric Dispersion Factor

A computer code XOQDOQ [2] has been developed to evaluate atmospheric dispersion in a routine release of radioactive effluents according to methodology recommended in the U.S. NRC's Regulatory Guide 1.111

A straight-line Gaussian plume model has been adopted to calculate annual averaged atmospheric dispersion factor (χ/Q, sec/m^3), which represents a dispersion capability of radioactive effluents released into the environment.

2.2 Meteorological Data Analysis

Joint Frequency Distribution (JFD) is a statistical data representing occurrence probability as function of wind speed and wind direction according to atmospheric stability. It was obtained using measured data at 10m height of a meteorological tower of Kori nuclear power plant site for 3years from 2008 to 2010, as shown in Fig. 1.

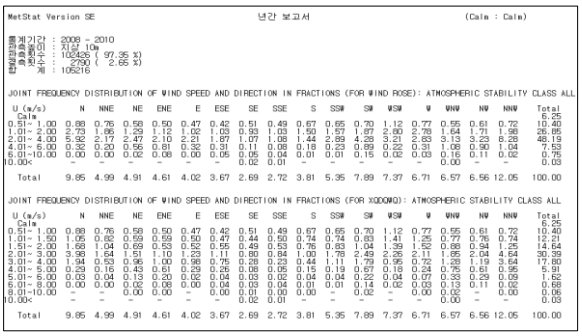

MetStat Version SE 년간 보고서 (Calm : Calm)

계기간 : 2008 ~ 2010
측풍계위 : 지상 10m
측풍유효 : 102426 (97.35 %)
측풍누수 : 2790 (2.65 %)
전체개수 : 105216

JOINT FREQUENCY DISTRIBUTION OF WIND SPEED AND DIRECTION IN FRACTIONS (FOR WIND ROSE): ATMOSPHERIC STABILITY CLASS ALL

U (m/s)	N	NNE	NE	ENE	E	ESE	SE	SSE	S	SSW	SW	WSW	W	WNW	NW	NNW	Total
Calm																	6.25
0.51~ 1.00	0.88	0.76	0.58	0.50	0.47	0.42	0.51	0.49	0.67	0.65	0.70	1.12	0.77	0.55	0.61	0.72	10.40
1.01~ 2.00	2.73	1.86	1.29	1.12	1.02	1.09	0.93	1.03	1.50	1.57	1.97	2.80	2.28	1.64	1.71	1.98	26.85
2.01~ 4.00	5.92	2.17	2.47	2.10	2.21	1.97	1.07	1.08	1.44	2.89	4.28	3.21	2.83	3.13	3.23	5.28	48.19
4.01~ 6.00	0.32	0.20	0.55	0.61	0.32	0.31	0.11	0.08	0.18	0.23	0.89	0.22	0.31	1.08	0.90	1.04	7.53
6.01~10.00	0.00	0.00	0.02	0.08	0.00	0.06	0.05	0.04	0.01	0.01	0.15	0.02	0.03	0.16	0.11	0.02	0.76
10.00<	-	-	-	-	-	-	0.02	0.01	-	-	-	-	-	0.00	-	-	0.03
Total	9.85	4.99	4.91	4.61	4.02	3.67	2.69	2.72	3.81	5.35	7.99	7.37	6.71	6.57	6.56	12.05	100.00

JOINT FREQUENCY DISTRIBUTION OF WIND SPEED AND DIRECTION IN FRACTIONS (FOR XOQDOQ): ATMOSPHERIC STABILITY CLASS ALL

U (m/s)	N	NNE	NE	ENE	E	ESE	SE	SSE	S	SSW	SW	WSW	W	WNW	NW	NNW	Total
Calm																	6.25
0.51~ 1.00	0.88	0.76	0.58	0.50	0.47	0.42	0.51	0.49	0.67	0.65	0.70	1.12	0.77	0.55	0.61	0.72	10.40
1.01~ 1.50	1.05	0.82	0.59	0.59	0.50	0.47	0.44	0.50	0.74	0.74	0.83	1.41	1.25	0.77	0.76	0.74	12.21
1.51~ 2.00	1.68	1.04	0.69	0.53	0.52	0.55	0.49	0.53	0.76	0.83	1.04	1.39	1.52	0.88	0.94	1.25	14.64
2.01~ 3.00	3.98	1.64	1.51	1.10	1.23	1.11	0.80	0.84	1.00	1.78	2.49	2.26	2.11	1.85	2.04	4.64	30.39
3.01~ 4.00	1.94	0.53	0.96	1.00	0.98	0.75	0.28	0.23	0.44	1.11	1.79	0.95	0.72	1.28	1.19	3.64	17.80
4.01~ 5.00	0.29	0.16	0.43	0.61	0.29	0.26	0.08	0.05	0.15	0.19	0.57	0.18	0.24	0.95	0.61	0.95	5.91
5.01~ 6.00	0.03	0.04	0.13	0.20	0.02	0.04	0.03	0.02	0.04	0.04	0.22	0.04	0.07	0.33	0.29	0.09	1.52
6.01~ 8.00	0.00	0.00	0.02	0.08	0.00	0.04	0.03	0.04	0.01	0.01	0.14	0.02	0.03	0.13	0.11	0.02	0.68
8.01~10.00	-	-	0.00	0.00	-	0.00	0.01	0.00	-	-	0.02	-	0.00	0.02	-	0.00	0.06
10.00<	-	-	-	-	-	-	0.02	0.01	-	-	-	-	-	0.00	-	-	0.03
Total	9.85	4.99	4.91	4.61	4.02	3.67	2.69	2.72	3.81	5.35	7.99	7.37	6.71	6.57	6.56	12.05	100.00

Fig. 1. Joint Frequency Distribution Data at Kori Site.

2.3 Comparison Between Different Approaches

The evaluation locations are 16 overall directions of Exclusion Area Boundary (EAB). In the conservative approach, the atmospheric stability classes are 7 (A-G), and effect of recirculation and stagnation is considered, while in the realistic approach, the atmospheric stability classes are 6 (A-F), and effect of recirculation and stagnation is not considered.

Table 1. Major items between conservative and realistic approaches

Items	Conservative approach	Realistic approach
Atmospheric stability class	7 classes (A-G)	6 classes(A-F)
Recirculation and Stagnation	Considered	Not considered

Table 2. Results between the conservative and realistic approaches

	Conservative(C) (χ/Q, sec/m^3)	Realistic(R) (χ/Q, sec/m^3)	Ratio (C / R)
S	4.499×10^{-5}	1.099×10^{-5}	4.09
SSW	2.789×10^{-5}	6.877×10^{-6}	4.06
SW	2.190×10^{-5}	5.370×10^{-6}	4.08
WSW	1.722×10^{-5}	4.168×10^{-6}	4.13
W	1.941×10^{-5}	4.534×10^{-6}	4.28
WNW	1.903×10^{-5}	4.534×10^{-6}	4.19
NW	1.959×10^{-5}	4.724×10^{-6}	4.15
NNW	1.841×10^{-5}	4.424×10^{-6}	4.16
N	2.393×10^{-5}	5.589×10^{-6}	4.28
NNE	3.289×10^{-5}	7.450×10^{-6}	4.41
NE	3.793×10^{-5}	9.066×10^{-6}	4.18
ENE	4.563×10^{-5}	1.110×10^{-5}	4.11
E	3.325×10^{-5}	8.215×10^{-6}	4.04
ESE	2.641×10^{-5}	6.541×10^{-6}	4.04
SE	3.226×10^{-5}	7.908×10^{-6}	4.08
SSE	4.333×10^{-5}	1.065×10^{-5}	4.07

The results of the atmospheric dispersion factor using conservative approach were predicted about 4 times higher than those using realistic approach for every 16 overall directions.

Additionally, we evaluated the atmospheric dispersion factor for the distance of 3 inland directions (N, NNE, NE) at the site boundary using conservative approach.

Table 3. The distance of 3 directions at the site boundary

Direction	N	NNE	NE
Distance(m)	1200	2550	3350
Atmospheric Dispersion Factor (χ/Q, sec/m^3)	9.137×10^{-6}	1.991×10^{-6}	1.257×10^{-6}

Table 4. Comparison of maximum Atmospheric Dispersion Factor at EAB and Site boundary

	EAB (E)	Site Boundary (S)	Ratio (E / S)
Max. Atmospheric Dispersion Factor (χ/Q, sec/m^3)	4.499×10^{-5} (Direction: S)	9.137×10^{-6} (Direction: N)	4.92

3. Conclusions

According to the conservative and realistic approaches, we compared the results of the atmospheric dispersion factors using XOQDOQ code. It was shown that there were a great difference between the conservative and realistic approaches. And the results were also depends on the location of the estimation.

It is desirable to evaluate the dose by the radioactive effluents released into the environment separately according to the purpose.

ACKNOWLEDGEMENT

This research was supported by the Nuclear Safety Research Program through the Korea Foundation resource from the Nuclear Safety and Security Commission (NSSC), Republic of Korea (No. 1605008).

REFERENCES

[1] U. S. NRC, Methods for Estimating Atmospheric Transfer and Dispersion of Gaseous Effluents in Routine Releases from Light Water Cooled Reactors, Regulatory Guide 1.111, 1977

[2] U. S. NRC, XOQDOQ: Computer Program for the Meteorological Evaluation of Routine Release at Nuclear Power Stations, NUREG/CR-2919, 1982

Radioactive Waste Management System of ARTI

Hyun-Jin Lee[1,2,*], Chong-Yeal Kim[2], Jin-Woo Lee[1], Gyo-Seong Jeong[1,2], and Sang-Bong Lee[1,2]
[1]Advanced Radiation Technology Institute, Korea Atomic Energy Research Institute, 29, Geumgu-gil, Jeongeup-si, Jeollabuk-do, Republic of Korea
[2] Chonbuk National University, 567 Baekje-daero, Deokjin-Gu, Jeonju, Jeollabuk-Do, Republic of Korea
[*]hyunjinlee@kaeri.re.kr

1. Introduction

Generating radioactive waste is inevitable in use and production facility of unsealed radionuclides. Therefore, licensee should establish waste minimization strategy prior to use, the wastes generated during use should be managed thoroughly with proper management system to prevent hazards from them and finally contribute workers safety. So in this paper, waste management system is proposed based on the ARTI system and we are going to draw improvement on system.

2. Management system

2.1 Facility Centralization

If there are multiple unsealed radioisotope use or production facilities within the boundary of the business establishment, it is hard to manage radioactive waste properly with limited manpower. Therefore, more efficient waste management can be achieved by concentrating the use and production facilities in a certain building or zone. ARTI has centralized total 23 unsealed radioisotope use and production facilities in RI-Biomics and Cyclotron Research center so as to focus on management.

2.2 Radioactive Waste Storage Facility Control

Radioactive waste storage facility should be accessible only by authorized person otherwise unauthorized disposal or store of unrecognized waste could be happen. To prevent this, installation of locked device and CCTV at the entrance of waste storage facility is preferred. In addition, there is a need for the way to check integrity of stored waste. To do this, ARTI has installed gamma detectors inside of a storage facility to monitor dose rate continuously. Periodic physical check also has been conducting to verify its integrity.

2.3 Carry In/out Items Monitoring

Since the items used in the RCA (Radiation Controlled Area) are potential radioactive waste, it's important to minimize the amount of material entering the RCA. So every item should be unpacked before carrying in to the RCA unless packing is essential. There is also a need for measures for monitor unauthorized release of waste from the RCA. For this purpose, ARTI has installed portal monitors which have large plastic scintillation detectors at all exit door from the RCA.

2.4 Radioactive Waste Inventory

Waste inventory should be carried out to verify the quantity and location by nuclide, type and occurrence date. This provides a means to confirm whether waste is discarded without authorization and to be used basic data for final disposal of waste.

2.5 Waste Management Process

Waste generated in ARTI is managed through the procedure shown in Fig. 1.

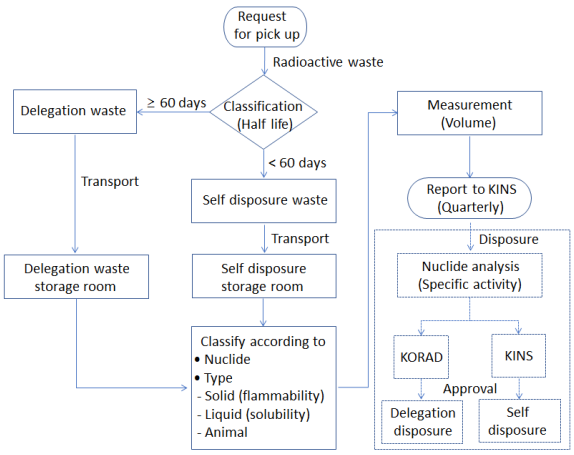

Fig. 1. Waste management flow.

3. Discussion

3.1 Waste Management System Computerization

Waste management is performed based on handwriting which has possibility of data omission or manipulation. Therefore, it's necessary to consider adopting a system for providing bar codes to each unit waste and managing them by computerization to secure waste management reliability.

3.2 Waste Quantification

Licensee should reports to the KINS the amount of radioactive waste periodically and volumetric unit is using for quantification. But using volumetric unit can causes difference between actual holdings and reported amount especially for non-flammable waste. Therefore, it is necessary to consider introducing the weight unit (kg) to present the amount of waste at least for some situations.

4. Conclusion

The waste management system of ARTI that is presented in this paper will be optimized continuously through vulnerability assessment of the system. In addition, radioactive waste generated in ARTI will be managed more thoroughly through the system improvement such as introducing computerization system.

REFERENCES

[1] Korea Act No.15749, Nuclear Safety Act.

[2] Korea NSSC Notice 2017-65, Regulation for radioactive waste classification and criteria for self-disposal.

Human Exposure to High Natural Background Radiation in Bangladesh

Gazi Muhammad Borhan Uddin and Juyoul Kim*
KEPCO International Nuclear Graduate School, 658-91, Haemaji-ro, Seosaeng-myeon, Ulju-gun, Ulsan, Republic of Korea
*jykim@kings.ac.kr

1. Introduction

Natural radioactivity is widely found in soil, sand, water, air, rocks and plants of the environment. According to UNSCEAR (1993), about 87% of the radiation dose received by mankind is due to natural radiation sources and the remaining is due to anthropogenic radiation [1]. It is observed that most of natural radioactive elements present in soil are primordial radionuclides from the uranium series, thorium series, and ^{40}K [2]. There are few sea beach in the world such as Brazil, China, India, Iran and France where the background radiation levels were found very high, varying over an order of magnitude depending upon the site-specific terrestrial radioactivity. Following that, this study was carried out to find out the effect of radiation to the people and environment in the Kuakata Sea beach which is located at Patuakhali district in Bangladesh.

Fig. 1. Kuakata sea beach in Bangladesh.

Assessment of any release of radioactivity to the environment is important for the protection of public health; especially if the released radioactivity is a matter of direct population exposure and can enter into the food chain. The RESRAD family of codes is developed at Argonne National Laboratory for estimating radiation doses and cancer risks to an individual located on top of radioactively contaminated soils. RESRAD-ONSITE code was used to assess radiation exposures of a human receptor located on top of soils contaminated with radioactive materials [4]. The study was carried out for the people who are working in the sea beach, living in the sea beach.

2. Methods

Kuakata Sea beach is the area of interest in the present study, which is located at 65 kilometers away from Patuakhali district is one of the attractive tourist place in Bangladesh. A simulation was conducted earlier using a high resolution high purity germanium detector of relative efficiency 40% where the activity concentrations of ^{226}Ra, ^{232}Th and ^{40}K were found in the soil samples were found 20.98±3.96 to 42.92±4.76 Bq/Kg, 59.25±15.62 to 144.34±18.52 Bq/Kg and 570.43±100.3 to 1165±166.27 Bq/Kg respectively [3].

Table 1. Soil samples of this study

Name of the Nuclide	Activity (Bq/kg)
^{226}Ra	23
^{232}Th	80
^{40}K	700

Different pathways such as Inhalation, Aquatic foods and Soil ingestion were considering for this study. Using above radio nuclides and their corresponding activities in the RESRAD-ONSITE Code the following outputs were found.

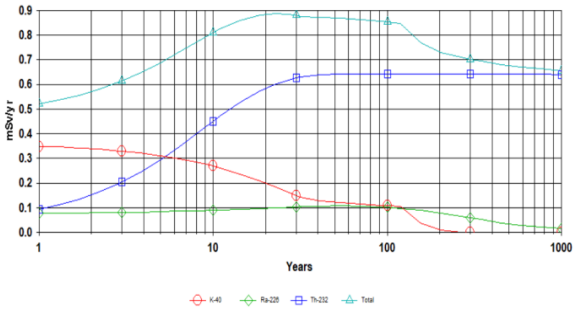

Fig. 2. Dose: all nuclide summed, all pathways summed.

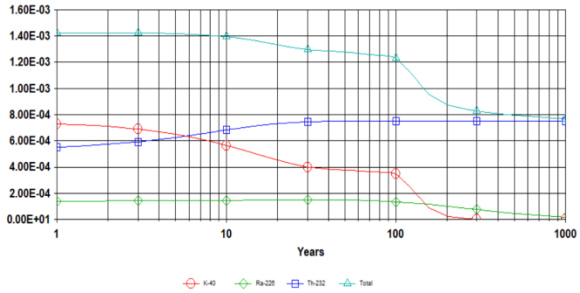

Fig. 3. Cancer risk assessment for all pathways.

3. Results

After the simulation it is shown that the total effective dose was increasing with time until 30 years, after 30 years it is decreasing. The maximum effective dose for all pathways was 0.888 mSv at 23 years. The cancer risk assessment for all pathways was 1.40E-03 after 1 year and it is saturated until 10 years. After 10 years' cancer risk assessment is decreasing with increasing time. So, Cancer risk in the Kuakata sea beach area is very low.

Table 2. Individual dose and total dose with time

Time (year)	Name of the nuclide (mSv/year)			Total Dose (mSv/year)
	^{40}K	^{226}Ra	^{232}Th	
0	0.359	0.077	0.033	0.469
1	0.349	0.078	0.094	0.522
3	0.329	0.081	0.204	0.615
10	0.269	0.090	0.451	0.810
30	0.150	0.104	0.626	0.880
100	1.080	0.102	0.642	0.852
300	0.000	0.059	0.642	0.702
1000	0.000	0.015	0.641	0.656

4. Conclusion

For assessing radiation exposures of a human receptor located on top of the contaminated soils with radioactive materials RESRAD-ONSITE code was used. In the Kuakata sea beach the mainly dominating nuclide particle is ^{40}K for certain time, then ^{232}Th is dominated. The effect of ^{226}Ra nuclide is not significant. Finally, it can be concluded that the Kuakata Sea Beach is not harmful for fisherman, as well as for tourist.

ACKNOWLEDGEMENT

This research was supported by 2019 Research Fund of the KEPCO International Nuclear Graduate School (KINGS), Republic of Korea.

REFERENCES

[1] V. Kannana, M. P. Rajana, M. A. R. Iyengara and R. Rameshb, "Distribution of Natural and Anthropogenic Radionuclides in Soil and Beach Sand Samples of Kalpak-kam (India) Using Hyper Pure Germanium (HPGe) Gam- ma Ray Spectrometry," Applied Radiation and Isotopes, Vol. 57, No. 1, pp. 109-119 (2002).

[2] S. U. El-Kameesy, S. Abd El-Ghany, S. M. El-Minyawi, Z. Miligy and E. M. El-Mabrouk, "Natural Radioactivity of Beach Sand Samples in the Tripoli Region, Northwest Libya," Turkish Journal of Engineering & Environmental Science, Vol. 32, No. 1, pp. 245-251 (2008).

[3] K M Nazrul Islam, Debasish Paul, Md. Mahbubur Rahman Bhuiyan, Amina Akter, Budrun Neher, S M Azharul Islam, "Study of Environmental Radiation on Sand and Soil Samples from Kuakata Sea Beach of Patuakhali", Journal of Environmental Protection, Vol. 3, pp. 1078-1084 (2012).

[4] RESRAD Codes, http://resrad.evs.anl.gov/

Assessment of Annual Indoor Effective Dose Around Mrima Area in Kenya

Tarus Kiplabat and Juyoul Kim*

KEPCO International Nuclear Graduate School, 658-91, Haemaji-ro, Seosaeng-myeon, Ulju-gun, Ulsan, Republic of Korea

*jykim@kings.ac.kr

1. Introduction

Several areas of the world show anomalies in the concentrations of Naturally Occurring Radioactive Materials (NORMs). The Mrima area in coastal Kenya has been extensively studied for its high concentration of NORMs [1]. The impact of constructing houses from materials derived from such an environment has however not been fully studied. RESRAD-BUILD is a computer code designed for analysing radiation exposures resulting from occupying buildings contaminated with radioactive materials. Modelling takes into consideration the number and type of contaminated rooms, type and of radionuclides, the receptors, nature of construction material, geometry of source, shielding between source and receptor, and room use. It also offers analysis of exposure pathways (ingestion, inhalation, radon, and external gamma exposure) and the layer thickness of walls [2]. Three NORMs are considered; K-40, U-238, and Th-232.

2. Methodology

In this study, assumptions are made on the nature of construction material in Mrima. The majority of people dwell in all-mud floor and wall houses, derived from the same area. The roof is grass/reed thatched. A typical room is rectangular with one door and one window. Subsistence farming is the main activity for the locals during the day.

Table 1. Radionuclides, activity concentrations and half-lives considered for RESRAD- BUILD [3]

Nuclide	Activity (mBq g^{-1})	Half-life ($\times 10^9$) years
K – 40	600	1.251
U – 238	325	4.5
Th – 232	1815	14.05

The activity concentration is relatively high for K–40 and U– 238. Th– 232 has higher activity concentration. These figures are conservative for radiation protection purposes. The time fraction spent indoors was set to 0.5 for 365 days. Evaluation time intervals was set to 1, 2, 5, 10, 25, and 50 years. One room was considered with an area of 25 m^2 and a height of 2 meters. Deposition velocity of 0.01 m/s was also considered. Other parameters are summarized in the table below [4].

Table 2. Other relevant parameters set

Parameter	Value/Unit
Receptors	1 person (adult)
Breathing Rate	18 m^3 d^{-1}
Height receptor	1.6 meters
Thickness of walls	20 Centimetres
Density of walls	1.5 g cm^{-3}
Porosity	0.1

3. Results

Simulations of annual effective dose and cancer risk were performed in this study. Fig. 1 shows the dose contribution per exposure pathway; Radon, inhalation, external exposure, deposition, immersion and ingestion for a recipient in the room were generated. A summary of dose contribution per radionuclide is shown in fig. 2.

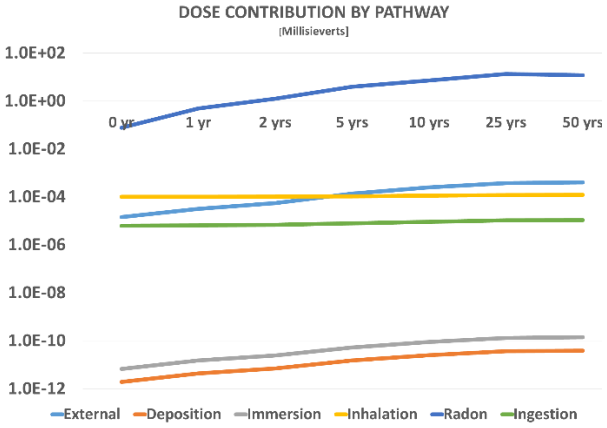

Fig. 1. Dose contribution by pathway.

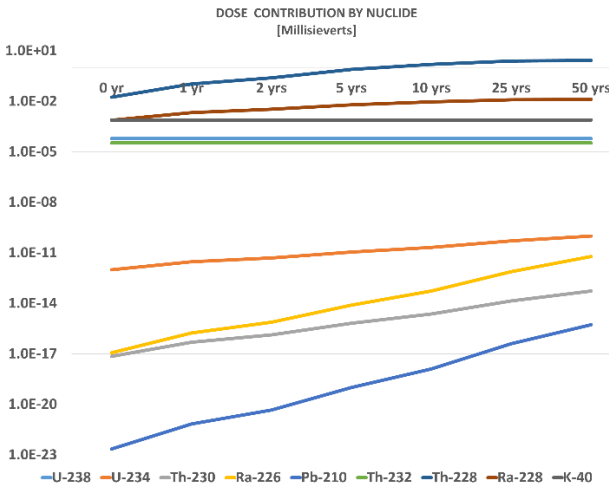

Fig. 2. Dose contribution by radionuclides.

4. Conclusion

The annual effective dose and cancer risk received by dwellers in Mrima was simulated using RESRAD-BUILD computer code. The results show that the dose rates through all pathways increased from 76 μSv/yr to a maximum of 13.4 mSv/yr in the first 25 years. According to Fig. 1, it was observed that Radon contributed the highest dose overall compared to other pathways. In addition, Fig. 2 shows that Thorium-228 contributed the highest fraction to the annual dose. The calculated cancer risk associated with inhalation of Radon at 25 years is 5.82E-06. This is below the recommended UNSCEAR cancer risk factor of 5E-05 per mSv [5]. This study concludes that there is no risk of cancer to the residents of Mrima.

REFERENCES

[1] J. Patel, “Environmental radiation survey of the area of high natural radioactivity of Mrima hill of Kenya”, Discovery and Innovation, 3(3): 31-35, (1991).

[2] C. Yu., “User’s Manual for RESRAD-BUILD Version 3”, (2003)

[3] M. Kaniu, “Rapid in-situ radiometric assessment of the Mrima-Kiruku high background radiation anomaly complex of Kenya”, Journal of Environmental Radioactivity, (2017).

[4] M. Festus, “Factors affecting use of Appropriate Building Materials and Technologies in Kenya”, University of Nairobi erepository, (2016).

[5] UNSCEAR, “United Nations Scientific Committee on the Effects of Atomic Radiation”, Report to the General Assembly, (2000).

Derivation and Comparison of Preliminary Derivation Concentration Guideline Level (DCGL) According to Scenarios of Kori Unit 1 Using RESRAD-BUILD

SangJune Park*, Jihyang Byon, and Seokyoung Ahn
Pusan National University, 2, Busandaehak-ro 63beon-gil, Geumjeong-gu, Busan, Republic of Korea
*xelidake2@pusan.ac.kr

1. Introduction

This study provides a method of calculating a Kori Unit 1 preliminary DCGLs by using RERAD-BUILD code and, for radionuclides on the surface of buildings. Additionally, this study provides a method for calculating the exposure dose to receptors such that it satisfied the site release criteria of South Korea.

2. RESRAD-BUILD Code Description

The RESRAD-BUILD code is an exposure path analysis code for assessing the potential exposure dose of an individual or worker in a building contaminated with residual radioactive material. In the RESRAD-BUILD code, radioactive particulates in the air, aerosol indoor radon decay products, and tritium water vapor, including external exposure to penetration radiation, due to the air submersion of the radioactive material and radioactive particulates that have accumulated at the source, are considered. Additionally, consideration is given to the intake and ingestion pathways of materials emitted from the source and to materials that have accumulated on the building surface. The Fig. 1 shows exposure pathway of RESRAD-BUILD

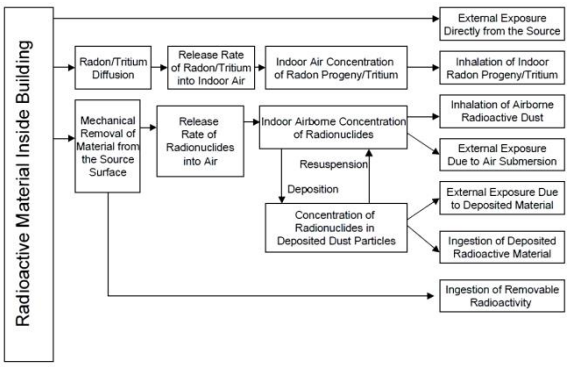

Fig. 1. Exposure pathway considered in RESRAD-BUILD [1].

RESRAD-BUILD allows the conduct of probabilistic analysis by the input of various parameters. The deterministic analysis derives a single output dose value according to the each single input parameters, while the probabilistic analysis uses the probability distribution of the input parameters to derive various output values. The Fig 2 shows difference of deterministic analysis and probabilistic analysis.

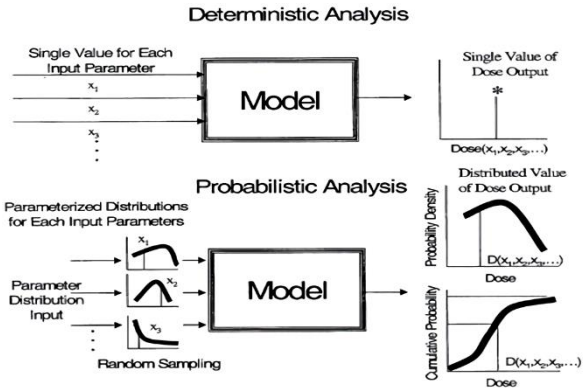

Fig. 2. Difference of deterministic analysis and probabilistic analysis [1].

3. Input Values for RESRAD-BUILD

The dose/risk library used in this study was ICRP 60. This library contains the latest data and is suitable to industrial workers. In this scenario, the ceilings were not considered because their contamination was assumed to be negligible.

The Indoor fraction was 97.4 $d \cdot yr^{-1}$ which based on the occupancy scenario in NUREG/CR-5512, Vol. 3 [2]. The direct ingestion rate is 0.88×10^{-6} $1 \bullet h^{-1}$ that was 1.1×10^{-4} $m^2 \bullet h^{-1}$ divided by the total contaminated area of 124.8 m^2. When entering a deterministic value, for which a probability distribution is developed, the most conservative dose is derived using the mean, median, or most likely value (for the triangular distribution) in the parameter distribution. Therefore, the area of Source 1 is the most likely value of triangular distribution, section A.1.3 Room area of NUREG/CR-6755. The area of source 2, 3, 4, 5 is calculated by multiplying the square root of 36 which is the most likely value of triangular distribution, NUREG/CR-6755 section A.1.3 Room Area and 3.7 that is most likely value of triangular distribution, NUREG/CR-6755 section A.1.4 Room Height [3].

With regard to the area and height of the room, the room size was set to the median value of the distribution in the RESRAD-BUILD code (based on NUREG/CR-5512, Vol. 1 [4]) and fixed at an area of 64 m^2 and height of 3 m. We assumed that the variation of the structure was large; therefore, we input it as a distribution.

The radionuclides for calculating DCGL were selected from the radionuclides detected both at the Zion NPP and Rancho Seco NPP, which was selected as a reference NPP. Table 1 shows the radionuclides used in this study.

Table 1. Radionuclides detected in Rancho Seco and Zion NPP buildings [5, 6]

Radionuclide			
^{3}H	^{90}Sr	^{137}Cs	^{239}Pu
^{14}C	^{94}Nb	^{152}Eu	^{240}Pu
^{55}Fe	^{99}Tc	^{154}Eu	^{241}Pu
^{59}Ni	^{108m}Ag	^{155}Eu	^{241}Am
^{60}Co	^{125}Sb	^{237}Np	^{244}Cm
^{63}Ni	^{134}Cs	^{238}Pu	

4. DCGL Calculation

To derive the DCGL, it was assumed that there was a large variation in the size of the indoor structure that will be left on the Kori Unit 1 site. Additionally, the assigned value of the room height and room area were selected and calculated conservatively. With regard to the deposition rate, receptor breathing rate, and source life, the value was assigned in order to provide consistency during the calculation process.

Table **2**. DCGL according to scenario (dpm/100cm^2)

Radio-nuclides	0.1 mSv/yr	Radio-nuclides	0.1 mSv/yr
^{3}H	1.33×10^{8}	^{137}Cs	2.26×10^{4}
^{14}C	3.64×10^{6}	^{152}Eu	1.31×10^{4}
^{55}Fe	1.39×10^{7}	^{154}Eu	1.20×10^{4}
^{59}Ni	3.18×10^{7}	^{155}Eu	2.28×10^{5}
^{60}Co	6.17×10^{3}	^{237}Np	1.17×10^{3}
^{63}Ni	1.32×10^{7}	^{238}Pu	1.67×10^{3}
^{90}Sr	3.72×10^{4}	^{239}Pu	1.49×10^{3}
^{94}Nb	9.52×10^{3}	^{240}Pu	1.49×10^{3}
^{99}Tc	5.32×10^{6}	^{241}Pu	8.06×10^{4}
^{108m}Ag	9.09×10^{3}	^{241}Am	1.46×10^{3}
^{125}Sb	3.34×10^{4}	^{244}Cm	2.41×10^{3}
^{134}Cs	9.00×10^{3}		

The scenario 1 is on-site building worker scenario and scenario 2 is containment building worker scenario.

Table 3. Comparison of DCGLs (dpm/100cm^2)

Radio-nuclides	Scenario1	Scenario2	Radio-nuclides	Scenario1	Scenario2
^{3}H	1.33×10^{8}	1.70×10^{8}	^{137}Cs	2.26×10^{4}	2.18×10^{3}
^{14}C	3.64×10^{6}	8.13×10^{5}	^{152}Eu	1.31×10^{4}	1.49×10^{3}
^{55}Fe	1.39×10^{7}	7.84×10^{7}	^{154}Eu	1.20×10^{4}	1.87×10^{3}
^{59}Ni	3.18×10^{7}	8.06×10^{6}	^{155}Eu	2.28×10^{5}	6.77×10^{6}
^{60}Co	6.17×10^{3}	1.65×10^{3}	^{237}Np	1.17×10^{3}	3.67×10^{2}
^{63}Ni	1.32×10^{7}	3.22×10^{6}	^{238}Pu	1.67×10^{3}	5.79×10^{2}
^{90}Sr	3.72×10^{4}	1.45×10^{4}	^{239}Pu	1.49×10^{3}	4.70×10^{2}
^{94}Nb	9.52×10^{3}	5.55×10^{2}	^{240}Pu	1.49×10^{3}	4.73×10^{2}
^{99}Tc	5.32×10^{6}	1.16×10^{6}	^{241}Pu	8.06×10^{4}	1.80×10^{4}
^{108m}Ag	9.09×10^{3}	6.72×10^{2}	^{241}Am	1.46×10^{3}	4.67×10^{2}
^{125}Sb	3.34×10^{4}	7.27×10^{4}	^{244}Cm	2.41×10^{3}	1.35×10^{3}
^{134}Cs	9.00×10^{3}	4.62×10^{4}			

5. Conclusion

In this study, DCGL is derived through the probabilistic analysis of the RESRAD-BUILD code. Deterministic and probabilistic parameters that reflect the characteristics of Kori Unit 1 are applied then sensitivity analysis are performed for the scenario. Through this process, we derived the Kori Unit 1 preliminary DCGL.

The DCGL of Containment building worker scenario (scenario 2) is lower than on-site building worker scenario (scenario 1) except ^{134}Cs, ^{155}Eu.

Scenario 2 shows a lower DCGL than scenario 1 because of receptor location, source location, source area and other parameter difference. Additional research is needed to determine why the DCGL values of ^{134}Cs and ^{155}Eu are higher.

REFERENCES

[1] C. Yu, D.J. LePoire, J.J. Cheng, E. Gnanapragasam, S. Kamboj, J. Arnish, B.M. Biwer, A.J, Zielen, W.A. Williams, A. Wallo Ⅲ, H.T. Peterson, Jr, "User's Manual for RESRAD-BUILD Version3", Argonne National Laboratory (2003).

[2] U.S. Nuclear Regulatory Commission (NRC), NUREG/CR-5512, Vol.3, "Residual Radioactive Contamination from Decommissioning-Parameter Analysis", Sandia National Laboratories (1999).

[3] U.S. Nuclear Regulatory Commission (NRC), NUREG/CR-6755, "Technical Basis for Calculating Radiation Doses for the Building Occupancy Scenario Using the Probabilistic RESRAD-BUILD 3.0 Code", ANL/EAD/TM/02-1, Argonne National Laboratory (2002).

[4] U.S. Nuclear Regulatory Commission (NRC), NUREG/CR-5512, Vol.1, "Residual Radioactive Contamination From Decommissioning-Technical Basis for Translating Contamination Levels to Annual Total Effective Dose Equivalent", Pacific Northwest Laboratory (1992).

[5] ZionSolutions, TSD14-019, "Radionuclides of Concern for Soil and Basement Fill Model Source Terms" (2014).

[6] Sacramento Municipal Utility District, DTBD-05-007, "Rancho Seco Nuclear Generating Station Decommissioning Technical Basis Document, Containment Buildings DCGLs" (2006).

Development of a Numerical Model to Evaluate the Terrestrial Behavior of Radionuclides

Byung-Il Min*, Kihyun Park, Sora Kim, Byung-Mo Yang, Jiyoon Kim, and Kyung-Suk Suh
Korea Atomic Energy Research Institute, 111, Daedeok-daero 989beon-gil, Yuseong-gu, Daejeon, Republic of Korea
*bimin@kaeri.re.kr

1. Introduction

A numerical model is needed to evaluate the long-term movement of radionuclide to land, river, lake, and ocean after an nuclear accident such as Fukushima accident. In this study, we develop a numerical model using a traditional kinematic wave equation.

2. Wave Equation

2.1 Kinematic Wave Equation

Fluid mechanics is used in various fields, and appropriate governing equations should be used according to the purpose of use. Generally, Saint Venant equation is used to express the flow of the river. The equation is as follows.

$$\frac{\partial A}{\partial t} + \frac{\partial Q}{\partial x} = q + (i - \Phi)$$
$$\frac{\partial u}{\partial t} + u\frac{\partial u}{\partial x} + g\frac{\partial y_0}{\partial x} = g(s_f - s_0) - q(\frac{u-v}{A}) \quad (1)$$

The equation (1) may be rewritten in the following form for a ready reference to the various types of wave models that are recognized.

$$\frac{1}{g}\frac{\partial u}{\partial t} + \frac{u}{g}\frac{\partial u}{\partial x} + \frac{\partial y_0}{\partial x} + (s_f - s_0) = 0 \quad (2)$$

The unknown parameters for the channel shapes under consideration α_k and mk being the unknown functions. The Kinematic Wave equation for the channel flow can be written as given below:

$$\frac{\partial A}{\partial t} + \frac{\partial(\alpha_k A^{mk})}{\partial x} = q \quad (3)$$

2.2 Kinematic Wave Equation Solution

As illustrated in Fig 1, an overland flow starts from the upstream boundary without any inflow. This water deficit propagates into the downstream reach. The water surface profile is continually being increased until it reaches its equilibrium.

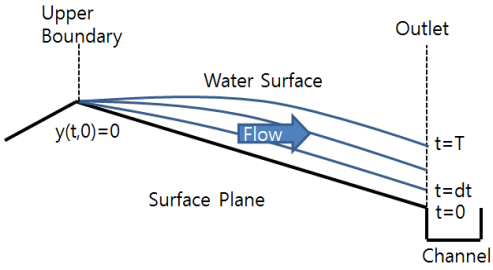

Fig.1. Illustration of one-dimensional Overland Unsteady Flow Profile.

The initial conditions for the Kinematic Wave equation overland flow include the dry bed condition everywhere on the ground before it rains.

$$y(t,x) = y(0,x) = 0.0$$
$$q(t,x) = q(0,x) = 0.0 \quad (4)$$

Guo and Urbonas (2009) and Guo et al. (2012) applied watershed shape factor to convert a natural watershed into its equivalent rectangular plane so that the unit-width KW theory can be used to predict overland flow from a given rainfall.

$$\frac{L_w}{L} = (1.5 - \frac{A_m}{A})(\frac{2}{\sin\frac{\pi}{8}}\sin(\frac{\pi A}{8L^2}))$$

$$X_w = \frac{A}{L_w} \quad (6)$$

in which A= watershed area, B= watershed width, Am = larger half area between left and right areas along the waterway through the catchment, L = length of waterway, Xw= length of overland flow, and Lw= width of plane as illustrated in Fig. 2.

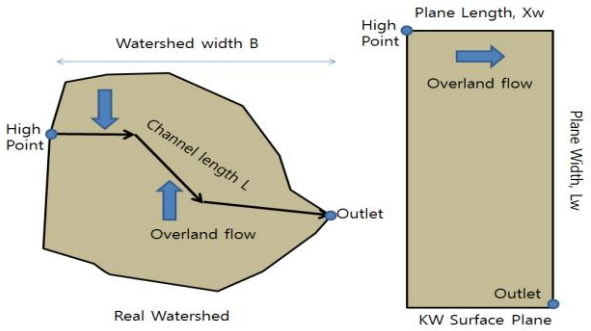

Fig. 2. Conversion of Natural Catchment into Kinematic Wave Rectangular Plane.

3. Numerical Results

Please follow this Author's Guide. The developed numerical model has been applied to the field and will be compared with observation data in future studies.

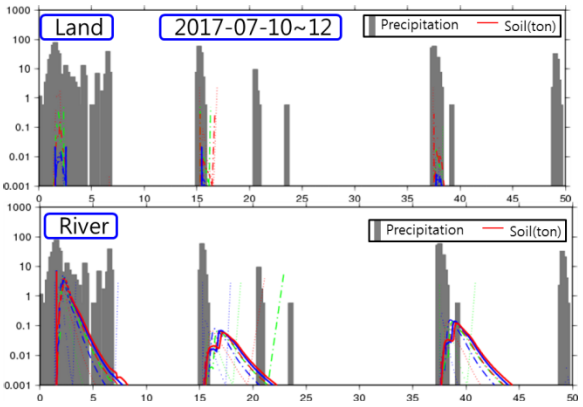

Fig. 3. Computation results of precipitation and eroded soil weight.

REFERENCES

[1] Guo, J. C.Y. and Urbanos B. (2009). "Conversion of Natural Watershed to Kinematic Wave Cascading Plane," Journal of Hydrologic Engineering, Vol 14, No 8, August, pages 839-846

[2] Guo, James C. Y. Cheng, Jeff, Wright, L.(2012) "Field Test on Conversion of Natural Watershed into Kinematic Wave Rectangular Planes," ASCE J. of Hydrologic Engineering, Vol. 17, No. 8, August.

Analysis of Area Factor According to Scenario

Jihyang Byon, Sangjune Park, and Seokyoung Ahn*
Pusan National University, 2, Busandaehak-ro 63beon-gil, Geumjeong-gu, Busan, Republic of Korea
*sahn@pusan.ac.kr

1. Introduction

An assessment of the elevated residual radioactivity is required to monitor decontamination levels and effects, in remedial action support survey for FSS (final status survey) at MARSSIM, which may limit activities such as direct measurements and scan surveys. In this study, area factors for class 1, which exceeds $DCGL_W$, were derived to evaluate elevated residual radioactivity in a locally small region. The selected list of potential radionuclides in the preceding studies was used to identify affected pathways and sensitive parameters in the preliminary impact areas according to the scenarios.

2. Description of Area Factor

An evaluation should be performed to take into account the possibility that there is a small area of elevated residual radiation outside the fixed measurement range during scanning. $DCGL_{EMC}$ is a guideline value that applies to an area where there is a locally elevated residual radioactivity in a small area to be measured. In other words, it is a site release standard concentration applicable to hot spot area, Class 1. The area factor for use in the comparison of EMC during the FSS is defined as follows [1]:

$$\text{Area Factor} = \text{DCGLEMC/DCGLw} \quad (1)$$

In other words, $DCGL_{EMC}$ is a $DCGL_W$ calibrated to an area factor considering a small area. As shown in Fig. 1, Area factors are defined according to their ratio by calculating the dose-to-source ratio (DSR) for each specific contaminated area, including the baseline area.

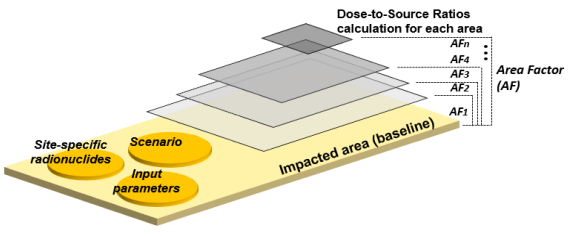

Fig. 1. Schematic representation of area factor derivation.

Potential radionuclides of the Kori Unit 1 were selected by combining the methodologies used in Rancho Seco and Zion NPP. Firstly, a suite of theoretical radionuclides with a half-life of more than two years is determined through the related documents, then site-specific radionuclides for soil are selected through the preceding characterization surveys. Since the characterization survey of Kori Unit 1 has just started, there is not enough information about radionuclides that can be directly applied to soil of the site. Therefore, concerned radionuclides for soil at Kori Unit 1 were selected as ^{14}C, ^{60}Co, ^{134}Cs, ^{137}Cs, ^{63}Ni, ^{90}Sr in the same manner as Rancho Seco NPP, which was confirmed as the same as Zion NPP except ^{14}C [2,3]. The preliminary security protected area of the Kori Unit 1 was designated as 39,000 m^2 including Unit 2. The area factor is determined from the ratio of the dose for each smaller area evaluated relative to the dose of the base case, so that the total dose of the considered pathways is calculated for each radionuclide and each contaminated area.

3. Analysis of Area Factors According to Scenario

When baseline area was designated as the specific area of Kori Unit 1 site of 39,000 m^2 in industrial worker scenario, maximum difference of area factors of gamma emitters was 1% increase of ^{60}Co based on the contaminated area of 1 m^2. ^{60}Co was confirmed that changes in dose due to differences in baseline area are negligible in industrial worker scenario. In the case of ^{134}Cs and ^{137}Cs, difference from the area factors of the Zion NPP and Kori Unit 1 in the same residential farmer scenario was greater than the difference due to the scenario change. This is because the transfer factors, which are ratios of radioactivity concentration between the two receptors when the radionuclides are transferred to a receptor associated with ingestion, are identified as a sensitive parameter with increasing contaminated area. In the case of beta emitters, the difference in area factors for the same scenario and for scenario changes was much greater than gamma emitters. The contributions resulting from components

of exposure pathways in residential farmer scenario based on the contaminated area 39,000 m^2 is as follows;
^{90}Sr:plant(53%)>milk(28%)>meat(16%)>ground(1.38%)>inhalation (0.01%),^{63}Ni: milk(85%)>plant(9.8%)>meat(4.2%)>soil(0.25%). Here, *ground* refers to direct exposure to external radiation from the contaminated soil material, and incidental ingestion of contaminated soil was expressed as *soil*. Because the ingestion pathways contribute up to 99% of the dose, there is a significant difference in the area factors due to the scenario change. All gamma emitters showed full contribution of exposure through the ground pathway at least 86% in the contaminated zone of 39,000 m^2 and at least 97% below 1,000 m^2. However, the order of the main exposure pathway of beta emitters, ^{90}Sr, ^{14}C, and ^{63}Ni, changes with the contaminated areas 10, 100, and 1,000 m^2 respectively when applying the residential farmer scenario. The most prevalent exposure pathway for each contaminated area is shown in Fig. 2.

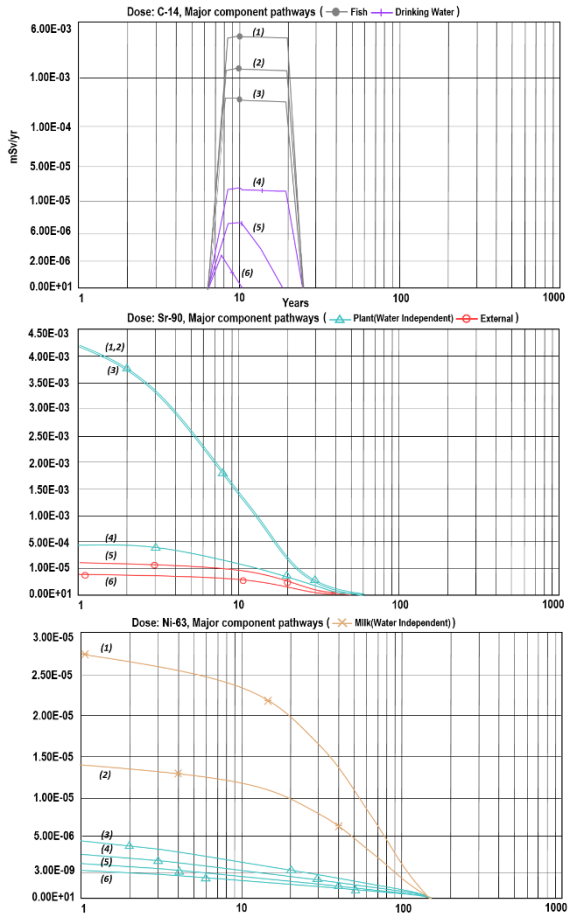

Fig. 2. Predominant exposure pathway of beta emitters in residential farmer scenario.
(1): 39,000 m^2, (2): 10,000 m^2, (3): 1,000 m^2, (4): 100 m^2, (5): 10 m^2, (6): 1 m^2

4. Conclusion

The preliminary area factor for class 1 was derived in consideration of the presence of elevated residual radioactivity in the affected area for further investigation of the FSS of Kori Unit 1. Area factors were evaluated for two scenarios for residential farmer scenario and industrial worker scenario for various reuse purposes of Kori Unit 1 site. Area factor of gamma emitters was less affected by the scenario or within the same scenario than the beta emitters. Overall, the effect of direct exposure to external radiation was greatest for gamma emitters. In the case of beta emitters, there was a significant difference in the value of the area factors while being dominantly influenced by internal exposure pathways.

ACKNOWLEDGEMENT

This work was supported by the National Research Foundation of Korea (NRF) grant funded by the Korea government [No. NRF-2018M2B2B1065637]; and was supported by New and Renewable Energy Program [No. G032181012] of Korea Institute of Energy Technology Evaluation and Planning (KETEP).

REFERENCES

[1] NRC, EPA, DOD, DOE, “Multi-Agency Radiation Survey and Site Investigation Manual (MARSSIM)”, 2000.
[2] Zion Solutions Inc., TSD 14-019, Radionuclides of Concern for Soil and Basement Fill Model Source Terms, 2014.
[3] United States Nuclear Regulatory Commission, “Rancho Seco License Termination Plan”, 2014.

Measurement of the Radioactivity on the Air Sampling Filter Using the Alpha Spectrometer

Sung-Kyun Park*, Jeong-Min Park, and Yi-Sub Min

Korea Atomic Energy Research Institute, 181, Mirae-ro, Geoncheon-eup, Gyeongju-si, Gyeongsangbuk-do, Republic of Korea

*skpark4309@kaeri.re.kr

1. Introduction

In order to check out systematically the radioactivity of the airborne particulates in the space, the way to measure the radioactivity on the filter of the air-sampler is used. That is, the air-sampler captures the air in the space with 120 LPM during 3 hours and then on the filter in the air-sampler, the airborne alpha and beta particulates are accumulated. The low alpha-beta counter can measure the total alpha and beta activity of the filter and the airborne concentration, C of the space to determine the airborne radioactivity can be calculated from this total activity, A_0 using the following:

$$C = \frac{A_0}{F \cdot t_0 (1 - e^{-\lambda \cdot t_0})} \quad (1)$$

where the parameter F is the flow rate of the air sampler. The parameter λ is the decay constant of the unknown radioactivity measured on the filter installed in air-sampler. The parameter t_0 is the air sampling time. Generally, the alpha radioactivity measured on the environmental sample like the air-sampler filter is from the natural activity, especially, the radon decay products called as the radon progeny is one of the most influential parameters. So the process to identify the nuclide of the filter is needed.

In this research, the procedure to analyze the alpha nucleus on the filter using the alpha spectrometer would be shown.

2. The Nuclide Analysis of the Filter

In order to identify unknown radionuclides detected on the air-sampler filter, the alpha spectrometer should be used. The filter shape used to analyze is processed into the disk-shape with the diameter of 24 mm. The standard source used to calibrate the alpha spectrometer has the same shape. Fig. 1 shows the result of the nuclide analysis measured during 12 hours and there are one main peak observed distinguishably in the energy 7608keV. The potential candidate for this main peak is Po-214. Since Po-214 is decayed from Radon (Rn-222), the alpha radioactivity measured on the filter might be produced from the radon or radon progeny.

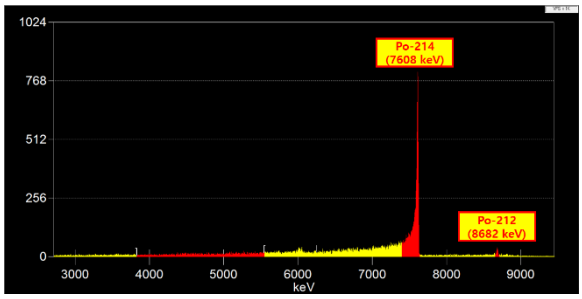

Fig. 1. The result of the nuclide analysis of the disk-shaped filter measured as soon as the air sampling during 43200 sec using the alpha spectrometer.

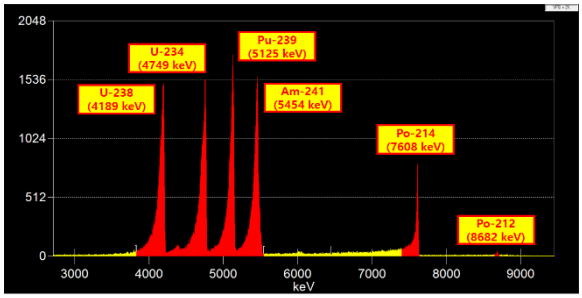

Fig. 2. The result of analyzing the nuclide of the standard source during 43200 sec using the alpha spectrometer after measuring the filter.

After finishing the first alpha nuclide analysis, the standard source is installed into the alpha spectrometer instead of the disk-shaped filter and then the measurement continue to be processed on the same window shown as Fig. 2. This standard source is composed of U-238, U-234, Pu-239, and Am-241, shown as Fig. 2 and their total activity is 6.727 Bq. By comparing between the analyzing data shown in Fig. 1 and Fig. 2, the pure area of the source peaks is 87440 count and the area of Po-214 is 807. The radioactivity of Po-214 on the filter with the diameter of 24 mm can be calculated into 0.0621 Bq.

Table 1. The result of the nuclides analysis of the filter

Peak	Energy range (keV)	Area (Count)	Activity (Bq)
Source Peak	3827 ~ 5539	90069 (2629)	6.727
PO-214	7397 ~ 7634	807	0.0621

3. Calculation of the Activity on the Filter

At the same place where the air was collected, the airborne concentration of Rn-222 measured is about 22.0 Bq/m^3. It assumes that the all radon gas in the air collected is accumulated on the filter. From the decay of the initial quantity of this parent radon, the concentration of the radon progeny can be calculated using the Bateman equation. The activities of the radon progeny on the filter can also be calculated from the concentrations of the radon progeny shown as Fig. 3 [1]. The activity on the filter with the diameter of 40 mm is calculated as 180 Bq. This activity calculated can be converted into 64.8 Bq under the same area of the standard source.

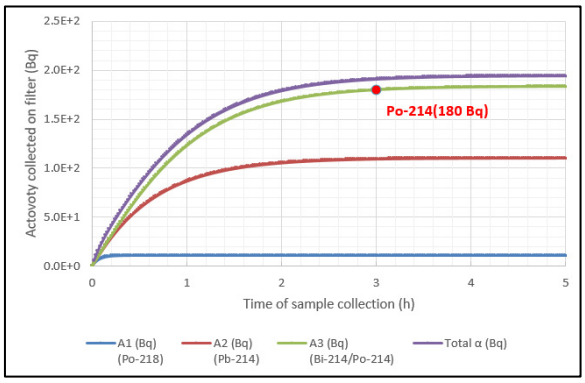

Fig. 3. Activities calculated of radon progeny collected on the filter with the time sample collection.

4. Conclusion

The activity of Po-214 measured on the filter is 0.0621 Bq and the activity calculated from the Bateman equation is 64.8 Bq. This means that only 0.096 % of the radon gases in the air accumulates on the filter. If the filter is preprocessed, the activity can be measured more exactly. This result shows that the most of the radon gas are not filtered.

REFERENCES

[1] S. Park, Y. Min, J. Park, “The theoretical calculations of the airborne natural activities monitored in KOMAC”, Proc. of the KNS 2018 Autumn Conference, Oct 25-26, 2018.

The Annual Environmental Radiation Measurement and Analysis in KOMAC

Jeong-Min Park*, Yi-Sub Min, Sung-Kyun Park, and Jin-Nyeong Choi
Korea Multi-purpose Accelerator Complex, Korea Atomic Energy Research Institute, 181, Mirae-ro, Geoncheon-eup, Gyeongju-si, Gyeongsangbuk-do, Republic of Korea
*jmpark027@kaeri.re.kr

1. Introduction

Tritium is a representative low-energy beta emitter, and its risk of internal exposure is low. However, it can be easily absorbed by the skin or ingested orally. The human body contains more than 80% water and the tritium uptake into the body is reacted with the beta rays emitted by the body of water. When water is irradiated, the ionization occurs and primary free radicals are generated. This is relatively large risk of tritium in the internal exposure which cause damage to body tissue in conjunction with a human body component [1] therefore, in the radiation safety team of the Korea Multi-purpose Accelerator Complex (KOMAC), after the test measurement period in the second half of 2017, a sample analysis focusing on the tritium of the water sample, which is generally absorbed into the body from 2018, has been carried out in earnest. The measurement sample is the surface water or rainwater and reservoir water in the site, and tritium is used as an object nuclide. In this research, the tritium is measured and analyzed quarterly using Liquid Scintillation Counter (LSC), and their change trend is checked.

2. Measurement and Result

In order to obtain an accurate measurement value, the calibration is performed on the equipment before the measurement to optimize the measurement capability. Then, an efficiency correction curve for the unknown sample is derived using the standard source. After the calibration of the measuring equipment is completed, the sample measurement is started.

2.1 Calibration of Measurement Equipment

The liquid scintillation counter (LSC) should be calibrated for the mechanical efficiency and the unknown source calibration of the equipment in advance to obtain precise measurements. In this measurement procedure, the tritium was used as the object nuclide. And the machine efficiency calibration of the equipment and the efficiency calibration for the unknown sample measurement were carried out. [2] The machine efficiency calibration aims to maintain the instrumentation performance of the equipment optimally and to confirm the integrity of the equipment operation. In this procedure, the unquenched source (15 ml) in the glass vial form is used as a standard sample. The calibration for the unknown sample is carried out using the Quenched standard Source and the efficiency correlation curve is derived to obtain the measurement efficiency for the unknown sample.

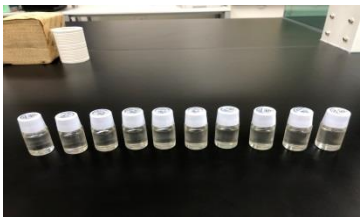

Fig. 1. The Quenched standard Source.

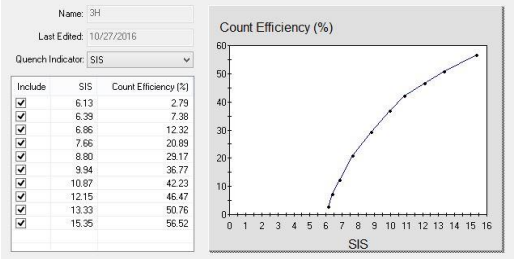

Fig. 2. The coefficient efficiency curve for the spectral index.

2.2. Measurement and Analysis

For the analysis of tritium, a sampling point in the site is designated and samples are taken quarterly. Samples to be used for analysis are collected at designated sites and quantitated in 2 ml using a micropipette. Then 10 ml of scintillator solution has been mixed and the sample for one day has been stabilized. The sample stabilized is measured once every 1800 minutes using the LSC instrument and the Becquerel value for 2 ml of sample is converted to Becquerel per liter (Bq/L). Fig. 3 show the collected samples and the mixed with scintillator solution.

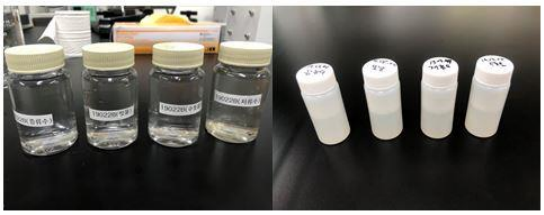

Fig. 3. The collected sample (right) and the sample mixed with scintillator solution.

2.3 Result

For the analysis of tritium in the water in the facility, environmental samples were taken quarterly and the results are shown in Table 1.

Table 1. Quarterly for measurement value of environmental samples (water) in 2018

Sample	1st Quarter [Bq/L]	2nd Quarter [Bq/L]	3rd Quarter [Bq/L]	4th Quarter [Bq/L]
Drinking water	> MDA	> MDA	> MDA	> MDA
Rain water	> MDA	> MDA	> MDA	> MDA
Reservoir	> MDA	> MDA	> MDA	> MDA

The unit of the measured value was converted to the becquerel per liter (Bq/L) in order to compare with the 'Tritium management standard value for each national drinking water'. Fig. 4 shows a comparison of the measured values for each quarter.

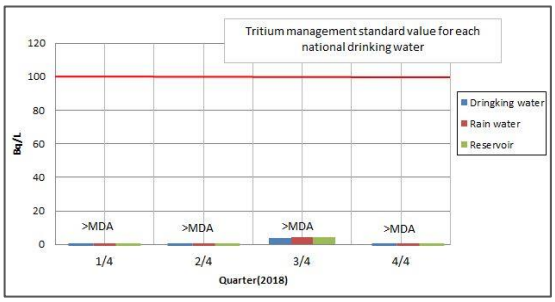

Fig. 4. Comparison of measurement value on site samples (Quarterly).

3. Conclusion

The Radiation Safety team of the KOMAC is measuring and analyzing the tritium value in the water by sampling the environmental samples quarterly as the part of the radiation and radioactivity monitoring in the general environment. As a result of comparing the tritium measurement value of the water samples in the facility quarterly, it was confirmed that it is below the minimum detectable activity (MDA). In addition, it can be seen that it is significantly lower than the European standard, which is the 'tritium management standard value for each national drinking water'

REFERENCE

[1] Osborne RV. Absorption of Tritiated Water Vapour by People. 1966;12:1527-1537.

[2] Michael F.L'Annunziatia, Handbook of Radioactivity Analysis, 3rd edition.

Study on the Calculating Method of Atmospheric Diffusion Coefficient Using Turbulence Observation Data on Field Experiments

Yoonhee Jung*, Jeong-mi Kim, and Hyun-jun Jo
KHNP Central Research Institute, 70, Yuseong-daero 1312beon-gil, Yuseong-gu, Daejeon, Republic of Korea
*yhjung89@khnp.co.kr

1. Introduction

According to the Nuclear Safety and Security Commission (NSSC), the dose of residues by released radioactive materials should be assessed.

At KHNP NPPs, a straight-line Gaussian plume model (e.g., PAVAN) based on U.S. NRC Regulatory Guide 1.145 is used to estimate the atmospheric dispersion and surface deposition of the released radioactive material from nuclear facilities. The Pasquill- Gifford (P-G) curve, which is function of distance and atmospheric stability classes, is used to evaluate the atmospheric dispersion. This method has been widely applied because it allows simple and conservative evaluation. Based on Notice of the NSSC No. 2017-26, feasibility analysis has been required to determine whether the method could be applied to the characteristics of domestic nuclear sites.

In this study, the atmospheric diffusion coefficient using the observed turbulence at Hanul NPP site was examined for the validity of the atmospheric diffusion coefficient by the P-G curve applied in Korea.

2. Materials and Methods

2.1 Monitoring and Equipment Installation

The three-dimensional ultrasonic anemometer was installed at Hanul NPP site. Atmospheric diffusion coefficient was calculated using the observed turbulence for 12 month (11.1.2017 ~10.31.2018).

2.2 Comparison of Methods for Assessing Atmospheric Diffusion Coefficients

Horizontal diffusion coefficient (σ_y) and vertical diffusion coefficient (σ_z) in Gaussian model are described by Taylor's turbulence hypothesis. (Equation 1).

$$\sigma_y = \sigma_v t f_y(t/T_{Ly})$$
$$\sigma_z = \sigma_w t f_z(t/T_{Lz}) \quad (1)$$

σ_v : horizontal standard deviation(m)
σ_w : vertical standard deviation(m)
f_y : non-dimensional horizontal diffusion function
f_z : non-dimensional vertical diffusion function
t : travel time of the diffusing material

There are several methods available to calculate the Lagrangian integral timescale, T_{Ly} and T_{Lz}. In this study, Draxler's method and Eulerian autocorrelation function were chosen for these calculations.

The atmospheric diffusion coefficients calculated by these two methods were classified by atmospheric stability and compared with P-G values.

3. Results

The horizontal and vertical atmospheric diffusion coefficients were calculated using the observed turbulence for 12 months at Hanul site (Fig. 1-2).

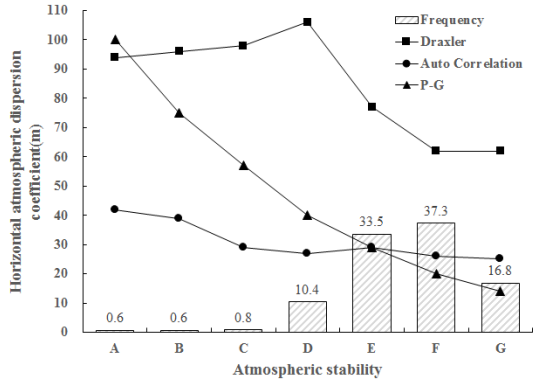

Fig. 1. Horizontal atmospheric diffusion coefficient with atmospheric stability.

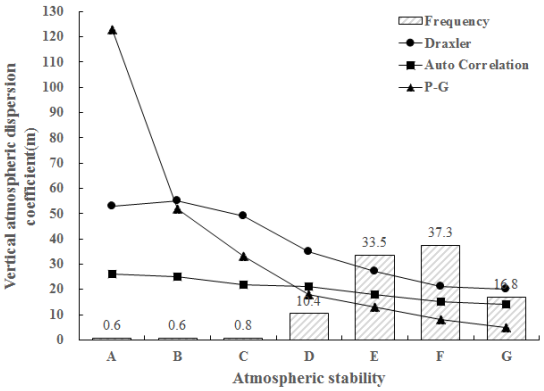

Fig. 2. Vertical atmospheric diffusion coefficient with atmospheric stability.

In the case of Draxler's method, the horizontal and vertical coefficients tend to decrease as the atmosphere stabilized. Draxler and P-G values were compared at atmospheric stability B to G. The coefficients of Draxler were 1.3~4.4 times and 1.1~4.0 times larger than P-G values, respectively.

On the other hand, when the horizontal and vertical atmospheric diffusion coefficients were calculated by autocorrelation function, atmospheric diffusion coefficient did not change with atmospheric stability. Especially, if the atmosphere was unstable (A~C), they were 2.0~2.4 times and 1.5~4.7 times lower than the P-G value. The results show that the relationship between turbulence and atmospheric diffusion coefficients is not consistent.

4. Conclusion

In order to evaluated the feasibility of the atmospheric diffusion coefficient currently used in domestic nuclear power plants, the method of estimating the atmospheric diffusion coefficient was reviewed.

As a result, Draxler's method is considered to be a comparison value for evaluating the suitability of atmospheric diffusion coefficient by the P-G curve.

REFERENCES

[1] KHNP, "Suitability validation of radioactivitiy atmospheric diffusion assessment model for hanul site", 2018-50003339-DAN-TR, 2018.

Status of Overseas Technical Standards for Exemption Levels of NORM and Disposal Limits of NORM Waste

Na Yoon Choi and Jae Hak Cheong*
Kyung Hee University, 1732, Deogyeong-daero, Giheung-gu, Yongin-si, Gyeonggi-do, Republic of Korea
*jhcheong@khu.ac.kr

1. Introduction

Products (referred to as "NORM products") containing natural occurring radioactive materials (NORM) at domestic and abroad are continuously produced, used and disposed annually. Typically, ionization chamber smoke detector, incandescent gas mantle, and uranium in counterweights are used. As like other radioactive products or wastes, radioactive materials which are contained in NORM product cause radiological effects on users and the environment.

From the issue about incandescent gas mantle in 1970 to the issue about Daejin bed in 2018, there has been brought up many problems of the safety for NORM products. In relation to Daejin bed issue, it was calculated to exposure dose up to 9.35 mSv/y in a specific exposure situation [1]. NORM products are directly and easily accessible to the living environment than other radioactive material. So if adequate level of regulation is not achieved, it can be occurred radiological effect above the limit value for a wide population range. Therefore, appropriate regulatory standards should be prepared in various situations such as production, use, transportation, and disposal of NORM products. In this study, in order to comparison the regulatory status, exemption level for NORM and disposal limits for NORM wastes in domestic and abroad.

2. Methods and Results

2.1 Comparison of Exemption Level of NORM in Overseas

First, exemption level for natural Uranium and Thorium in IAEA, EU and six foreign nations are investigated. Exemption level are divided into 3 standards, as like radioactivity concentration, total radioactivity and annual exposure dose. In addition, there are different effects by equilibrium state with daughter nuclides of Uranium and Thorium, exemption levels are different with each equilibrium states. Table 1 shows the exemption level for Uranium and Thorium in each countries and organizations.

Internationally, exemption level for Uranium and Thorium is similar to that 10 Bq/g, 10^4 Bq for ^{238}U+ and 1 Bq/g and 10^3 Bq for ^{232}Th and ^{238}Usec. However, in Canada, has more conservative radioactivity concentration level as 0.3 Bq/g for ^{232}Th and ^{238}Usec. In Japan, the exemption level for total radioactivity is unified to 8,000 Bq for all Uranium and Thorium under permanent equilibrium.

The annual dose is usually limited to 1 mSv/y, but limited to a lower level of 0.3 mSv/y in Canada and Sweden.

Table 1. Exemption level of NORM for U and Th

Nation	Nuclide	Radioactivity Concentration	Total Activity	Annual Dose
Unit		Bq/g	Bq	mSv/y
IAEA [2]	^{238}U+ ^{232}Th	10	1×10^4	1
EU [3]	^{238}U+	10	1×10^4	1
Canada [4]	^{238}U+	10	1×10^4	0.3
	^{238}Usec	0.3	1×10^3	
	^{232}Th	10	1×10^3	
	^{232}Thsec	0.3		
United Kingdom [5]	^{238}U+	10	1×10^4	0.3 (residence)
	^{238}Usec	1	1×10^3	
	^{232}Thsec	1	1×10^3	1 (worker)
Germany [6]	^{238}U+	10	1×10^4	1
	^{238}Usec	1	1×10^3	
	^{232}Th	10	1×10^4	
	^{232}Thsec	1	1×10^3	
Sweden [7]	^{238}U+	10	1×10^4	0.3
	^{238}Usec	1	1×10^3	
	^{232}Thsec	1	1×10^3	
Finland [8]	^{238}U+	10	1×10^4	1
	^{238}Usec	1	1×10^3	
	^{232}Thsec	1	1×10^3	
Japan [9]	^{238}U	10	8×10^3	1
	^{238}Usec	1		
	^{238}Usec	1	1×10^3	

* '+' means permanent equilibrium with daughter nuclide ^{234}Th, ^{234m}Pa.
* 'sec' means permanent equilibrium for ^{238}U with ^{234}Th, ^{234m}Pa, ^{234}Pa, ^{234}U, ^{230}Th, ^{226}Ra, ^{222}Rn, ^{218}Po, ^{214}Pb, ^{214}Bi, ^{214}Po, ^{210}Pb, ^{210}Bi, ^{210}Po and permanent equilibrium for ^{232}Th with ^{228}Ra, ^{228}Ac, ^{228}Th, ^{224}Ra, ^{220}Rn, ^{216}Po, ^{212}Pb, ^{212}Bi, ^{208}Ti (0.36), ^{212}Po (0.64).

2.2 Comparison of Disposal Limits of NORM waste in Overseas

Second, disposal limits for six abroad nations are investigated. Table 2 lists disposal options in overseas according to radioactivity concentration and total activity for Uranium and Thorium.

Table 2. Disposal Options for radioactivity concentration of U and Th in abroad

Nation	Radioactivity Concentration	Disposal Option	Note[1)]
United Kingdom	5 Bq/g	Incineration	< 100 Bq/y
	5 Bq/g	Unlimited Landfill	< 50 GBq/y
	5 Bq/g	Licensed Acceptor	-
	5 Bq/g	Landfill with Evaluation	> 50 GBq/y
	10 Bq/g	Landfill with Evaluation	-
Belgium	0.1 Bq/g	Unlimited Landfill	Single Site C_{Avg} < 0.1 Bq/g
	10 Bq/g	Landfill	C_{Avg} < 0.2 Bq/g
	50 Bq/g	Landfill in Harzard Waste Disposal site	C_{Avg} < 0.2 Bq/g
Germany	10 Bq/g	Landfill (< 150,000 m^2)	C_{Avg} < 0.05 Bq/g
		Landfill (> 150,000 m^2)	C_{Avg} < 0.1 Bq/g
		Licensed Landfill	C_{Avg} < 1 Bq/g
		Underground Disposal	C_{Avg} < 5 Bq/g
Sweden	< 10 Bq/g	Landfill	Dose Criteria 1 mSv/y
Netherland	1-10 Bq/g	Landfill	Need to report
	> 10 Bq/g	Licensed Acceptor	Need to permit
Norway	< 1 Bq/g	Landfill	-
	1-10 Bq/g	Landfill in Harzard Waste Disposal site	-
	> 10 Bq/g	Disposal in RW Disposal Site	-
Spain[2)]	< 10 times of EL	Landfill	-
	10-50 times of EL	Landfill in Harzard Waste Disposal site	-
	> 50 times of EL	Disposal in RW Disposal Site	-

[1)] C_{Avg} means average radioactivity concentration after the disposal.
[2)] EL means exemption level

It is not easy to unify or classify disposal limits by disposal options. As a results, it has shown that NORM wastes with radioactivity concentrations between 1-10 Bq/g are usually treated as general wastes and disposed at landfill site. But above 10 Bq/g are treated as radioactive wastes and disposed of at licensed landfill sites or radioactive waste repositories. On the other hand, in Korea, it does not specify radioactivity concentration and quantity limits for self-disposal of natural Uranium and Thorium in Notice of Nuclear Safety and Security Commission [10].

3. Conclusions

In this study, according to various issues about NORM product, in order to analyze relevant standards, the various exemption level and disposal limits for Uranium and Thorium are investigated in overseas countries, IAEA and EU. As a result, exemption levels specified in many countries and organizations have similar form of classification and have like values. Also, there are various criteria for disposal of NORM waste according to disposal options. Normally, NORM wastes with radioactivity concentrations between 1-10 Bq/g are treated as common wastes and disposed at landfill site. But above 10 Bq/g are treated as radioactive wastes and disposed of at licensed landfill sites or radioactive waste repositories. It can be used as a reference to seek management plans for NORM or disposal limits for NORM waste in domestic.

REFERENCES

[1] http://www.nssc.go.kr/nssc/information/radon/20180515_ 2.pdf
[2] International Atomic Energy Agency, Radiation Safety for Consumer Product, IAEA-SSG-36, 2016.
[3] European Union, 2013/59/EURATOM, 2013.
[4] Canadian NORM Working Group of the Federal Provincial Territorial Radiation Protection Committee, Canadian Guidelines for the Management of NORM, 2011.
[5] United Kingdom, Exemption Guidance, Guidance for NORM Industrial Activities on How to Comply with the Radioactive Substances Exemption Regime, 2013.
[6] The Federal Office for Radiation Protection (BfS), Radiation Protection Ordinance, 2016.
[7] Swedish Radiation Safety Authority, Strålsäkerhetsmyndighetens föreskrifter om naturligt förekommande radioaktivt material och byggnadsmaterial, SSMFS 2018:4, 2018.
[8] STUK, Radiation Safety in Practices causing Exposure to Natural Radiation, ST 12.1, 2011.
[9] The Nuclear Regulation Authority, Guideline for Ensuring Safety of Raw Materials and Products Containing Uranium or Thorium , 2009.
[10] Nuclear Safety and Security Commission, Regulation on the classification of radioactive waste and standard for self-disposal, Notice 2017-65, 2017.

Radiation Hazards to Consider During the Decommissioning of NPP for Radiation Protection

Gi-Lim Kim and Hyung-Woo Seo*

KHNP Central Research Institute, 70, Yuseong-daero 1312beon-gil, Yuseong-gu, Daejeon, Republic of Korea

*sehywo1727@khnp.co.kr

1. Introduction

The final goal of decommissioning of nuclear facilities is to safely eliminate the exposure risk, and release facilities and sites form regulation applied for operation. The Dismantling and Decontamination (D&D) works involve all the elements of the site from the facility's main components and systems to the buildings, and it is necessary to secure the safety of workers, general public and the environment from the radiation hazards. To do this, the decommissioning plan for various activities should be well prepared, and the radiation protection plan for the workers should be appropriately (As Low As Reasonably Achievable) performed at the stage of executing the D&D activities.

However, the radiation hazards during the operation of nuclear facilities are different from that at the time of decommissioning. Therefore, from this understanding, the radiation hazards for decommissioning could be adequately addressed to minimize its effect. The purpose of this study is to review the contents that need to be described in decommissioning plan in terms of radiation protection and to investigate the radiation hazards based on Jose Cabrera nuclear power plant's decommissioning characteristic, which is a basic point for radiation protection plan for the safety of workers.

2. Methods

2.1 Contents of Radiation Protection in Final Decommissioning Plan

In Korea, according to Nuclear Safety and Security Commission (NSSC) Notice No. 2018-10 (Regulation on creation of nuclear power plants decommissioning plans, etc.) [1], the contents to be described in the Final Decommissioning Plan (FDP), which is a licensing document that must be approved for the decommissioning of nuclear facilities, are specified.

The FDP composed of 13 chapters, of which the radiation protection is included in chapter 7. There are four items to be described: ALARA application, radiation protection design characteristics, dose assessment, and radiation protection plan. In order to properly cover these contents, it is necessary to understand the radiation hazard from the aspect of radiation protection in decommissioning as mentioned in the introduction. Therefore, this study refers to technical report of EPRI [2]. In this report, radiation exposure data is based on Jose Cabrera nuclear power plant in Spain, which is currently toward the end of decommissioning phase. As a risk that can occur during decommissioning, the two aspects of hazards from the building and from the contamination are largely discussed.

3. Results & discussion

3.1 Radiation Hazard From Buildings During Decommissioning

Considerations for radiation protection during decommissioning include D&D plans for large components and radioactively contaminated equipment, handling of radioactive wastes and spent nuclear fuels, level and classification of risks, standards and measures, controls, decontamination of structures or facilities, area classification, etc. In summary, when taking into account the effects of radiation on major components, equipment and systems during decommissioning period, the buildings arising hazard are as follows.

- Reactor building
- Auxiliary building
- Waste treatment facility (Evaporator)
- Radioactive waste storage building
- Dismantling auxiliary building
- Cutting and decontamination workshop (turbine building if it is renovated)
- Spent nuclear fuel storage

In addition, the main materials of radiation that should be noted are as follows.

- Systems, structures and radioactive materials or contaminants
- Radioactive waste
- Radioactive material in case of accidents
- Spent nuclear fuels

3.2 Exposure Activities in Each Building

Among major exposure cases in various areas of facility, in case of reactor building, the most important ones in terms of hazard of external exposure are:

- RVI disassembly, cutting and treatment of RV and large components
- Dismantling of radioactive equipment
- Bioshield and demolition of contaminated concrete
- In-situ decontamination of parts and walls

The turbine building is basically a non-radioactive area, but if it is renovated to use for storage, cutting and decontamination, the radiation exposure is related to the treatment of radioactive materials. In the auxiliary building, the radiation exposure is caused by contaminated walls inside or outside the building, or by internal dismantling equipment. In the waste treatment building, there is exposure risks from waste treatment system such as concentration tanks or pumps, drainage tanks or pumps, recirculation pumps, analyzers, separators, heaters, condensers, coolers and steam and ventilation. In the radioactive waste storage, its function of storage is maintained during decommissioning and the exposure will be from the operation of radioactive materials. In the spent nuclear fuel storage, when decommissioning is initiated, all spent nuclear fuels will be transported to the spent nuclear fuel storage and the activated part of the reactor vessel and its internal parts above the waste classification of intermediate level will also be stored. The risk of exposure to the spent nuclear fuel storage will be caused by facility operation.

3.3 Radioactive Contamination of Nuclear Facilities

For most nuclear power plants, mostly radiation controlled area, the main radiological hazard is from beta or gamma radionuclides; Co-60, Fe-55, Cs-137, Ni-63, and so on. Alpha radionuclides (Am-241 and Pu-238) are also present in the facility. But among them, the most contributions are attributed to Co-60 and most of them are similar in each buildings.

The contamination caused by decommissioning activities, full system chemical decontamination before dismantling, metal or concrete segmentation, etc., are different in each type of building. Most of the contaminated Structure, System, and Components (SSC) are located inside the reactor building, and the proportion of the contamination of the reactor building is the highest among the dismantling facilities. It should be noted that contamination occurs mainly from activities like cutting, dismantling, and managing contaminants.

3.4 Categorize of Decommissioning Tasks for Radiation Protection

During the decommissioning, the exposure activities could be classified into 13 contents:

a. Transfer of spent nuclear fuel to dry storage
b. Defueling, modifications and disposal of operational waste
c. Full system chemical decontamination
d. Maintenance, Engineering and management
e. Radiation protection
f. Operations and inspections
g. Segmentation/Removal of large components (reactor internals, reactor vessel, steam generator, pressurizer, reactor coolant pump, reactor coolant piping, etc.) and metal components
h. Biological shield removal
i. Spent fuel pool decontamination
j. Dismantling work in containment and other buildings
k. Other concrete decontamination
l. Radioactive waste management
m. Miscellaneous

4. Conclusion

On the basis information of the 13 contents in section 3.4, the common considerations in term of presence of radiation hazards for all of building are related with items of d, e, f, j, k, and l. Except these 5 items, the reactor building contains most of radiological hazards; b, c, g, h and i. However, the hazardous items of other buildings are rather simple. The turbine building, if renovated, contains only g. Also, the spent nuclear fuel storage includes a. The auxiliary building contains c and g. And then, both of the waste treatment facility and the radioactive waste storage building are connected to l. By identifying the radiation hazard from each building and its activities during the decommissioning, we expect that it will contribute to the prediction and reduction of the risk to the radiation.

REFERENCES

[1] Nuclear Safety and Security Commission, Regulation on creation of nuclear power plants decommissioning plans, etc., Notice No. 2018-10, 2018 (In Korean).
[2] Analysis of Dose Reduction Technology During Decommissioning, EPRI, Palo Alto, CA: 2018, 3002013095.

A Study on the Radiological Safety Assessment Method Establishment of Recycling Workers of Very Low Level Radiological Metallic Wastes in Decommissioning Nuclear Power Plants

Sang Heon Lee[1,*], Jong Soon Song[1,*], Byung Gi Park[2], and Hwa Jeong Han[2]

[1] Chosun University, 309, Pilmun-daero, Dong-gu, Gwangju, Republic of Korea

[2] Soonchunhyang University, 22, Soonchunhyang-ro, Sinchang-myeon, Asan-si, Chungcheongnam-do, Republic of Korea

[*]leesanghoen@naver.com

1. Introduction

Most metal wastes, generated during NPP decommissioning, are very low level radioactive wastes, and it seems necessary to calculate recyclability in consideration of the licensing procedure involving regulatory agencies. This study examined establishment of assessment plans prior to assessment of the radiologic stability of very low level radioactive metal wastes.

2. Method Establishment

2.1 Radionuclide Selection and Concentration

For radiologic assessment for Clearance waste, it was believed that utilization of the nuclides mentioned in foreign literature for assessment of nuclides would enhance the reliability of the result of assessment. To this end, the considered nuclides, mentioned in IAEA-TECDOC-855, NUREG-1640 and Rp-117, were compared, and nuclides were derived within the scope applicable in RESRAD-RECYCLE, and they will be used for assessment. As for the concentration of nuclides, 100 times the permissible concentration of Clearance level in Korea was considered for assessment.

2.2 Radionuclide Partitioning Factor

Because of the division of radioactive nuclides and the distribution of the mass of by-products, the concentration of some radioactive nuclides may be much higher than the original concentration of the waste metal in one of the by-products. For the concentration of the radioactive nuclides of the various smelting by-products, the Radionuclide Partitioning Factor value, mentioned in the Radiation Protect 89 and 117 report, was used.

2.3 Mass Partitioning Factor

As the induction furnace is used for melting in this study, it is necessary to modify the dust and slag contents. Ingot (78.5%) - slag (1.5%) - dust (20%) were applied as fixed values.

Type of furnace	Kg dust /tonne of steel	Kg slag /tonne of steel
Electric furnace	15	140
Induction furnace	1.5	20
Oxygen blast furnace	15	90

2.4 Recycling Scenario

Recycled metal wastes can be classified into the construction materials of nuclear facilities, containers for radioactive wastes, materials for disposal of radioactive wastes and radiation shield materials, and the detailed scenario is as shown in Table 1.

Table 1. Recycling Scenarios

Recycling Scenario	note
Nuclear Facility Construction Material	- Reinforcement concrete of spent nuclear fuel storage facilities - Reinforced concrete at the disposal facility on the near-surface
Radioactive Waste Container	- Drum. - Disposal containers (steel and carbon steel casting containers) - Packing container - Disposal containers of SNF copper - Aluminium storage container for HLW
Radioactive Waste Disposal Material	- Disposal container filled (metallic aggregate, wire mesh)
Radiation Shielding Material	- Fixed shielding walls (radiation source shield reinforcement) - Radioactive waste transport shielding

3. Selection of Evaluation Code

Among the metal wastes, generated during the decommissioning of an NPP, to know that the regulatory requirements for Clearance level of the very low level radioactive wastes in SG are satisfied, the assessment tool (RESRAD-RECYCLE Code) was selected, and this study will evaluate whether the permissible concentration of workers and the permissible dose are satisfied.

4. Conclusion

This study investigated methods fit for domestic conditions and conducted analysis to assess the exposure dose of workers who recycle metal wastes, generated during the decommissioning of an NPP. Assessment results (individual doses and collective doses) will be derived, and the sensitivity analysis of input variables will be conducted in the future.

REFERENCES

[1] European Commission, “Methodology and models used to calculate individual and collective doses from the recycling of metals from the dismantling of nuclear installations”, Radiation protection-117, (2010).

[2] European Commission, “Recommended radiological protection criteria for the recycling of metals from the dismantling of nuclear installations”, Radiation protection-89, (1998).

[3] NRC, “Radiological Assessment for Clearance of materials from nuclear Facilities”, NUREG-1640 Vol.1 (2003).

[4] AVL/EAD-3, “RESRAD-RECYCLE – a computer model for analyzing the radiological doses and risks resulting from the recycling of radioactive scrap metal and the reuse of surface contaminated material and equipment”, ANL/EAD-3 (2003).

7분과

방사화학 (Oral)

DFT Study on the Actinide Complexes in Water

Keunhong Jeong
Korea Military Academy, 574, Hwarang-ro, Nowon-gu, Seoul, Republic of Korea
doas1mind@kma.ac.kr

1. Introduction

Nuclear power industries are on the concern over the management of irradiating nuclear fuels in long-term safety assessment of the waste management. Liquid waste from the radioactive waste management contains highly toxic actinides including plutonium, americium, and uranium which are needed to be extracted thoroughly before contaminating the nature and environment. Research has been focused on the fate of various radioactive actinides in environmental chemistry in order to manage and remediate contaminated sites [1, 2]. Since most experimental researches with those actinides have technical difficulties in dealing with, theoretical researches have been considered as the supporting and/or alternative methods for understanding the actinide chemistry in conjunction with exponentially increasing calculation capacity despite its relatively initial stage of study [3].

Especially, density functional theory (DFT) study can provide valuable information on the molecular level structure, investigating the various properties of molecules, and even designing new organic ligands for actinide detection or extraction [4].

Herein, I will introduce several interesting theoretical results with several actinide complexes.

2. Quantum Calculation on Actinides

2.1 Half-sandwich Structure With Yb

After synthesizing uranocene, several actinides and lanthanides with sandwich and half-sandwich structures have been highlighted in the heavy metal ion structure study[5]. After theoretical investigating several heavy metal ion- ligand complexes including Yb(III)-C_7(C_8) stable half sandwich, several interesting structural properties were successfully analyzed.

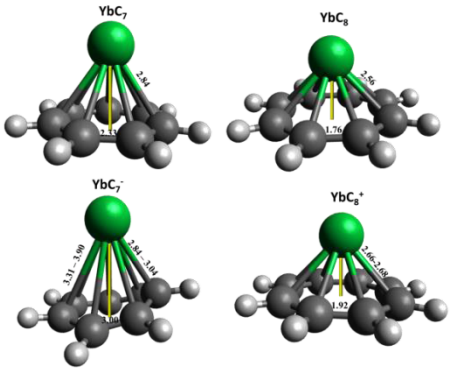

Fig. 1. Optimized half sandwich structures of Yb(III)-C_7(C_8).

2.2 Pu(III) and Pu(IV) Chloro Complexes

To understand the structures of Pu(III) and Pu(IV) in molten salt, quantum calculations on the plutonium chloro complexes were performed. Moreover, the NPA and QTAIM studies were harnessed for unveiling the electron structure of the complexes, which provide the electronic properties in bonding and NMR characteristics [6].

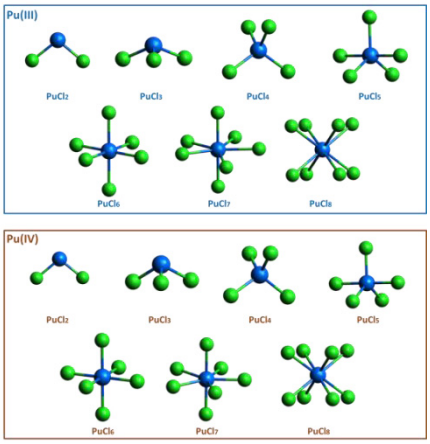

Fig. 2. Optimized structures of Pu(III, IV) chloro complexes.

2.3 Hydrolyzed Pu(III) and Pu(IV) Complexes

Plutonium chlorides in pyroprocessing molten salt can be hydrolyzed by water. Early detection and monitoring those reactions are highly important not only because of safety requirements but also because of its environmental issues. Therefore, possible reaction products from Pu(III)/Pu(IV) chlorides by water were investigated by DFT study.

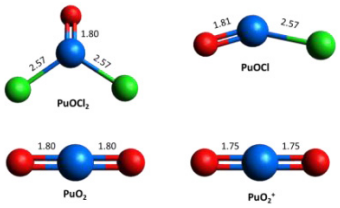

Fig. 3. Theoretically studied structures of hydrolyzed Pu(III, IV) chloro complexes.

2.4 U(IV)-PNPP Complex in Water

The DFT study on the complexation between U(IV) and PNPP was carried out in order to investigate important chemical properties of the U(IV)-PNPP complex in water including their stable structures, spin state, and infrared spectra.

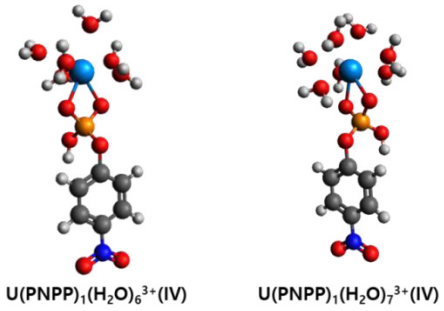

Fig. 4. Optimized structures of U(IV)-PNPP complex in water and energies of possible spin states in each complex.

2.5 Am(III)-Oxalate Complex in Water

Structures and bonding properties Am(III)-Oxalate complex were predicted by DFT calculations and several thermodynamic properties were analyzed.

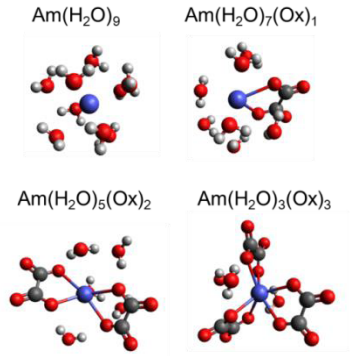

Fig. 5. Theoretically relaxed structures of Am(III)-Ox complexes in water.

3. Conclusion

Herein, theoretical studies were performed on various actinide complex structures. The analyses after extensive quantum calculations can provide valuable information both for confirming the experimental data and predicting the properties of actinides before/after the experiments.

REFERENCES

[1] J. Serp, R. J. M. Konings, R. Malmbeck, J. Rebizant, C. Scheppler, J. P. Glatz, “Electrochemical Measurement of Diffusion Coefficient of Pu in Liquid Cd”, Journal of The Electrochemical Society, 561, 143–148. (2004).

[2] S. E. Bonea, J. J. Dynes, J. Cliffc, and J. R. Bargar , “Uranium(IV) adsorption by natural organic matter in anoxic sediments”, Proceedings of the National Academy of Sciences of the United States of America, 114(4),711-716 (2017).

[3] K. Maher, J. R. Bargar, and G. E. Brown Jr, “Environmental Speciation of Actinides”, Inorganic Chemistry, 52(7), 3510-3532 (2013).

[4] Z. Wang|, N. Pu, Y. Tian, C. Xu, F. Wang, Y. Liu, L. Zhang, J. Chen, and S. Ding, “Highly Selective Separation of Actinides from Lanthanides by Dithiophosphinic Acids: An in-Depth Investigation on Extraction, Complexation, and DFT Calculations”, Inorganic Chemistry, in press (ASAP) (2019).

[5] J. Jiang and D. K. P. Ng, “A Decade Journey in the Chemistry of Sandwich-Type Tetrapyrrolato−Rare Earth Complexes”, Accounts of Chemical Research, 42(1), 79–88 (2009).

[6] K. Jeong, S. M. Woo, S. Bae, “DFT study on the bonding properties of Pu (III) and Pu (IV) chloro complexes”, Journal of Nuclear Science and Technology, 55(4), 424–428 (2018).

Chemical Behavior and Solubility of $Ca_2UO_2(CO_3)_3 \cdot 10H_2O$(cr) at T = 22 and 80°C in Dilute and Saline NaCl Systems

Jun-Yeop Lee[1,2,*], Vanessa Montoya[1], David Fellhauer[1], Xavier Gaona[1,*], and Marcus Altmaier[1]

[1]Karlsruhe Institute of Technology, Hermann-von-Helmholtz-Platz 1, 76344 Eggenstein-Leopoldshafen, Germany

[2] Pusan National University, 2, Busandaehak-ro 63beon-gil, Geumjeong-gu, Busan, Republic of Korea

[*]jylee@pusan.ac.kr; [*]xavier.gaona@kit.edu

1. Introduction

A comprehensive knowledge of uranium chemical behavior is indispensable for the prediction of radionuclide migration in contaminated sites in the environment. According to the omnipresence of carbonate and calcium ions, aqueous ternary Ca-UO_2-CO_3 species are foreseen to be predominant complexes in natural groundwater system. Particularly, the solubility of U(VI) could be controlled by $Ca_2UO_2(CO_3)_3 \cdot 10H_2O$(cr) solid phase (also known as liebigite) where aqueous Ca-UO_2-CO_3 complexes dominate the overall aqueous U(VI) species. Although of the relevance of the Ca-UO_2-CO_3 system, there are still significant lack of relevant experimental data for determining thermodynamic data for the solid $Ca_2UO_2(CO_3)_3 \cdot 10H_2O$(cr), which is essential for the reliable interpretation of U(VI) migration behavior in nature.

The objective of the present work is to investigate the solubility and stability of $Ca_2UO_2(CO_3)_3 \cdot 10H_2O$(cr) in various NaCl concentrations at T = 22 and 80°C, under weakly alkaline pH condition.

2. Experimental

Batch-series solubility experiments were performed under ambient air condition. Well-characterized $Ca_2UO_2(CO_3)_3 \cdot 10H_2O$(cr) solid phase provided by Helmholtz-Zentrum Dresden-Rossendorf was equilibrated with ≈ 0.03, 0.51, and 5.61 m NaCl solutions for 132 days at two different temperatures of T = 22 ± 3 and 80 ± 5°C. The pH_m ($-\log m_{H^+}$) values were initially adjusted to be pH_m = 7.9 – 8.2 by using HCl/NaCl solutions. After reaching equilibrium, post-experimental analyses of the solid were performed by means of powder XRD, SEM-EDX, and chemical analysis digestion (ICP-MS/OES).

3. Results

The experiment results showed the clear presence of $Ca_2UO_2(CO_3)_3 \cdot 10H_2O$(cr) solid phase, controlling the solubility of U(VI) in ≈ 0.03, 0.51 m NaCl solutions at T = 22°C. However, notable transformation from the initial U(VI) solid phase to $Na_2CaUO_2(CO_3)_3 \cdot 6H_2O$(cr) (also known as andersonite) was observed for 5.61 m NaCl solution at T = 22°C, (based on the characteristic XRD patterns and quantitative chemical analysis by ICP-MS/OES). Similarly, dramatic changes in U(VI) solid phases were identified for all samples equilibrated at elevated temperature, indicating remarkable transformation of initial $Ca_2UO_2(CO_3)_3 \cdot 10H_2O$(cr) to $CaU_2O_7 \cdot 3H_2O$(cr) and/or $Na_2U_2O_7 \cdot H_2O$(cr) along with calcite.

As shown in Fig. 1, the solubility data presented significantly high U(VI) concentrations at [NaCl] ≤ 0.51 m at T = 22°C. The stoichiometric ratio of [Ca] : [U] ≈ 2 : 1 derived by ICP-MS/OES analysis supported the presence of $Ca_2UO_2(CO_3)_3 \cdot 10H_2O$(cr)

after the solubility experiments. On the other hand, relatively decreased concentrations of aqueous U(VI) were determined at [NaCl] = 5.61 m at T = 22°C, in accordance with the presence of transformed $Na_2CaUO_2(CO_3)_3 \cdot 6H_2O$(cr) based on the solid phase characterization after solubility experiments.

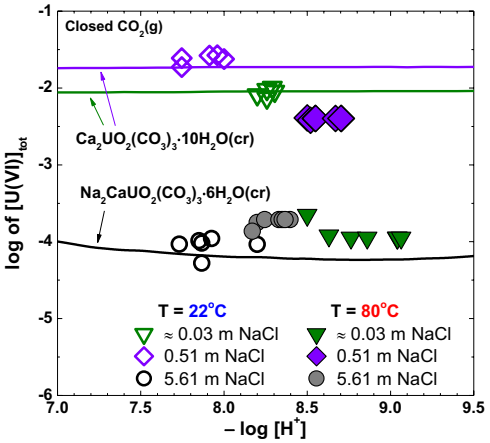

Fig. 1. Solubility of U(VI) observed at T = 22 and 80°C (symbols). Lines represent the calculated solubility at T = 25°C based on chemical thermodynamic data obtained in the present work and taken from the literatures [1,2].

In addition, remarkably changed solubility tendency was identified at T = 80°C, compared with that obtained at T = 22°C. Relatively shifted pH_m values towards further alkaline condition referred to the degassing of CO_2(g) driven by the elevated temperature. Considerably lower concentrations of U(VI) were measured for samples at [NaCl] ≤ 0.51 m at T = 80°C in comparison to analogous samples equilibrated at T = 22°C, complementally indicating the transformation of initial U(VI) solid phase.

The solubility results, quantitatively obtained in this work, and chemical thermodynamic data describing the formation of aqueous Ca-UO_2-CO_3 complexes [1] were employed to derive solubility products of $Ca_2UO_2(CO_3)_3 \cdot 10H_2O$(cr) and $Na_2CaUO_2(CO_3)_3 \cdot 6H_2O$(cr).

4. Conclusion

The stability and aqueous solubility of $Ca_2UO_2(CO_3)_3 \cdot 10H_2O$(cr) was investigated at various NaCl concentrations at T = 22 and 80°C. The experimental evidences and chemical thermodynamic data obtained in the present work provide better understating of chemical behavior of U(VI) in the context of geologic disposal of radioactive waste.

ACKNOWLEDGEMENT

The authors are indebted to Robin Steudtner and Vinzenz Brendler (HZDR–IRE) for providing and organizing the transportation of the liebigite utilized in this work. Ezgi Yalçıntaş (LANL), Melanie Böttle, Frank Geyer, Cornelia Walschburger, Stephanie Kraft, and Dieter Schild (all KIT–INE) are kindly acknowledged for their scientific and technical support. This work was partly supported by the German Ministry of Economic Affairs and Energy (BMWi) (EDUKEM project, contract no. 02E11334) and by the German Federal Ministry for Education and Research (BMBF) (ThermAc project, contract no. 02NUK039A)

REFERENCES

[1] J.-Y. Lee, et al., "Formation, stability and structural characterization of ternary $MgUO_2(CO_3)_3^{2-}$ and $Mg_2UO_2(CO_3)_3$(aq) complexes." Radiochimica Acta 105(3), 171-185 (2017).

[2] R. Guillaumont, et al., “Chemical Thermodynamics Vol. 5: Update on the Chemical Thermodynamics of Uranium, Neptunium, Plutonium, Americium and Technetium”, OECD-NEA (2003).

Luminescence Properties of U(VI) Surface Species on Amorphous Silica

Euo Chang Jung[1,*], Yongheum Jo[2], Tae-Hyeong Kim[1], Hee-Kyung Kim[1], Hye-Ryun Cho[1], Wansik Cha[1], Min Hoon Baik[1], and Jong-Il Yun[2]

[1]Korea Atomic Energy Research Institute, 111, Daedeok-daero 989beon-gil, Yuseong-gu, Daejeon, Republic of Korea

[2]Korea Advanced Institute of Science and Technology, 291, Daehak-ro, Yuseong-gu, Daejeon, Republic of Korea

[*]ecjung@kaeri.re.kr

1. Introduction

U(VI) (hexavalent uranium) in an aqueous solution is easily adsorbed onto solid surface under near neutral pH condition. Thus, the interactions of U(VI) with a variety of minerals have been widely studied to understand its migration behavior in groundwater system. The sorption characteristics of U(VI) onto SiO_2 surfaces were investigated at a molecular scale using several spectroscopic techniques, such as X-ray photoelectron spectroscopy, extended X-ray absorption fine structure spectroscopy, and time-resolved laser fluorescence spectroscopy (TRLFS). Among these techniques, TRLFS has received considerable attention because of its superior speciation sensitivity.

A lot of data on the luminescence characteristics (peak wavelengths in the spectrum and lifetimes of excited state) of U(VI) species adsorbed onto SiO_2 surface has been accumulated in literatures. However, the values of luminescence lifetimes of U(VI) surface species obtained by different groups differ significantly. Until now, the reason for these inconsistent luminescence lifetime values had not been clarified.

The objective of the present TRLFS study is to understand the origin of the inconsistent luminescence lifetime values of U(VI) species on SiO_2 surface reported in previous studies. We focus on the luminescence lifetimes of the U(VI) surface species which depend on the specific surface area (SSA) of SiO_2 samples and the incident laser pulse energy at UV wavelength. Other experimental parameters (aging effect of the sample and several instrumental parameters) are also examined.

2. Experimental Conditions

Four different SiO_2 powders are used in the present study. The first is a high-purity grade SiO_2 gel with a particle size of 40–63 μm (Sigma-Aldrich, 227196). The pore size of the SiO_2 gel is approximately 6 nm (0.8 cm^3/g pore volume) with a SSA of approximately 477 m^2/g. The second is hydrophilic fumed SiO_2 with a diameter of a few tens of nm (Evonik, Aerosil 200). It is a nonporous, amorphous material composed of spherical particles with a SSA of approximately 156 m^2/g. The third is a spherical SiO_2 powder with a particle size of 1.5 μm and a SSA of approximately 2 m^2/g (Alfa Aesar, L1698). The fourth is crystalline silica (α-quartz) with a particle size of approximately 5 μm and a SSA of approximately 7 m^2/g (U.S. Silica, Min-U-Sil 5).

All the sample preparations are performed in an Ar-conditioned glove box with continuous stirring. The desired pH conditions are achieved by adding known amounts of 0.1 M NaOH or $HClO_4$ determined from pre-titration processes. Samples are further equilibrated in a rotary shaker for two or more days, after which the pH of the samples is measured using a glass combination electrode (Orion™, Ross Ultra).

The luminescence intensities were measured using the kinetic mode of the intensified charge-coupled device with a gate delay time of 1 μs, a gate width of 1000 μs, and a gate delay step of 50 μs for the luminescence lifetime determination.

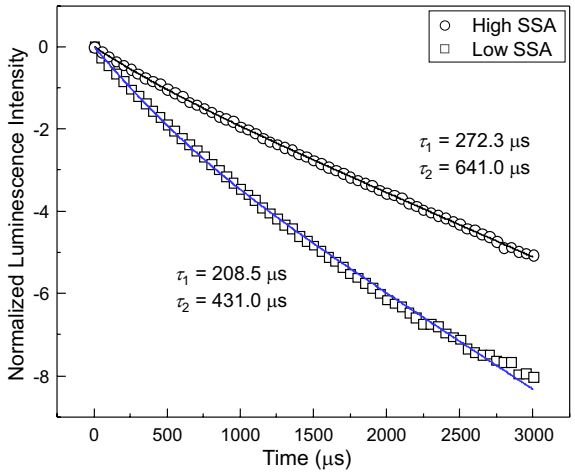

Fig. 1. Luminescence lifetimes measured from silica samples at pH 7.5. The luminescence lifetimes of the low SSA sample are shorter than those of the high SSA sample.

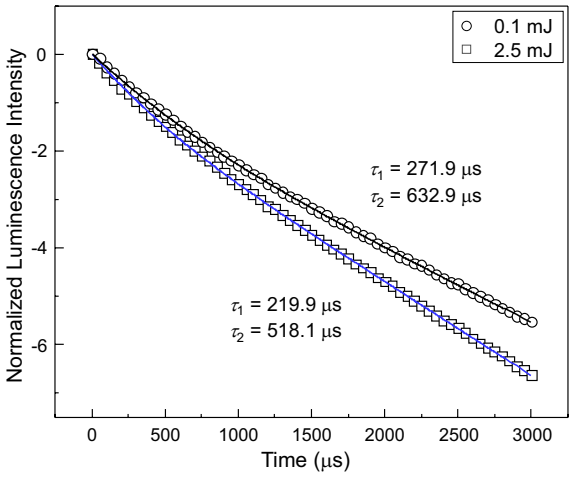

Fig. 2. Luminescence lifetimes measured from silica samples at pH 6.5. The luminescence lifetimes measured at 2.5 mJ are shorter than those measured at 0.1 mJ.

3. Results and Discussion

Fig. 1 shows luminescence lifetimes of U(VI) (concentration of 3.4 μM) measured from the low and high SSA SiO_2 samples at pH 7.5. The symbols depict the normalized luminescence intensities in the natural logarithmic scale. The solid lines represent the result of fitting the data to the double exponential decay equation. In Fig. 1, the luminescence lifetimes of the short- and long-lived species were determined to be τ_1 = 208.5 and τ_2 = 431.0 μs, respectively, for the low SSA sample (approximately 2 m^2/g). Whereas, the luminescence lifetimes were determined to be τ_1 = 272.3 and τ_2 = 641.0 μs, respectively, for the high SSA sample (approximately 477 m^2/g). The difference in the luminescence lifetime between the high and low SSA silica samples reflects that U(VI) species encounter a different distribution of surface sites.

Fig. 2 shows luminescence lifetimes of the high SSA silica sample at pH 6.5 measured using the weak and strong laser pulse energies. The luminescence lifetimes measured at a strong laser pulse energy (2.5 mJ) are clearly observed to have become shortened. The reason of this phenomenon seems to be related to the laser-induced reaction such as a laser-induced desorption of adsorbates and the excited states annihilation.

4. Conclusion

We observed the differences in the luminescence characteristics (both the luminescence spectra and lifetimes) of the U(VI) surface species between the high and low SSA silica samples. It means that the distribution of surface sites has an important influence on luminescence characteristics of adsorbed U(VI) species. It is also observed that laser irradiation with a strong pulse energy at UV wavelength triggers a laser-induced reaction which results in the change of the luminescence characteristics. These phenomena can be pointed out as the origin of the inconsistent luminescence lifetime values reported in previous studies.

Spectroscopic and Computational Studies on Am(III)-Dicarboxylate Complexes

H.–K. Kim[1,*], K. Jeong[2], H.–R. Cho[1], E. C. Jung[1], K. Kwak[3], and W. Cha[1]

[1] Korea Atomic Energy Research Institute, 111, Daedeok-daero 989beon-gil, Yuseong-gu, Daejeon, Republic of Korea

[2] Korea Military Academy, 574, Hwarang-ro, Nowon-gu, Seoul, Republic of Korea

[3] Korea University, 145, Anam-ro, Seongbuk-gu, Seoul, Republic of Korea

*hkim11@kaeri.re.kr

1. Introduction

The long-term safety assessment of the deep geological disposal of spent nuclear fuel requires a thorough understanding of the actinide chemistry in natural aquatic systems. Organic matter including humic acids in groundwater is one of the major components that increase the mobility of the actinides by a strong complexation with highly positively charged actinide ions [1]. Carboxylate in organic matters is a key functional group directly interacting with actinide ions, and small carboxylate ligands are abundant in aquatic systems. To understand the chemical interactions of organic carboxylate groups with Am(III), we investigated the Am(III) interactions with a series of alkyl dicarboxylate ligands with an increasing carbon chain length: oxalate (Ox), malonate (Mal), and succinate (Succ).

UV-Vis spectrophotometry coupled with liquid waveguide capillary cell (LWCC) and time-resolved laser fluorescence spectroscopy (TRLFS) were employed for monitoring the complex formation reactions. The speciation and formation constant of each complex estimated from the experimental results will be discussed in this presentation. Probable molecular structures of the complexes optimized through DFT calculations will also be discussed.

2. Experimental

2.1 Sample Preparations

^{241}Am was purified as described in our previous study [2]. Quantitative and qualitative analysis of the purified ^{241}Am were carried out by using liquid scintillation counting, gamma and alpha radiation spectrometry [2]. Sodium dicarboxylate solutions were prepared in 0.1 M $NaClO_4$ and pH was adjusted to be in the range of pH 6 – 6.3 by adding $HClO_4$. Am(III) solutions were also prepared in 0.1 M $NaClO_4$ and pH 6 – 6.3. Am(III)-dicarboxylate samples were prepared by adding dicarboxylate solutions into fixed volume of Am(III) solutions.

2.2 UV-Vis-LWCC and TRLFS

UV-Vis absorption spectra were measured by using Cary3 (Varian) coupled with a LWCC (WPI) with an optical path-length of 100 cm. Luminescence spectra were collected by TRLFS equipped with a nanosecond pulsed laser (OPO, Vibrant B, OPOTEK Inc.) as an excitation source (503 – 507 nm, ~3.5 mJ), a spectrograph (SR-303i, Andor Technol.), and an intensified CCD (ICCD, iStar, Andor Technol.). All the measurements were carried out at 25℃. Absorption spectra were deconvoluted to individual spectra by using the HypSpec program.

3. Results and Discussion

Absorption and luminescence spectral shifts towards the longer wavelength direction were observed as the concentrations of the ligands increased. Fig. 1 shows a representative spectral changes of Am(III) upon reaction with Ox as an example. Ligand-dependent molar absorption

coefficient changes and formation constants changes were investigated. Speciation of each complex was conducted by deconvolution of the absorption spectra. Formation constants obtained from the deconvolution processes are in good agreements with those estimated in the NEA-TDB review [3].

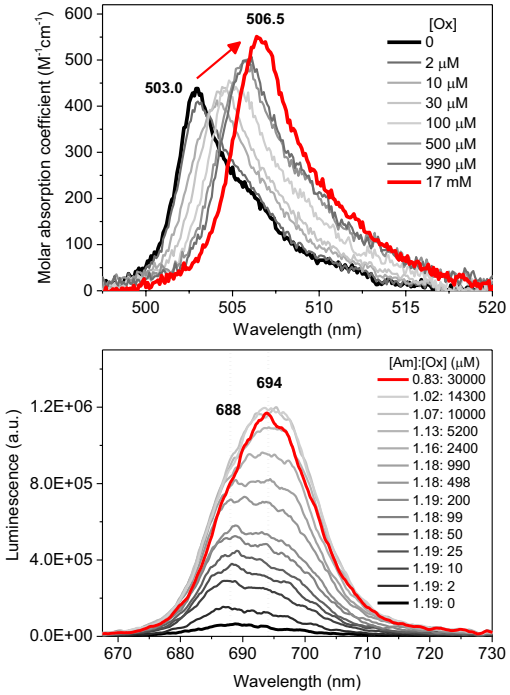

Fig. 1. Absorption (upper) and luminescence (bottom) spectra of Am(III) in the presence of various Ox concentrations. Concentrations of the Am(III) and Ox varied between 1.19 – 0.83 μM and 0 – 30 mM, respectively.

Luminescence spectra of Am(III) in the presence of the each ligand exhibited significantly enhanced intensities with prolonged lifetimes. Am(III)-Ox complexes induced the most pronounced changes in the absorption and luminescence spectral properties followed by the Mal and Suc ligands in the order. Luminescence lifetime changes measured by TRLFS suggest that the examined dicarboxylic ligands bind to Am(III) via a bidentate binding mode. Optimized structures by DFT calculations further suggest side-on bidentate bindings of the ligands that are stabilized by forming 5, 6, and 7-membered rings for the Ox, Mal, and Suc ligands, respectively.

In this presentation, we will discuss on the detailed spectral property changes of Am(III) and strength of chelating effects by the two carboxylic groups depending on the distance between them. The results will also be discussed in comparisons to those reported for Eu(III) and Cm(III) complexes with the aliphatic dicaboxylate ligands [4,5].

REFERENCES

[1] McCarthy JF, Sanford WE, Stafford PL: "Lanthanide Field Tracers Demonstrate Enhanced Transport of Transuranic Radionuclides by Natural Organic Matter". *Environmental Science & Technology*, 32:3901-3906 (1998).

[2] Kim H-K, Cho H-R, Jung EC, Cha W: "Radioanalytical and spectroscopic characterizations of hydroxo- and oxalato-Am(III) complexes". *Journal of Nuclear Fuel Cycle and Waste Technology* 16:397-410 (2018).

[3] Hummel W, Anderegg G, Rao L, Puigdomenech I, Tochiyama O: *Chemical thermodynamics Vol. 9: Chemical thermodynamics of compounds and complexes of U, Np, Pu, Am, Tc, Se, Ni and Zr with selected organic ligands*. Amsterdam, The Netherlands: Elsevier 2005.

[4] Wang Z-M, van de Burgt LJ, Choppin GR: "Spectroscopic study of lanthanide(III) complexes with aliphatic dicarboxylic acids". *Inorganica Chimica Acta*, 310:248-256 (2000).

[5] Fröehlich DR, Trumm M, Skerencak-Frech A, Panak PJ: "The complexation of Cm(III) with succinate studied by time-resolved laser fluorescence spectroscopy and quantum chemical calculations". *Inorganic Chemistry*, 55:4504-4511 (2016).

Performance of Mullite as Reference Electrode Membrane During the Electrochemical Reduction and Electrorefining Process

Seokjoo Yoon, Dokyu Kang, and Sungyeol Choi*

Korea Advanced Institute of Science and Technology, 291, Daehak-ro, Yuseong-gu, Daejeon, Republic of Korea

*sungyeolchoi@kaist.ac.kr

1. Introduction

The purpose of this paper was to investigate the performance of mullite as the reference electrode membrane for the electrochemical reduction and electrorefining processes. The comparison of reproducibility and the potential stability was made against the pyrex[1] and quartz[2] membrane, which are widely used as the reference electrode membrane for high temperature electrolytes. Also, the mullite membrane was tested using different concentrations of reference electrode solutions, which is composed of AgCl in LiCl-KCl eutectic.

2. Experimental Setup

2.1 Reference Electrode Setup

The silver wire and the reference electrode solution enclosed in the membrane was utilized as the reference electrode. LiCl-KCl eutectic was chosen as an electrolyte, since it is widely used in the electrorefining processes. The concentrations of reference electrode solution were 1wt%, 1.6wt% and 1mol%(2.5wt%).

2.2 Experimental Setup

The experiments are carried under Argon (99.99%) environment with moisture and oxygen level kept around 1ppm. The furnace which can go up to 900°C and potentiostat which can provide voltage from -4 to 4V and current range up to 20A are utilized in this experiment to measure the electrochemical data.

2.3 Experiments

To test the reproducibility of the reference electrodes, the open circuit potential between the two reference electrodes with same membranes was measured. In this experiment, 1wt% of reference electrode solution was used. After this process, the potential difference of the mullite membrane with different concentrations of reference electrode solution was measured against the tungsten wire.

3. Results and Discussion

3.1 The reproducibility of the Reference Electrodes

The open circuit potential of the two reference electrodes with same membranes are shown in Table 1. The potential difference of the mullite membrane decreased with increasing temperature. In contrast, the pyrex membrane showed increasing potential values with increasing temperature, and the quartz membrane showed much higher potential difference than the other two membranes.

Table 1. The Potential Difference of the two Reference Electrodes with Same Membrane Material

	Mullite	Pyrex	Quartz
500C	103mV	49mV	283mV
650C	68mV	62mV	285mV
800C	26mV	71mV	97mV

3.2 Reference Electrodes With Different Concentrations of AgCl in LiCl-KCl Solution

The potential differences of the reference electrodes with different concentrations of AgCl in LiCl-KCl eutectic are given in Fig. 1. The potential difference between different concentrations of reference electrode solution was in the range of the results from Table 1, which shows that the effect of the concentration of AgCl can be considered negligible.

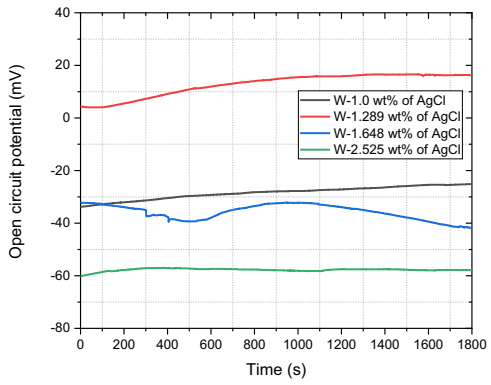

Fig. 1. The Potential Difference of the Two Reference Electrodes with Different Concentrations of Reference Electrode Solution.

4. Conclusion

The performance of the mullite as the reference electrode membrane was tested in different conditions for the electrochemical reduction and electrorefining processes. The potential difference of the two reference electrodes with mullite membranes may imply that the mullite might be suitable as the reference electrode membrane at higher temperatures.

ACKNOWLEDGEMENT

This work was supported by the National Research Foundation of Korea (NRF) funded by the Ministry of Science and ICT (The grant number: NRF-2016M2B2B1945249).

REFERENCES

[1] Ling Yang, Robert G. Hudson, Some Investigations of the Ag/AgCl in LiCl-KCl Eutectic Reference Electrode, Journal of the Electrochemical Society, November 1959, 986-990.

[2] Pei Gao, Xianbo Jin, Dihua Wang, Xiaohong Hu, George Z. Chen, A quartz sealed Ag/AgCl reference electrode for CaCl2 based molten salts, Journal of Electroanalytical Chemistry, 579 (2005) 321-328.

[3] Han Wang, Nancy J. Siambun, Linpo Yu, George Z. Chen, A Robust Alumina Membrane Reference Electrode for High Temperature Molten Salts, Journal of The Electrochemical Society, 159 (2012) 740-746.

Desorption of α, β, and γ Emitting Nuclides in the Mixed Ion-Exchange Resin Using High-Performance Microwave Digestion System

Kwang-Soon Choi*, Jae-seok Lee, Simon Oh, and Tae-Hong Park
Korea Atomic Energy Research Institute, 111, Daedeok-daero 989beon-gil, Yuseong-gu, Daejeon, Republic of Korea
*nkschoi@kaeri.re.kr

1. Introduction

A cave repository in Korea has been operated to permanently dispose the radioactive wastes generated from nuclear power plants. To take over radioactive waste in the repository, > 95 % of the total activity in a drum should be accounted for based on the radioactive waste acceptance criteria specified by nuclear safety and security commission (NSSC) [1]. And activity concentration (Bq/g) of 13 nuclides, such as ^{14}C, ^{144}Ce, $^{58,60}Co$, ^{137}Cs, ^{55}Fe, ^{3}H, ^{129}I, $^{59,63}Ni$, ^{94}Nb, ^{90}Sr, ^{99}Tc, and total alpha activity should be identified.

Thirteen nuclides and alpha emitting nuclide are divided into two groups, volatile and nonvolatile nuclide. The identical solution was used to measure radioactivity of nonvolatile nuclide such as ^{144}Ce, $^{58,60}Co$, ^{137}Cs, ^{55}Fe, $^{59,63}Ni$, ^{94}Nb, ^{90}Sr, ^{99}Tc, and alpha emitting nuclide. To evaluate the radioactivity of nuclides in the spent ion exchange resin, it is necessary to make a solution where the nuclides are dissolved. We herein study desorption of mixed ion exchange resin using a high-performance microwave digestion system (HP-MDS) and a dry ashing method.

2. Experiments

2.1 Adsorption Tests

One gram of inactive mixed (anion and cation) ion exchange resin was weighed using a weighing plastic dish. It was transferred to a centrifuge tube and 20 mL of distilled and demineralized water (DDW) was added. Nine elements (Ce, Co, Cs, Fe, Nb, Ni, Re, Sr and U) were added to the tube. The amount of element added was as follows; (1) 1 mg of Ce, Co, Ni, (2) 2 mg of Fe, Nb, Re, Sr, (3) 0.1 mg of Cs, (4) 0.2 mg of U. After 1 day passed, the supernatant was separated from the mixed ion exchange resin using a Whatman No 42 filter paper. The amount of adsorbed 9 elements was calculated after the measurement of element in the supernatant using ICP-AES and ICP-MS.

2.2 Desorption Tests Using a High-Performance Microwave Digestion System

To desorb the adsorbed element in the mixed ion exchange resin using an HP-MDS, three kinds of mixed acid was tested as follows; (1) 7 mL of conc. HNO_3 and conc. HCl plus 0.25 mL of conc. HF, (2) 10 mL of conc. HNO_3 plus 4 mL of conc. HCl plus 0.25 mL of conc. HF, (3) 10 mL of conc. HNO_3 plus 3 mL of H_2O_2 plus 1 mL of conc. HCl plus 0.25 mL of conc. HF. The operating conditions of an HP-MDS are shown in Table 1.

Table 1. Operating conditions of an HP-MDS

Step	Power (W)	Time (min)
1	290	5
2	400	10
3	300	20
4	250	10

The amount of desorbed 9 elements in the obtained solution was measured using ICP-AES and ICP-MS.

2.3 Dry ashing pretreatment

After desorption of the adsorbed 9 elements in the

mixed ion exchange resin using an HP-MDS [2], the mixed ion exchange resin used was transferred to a Pyrex beaker and heated till 450 ℃ to make sure that Ce remains in the ion exchange resin. To dissolve the ash produced using an HP-MDS, conc. HNO_3 (4 mL), H_2O_2 (1x3 mL), conc. HCl (1 mL) was added to the beaker and it was transferred to a microwave digestion (MD) vessel including conc. HF (0.25 mL). The beaker was washed with conc. HNO_3 (2x3 mL) and the washed solution was transferred to the MD vessel. Following the operation of an HP-MDS, the contents of 9 elements in the ash were measured using ICP-AES and ICP-MS.

3. Results & Discussion

The recovery of Fe was not largely differed between 4 M HCl and 10 M HCl using an HP-MDS, although the distribution coefficient of Fe in cation ion exchange resin with 3.5 M HCl is minimum value. Eight elements except Ce, as shown Table 2, were quantitatively recovered using an HP-MDS in the mixture of conc. HNO_3 (7 mL)-4 M HCl (7 mL)-conc. HF (0.25 mL). However, the Ce in the mixed ion exchange resin adsorbed was not quantitatively desorbed irrespective of the heating time of an HP-MDS and the amount of HNO_3 and HCl, respectively. In addition, following two operations of an HP-MDS, it was confirmed that there was Ce in the ash produced.

Thus, to increase the Ce recovery, H_2O_2 as an oxidizing agent was added to a microwave digestion vessel, and an HP-MDS was operated in the mixture of conc. HNO_3 (10 mL)-H_2O_2 (3x1 mL)-conc. HCl (1 mL)-conc. HF (0.25 mL). It was found that Ce, Co, Cs, Fe, Nb, Ni, Re, Sr and U elements were quantitatively recovered. The recovery of Ce was increased from 64.0 % to 92.4 % using an HP-MDS in the mixture of HNO_3-H_2O_2-HCl-HF. It is very important to add H_2O_2 in three times (3x1 mL) to prevent the solution from overflowing.

Table 2. Recovery of 9 elements using an HP-MDS

Element	Recovery (%)	Element	Recovery (%)
Ce	57.2	Ni	102.0
Co	100.2	Re	85.0
Cs	97.3	Sr	95.7
Fe	96.8	U	87.0
Nb	97.0		

4. Conclusions

We developed a pretreatment procedure for the measurement of radioactivity in mixed ion exchange resin radioactive waste samples. The ICP-AES and ICP-MS analytical results showed that 9 elements were quantitatively recovered in mixed ion exchange resin with a mixture of HNO_3-H_2O_2-HCl-HF using an HP-MDS. This procedure will be applied to pre-treatment of radioactive ion exchange resin samples to measure α, β, and γ ray-emitting nuclides.

REFERENCES

[1] Notice No. 2017-60 of the Nuclear Safety and Security Commission (NSSC) (2017).

[2] Fiona L., Lian Z., “Microwave digestion for the quantification of inorganic elements in coal and coal ash using ICP-OES”, Talanta, 101 346-352 (2012).

Feasibility Study on Hydrogen Isotope Exchange Reaction by Ultraviolet Light

JiEun Yang[1,3], TaeJun Kim[2], Minsik Kim[2,3], and Jei-Won Yeon[3,*]

[1]Chungnam National University, 99, Daehak-ro, Yuseong-gu, Daejeon, Republic of Korea

[2] University of Science & Technology, 217 Gajeong-Ro, Yuseong-gu, Daejeon, Republic of Korea

[3] Korea Atomic Energy Research Institute, 111, Daedeok-daero 989beon-gil, Yuseong-gu, Daejeon, Republic of Korea

[*]yeonysy@kaeri.re.kr

1. Introduction

The methods of tritiated wastewater treatment, which has been studied so far, are composed of a combined process of electrochemistry, catalyst, metal materials, and laser technology [1]. Among them, hydrogen isotope exchange reaction has been known an efficient method for treating tritiated wastewater [2-3]. For this reason, most of study has been mainly directed toward increasing the efficiency of hydrogen isotope exchange. Until now, the most economical separation method for the tritium is known to be the liquid catalytic exchange reaction. However, since this method has to be operated at high temperature (> 80^{o}C) and to be carried out under deaerated condition, it needs lots of energy and complicated system for the treatment of tritiated wastewater.

In present work, we analyzed the principle of the liquid catalytic exchange reaction and then modified it as introducing UV light instead of platinum catalyst. This article mentions about the feasibility of this modified technique.

2. Feasibility of Hydrogen Isotope Exchange Under Ultraviolet Light Conditions

2.1 Experimental

The experimental equipment for the hydrogen isotope exchange reaction consists of a reaction vessel, UVC lamps (254 nm, 24 W × 2), and a hydrogen gas (H_2) supply unit. The basic configuration of the experiment is shown in Fig. 1.

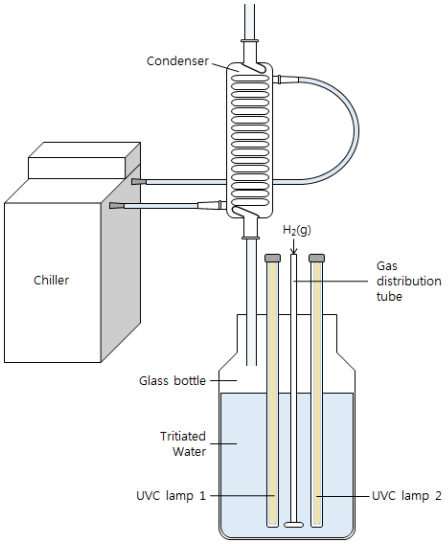

Fig. 1. Experiment system of UV-based the hydrogen exchange reaction.

The tritium radioactivity of the solution used for the experiment was in the range of 300 - 500 Bq·g^{-1}. Hydrogen gas (99.999 vol%) was supplied to the bottom of the solution with 200 mL·min^{-1} of the flow rate.

2.2 Results

The experiments were conducted to confirm the hydrogen isotope exchange reaction between hydrogen in water molecules and gaseous hydrogen atoms under UV light conditions. Under non-irradiated condition, only the hydrogen gas was

supplied in the solution. Table 1 shows the comparison of the reduction of tritium radioactivity with and without UV light. Without UV light, the tritium radioactivity little changed after supplying hydrogen gas. With UV light, the radioactivity decreased significantly after supplying hydrogen gas.

Table 1. Reduction of tritium radioactivity in the solution at the room temperature

Reaction time (h)	w/o UV (Bq/g)	with UV (Bq/g)
0	452.13	403.42
3	451.99	401.75
6	450.97	398.63

At our experimental condition, as UV light and hydrogen gas supply conditions are constant, the isotope exchange reaction may follow the first order reaction rate as follow:

$$\ln \frac{[C_a]}{[C_{a0}]} = -kt \qquad (1)$$

Where, C_a is the tritium concentration at time t, C_{a0} is the initial concentration of tritium, k is the reaction rate constant, and t is reaction time.

Using the equation 1, we plotted the data denoted in Table 1 as shown in Fig. 2. We confirmed that the decrease of radioactivity follows the first order reaction rate under UV light condition. And the reaction rate was calculated to be 0.0038 $Bq \cdot g^{-1} \cdot h^{-1}$. The results indicates that the hydrogen isotope exchange reaction is feasible under UV light condition.

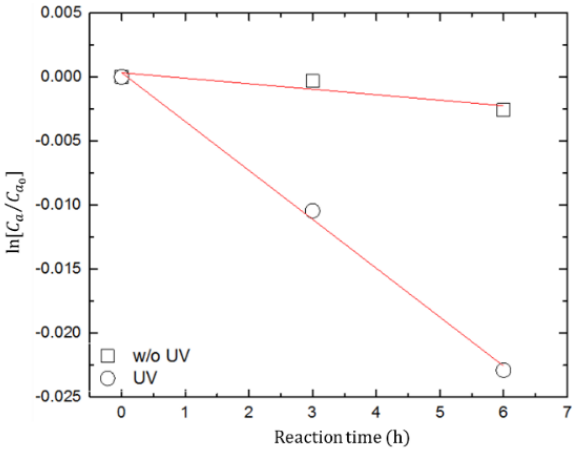

Fig. 2. Relationship between $\ln[C_a/C_{a0}]$ and reaction time with and without UV light.

3. Conclusion

The feasibility experiments of hydrogen isotope exchange reaction were carried out under UV light conditions. With UV light, the decrease of tritium radioactivity follows the first order reaction rate. The reaction rate was calculated to be 0.0038 $Bq \cdot g^{-1} \cdot h^{-1}$. We confirmed that the hydrogen isotope exchange reaction could be possible by UV light.

REFERENCES

[1] W.L. Allen, “Tritiated Wastewater Treatment and Disposal Evaluation for 1995”, U.S. Dept. of Energy, DOE/RL-95-68 (1995).

[2] J.P. Butler et al., “Novel catalysis for Isotope Exchange between hydrogen and Ligand Water”, ACS Symp. Series No.68, 110 (1978).

[3] G. Vasaru, “Tritium Isotope Separation”, CRC Press (1993).

7분과

방사화학 (Poster)

Use of Macroporous Resin to Reduce Released Corrosion Products During Shutdown Evolution

Jinsoo Choi, Kahee Jeong, and Wook Sohn
KHNP Central Research Institute, 70, Yuseong-daero 1312beon-gil, Yuseong-gu, Daejeon, Republic of Korea
jinsoochoi@khnp.co.kr

1. Introduction

During refueling outages of PWRs, the shutdown evolutions are performed to reduce corrosion products from the primary coolant water by controlling chemistry environments for the integrity of fuel performance. During the shutdown evolutions, the corrosion products, which are released from fuel and system surfaces, are removed by resin and filters at Chemistry and Volume Control System (CVCS). Recently, significant increases in activity releases have occurred during several PWRs shutdown evolutions as a result of changes in fuel duty, particularly excessive subcooled nucleate boiling, increases in cycle length and replacement of steam generators. The removal of activated corrosion products such as ^{58}Co and ^{60}Co which are released after hydrogen peroxide addition has been challenges for meeting cleanup limits for the corrosion products among PWRs, especially particles of less than 0.45 micro meter whose concentration is 2~5%.

For this reason, more than 33 PWRs in the world started using macroporous resins to improve the removal efficiency. Macroporous resins are known for their effective removal of micro particles by static electricity. Therefore, domestic Plant A applied a macroporous resin to increase the removal of micro insoluble corrosion products during shutdown evolutions. In this paper, we give preliminary results for effects of using macroporus resin at Plant A.

2. Materials and Methods

Macroporous resins are strong exchange resin with large pores which can capture effectively fine particulates associated with metal oxides. Plant A used a macroporous-type Purolite® NRW5070 during refueling outage (RFO) 20 and 21.

The macroporous resin of 100 L was added with the mixed resin of 700 L into the CVCS resin beds (800 L) before shutdown, as can be seen from Fig. 1. We added macroporous resin at the top of mixed resin and newly filled ion exchange resin bed was used during shutdown evolutions.

Table 1. Purolite® NRW5070 Information

Items	Contents
Total Capacity	1.0 eq/l (OH- form)
Moisture Retention	50 - 55 % (Cl- form)
Particle Size Range	425 - 1200 μm
Uniformity Coefficient (max.)	1.7
Conversion (min.)	95% (OH- form)

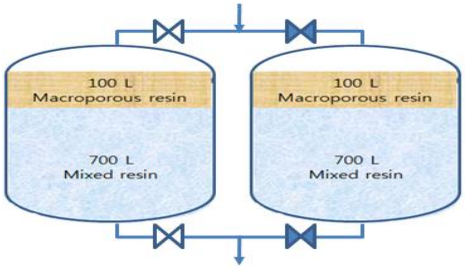

Fig. 1. CVCS resin bed loading.

After peroxide addition, the RCS purification was started following ^{58}Co peak detection. The clean-up continued with the purification flow rate of 20~28 m^3/hr until reaching 24 hour cleanup or ^{58}Co concentration peak being less than 3.7E+4 Bq/g..

The key corrosion products (^{58}Co and ^{60}Co) were monitored to evaluate the total release of corrosion products by using HPGe (CAMBERRA, DSA1000). The corrosion product parameters and monitoring frequencies during shutdown are shown in Table 2.

Table 2. Monitored Primary Water Parameters

Parameters	Minimum Sample Frequency
^{58}Co (without filtering)	Every 4 hours
^{60}Co (without filtering)	Every 4 hours

3. Results and Discussions

During shutdown evolutions in RFO 19~21, hydrogen peroxide of 25 ~ 45 kg was added to produce acid oxidizing conditions which solubilizes corrosion products such as radiocobalts. Fig. 2 shows that ^{58}Co release trends during shutdown evolutions during the RFOs. ^{58}Co release shows a steep increase following peroxide addition until reaching its peaks. After the peaks, ^{58}Co concentration decreased during the following clean-up by filters and ion exchangers at CVCS.

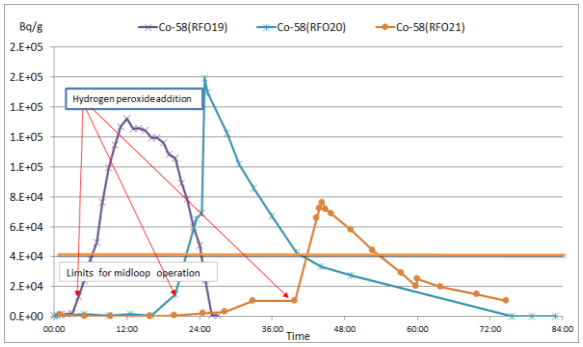

Fig. 2. ^{58}Co trends during shutdown chemistry for RFO 19~21.

^{60}Co concentration also showed a similar trend as observed for ^{58}Co after hydrogen peroxide addition as in Fig. 3. Especially, ^{60}Co activity at RFO19 is higher than at RFOs 20 and 21 where the macroporous resin was applied, showing that ^{60}Co activity is effectively removed by the macroporous resin. As for ^{60}Co purification trends, ^{60}Co's activity behavior is similar to ^{58}Co after ^{58}Co peak. These results shows that ^{60}Co micro-particles were removed effectively by macroporous resin at Plant A.

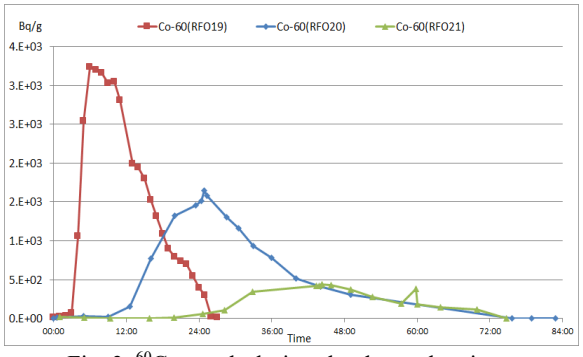

Fig. 3. ^{60}Co trends during shutdown chemistry for RFO 19~21.

Fig. 4 shows purification periods after hydrogen peroxide addition. At RFO 20 and 21 using macroporous resin, the clean-up took 19 and 13 hours which are shorter than 22 hours of RFO 19. Moreover, ^{58}Co concentration at RFO 20 and 21 was significantly lower than that of RFO 19. Although cleanup were not effective at low ^{58}Co concentration because micro particles mostly affect the RCS activity at that time, ^{58}Co concentration was lowered effectively at RFOs 19 and 20 by using macroporous resin.

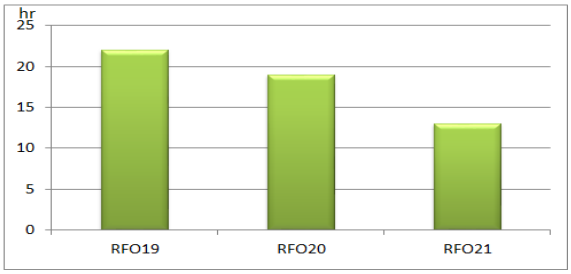

Fig. 4. Purification Time after ^{58}Co peak.

4. Conclusion

Macroporous resin was applied at Plant A to remove micro particles which are not readily captured by filters resulting in problems of RCS purification. During shutdown evolutions at RFO 20 and 21, macroporous resin was applied as CVCS demineralizers. As results, cleanup periods which were needed for meeting cleanup limit (3.7E+4 Bq/g) were reduced by 15~51%.

Therefore, it was found that macroporous resin is an effective method to capture the micro particles at primary coolant water in PWRs thus thereby contributing to the reduction of cleanup time and RCS activity during shutdown evolutions.

REFERENCES

[1] PWR Primary Water Chemistry Guidelines, Rev. 6. EPRI, Palo Alto, CA:2007, TR-1014986.

[2] Benchmarking Shutdown Chemistry Control Recommendations in the Pressurized Water Reactor Primary Water Chemistry Guidelines. EPRI, Palo Alto, CA:2006, TR-10117803.

[3] Shutdown and startup Chemistry Guidelines, KHNP, 2013.

[4] Hanbit-1 Shutdown and startup report, KHNP, 2009~2013.

[5] Material Safety Data Sheet of NRW5070, Puriolite, 2012.

Study on Cell Design of Electrorefining Process for Decontamination Using Molten Salt

Jungho Hur, Gwan Yoon Jeong, Younghwan Jeon, Hyeongjin Byeon, and Jaeyoung Park*
Ulsan National Institute of Science and Technology, 50, UNIST-gil, Eonyang-eup, Ulju-gun, Ulsan, Republic of Korea
*jypark@unist.ac.kr

1. Introduction

Lab-scale electrorefining experiments have been conducted to investigate decontamination capability of electrorefining using molten salt [1]. Electrochemical cells have a simple design which is composed of three electrode systems, electrolyte and quartz cell. If the electrorefining process is scaled up to engineering scale or commercial scale, rotating electrode or stirring is essential for better ion transfer. Particle mixing problem in a cell will be more serious than lab-scale experiments. Particles which more reductive in the anode can drift in molten salt and some which are detached from the cathode can exist as well. The problem can affect recovery factor of cathode and purity of bulk salt which is important to the secondary waste issue. To relieve this problem, baskets for both electrodes were introduced into a cell. But there is an IR drop problem due to long diffusion path of ions in salt. Therefore, a porous basket design was suggested and impacts on IR drop and particle floating were studied.

2. 3-D Hydrodynamic modeling

2.1 ANSYS-CFX

ANSYS-CFX code is a software tool for high performance computational fluid dynamics. It has been broadly used for CFD and multiphysics applications such as simulating pumps, fans, compressors and so on. Electrorefining modeling can be also modeled as well [2].

2.2 Modeling Condition

To model electrorefining cell with rotating electrodes, several assumptions for simulation was set.

1) Rotating speed of Anode and Cathode: 5 rpm [3]
2) Current density: 100 mA/cm^2
3) Anode potential: 0 V vs. 1 wt. % Ag/AgCl
4) A diameter of particle: 1.0E-06 m
5) Particle tracking time: 2000 sec
6) Number and diameter of holes: 16 / 1 mm

3. Results

3.1 IR Drop

Anode potential keeps 0 V vs 1wt. % Ag/AgCl as set. Cathode potential drops from top to end because of increasing diffusion path from the anode to the cathode. The lowest electrical potential on cathode in a non-porous case was -2.87E-01 V. However, the potential is reduced from -2.87E-01 V to -1.35E-01 V when basket design with symmetrical 16 holes of 1 mm diameter is applied. The IR drop between anode and cathode become smaller by more than 2 times, as shown in Fig. 1 and Fig. 2.

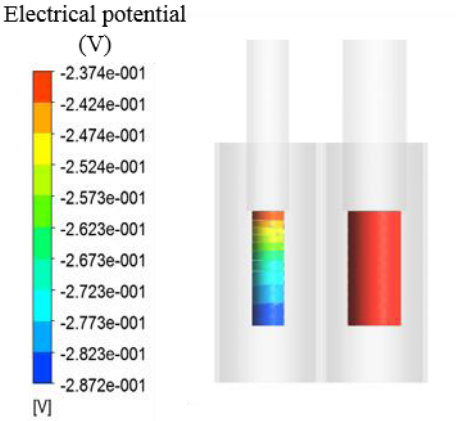

Fig. 1. IR drop simulation result with non-porous baskets.

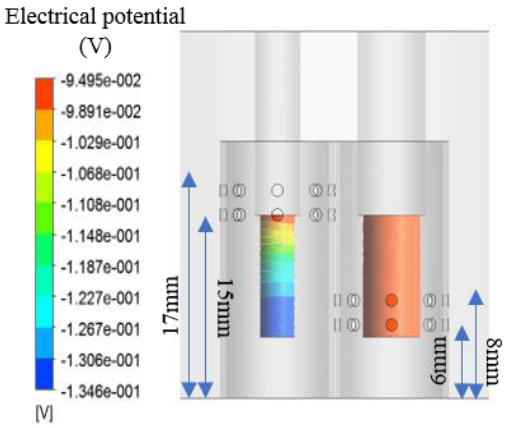

Fig. 2. IR drop simulation result with porous baskets.

3.2 Particle Tracking

A Velocity of electrolyte around electrodes and particle tracking path are shown in Fig. 3 and Fig. 4. Fastest velocity recorded in both cases is 1.34E-02 m/s. There was no escape of particles from the basket in non-porous design. They only drift inside anode basket and go under down part. It means that even if a particle falls out from the anode, it does not contaminate bulk salt in electrorefining cell. Side view and top view of the porous basket design model were shown in Fig. 4 for better understanding. Particles rarely came out from the anode basket through tiny holes in the porous design. Most particles in anode basket are staying at bottom and escaped particles are falling down because of flow. Additionally, no intrusion of particles into cathode basket is observed.

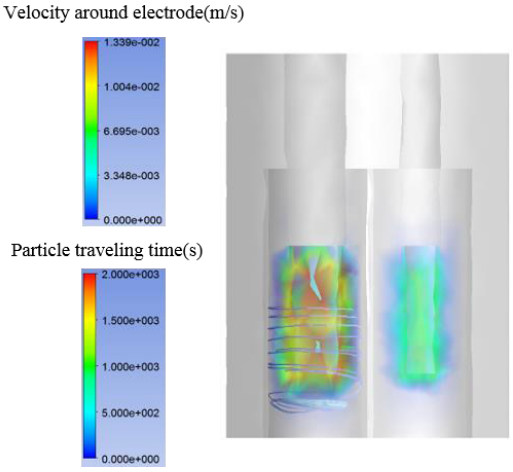

Fig. 3. Particle tracking simulation result with non-porous baskets.

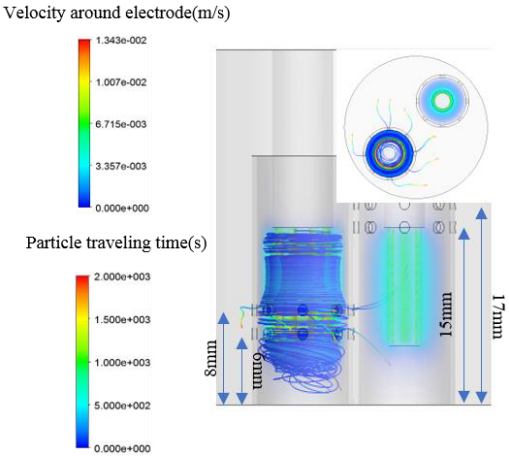

Fig. 4. Particle tracking simulation result with porous baskets.

4. Conclusion

Electrode baskets were introduced for collecting detached particle from both electrodes. However, they may cause a long diffusion path which makes large IR drop from the anode to the cathode. A porous basket was designed to reduce IR drop in the cell but it may occur the particle mixing problem which means contamination of electrolyte. Through 3-D hydrodynamic modeling code, ANSYS-CFX, it is shown that porous basket design can alleviate IR drop and there is possibility of no contamination and less IR drop effect by balancing the number and size of holes.

REFERENCES

[1] Jungho Hur, “Pyrochemical decontamination Process development for Volume Reduction of Intermediate Level Waste from PWR decommissioning”, Master’s dissertation, (2019).

[2] Jaeyeong Park, “Electrorefining of Irradiated Spent Nuclear Fuel Zircaloy-4 Cladding in LiCl-KCl Molten Salts”, Doctoral dissertation, (2014).

[3] Shelly X. Li, Thomas A. JOHNSON, Brian. R. WESTPHAL, Kenneth M. GOFF, and Robert W. BENEDICT, “Electrorefining Experience For Pyrochemical Processing Of Spent EBR-II Driver Fuel”, Proc. Of GLOBAL 2005, (487)1, Oct 9-13, 2005, Tsukuba, Japan.

Meso-scale Multi-physics Modeling of CRUD Layer With Water Radiolysis Reactions

Seungjin Seo[1], Byunggi Park[2], and Sungyeol Choi[1,*]

[1] Korea Advanced Institute of Science and Technology, 291, Daehak-ro, Yuseong-gu, Daejeon, Republic of Korea

[2] Soonchunhyang University, 22, Soonchunhyang-ro, Sinchang-myeon, Asan-si, Chungcheongnam-do, Republic of Korea

[*]sungyeolchoi@kaist.ac.kr

1. Introduction

During operation of nuclear power plant, axial shift of power distribution has occurred. CRUD (Chalk River Unidentified Deposit or Corrosion Related Unidentified Deposit) layer and boron hideout has been considered as one of the reason of the axial shift. Water radiolysis is one of main part within the CRUD layer due to its influence of chemical environment. This model treats the fully coupled multi-physics within the meso-scale CRUD layer by using COMSOL Multi-physics software for predicting the behavior of radiolysis products within the CRUD layer.

2. Method for Multi-physics Modeling

2.1 Geometry of Model

A meso-scale geometry of CRUD layer with uniform thickness and uniform porosity was used. The cell included the four boundary; cladding interface, coolant interface, steam chimney interface and symmetry line.

2.2 Each Physics Within CRUD Layer

In the CRUD layer, conductive heat transfer with evaporative heat on the surface of steam chimney considered. Due to evaporation, mass flux occurs on the surface of steam chimney, and to satisfy the mass conservation capillary flow occurs through the porous layer. Mass transport occurs by diffusion and convection due to the capillary flow. Numerous chemical reactions occurs within the layer during mass transport, and they act as source/sink term of species.

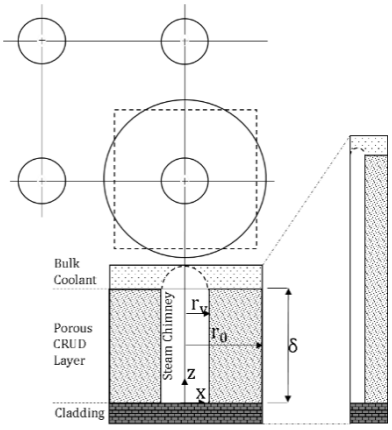

Fig. 1. Geometry of CRUD layer.

2.3 Water Radiolysis

During the radiolysis of water, the molecular products are produced by alpha particles and neutrons. Also, the radical products are produced by gamma rays. With the G-valued related with these phenomena and dose rate data, radiolysis reaction rate for thirteen radiolysis products are calculated. These products are also undergone the overall 37 recombination and decomposition reactions and some of them contributes on the chemical reactions as source/sink term of concentration distribution.

3. Results of Meso-scale CRUD Model

Radiolysis products undergo mass transport according to multi-physics. Especially, H^+, and OH^- quietly contributes on chemical reactions, so they have special distribution behavior within the CRUD layer, as shown in Fig. 2. H_2, O_2 undergo the partitioning volatilization on the surface of steam chimney, so their concentration near the surface of steam chimney is relatively low compared with CRUD layer.

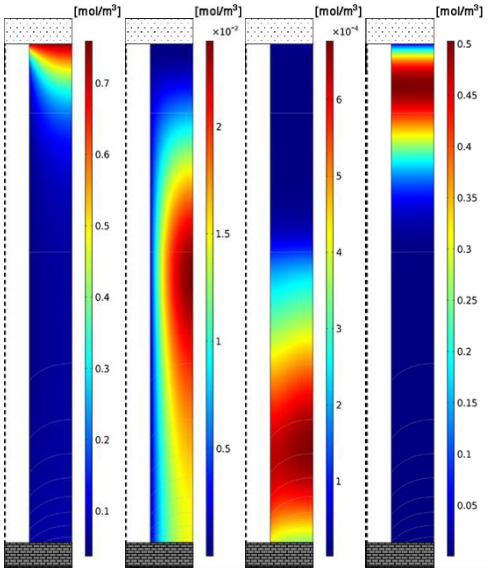

Fig. 2. Concentration distribution of H_2, O_2, H^+, and OH^-.

4. Conclusion

The behavior of radical and molecular products generated from radiolysis of water was analyzed by using meso-scale CRUD multi-physical model with COMSOL multi-physics software. Thirteen radiolysis products with 37 reactions are calculated with heat transfer, capillary flow, transport and five categories of chemical reactions.

REFERENCES

[1] J. Henshaw et al., “A model of chemistry and thermal hydraulics in PWR fuel crud deposits”, Journal of Nuclear Materials, 353(1), 1-11 (2006).

[2] J. Deshon, “PWR Axial Offset Anomaly (AOA) Guidelines, Revision 1”, EPRI, Palo Alto, CA, p. 1008102 (2004).

[3] S.J. Seo et al., “Meso-scale multi-physics full coupling within porous CRUD deposits on nuclear fuel”, Journal of Nuclear Materials, 512 100-117(2018).

[4] D.D. MacDonald et al., “A coupled environment model for stress corrosion cracking in sensitized type 304 stainless steel in LWR environments”, Corrosion Science, 32(1), 51-81 (1991).

[5] H. Christensen, “Fundamental Aspects of Water Coolant Radiolysis”, SKI, (2006).

Nonlinear Dynamic Partial Least Squares Modeling for Prediction of Strontium Concentrations in Underground Water (South Korea)

Jiseon Jang[1], Soon Il Ok[2], Jae-Yeol Cheong[1,*], and Dae Sung Lee[3,*]

[1]Korea Radioactive Waste Agency, 174, Gajeong-ro, Yuseong-gu, Daejeon, Republic of Korea

[2]Korea Radioactive Waste Agency, 19, Chunghyocheon-gil, Gyeongju-si, Gyeongsangbuk-do, Republic of Korea

[3]Kyungpook National University, 80, Daehak-ro, Buk-gu, Daegu, Republic of Korea

[*]jsjang@korad.or.kr, [*]daesung@knu.ac.kr

Strontium and its isotopes as effective tracers are monitored for characterizing geochemical behaviors in underground water. However, intrinsically complex and nonlinear dynamics of water variables and their interactions make it difficult in predicting strontium concentration in the system. Therefore, it is strongly necessary to develop a reliable model to predict the dynamic behaviors of strontium in underground water. In this study, different partial least square (PLS) models were combined with finite impulse response (FIR) and auto-regressive with exogenous (ARX) inputs to predict strontium concentrations in an underground water system. Initially, water quality monitoring variables in the underground water from 2010 to 2018 were analyzed using principal component analysis. Then the effectiveness of proposed PLS methods was evaluated by modeling strontium concentrations in the underground water. Neural network PLS with ARX inputs gave much improved prediction performance over the conventional linear PLS model and was successfully capable of predicting strontium dynamics in the underground water.

Keywords: Strontium and its isotopes, Principal component analysis, Partial Least Squares, Neural network, Dynamic behavior, Nonlinear system

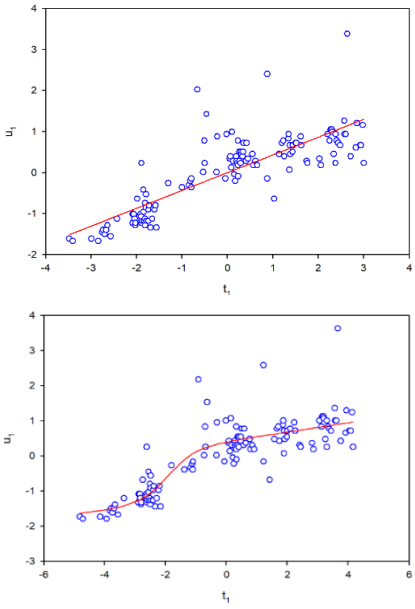

Fig. 1. Score plot of the first latent factor (linear PLS and nonlinear NNPLS).

REFERENCE

[1] D.S. Lee, P.A, Vanrolleghem, Biotechnol. Bioeng. 82, 489–497 (2003).

[2] Y. Wang, Q. Guo, C. Su, T. Ma, J. hydrol. 328, 592-603 (2006).

[3] E.L. Brinck, C.D. Frost, Groundwater. 45, 418-432 (2007).

[4] R.B. Goldberg, E.M. Griffith, J, Chin. Environ. Geosci. 24, 151-165 (2017).

Experimental Study on Mass Transfer of Lanthanide Ions During Reduction by Li Metal in Molten LiCl-KCl/Bi System

Jae Hong Yim, Beom Kyu Kim, Hwa Jeong Han, and Byung Gi Park*
Soonchunhyang University, 22, Soonchunhyang-ro, Sinchang-myeon, Asan-si, Chungcheongnam-do, Republic of Korea
*byunggi@sch.ac.kr

1. Introduction

In the molten salt-liquid metal extraction process, the rate of mass transfer through the interface plays an important role in the process design for group separation of elements. The exchange reaction of chemical species through the interface between the molten salt and the liquid metal, regardless of the characteristics of the apparatus in terms of mass transfer, can be divided into three steps, which are mass transfer by convection on the molten salt and liquid metal forming the interface, mass transfer by the diffusion of the species participating in the reaction through the boundary layer formed on both sides of the interface, and chemical reaction at the interface. Thus, the step of determining the reaction rate can be one of interfacial reaction, mass transfer by diffusion at the boundary layer, or mixing by convection at each phase. Since the molten salt-liquid metal extraction process is operated at a high temperature, it is assumed that the chemical reaction at the interface is usually very fast, so that it is predicted that mass transfer by convection or diffusion by diffusion in each phase will dominate the reaction rate.

2. Experimental

In order to observe the kinetics of exchange reaction in the LiCl-KCl/Bi system by using the Li reducing agent, a simple sampling method using test tubes was devised and prepared as shown in Fig. 1. In a glove box with controlled atmosphere, LiCl-KCl molten salt, lanthanide chloride, Bi metal, and Li metal were added to each test tube under the same conditions and heated at a high temperature, and the test tube was recovered and the concentrations were analyzed by ICP-AES. The Li reductant was prepared by using Bi-Li (10mol%) alloy, and the concentration of Li metal was controlled by adding Bi-Li alloy. The initial conditions were set so that the molar ratio of lanthanide chloride to lithium metal in the molten salt was 1:3. The masses used in the experiments for different types of lanthanide chloride are given in the table.

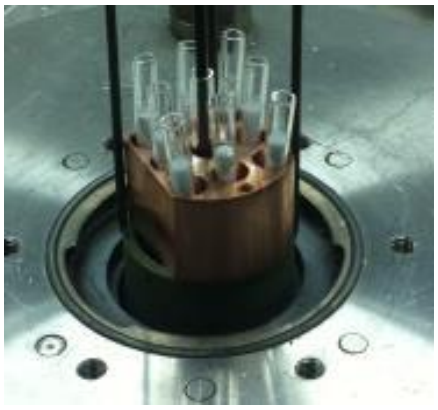

Fig. 1. Experimental setup for LiCl-KCl/Bi(Li) system.

3. Results and Discussion

The lanthanide chloride dissolved in the molten salt reacts with the Li metal dissolved in the Bi liquid metal as follows.

$$LnCl_n + nLi \leftrightarrow nLiCl + Ln \quad (1)$$

According to this reaction, the lanthanide elements in the molten salt are reduced to the Bi liquid metal. The concentration of the remaining lanthanide in the molten salt was measured and the concentration was calculated as a percentage of the initial amount of the lanthanide salt, which is listed in Table 1. As shown in Table 1, after the reduction of the lanthanide element by the Li reducing agent and the mass transfer on the molten salt proceeded very quickly, only a very small amount of lanthanide remained in the molten salt after 30 minutes passed respectively. As to each of the lanthanide elements, about 5.6% of La, about 1% of Ce, about 3.6% of Pr, about 3% of Nd and about 14% of Sm remain in the LiCl-KCl molten salt. According to this concentration change, the mass transfer rate of the lanthanide elements has the following order.

$$\mathrm{Ce} > \mathrm{Nd}{\sim}\mathrm{Pr} > \mathrm{La} > \mathrm{Sm} \quad (2)$$

Table 1. Lanthanide concentration in LiCl-KCl according to elapsed time

Time (hour)	La	Ce	Pr	Nd	Sm
0.5	5.56%	0.93%	3.59%	3.03%	13.60%
1	3.03%	1.00%	1.98%	2.30%	11.10%
1.5	1.69%	0.36%	0.40%	1.24%	11.38%
2	1.10%	1.61%	1.42%	0.90%	8.54%
3	1.39%	0.09%	1.34%	0.77%	5.75%
5	0.34%	0.28%	1.32%	0.41%	5.76%
7	0.21%	0.25%	0.15%	0.54%	5.38%
9	0.18%	1.71%	0.40%	0.26%	4.90%

The mass transfer coefficients were estimated using the concentration change after 30 minutes. Mass transfer coefficients were obtained by performing curve fitting on the concentration measurement data. Mass transfer coefficients of La, Ce, Pr, Nd, and Sm were to be estimated to 0.3854, 0.0006, 0.2338, 0.2468, and 0.1144, respectively.

4. Conclusion

In the molten salt - liquid metal extraction process, the rate of reduction of the lanthanide ion to the lithium reducing agent was measured. The reduction reaction was so rapid that within 90 minutes of initial lanthanide ions were reduced to liquid metal within 30 minutes and then the reaction rate was estimated according to the general linear diffusion theory. The mass transfer coefficient is the largest at 30 minutes after the start of the reaction, but the rate of reduction of cerium is estimated to be the fastest since cerium tends to be reduced to 99% or more within 30 minutes. Samarium has a relatively slow reaction rate and remains in the molten salt at a rate of about 5% even at a sufficient reaction time, which is considered to be a chemical species difficult to reduce to lithium reductant.

ACKNOWLEDGEMENT

This work was supported by a grant from the Nuclear R&D Program of the National Research Foundation of Korea funded by the Korean Ministry of Science and ICT (Grant codes: 2016M2B2B1945263).

Effect of Scavengers on Oxalic Acid Degradation Using Ionizing Radiation

Kang Lee[1,2], TaeHun Kim[1], JaeSon Kim[1], Seungjoo Lim[1], Joonpyo Jeun[1], and Seungho Yu[1,*]

[1] Korea Atomic Energy Research Institute, 29, Geumgu-gil, Jeongeup-si, Jeollabuk-do, Republic of Korea

[2] Korea University, 145, Anam-ro, Seongbuk-gu, Seoul, Republic of Korea

[*]yuse@kaeri.re.kr

1. Introduction

Organic acids such as oxalic acid, citric acid, and formic acid are commonly used as cleaning agents to remove metal scales [1].

Various studies are being conducted regarding the removal of organic acids used in advanced oxidation processes (AOPs) [2].

Highly reactive species such as •OH, •H, and e_{aq}^- can be generated to remove organic pollutants by water radiolysis using gamma radiation [3].

The objectives of this study were to demonstrate the radiolytic degradation of oxalic acid and to demonstrate the effect of radical scavengers on oxalic acid degradation using gamma radiation.

2. Materials and Methods

2.1 Materials and Sample Preparation

Oxalic acid, tert-butanol (BuOH), and 2-propanol (PrOH) were purchased from Sigma-Aldrich. All solutions were prepared with distilled water. The initial concentration of the oxalic acid was 20 mM. Radical scavengers (BuOH and PrOH) were added to the oxalic acid solution before irradiation.

2.2 Irradiation Sources

Gamma radiation was achieved using a high-level ^{60}CO source (Nordion Inc., Canada) at Korea Atomic Energy Research Institute (KAERI), Jeongeup, Rep. of Korea. Samples were irradiated at absorbed doses of 5 kGy to 50 kGy.

2.3 Analysis Methods

Oxalic acid was determined using high-performance liquid chromatography (HPLC), with a UV detector at a wavelength of 220 nm. Separation of oxalic acid was achieved using a Synergi 4 um Hydro-RP 80 Å (250 x 4.6 mm). The mobile phase comprised 20 mM potassium phosphate at a flow rate of 0.7 ml/min.

3. Results and Discussion

3.1 Radiolytic Degradation of Oxalic Acid

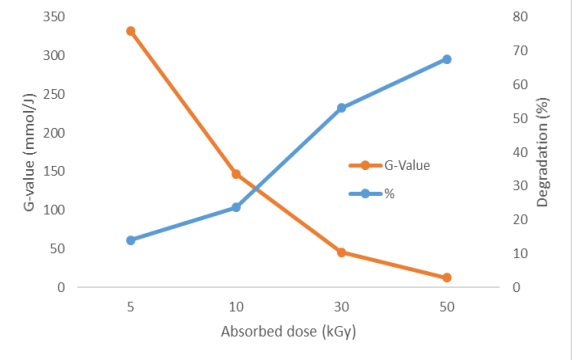

Fig. 1. The relationship between degradation efficiency (%) and G-value of oxalic acid using gamma radiation ([oxalic acid]$_0$ = 20 mM, pH = 2.5).

Fig. 1 shows a comparison between the degradation efficiency and the G-value of oxalic acid using gamma radiation. The degradation efficiency of

oxalic acid was 14, 24, 53, and 68 % for an absorbed dose of 5, 10, 30, and 50 kGy, respectively. The degradation efficiency of oxalic acid increased with an increase in the absorbed dose, whereas the G-value of oxalic acid decreased with an increase in the absorbed dose. In other words, the concentration of reactive radical species was decreased with increasing radical–radical recombination reactions.

3.2 Effect of Scavengers on Oxalic Acid Degradation

Fig. 2 shows the degradation of oxalic acid in the presence of scavengers using gamma radiation. Effective radicals were investigated for the radiolytic degradation of oxalic acid. The most active species were •OH, •H, and e_{aq}^- for organic compounds degradation.

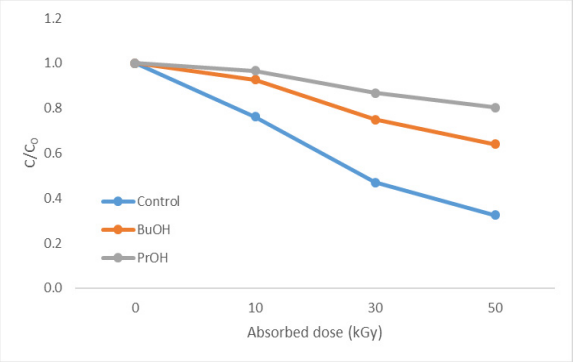

Fig. 2. Effect of scavengers on oxalic acid degradation using gamma radiation ($[oxalic\ acid]_0 = [BuOH]_0 = [PrOH]_0 = 20$ mM, pH = 2.5).

BuOH was used as a scavenger of •OH. Therefore, •H and e_{aq}^- play the dominant roles. PrOH can scavenge •OH and •H; thus, e_{aq}^- plays the superior role. As a result, the most active species for oxalic acid degradation is •OH.

4. Conclusion

The G-value of oxalic acid was inversely proportional to the dose constant, whereas the degradation efficiency was directly proportional to the dose constant. The predominant radical species for oxalic acid degradation were investigated. The radical species on oxalic acid degradation were as follows: •OH > •H > e_{aq}^-. Consequently, the most active radical species for oxalic acid degradation was identified as •OH.

REFERENCES

[1] Angel Hernandez Hernandez, R., et al., Statistical Treatment of Bleaching Kaolin by Iron Removal. Vol. 57. 2013. 261-266.

[2] AlSalka, Y., et al., Understanding the degradation pathways of oxalic acid in different photocatalytic systems: Towards simultaneous photocatalytic hydrogen evolution. Journal of Photochemistry and Photobiology A: Chemistry, 2018. 366: p. 81-90.

[3] Shah, N.S., et al., Synergistic effects of HSO5− in the gamma radiation driven process for the removal of chlorendic acid: A new alternative for water treatment. Chemical Engineering Journal, 2016. 306: p. 512-521.

A Study on the Pure Separation for Determination of Molybdenum Isotopes in a Simulated Fuel Solution

Jung Suk Kim*, Kyungwon Suh, Byungman Kang, Yang-Soon Park, and Yeong Keong Ha

Korea Atomic Energy Research Institute, 111, Daedeok-daero 989beon-gil, Yuseong-gu, Daejeon, Republic of Korea

*njskim1@kaeri.re.kr

1. Introduction

One of the important parameters required for the study of a nuclear fuel is its burnup, which is the number of fissions per 100 heavy nuclide atoms (mass ≥232) initially present in the fuel. The burnup of important fissile isotopes and the composition of an irradiated fuel depend on the nature of the fuel and on the conditions of an irradiation. A detailed knowledge of these quantities is useful for a reactor work as well as for the effective utilization of a nuclear fuel. Of the many stable nuclides formed in the fission, Some Mo isotopes (^{97}Mo, ^{98}Mo and ^{100}Mo) satisfied most of the necessary requirements for a burnup monitor as Nd, Cs and Ce monitor isotopes. U and Mo isotopes can be measured using isotope dilution mass spectrometric techniques (IDMS), and U and Mo elements can be also determined with by inductively coupled plasma atomic emission spectrometry (ICP-AES) [1-3].

The aim of the present work is to separate individually without the isobaric interferences the U and Mo from a simulated fuel solution by using anion exchange chromatographic techniques.

2. Experiments

2.1 Chemicals

The Certified ^{96}Mo (95.78 atom%) spikes was obtained from Oak Ridge National Laboratory (ORNL). This spike solution was prepared by dissolving its oxide in 8 M HNO_3-0.01 M HF. The concentration of the spike solution was determined by calibrating that with a standard solution and ICP-AES. The simulated fuel solution was prepared by mixing with the ^{96}Mo spike and fifteen standard solutions (Table 1). All standard solutions were obtained from AccuTrace and Spex Industries Inc.

Table 1. Compositions of a Solution Simulated for Irradiated Nuclear Fuel

Element	Quantity added (μg)	Remark
^{96}Mo	40	ORNL
U	100	Certified standard solution
Nd	40	
La	40	
Ce	40	
Pr	40	
Sm	40	
Eu	40	
Gd	40	
Sr	40	
Ba	40	
Zr	40	
Cs	40	
Ru	40	
Rh	40	
Pd	40	

2.2 Separation and Determination by ICP-AES

The separation procedure of the U and Mo from the simulated fuel solution was carried out by two analytical schemes. Analytical scheme-I was composed of the two-steps sequential anion exchange separations in media HCl and HNO_3 (Fig. 1). Analytical scheme-II was composed of the one-step sequential anion exchange separation in media HCl and HF. The concentrations of U, Mo, and Ru and Zr, which are considered as the isobaric elements in the separated solutions were determined using a ICP-AES (Jobin Yvon).

3. Results & Discussion

3.1 Determination of Mo and U by ICP-AES

Table 2 shows the concentrations of Mo and U

sepatated from the simulated fuel solution sample by the analytical scheme-I. The U was separated purely without interference of Mo, which is appeared the similar anion exchange behavior in HCl solution. The Mo was separated purely without the interference of the isobaric elements, Ru and Zr through two-steps anion exchange separations.

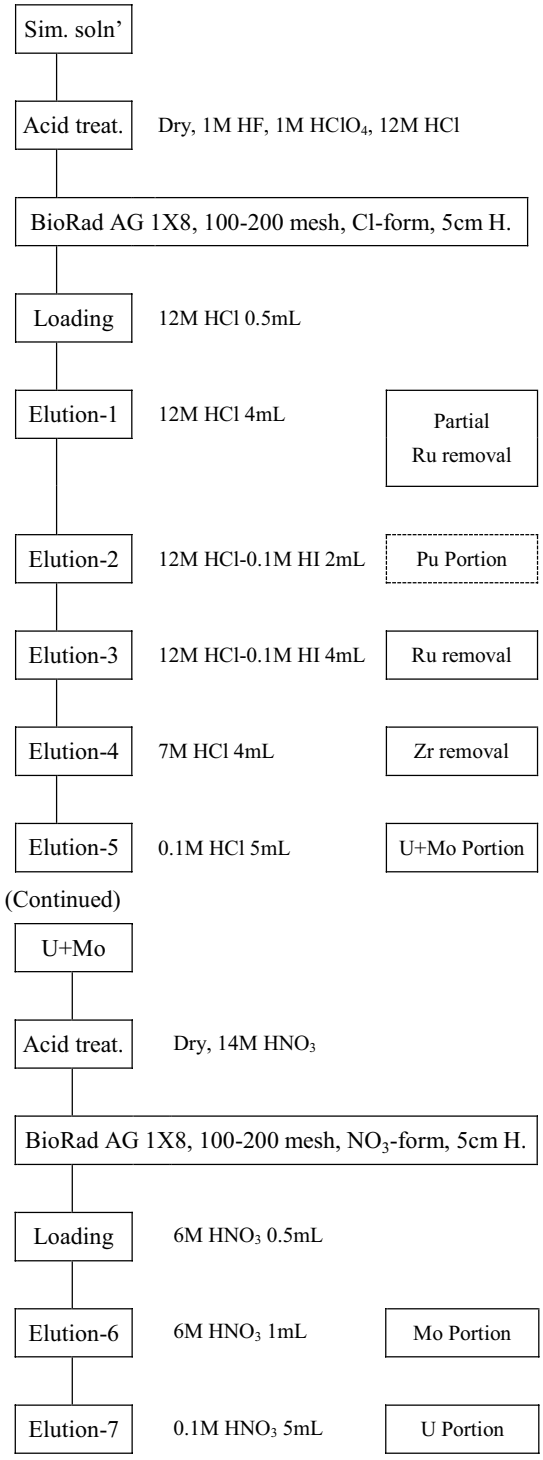

Fig. 1. Analytical Scheme-I for the Mo and U Separations

.

Table 2. ICP-AES results for Each Portions Separated from the Simulated Fuel Solution

Sample	μg/mL			
	Mo	U	Ru	Zr
S-21	<0.10	<0.10	0.389	<LOD
S-22	<0.10	<0.10	<0.10	2.398
S-23	1.767	<0.10	<0.10	<LOD
S-24	<0.10	5.954	<0.10	<LOD

LOD(Zr) : 0.169 μg/mL

4. Conclusion

The Mo and U in the simulated fuel solution can be separated and determined simultaneously by the inductively coupled plasma atomic emission spectrometry. It is expected that the contents of U, Mo and their isotopes in the simulated fuel solution and the real irradiated fuel solution can be determined simultaneously by the isotope dilution mass spectrometric method using ^{233}U and ^{96}Mo as spikes. A comparison between values determined by two analytical techniques provides a check on the validity of the results. The separation procedures established in the present work would be applied for burnup determination by the isotope dilution mass spectrometric method by using quadrupole spikes (^{233}U, ^{242}Pu, ^{150}Nd and ^{96}Mo).

REFERENCES

[1] J. S. Kim, Y. S. Jeon, S. D. Park, S. H. Han, and J. G. Kim, "Burnup Determination of High Burnup and Dry Processed Fuels Based on Isotope Dilution Mass Spectrometric Measurement", J. Nucl. Sci. Technol, 44(7), 1015-1023 (2007).

[2] F. L. Lisman, W. J. Maeck, and J. E. Rein, "Determination of Nuclear Fuel Burnup from Fission Product Analysis", Nucl. Sci. Eng., 42, 215-219 (1970).

[3] P. W. J. M. Boumans, "Inductively Coupled Plasma Emission Spectroscopy", Chemical Analysis: Volume 90, John Wiley & Sons, Inc. (1987).

Study on Decomposition Characteristics of Oxalic Acid and Hydrazine by Electron Beam Irradiation

DongWoo Kim[1,2], Kang Lee[1], KiHwan Park[1], KyungHoon Jung[1], and Seungjoo Lim[1,*]
[1] Korea Atomic Energy Research Institute, 29, Geumgu-gil, Jeongeup-si, Jeollabuk-do, Republic of Korea
[2] Jeonju University, 303, Cheonjam-ro, Wansan-gu, Jeonju-si, Jeollabuk-do, Republic of Korea
[*]seungjoolim@gmail.com

1. Introduction

In the nuclear industry, organic acids (oxalic acid, citric acid, formic acid, etc.)

Various organic solvents such as ascorbic acid, di-2ethylhexylphosphoric acid (HDEHP), and tributyl phosphate (TBP) have been used.[2)]

Of the above organic solvents, oxalic acid ($C_2H_2O_4$) Sedimentation agents for sedimentation, extraction agents for decontamination of radioactive materials, and general decontamination agents.[2)]

In addition, in nuclear power plants, oxalic acid is used to remove the oxide film formed on the internal surfaces of various facilities such as piping, pumps, heat exchangers, etc. related to power generation.[1)]

It is combined with the oxidized precipitate and is present in water in complex form.

As the removal process of oxalic acid, various methods such as a method using an oxidizing agent such as KMnO4, chromic acid, and an ion exchange method are suggested.3)

However, the conventional methods have a problem that the metal ions remain in the final treatment liquid, the treatment chemicals are consumed excessively, and the waste liquid and waste are excessively generated.

Hydrazine(N_2H_4) is a weak base and is a strong reducing agent and is mainly used for rocket propellants, reactants for military fuel cells, plating, polymerization, and removal of dissolved oxygen from boiler feedwater causing corrosion.

Hydrazine solution is used in water treatment process of boiler because it suppresses oxidation of metal in low or high pressure steam environment and maintains weak reduction state.

It is used in applications such as metal corrosion inhibition, dissolved oxygen removal, etc. in addition to oxalic acid in nuclear power plant, and it is mainly used in the first system cooling water.

Recently, new elimination methods such as advanced oxidation have been actively studied.

In this study, we compared the treatment effects of excess hydrazine and oxalic acid in the waste and waste through electron beam irradiation.

2. Main subject

2.1 Materials and Methods, Analysis

2.1.1 Sample Preparation. The initial concentration of oxalic acid (Oxalic Acid, 99 +%, 144-62-7, Aldrich Chemical Company, Inc.) were set at 2, 5, 10 and 20 mM.

The initial concentration of hydrazine(Hydrazine monohydrate 98%, N_2H_4 64-65%, Lot#BCBX7481, Sigma-Aldrich Chemical company, Inc.) was set at 20 mM.

2.2 Radiation (Electron Beam) Irradiation

All the irradiation experiments were carried out with the electron beams of the electron beam accelerator units 2 of EB-Tech (170-9, Techno 2-ro, Yuseong-gu, Daejeon, 34028, KOREA). The maximum electron energy is 2.5 MeV(19 mA, 100kW).

All investigations were carried out at room temperature. The absorbed dose of radiation was 5, 10, 30, 50 kGy. The sample was allowed to have a depth of 0.7 cm in a beaker so that the electron beam could be irradiated uniformly.

2.3 Experimental Apparatus and Analysis Apparatus

The concentration of oxalic acid was analyzed using High Performance Liquid Chromatography (HPLC) (Agilent Technologies, 1200 series). Rezex ROA-Organic Acid H + (8%) (300 × 7.8 mm) was used as the column. The mobile phase used 20 mM $KHPO_4$. TOC-VCSN TOC analyzer (Shimazu, kyoto, Japan) was used to measure total organic carbon.

The concentration of hydrazine was measured by UV-VIS (DR-5000, HACH).

3. Result

Fig. 1 shows the degradation of oxalic acid by concentration.

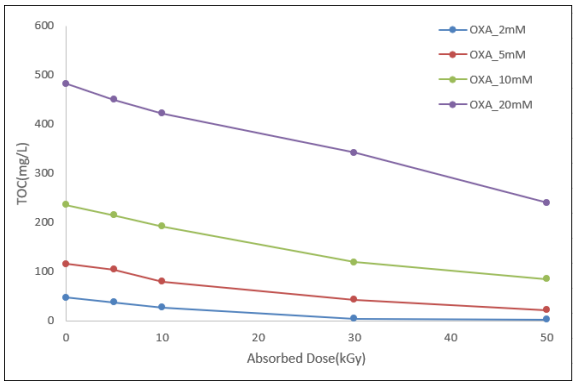

Fig. 1. Degradation of oxalic acid by electron beam irradiation (by concentration).

Fig. 2 shows decomposition of hydrazine by electron beam irradiation.

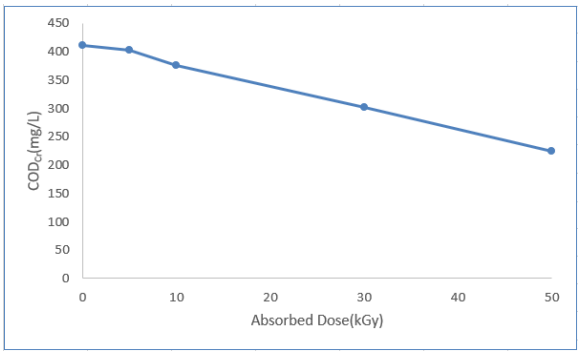

Fig. 2. Decomposition of hydrazine by electron beam irradiation (= 20 mM).

4. Conclusion

The decomposition characteristics of oxalic acid and hydrazine were investigated using electron beam, which is one of the advanced oxidation methods. In the case of oxalic acid, the decomposition efficiency was decreased as the concentration increased. Hydrazine also had the same results as oxalic acid. It is necessary to further decompose organic materials by promoting the generation of OH radicals in water through irradiation with an electron beam after using an oxidizing agent.

REFERENCES

[1] Dong Yun Ha, Soon Haing Cho, Young Soo Choi ,Gyu Seok Kyung, Dong Hyun Kim, “Degradation Characteristics of Oxalic Acid and Citric Acid by UV/H_2 O_2 Oxidation”, KOSENV, 22(7), 1307~1318 (2000).

[2] Eung-Ho Kim, Young-Hwan Kim, Dong-Yong Chung and Jae-Hyung Yoo, “Decomposition of Oxalic Acid in Nitric Acid by UV Radiation”, J. of Korean Ind. & Eng. Chemistry Vol.8,No.1, 108~113 (1997).

[3] Gyu Seok Kyung, Soon Haing Cho, Young Soo Choi, Dong Hyun Kim, Dong Yun Ha “Degradation Characteristics of Oxalic Acid and Citric Acid by TiO_2 Photocatalytic Oxidation”, KOSENV, 25(3), 393~400 (2003).

[5] Sang Dae Kim, Hyun Kyoung Ahn, Hyoung Jun Yoon, In Hyoung Rhee “A study on Decomposition Characteristics of Hydrazine”, KAICS, 2004.11, 255~258 (2004).

2019 춘계학술논문요약집

발행인 김창락

발행처 한국방사성폐기물학회

주 소 대전광역시 유성구 대덕대로 989번길 111
한국원자력연구원 원자력성과확산관(E7) 202호

연락처 **Tel** +82-42-861-5851, +82-42-866-4205
Fax +82-42-861-5852 **E-mail** krs@krs.or.kr

인쇄처 신진기획인쇄사 **Tel** +82-42-638-7887

Abstracts of Proceedings of the
Korean Radioactive Waste Society Spring 2019

www.krs.or.kr

KOREAN RADIOACTIVE WASTE SOCIETY

사단 한국방사성폐기물학회
법인 Korean Radioactive Waste Society